UNIVERSITÀ DEGLI STUDI DI PADOVA

Sede Amministrativa : Università degli Studi di Padova

Dipartimento di Ingegneria Meccanica – Settore Materiali

SCUOLA DI DOTTORATO DI RICERCA IN SCIENZA ED INGEGNERIA DEI MATERIALI

CICLO XXII

Tesi di Dottorato

FABRICATION AND CHARACTERIZATION OF POROUS CERAMICS WITH HIERARCHICAL POROSITY

Direttore della Scuola: Ch.mo Prof. Gaetano Granozzi

_____

Supervisore: Ch.mo Prof. Paolo Colombo

_____

Dottorando: Çekdar Vakıfahmetoğlu

_____

ANNO 2009

ABSTRACT

FABRICATION AND CHARACTERIZATION OF POROUS CERAMICS WITH HIERARCHICAL POROSITY

January 2010, 364 pages

The research work presented in this thesis is concerned with the production of porous components by using preceramic polymers as a starting precursor. During the preliminary studies on which the production of polymer derived cellular ceramics was based; various compositions have been investigated. Cellular SiOC ceramics having a complex morphology were produced using three different types of polysiloxane precursors. Pore formation was attributed to the different polymer architecture which resulted in a different behavior (larger weight loss, shrinkage and gas evolution) upon pyrolysis. In this context; polysiloxane precursors were crosslinked, crushed, sieved and pressed to form compacts yielding with porous SiOC monoliths by pyrolysis. The resulted ceramic bodies showed compressive strength values reaching to 37.4MPa (~53vol% porosity). Hot-isostatic pressing enabled the formation of SiOC(N) tablets having extremely high piezoresistivity in between 100-1700 at high temperatures (700-1000°C). By using a polysilazane precursor microcellular SiOCN and macrocellular SiCN foams were produced via sacrificial templating or a physical blowing agent. Foams had mostly interconnected porosity ranging from ~60 to 80 vol% and possessing a compressive strength in the range ~1 to 11 MPa. By following the similar strategies boron including porous (70 vol%) PDC monoliths have also been produced.

In the direction to produce high specific surface area (SSA) hierarchically porous PDC components; Periodic Mesoporous Organosilica (PMO) particles were embedded into a

foamed polysiloxane polymer, and by pyrolysis, permeable SiOC monoliths having SSA of 137 m^2/g were obtained. In the method; catalyst assisted pyrolysis (CAP), silicon nitride, silicon oxynitride or silicon carbide nanowires were formed directly during the pyrolysis of highly porous monoliths. Increasing the pyrolysis temperature caused an increase in the length and the amount of nanostructures produced. The growth mechanisms for the nanowires depended on the pyrolysis conditions and catalyst type. The presence of the nanowires afforded high SSA values to the macro-porous ceramics, ranging from 10 to 110 m^2/g. The differences were explained in terms of the morphology and amount of the nanowires that were produced using the two different catalysts (Co or Fe). High temperature etching of SiCN ceramics yielded with disordered or graphitic carbon materials possessing a hierarchical bi-modal pore structure (micro-mesopores with mean pore size, 3-11 nm) and large SSA, up to 2400 m^2/g. The resulting porosity (pore size, PSD, and SSA) strongly depended on nanostructural phase evolution of the PDC material, as well as on etching conditions. The mean pore size increased with increasing pyrolysis temperature.

Keywords: Preceramic polymers, cellular ceramics, nanowires, specific surface area, hierarchically porous carbon.

.

RIASSUNTO

SVILUPPO E CARATTERIZZAZIONE DI CERAMICI POROSI A POROSITÀ GERARCHICA

Gennaio 2010, 364 pagine

Il lavoro di ricerca esposto nella presente tesi riguarda la produzione di componenti porosi mediante l'uso di polimeri preceramici quali precursori iniziali. Durante una fase preliminare del lavoro di ricerca, sulla quale si è basata la produzione di ceramici cellulari derivati da polimeri, sono state studiate varie composizioni. Ceramici cellulari di SiOC aventi una morfologia complessa sono stati realizzati usando tre diversi tipi di precursori polisilossanici. La formazione di pori è stata attribuita alle differenti strutture dei polimeri, che hanno comportato differenti comportamenti durante la pirolisi (maggiore perdita in peso, diminuzione del volume e sviluppo di gas). In tale contesto, precursori polisilossanici sono stati reticolati, ridotti in polvere, setacciati e pressati al fine di ottenere campioni risultanti in monoliti di SiOC poroso, mediante pirolisi. I campioni ceramici cosí ottenuti esibivano valori di resistenza a compressione fino a 37,4 MPa (con una porosità pari a circa il 53% in volume). La pressatura isostatica a caldo ha consentito la formazione di campioni di SiOC(N) aventi piezoresistivitá estremamente elevata, compresa tra 100 e 1700 ad alte temperature (700-1000°C). Utilizzando un precursore polisilazanico, sono state prodotte schiume microcellulari di SiOCN e macrocellulari di SiCN, mediante l'impiego di fillers sacrificali o di un agente schiumante fisico. Le schiume presentavano una porosità prevalentemente interconnessa compresa tra ~60 e 80 vol% ed una resistenza a compressione compresa

tra ~1 e 11 MPa. Utilizzando procedimenti simili, sono stati inoltre prodotti campioni monolitici porosi (70 vol%) di PDC contenenti boro.

Al fine di produrre componenti ceramici derivati da polimeri, dotati di porosità gerarchica e di elevata area superficiale specifica (SSA), particelle di PMO (Periodic Mesoporous Organosilica) sono state immerse in un polimero polisilossanico schiumato e, mediante pirolisi, sono stati ottenuti campioni monolitici di SiOC permeabili dotati di una elevata SSA, pari a 137 m^2/g. Mediante tale metodo, pirolisi catalizzata assistita (CAP), nanofili di nitruro di silicio, di ossinitruro di silicio o di carburo di silicio sono stati formati direttamente durante la pirolisi di campioni monolitici altamente porosi. L'aumento della temperatura di pirolisi ha provocato un aumento nella lunghezza e nella quantità di nanostrutture prodotte. Il meccanismo di crescita dei nanofili dipende dalle condizioni di pirolisi e dal tipo di catalizzatore. La presenza dei nanofili ha permesso di raggiugere elevati valori di SSA nei ceramici macroporosi, compresa tra 10 e 110 m^2/g. Le diversità in tali valori sono state spiegate in termini di morfologia e quantità dei nanofili prodotti impiegando due diversi catalizzatori (Co e Fe). L'ablazione superficiale (etching) ad elevate temperature di ceramici di SiCN ha condotto a materiali contenenti carbonio amorfo o grafitico dotati di una struttura gerarchica bimodale dei pori (micro-mesopori con dimensione media dei pori di 3-11 nm) ed elevata SSA, fino a 2400 m^2/g. La porosità risultante (dimensione dei pori, PSD e SSA) dipendeva fortemente dall'evoluzione della fase nanostrutturale del materiale PDC, nonché dalle condizioni di etching. La dimensione media dei pori aumentava all'aumentare della temperatura di pirolisi.

Parole chiave: Polimeri preceramici, ceramici cellulari, nanofili, area superficiale specifica, carbonio a porosità gerarchica.

To my

Lovely mother;

Esma Duman

ACKNOWLEDGEMENTS

I wish to express my deepest gratitude to my supervisor Prof. Ing. Paolo Colombo for his firm guidance, helpful suggestions and endless creative ideas, prompt feedbacks, everlasting patience, encouragements, and the trust he showed in me which supplied me the freedom to implement my ideas. This dissertation would not have been possible without his support.

I express my gratitude for the chance and financial support provided by the Marie Curie Research Training Network (MRTN-CT019601) called PolyCerNet to realize this research.

The author also wants to express sincere thanks to Claudio Furlan for taking SEM micrographs and EDS analyses, and Mauro Gobbin for assisting every time I need a help in the laboratory and as well for his endless patience.

I especially would like to give thanks to my family; starting from my grandmother Beser Duman, my mother Esma Duman, and my aunts Nurcan Taş, Şengül Duman, Mehtap Duman, my uncles Mustafa and Zeynel Duman, as well as my cousins Baran and Deniz Taş for their moral support, encouragement and unselfish love throughout my life.

I would like to express my sincere appreciation and heartfelt thanks to all friends who have shared good times and helped me out in all difficult times. I appreciate the help from all my colleagues, apart from the scientific career that I earned at UNIPD is the friendship, so “grazie mille” to all of you.

TABLE OF CONTENTS

LIST OF TABLES

LIST OF FIGURES

CHAPTER I

INTRODUCTION & MOTIVATION

Oldest Human made ceramics dates back to the upper Paleolithic period. Clay which is an important ceramic and the backbone of the traditional ceramic industry was first processed on the cooking fire of this era. Since these ancient times, the technology and applications of ceramics (including glass) has steadily increased. While industrial revolution made a rapid enhancement in the processing of ceramics, scientific understanding of the 20th century allowed human being to "design" new ceramic types from the combinations of existing materials. These designed ceramics are called advanced or fine ceramics and they exhibit unique or superior functional attributes that can be "precisely specified" by careful processing and quality control.

Like their traditional counterparts, advanced ceramics are often made by mixing and heating the precursor powders which are not naturally occurring raw materials as in the case of traditional ceramics. In recent years, besides traditional manufacturing processes, more sophisticated methods such as chemical vapor deposition (CVD), sol–gel and polymer pyrolysis techniques have been realized to create high-purity starting materials and bulk components with well defined properties. In all three processes, the ceramic solid is synthesized by using the lower molecular, inorganic or elemental organic precursors to develop concepts for the production of novel multifunctional inorganic materials with a tailor-made, nanoscaled structure.[1]

Starting from early 1960s polymeric precursors have been used to produce advanced ceramics at significantly lower temperatures ($T<1500°C$) than the conventional powder sintering processing. The interest in this approach has increased steadily in the last three decades after the commercialization of preceramic polymers.[2] These precursors (preceramic polymers) are organic inorganic polymers with backbone contains usually Si atoms, which give a ceramic residue through the elimination of organic moieties. Polymer to ceramic conversion is achieved either

thermally (pyrolysis, via conventional oven annealing, microwave or laser heating) or non-thermally (for instance by irradiation with ions), usually by processing in inert atmosphere.[3] The thermolysis of silicon-based polymeric precursors under controlled gas atmosphere has proven to be promising route for the production of advanced ceramic components such as fibers, coatings, porous media, or complex-shaped bulk parts. Many examples of polysilanes, polycarbosilanes, polysilazanes and polysiloxanes as precursors for the production of silicon based ceramics have been reported in recent years.[1] In Chapter 2, more detailed information related with preceramic polymers will be given.

The control of porosity during ceramic manufacture is one of the most critical issue and for many years, the presence of porosity in ceramics was often seen to be problematic and a significant scientific effort was made to define the paths for the production of pore free, dense materials.[4] Until recently, engineering the porosity was not realized as a methodology to tailor the materials properties which are of interest for many diverse applications. An exception to this issue could be found in refractory industry where it was understood that porosity is a critical parameter in controlling the thermal conductivity of a material. A considerable effort has recently been directed toward developing porous ceramic materials for the applications including filtration, catalyst supports, biomedical devices, reinforcement for metal matrix composites, bioreactors, thermal protection systems, supports for space mirrors, components in solid oxide fuel cells, lightweight sandwich structures, etc.[4]

The features gained by the replacement of solid material by voids such as low thermal mass, low thermal conductivity, controlled permeability, high surface area, low density, high specific strength, and low dielectric constant, when combined with the inherit properties of ceramic materials like high melting temperature, high corrosion, and wear resistance makes porous ceramics indispensable. All these properties can be tailored for the desired application by controlling the composition and microstructure of the porous ceramic that is; the processing route used for the production of the porous material has to be selected carefully. Changes in open and closed porosity, pore size distribution, and pore morphology can have a major effect on a material's properties.[5]

The simplest processing route for the preparation of porous ceramics is the partial sintering of ceramic powders. This method often results in a relatively low porosity (<60 vol%). Nevertheless, for many applications mentioned before, it is necessary to have high porosity (>60 vol%) ceramics, so called "cellular ceramics". Cellular ceramics are a class of high porosity materials, comprising foams, honeycombs and fiber felts or mats, a recent book edited by Scheffler and Colombo[4] gives a comprehensive info on the fabrication and use of cellular ceramics in a vast number of different applications. The production of porous ceramics from preceramic polymers offers unique opportunities, especially from a processing point of view. In fact, the first suggestion that porous ceramics could be produced from preceramic polymers dates back to early 1990s where blowing agents was used for foaming. Several papers have been since then published in the scientific literature concerning polymer derived porous ceramics.[3, and references therein]

According to IUPAC classification a porous solid falls into one of three categories according to its pore dimension (d): micro-porous if d is less than 2 nm, meso-porous if d is between 2 to 50 nm and macro-porous if d is bigger than 50nm. A porous component containing pores on two or more length scales is referred to as a material with hierarchical porosity. Different types of hierarchical porosity may exist according to the range of pore sizes that are involved in the porous structure, that is, bimodal size distribution (micro–meso, meso–macro, micro–macro), or trimodal (micro–meso–macro). When porous materials are required to perform multiple functions, hierarchical porosity constitutes a means to accomplish these multiple tasks. For example, for various applications such as catalysis, adsorption and support materials, a high surface area and a low pressure drop is needed. This can easily be provided by producing a component with hierarchical porosity. Several routes have been explored to fabricate ceramics with hierarchical porosity[6-9, and references therein]. Commonly these routes can be divided into two main synthesis strategies; i) the use of structure-directing agent combinations (i.e. self assembling surfactants or block-copolymers in conjunction with other larger scale structure-directing agents like polymeric colloids, microemulsions, air bubbles, starch granules and natural biological templates[9]) that control the pore arrangement at different length scales, and ii)

controlled phase separation (i.e. sol-gel transition of the inorganic precursors or well-controlling the hydrodynamic conditions[9]) in a confined space. Recently, Vasiliev et al.[7] demonstrated that it is also possible to produce hierarchically porous (meso/macro) materials from an assembly of porous powders by rapid heating under a compressive pressure using pulsed current processing (PCP). In addition to these methods, in our laboratories preceramic polymers have been used for this purpose; hierarchical porosity was achieved by a controlled thermal treatment[10-12] and/or the addition of suitable fillers such as by depositing zeolites onto the cell walls of SiOC microcellular foams,[13] by coating with a mesoporous film or by selective etching.[14] These studies confirmed the processing flexibility of the preceramic polymer pyrolysis technique to produce hierarchical porosity ceramics. In Chapter 2.3.3, a detailed review on the hierarchically porous ceramics can be found, and as one can see, despite the significant progress in synthesizing hierarchically porous materials, the preparation of such materials with well-defined properties (e.g. pore architecture with all length scales –micro/meso/macro-, high specific strength, high specific surface area, etc.) in a rapid and facile technique remains a challenge.

In the present thesis study, it was aimed to explore simple, cost effective and one-pot novel strategies in order to produce hierarchically porous ceramic monoliths via preceramic polymer pyrolysis route. During the course of the present study, initially a variety of methods have been investigated to fabricate macro-porous Silicon OxyCarbide (SiOC), Silicon OxyBoronCarbide (SiOBC), Silicon OxyCarboNitride (SiOCN), Silicon CarboNitride (SiCN) and Silicon BoronCarboNitride (SiBCN) monoliths. These porous components have been characterized in detail and the data collected is given in Chapter III: *Production and properties of polymer derived cellular ceramics*. Subsequently investigations mainly focused on the fabrication of porous components with hierarchical pore architecture and high specific surface area (SSA). Different routes were followed to obtain different type of hierarchical porous components. Initially, via pyrolysis of macro-porous polysiloxane bodies including the Periodic Mesoporous Organosilica (PMO) particles stuck onto their pore walls; hierarchically porous permeable SiOC monoliths were produced. Afterwards, Catalyst Assisted Pyrolysis (CAP) of polysiloxane foams let us to discover the fruitfulness of the preceramic polymer route to produce hierarchical porous high specific surface area SiOC ceramics composites including either Silicon Carbide (SiC) or

Silicon Nitride (Si_3N_4) nanowires (depending on thermolysis atmosphere) protruded from the cell walls of macro-porous bodies. Finally, high temperature chlorination of some PDC systems was investigated. The results showed also here the usefulness of preceramic polymers; high temperature chlorination of SiCN ceramics derived from polysilazane precursor resulted in a hierarchically porous carbon with an extremely high specific surface area reaching 2400m^2/g. More detailed information for these investigations could be found in Chapter IV: *Production and properties of high specific surface area components from preceramic polymers.* The thesis will be finalized with the general conclusions given in Chapter V.

1.1. References

[1]R. Riedel, E. Ionescu, and I.-W. Chen, "Modern Trends in Advanced Ceramics," pp. 3-38 in Ceramics Science and Technology, Volume 1: Structures. Edited by R. Riedel and I.-W. Chen. WILEY-VCH Verlag GmbH & Co. KGaA Weinheim, 2008.

[2]Y.D. Blum, K.B. Schwartz, and R.M. Laine, "Preceramic polymer pyrolysis," *Journal of Materials Science*, 24 [5] 1707-18 (1989).

[3]P. Colombo, "Engineering porosity in polymer-derived ceramics," *Journal of the European Ceramic Society*, 28 [7] 1389-95 (2008).

[4]M. Scheffler and P. Colombo, "Cellular ceramics: structure, manufacturing, properties and applications," WILEY-VCH Verlag GmbH, Weinheim, Germany, 2005.

[5]A.R. Studart, U.T. Gonzenbach, E. Tervoort, and L.J. Gauckler, "Processing Routes to Macroporous Ceramics: A Review," *Journal of the American Ceramic Society*, 89 [6] 1771-89 (2006).

[6]J.-H. Smatt, S. Schunk, and M. Linden, "Versatile Double-Templating Synthesis Route to Silica Monoliths Exhibiting a Multimodal Hierarchical Porosity," *Chemistry of Materials*, 15 [12] 2354-61 (2003).

[7]P.O. Vasiliev, Z. Shen, R.P. Hodgkins, and L. Bergstrom, "Meso/Macroporous, Mechanically Stable Silica Monoliths of Complex Shape by Controlled Fusion of Mesoporous Spherical Particles," *Chemistry of Materials*, 18 [20] 4933-8 (2006).

[8]T.-Z. Ren, Z.-Y. Yuan, A. Azioune, J.-J. Pireaux, and B.-L. Su, "Tailoring the Porous Hierarchy of Titanium Phosphates," *Langmuir*, 22 [8] 3886-94 (2006).

[9]Z.-Y. Yuan and B.-L. Su, "Insights into hierarchically meso-macroporous structured materials," *Journal of Materials Chemistry*, 16 [7] 663-77 (2006).

[10]H. Schmidt, D. Koch, G. Grathwohl, and P. Colombo, "Micro-/Macroporous Ceramics from Preceramic Precursors," *Journal of the American Ceramic Society*, 84 [10] 2252-5 (2001).

[11]M. Wilhelm, C. Soltmann, D. Koch, and G. Grathwohl, "Ceramers--functional materials for adsorption techniques," *Journal of the European Ceramic Society*, 25 [2-3] 271-6 (2005).

[12]A.V. Belyakov, N.N. Fomin, and D. Koch, "Nanoporous Ceramics Based on Organosilicon Polymers," *Glass and Ceramics*, 59 [1] 54-7 (2002).

[13]A. Zampieri, P. Colombo, G.T.P. Mabande, T. Selvam, W. Schwieger, and F. Scheffler, "Zeolite Coatings on Microcellular Ceramic Foams: A Novel Route to Microreactor and Microseparator Devices," *Advanced Materials*, 16 [9-10] 819-23 (2004).

[14]S. Costacurta, L. Biasetto, E. Pippel, J. Woltersdorf, and P. Colombo, "Hierarchical Porosity Components by Infiltration of a Ceramic Foam," *Journal of the American Ceramic Society*, 90 [7] 2172-7 (2007).

CHAPTER II

MATERIALS & RELATED LITERATURE

2.1. Preceramic Polymers

Preceramic polymers are inorganic and organometallic polymers in which unlike conventional organic polymers, which contain a chain of carbon atoms, the chain backbone contains other elements (such as Si, B, and N) than carbon or in addition to carbon.[1] Pyrolytic decomposition of metal-organic polymeric compounds to produce ceramics is described as polymer pyrolysis. The schematic transitions during ceramic manufacturing from preceramic polymers are shown in **Figure 2.1-1**.[2]

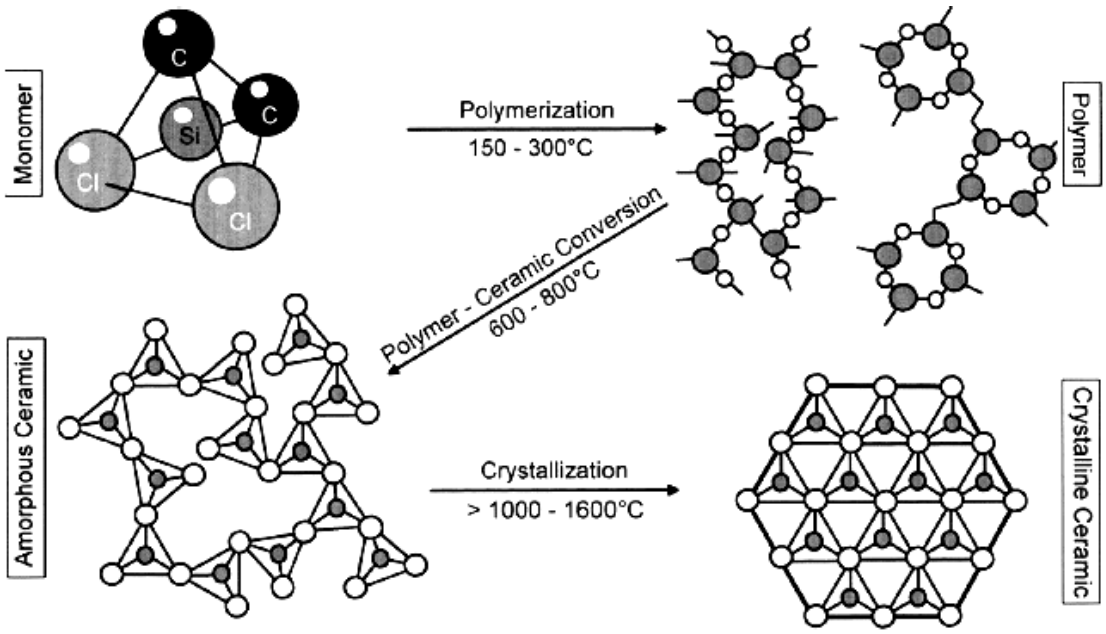

Figure 2.1-1. Scheme of molecular and microstructural transitions during ceramic manufacturing from preceramic polymers.[2]

It is know that the resulting chemistry of the preceramic polymer dictates the final properties of ceramic material.[3-5] Therefore in order to obtain a ceramic with high-quality properties one has to satisfy the general requirements for a precursor suitable for pyrolysis processing. Rahaman M. N.[1] summarized these key factors as; (a) the ability to be synthesized from low-cost starting materials and polymerization reactions, (b) fusibility at moderate temperatures or solubility in solvents for formation into the required shape, (c) high ceramic yield on pyrolysis (greater than -75 wt%) to minimize volume changes and so shrinkage stresses, and (d) pyrolysis to give desired chemical composition and microstructure for property optimization.

Currently two most important methods are in use for the synthesis of ternary or quaternary glasses in the Si-O-C-N-B system namely; sol-gel processing of organosilicon compounds and pyrolysis of preceramic polymers. Although sol-gel process can be versatile because of the advantage of low temperature processing, drawbacks such as shrinkage and cracking caused by solvent or byproducts evolution during drying and pyrolysis have motivated research on new synthetic methods for this class of materials.[6] Therefore, a large variety of silicon containing polymers which are well suited to fulfill above requirements, were developed (see **Figure 2.1-2**) in the last decade, albeit still only few of them are commercialized and most of them are in laboratory scale.[2]

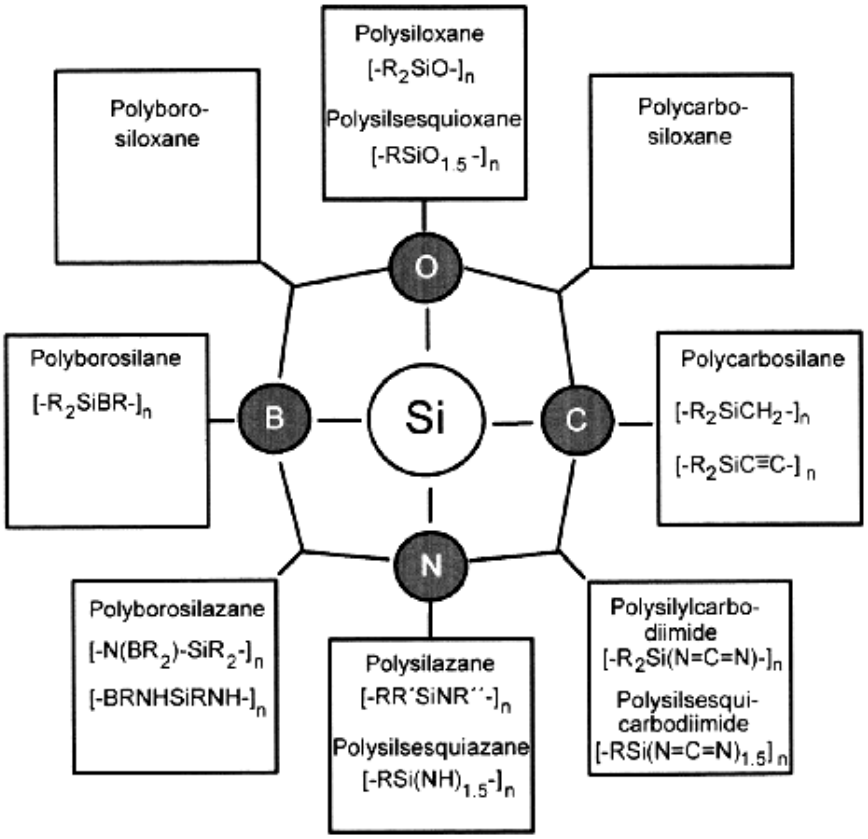

Figure 2.1-2. Preceramic polymer compositions in Si-O-C-N-B system.[2]

Binary compounds can also be prepared by the polymer pyrolysis of appropriate organometallic precursor. For example among the given silicon containing preceramic precursors in **Figure 2.1-2**; polycarbosilanes have been the subject of much interest and were widely studied in the last three decades particularly as a precursor for SiC materials. This was because silicon carbide formation via the preceramic polymer route is advantageous compared with conventional techniques (e.g. Acheson process) in that lower formation temperatures (800–1500°C) are used.[7]

Recently, polysiloxanes and polysilazanes have been used to fabricate ternary and quaternary ceramic components in Si-O-C-N system. While polysilazanes are still expensive precursors to produce SiCN ceramics and pose problems in handling as they are sensitive to ambient atmosphere, polysiloxanes are readily available, cheap in cost and can be converted to SiOC ceramic by following very easy processing strategies (see later).[8]

In the present study chiefly commercially available polysiloxanes were used in order to obtain cost effective ceramic components. Some additional experiments have been conducted by using commercially available polysilazanes and lab scale synthesized boron modified polysilazanes. Although every company has its own price criteria and difficult to give a generalized costs, for the reader we can comment that the market prices for these precursors, roughly speaking with 2010 costs are; ~20euro/kg for polysiloxane resins, ~800euro/l for polysilazane and ~1000euro/l for polycarbosilane. Due it was aimed to utilize preceramic polymer technology to develop new ceramic formations from the commercial precursors, the following sections will not cover preceramic polymer synthesis methodologies in detail, but will only be a brief review focusing mainly on their general characteristics. Moreover, information related to polysilane and polycarbosilane polymers is excluded from the following sections. This is mainly due to a) compared to polysiloxane and polysilazanes they are much more expensive, and b) they have already been subjected to a large number of investigations starting from the first synthesis of a SiC material from polycarbosilane precursor dating back to late 70s.[3, 9, and references therein]

2.1.1. Poly(organosiloxane) and its derivatives.

Definition of siloxane is; any chemical compound composed of R_2SiO units, where R is a hydrogen atom or a hydrocarbon group. According to the main rules for classification of chemicals (The International Union of Pure and Applied Chemistry, IUPAC) these R_2SiO compounds are designated siloxanes, but most often the term "silicones" are used to describe the product made from siloxane units. Therefore, silicones which are actually the polymerized siloxane blocks, are called as polysiloxanes or poly(organosiloxanes). Polysiloxanes are silicon analogues of carbon based organic compounds, and can form (relatively) long and complex molecules based on silicon. Backbone is formed of alternating silicon-oxygen atoms (...Si-O-Si-O-Si...) or siloxane, rather than carbon atoms (...C-C-C-C...). Other species attach to the tetravalent silicon atoms and not to the divalent oxygen atoms which are fully committed to form siloxane chain. A typical example is polydimethylsiloxane (PDMS), where two methyl groups attach to each silicon atom to form the structure. The carbon analogue

would be an alkane, i.e. dimethylpropane, see **Figure 2.1-3** (a) and (b) for the comparison of backbone structures given for these two polymer types. Enthalpy of dissociation (in kilojoules per mole) and bond length (in picometers), respectively, are given for the following covalent bonds: Si-O, 452 and 166; C-C, 346 and 154; C-O, 356 and 143; C-N, 305 and 147; and Si-C, 318 and 185. As seen the dissociation energy of Si-O bond (~452 kJ/mol) is considerably higher than those of C-C and C-O bonds.[10, 11] Consequently, the Si-O bond can withstand exposure to higher temperatures than the bonds normally found in organic polymers. This makes polysiloxanes as a class of materials exhibiting higher thermal stabilities than their C-C counterparts.[12]

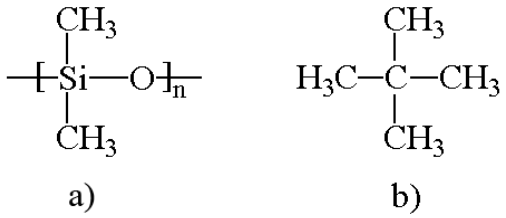

Figure 2.1-3. Backbone structure of a) polydimethylsiloxane, and b) dimethylpropane.

There are two general routes to form polysiloxanes polymers: the polycondensation of α,ω-functionalized linear silanes and the ring opening polymerisation (ROP) of cyclic silaethers.[13, 14] The details for these synthesis methods could be found in recent reviews.[13, 15, 16] Polysiloxanes are one of the most common precursors having the general formulae $[RR'SiO]_n$ where R and R' = hydrogen, methyl, vinyl, phenyl, OH, OEt, etc. These groups can further condensed, to give highly crosslinked, insoluble polysiloxane networks (thermosets). Several abbreviations are used for naming of polysiloxanes. "M" stands for R_3SiO that is mono-functional unit while "D" for di-functional: R_2SiO_2, "T" for tri-functional: $RSiO_3$ and "Q" for quadric-functional SiO_4 units (a network of only Q groups becomes fused silica). A majority of polysiloxanes contains all above units in a mixed state where each R independently stands for hydrogen atoms or some radicals (e.g. alkyl, phenyl and vinyl). They can be classified into three types depending on the length of the backbone, the extent of crosslinking and the type and number of organic groups attached to the silicon atoms: i) silicone fluids (oils), ii) silicone elastomers, and iii) silicone resins. Polysiloxanes can be handled in air and are available in

liquid, semi-solid (viscous) as well as solid (powder, resins) form. Polymeric applications of polysiloxanes (cured or uncured) are beyond the scope of this work (the reader interested in these cases is referred to reference[17]) and thus there will be only some basic info about their structures and the curing mechanisms in the following subsections.

2.1.1.1. Silicone fluids (oils)

Silicone fluids (also called as silicone oils) include silicon and oxygen atoms which might be linked into linear or cyclic structures. Linear polysiloxanes are characterized by the functional side chains attached to the Si-O backbone and the end groups terminating the structure. As an example in Figure 2.1-4(a) the structure of vinyl-terminated polydimethylsiloxane while in Figure 2.1-4(b) polyphenyldimethylsiloxane structure is demonstrated.

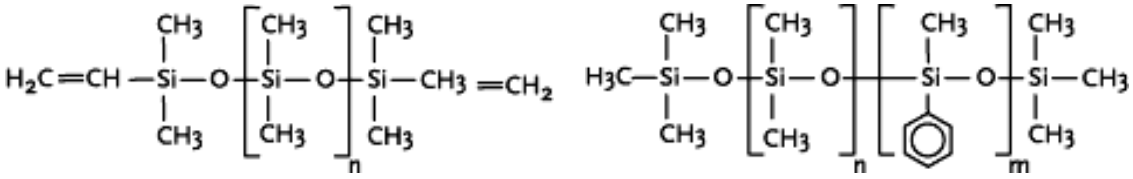

(a) (b)

Figure 2.1-4. The plausible chemical structures of a) vinyl-terminated polydimethylsiloxane, and b) polyphenyldimethylsiloxane.

Cyclic siloxanes are generally used as intermediates for the production of higher molecular weight linear polysiloxanes, and partly used directly as fluids. In the cyclic siloxanes the Si-O backbone forms a cyclic structure with two substituent attached to each silicon atom.The nomenclature for cyclosiloxanes is often designated with reference to the number of silicone atoms: D3 cyclotri-, D4 cyclotetra-, D5 cyclopenta- and D6 cyclohexa-siloxane, see Figure 2.1-5 for the representative image of decamethyl-cyclo-pentasiloxane, D5, structure.

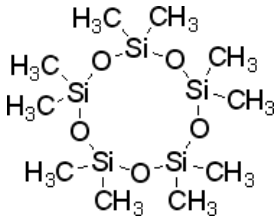

Figure 2.1-5. The plausible chemical structure of D5, decamethyl-cyclo-pentasiloxane.

Cross-linking of polysiloxane polymers results in an insoluble thermoset which might be used as a preceramic precursor. Quality preceramic precursor should have at least two inherent characteristics: latent reactivity and branched structures. The latent reactivity can provide the opportunity for cross-linking and so works in maintaining appropriate shape during processing and high ceramic yield. Linear polymers generally give low ceramic yield owing to backbone reactions that lead to escape of volatilities. Branched structures can, however, slow down the backbone reactions due to steric hindrance or steric resistance which occurs when the large size of groups within a molecule prevents chemical reactions that are observed in related smaller molecules. Silicone fluids generally increase in viscosity with increasing chain length. Their properties are strongly dependent on the functional groups. These precursor can easily be transformed into a three dimensional network via a crosslinking reaction, which allows the formation of chemical bonds between adjacent chains. This is achieved according to one of the following mechanisms: by, addition (hydrosilylation), condensation or radical reaction.

Polysiloxanes having vinyl groups and hydrogen are often preferred since these groups can provide a mechanism for curing by hydrosilylation reaction. Hydrosilylation (addition curing), which involves the addition of a silicon hydride to an unsaturated carbon-carbon bond (vinyl or other alkenyl functionality) can be catalyzed radically, ionically, or by noble metal complex such as platinum, rhodium or palladium. These metal complexes are usually added at concentrations of 10-500 ppm, preferably of 50-300 ppm. For example Pt-catalyzed hydrosilylation reaction of poly(methylhydrosiloxane) and 1,3,5,7-tetramethyl-1,3,5,7-tetravinylcycletetrasiloxane (D_4Vi), yields with a highly branched thermoset which gives a high ceramic yield > %86 upon pyrolysis.[6] As in the given example, usually the polymer-base contains Si-vinyl groups in the side chains. Methylhydrogensiloxane compounds (cyclic or

polymeric), can be used as cross-linking agents and the addition reaction is selective, giving rise mainly to –(Si-CH_2-CH_2-Si-) bridges, see curing schema given in Figure 2.1-6. A major advantage of hydrosilylation is that the curing reactions do not produce byproducts.

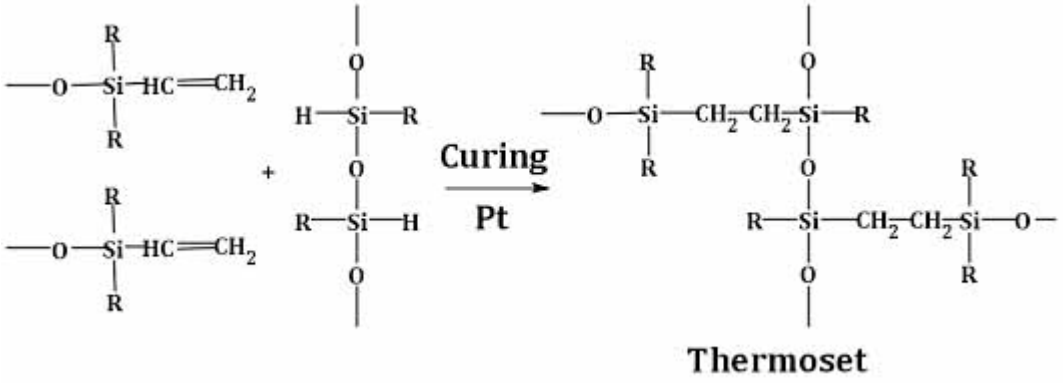

Figure 2.1-6 Addition curing of vinyl containing siloxane with hydro-siloxane under Pt catalyst.

In condensation curing mechanism, the presence of organometallic zinc or tin compounds such as zinc acetylacetonate, zinc octoate, stannous (tin) octoate, tin diacetate, etc. is required to catalyze silanol (hydroxy end-blocked) containing polysiloxanes. A representative example is given in Figure 2.1-7, where the presence of tin diacetate lets α,ω-dihydroxypolydimethylsiloxane reacts reversibly with silicic acid ester and releases alcohol as by-product. General by-products of the condensation curing are water, alcohols, and acids which might cause some problems concerning chemical shrinkage or corrosion.

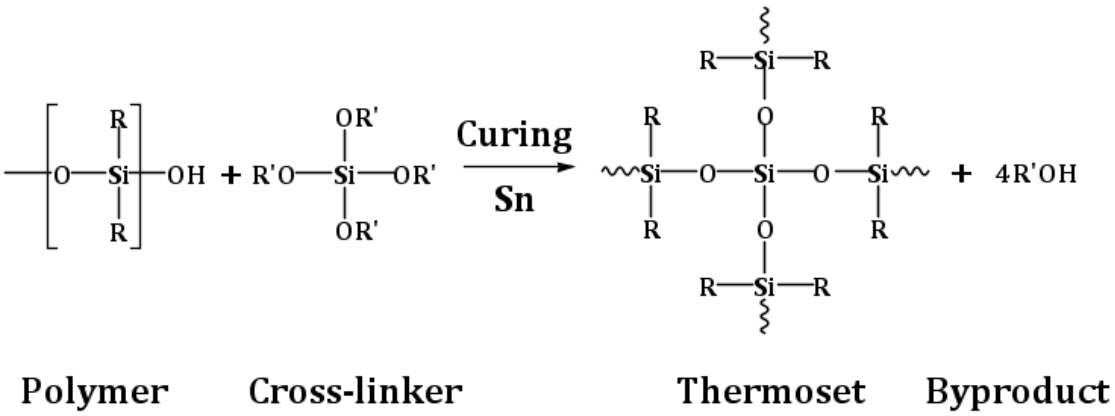

Figure 2.1-7. Condensation curing of hydroxyl terminated polysiloxane with stiric acid crosslinker under Sn catalysis.

Curing of polysiloxanes can also be done by peroxide addition. Peroxide curing systems require energy (heat or radiation) to enable the peroxide (radical generator) catalyst to decompose into two free radical-containing components. Cross-linking occurs as the free radicals on one polymer chain react and bond with alkyl species on another polymer chain (generally with vinyl groups), see Figure 2.1-8 for representative curing mechanism. Different organic peroxides may serve as free-radical generators for initiating this type of curing. Like any other compounding ingredients, choice of peroxide is dictated by technical reasons such as the peroxide reactivity, polarity, transparency, and cure temperature required. Dicumyl Peroxide (DCP, Cumene peroxide), one of the cheapest peroxide, is found to effectively polymerize many preceramic precursors.

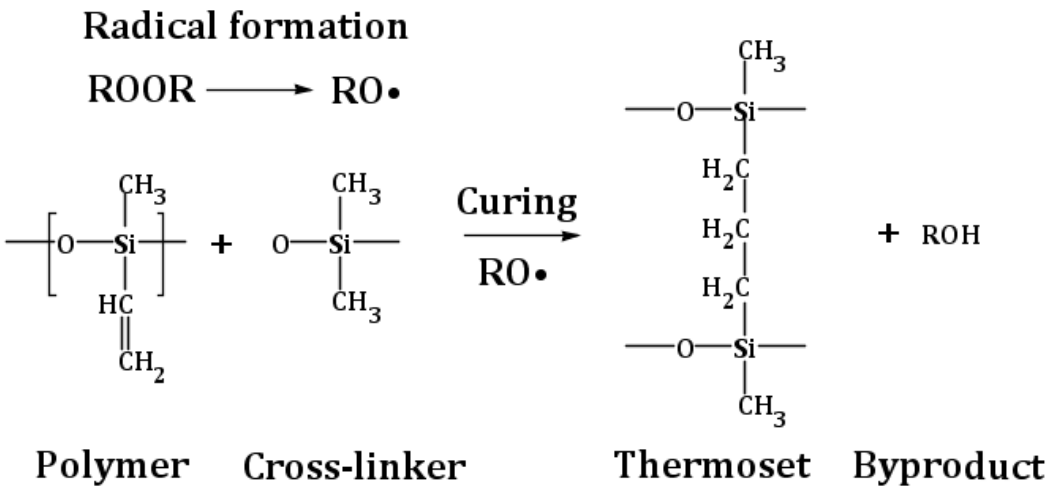

Figure 2.1-8. Representative cross-linking mechanism for peroxide curing.

2.1.1.2. Silicone elastomers (rubbers)

Elastomers are formed from silicone fluids by the formation of cross-links between linear precursor and cross-linking agent. This process is called “curing”, but also “vulcanization” differently from terminology of plastics technology where it usually means the sulfur treatment. Normally, heat is required to cure (vulcanize) the rubber. Usually, elastomers are categorized in four main types: one component RTV (room temperature vulcanizing), two component RTV elastomers, HTV (high temperature vulcanizing), and LSR (liquid silicone rubber) elastomers. One of the most common and cheap elastomer; poly(dimethyl-siloxane) (PDMS) could easily be prepared by mixing ten parts of vinyl-type PDMS (generally sold as “part A”, also called as “oil A”) with one part of hydrosilyl-type PDMS (generally sold as “part B”, also called as “oil B”). Hydrosilylation reaction catalyzed by platinum ions in oil A forming a PDMS thermoset with a linear structure. Silicone rubbers offer excellent electrical insulating properties, inertness, low toxicity and resistance to ozone, weathering, and finally a wide range of application temperature, being able to operate between -100°C to 500°C. However, since generally rubbers have linear backbone structure, during pyrolysis they give a low ceramic yield so that their use as a preceramic polymer is highly limited.

2.1.1.3. Silicone resins

Whereas silicone oils and elastomers are based on cyclic or linear polymers, silicone resins are highly branched polymers. Due to this phenomena during thermolysis under inert gas atmosphere these precursors generally gives high ceramic yield. Poly(organosilsesquioxanes) (interchangeable with polysilsesquioxane) are a subgroup of the polysiloxanes and usually can be found as solid form, i.e. resin. The term silsesquioxanes denotes a polymer in which the ratio of silicon and oxygen in each moiety (sequence) is 1.5 (*latin: sesqui*). The polysilsesquioxanes are highly branched polymers and they can be described by a ladder structure, see **Figure 2.1-9**(a). More complex structures are also designated like "cage structure" and "random structure", see **Figure 2.1-9**(b) and (c), respectively for these structures. They have a general formulae $[RSiO_{1.5}]_n$ and they are generally solid in room temperature due to their higher Tg resulted from the higher backbone branching compared to that of polysiloxanes for which Si:O ratio is fixed to 1. At the present time, polysilsesquioxanes are unique among preceramic polymers and are most important ones with regard to commercial aspects of practical applications.

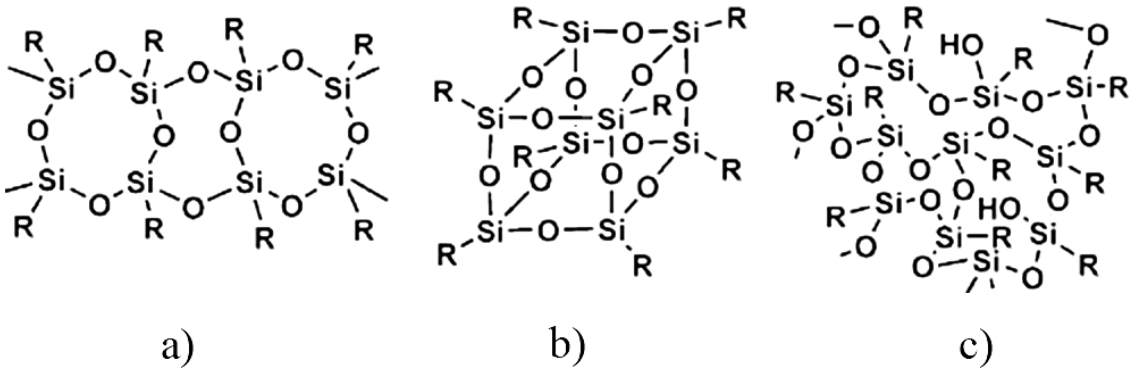

Figure 2.1-9. Hypothetical structures for polysilsesquioxanes a) ladder, b) cage like, and c) random amorphous.[18]

Silicon resins may include few amount of (generally 2-7wt%) functional cross-linking groups like hydroxy and ethoxy. In **Table 2.1-1**, organo and cross-linking functional groups of some commercial silicon resins are given.[19, 20] While H62C cures via addition mechanism due to

vinyl groups, all other resins given in table, can cross-link in air by condensation mechanism at low temperatures (between 100-300°C) without the need of any peroxide or catalyst additive. Cross-linking of these resins can be accelerated by a number of catalysts which can effect condensation curing over hydroxy groups; e.g. zinc acetylacetonate ($C_{20}H_{28}O_8Zr$).[8] The curing rate depends on the concentration and the type of curing agent, as well as on the curing temperature. Curing results in the release of reaction byproducts such as water, ethanol and oligomers, see reaction schema (2.1-1) and (2.1-2) below.[19] These byproducts could be used as intrinsic blowing agents to introduce porosity into the cured thermoset. This methodology will be discussed later in the thesis comprehensively.

$$\equiv Si - OH + HO - Si \equiv \rightarrow \equiv Si - O - Si \equiv + H_2O \qquad 2.1\text{-}1$$

$$\equiv Si - OC_2H_5 + HO - Si \equiv \rightarrow \equiv Si - O - Si \equiv + C_2H_5OH \qquad 2.1\text{-}2$$

Table 2.1-1. Functional groups of various commercial polysilsesquioxanes.*

Commercial: Chemical name	**Company / Form**	**Organo groups**		**Cross-linking groups**	
		R	**R′**	**O-R**	**O-R′**
MK: poly(methyl-silsesquioxane) (PMS)	Wacker / Solid	$-CH_3$	--	-OH	$-OC_2O_5$
H44:poly(methyl-phenyl-silsesquioxane) (PMPS)	Wacker / Solid	$-CH_3$	$-C_6H_5$	-OH	$-OC_2O_5$
601:poly(phenyl-silsesquioxane) (PPS)	Wacker / Solid	$-C_6H_5$	--	-OH	--
SR350:poly(methyl-silsesquioxane) (PMS)	General Electrics / Solid	$-CH_3$	--	-OH	--
H62C:poly(methyl-phenyl-vinyl-hydrido-silsesquioxane) (PMPVHS)	Wacker / Liquid	$-CH_3$ -H	$-C_6H_5$ $-C_2H_3$	Cures via addition mechanism of vinyl groups.	

*info is extracted from the data sheets

Technical properties of some polysilsesquioxane resins used during the present thesis study are listed in **Table 2.1-2**. Besides these resins, silicone oils and elastomers were also used for specific aims, information about these polymers will be given later on where these polymers utilized.

Table 2.1-2. Typical general characteristics of some commercial polysilsesquioxane resins.*

	MK	**H44**	**601**	**H62C**
Supply form	White powder	Colorless to yellowish powder	Colorless to yellowish flakes	Yellowish liquid
Melting point / Melting range	35-55 °C	45-60 °C	50-70°C	Viscosity, dynamic at 23 °C=900 mPa.s
Bulk density	0.5 g/cm³	0.45 g/cm³	n.a.	at 23 °C=1.13 g/cm³
Thermal decomposition	> 350°C	> 500°C	n.a.	n.a.

*info is extracted from the data sheets, n.a. : data not available

Among these resins MK and H44 were used more frequently. Both of these precursors are cheap and could easily be found in the market, while MK has methyl groups attached to its siloxane backbone, H44 includes phenyl groups which make the precursor higher in carbon content. See Figure 2.1-10(a) for the possible structure that is methyl network unit of MK precursor[8] and Figure 2.1-10(b) for methyl-phenyl unit of H44. Cross-linking active groups are illustrated in Figure 2.1-11(a) and (b).

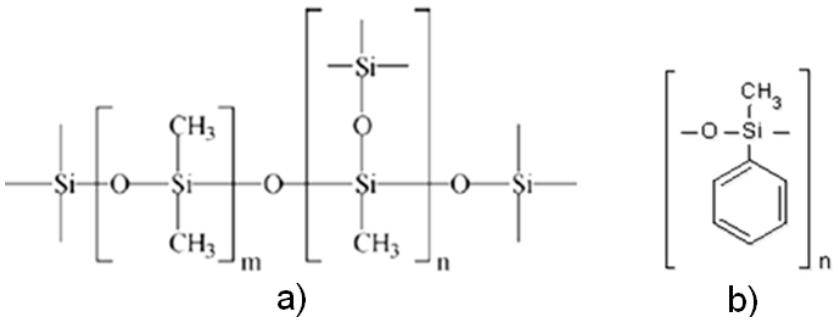

Figure 2.1-10. a) linear and branched network units of MK (PMS) and b) methyl-phenyl unit of PMPS (H44).

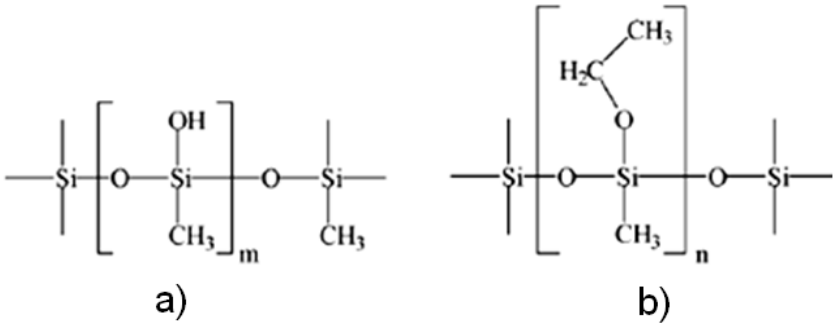

Figure 2.1-11. Structural units containing a) OH- and b) OEt-functional groups which are used for curing both for MK and H44.[8]

After cross-linking of such precursors, the obtained preceramic networks can be thermolyzed under inert gas atmosphere to obtain ceramic materials. During pyrolysis first elimination of the organic parts in organic/inorganic transformation is observed. This period is also called polymer decomposition or mineralization or ceramization and occurs roughly between 400-800°C depending on the polymer architecture. Through this period due to the released gaseous products like oligomers, CH_4, C_2H_4, C_6H_6, etc (depending on the precursor backbone, see **Figure 2.1-12**) a transient nanometric size porosity is generated. This transient (micro-) porosity is eliminated when the pyrolysis temperature leading to the completion of the ceramization process is increased, according to a densification mechanism based on surface reaction/pyrolysis accommodated by viscous flow.[21] On the other hand, larger pores resulted due to manufacturing (e.g insufficient powder compaction during warm-pressing) may stay in

the structure.[22] SiOC material obtained above 800°C remains predominantly amorphous up to 1200-1300°C.

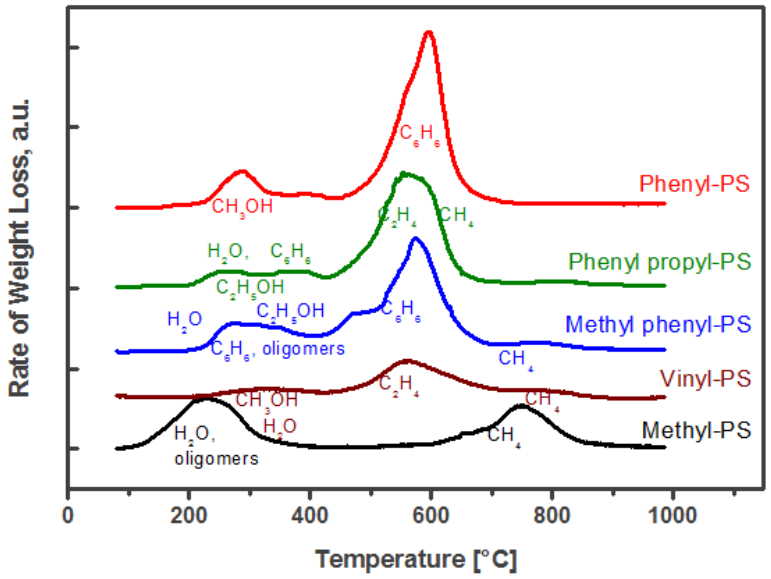

Figure 2.1-12. DTG curves of some commercial polysilsesquioxane (PS) resins.[19]

The chemistry of SiOxCy (x+y=4) compounds could be different relying on the precursor chemistry and pyrolysis conditions (atmosphere, heating & cooling rate, etc.). For example; when MK and H44 pyrolyzed in the same conditions (1050°C, 1h dwelling, 1C/min heating and cooling rate), they gave very different carbon yield; 12.8wt% and 39.1wt% of carbon yield, respectively.[19] As could be understood -organo groups attached to the main siloxane backbone dictates the final carbon yield of the formed ceramic when commercial resins are selected. Therefore selection of commercial resin has to be done concerning the requirements for the final product. As an alternative, polysiloxane oils can be intentionally modified to alter their carbon amount. For example; recently Blum et al.[23] have shown production of carbon-enriched silicon oxycarbides from the precursor synthesized by grafting and crosslinking polyhydridomethylsiloxane (PHMS) with divinylbenzene (DVB) using a hydrosilylation reaction in the presence of a very efficient platinum catalyst. These new high-carbon- SiOC materials demonstrated unexpectedly high thermal, chemical, and environmental stability, as well as remarkable microstructural stability at their amorphous stage (at least up to 1200°C).[23]

In Chapter 2.2.1 more detailed information related with the pyrolysis process of polysiloxane polymers and properties of polymer derived SiOC ceramics could be found.

Finally it has to be mentioned that, by chemical modification of the polysiloxane structure, the final composition of the produced ceramics can be tailored. This alteration in fact changes most of the materials' properties. For example; the modification of polysiloxanes by main group elements such as B and Al has attracted recent interest due to their strong influence on the thermo-mechanical properties and microstructure development of the formed new ceramics like SiOBC, SiOAlC.[12, 14, 24-28] Although the first publication on synthesis of polyborosiloxane precursors dates backs to 70s,[26] the commercialization of such precursors has always been limited. In the present study we have used a commercial polyborosiloxane in order to obtain porous SiOBC ceramics, the details for such experimenting will be given later in the thesis. Thermosetting properties (rheology) of such precursors are highly affected by hetero elements. Moreover, high-temperature properties (see later) of the produced ceramic, such as oxidation and creep resistance, can be influenced by the incorporation of additional elements to the SiOC matrix, such as Nb, Ta, Ti or Zr.[29-32] In fact, all these studies related with the "modification" in the SiOC structure clearly implies that through good polymer chemistry, PDC route might offer an exceptional opportunity to synthesize novel multi-component ceramics.

2.1.2. Poly(organosilazane) and its derivatives.

Compounds which contain one or more silicon-nitrogen bonds in which the nitrogen atom is bonded to at least two silicon atoms are classified as "silazanes". The terms "polysilazane" and "silazane polymer" are intended to include oligomeric and polymeric silazanes, i.e., compounds which include more than one type of monomeric silazane units. Although the synthesis of polysilazanes has been investigated vastly, there is still a lack of suitable synthesis methods for producing linear chains of really high molar mass. In fact many of the apparent routes to synthesize polysilazanes result not in polymers but in mixtures of cyclic compounds and linear oligomers with generally a rather complicated structure.[33]

Polysilazanes which contain Si-N-H structural units are isoelectronic to polysiloxanes, are precursors for the production of silicon nitride and silicon carbonitride ($Si_xC_yN_z$) ceramics through high-temperature pyrolysis. Although the bonding energy of the Si-O bond is higher than that of Si-N (452 and 355 kJ/mol, respectively[10]), polysilazanes have been shown to be more thermally stable than polysiloxanes. As in the case for polysiloxanes, the ceramic yield of polysilazanes strongly depends on their chemistry including backbone structure, the functionality as well as degree of cross-linking. For example cross-linked polysilazanes of the type ((R-Si-HNH)n and (R_2-Si-NH)m) gave a high ceramic yield of ~85 wt.% upon pyrolysis whereas uncross-linked silazane of the same types gave only 20 wt.% ceramic residue.[3] The polysilazane precursors which could be used as SiCN production can be made starting from chlorosilanes by means of ammonolysis reactions with ammonia or aminolysis with different amines, as shown in **Figure 2.1-13**.[14] Synthesized precursors are generally hydrolytically sensitive and generate a mild to strong ammonia or ammonia-like odor upon contact with moisture. Kroke et al.[3] recently reviewed most of the synthesis methodologies to produce polysilazane precursors and gave comprehensive information related with PDCs manufactured from these preceramic polymers.

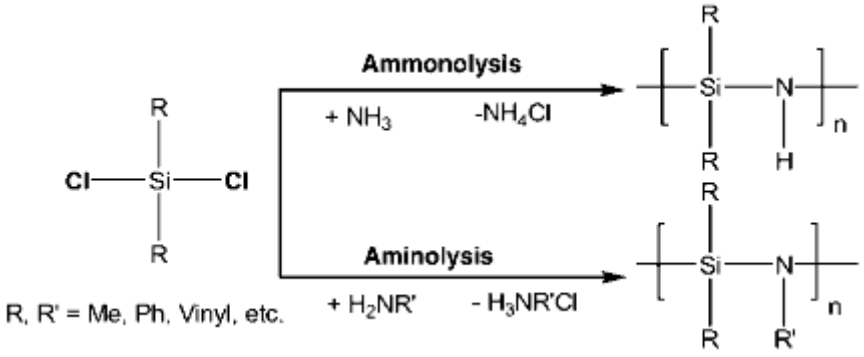

Figure 2.1-13. Synthesis routes to polycarbosilazanes starting from chlorosilanes.[14]

As demostrated by Kroke et al.[3] a great number of studies concerning the synthesis and modification of molecular, oligomeric and polymeric compounds containing Si-N-Si units have been done. Different laboratories have developed their own precursor systems and even synthesized the precursors on a semi-technical scale. However, the properties of the ceramic

products are known to be strongly influenced by the processing parameters and not only depend on the composition and structure of the starting precursor. Therefore, it should always be kept in mind that commercially available SiCN and Si(E)CN (E=B, P, Al, Ti, Ar, etc.) precursors can make the results of different studies comparable; meaning that the use of commercial products is recommended.[3]

As mentioned before, cross-linking of the oligomeric silazanes into large molecules with highly branched backbones is needed for high ceramic yield. Silazane oligomers can be cross-linked either thermally or chemically using radical initiators like peroxides or catalysts. Alternatively, these polymers may be cured by exposure to UV radiation in the presence of a UV sensitizer. The cross-linking conditions that are generally used in thermosetting of some commercial silazane oligomers vary depending on the type of functional groups in the silazane mixture. Roughly speaking; most of the commercial silazane oligomers-polymers are cross-linkable under heating in inert atmosphere. For example; crosslinking of polyhydridomethylsilazane (PHMS) (NCP200 (Nichimen Corp., Japan / not available in the market anymore) was done between 350-450°C to transform low viscous polymer into infusible thermoset.[3] Dehydrogenation (condensation curing via H_2 release) by using Si-H and N-H groups was the major cross-linking mechanism under these conditions, e.g. see reaction schema (2.1.3).

$$R_2SiH_2 + R'NH_2 \rightarrow \equiv SiR_2 - NR' \equiv + H_2 \qquad 2.1\text{-}3$$

While thermal crosslinking of Si-H free polyvinylsilazane (PVS) (e.g. VT50, Hoechst GmbH, Germany / not available in the market anymore) occurred differently, that is predominately via vinyl groups at lower temperatures (200-300°C). In the case of Si-H functionalized PVS, hydrosilylation of vinyl groups occurred.[34] Hydrosilylation reactions were also reported for the polyureamethylvinyl (PUMVS)[3, 35] and polymethylvinyl (PMVS)[36] silazane (Ceraset™ and VL20™, respectively, KiON Corporation, Clariant, USA; Ceraset™ is no more in market but VL20™ is still commercially available) precursors, see Figure 2.1-14 for the crosslinking schema of oligomeric silazanes by hydrosilylation reactions. Besides hydrosilylation, transamination was also detected during the cross-linking but to a smaller extent.[35] As

expected, the hydrosilylation of solutions of PHMS was faster when Pt catalyst was used: the liquid-solid transformation was complete in 10 min at 200°C.[3] In the same manner, the presence of 0.1-1.0 wt% of dicumyl peroxide induced low temperature (100-200°C) crosslinking of vinyl containing silazanes.[3, 35]

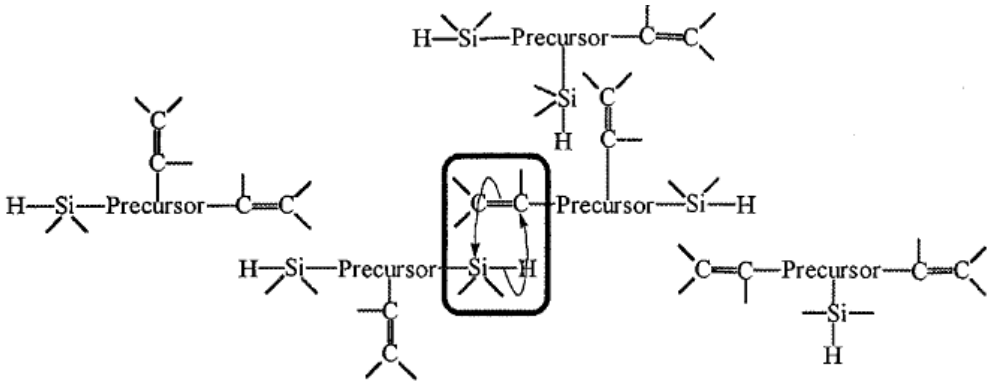

Figure 2.1-14. Crosslinking of oligomeric silazanes by hydrosilylation reactions.[37]

During the course of the present thesis study, commercial polysilazanes of Kion Corporation namely; liquid Ceraset™ (PUMVS) and VL20™ (PMVS) polysilazanes were used. Both of them are low viscous (50-200 mPa.s.) liquid mixtures of different liquid silazane oligomers-polymers and they have clear to pale yellow color, see Figure 2.1-15 for the molecular structure of these mixtures given by Kion corporation.[38] These patented polymers contain repeat units in which silicon and nitrogen atoms are bonded in an alternating sequence. Both of these polysilazanes contain cyclic and linear features. The distinguishing characteristic that differentiates Ceraset (PUMVS) from VL20 (PMVS) is that the former contains a small percentage of urea functionality. In addition, VL20 contains fewer low molecular weight polysilazane components so that a higher ceramic yield upon pyrolysis is expected.

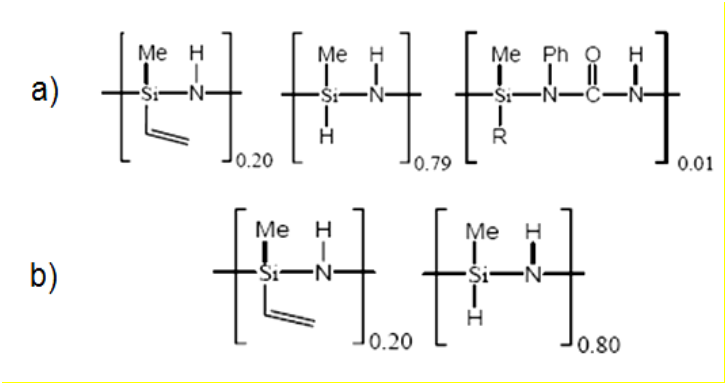

Figure 2.1-15. The molecular structure of KiON a) Ceraset (PUMVS), and b) VL20 (PMVS).

At temperatures around above 400°C decomposition of cross-linked polysilazane occurs with intermediate moieties such as Si-CH_3, N-H and Si-H. Generally, methane and hydrogen are the major volatile by-products of mineralization. Pyrolysis in the 800-1450°C range produces a ternary amorphous SiCN material (a-SiCN) consisting mainly of tetrahedral SiCxNy (x+y=4) units, and leads to a significant volume reduction. Further heat treatment above 1450°C under flowing N_2 promotes structural rearrangements in the amorphous phase leading to the formation of short or long-range ordered Si-N and Si-C rich regions, in addition to the free carbon. More detailed information on PDCs formed from polysilazanes precursor will be given in the following Chapter 2.2.2

Like in the case for polysiloxane, variations in polysilazane structure in order to obtain multinary ceramics and composite materials are of interest due to their superior properties such as enhanced thermal stability and oxidation resistance.[2, 7] Various kinds of metals can be incorporated as pendent groups or by modification into the polysilazanes backbone. For instance using the transamination reaction of polysilazanes with $Al(NR_2)_3$, $B(NR_2)_3$ or $P(NR_2)_3$ or $Zr(NR_2)_4$ corresponding quaternary ceramics have been produced.[3] Likewise, transition metals like Ti, Hf, Al and Zr could also be incorporated in polysilazane structure with alkoxide-based sol-gel methods (as discussed also for polysiloxanes). These elements can be added also as an external powder source (e.g. nano-powders of desired elements, see Chapter 2.2.3 for the details of passive/active filler pyrolysis). The effects of each element on the properties of precursor polymer can be different; for example; while it was shown that

fiber drawing from commercial polysilazane precursors such as PUVMS (Ceraset) is difficult because the polymerization apparently produces a three-dimensionally cross-linked network that causes a sharp increase in the viscosity of the polymer, but the addition of an zirconium alkoxide to the this precursor makes the polymer amenable to fiber drawing.[39] As this alkoxide modification method of polysilazanes has been claimed to be fairly general, alkoxides of different metals can be used for modifying the rheology of the polymers and preparing Si(E)CN-based ceramic fibers (E=B, P, Al, Ti, Ar, etc. Moreover, it was shown that addition of hetero elements effect the thermal stability of resulted PDC. For example, Boron addition to SiCN structure improved the thermal stability of the resulted material up 2000C, see later. The synthesis and properties of preceramic precursors (co-polymers, polyborosilazanes, etc) to produce SiBCN ceramics, will not be including in the present text since it varies and has been summarized in recent reviews.[3, 40, 41] In the present study we have conducted some experimenting on lab-scale synthesized boron-modified polysilazanes in order to produce micro-cellular SiBCN ceramics. The properties of such precursors and details for such experimenting will be given later in the thesis. To sum up, it can be said that the polymer modification significantly influences (a) thermosetting characteristics (b) the thermal stability (see later) and therefore the properties of the resulting advanced ceramic.[3]

2.2. Polymer Derived Ceramics (PDCs)

Compared to ceramics obtained by conventional methods such as sintering of powder compacts, polymer derived ceramics (PDCs) have the advantages of high chemical purity, homogeneous element distribution, low sintering temperatures, and the absence of sinter additives. A further advantage is the complex shaping possibility to produce ceramic fibers, coatings, bulk, and porous media in an easy manner. Following this route, novel ceramic materials can be synthesized which are not accessible by conventional methods. For example, while conventional synthesis of ternary SiOC by solid state reactions using SiO_2, SiC and C or Si powders as starting materials is not possible for thermodynamic reasons,[8] it is very easy to obtain SiOC by PDC route. Amorphous SiOC, SiCN, SiBCN, etc. solids can easily be prepared by the pyrolysis of preceramic polymers. The chemistry of the polymer and pyrolysis conditions dictates the final product which generally shows homogeneous elemental

distribution. For example; a single phase SiCN material with a homogeneous distribution of Si, C and N at an atomic level can be produced from the preceramic polysilazane polymer for which the ratio of these three elements may be modified and controlled by the selection and design of appropriate precursors.

Several studies conducted during the past few years have focused on the production and characterization of SiOC and SiCN ceramics from cheap commercial precursors.[16] In order to produce these ceramics, after molding the preceramic polymer, it has to be cured to form a non-fusible thermoset (shaping by cross-linking of polymer). Cross-linking depending on the precursor type is generally obtained by thermal treatment between 100-400°C in air (e.g. polysiloxane) or in inert atmosphere (e.g. polysilazane). Subsequent pyrolysis mechanism of cured polymer follows several distinct steps shown in **Figure 2.2-1**.

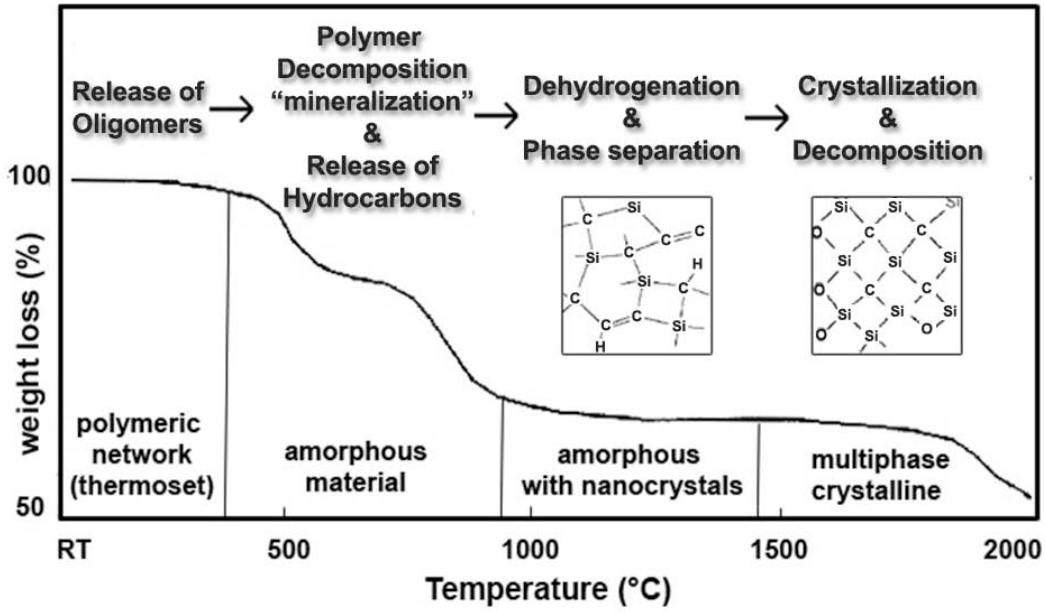

Figure 2.2-1. Structural transformations from thermal decomposition of preceramic polymers.[2]

Generally speaking for both polysiloxane and polysilazane systems, above 400°C rearrangement and radical reactions result in cleavage of chemical bonding and release of organic functional groups (CH_4, C_6H_6, CH_3NH_2, etc.). Logically, the release of these gaseous

species causes weight loss; as could be seen from **Figure 2.2-1**. "Mineralization" or "ceramization" that is the organic-inorganic transition terminates around 800-1000°C which is associated with a total weight loss of typically 10-30 wt.%.[2] During ceramization, the build-up of internal pressure in the component, provoked mainly by the decomposition of the organic moieties in the preceramic polymer leads to porosity (with pore size ranging from nanosized micropores[42-44] to the micronsize macro-pores (2μm)[45, 46]. Materials obtained from low temperature pyrolysis (500-800°C) shows a high SSA value due to micro-porosity in the amorphous network.[44, 47-49] This micro-porosity is however transient, and thus was drastically terminated when the pyrolysis temperature leading to the completion of the ceramization process is increased, according to a densification mechanism based on surface reaction/pyrolysis accommodated by viscous flow.[42]

Nanocrystals of different phases may nucleate in the amorphous matrix with the further heating. Excessive carbon presented as carbon clusters at lower temperatures is called basic structural units, BSUs, which are small stacks of 2–3 polyaromatic layers piled up in turbostratic order, with peripheral carbon atoms saturated with hydrogen atoms rather than other atoms from the surrounding medium. In fact the stability of the amorphous network which is formed upon polymer pyrolysis versus devitrification could be related with the presence of "network modifying elements" such as H.[2] Above around 1000°C generally H_2 release is observed where precipitation of nanocrystals start.[50] It is still a debatable question whether or not these BSUs act as nuclei for crystallization, but it is clear that BSUs develop a percolating network upon further thermal treatment.[22] Around 1200°C short range ordered environments (such as [SiO_4] [SiC_4] and [SiN_4] depending on the system) started to form. In **Figure 2.2-2** a tentative phase diagram, showing the temperature dependent structural transitions in preceramic polymers of various compositions derived from literature data, is demonstrated. As could be seen, for example, B introduction shifts the crystallization temperature above 1600°C.[12] Logically, it can also be inferred that dehydrogenation active elements can change the stability of employed systems.[46]

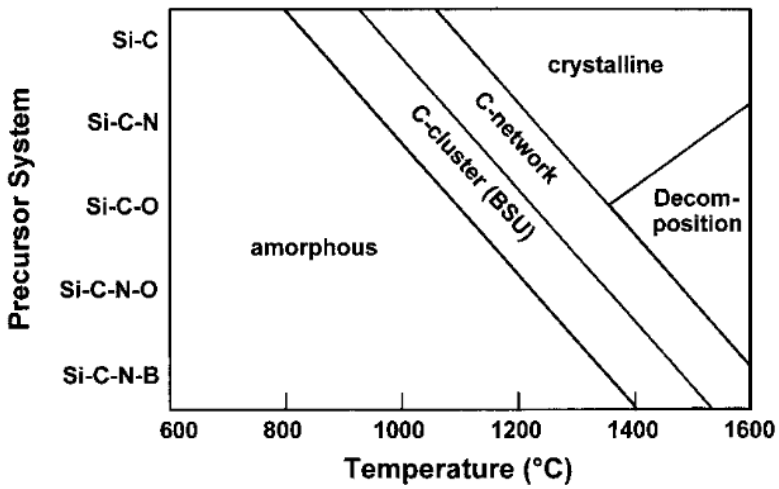

Figure 2.2-2. Tentative phase diagram of various preceramic polymers in Si-O-B-C-N system.[2]

Concerning the analyzed systems in the present study, namely SiOC and SiCN; both show higher resistance to crystallization than related binary amorphous compositions of SiC, Si_3N_4, and SiO_2. They are, indeed, distinguished from their binary constituents by the presence of excess carbon, as pointed out in **Figure 2.2-3**.[14, 51] Both possess a remarkable resistance to creep at high temperatures, even though they are apparently amorphous. The presence of some oxygen (1–5 wt%) in SiCN has no deleterious effect on the kinetic behavior also suggests that these two amorphous ceramics may share essentially the same basic nano-structural framework.[14]

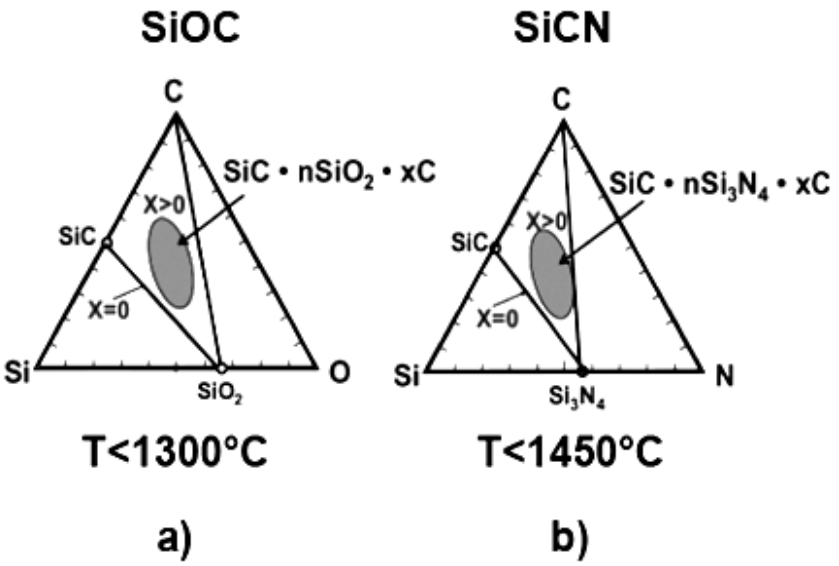

Figure 2.2-3. Composition regimes (gray areas) for two families of polymer-derived ceramics (PDCs): silicon oxycarbides and silicon carbonitrides.[51]

2.2.1. Silicon Oxycarbide (SiOC)

Several heat treatment atmospheres can be applied to polysiloxanes in order to obtain different type of final products. Basically as shown in **Figure 2.2-4**(a) thermolysis atmosphere dictates the formation of final ceramic product. While under inert conditions SiOC glass is obtained upon thermal treatment in between 800-1000°C, NH_3 pyrolysis causes a random structure similar to that observed for oxycarbide phase; i.e. silicon oxynitride (SiO_xN_y), with the difference that when crystallization occurs, a mixed phase exists in the Si-O-N ternary system: Si_2ON_2.[52] Air can also be used to obtain multi-component ceramics but one should keep in mind a decrease of ceramic yield due to high volatilization in air atmosphere.[53]

In the case for SiOC, during pyrolysis in inert atmosphere; following an organometallic-inorganic transition between 500-800°C, an amorphous hydrogenated solid a-SiOC(H) built on tetrahedral structures of the type SiOxCy with (x+y=4) and excess carbon, depending on the initial polymer composition, is observed at temperatures between 800-1000°C. The

structure of produced SiOC is based on a random network of Si-O and Si-C bonds in which all the possible Si sites (SiC_4, $SiOC_3$, SiO_2C_2, SiO_3C, SiO_4) can be found in different ratios.[54] Pantano et al.[55] proposed the schematic structure of SiOC obtained in this temperature range as given in Figure 2.2-4(b).

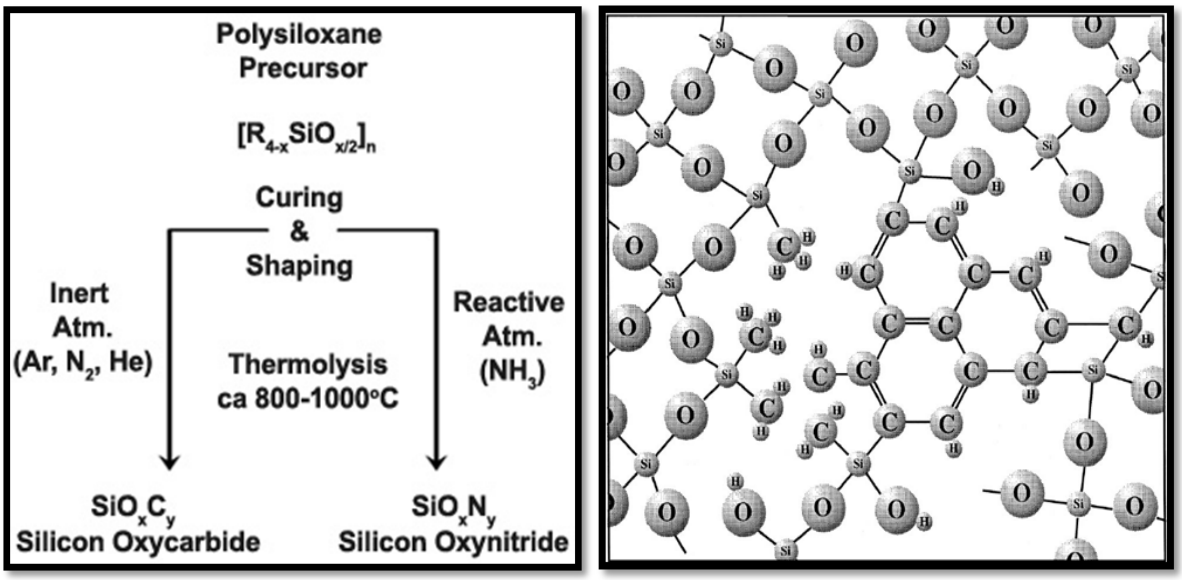

Figure 2.2-4. a) Preparation of silicon oxycarbide and oxynitride glasses by pyrolysis of polysiloxane precursors, and b) schematic representation of an amorphous 800–1000°C SiOC structure.[55]

Excess of carbon is well known in the literature as "free" carbon (C_{free}), and as mentioned before, the amount of free-carbon precipitates, depends on the nature of the organic groups in the polymer precursor. Methyl groups or linear alkyl groups lead to similar, moderate free-carbon contents. On the other hand, unsaturated groups which may undergo free-radical addition reactions, lead to higher free-carbon contents. Actually, free carbon is always the first phase to nucleate, generally as so-called Basic Structural Units (BSUs) which are small stacks of 2-3 polyaromatic layers (graphenes) of 1 nm in lateral extension and piled up as plates in turbostratic order (**Figure 2.2-5**).[50]

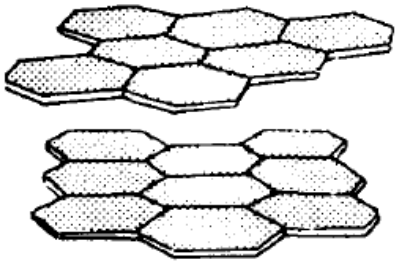

Figure 2.2-5. Sketch of a turbostratic ordered polyaromatic carbon layers (BSU).

Precipitation of these aromatic carbon clusters is seen due to the decomposition of hydrocarbon fragments in the organic-inorganic transition range resulting from cleavage of the functional groups bonded to silicon (Si-C_6H_5 and Si-CH_3, etc). BSUs are found to act as independent entities, and the peripheral carbon atoms of graphenes tend to be saturated with hydrogen atoms rather than to be linked to the surrounding medium. Aromatic CH groups are not stable at high temperature as in any carbon material, and as expected in SiOC system hydrogen is removed mainly as gaseous H_2 in the 1000-1250°C temperature range. H_2 release induces unsaturations on these carbon forms which are fixed by the forming a percolating network; that is these clusters of turbostratic carbon grow and coalesce by edge-to-edge linkage of neighboring BSUs to form an interconnected network (percolating, electrically conductive networks of turbostratic carbon).[43, 46] Depending on the precursor and pyrolysis atmosphere, the formation of this continuous network of polyaromatic turbostratic carbon results in distinct insulator-quasi metal transition. The percolation threshold depends on the carbon content in the polymer precursor and the processing conditions. **Figure 2.2-6** summarizes a model of the major structural transitions during heating of the two polysiloxane precursors having different amounts of carbon in their backbone. Note that PMPVHS (H62C: polyphenylmethylvinylhydrogensiloxane) has much higher carbon content than the PMHS (NH2100:polymethylhydrogensiloxane).[43] This interesting evolution of carbon precipitates effects materials properties. For example, it was shown that depending on the carbon structure in SiOC matrix, ceramic can be either electrically conductive via percolating network or semiconducting due to tunneling of localized electrons.[43] Furthermore it is proposed that such layers, forming a kind of percolation network in the otherwise amorphous matrix, act as

diffusion barriers that prevent local crystallization by keeping the size of the nucleus below the critical radius, *R*c.[56]

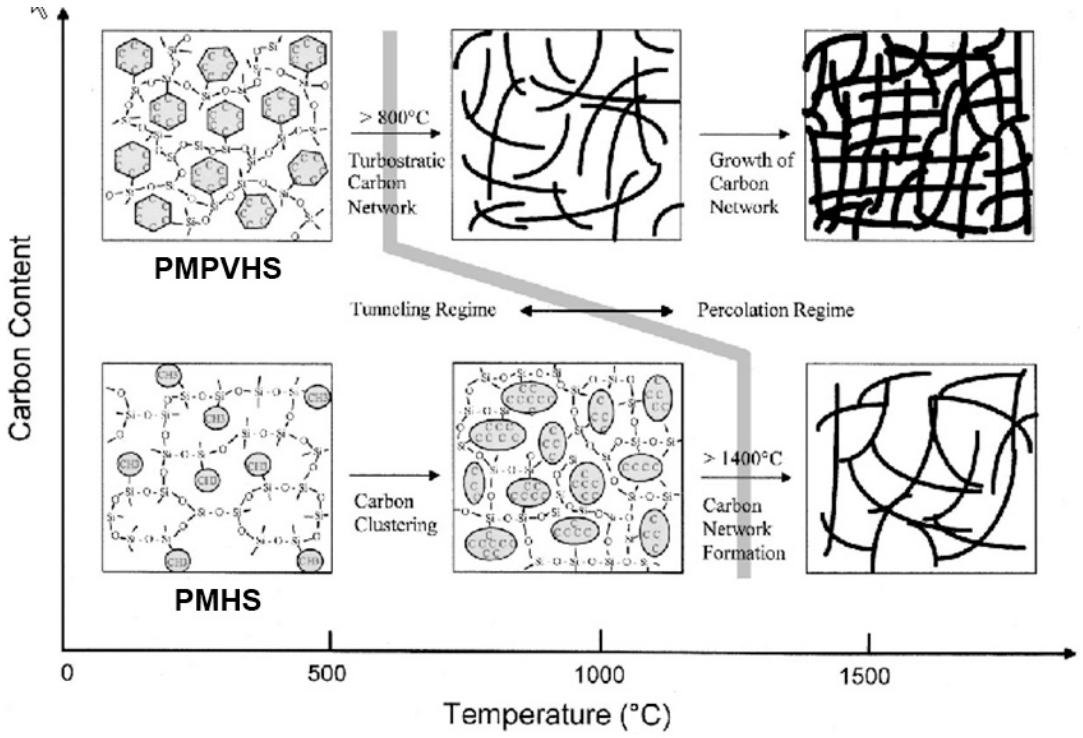

Figure 2.2-6. Model of carbon redistribution reactions during pyrolysis in (bottom) PMS and (top) PPS derived ceramic residue.[43]

The study of done by Pantano et al. on SiOC materials having different structural units by ^{29}Si NMR has shown that the formation of [SiC_4] species is significant in between 1200-1400°C.[55, 57] It is shown that the formation of SiC through carbothermal reduction of SiO_2 (by C) occurs only at much higher temperatures (≥1400°C, see later). Accordingly, it is likely that these primary [SiC_4] species are formed through exchange reactions and "local" decomposition of the [SiOxCy] species. The size of these primary domains is generally in 1-2nm range. It can be said that thermolysis temperatures exceeding 1000°C promotes local decompositions within the matrix due to redistribution reactions between different silicon sites and further heating results with the escape of gaseous species such as silicon monoxide (SiO), carbon monoxide (CO) and/or methane (CH_4).[43, 56, 58-61] Thermodynamic calculations showed that

above 1300°C where the temperature for the onset of crystallization in SiOC materials is reached, the partial pressure of CO approaches to 0.1 bar, large enough to cause significant volatilization.[62] The formation of nanosized SiC crystallites (or [SiC_4] domains) embedded in the amorphous matrix was also confirmed by comprehensive TEM study[63]. It is shown that this newly formed SiC still contains a high fraction of SiOC environment at the phase boundary.[63] This entire process is usually called as "phase separation" and yields with the formation of nanosized SiC precipitates finely dispersed in the amorphous SiO_2-rich bulk.[55, 63] The phase separation into nano-crystalline SiC and amorphous SiO_2 (a-SiO_2) together with free carbon phase was shown to progress with increasing temperature.[55] In **Figure 2.2-7**(a) and (b) HRTEM images of the SiOC sample annealed at 1200°C and 1400°C in Ar are given.[63] While 1200°C treated sample is completely amorphous (only weak phase contrast), with the exception of few lamellar features (BSU), given in the inset, 1400°C treated sample has SiC precipitates. The regions labelled as "SiC" are distributed in SiO_2-rich matrix as observed by HRTEM and EELS.[63] It should be noted that these new nano-sized crystals may be considered as nuclei for subsequent crystallization at higher temperatures.[55]

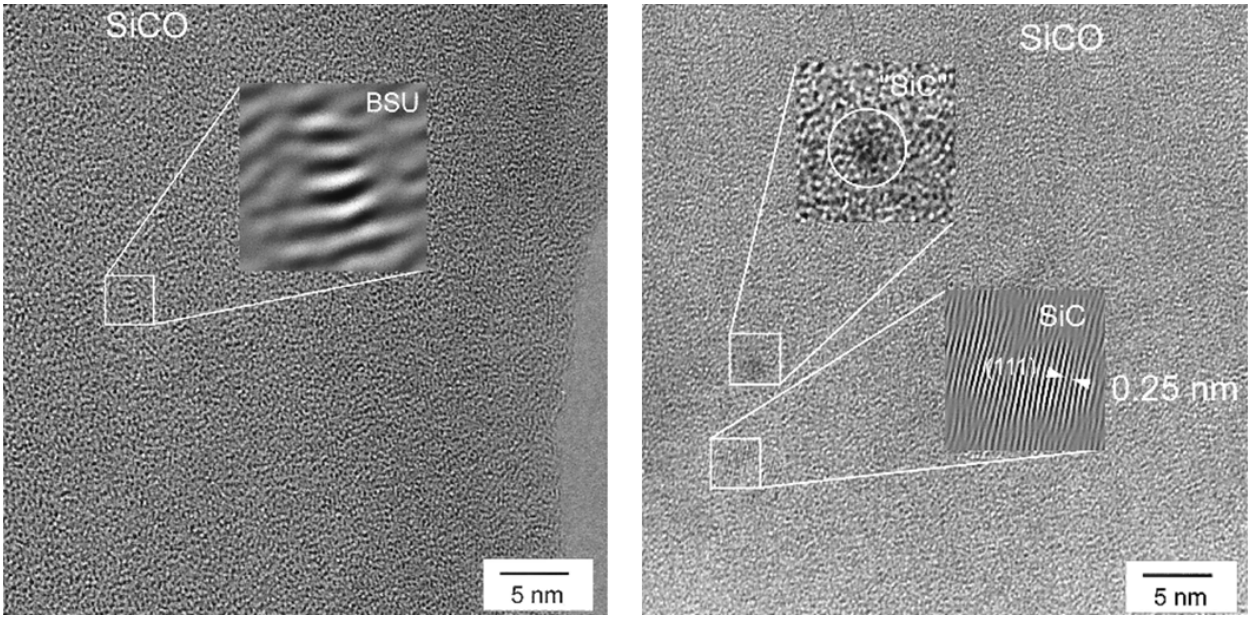

Figure 2.2-7. HRTEM images of the SiOC samples annealed in Ar at a) 1200°C and b) 1400°C (with lattice fringes, which could be assigned to SiC precipitates).[63]

Roughly speaking, the chemical durability of the formed system increases as the amount of phase separation decreases, because the system generally becomes more similar to SiOC (the addition of quaternary elements into SiOC may alter this generalization, see later). The presence and extent of the phase separation is related to the composition of the starting precursor; increases as the C/Si ratio decreases and the pyrolysis temperature; increases as the pyrolysis temperature increases. Other factors, such as the preceramic polymer architecture, also may have an influence on this process.[4, 5, 54] Although it is shown in polysilazane system that precursors with similar composition but different starting polymeric architecture undergo a network reconfiguration process that ultimately results in a very similar amorphous network structure.[64]

According to Saha et al.[65] nanoclusters of amorphous SiO_2 tetrahedras are confined in constrained domains which are defined by graphene sheets and oxycarbide phase on the phase boundary; see **Figure 2.2-8**(a). Such scaffold-like structure of nanodomains indeed explains several observed peculiar features of the oxycarbide materials, especially their high temperature (1000°C) viscoelastic behavior and outstanding creep resistance.[66, 67] The model matches also the crystallization resistance of these SiOC ceramics, as the finite domain size of amorphous silica possesses a domain size comparable to the critical size for the nucleation of the crystalline phases, such as cristobalite.[56, 67] The authors claims that the domain sizes greater than about 6 nm will yield materials that are likely to be more akin to silica than to polymer-derived ceramics in their creep and crystallization behavior, because these compositions lie very close to the SiO_2 corner. Nevertheless, there might be some deviations from this “ideal-static” model for such complex structured PDCs. This is recently observed for carbon enriched SiOC ceramics for which the overall nanostructure formed at high-temperature (1450°C) is characterized by 10-20nm SiO_2-rich regions engulfed by turbostratic carbon making an open network with nanocrystalline SiC bonding at their edges, see **Figure 2.2-8**(b).[68] The carbon-enriched SiOC materials, in contrast to other reports about the destabilization of SiOC and other PDCs in the presence of excessive amount of “free” carbon and having bigger SiO_2 domains, described in this study are shown to be thermally durable and chemically stable at high temperatures.[23]

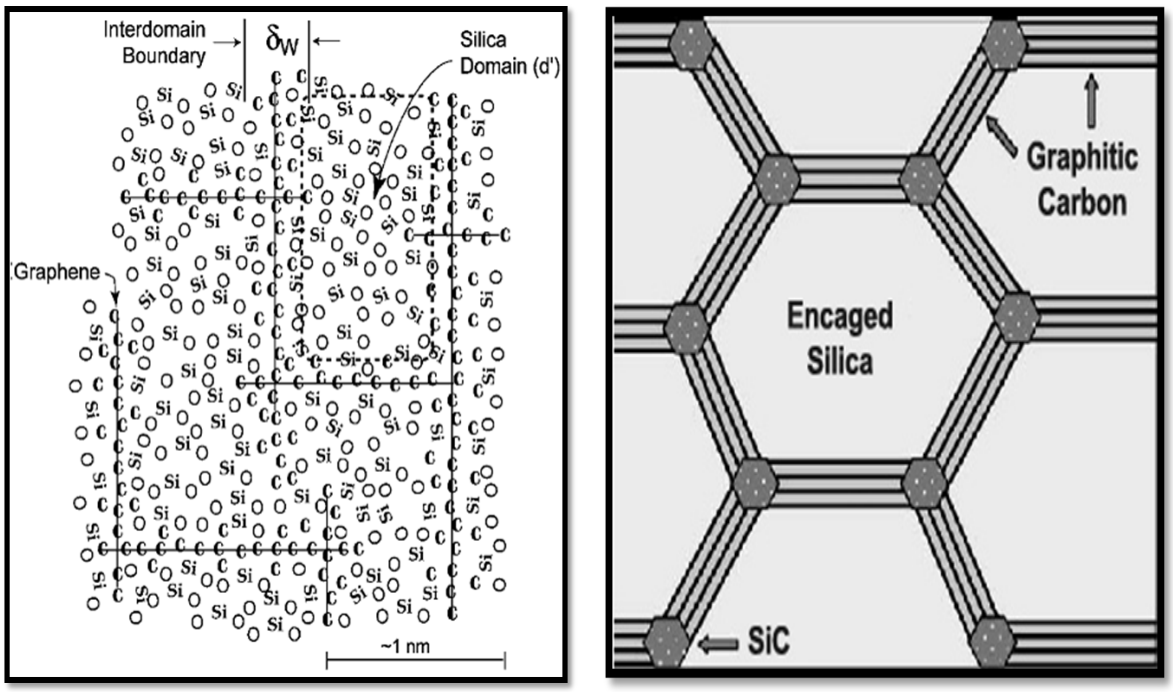

Figure 2.2-8. a) A concept of the molecular make-up of the nanodomains for low-medium carbon containing polysiloxane derived SiOC. Note that the interdomain boundary consists of graphene layers with mixed Si-O-C bonds forming the interface with the silica domains,[65] and b) A schematic microstructure of carbon enriched SiOC at high temperature (1450°C). Note that size of the cages filled with the amorphous SiO_2 phase at this temperature was found as 10-20nm.[68]

Comparing some recent studies dealing with hydrofluoric acid (HF) etching of SiOC ceramics (to etch out SiO_2 nanocrystals/domains) some new insights could be inferred related to the nanostructure of SiOC ceramics. For example, Pena-Alonso et al.[69] has shown that at low pyrolysis temperatures (<1200°C) SiOC glasses having low to moderate free carbon content, were mainly amorphous and the nanostructure was built up by mixed silicon oxycarbide units that could not be etched out by HF attack. The same sol-gel derived SiOC at around 1200°C presented some silica clusters that can be etched out by HF, producing a porous residue with a SSA of 204 m^2/g. The authors showed that increasing the pyrolysis temperature promoted (i) the crystallization of nanocrystalline SiC and precipitation of graphitic carbon and (ii) the formation of the silica-based clusters. The crystallite size of these phases increases with the

temperature. Consequently the material obtained at 1400°C and 1500°C pyrolysis yielded with 482 m^2/g and 562 m^2/g SSA, respectively. Biasetto et al.[67] recently demonstrated that HF etching of gel-derived and resin derived SiOC ceramics produced under the same pyrolysis conditions (1200°C/2h/N_2) yielded with different SSA values. Polysiloxane resin (MK resin with a low carbon content) derived SiOC showed modarate SSA (26.2 m^2/g) compared to the ones obtained by sol-gel derived SiOC (low or medium free carbon).[67] The authors explained this disparity focusing on the differences in the nanostructural phase evolution. Specifically, PMS (MK) derived SiOC thought to have smaller SiO_2 domains and/or more amorphous (less phase separated) structure. Similarly, Dibandjo et al.[70] has shown that etching of carbon enriched SiOC did not yield with nanoporous structure when ceramic is obtained at 1200°C (implying that the matrix is still amorphous with no interconnection in SiO_2 domains). But when pyrolysis temperature is increased to 1400°C where SiOC network is phase separated and SiO_2 domains presented in the glass structure, the same material gave high SSA around 400 m^2/g upon HF attack. It is clear from these studies that as the amount of phase separation increases, more interconnected silica-rich phase forms. The authors proposed that the nanostructure, end hence the properties, of SiOC (and of PDCs in general) are strongly dependent upon the architecture of the starting preceramic polymer,[5, 70] Kleebe and Blum,[56] more sceptically, suggested that the observed nanostructural evolution in PDCs may not only be a consequence of the specific polymer architecture employed during processing, but also a result of pronounced molecular rearrangements upon thermal annealing.[56] This conclusion is further corroborated by the comparative study of integral spectroscopic techniques, (solid-state NMR and Raman spectroscopy) with high lateral resolution techniques (electron energy-loss spectroscopy, high-resolution TEM and energy-filtered TEM) done on SiOC ceramics with or without carbon-enrichment.[68, 71] Consequently, we posit that the generalization of nanostructured assembly in SiOC (and generally in PDCs) to one type of “static” model seems insufficient to make rigorous predictions for such arrangement having “dynamic” microstructural phase evolution.

The proposed decomposition for SiOC can be separated into two regimes;[62] just above 1400°C, the weight loss occurs predominantly by Eq. (2.1-4) that is the carbothermal reaction between C and SiO_2 and above 1500°C, the reaction Eq. (2.1-5)[72] becomes

thermodynamically feasible leading to complete decomposition of the SiOC ceramic. The effect of CO partial pressure on these reactions is clearly demonstrated in a recent study done by Plachky et al.[73] The graphs implies if the CO partial pressure is kept between the two calculated equilibrium curves during thermolysis, the formation of SiC within the composite materials can be promoted, while its decomposition by Eq. (2.1-5) should be avoided. It is worth also to point out that the lower bound in **Figure 2.2-9** represents the total equilibrium pressure of CO and SiO gaseous species of reaction given in Eq. (2.1-5)[73] (note that the importance of pyrolysis conditions; i.e. if the pyrolysis is performed in a graphite tube/crucible,[74] it might be expected that the partial pressure of CO at the vicinity of the surface is high and suppresses the reactions given in Formulas (2.1-4) and (2.1-5)).

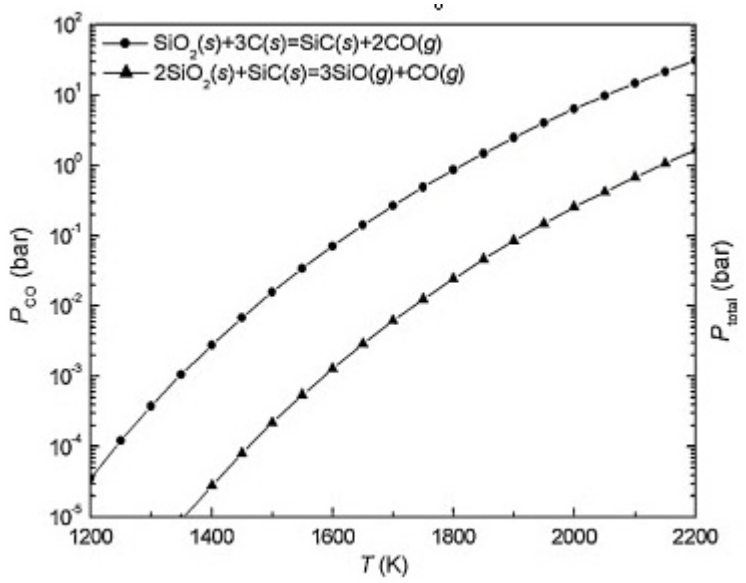

Figure 2.2-9. Calculated equilibrium pressures of CO(*g*) and SiO(*g*) for the reactions (2.1-4) and (2.1-5).[73]

The overall carbothermal reduction reaction given in Eq. (2.1-4) to synthesize SiC is shown to have a positive standard free energy change up to about 1500°C; thus, unless the produced CO is removed from the process, a higher temperature is needed to promote reaction at a reasonable rate (note that even around 1450°C calculated log[K_p] for reaction (2.1-4) is

negative (-1.14)[73], see also Figure 2.2-9).[75] In view of that, it was shown by Wiemer et al.[75] the formation of SiC appears to proceed through a rapidly formed SiO(g) intermediate[71] implying that reaction (2.1-4) is controlled by the reduction of SiO(g) via Eq. (2.1-6) ($\Delta G° = -132770 + 33.9T$, $\log[K_p]_{1300°C} = 2.6$).[59, 76] Generally it is excepted that SiO(g) forms due to solid/solid reaction by following Eq. (2.1-7). This reaction most likely occurs at the contact points of the C and SiO_2. In the absence of direct carbon and silica contact, SiO could also be generated by reaction (2.1-8).[75] However, both of these reactions require temperatures above approximately 1750°C to proceed under equilibrium conditions at atmospheric pressure.[75] Therefore, unlike in the SiO_2 reduction methods, SiO and CO gases involved in SiC formation is believed to come directly from the polymer precursor during heat treatment.[43, 56, 58-61] Above 1500°C the release of SiO gas is not anymore yield with SiC but only creates porosity in the system via reaction (2.1-5).

$$3C(s) + SiO_2(s) \rightarrow SiC(s) + 2CO(g) \qquad 2.2\text{-}1$$

$$SiC(s) + 2SiO_2(s) \rightarrow 3SiO(g) + CO(g) \qquad 2.2\text{-}2$$

$$2C(s) + SiO(g) \rightarrow SiC(s) + CO(g) \qquad 2.2\text{-}3$$

$$C(s) + SiO_2(s) \rightarrow SiO(g) + CO(g) \qquad 2.2\text{-}4$$

$$SiO_2(s) + CO(g) \rightarrow SiO(g) + CO_2(g) \qquad 2.2\text{-}5$$

The phenomena of crystallization and weight loss (decomposition) in SiOC ceramics appear to be intertwined. Around 1400°C, the oxycarbide structure completely separates into an amorphous mixture of SiO_4 and SiC species, as explained before.[55] Saha et al.[62] studied the crystallization of SiOC amorphous ceramics at temperatures up to 1500°C. In all instances,

the product of crystallization is reported to be β-SiC and their domain size are generally bigger than the initially precipitated SiC nanodomains. The other phase, a-SiO_2, remained non-crystalline. This observation is unusual because single-phase a-SiO_2 crystallizes into cristobalite at much lower temperatures (~1200°C). The explanations given by Saha et al.[62] concerning this phenomenon were based on both the assumption that crystallization of SiO_2 in SiOC is nucleation limited (the low interfacial energy between β-SiC and a-SiO_2 may be a possible reason) and the possibility that the silica phase is not interconnected in the SiC–SiO_2 composite, because if that was the case then silica would nucleate crystals of cristobalite at the free surface, which would then propagate into the interior of the specimen. The latter explanation seems less accurate since HF etching of SiOC even pyrolyzed at 1200°C gives high specific surface area interconnected porous structure due to SiO_2 etching. In addition to that contrary to nucleation limited crystallization theory, Kleebe et. al.[63] related this behavior to the presence of carbon (either as free C or residual carbon bonded in form of SiC) in the amorphous SiO_2 network. Excess free C is assumed to prevent nucleation of cristobalite or tridymite, because short-range diffusion is strongly impeded by the incorporation of carbon into the SiO_2 network. Later on by the same authors it was concluded that such layers, forming a kind of percolation network in the otherwise amorphous matrix, act as diffusion barriers that prevent local crystallization by keeping the size of the nucleus below the critical radius, Rc.[77] It is important to note, that, apart from the polymer architecture which defines the nanostructural assembly, the residual porosity may play a role with respect to crystallization of the bulk polymer-derived ceramics.[78]

Stability of SiOC system can be modified by the incorporation if hetero elements. These elements can be added either by modifying the polysiloxane structure with suitable chemicals (e.g metal alkoxides) or as an external powder source (e.g. nano-powders of desired elements as in the case for passive/(re)-active pyrolysis. Introduction of these additional elements by modifying the polysiloxane structure may result in a ceramic with different final properties compared to that of the (re)active filler pyrolyzed one where filler particle is added as a powder source. As an example; Ionescu et al.[79] has recently prepared SiOC/ZrO_2 ceramics both by adding zirconia powder to PMS (MK) and by chemical modification of PMS (MK) with a zirconium alkoxide. While ZrO_2-filled ceramics showed the presence of two ZrO_2

polymorphs (monoclinic and tetragonal) and an amorphous SiOC phase, alkoxide-modified materials were X-ray amorphous under the same pyrolysis conditions (1100°C). Experiments in this study revealed that the incorporation of ZrO_2 into the SiOC matrix remarkably increases the stability of the composite by strongly suppressing the decomposition of SiOC. Increasing the content of ZrO_2 clearly induced an increase in the thermal stability, whist by alkoxide modification the content of ZrO_2 was limited.[79] Alkoxide modification of polysiloxane by Al, B, Zr, Hf, etc. has also been shown to be an effective way to change the stability of SiOC system. Harshe et al.[25] demonstrated that Al introduction into SiOC ceramics clearly inhibits devitrification of the amorphous matrix at higher temperatures. The formation of mullite nano particles acts as cristobalite devitrification inhibitor during annealing. Carbon content of the resulted SiOC was also decreased by the Al addition.

Similarly, the presence of boron in SiOC glasses inhibited the separation of free carbon, thus provided higher electrical resistivity. The presence of boron induced a modified behavior in the microstructure development, in that an enhancement of finely dispersed β-SiC nanocrystallites throughout amorphous SiOBC matrix without the formation of α-cristobalite was observed.[12] Although the first publication on synthesis of polyborosiloxane precursors date backs to 70s[26], compared to pure SiOC system relatively few papers have been published concerning the properties of multi-component SiOBC glasses up to now.[24, 26, 80-84] This material was shown to have higher temperature resistance and more stable electrical properties compared to that of bare SiOC due to enhanced nanostructured assembly.[82] Zr and Hf modification in polysiloxane structure is also shown to yield with a suppressed carbothermal decomposition of the SiOC matrix due to zircon and hafnon formation, even if addition of these elements has shown to enhance phase separation.[79, 85] Ta and Nb modified polysiloxanes have also been produced. Though, the resulted final ceramics showed improved oxidation resistance, information on high temperature stability of these ceramics is not covered in the literature.[29, 86]

2.2.2. Silicon Carbonitride (SiCN)

In the case for SiCN, pyrolysis in inert atmosphere involves similar steps that were explained for SiOC in the previous subsection; roughly speaking in the first stage (up to 400°C), additional cross-linking reactions proceed and the loss of low molecular mass oligomers occurs. During the second stage (400–800°C) Si-C, Si-H and C-H bonds are broken and small molecules, mostly hydrocarbons, are evolved. This step is commonly called “mineralization” and consists of the organic–inorganic transition. At temperatures higher than 800°C, a mineral ceramic material is obtained consisting of free carbon and an amorphous SiC_xN_y (x+y=4) matrix with a completely homogeneous distribution of the elements.

Polysilazane derived amorphous SiCN ceramics were found to have a structural and chemical stability comparable to the binary SiC or SiN_X amorphous ceramics, derived from N or C free polysilane, oxygen-containing ternary or quaternary phases like Si-O-C and Si-O-C-N, derived from oxygen-containing polysilane precursors. As stated before most kinds of polysilazane derived ceramics are C rich with respect to stoichiometric Si_3N_4-SiC phases, see **Figure 2.2-3**(b). Analogous to the SiOC system, this excess carbon during pyrolysis precipitates as free carbon. The formation of a free carbon is shown to be caused by the cracking of aliphatic hydrocarbons, and its reorganization toward aromatic hydrocarbons around 600°C. In the temperature range between 800° and 1200°C, the residual -H bonded to the periphery of the free carbon is eliminated. During the following heat treatment at 1200-1450°C, the changes in Si-C-N network structure, density, and bonding are minimal, but, it was found that the growth and rearrangement of free-carbon regions lead to a carbon network with nanocrystalline graphitic-like clusters, as in SiOC system. Further heat treatment causes the decrease of the free-carbon content in the ceramic material because of its reaction with silicon carbonitride and Si_3N_4 to yield SiC and N_2, see later. The microstructural analysis of the amorphous SiCN ceramics demonstrated that ceramics derived from polysilazanes are the only ones that can be considered as single phase amorphous SiCN (see **Figure 2.2-10**(a)) while polysilylcarbodiimide derived SiCN consists of a bi-phasic matrix comprised of amorphous Si_3N_4-nanodomains and carbon segregations as illustrated in **Figure 2.2-10**(b). A schematic model for carbon enriched polysilylcarbodiimide derived SiCN is also given in

Figure 2.2-10(c), note that the similarity with the nanodomain model for carbon enriched SiOC given in **Figure 2.2-8**Figure 2.2-10(b).

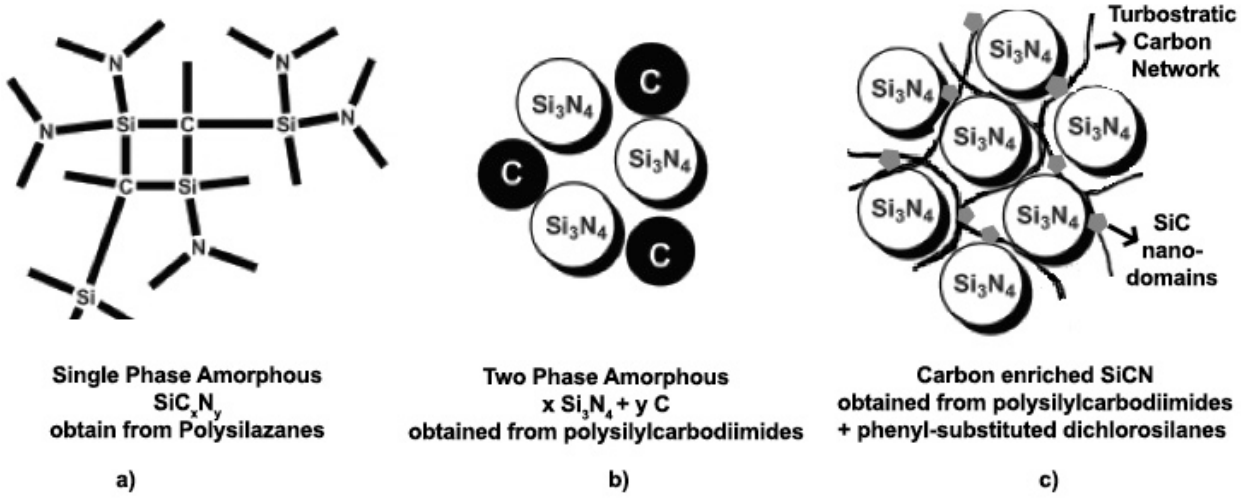

Figure 2.2-10. A schematic microstructures of SiCN ceramics derived from a) polysilazane precursor, b) polysilylcarbodiimide and c) carbon enriched polysilylcarbodiimide.[14, 87]

As stated before final chemistry and microstructure of SiCxNy depends on the precursor (synthesis -so S:C:N-, polymerization, degree of cross-linking), and the pyrolysis temperature, as well as on the atmosphere applied for the pyrolysis process. **Table 2.2-1** summarizes some of the literature data in order to show the differences in the final chemical composition of the Si-C-N ceramics derived from several kinds of polysilazanes under various pyrolysis conditions. As could be seen thermolysis above 1000°C is generally done using N_2 atmosphere in order to hamper the solid state reaction of nitride species with carbon to form SiC and N_2 which becomes relevant at temperatures above 1450°C. In addition to that, N_2 suppresses the self-decomposition of Si_3N_4 formed from the amorphous SiCN-phase (see later).[88]

Table 2.2-1. Chemical composition of the Si-C-N ceramics derived from several kinds of polysilazanes.[3]

Polysilazane	PDC Chemical composition	Pyrolysis conditions	C:Si	Ref
Polycarbosilazane (PCS), ABSE	$SiC_{1.25}N_{0.71}$	1000°C / N_2	>1	89
Polyhydridomethylsilazane (PHMS), NCP200	$SiC_{0.58}N_{0.90}$	1000°C / Ar	<1	3
Polyureavinylmethylsilazane (PUMVS), Ceraset	$SiC_{0.86}N_{0.82}O_{0.02}$	1000°C / Ar	<1	35
Polyureavinylmethylsilazane (PUMVS), Ceraset	$SiC_{0.90}N_{0.76}O_{0.14}$	1300°C / N_2	<1	90
Polyvinylsilazane (PVS), VT50	$SiC_{1.60}N_{1.33}$	1050°C / Ar	>1	91
Polyvinylsilazane (PVS), VT50	$SiC_{1.47}N_{0.98}O_{0.06}H_{0.06}$	1400°C / N_2	>1	3
Polymethylvinylsilazane (PMVSZ)	$SiC_{0.06}N_{0.01}O_{2.08}H_{0.18}$	800°C / O_2+He	<1	92
Polymethylvinylsilazane (PMVSZ)	$SiC_{1.08}N_{0.78}O_{0.16}H_{0.66}$	850°C / N_2	>1	92
Polymethylvinylsilazane (PMVSZ)	$SiC_{1.06}N_{0.86}O_{0.16}H_{0.96}$	1400°C / N_2	>1	92

The pyrolysis mechanism involved in the polymer-to ceramic transformation is a very complex process and is not completely understood. This is partly due to the poorly defined structure of the highly cross-linked polysilazanes and the resulting amorphous and crystalline composite ceramics. Roughly speaking, upon pyrolysis at temperatures exceeding 1000°C, structural changes occur in SiCN amorphous ceramics like in SiOC, the samples thermolyzed up to this temperature are amorphous as confirmed by XRD as well as by HRTEM. The phase separation in the material occurs generally ≥1200°C, beginning with the formation of

turbostratic graphite and the nucleation of nano-crystalline SiC at temperatures ≥1300°C , while the material remains x-ray amorphous up to ~1400°C. Such PDC glasses with high stability against (local) nucleation are considered to reveal metastable structures, which eventually will crystallize to the thermodynamically stable phases. Hence, these glasses can be described as kinetically stabilized metastable networks.[93] Very few studies in the literature discussed the relationship between microstructural evolutions (network rearrangements) below 1400°C and early stages of crystallization polysilazane derived SiCN.[34, 64]

Gregori et al.[64] has investigated the structure evolution of different precursor-derived SiCN ceramics upon exposure at temperatures ranging between 1000 and 1400°C by means of transmission electron microscopy (TEM), electron energy-loss spectroscopy (EELS), X-ray energy dispersive spectroscopy (XEDS), Raman spectroscopy and Neutron scattering. The results indicated that these materials remain structurally amorphous and can, therefore, be considered stable against devitrification within this temperature range. However, the amorphous structure of these ceramics does undergo short-order rearrangements (phase separation) which were recorded by several studies.[34, 78, 89, 93, 94] Several factors may play role in the final nanostructural assembly; polymer architecture and chemistry (so C:Si ratio of the obtained amorphous glass), pyrolysis conditions (atmosphere, dwell time and peak temperature).[93, 94] For example; it was shown by comprehensive solid state NMR study that during pyrolysis of polysilazanes having different structural units (di-D, or tri-T, etc.), short range ordering could be controlled. Precursor made with T-units (TVS) yields an amorphous pyrolysis residue containing mainly SiN_4 sites (even as low as 1200°C pyrolysis) whereas the pyrolysis of the polymer consisting of D-units leads to an amorphous ceramic containing a broad distribution of SiC_xN_y environments. The formation of both CSi_4 and SiN_4-environments with a short range order is observed for the precursor including both D- and T-units (NVGN with $SiC_{0.96}N_{1.08}$ empirical formula (C:Si<1)). The authors proposed that the presence of T-units is pre-structuring the architecture for the precursors. Consequently, structural rearrangements during pyrolysis are limited, whereas difunctional units (D-units) enable a broader distribution of Si sites. This result, indeed, supports that the initial polymer architecture governs the resulting SiCN glass network or, in other words, “memorizes” the intrinsic architecture of the starting polymer. It should be noted here that although by solid

state NMR, it is possible to define short range ordered Si-N sites, apart from the precipitation of nanocrystalline SiC, HRTEM did not allow a distinction between the different amorphous nanodomains and, consequently, between the different amorphous glass networks for these ceramics. This is also consistent with the XRD data showing amorphous phase only up to temperatures around 1450°C. In addition to that it should be noted that after BSU carbon, SiC is commonly the second phase to nucleate in the precursor derived SiCN ceramics (and seemingly for all PDC systems).

The further heating of obtained material induces crystallization by rearrangements in the silicon sites and also by decomposition depending on the chemistry of the precursor and pyrolysis conditions.[95] The formation of SiC and Si_3N_4 crystalline phases for the sample pyrolyzed in N_2 atmosphere, and SiC phase, under Ar atmosphere, can be observed. In general, the compositions of silicon carbonitride ceramics $Si_xC_yN_z$ obtained from molecular precursors are located either on the Si_3N_4-C tie line (if obtained from nitrogen-rich polymers) or in the SiC-Si_3N_4-C three-phase field. A recent work devoted on to synthesize carbon enriched precursors in order to process high carbon SiCN ceramics has shown that these ceramics also locates near to Si_3N_4-C tie line but close to the carbon corner.[87] Therefore, concerning SiCN composition diagram, it can be said that stable crystalline phases at 1450°C (0.1 MPa, N_2) are SiC, Si_3N_4 and C for the precursor derived SiCN ceramics. The reaction paths given in Formulas (2.1-9) and (2.1-10) indicate the change of the gross composition of the solid samples due to the loss of nitrogen according to the nonvariant reactions around 1450°C and 1850°C, respectively.

$$Si_3N_4(s) + 3C(s) \rightarrow 3SiC(s) + 2N_2(g) \qquad \textit{2.2-6}$$

$$Si_3N_4(s) \rightarrow 3Si(l) + 2N_2(g) \qquad \textit{2.2-7}$$

The aforementioned reactions are dictated by the C:Si ratio of the mineral as can be seen from the isobaric sections in the Si–C–N system given in **Figure 2.2-11**(a) and (b). The material

with C:Si ratio >1 produces nitrogen until the indicated reaction path ends on the tie line graphite–SiC whereas the material with C:Si ratio <1 produces nitrogen and changes the composition to the SiC-Si_3N_4 tie line. At temperatures above 1850°C, the latter ceramic again loses nitrogen because of the residual Si_3N_4 dissociation into liquid silicon and nitrogen gas according to reaction (10).

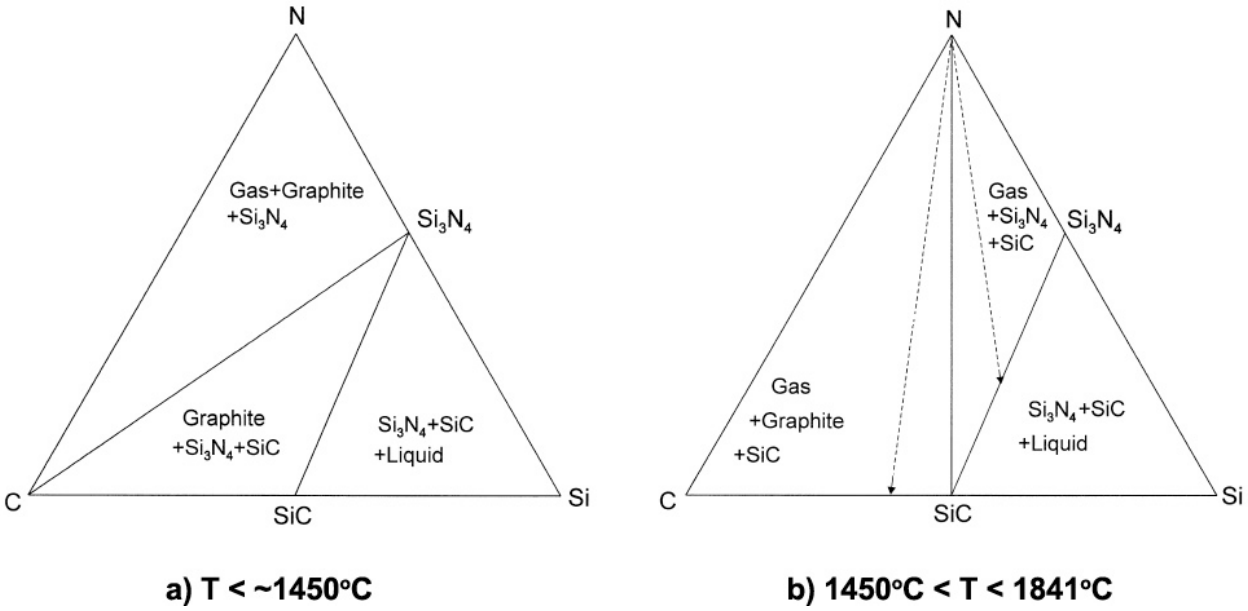

Figure 2.2-11. Isothermal, isobaric sections in the Si–C–N system at 1 bar/N_2. (a) T< 1450°C, and (b) 1757<T<1850°C (reaction paths are indicated by arrows).[91]

The study of Trassl et al.[96, 97] on different free carbon containing polysilazanes has shown that finely dispersed carbon, with cluster sizes around 1-2 nm, in the form of percolation network acts as an effective diffusion barrier, hence, inhibits rearrangement and crystallization within the amorphous Si-C-N phase. Although the authors observed the formation of turbostratic carbon for all their samples, the one with the highest amount of free carbon remained amorphous and more conductive whilst for the ones with less free carbon crystallization has already been induced upon same pyrolysis conditions. Similarly, other studies were also reported that the presence of carbon segregations helps to reduce coarsening of SiC and Si_3N_4 particles in polysilazane-derived polycrystalline ceramics.[77, 94, 98] In a comprehensive study

related to the thermal stability of SiCN ceramics, Iwamoto et al.[99] discussed the specific crystallization behavior of polysilazane and polysilylcarbodiimide derived ceramics. The authors used solid-state NMR and X-ray diffraction (XRD) to show that carbon segregation found in polysilylcarbodiimide-derived SiCN hinders the crystallization of amorphous Si-N. Although polysilylcarbodiimide derived SiCN is not the interest of the present study, the properties of such ceramics are useful to understand the polysilazane derived SiCN. In this manner; recently carbon enriched SiCN ceramics has been produced from carbon rich polysilylcarbodiimide precursors that were synthesized by the reaction of bis(trimethylsilylcarbodiimide) with phenyl-substituted dichlorosilanes.[87, 100] Even if the synthesized precursors for these SiCN derivatives give low ceramic yield (<50%), it was shown that improved carbon content seals off the SiN_x domains leading to an enhanced thermal stability of the SiCN with respect to crystallization. The authors claimed that graphene layers surrounding amorphous SiN_x domains prevents out diffusion of N_2 and therefore increases the stability of nitride clusters. The C-rich SiCN proved to be more temperature resistant than that of the published SiCN ceramics with lower C-content, reveling the importance of "free carbon" phase in such ceramics.[87] Note that the organization of the graphitic phase starts as early as by 800°C pyrolysis, however, the size of the these domains remain below the critical level in order to be identified as separate phase, generally up to 1200°C. In short; it can be inferred that increasing the carbon content of polysilazane (or better to say utilization of high carbon containing polysilazanes) seems a proper way of improving the high temperature stability of resulted SiCN ceramic, yet the oxidation resistance of the final components are doubtful.

The effect of polymer architecture on crystallization behavior and the thermal stability of SiCN ceramic were also examined with polysilazanes having different starting structural units. The amorphous structure of the precursor, with T-unit derived material, which consists of pure SiN_4-units together with a rather high volume fraction of a free carbon phase revealed the highest thermal stability, i.e., resistance against nucleation. The effect is attributed here also to the carbon network covering the nitride species. Therefore, the thermal stability of these "kinetically stabilized metastable networks" highly depends on polymer architecture yielding with an amorphous nanostructured network for which nanodomain structure of each

Si-N, Si-C and free carbon phase dictates the final properties.[93] Actually, it is more reasonable to think that polymer derived SiCNs are ceramics containing graphitic carbon and amorphous matrix including nanodomains of SiC, Si_3N_4 which prone to crystallization with further heating, in an interpenetrated network. Meaning that carbon may not be the only "network" forming element in SiCN (an in general PDC) structure but instead it should be one-part of the interpenetrated network.

While rearrangements below 1400°C results with Si-N and Si-C short range orders (phase separation), Further heat treatment above 1400°C under flowing N_2 promotes structural rearrangements in the amorphous phase leading to the formation of long-range ordered Si–N and Si–C rich regions, in addition to the turbostratic carbon (depending on the precursor). Crystallization is promoted when these regions exceed the critical nucleation radius while turbostratic carbon regions making a barrier for growth (similar to the SiOC situation where carbon hinders silica crystallization). It is important to note, that, apart from the nanostructural assembly, the residual porosity plays a dominant role with respect to crystallization of the bulk SiCN ceramics.[78] The final crystalline phases are mainly determined by the composition of the amorphous Si-C-N materials obtained at lower temperatures (800-1200°C). Thus, analysis of the ternary Si-C-N phase diagrams provides a very useful way to evaluate the composition of the amorphous Si-C-N ceramics or to predict the final crystalline phases.

Upon crystallization, density increases o ~3.25g/cm^3 (corresponding to SiC) with a substantial mass loss (26%) due to the decomposition of amorphous Si-C-N and Si_3N_4. These structural changes were particle size dependent, illuminating the importance of the kinetic aspects. Using particles sizes >1 mm, the structural changes were shifted to higher temperatures, indicating that rearrangement is affected by both bond cleavage and diffusion of gaseous species. Moreover, the influence of the gas phase on the phases (Formula (2.1-9) and (2.1-10)) is shown in **Figure 2.2-12**(a) and (b) by the calculated potential phase diagrams for C:Si >1 (a) and <1 (b). As seen thermal stability can be highly affected by N_2 partial pressure. Crystallization of Si-C-N ceramics is therefore dominated by (i) structural rearrangement causing phase separation, and (ii) chemical degradation (nitrogen escape).[77, 89, 94]

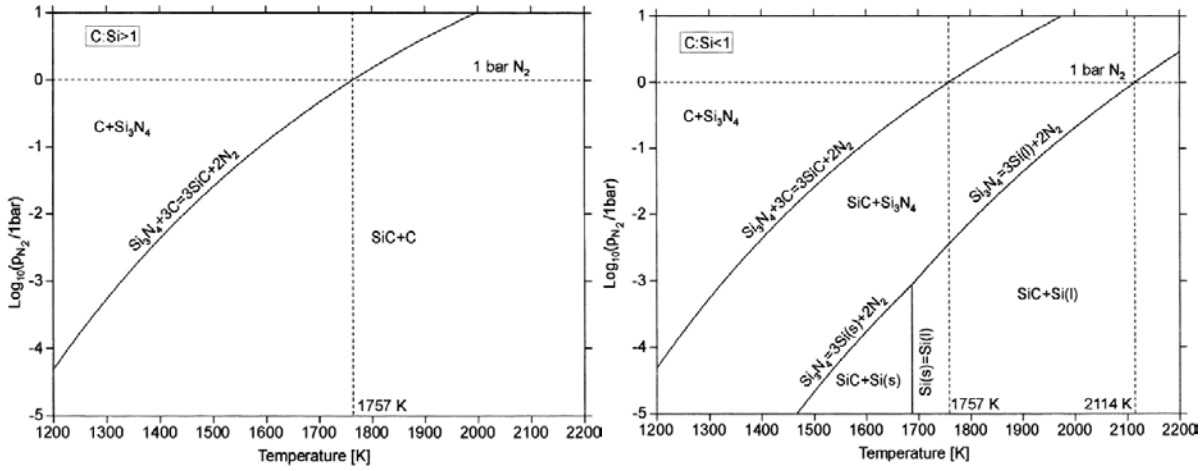

Figure 2.2-12. Potential phase diagrams for the Si–C–N system; a) C:Si>1, and b) C:Si<1.[91]

Considering all these observations, it can be concluded that for the high temperature stability of pure SiCN system; analogous to SiOC, a unique self-assembled nanodomain structure is required. Stability of such system can be modified by the incorporation if hetero element in polysilazane structure which may affect this unique assembly. Several methodologies in order to synthesize Si(E)CN-based (E=B, P, Al, Ti, Ar, etc.) ceramics from polymeric precursors has recently reviewed. Basically; these elements can be incorporated either as an external powder source (e.g. nano-powders) or by incorporation into the precursor structure with suitable chemical (either by pendent group or by modification). Each method may yield with a ceramic having different final properties. Moreover, the effect of each element on the properties of precursor polymer and final ceramic were also diverse. For example; it was found that SiPCN ceramic tend to crystallize more rapidly than SiCN material which was opposite to the behavior of corresponding SiBCN ceramic.[3] Similarly, SiCN materials containing oxygen may show enhanced crystallization and grain growth. These effects of oxygen are due to various vapor phase reactions involving SiO and/or CO_2/CO gases producing Si_3N_4 or SiC in the form of needles or whiskers, as frequently observed after thermal annealing of the amorphous material. A promising candidate is Al as in the case for SiOC polysilazane derived ceramic materials in the Si-Al-O-N system have been found to

show suppressed grain growth compared to Al-free analogues. Transition metals like Ti or Zr may be incorporated in silazane precursors also. This is a useful task since cross-linking and curing may be positively influenced by the presence of these metals, for example giving higher ceramic yields. In fact some few studies conducted for the molecular and polymeric Si-Ti-C-N precursors and their thermal transformation into ceramic material.

Among all the SiCN systems including hetero elements; boron doped SiCN ceramics have a number of advantages. The most significant property of these materials is their extraordinary thermal stability which usually do not show essential mass loss during annealing up to 1600°C and outstanding representatives withstand at temperatures above 2000°C without essential sign of decomposition.[101] This high temperature stability is as like other PDCs due to unique nanostructural phase formation including turbostratic structures of B–N–C domains probably including intercalating carbon and boron nitride (BN) layers which surrounds amorphous SiCN phase having Si-C and Si-N domains. The fabrication of boron containing SiCN ceramics, including fibers and coatings, is currently under development, with the target to produce composites for aircraft and spacecraft components as well as other applications. Consequently, it can be said that the addition of hetero elements significantly influences (a) the crystallization behavior, (b) the thermal stability and (c) the properties of the final ceramic.[3]

2.2.3. Manufacturing and Properties.

The properties of PDCs may vary because different starting precursors and various processing techniques make impossible to obtain “identical” final material in order to obtain accurate comparison. Differences in characterization techniques pose another difficulty. All of these cause some uncertainties in the published literature data, especially concerning the mechanical properties. For example, Shah et al.[102] found that the Vickers hardness of the dense flawless SiCN ceramic increases from 15 GPa at an applied load of 1 N to 26 GPa at 3 N, contrary to this observation Nishimura et al.[103] showed that increases the indentation load decreases Vickers hardness massively. This is explained due to the differences between powder processing (so the residual porosity, surface properties) and casting methods, therefore, the

reported values for the hardness of SiCN (6-16 GPa)[103] has been found significantly lower than the 25-27 GPa measured for the cast specimens.[102] Likewise fracture strength (bending strength, modulus of rupture, MOR) values which can be found in literature ranges from ~100MPa[78] for a powder processed to the values as high as 1100 MPa for cast and polished dense SiCN.[102, 103] The same data for SiOC also varies; for example fracture strength of sol-gel derived SiOC was found as high as 700 MPa[104] while that of precursor derived one was found lower than 400 MPa.[105] Therefore, in **Table 2.2-2**, only the values acquired from dense/almost dense samples are included, for PDC materials only amorphous components obtained by the pyrolysis of polymeric precursors (any data obtained by sol-gel routes is excluded from the table) between 1000-1200°C is included. It should be underlined that the parameters affecting the final properties are not merely bulk density and surface properties but also nanostructural evolution may be different so that all the properties may fluctuate. Therefore all the properties listed in this table are strongly dependent on the chemical composition, preparation technique, and thermal history of PDCs, but given here in order to have a rough estimation about the properties of PDCs.

Table 2.2-2. A Some elected properties of PDCs together with that of vitreous SiO_2, Si_3N_4 and SiC.

Property	**Vitreous SiO_2[105, 106]**	**SiC[107]**	**Si_3N_4[107]**	**SiOC[105]**	**SiCN[102, 103, 108, 109]**
Glass Transition (°C) (Viscosity of ~10^{13} P)	1200	crystalline	crystalline	1350	1450
Density (g/cm^3)	2.20	3.10	3.20	2.35	2.23
Elastic Modulus (GPa)	70	410	310	100	155
Fracture Strength, MOR (MPa)	60	483	896	385	1100
Fracture Toughness, K_{1C} ($MPa^{0.5}$)	0.8	3	5	1.6	2.5
Coefficient of Thermal Expansion, CTE (1/K)	$0.5*10^{-6}$	$4.3*10^{-6}$	$3.2*10^{-6}$	$3.14*10^{-6}$	$3.96*10^{-6}$
Thermal Conductivity ($W.m^{-1}.K^{-1}$) @RT	1.4	84	25	-	-

It is known that, both SiOC and SiCN show higher resistance to crystallization than the binary amorphous compositions of Si_3N_4, SiC or SiO_2.[14] Studies on these properties showed that, in general, non-oxide ceramics (e.g., SiC, Si_3N_4) are promising for applications at high temperatures, but are unlikely to operate above 1500°C. While ceramic oxide/non-oxide composites may react at temperatures above 1200°C, oxide-based ceramics can be designed to have, for example, remarkable resistance to creep in the range of 1500 to 2000°C.[14] It is shown that both pure SiOC and SiCN have negligible steady-state creep up to 1300°C and 1550°C, respectively. Indeed the fact that the presence of some oxygen <5 wt% in SiCN has no deleterious effect on the kinetic behavior also suggests that these two amorphous ceramics may share essentially the same basic nanostructural framework.

There are virtually no studies on the oxidation behavior of PDCs aiming to compare the properties of different PDCs systems. This is because the comparison is often rendered difficult by the different characteristics of the ceramic (e.g., specific surface area, open porosity, nanostructural assembly, etc.) and the variable composition of the resulting compounds. Moreover, there are no studies concerning the active oxidation which mimics real conditions better than other methods (at high temperature/low pressure) and/or corrosion (in presence of H_2O or other combustion gases). Although oxidation data will not be sufficient since in real application, PDC is likely to be associated with different materials, submitted to other corrosive species than O_2 and often to stress, it should be noted that roughly speaking PDCs are generally oxidation resistant materials.[16] For example, despite the presence of high amounts of carbon (near one third molar), the oxidation resistance studies on SiOC system suggests that carbon activity is much less than unity.[110] Similarly, oxidation resistance of SiCN ceramics was found comparable to the best known resistance in crystalline materials, i.e. CVD Si_3N_4 and SiC.[14] Within the intrinsic thermal stability domain (till to the beginning of decomposition), the parabolic rate Kp (the oxide thickness parabolic constant) is shown to depend essentially on the nature of the oxide. While Ea (activation energy) was around 100 kJ/mol for SiOC, the increase of the nitrogen concentration in Si-C-N-(O) ceramics gives rise to an increase of Ea (up to ~300 kJ/mol) and decrease of Kp (so more resistant) at low temperatures, close to the values for Si_3N_4. This specific property of nitrogen-containing PDC was related to the well distinct oxidation behavior of SiC and Si_3N_4 and particularly the

significantly higher *Ea* value for the latter. Although, introduction of hetero elements are advisable to improve the oxidation resistance like Al, B, Zr, etc. (comprising neither H nor O) [111], the influence of these elements on oxidation resistance has not been fully elucidated for all PDC systems.[16]

Among the phases occurring in the polymer derived Si-O-C, Si-C-N, Si-O-C-N and Si-B-C-N materials SiO_2, BN, and Si_3N_4 are insulators (σ_{dc}(RT) = 10^{-14}-10^{-12} $(\Omega cm)^{-1}$) whereas SiC, and amorphous carbon are semiconductors (σ_{dc}(RT) = 10^{-4}-10^{2} $(\Omega cm)^{-1}$). Turbostratic carbon and graphite have a significantly higher conductivity (σ_{dc}(RT) = 1-10^{5} $(\Omega cm)^{-1}$). Recent studies in order to define the electrical properties of SiOC have shown that kinetics of carbon precipitation and subsequent cluster growth governs the electrical behavior of SiOC. Depending on the carbon content in the polymer two different temperature regimes have been distinguished: at low temperatures (<800°C for low carbon SiOC, <1400°C for high carbon SiOC) semiconduction and at higher temperatures due to percolation network of precipitated turbostratic carbon electron conduction. Generally, the conductivity increases upon heating resulting in an insulator-conductor transition after the polymer-ceramic conversion is completed above 1400°C ($\sigma_{\text{low carbon SiOC}}$ (1400°C)=10^{-2} $(\Omega cm)^{-1}$, $\sigma_{\text{high carbon SiOC}}$ (1400°C)=10^{0} $(\Omega cm)^{-1}$).[43]

The electrical properties of amorphous SiCN ceramics are in the range between the electrical properties of semi-conducting SiC and that of insulating Si_3N_4. Similarly to SiOC, increase of the conductivity of the amorphous SiCN matrix up to ~1300°C caused by an enhanced organization of the carbon atoms, while with a further heating a strong increase of the conductivity due to the formation of SiC and the loss of nitrogen is observed.[112] This enables to synthesize a variety of materials for electrical and electronic applications just by changing composition and structure of the amorphous silicon carbonitride ceramics. As predictable, amorphous SiBCN pyrolysis products of poly(borosilazane) was found to behave as electron semiconductors as well.[14] Electrical properties of PDCs can easily be altered by introduction of hetero elements or compounds, for example boron addition to SiOC suppress the carbon precipitation so improves the insulator properties, in contrast Cu_2O or $MoSi_2$ addition to same system enhances the electrical conductivity.[113] Although, considerable difference of materials

studied as well as pyrolysis conditions lead to significant variation of room temperature conductivities of the PDCs. According to the majority of the experimental investigations, PDCs pyrolyzed at low temperatures can be better described as insulators because they exhibit the room temperature dc below 10^{-10} $(\Omega cm)^{-1}$. In contrast, PDCs either after high pyrolysis temperatures or with high carbon content appear to be described as amorphous semiconductors.[16]

The piezoresistive behavior of some PDCs has been recently reported. It was shown that SiCN exhibits extremely high room temperature piezoresistive coefficients (gauge factor) of ~1000-4000, which is much higher than that of any existing ceramic. Typically, such a high gauge factor has only been observed in conductor-filled insulating polymer composites.[114] The particularly high piezoresistivity of the polymer-derived SiCN materials following the tunneling–percolation mode provides strong evidence supporting the formation of conductive graphene sheets within the framework of the nanodomain structure. The recent study done on high temperature (700-1000°C) piezoresistivity of SiOC(N) has shown that the piezoresistive behavior (gauge factor as high as 1700) of the produced ceramic far exceeds the performance of any known material in this temperature range (keep in mind that vitreous silica shows virtually no piezoresistivity).[115] A very recent study showed also that SiOC ceramic synthesized at 1400°C exhibits high room temperature piezoresistivity, leading to strain sensitivities (k factors) of ~145, while lower pyrolysis temperatures (1000-1300°C) do not show a RT piezoresistive effect. Similarly, it was obviously be concluded that the presence of a percolating network comprising electrically conductive free carbon is responsible for the measured piezoresistive behavior.[116]

PDCs sometimes called as “black diamond”, due most probably to the black color of final product optical properties of these materials have received little attention. The results of recent studies on the optical properties of both SiOC[117] and SiCN[118] have proven that these materials have very promising photoluminescence properties. Besides all these properties PDCs can be functionalized by incorporating of magnetic species into the PDC framework. SiOC foams possessing magnetic functionalization have been produced from a pre-ceramic polymer and iron silicide filler.[119] The final iron silicide phase consisted of fine cubic Fe_3Si particles

embedded in a SiOC matrix and exhibited M_s in the range of 9.5–17 emu/g, depending on the amount of fillers introduced. Composites consisting of particles of α–Fe dispersed in SiCN have been fabricated by incorporating Fe_3O_4 powder into liquid polysilazane precursor followed by reduction with graphite.[120] The composites had iron inclusions with the same magnetization as bulk iron, but they resisted oxidation up to 500°C. The same authors mixed different metal elements and alloys (Fe, Mn, Co, Ni, Ni-Mn, Co-Mn, Fe-Mn) with pre-crosslinked polysiloxane and found that the composites showed good soft magnetic properties.[121] Similarly, soft ferromagnetic micrometer-sized Fe-SiCN composites with a high Ms of ~57 emu/g have been obtained from direct mixing and ball milling of Fe powder with polysilazane precursor (cured).[16, 122]

As could be understood preceramic polymer pyrolysis is a very suitable process to produce oxide/non-oxide based ceramic materials which may show various type of properties underlined before. Moreover, manufacturing of glass and/or ceramic components from preceramic polymers can be achieved at significantly lower temperatures compared to conventional sintering, e.g., SiC from poly(carbosilane) is formed at 800-1500°C compared to 1900-2200°C for sintering. The organometallic polymers can easily be purified and a large variety of shaping processes are available; casting, injection molding, tape casting, pressing, impregnation, coating, fiber drawing, rapid prototyping, blank machining, etc. Nevertheless, there are some basic limitations for the production of components from polymeric precursors due to extraordinary high volume shrinkage deriving from the gas release occurring during the polymer-to-ceramic conversion and a pronounced density increase during thermolysis. For example, density typically increases by a factor of 2 to 3 from the precursor (1 g/cm3) to the ceramic residue (SiO_2, 2.2-2.6 g/cm3, Si_3N_4 and SiC, 3.0-3.2 g/cm3); and volume shrinkage may exceed 50 %. When the structural changes in the polymer-derived phase cannot be relaxed by viscous flow or diffusional material transport, extensive cracking and pore formation generally occurs. Thus, direct conversion of a polymer to dense ceramic compact is almost impossible to achieve, while to minimize these difficulties, especially crack formation due to shrinkage-induced tensile stresses, the size of the component can be reduced. Accordingly, flawless thin coatings and fibers can easily be produced from preceramic polymers but dense components necessitate more attention and carful work.

The pioneering research carried by Peter Greil[2, 123, 124], showed the possibility of both controlling the shrinkage and density by simply adding so-called “active fillers” to the preceramic polymers. In active-filler controlled pyrolysis process, a polymer that decomposes to a ceramic material is partially filled with active powder particles (metals or intermetallics). These filler particles react with the decomposition products of the polymer or a reactive gas atmosphere, the volume expansion (e.g. Ti to TiC) resulting from this reaction counters the shrinkage that occurs during sintering and allows the fabrication of bulk, flawless, near-net shape components. This process can be used as a possible route to produce various ceramic components. Suitable active fillers are elements or compounds forming carbide, nitride, or oxide reaction products such as Al, B, Si, Ti, $CrSi_2$, $MoSi_2$, etc., which are typically 1-10 μm and exhibit a high specific volume increase upon reaction.

As an alternative method, shrinkage and porosity during polymer-ceramic conversion can be decreased when the polymer matrix is filled with inert SiC, Si_3N_4, B_4C, BN, TiC, AlN, NbC powders so that the fraction of shrinking polymer phase is reduced according to the filler volume effect, see **Figure 2.2-13** for the schematic draw of probable microstructural chances during polymer thermolysis. In other words fillers simply partially reduce the total shrinkage in the component, by diluting the transforming mass.[2, 123, 125] As could be understood, incorporation of fillers offers the possibility to influence aforementioned mechanical as well as the physical and chemical properties of polymer derived ceramics in a wide range. For optimum combinations of reactive/inert filler, and pyrolysis atmosphere, zero net shrinkage is predicted for filler volume fractions which can be as low as 20%.[124] Generally, the mechanical properties increase with increasing filler volume fraction up to a maximum at approximately 40-50 vol% followed by a pronounced decrease at higher filler fractions due to enhanced porosity formation.[2] The size of the particles depends on the desired aim but if high reactivity is requested then nanosized powders with high specific surface area is advantageous.[53]

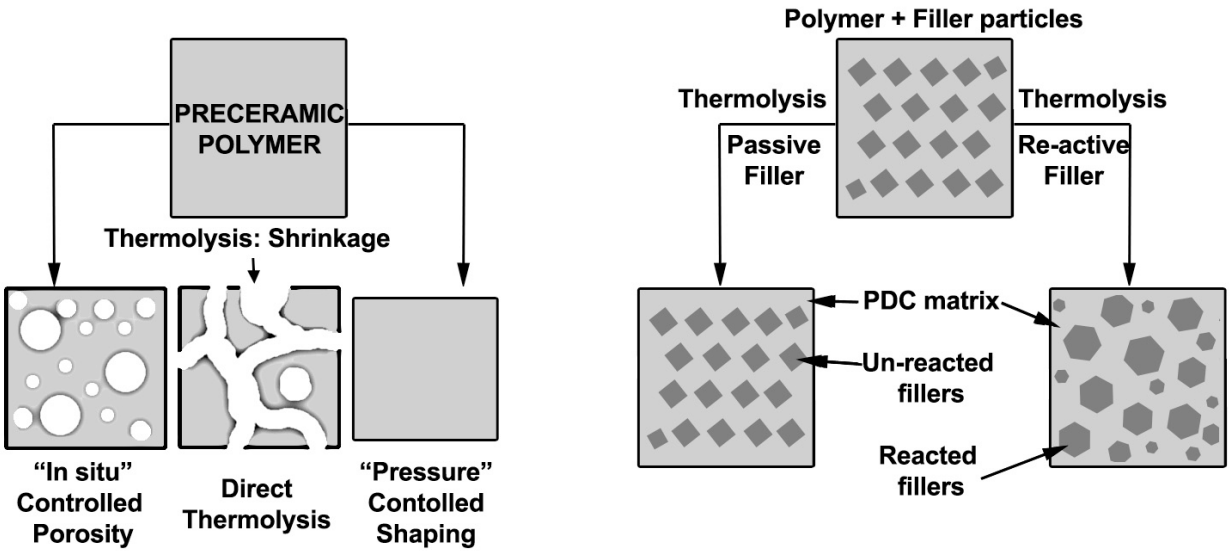

Figure 2.2-13. Probable microstructural chances during polymer thermolysis (Ar, N_2, air, etc.).[123]

Dense PDCs can be manufactured with sintering additives such as Y_2O_3-Al_2O_3 and Y_2O_3-Yb_2O_3. Even though, the technique is not an alternative to stabilize volumetric shrinkage, bulk density can be improved and flawless ceramic components can be produced.[73, 126, 127] Preceramic polymers can also be used to produce muti/single phase ceramic components. The general aim in these studies is not to keep the shaping or chemical stability of PDC but instead to use preceramic polymer as a reactive agent. While active filler pyrolysis derived materials with the aforementioned active fillers yield ceramic micro-composites, highly reactive powders is shown to afford synthesis of the different materials. For example; by using high reactivity of the electropositive magnesium metal with the organosilicon polymers, it is possible to synthesize title ceramics like $MgSiN_2$, where a homogeneous distribution of Mg at a length scale above 100 nm is realized. Furthermore, some recent studies highlighted the potential of using oxide fillers in combination with preceramic polymers.[53, 125, 128-132] Highly reactive nano-sized fillers, such as γ-Al_2O_3 nano-particles, allowed to produce a large amount of mullite at low temperature (by reaction in oxidative atmosphere)[53] and SiAlON ceramics (in N_2 atmosphere).[133] Other multi-component ceramics including biocompatible phases like wollastonite and hydroxyapatite were also produced by similar approaches.[125, 130, 131, 134] A more recent method to utilize preceramic polymers can be entitles as catalyst assisted

pyrolysis (CAP) which is thermolysis of the preceramic precursors with catalytic powder sources (Ni/Fe/Co/Pt/etc. generally below 10wt%) and following the formation of new structural formations like Carbon nanotubes (CNTs), SiC, Si_3N_4, SiO_2 1D nanostructures, see Chapter 4.2, for more details on CAP.

PDCs can also be combined with oxides to achieve synergetic enhancements in high-temperature properties. In this manner two methodologies have been postulated; i) "particulate composites"; pyrolysis of precursor to obtain ceramic powder (generally ball milled and sieved to few micron size), which can then be mixed with the powder of the conventional ceramic and then sintered, ii) "interface composites" coating a ceramic powder with the polymer precursor of the PDC.[132] The polymer coating is expected to develop a reactive liquid-like phase upon pyrolysis. Therefore, precursor is generally added in few amounts analogues to reactive liquid phase sintering studies where frit volume is generally less than 10%. Brahmandam et al.[132] in the study to produce HfO_2-SiCN composites has shown that while the interface composites (having the highest strength) and single-phase hafnia specimens remained immune to hydrothermal exposure, the particulate composite suffered a dramatic loss of strength, which coincided with the onset of weight loss in these specimens. Consequently, the authors claimed that the interface composites, with their highly refractory grain boundaries, represent a new class of ceramics for structural applications in harsh environments and at ultrahigh temperatures.[132]

As a sum preceramic polymers offer a great variety of chemical and structural modifications which allow molecular tailoring of ceramic materials with improved properties compared to conventional ceramic materials. Development of high temperature resistant ceramic components (fibers, coatings, tapes, foams, bulk, etc.) from less expensive polymers gain in significance for current and future applications, in **Figure 2.2-14** preparation of different ceramic forms by using polymeric precursors is schematically summarized. Note that interface/particulate composite approaches have not been applied to produce some forms given in table like foams, fibers and coatings. Since sintering is the main situation in these approaches and generally bulk component is expected, yet it is also possible to produce even foam by following these approaches. Moreover, replacement of Si by further hetero atoms

such as Al, Ti, etc. in the polymer backbone may yield new type of precursors to manufacture functional ceramics with particular electrical, thermal, chemical and biological properties.[2, 14, 135]

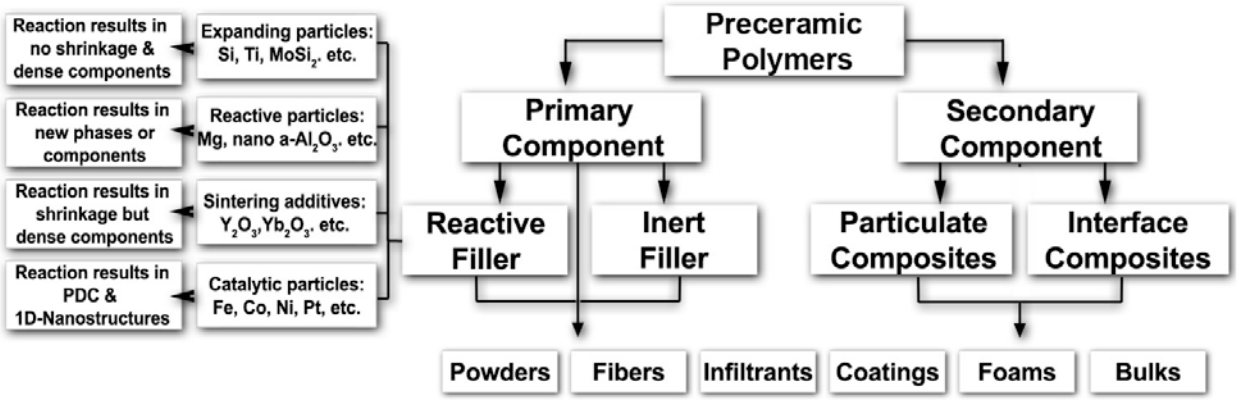

Figure 2.2-14. Utilization of preceramic polymers.

Although groundwork for PDCs focused on fiber processing and coatings, more recently bulk components and porous bodies are of particular interest to produce high temperature stable PDCs. The present thesis study attempts to provide methodologies to explain how preceramic polymers can be use to produce porous components especially the ones having high specific surface area. In this manner, in the following chapter we will give some fundamental info on porous materials and especially on porous ceramics; particularly giving an emphasis on reviewing the polymer derived porous components and hierarchical porous ceramics.

2.3. Porous Materials

Materials containing tailored porosity exhibit special properties and features that usually cannot be achieved by their conventional dense counterparts (see **Figure 2.3-1**). Therefore, porous materials find nowadays many applications as end products and in several technological processes.[136] Particularly, porous ceramics find use in several key engineering applications, such as thermal insulation, filtration, absorption, catalyst support, load-bearing lightweight structures, etc.[137] The properties of porous ceramics are affected by various

parameters, including their relative density (amount of porosity), morphological characteristics (cell size and shape), distribution of the pores (pore interconnectivity and cell wall/strut porosity), and finally the material type. The porosity characteristics can be varied in a wide range of values depending on the production method. Several processing methods have been proposed for the fabrication of porous ceramics, among which are the replication of the structure of polymeric foams, direct blowing, the use of sacrificial fillers, extrusion through special dies (for honeycombs), solid freeform techniques, the mimicking of natural templates (e.g. wood) or the assemblage of fibers or hollow bodies, partial sintering and powder processing, emulsion processing, etc.[42, 136] In addition to the composition of the ceramic material constituting the solid skeleton of a porous component, the characteristics of its porosity (total amount, ratio closed/open porosity, average pore size and distribution, pore shape, tortuosity and interconnectivity, presence of graded porosity), which are dictated by manufacturing process employed, determine its properties and suitability for potential applications.

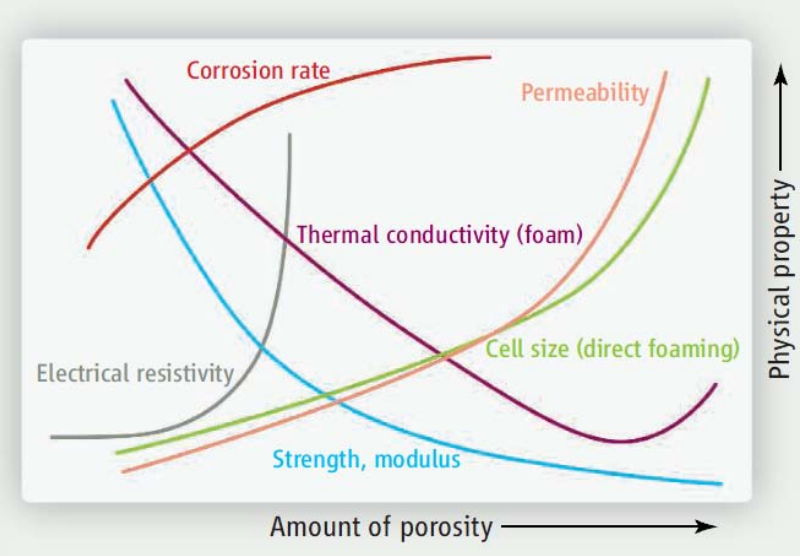

Figure 2.3-1. The amount of porosity versus some physical properties, no distinction is made in the graph between open and closed porosity.[138]

2.3.1. Cellular Ceramics

Cellular ceramics constitute a specific class of materials containing a high level of porosity (> 60 vol%) which are characterized by the presence of a recognizable "cell", that is an enclosed empty space possessing faces and solid edges (see **Figure 2.3-2**). The faces can either be fully solid or void, giving a closed cell or an open cell material, respectively. In some cases, pores can exist in the cell walls (pore windows or cell windows), or the material can have a mixed morphology containing both closed and open cells. The structure of a cellular ceramic consists of polyhedral cells that are arranged three-dimensionally to efficiently fill the space, and depending on the overall morphology a structure typical of a honeycomb (possessing parallel prismatic cells) or of a foam (for which cell walls are randomly oriented in space) can be identified.[139, 140] Furthermore, cells can be regular or exhibit random or graded variations in size, shape and distribution, thus further extending the range of morphologies that cellular materials can exhibit. Besides foams and honeycombs, connected rods, connected fibres, connected hollow spheres and materials obtained from the replica of biological templates are also examples of cellular structures that are being produced nowadays.

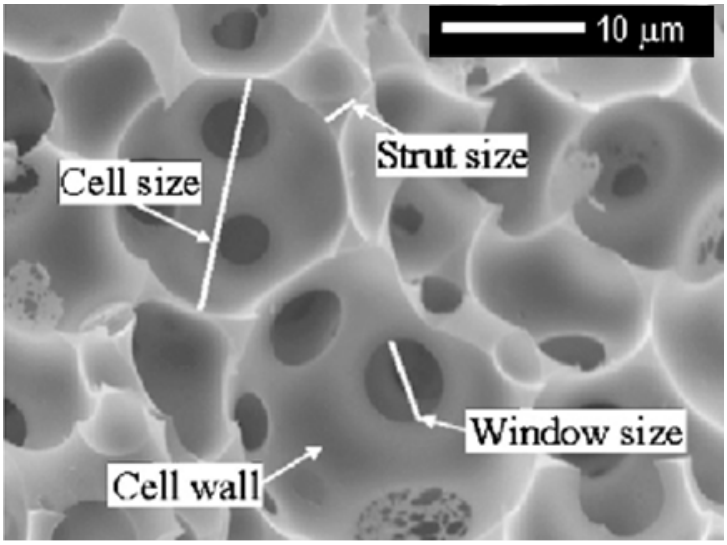

Figure 2.3-2. Micrograph showing the dimensional characteristics (pore-cell size, strut thickness, cell window) of a ceramic foam.[141]

It must be observed that the terminology used to classify the porosity of materials (i.e. microporosity when the pore size is < 2 nm, mesoporosity 2-50 nm and macroporosity >50 nm), which was developed by IUPAC chiefly with the aim of helping in the characterization of catalytic materials,[142] is not particularly of assistance in the description of the porosity of cellular materials. In fact, it defines a porous solid as "a solid with pores, i.e. cavities, channels or interstices, which are deeper than they are wide" (which is not always the case, as for instance in foams) and the pore size (generally pore width) as "the distance between two opposite walls of the pore" (therefore failing to take into account asymmetric pore shapes). More importantly, according to this definition, all cellular ceramics are constituted of macropores, a generalization which does not help in describing the architecture of their porosity in a detailed and meaningful way. However, the technical literature, borrowing from what has been proposed for plastics,[143] started distinguishing between macro-cellular and micro-cellular foams[144] the latter possessing cells with a size smaller than 30-50 μm and a cell density (number of cells per unit volume) greater than 10^9 cells/cm^3. Therefore it is possible to accept that microcellular material is the one with cell sizes smaller than about 100 μm and ideally in the range of about 30 to about 50 μm, while macrocellular ones with cell sizes bigger than 100 μm.

A cellular ceramic when it is in bulk form sometimes referred as a "monolith", here in the remaining part of the text "monolith" and "cellular ceramic" will be used interchangeably. In the present study we will not discuss powder components and ceramic membranes, and will give an emphasis more on monolithic structures. Most common monolithic forms are honeycombs (**Figure 2.3-3**(a)-(c)) and foams (**Figure 2.3-4**(a)-(c)) and the latter will be the focus of the present study. Honeycombs are composed of regularly arranged parallel channels. The most important characteristics are the channel size, expressed as channel per square inch (cpsi), and the open frontal area, which amounts to 63-87vol% (ceramic bodies) and to ~ 90vol% (metallic honeycombs). The main advantage of honeycombs reside in their low-pressure drop, high-geometric surface, robustness, strength and low weight. The ceramic monoliths are operated essentially adiabatically, because of their low thermal conduction and the lack of radial mixing that yield a poor heat transfer to the walls.[145]

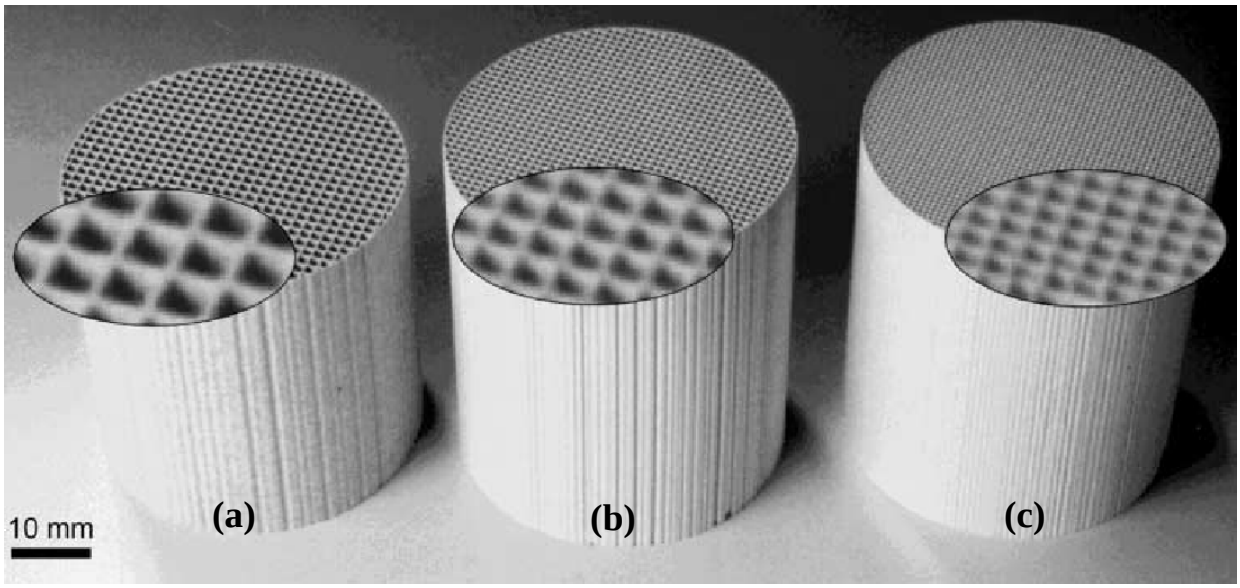

Figure 2.3-3. Photographs of a) 200, b) 400, and c) 600 cpsi ceramic monoliths (cordierite).[146]

Ceramic foams are used commercially for the filtration of molten metals, and are attracting increasing attention as catalyst supports due to high thermal stability, high porosity and increased tortuosity with respect to honeycombs. Ceramic foams have open porosities of >75% and the metallic foams of about 95%. According to Gibson and Asbhy,[139] one can properly speak of foams only when the relative density (bulk density / theoretical density) of the material is <0.3, while for higher densities it should be classified as a generic (macro) porous material. The main characteristic is the size of pores, which is usually expressed as the pore count "pores per inch" (ppi). Commercial foams have pore counts between 5 to 100 ppi, see Figure **2.3-4**(a)-(c) for some foam structures having different ppi. The structure of foams allows low-pressure drop flowing with radial mixing, tortuous flow paths and enhanced turbulence in the pores. The heat transport to the walls occurs not only by conduction, as in honeycombs, but also by convection and radiation.[145]

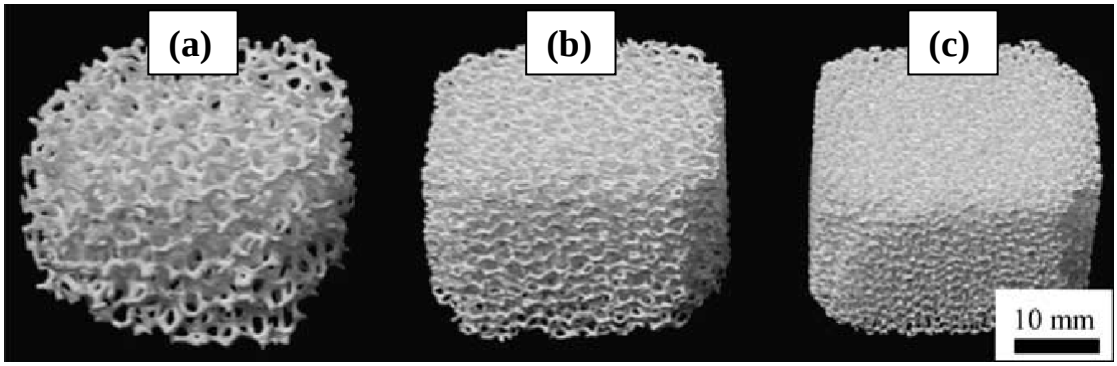

Figure 2.3-4. Photographs of foam structures with different porosities, a) 10, b) 20, and c) 35 ppi.[147]

Because of their structure, cellular ceramics display a rather unique combination of properties, such as low density, low thermal conductivity, low dielectric constant, low thermal mass, high specific strength, high permeability, high thermal shock resistance, high resistance to chemical corrosion and high tortuosity of flow paths, making them indispensable for various engineering applications.[148] But generally speaking exhibiting low SSA values (<2 m^2/g). These materials offer also the advantage of a much higher temperature and environmental stability in comparison to conventional polymers or metals, and typical materials used for manufacturing cellular ceramics include crystalline inorganic materials such as silicon carbide, alumina, zirconia, cordierite, mullite, but also silicate glass and carbon as well as concrete. Depending on their nature and structure (e.g. open versus closed cells), typical and novel applications for cellular ceramics include: filtration of molten metals or of particulate from exhaust gases; radiant burners; catalyst supports; biomedical devices; kiln furniture; reinforcement for metal or polymer matrix composites; bioreactors; fibre-free thermal management components; supports for space mirrors; components in solid oxide fuel cells; lightweight sandwich structures; heat sinks; electrodes; and heat exchangers.[149] All these applications require the porous component to possess a specific range of values for different properties (permeability, thermal conductivity, strength, stiffness, chemical durability, etc.), and this can be achieved by selecting the appropriate fabrication method. A wide range of

processing routes have in fact been proposed for the production of cellular ceramics, employing raw materials of various nature and leading to a variety of morphologies

A detailed work by Gibson and Ashby[139] gives a comprehensive info on cellular materials (metals, polymers and ceramics), while Brezny and Green[150] reviewed their work concerning the mechanical behavior of cellular ceramics. The main processing methods used for the preparation of cellular ceramics such as foams, honeycomb structures, etc. can be found in the recent review of Colombo.[140] The fabrication and the use of cellular ceramics in a vast number of different fields has also been described in a recent book edited by Scheffler and Colombo[149] and in a review paper by Colombo.[42] Moreover, the processing microstructure property relations for these materials are also comprehensively reviewed by Studart et al.[136] As seen, literature holds sufficient info related with the production and properties of cellular ceramics, consequently in the following sections we will exclude general properties and production methods for these materials but discuss ceramic foams which are produced by using preceramic polymers, i.e. polymer derived micro-macro cellular foams. Moreover, concerning the main scope of the present thesis study, i.e. to produce high SSA porous components, hierarchically porous ceramics will be reviewed in depth.

2.3.2. Cellular PDCs

Preceramic polymers, in particular silicones, have been successfully used for obtaining ceramic components (such as foams and membranes) possessing a large amount of porosity, in the micro-, meso- and macro-size scale.[42] The first suggestion that porous ceramics could be produced from preceramic polymers can be found in the patent literature -by direct blowing[151] or by solvent extraction from a phase-separated polysilane gel.[152] Several papers have been since then published in the scientific literature by the present author and various collaborators, detailing a range of processing procedures, reporting extensive characterization of the products and describing their testing for diverse applications.[42, and references therein] Alternative processing methods for the production of open cell (macro-)porous ceramic foams have also been proposed by different researchers. These include the use of preceramic polymer blends,[153-155] infiltration of a porous salt preform using a molten preceramic

polymer,[156, 157] utilization of sacrificial polymer as a substrate[158-160] or both as a blowing aid and as a template,[113, 161-166] self-foaming by in situ evaporation of volatile condensation products generated during silicone crosslinking reactions,[38, 167-171] freeze-drying processing,[172, 173] foaming by physical blowing agent,[49, 174, 175] dissolution of CO_2 gas into a preceramic polymer under pressure followed by introducing of a thermodynamical instability,[176-180] dissolution of colloidal silica sub-micron spheres,[181-184] utilization of biotemplates,[185] emulsion processing,[186] the use of sacrificial polymeric microspheres.[67, 119, 125, 144, 175, 187-195] In **Figure 2.3-5**(a)-(l) a collection of SEM micrographs taken from the cellular PDCs produced by aforementioned processing strategies is given. Note that these microstructures are given in order only to have an idea about the rough morphologies for the produced bodies and undoubtedly changing the processing condition affects the given microstructures.

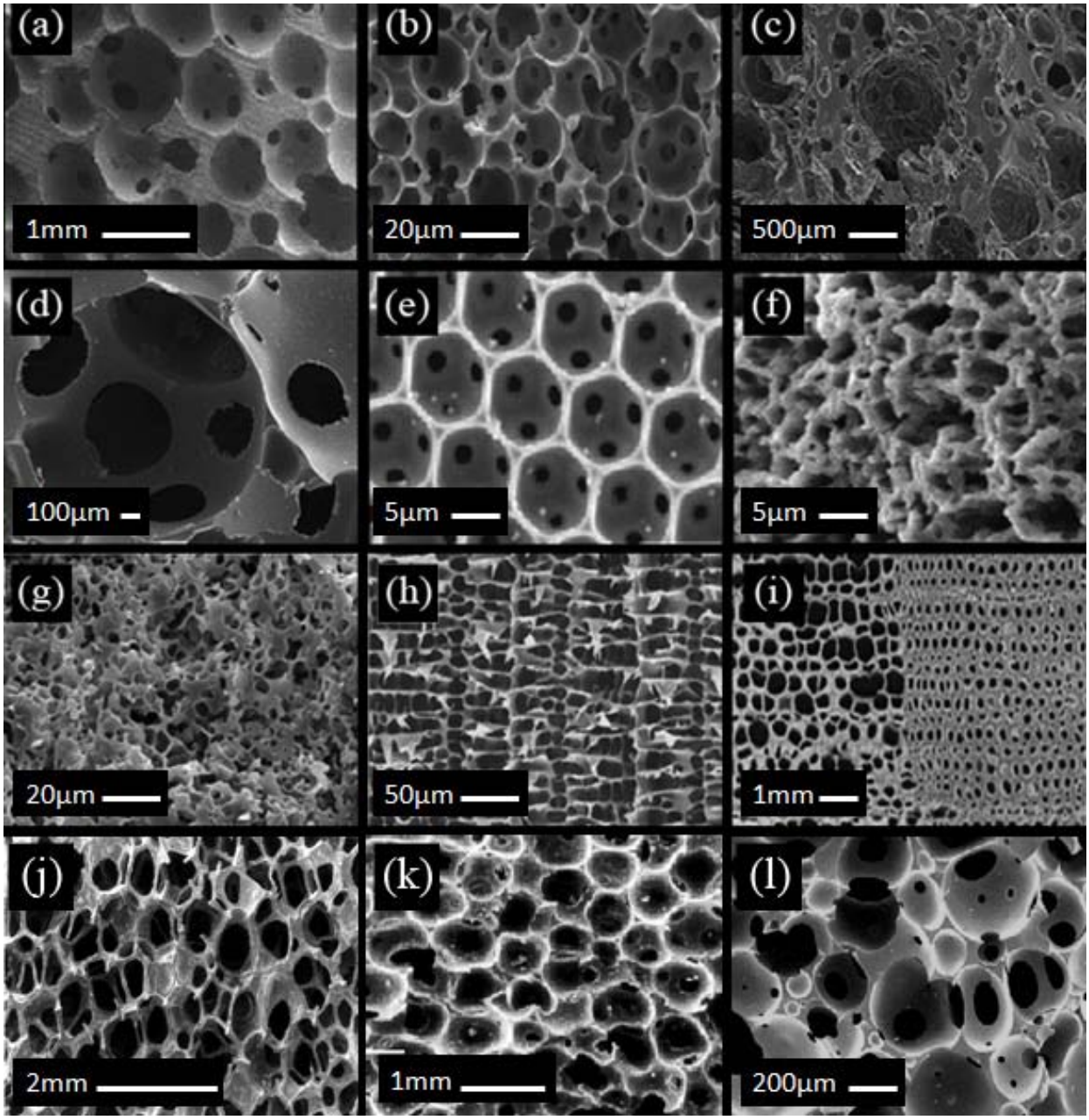

Figure 2.3-5. SEM-micrographs of polymer derived ceramic foams processed via different routes; a) Utilization of PU-preceramic polymer blend,[42] b) via sacrificial PMMA microbead templating,[42] c) blending of preceramic polymers,[42] d) physical blowing agent,[175] e) colloidal silica templating,[184] f) emulsion processing,[186] g) dissolution of CO_2,[178] h) freeze casting,[173] and i) biomimetic templating,[185] j) reticulated foam by using PU foam,[159] k) self foaming due to volatile release during thermal curing,[168] l) self foamed via electron beam irradiation.[171]

Each of these mentioned processing methods utilizing preceramic polymers has its own benefits and drawbacks as regards to manufacturing. For instance; direct foaming techniques often lead to a gradient in the porosity amount and pore size along the main expansion axis;[38, 161, 175] while infiltration of a silicone resin within organic sacrificial fillers requires a burn out step that has to be carried out in a very controlled fashion in order to produce components without defects (besides often requiring warm pressing -depending on the rheological characteristics of the preceramic polymer- to obtain a well controlled morphology),[144] thus limiting the size and shape of the component that can be produced; similarly colloidal silica templating necessitates etching which may disturb the structure and results in a small size pores and pore openings;[182] similarly the use of supercritical CO_2 is regulated by the diffusion within the solid polymer, and works well only for components of limited thickness, and enables to obtain only micro-cellular foams.[177] The comparison of these techniques has already been done by Colombo[42] in a recent comprehensive review together with possible applications for these materials. Concerning the main properties of ceramics obtained from PDC foams; data for the SiOC system shown in **Table 2.3-1** was taken from this recent review[42] and given together with the other studied PDC system in the present thesis study; i.e. SiCN. More detailed discussions on processing of macro porous PDC components will later be given in the following chapters where it is needed.

The most important parameters to realize application of a component produced from preceramic polymers are the cost and reproducibility of the final component. Polysiloxanes in this manner offer exceptional opportunity. SiOC based porous ceramics have been so far tested including thermal protection components for space vehicle re-entry, micro-reactors for chemical engineering applications, aerosol filter components and gas absorbers. It is believed that these materials could find also use as high temperature acoustic insulation, as well as thermal shock-resistant components.[42]

Table 2.3-1. Main characteristics of PDC porous components, data for SiOC components is taken from ref[42].

Property	Macro-cellular SiOC foams	Micro-cellular SiOC foams	Porous SiOC components	Macro-cellular SiCN foams[175]	Micro-cellular SiCN foams[184]
Porosity (vol%)	68-90	72-88	55-80	64-71	>70
Average cell size (μm)	100-2000	1-185	100-500	500-1000	1-10
Compression strength (MPa)	1.2-12.5	nm	nm	1.08-3.31	nm
$CTE_{20–1100}$ °C ($\times 10^{-6}$ K^{-1})	3.75±0.19	4.40±0.20	4.60±0.15	nm	nm

2.3.3. Hierarchically Porous Ceramics – A Review

To be published in a review article: P. Colombo, C. Vakifahmetoglu, and S. Costacurta, "Ceramic Components with Hierarchical Porosity," Journal of Material Science, 2010.

A porous component containing pores on two or more length scales is referred to as a material with hierarchical porosity. Different types of hierarchical porosity may exist according to the range of pore sizes that are involved in the porous structure, i.e. bimodal size distribution (micro-meso, meso-macro, micro-macro), or trimodal (micro-meso-macro). Graded or oriented porosity is also sometimes desirable for specialized applications. A component containing hierarchical porosity typically possesses simultaneously a wide range of desirable characteristics, which include high accessibility, rapid transport of fluid and gases, high selectivity, fast uptake and release, the possibility of rapid thermal cycling, chemical and mechanical stability and efficient use of volume. The presence a small pores (particularly micropores) provides a high specific surface (SSA), that is geometric area per unit mass of the part. These components are therefore of significant technological interest, and are successfully used in several industrial processes and household products. Applications include catalysis, filtration (of liquids or gases), extraction, separation, sorption and scaffolds for biological

applications.[196] However, several challenges remain, in particular limited mechanical strength (especially for components with micro-meso porosity), a poor structural control at all length scales and the requirement of elaborate processing methods to achieve such a complex, multiscale microstructure

Several processing routes have been proposed to fabricate ceramics with hierarchical porosity[197-200, and references therein]. Here we will try to make a new wider categorization dividing the strategies into two main processing: I) production of micro- or meso-porous ceramic materials followed by the introduction of macro-porosity, and II) production of macro-porous ceramics followed by the introduction of micro/meso-porosity. Both routes include one-pot or multi-pot processing strategies. Since the production of micro- and meso-porous ceramics as well as their combination (i.e. micro-meso hierarchical porosity) has been covered recently by several authors,[200-203] in this part of the study we will focus mainly on ceramic components which also contain macro-porosity (ranging from a few microns to a few millimeters) in their pore architecture, which is therefore classifiable either bimodal (micro-macro and meso-macro) or trimodal (micro-meso-macro).

2.3.3.1. From micro/meso-porosity to a multi scale pore hierarchy

In the excellent review Schuth,[202] divided templating approaches that will be used in the synthesis of porous solids into two different modes (I) endotemplate and (II) exotemplate. In endotemplating template specie which is an isolated precursor and is included as an isolated entity into the growing solid particle is used, while exotemplating describes a structure providing a scaffold with voids. If this scaffold including pore channels is removed after filling of the voids, either a small-particle/high-surface-area material or a porous solid is generated, depending on the 3D interconnectivity of the templating material.[202] Later on; Tiemann[204]underlined the difference in replication procedures involving solid-state matrices and true liquid-crystal templating (colloidal templating) in a way that the latter method is not though as an exact case of exotemplating or nanocasting. Here, we will follow the same way of thinking but as well including the polymeric templating approaches in this part of the review; meaning that via dividing the templating approaches as “soft” and “hard”.[205] Thus; all

the methods utilizing templating agents that could be thought as “soft” (polymeric particles, beads, foams and emulsions), and bio templates, inorganic salts, ice crystals when used together with particles having mirco/meso porosity or structure directing agents to produce this type of porosity is included in the present subsection.

Generally speaking; in the production of hierarchical porous cellular ceramics; self-assembled molecular aggregates or supramolecular assemblies are employed as the structure-directing agent of mesostructures/pores. Instead, bigger-sized substances, such as colloidal crystals, polymeric substances, bio-celluloses, emulsions, vesicles, inorganic salt and ice crystals, are added in the synthesis to create macroporosity, while for the micropore templating the function of the templates is still little understood.[202] Yuan et al.[200] in the recent comprehensive review gave a detailed description of most of the synthesis strategies to produce hierarchical meso-macroporous materials. Concerning sufficient literature info in the field, in the following subsections we will restrict reviewing by focusing mainly on the production of cellular ceramics by templating approach.

a) Colloidal templates

Colloids are nanosized particles with at least one characteristic dimension reaching to one micrometer size.[206] Colloidal crystals (silica or polymer spheres) together with appropriate structure directing agents has been widely used to form bead inverse structured porous ceramics and carbon. Different types of cellular macroporous materials are accessible by templating with colloidal crystals of monodisperse spherical particles.[200, 202] In a typical processing of utilizing colloidal particles; first regular aggregates (called as opals) of these species are made. Then inorganic precursor together with structure directing agents (such as surfactants or copolymers) is allowed to infiltrate the voids (spaces between the spheres) in the formed aggregate, which is followed by condensation and crystallization. Alternatively, colloidal particles can be coated with the precursor of desired material to process which is then used to form an opal structure; that is the pores of the opal are incompletely filled. The removal of the surfactant and colloidal latex species, by either high-temperature calcination or solvent extraction, leads to the formation of three-dimensional (3D) ordered meso-

macroporous materials. Various compositions including titania,[207] silica,[208, 209] niobia,[207] alumina[210-212] and silica-alumina (by applying 275 nm size PMMA beads as macroporosity generator)[213] with macroporous walls having mesoporosity have been prepared by following this route.[200] Furthermore, by using different diameter-sized colloidal crystals together with different types of structure directing agents variable pore hierarchy and graded pore systems can also be successfully formed, see **Figure 2.3-6** for a representative schema of this processing type.[200, 214] For example; 3D cubic ordered macroporous (140 nm) and binary macroporous (140, 80 nm) silica structures having ordered mesoporous (7.7 nm) walls have been synthesized by Luo et al.[215] Instead, Kuang et al.[216] used PS (560 nm particles), a novel block copolymer, and an "ionic liquid" (IL) as templates in order to produce meso(in bimodal manner)-macro porous materials. The material represented a 3D macroporous structure (~360nm cell size) with long-range order and interconnecting windows of ~80 nm. The surface of the cell walls is shown to be covered by two types of mesopores that is; large spherical mesopores (~ 12 nm), and small elongated mesopores (2-3 nm) leading to a high SSA (244m^2/g) silica material.

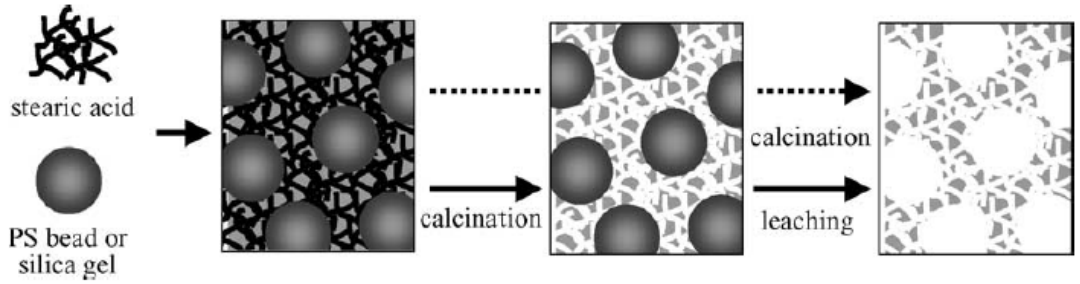

Figure 2.3-6. Processing schema for the synthesis of porous alumina with a bimodal pore size distribution. Template removal steps are indicated by a dotted-arrow for polystyrene beads and a solid-arrow for silica gels as physical templates.[212]

Ionic liquids used in the mentioned study are salts with melting points of below ca. 100 °C, and sometimes as low as –96 °C, so that they can be used as solvents under conventional organic liquid-phase reaction conditions.[217] These materials have recently used as templates for the synthesis of mesostructured silicas consequently is adopted in engineering porosity applications to produce hierarchical porosity components.[200] In this way, bimodal micro

(~1.3nm) /macro (175nm) porous silica material was produced by using PS bead packing and an amphiphilic ionic liquid as dual templates.[218] The overall BET surface of the hierarchical porous silica formed in the study was very high reaching to the values higher than 1000 m^2/g. Due to the high flexibility of the method tri-modal pore hierarchy is also obtained. Sen et al.[210, 219] produced a hierarchically porous high SSA (531m^2/g) silica with ordering on three different scales, that is, macropores (200–800 nm), interconnecting windows (70–130 nm), ordered mesoporous walls (80 nm) with narrow micropores <2 nm in the presence of multiple templates, that is, PS latex spheres, surfactants (triblock copolymers) and cosurfactants (butanol or pentanol). Recently in a same methodology Suzuki et al.[220] produced high SSA trimodal porous silica (356m^2/g, see electron microscopy images given in **Figure 2.3-7**) and alumina (329m^2/g). The obtained products had three types of pores (macropores ~200 nm, mesopores (cage-type) ~4nm and micropores <2nm) originating from PS spheres, triblock copolymer spheres and the tails of the copolymer, respectively. The major drawbacks of these studies can be listed as the limited product and its restricted macropore size (<1µm), small pore openings (window) between interconnected cells combined with high production costs due to expensive templates.[221]

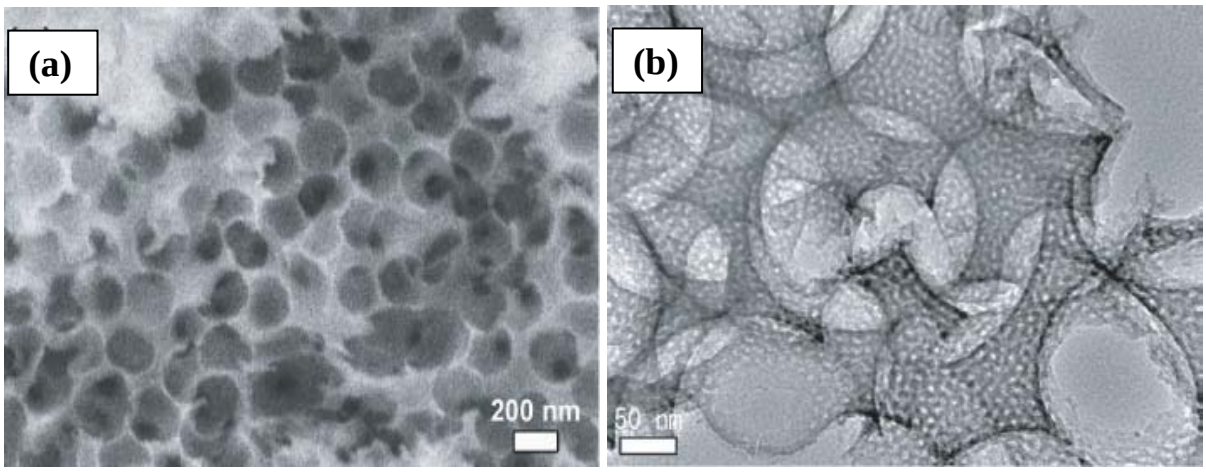

Figure 2.3-7. a) SEM, and b) Bright-field TEM images of the trimodal hierarchically porous silica samples produced by Suzuki et al.[220]

b) ***Polymeric foams, biomimetics, emulsions, inorganic salts and ice templating***

In order to answer the requirements for larger macropores, more recently, monolithic polystyrene (PS) foams, preformed by polymerization of styrene either in the continuous or the dispersed phase of highly concentrated water/oil emulsions, have been used to synthesize meso/macroporous inorganic oxide monoliths by using block-copolymer/sol-gel mixture. After calcination to remove the organic components, the resulting meso–macroporous silica, titania, and zirconia materials is shown to retain their macroscopic shapes and possessed independently adjustable meso- and macropore structures. The meso–macroporous silica monoliths prepared from the W/O-PS foams together with PEO-PPO-PEO triblock copolymer species consisted of cellular macropores 0.3-2 μm in diameter, (pore windows had 0.2-0.5 μm in diameter), and highly ordered mesopores of 5.1 nm in size.[222] Alternatively, preformed high SSA, mesoporous silica nanoparticles can be used as building blocks to coat polyurethane (PU) foam.[223, 224] Following by mineralization, and subsequent elimination of the organic foam (therefore porous struts) by calcination, monolithic macrocellular silica foams with a trimodal pore system (small mesopores-large mesopores-macropores) were obtained. Textural large-mesopores/macropores (in the 20-70 nm range) have their origin in the inter-particle voids, and the small intra-particle mesopore system (2-3 nm in diameter) is due to the supramolecular templating effect of the surfactant. The obtained meso-macro porous silica can further be utilized as a sacrificial foam to obtain meso-macro porous carbon monoliths[225, 226] which can later be used to produce zeolite monoliths as well (see layer).[227] Almost the same methodology is followed very recently by Li et al.[228] to produce macroporous γ-Al_2O_3 foams with highly ordered (2D) crystalline mesoporous walls, but in a slight modification; i.e. by utilizing a triblock copolymer P123 as mesoporous structure-directing agents.

It is know that PU and PS polymeric foams are hydrophobic, contrary to these materials hydrophilic urea-formaldehyde (UF) resin monolith (foam) can be used as a template material. Since UF resin possesses hydrophilic characteristics, organic solvent free precursors can be also utilized for “soft” nanocasting, which should be benign to the environment.[229] Shi et al.[229] recently used UF resins as a template for preparing series of inorganic oxide monoliths including silica, zirconia and titania by nanocasting. Later on by using the same type of

polymeric template, high SSA (324m^2/g) silica monoliths having meso (~4.5nm)-macro porosity are produced.[230] While with the use of UF templating, it is shown that macropore size can be tailored below 5μm by changing the processing conditions of polymer production, no information was given concerning the mechanical properties of the produced foams.

Some other hybrid techniques are also used to synthesize hierarchical porous ceramics; for example Ocampo et al.[231] prepared a hierarchically porous glass monolith via combination of the sol-gel, double polymer templating, and rapid prototyping (RP) techniques. The monolith produced in this way exhibited three pore families in bimodal length scale that is macro-meso with macropores around 300-500 μm produced by the RP technique, and around 10-100 μm made by using a methyl cellulose template, and finally mesopores around 4-5 nm with 2D hexagonal pore structure produced by P123 triblock copolymer self-assembly. Several other studies followed hybrid methods to produce pore hierarchy. Yun et al.[232] recently produced hierarchically mesoporous–macroporous bioactive glasses scaffolds for bone tissue regeneration by sol–gel method and evaporation-induced self-assembly process in the presence of both nonionic triblock copolymers, (P123 or F127), inorganic templates and methyl cellulose template, see **Figure 2.3-8** for the schematic description of the hybrid processing proposed by the mentioned authors.

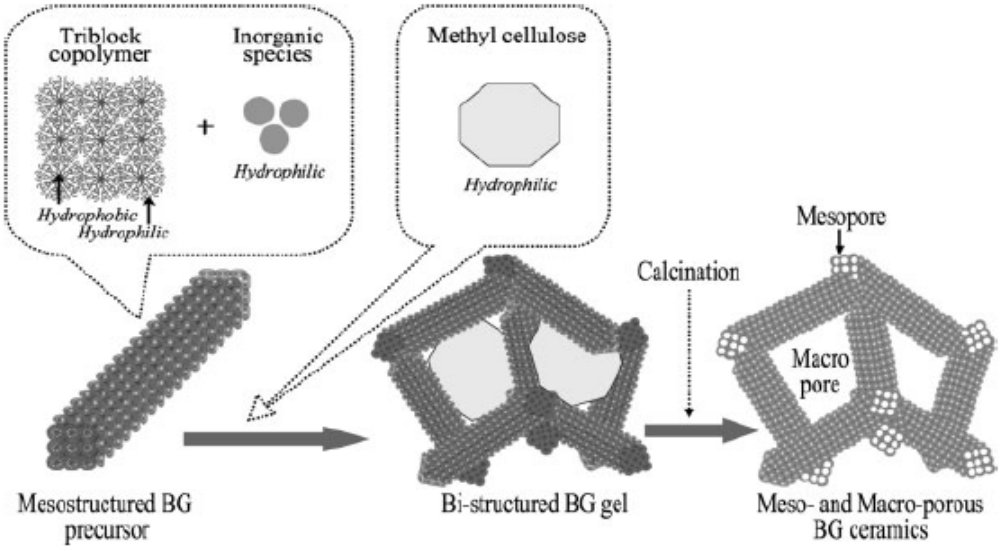

Figure 2.3-8. Synthesis of hierarchically porous bioactive glasses.

Templating strategy has also been applied to produce hierarchically porous zeolite monoliths since utilization of sacrificial templates supplies higher purity to a cellular monolith (self-supporting) compared to that of the coated one. For example; apart from the pelletization or extrudation studies, template-directed processes involving polymeric templates, starch, biological tissues, etc. are used to prepare hierarchical porous phase pure zeolite frameworks through hydrothermal synthesis or a secondary-growth process of zeolites. In a typical procedure, zeolite nanoparticles or their precursors are assembled around the skeleton of a template to form the coating (or seeding) followed by processing to form zeolite monolith via elimination of the template to form self supporting zeolitic monoliths. PU among other templating materials have been used more commonly in this field since it is readily available in the market with nearly unlimited variation of the pore window size and volume.[233] PU supported ZSM-5, silicalite (see **Figure 2.3-9** sample for the sample morphologies prepared by Lee et al.[147]) and TS-1 samples have been utilized to produce zeolite self supported foams having high SSA reaching to the values of ~450m^2/g.[147, 233-235] Other polymeric template alternative; PS has also been used for the synthesis of silicates with bimodal pore structures of macropores (250 nm average diameter) that are surrounded by microporous zeolithic walls.[236] Dual templating method is employed to control the hierarchichal pore system where macropores are formed by using arrays of monodisperse PS spheres as templates, and micropores are governed by structure directing agent.[236]

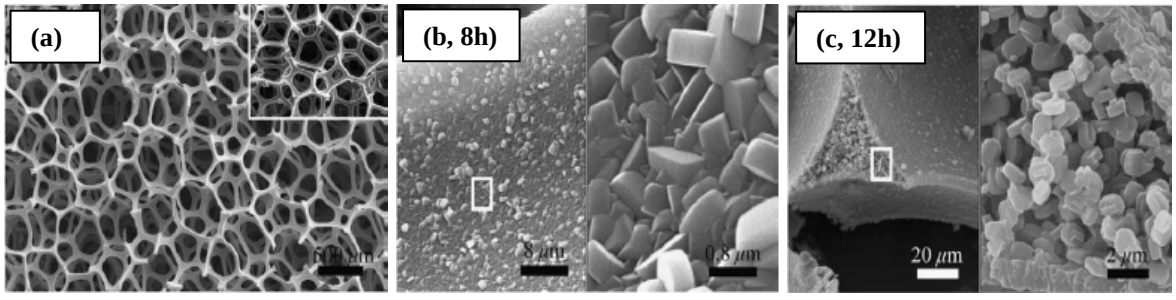

Figure 2.3-9. SEM images of; a) Ester derived no membrane PU foam, b) the surface detail after 8h of zeolitization, and c) strut detail after 12h of reaction.[147]

Compared to synthetic templates, natural tissues are not only inherently complex and hierarchical but also different from species to species even within the same genus, making it possible to synthesize materials with unique multilevel structures and morphologies (biomimetic materials). Biological templates are generally inexpensive, abundant, renewable, and environmentally benign. As an alternative to conventional extrusion technologies, biotemplating (biomimetics) have been developed in order to replicate the hierarchical porous structures of biological materials for the development of ceramic materials.[237, 238] For example, in addition to aforementioned artificial templates, natural complexes; such as starch gel,[239] wood,[240-242] equisetum arvense,[243, 244] cellulose acetate,[245] palm fibers,[246, 247] cuttlebone,[248] diatom, [249-251, and references therein] etc. have been used as a macrotemplate to produce micro/macro porous zeolite components, see **Figure 2.3-10** for the SEM images of the samples prepared by Zampieri et al.[242] using rattan derived SiSiC foam to produce ZSM-5 type zeolite coatings. However, zeolitization throughout the entire structure of the biological structure would not be achieved if the zeolite crystallization process did not take place within the tissue.[244] This limits the utilization of bare biological tissues; with an exception offered by some plants which are rich in silica, like the ones from the *Equisetaceae* family.[244] Moreover, it should be noted that most of these studies which let to obtain micro-macro porous components are laboratory scale and the final product size is dictated by the pre-form of the biological material which is not practical to manufacture large components. Though, the excellent strength and specific stiffness of the biomorphic ceramics open a wide range of applications for these attractive materials.[252] Templating strategies with natural materials can be extended to several compositions; for example Iwasaki et al.[253] prepared starch sponges with high internal macroporosities by freezing and thawing of starch gels. Produced sponges were then infiltrated with colloidal suspensions of titania nanoparticles and air-dried to produce TiO_2-starch foams with pores up to 200 μm depending on the starch concentration and the TiO_2 loading. No organic fragment remained in the TiO_2 sponge after heating at 600°C and the produced foam had 65m^2/g SSA including meso(6.5nm)-macro porosity, no information was given about mechanical properties of the TiO_2 foam.

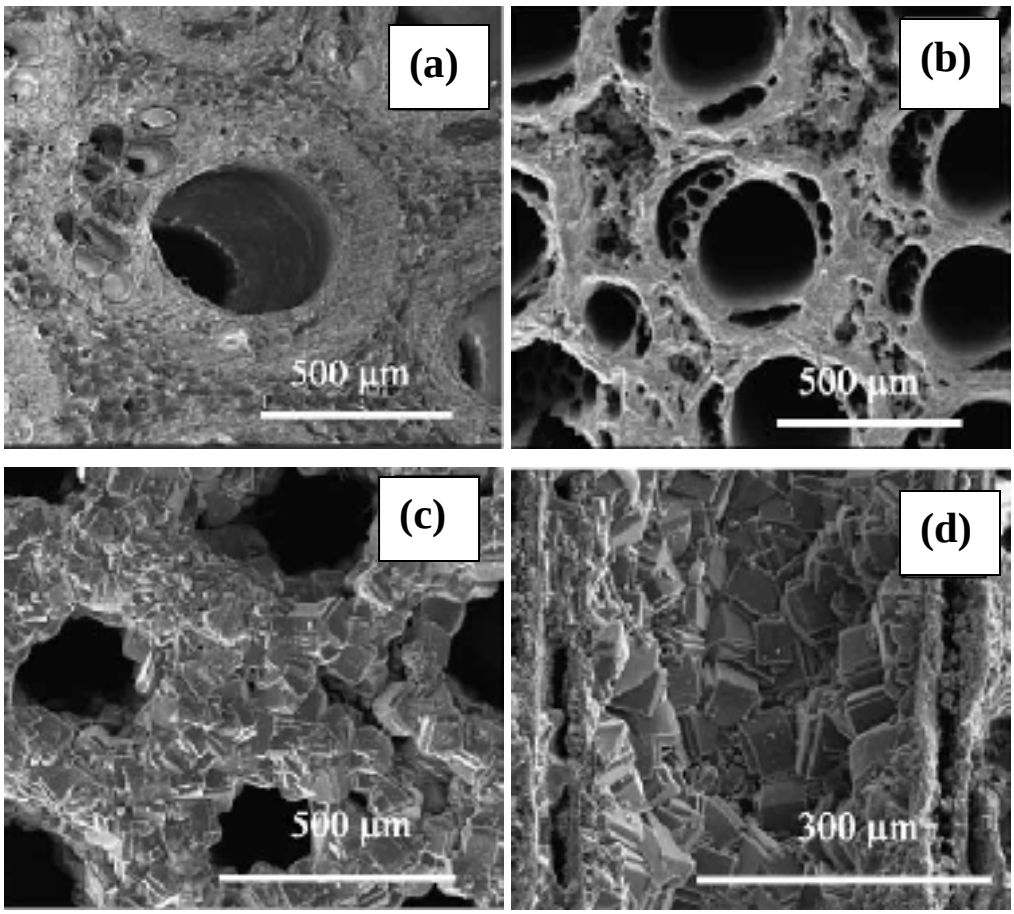

Figure 2.3-10. SEM micrographs of; a) native Rattan stem, b) SiSiC replica, c&d) ZSM-5 coatings in the channels of the Rattan-derived SiSiC monoliths; (c) from top view, and (d) taken along the channels.[242]

The microstructural features of wood range from mm (growth ring patterns) via µm (tracheidal cell patterns, macro- and microfibril cell wall textures) down to nm scale (molecular cellulose fiber and membrane structures of cell walls.[254] Thus, compared to the several natural systems wood could readily be used as a template to generate cellular ceramics with multi-modal pore hierarchy.[237, 238, 242, 252, 255] Cellular β-SiC ceramics have been synthesized at 1400°C from pine wood infiltrated with silica gel.[252] In a very easy processing, the presence of both long cylindrically shaped macropores and slit-shaped mesopores, with the formation of SiC whiskers in a diameter of 20-400 nm and a length of 5-20 µm inside the macropores has been detected. While this material showed medium SSA ~14 m^2/g, in a

similar manner but adding structure directing agents during mineralization, high SSA cellular ceramics is also produced. In this vial; mineralization of wood cellular structures by using a surfactant-templated sol-gel solutions has been investigated by Shin et al.[256]. The authors successfully prepared both positive and negative replicas of the wood by changing the pH values,[257] and utilization of surfactants resulted in a high SSA samples (350-650 m^2/g) which is one order of magnitude larger than for the samples prepared without the use of surfactant ($SSA<45m^2/g$).[256, 257] The surfactant micellar structures incorporated in the silica network, which produced organized nanoporous channels during calcination was found critical in maintaining the structural integrity because they provided pathways for the decomposed organic contents to leave without degrading the whole structure. In a later study,[255] high SSA cellular SiC ceramics are obtained via carbothermal reduction of silica mineralized wood. It was reported that the synthesis using acidic conditions, resulted in a high SSA (60-100 m^2/g) ceramic, where the pore sizes were randomly distributed from nanometres to micrometres implying that hierarchically ordered architectures with organized nanoporous channels within the cell walls are formed.[257] It should be noted that similar to extrudates, the main drawback of all sacrificial sacrificial-templating processes to form zeolite monoliths is the low mechanical properties of the produced self supported body compared to that of the coated ones.

A promising approach to generate hierarchically organized materials with macropore diameters ranging from 5 to 600 μm involves the use of complex fluids such as biliquid or air-liquid foams. Emulsion technique is shown to be very easy method for the fabrication of meso/macroporous nanostructured silica foams based on the rearrangement of SiO_2 nano-building blocks along the confined geometry of a tailored air-liquid foam structure acting as a macroscopic pattern.[258] A multiphase process of acid catalyzed silica sol-gel chemistry in the presence of inorganic salts and self-assembling block copolymers is described by Zhao et al.[259] In the study spongelike silica membranes with 3D structures that have adjustable mesoscopic and macroscopic porosities is produced. The process utilizes multiphase media comprised of a mesoscopically ordered block copolymer/silica phase that macroscopically separates from an electrolyte phase. This result in a hierarchically organized composite structure whose different characteristic length scales can be independently adjusted.

Macropore dimensions are established by the sizes of droplets of aqueous electrolytes, such as NaCl, LiCl, KCl, NH_4Cl, or $NiSO_4$.

Ice crystals can also be used as macrotemplates, Nishihara et al.[260] showed that the ice-templating method can be used as a new processing technology for the preparation of ordered macroporous materials with micro-/mesoporosity. By this method it is possible to precisely control the macroporosity, wall thickness, and micro-/mesoporosity of silica materials via extremely simple procedures. When compared with conventional methods, the ice-templating method has many advantages such as flawless materials with monolithic shape can be produced, it does not require the addition of special templates which usually leads to high production costs and requires severe removal processes, such as calcination and chemical etching, using a strong base.

c) ***Other methods utilizing structure directing agents***

Other than these hybrid methods some powder processing routes such as Plasma assisted sintering" (PAS), "Field assisted sintering technique" (FAST), "and "spark plasma sintering" (SPS) can also be used. In this manner, Vasiliev et al.[198, 261] used a more neutral term "pulsed current processing" (PCP) which that solely relates to the process without indicating a specific brand of machine or an assumption about the nature of the process, and produced hierarchically porous ceramics from diatomite powders by PCP very recently.[261] The PCD process for producing mechanically stable meso/macroporous monoliths of complex shape is schematically illustrated in **Figure 2.3-11** by Vasiliev et al.[198, 262] Another, possible novel processing has been applied in our laboratories in which we have mixed high SSA periodic mesoporous organosilica (PMO) particles with ordinary commercial elastomer which acted both as a foaming agent and high temperature binder during pyrolysis and finally high SSA ~100m^2/g SiOC foams have been formed, see Chapter 4.1 for more details.

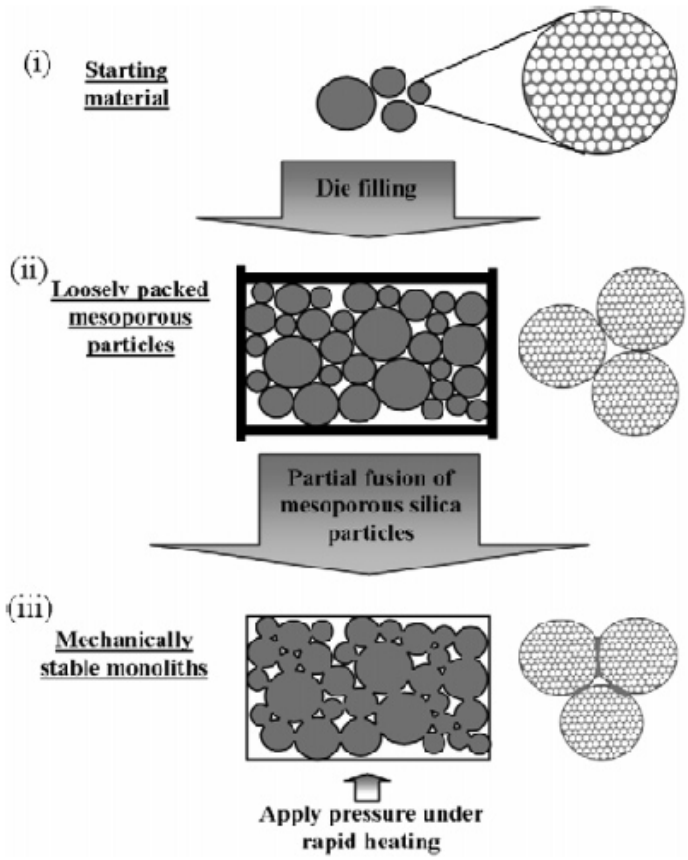

Figure 2.3-11. Schematic illustration of the process used to prepare bimodal porous monoliths from mesoporous particles.[198, 262]

2.3.3.2. From macro-porosity to a multi scale pore hierarchy

A macroporous monolith serves as a host matrix, to which micro- and/or meso-pores are added using different strategies. By the term "macroporous monolith," we mean a porous ceramic that exhibits a total porosity higher than 60 vol% (i.e. specifically a cellular ceramic; in this review we will not consider powder compacts and ceramic membranes, which are asymmetric layered porous structures composed of a separation layer which fulfills the actual filtration function, and a ceramic support structure comprising up to 5 different layers providing mechanical stability, typically produced from sintering of powder compacts. Depending on the degree of separation required (i.e. micro-, ultra-, hyper-filtration, gas separation or pervaporation), the pore size ranges from a few angstrom in the top membrane

(which could also be partially infiltrated into the substrate) to a few microns in the support (typically < 15 μm), and therefore such a component possesses hierarchical porosity), with an average cell size of the order of several microns to a few millimeters.[263] Futhermore; it should be noted that cellular ceramics or monoliths typically posses low SSA values (<2 m^2/g), and thus adding smaller length scale pores to the macroporous network results in an increase in SSA of the cellular component. Processing strategies to add micro- and/or meso-pores, or high SSA, to a cellular ceramic include coating (deposition of thin continuous films or surface attachment of discrete micro/meso-porous particles), growth of 1D-nanostructures (nano-fibers or nano-tubes), selective etching, full infiltration with a micro/meso-porous material or the exploitation of the inherent characteristics of preceramic polymers.

a) Coating

Coating the cell wall surface of a macro-porous ceramic with a high specific surface area layer is a well established route, which has been widely used to fulfill the specific requirements of industrial applications (such as catalytic converters in automobile industry) for several decades. In particular, the high geometric surface area (of the order of tens of cellular materials provides a wide area for the deposition of coatings possessing micro/meso-porosity, and the complete interconnection among the cells supplies easy access to the coating solution or slurry. In principle, any high SSA material can be used as a material for coating/deposition on macroporous cellular ceramics, provided that the introduction of this secondary phase maintains the permeability of the structure. Typically, this approach leads to components having bimodal porosity (micro/macro or meso/macro), with only a few examples of trimodal pore architecture. The thickness of the deposited layer (commonly termed a “washcoat”) is a parameter which strongly influences the final SSA value of the component, as well as other characteristics (such as adhesion, scratch resistance, catalyst loading, etc.), and it depends on the deposition technique (which range from solution-based dipping and spraying to slurry coating, electrophoretic or electrochemical deposition, chemical or physical vapor deposition).[146, 206, 264-266] For example, the sol-gel method typically allows to form <10 μm thick layers, whereas by vapor deposition methods layers thinner than 1 μm are typically obtained, and suspension-based methods lead to layers with a thickness ranging from ~1 to

~100 µm. As some reviews have already comprehensively illustrated the different coating methods,[146, 206, 264-266] here we will focus on the type of material that is deposited on the macroporous substrate.

Analogous to anodic oxidation, which is generally applied to aluminum structures in order to obtain a porous alumina layer at the surface,[206] γ-Al_2O_3 (SSA~250 m^2/g) is commonly used as a coating material for cellular ceramics. This material, deposited on several substrates (foams, honeycombs and ceramic fibers, all typically made of α-Al_2O_3, cordierite, zirconia or silicon carbide) using several methods, [146, 206, 264] increases the SSA of the porous body[146, 267, 268] and the structure remains stable up to temperatures of ~700-800°C.[269] Typically, a dilute slurry containing the washcoat precursors (particle/colloidal suspension or sol with binders and small amounts of viscosity-modifying agents) is deposited on the substrate, which is then dried and calcined at moderate temperatures (~500°C).[146] Using a suspension, thicker layers can be produced than by sol-gel,[206] although repeating the solution coating procedure leads to an increase in coating thickness and specific surface area value (for example the SSA of α-Al_2O_3 foam (~1m^2/g) can be increased linearly with the γ-Al_2O_3 (SSA~205 m^2/g) washcoat allowing to reach final values of ~33 m^2/g with repeated coating cycles giving a loading of 17 wt%,).[268] The final characteristics of a washcoat are a complex function of the slurry properties: nature and particle size the precursor powder, loading amount, nature and concentration of dispersants, temperature of the slurry, and the presence of binders in the slurry.[267, 269-271]

Although coating of porous ceramic monoliths by γ-Al_2O_3 is well established, and improvements in processing methods have led to an increase in SSA up to ~45m^2/g (starting from the low SSA ~1m^2/g porous sample) [268, 272, 273] the final pore characteristics of the coated cellular monolith is scarcely documented, probably because the aim of most studies is simply to obtain a moderate-to-high SSA value (20 to 60 m^2/g) or barely a rough surface, and not to produce hierarchical porosity.[269, 271, 274] The pore nature (micro or meso) of the alumina washcoat is anyway shown to be dictated by the processing and especially by the type of the precursor used to synthesize alumina powders.[275] Agrafiotis et al.[270, 276-278] studied the effect of powder characteristics and processing parameters on the properties of various washcoats

such as alumina, zirconia and titania for ceramic honeycombs. Using a sol prepared with a dispersible commercial colloidal pseudo-boehmite (γ-AlOOH) powder, they formed a mesoporous (mean pore size ~7.0 nm) γ-Al_2O_3 coating on cellular cordierite honeycombs (400cpsi).[267] Jarrah et al.[272, 273] also mentioned mesoporous alumina coatings possessing pores of 5-20 nm on 600 cpsi cordierite monoliths.

An alternative coating material commonly used is zeolite. Pure zeolite has a SSA in the range of 400 to 600 m^2/g and a regular internal channel structure with pores <2 nm; therefore a monolayer of zeolite may satisfy the need for specific surface area requirements for many applications such as adsorbents, catalysts, and pollution abatement.[279] Strategies for the preparation of zeolite layers and membranes (thin films) on different substrates have been reviewed comprehensively.[280, 281] In general, zeolite coatings on cellular ceramic (and in most cases for all types of substrates) can be made either by in situ crystallization through wet hydrothermal methods (direct synthesis, seeded growth - also termed secondary growth -) or through vapor phase synthesis that is dry gel conversion, or by depositing an existing zeolite phase as slurry (having either large single crystals or small crystallites) on the support.[264] The direct hydrothermal synthesis of zeolite crystals on ceramic surfaces is performed by prolonged contact of a cellular body with an aged zeolite gel inside an autoclave and heating according to a precisely defined schedule. In the case of the dry gel conversion method, sol or sol containing template is deposited on the substrate, dried and treated with vapors of a template to form a zeolite layer. While in the secondary growth procedure, zeolite nanoparticles are layered or seeded on a substrate and grown to the continuous thin film by usual hydrothermal synthesis.[201, 206] These synthesis methods have the advantage of achieving a stronger adhesion without the use of any binder, and the possibility of controlling crystal orientation[264] but, on the other hand, they are considerably more complex than slurry-coating and can hinder diffusion if a dense layer is formed.[282, 283] Some recent publications have however shown the possibility of overcoming this problem.[146, 284] Utilization of zeolite crystals by a slurry coating technique results in a coating consisting of randomly oriented zeolite crystal layers, useful for adsorption and catalysis purposes.[206] Slurry coating usually involves the addition of a binder material to the zeolite slurry in order to obtain a strong adherent coating. However the binder (colloidal particles such as silica), which has mostly

smaller size crystals than the zeolite, may block the access to the micropores by surrounding the zeolite crystals.[266] Fortunately, it has been reported that the use of a binder is not essential for washcoating using zeolite powders with small particle size.[266, 276, 285]

These processing strategies have been used to create coatings of various zeolites (silicalite-1, HZSM-5, ZSM5, mordenite and Zeolite Y, etc.) on the surface of different cellular ceramics.[266, 282, 283, 285-307] The SSA value of the final component, which is a consequence mostly of the microporosity of the zeolite crystals, depends on the intercrystalline porosity, the orientation of the zeolite crystals with respect to the support, the uniformity and degree of coverage ($g_{zeolite}/m^2$ support surface) and the thickness of the coating.[292] Excluding the studies quoted in the recent reviews of Mielle et al.[206] and Avila et al.[264] and focusing only on studies concerning zeolite coatings on cellular ceramics, we can state that most of the work in this field has been devoted to coat commercial cordierite honeycombs (200-600 cpsi), for several industrial applications. Components with SSA values up to 200 m^2/g and high mechanical integrity have been produced. Zeolite coated honeycombs have shown to posses higher mechanical integrity than monolithic bodies produced by extrusion of zeolites, and several coating approaches have been used. By in situ hydrothermal method, without organic templates, deposition of several zeolites types (ZSM-5, Linde A, Linde Y, and mordenite) on cordierite supports has been demonstrated. [282, 286-291] Mullite honeycombs have also been coated by a continuous ZSM-5 film (150-200 μm thick) by hydrothermal synthesis, and the final component had a hierarchical pore architecture with micropores (0.5 nm in diameter) and macropores (0.5-0.6 mm) and high SSA (~90 m^2/g).[302] The preparation of a continuous monocrystal zeolite thin film on cordierite honeycombs via in situ crystallization was also reported by Madhusoodana et al.[283] and other authors.[287-289] In a different way; slurry coating was applied by Beers et al.[303, 304] Zamaro et al.[305, 306], and lately by Mitra and Kunzru,[265] to produce a washcoat on cellular cordierite monoliths with various types of zeolites such as mordenite, ZSM5, β zeolite, Zeolite Y, BEA (generally wet ball-milled to 2-3 μm size), leading to a significant increase in SSA in the final component.

Ceramic foams are used commercially for the filtration of molten metal, and are attracting increasing attention as catalyst supports due to their high thermal stability, high porosity and

increased tortuosity with respect to honeycombs. Seijger et al.[292, 293] studied hydrothermal synthesis of ZSM-5 zeolite coatings on α-Al_2O_3, SiC/Al_2O_3 and ZrO_2/Y_2O_3 foam supports (cell size ~0.04-1.5 mm and porosity ~80-90 vol%), and demonstrated that SSA of ceramic foams can be increased from <1 m^2/g to >200 m^2/g by the in-situ formation of 5-10 μm size zeolite crystals. Falamaki et al.[295] deposited a silicalite zeolite layer via both in situ crystallization and dip-coating on porous alumina and zircon supports, and dip coating the silicalite seeds followed by hydrothermal fixation resulted in a zeolite possessing a preferred orientation along the 200/020 planes. Other authors used a seed-film method to produce zeolite thin coatings on ceramic foams and documented the resulting increase in SSA values.[286],[294] Buciuman et al.[266] demonstrated the possibility to coat and enhance the SSA of ceramics foams (alumina–mullite, china, cordierite or steatite, 10-80 ppi) without binder addition by simply dipping the ceramic body in an aqueous suspension of zeolite (silicalite - particle size 100 nm - and HZSM-5 - particle size 650 nm). Patcas et al.[307] used 500 nm size ZSM-5 particles to washcoat mullite-bonded alumina foams (45 ppi) and showed the formation of a bimodal pore size distribution. In a very recent modified washcoating approach, cordierite foams (porosity ~80vol%) were coated with ZSM-5 zeolites after treating the surface of ceramic foams with an aqueous cationic polymer solution, which increased significantly the amount of zeolite loading in the final component, see **Figure 2.3-12** for the illustration of this modified washcoating method.[285]

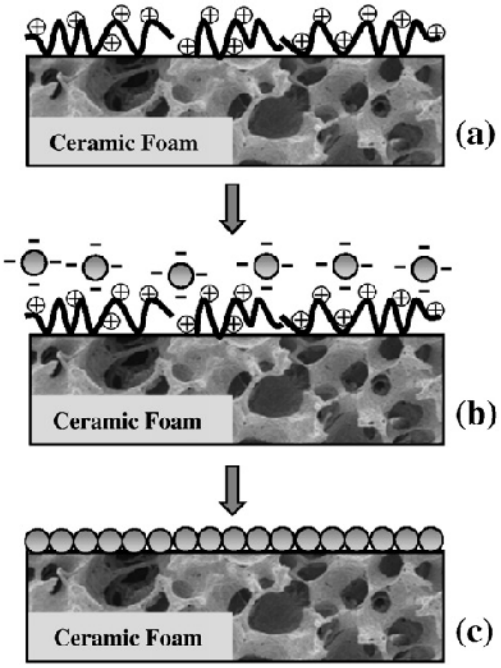

Figure 2.3-12. Illustration of the three steps of washcoating method described by Silva et al.[285]: (a) surface foam modification by cationic polymer solution; (b) surfactant–zeolite particles adsorption onto foam surface; (c) zeolite coated foam.

In most of these aforementioned studies, the ceramic cellular support is considered to be inert under zeolite synthesis conditions, although the high pH present during hydrothermal synthesis[266, 292, 293] can lead both to the deterioration of the support and a modification of the gel composition.[308] This feature has however been exploited in a novel approach, which utilizes the partial dissolution of the substrate to supply the Si or Al atoms needed for the in-situ formation of zeolites. A significant advantage of this approach is a higher degree of adhesion to the substrate, reduced difference in coefficient of thermal expansion between substrate and coating, and a high zeolite loading. Crystallization of zeolites on different supports has been reported, including porous glasses,[309, 310] SiC[308] or polymer-derived-ceramic foams[168, 169, 311] and biologically-derived substrates. In the case of biologically-derived substrates,[242, 312] micro-meso-macro porous components were produced (tri-modal pore hierarchy). Preceramic polymer-derived microcellular foams were also used as reactive substrate for the formation of Silicalite-1 and ZSM-5 zeolites layers, giving high SSA (~342 m^2/g) and a relatively strong component possessing hierarchical porosity (mean cell size ~ 8

µm, porosity ~84 vol%; compression strength 1-44 MPa) and high thermal stability (600°C, air), see **Figure 2.3-13** (a-c) for the SEM images of zeolite coated and uncoated SiCO microcellular samples prepared by Zampieri et al.[311] Tong et al.[227] prepared zeolite beta monoliths with a trimodal pore structure of interconnected macropores, mesopores and micropores via the transformation of the amorphous silica walls of a macroporous monolith using carbon as a transitional template. Similarly, Lei et al.[313] synthesized hierarchically structured monolithic silicalite-1 by transforming the skeleton of a macroporous silica gel into silicalite-1 crystals through steam-assisted conversion followed by layer by layer coating.[314] Ocampo et al.[231], working with a glass macro-porous monolith, produced components with high SSA (400-450 m^2/g) with hierarchically (tri-modal) porosity by using the substrate in a reactive manner. All the coating methods described above deposit zeolites layers in the form of stable particles covering the cell surface of a macroporous ceramic support, resulting in a porous monolith with hierarchical porosity (typically micro-macro; rarely micro-meso-macro). However, coating routes generally result in a composite ceramic which suffers from a low zeolite-to-support weight ratio, single-sided mass transport to and from the layers, and probable loss of zeolite layer from the supports upon repeated heating due to the difference in the thermal expansion coefficients of the components, namely zeolite and substrate material.[233]

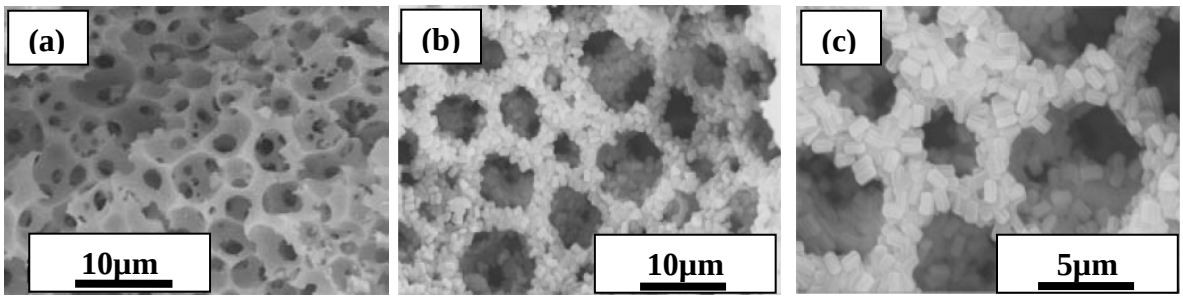

Figure 2.3-13. SEM images of a) as-prepared SiOC microcellular ceramic foam supports, b&c) fracture surface of the same foam coated with Silicalite-1 synthesized at 150°C.

An alternative coating material is meso-porous silica. Mesoporous MCM-41-like molecular sieves (M41S) are very useful in applications where pore sizes larger than those typical of zeolites (micropores) are required.[315] Only one study focused on the use of pre-formed

mesoporous silica nanoparticles as coating particles. Huerta et al.[315] produced a multiphase (silica rich glass with mullite and quartz) foam using the replica technique, and then deposited UVM-7 mesoporous particles by multiple impregnations in a slurry. The stabilization of the particles on the ceramic surface was achieved by a low temperature treatment (120°C), leading to a component with 229 m^2/g SSA, high coverage values (~17wt%) and good compression strength (3-4 MPa). However, every impregnation cycle caused a decrease in the pore window diameter and, after five dip-coating cycles, blockage of the macropores, see **Figure 2.3-14** for the SEM images of bare PU foam template, after ceramization and coating with UVM-7 particles**.** In a different approach, which does not require the pre-formation of particles, Costacurta et al.[189] prepared microcellular SiOC foams, which were shown to have good mechanical properties and high chemical durability, and deposited a mesoporous silica coating by dipping into a TEOS solution containing a templating agent. After calcination at 350°C, the cell walls were uniformly covered by a mesoporous silica layer with a thickness ranging from <1 to ~5 μm, thus producing a meso-macro porous component with a SSA of ~60 m^2/g.

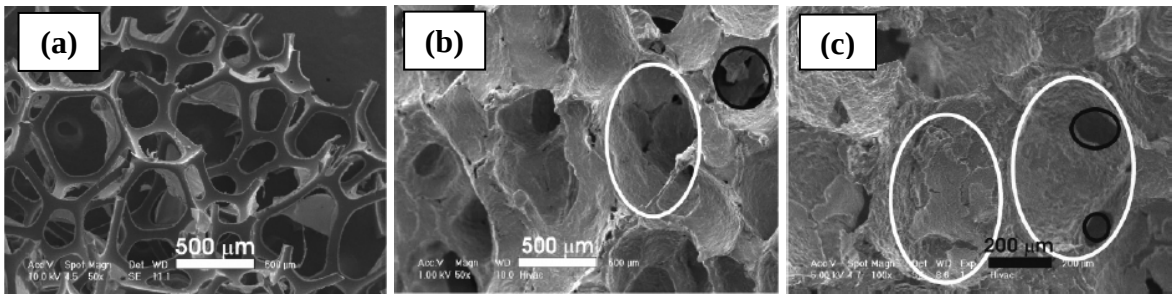

Figure 2.3-14. SEM images of; a) the commercial PU foam used, b) ceramic foam before coating (open cells and their windows are marked in white and black circles respectively), and c) ceramic foam after seven UVM-7 impregnation cycles, showing the pore closure with white circles and open pore windows by black circles.

Carbon coatings have also been deposited on cellular ceramic substrates in order to enhance SSA while obtaining hierarchical porosity; the tunable porosity and chemical surface properties of carbon coatings permit to adjust the characteristic of the coating for specific applications.[316] Carbon-coated ceramic honeycombs (clay containing,[317] cordierite[318-327] and

acicular mullite[328]) and foams (commercial zirconia,[329] alumina[329] and cordierite[330]) have been produced. In a typical process, these cellular ceramic supports are coated with a polymer solution (such as novolak, furan, etc.), dried and then heated at high temperature (500-1000°C) in inert atmosphere to produce a porous carbon layer.[316] These coatings have been showed to enhance SSA and mechanical strength of the honeycomb substrates. The carbon layer typically contains micro-porosity, but the presence of carbon accumulations forming spherical particles induces also a meso-macro porosity.[330] By the activation of the carbon layer (for instance by heating for 4h at 900°C in CO_2) very high SSA values up ~1400 m^2/g can be obtained for the coat layer.[329]

If vanadia/titania (V_2O_5/TiO_2 : high anatase fractions (>90%, w/w), containing 0-10% (w/w) V_2O_5) synthesized in vapor-fed flames, it results in a high SSA reaching 120 m^2/g powder. Schimmoeller et al.[331] deposited (dip coating) this type of flame-made airborne V_2O_5/TiO_2 nanoparticles onto mullite foam supports to create ready-to-use catalysts. Although the porosity of the layer on the foams was not determined, the authors assumed to have pore size ranging from 10 to 100 nm in the deposited layer of the coating which is comparable to those in the nanoparticle beds. Thus meso/macro porous cellular material having enhanced SSA compared to that of bare body is obtained.

b) Growth of 1D-nanostructures

Despite the fact that, strictly speaking, the presence of nanofibers does not add porosity to a dense material, it is appropriate to discuss their growth on the surface of macroporous ceramics in the context of this review, as it has been demonstrated that their presence leads to an increase of the specific surface area of a part, therefore enabling it to fulfill similar applications than those of a properly termed hierarchical porosity component. Moreover, this approach allows to produce alternative phases in the material, which can further functionalize the system (for example altering its mechanical, magnetic or electrical properties). A pioneering work in this field was reported by Jarrah et al.[272, 273], in which cordierite honeycombs (600 cpsi) were washcoated with a γ-alumina layer (enhancing the SSA from <1 m^2/g to values of ~25-45 m^2/g, depending on the layer thickness). Nickel was then deposited

on the honeycombs and samples were heated in a reactive gas mixture (CH_4 or C_2H_4), leading to the formation of ~1 µm thick layer of carbon nanofibers (CNF, diameter of 10-30 nm) which caused an increase of the surface area of the cellular substrates up to 63 m^2/g.[273] The fiber diameter was controlled by the size of the deposited Ni particle, by the reactivity of the gas used over this particle, and by the duration of thermal treatment and this parameter, together with the total amount of fibers formed, affected the final SSA of the component.[272] The total porosity component decreased with the amount of CNFs whereas the surface area per gram of monolith increased. BET analysis showed the presence of micropores, which were attributed to the space between the fibers and the pore walls of washcoat layer, and therefore not to the presence of pores in the substrate or washcoat layer which was previously characterized as mesoporous (pore size 5-20nm) before fiber formation.[272] de Lathouder et al.[326-328] followed the same strategy using both silica-coated cordierite and alumina-coated highly porous acicular mullite honeycombs (200/400cpsi). The authors demonstrated that CNF-containing cordierite monoliths had ~8nm mesopores which were attributed to the space among the fibers and therefore not to the presence of pores in the substrate, causing a high enzyme activity for the CNF-containing cellular ceramics. A correlation between fiber diameter and the surface area was given in a way that increasing the fiber diameter causes a decrease in the surface area while the carbon yield is assumed to be constant.[327] Further improvements by García-Bordeje et al.[332], using a thin (~0.1 µm) alumina washcoat which prevented CNFs from being trapped inside its pores, have led to the increase of the CNF layer to ~4 µm. The authors underlined the significant influence of the fiber diameter and degree of entanglement on the morphology (density and uniformity) of the formed layer and resulting SSA of the porous components.[333] Interestingly, they showed also that the mechanical strength of the cordierite honeycomb (crushing strength of pure cordierite monolith was 22 MPa, 400cpsi) was affected, with higher strength (30-35MPa) achieved for a stronger adhesion of the CNF layer to the substrate.

Ulla et al.[334] more recently studied the catalytic decomposition of C_2H_2 over a cordierite monolith previously coated with cobalt including mordenite (see Figure 2.3-15(a)) synthesized by a hydrothermal route, leading to the formation of ~20 µm thick layer of CNFs shown in Figure 2.3-15(b) (hollow fibers 40-50 nm in diameter with closed ends thus can be

thought as tubes with closing ends) which increased the SSA of the component. Wang et al. circumvented the presence of the washcoat and synthesized carbon nanotubes (CNTs) directly on cordierite honeycombs (300 cpsi) via in situ catalytic chemical vapor deposition (CCVD) of a C_2H_2:H_2 mixture over Fe or Co catalyst deposited by impregnation from a nitrate solution.[335, 336] The honeycombs possessed a SSA value of 30-40 m^2/g, suitable pore size distribution and good attachment of the CNTs layer (< 1 μm thick) to the substrate. Jayaseelan et al.[337], produced SiC nanofibers on the surface of cordierite honeycombs via the carbothermal reduction reaction of carbon added to the oxide raw materials, when processing in inert atmosphere, leading to a SSA value of 36 m^2/g.

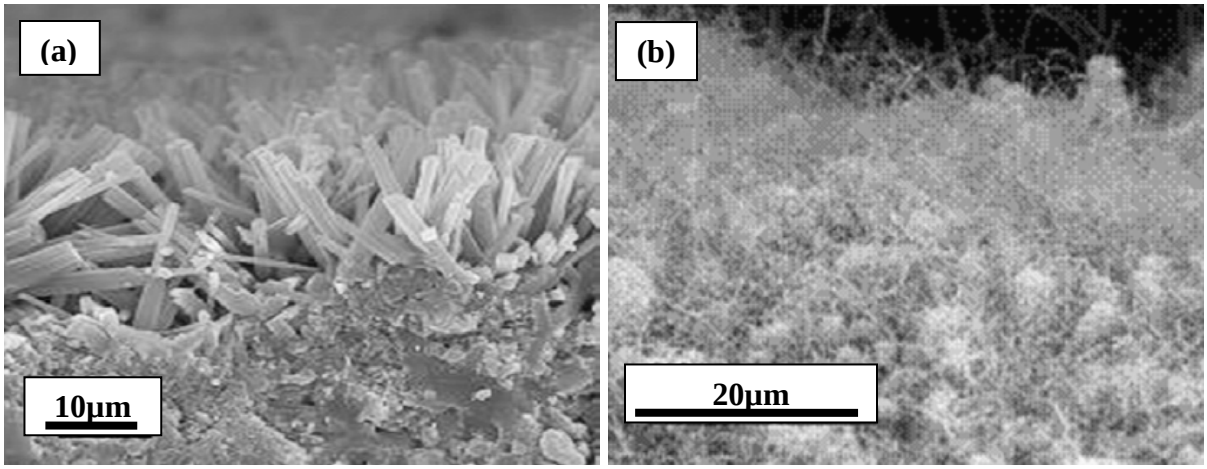

Figure 2.3-15. SEM images showing the morphology of; a) Co-mordenite coating on the cell wall of cordierite monolith, and b) CNF coating on the cell wall.[334]

Ceramic foams have also been used as substrate for the growth of nanofibers and nanotubes. It has been shown that a $Mg_{0.9}Co_{0.1}Al_2O_4$ solid solution foam prepared by gelcasting (total porosity 98%, cell window size < 300 μm), instead of the corresponding powder, gave a four-fold increase in the production of CNT (> 95% with only 1 or 2 walls, and ~ 70% single wall nanotubes, SWNT), because it allowed for a higher quantity of metal nanoparticles on the surface, a better dispersion of the metal particles (which hampers growth and therefore favours selectivity for CNT formation), and for more space available to the CNT to grow.[338] A commercial, conventional, open cell ceramic foam (containing α-alumina (>80wt%), mullite

and cristobalite; 50 ppi, cell size 0.5-1.5 mm) was also impregnated by a slurry of α-$Al_{1.8}Fe_{0.2}O_3$ and covered by CNTs via CCVD.[339] In a similar way α-$(Al_{1-x}Fe_x)_2O_3$ foam was also used to form CNTs via CCVD very recently.[340] As the above studies were more concerned with the production of CNTs per se, rather than in the development of components with high SSA, no information were given on the SSA and the mechanical properties of the final foam. In the study Cordier et al.[341] where 50ppi commercial alumina-silicate foams were impregnated with a slurry of $Mg_{(1-x)}(Co_{0.75}Mo_{0.25})_xO$ (X=0.01-0.2) followed the formation of CNTs via CCVD, clearly showed the formation of composite foam with a multi-scale pore structure including very well distributed CNTs which gives a surface area of ca. 15 m^2 for each gram of foam.[341]

Wenmakers et al.[342] recently deposited Ni on reticulated vitreous carbon (RVC) (60 ppi, porosity 97 vol%) and produced CNFs by reaction with ethylene at 500°C. Although, different types of CNF structures with a large fiber diameter distribution (30 to 1100 nm) were observed, no correlation could be made between fiber diameter and specific surface area (which ranged from 118 to 146 m^2/g). Mukhopadhyay et al.[343] also utilized commercial carbon foams (porosity 80 vol%) to grow CNTs via two stage CVD, using a ferrocene catalyst, and showed that that with a silica coating, not only higher iron deposition level could be obtained, but also the bond strength between CNTs and substrate was improved. By following a parallel strategy, Vanhaecke et al.[344] produced SiC nanofibers (NFs) in the macropores of a SiC foam (45ppi, cell size ~1.9 mm and SSA~10m^2/g) by converting the CNFs that had formed on the SiC host structure via CCVD, using SiO vapor as a reactant at 1300°C. The final SSA value for SiC-NFs/SiC foam was 50 m^2/g, lower than that of the foam covered with CNFs, because of the increase of the nanofibers diameter after reaction. The produced samples were tested in a diesel particulate filtration system, and the microstructure of the composite foam, comprising a macroscopic interconnected porosity and walls covered with nanofibers, led to a small pressure drop and high trapping efficiency during the filtration step of fine and ultrafine soot.[344, 345]

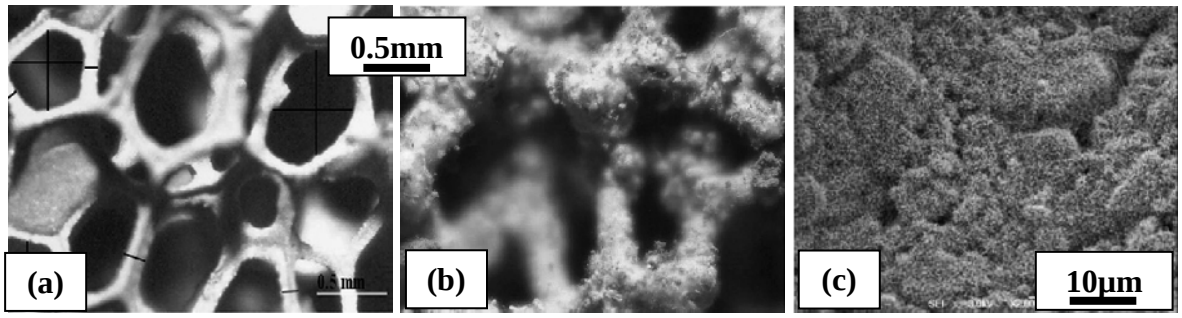

Figure 2.3-16. Optical images of a) bare 1900 µm SiC foam, b) the same foam with 39 wt% SiC nanofibers/SiC struts, and c) SEM micrograph of SiC nanofibers on SiC surface (39 wt% NFSiC/SiC sample).[344, 345]

The release of decomposition gases when pyrolyzing preceramic polymers at high temperature in inert atmosphere, has led some researchers to develop 1D-nanostructures in the pores of the these ceramics via catalyst assisted pyrolysis (CAP).[46, 346] In situ formation of β-SiC nanowires was observed in the channels of porous SiC ceramics fabricated from -SiC powder and polycarbosilane (PCS) precursor used as a binder.[347, 348] Catalyst particles for the growth of the nanowires were considered to originate from unwanted iron impurity in the starting SiC powder,[347, 348] but the amount of nanofibers formed was quite limited. Segatelli et al.[61] showed also that the pyrolysis of a preceramic polymer together with Ni catalyst source, caused a variation in the microstructure of the final ceramic.[60] While no clear macroporosity was present in the samples, increasing the pyrolysis temperature from 950 to 1500°C led to different SSA values due to the formation of micro- and meso-pores (as indicated by BET data).

An application of this processing concept to the growth of nanofibers on the surface of cellular polymer-derived-ceramic has been recently pursued by Yoon et al.[172] and in our laboratories.[349-351] The first authors reported the formation of highly aligned macro-porous SiC ceramics decorated with homogenously distributed SiC nanowires, produced by unidirectional freeze casting of SiC/camphene slurries with different amounts of the PCS precursor. Iron originated again from the starting SiC powder, and was found in the tips of the nanowires. The presence of nanostructures led to a remarkable increase of SSA (from 30 to 86

m^2/g), when the initial PCS content was varied from 5 to 20 wt%, due to enhanced growth of the SiC nanowires, see **Figure 2.3-17** for the microstructural evolution for the samples prepared with or without preceramic polymer addition.

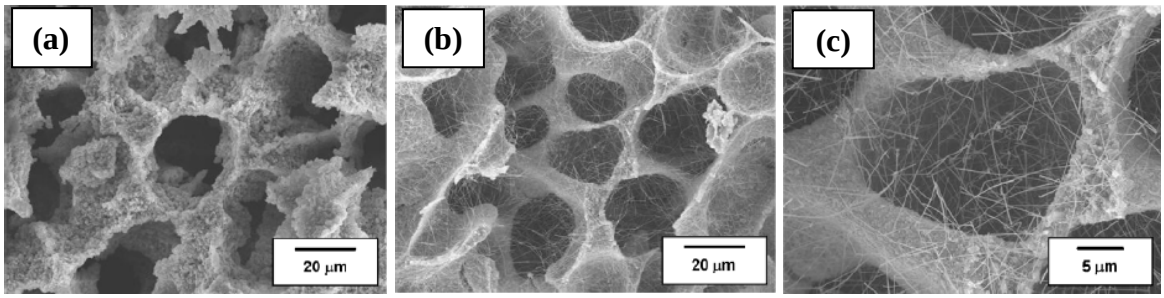

Figure 2.3-17. SEM images of the porous SiC samples produced; a) without polycarbosilane, b) with 20wt% of polycarbosilane upon pyrolysis at 1400°C for 1 h in Ar.[172]

The work in our laboratory has focused on the deliberate one-pot synthesis of foams with hierarchical porosity via catalyst assisted pyrolysis (CAP) using different catalysts (Fe, Co, Pt) and polysiloxanes (see Chapters 4.2. for the details).[349-351] Cellular SiOC ceramics, possessing a large amount of interconnected porosity (>60vol%), were produced by direct foaming and the addition of a catalyst enabled the formation of 1D-nanostructures (nanowires) in large quantity on the surface of the cell walls. The characteristics of the nanostructures depended on the preceramic polymer (Si:C:O ratio) and pyrolysis conditions (atmosphere and temperature). In particular, when heating in N_2, single crystal Si_3N_4 nanowires were obtained, while pyrolysis in Ar produced SiC nanowires. The formation of nanowires and their structural evolution (thickness, entanglement) caused a variation in the final SSA of the produced composite foams, which ranged from 10 to 120 m^2/g. The use of a Pt catalyst led to the formation of Pt-silicide tips which were active in the CO oxidation reaction; it is forecasted that the immobilization of the catalyst on the tip of nanofibers exposed to the environment could lead to increased efficiency and reduced catalyst loss during operation. Moreover, in a separate experiment, the presence of long fiber bundles decorating the cell walls have been demonstrated to be very effective in the trapping of nanopowders (diameter ~ 90 nm) contained in a gas stream.

c) Etching

In the classical "Vycor" process; a homogeneous glass (usually in Na_2O-B_2O_3-SiO_2 system) is prepared by the melt-quench method and heat treated to produce spinodal decomposition into two interconnected phases. After that one phase is preferentially etched in a suitable acid, leaving behind glass with 3D porosity. This method has recently been successfully used in making hierarchically porous bioglass samples which had multi-modal meso-macro interconnected porosity (the average size of the macropores is about 32 μm with additional distinct pores within the 0.1-8 μm range and mesopores with average size 15 nm).[352, 353]

Very limited studies have used this concept to create multi-modal pore architecture due most probably to the difficulty in controlling the phase separation and the harsh processing conditions. Polymer derived ceramics, in this manner, are very advantageous since phase separation is a common phenomenon for these materials.[42, 63] Wilson et al.[354] have shown that dilute hydrofluoric (HF) etching of bulk SiOC glasses results in a microporosity and a mass loss up to a 40%. This approach has been followed by the group of Soraru G. D.[69, 70, 355] on sol-gel derived SiOC ceramics with different chemical compositions (varying Si:C) and the results showed that high SSA, reaching to the values as high as 600 m^2/g samples can be produced. While these samples did not include intentionally introduced macro porosity, Biasetto et al.[67] recently showed that microcellular SiOC samples (84vol% porous with ~35μm average cell size) can be treated by HF attack to produce high SSA (up to 65m^2/g) foams with multi-modal porosity.

Although no other studies have been published specifically concerning etching to introduce micro/meso porosity into macroporous cellular ceramics, it should be noted that selective phase/element etching has been applied to several materials, as for instance in the nitric acid treatment of honeycombs (cordierite) to increase their specific surface area and reduce the thermal expansion coefficient[264, 356] or the chlorination of carbides to manufacture ultra high SSA (~3000 m^2/g) carbon materials (this micro-porous carbon is also termed carbide derived carbon – CDC),[357] In this way, very recently hierarchically porous (meso/micro) high SSA carbon samples have also been prepared from polymer derived SiCN[358] (see also Chapter 4.3)

and SiC[359, 360] ceramics. Alternatively, in order to form hierarchically porous carbon monoliths, a silica/carbon composite material can be formed by nanocasting of a carbon source into a porous silica monolith, followed by the leaching out the silica phase via chemical etching, to obtain a negative porous carbon replica.[221, 361-363]

d) Infiltration

The full or partial infiltration of a cellular ceramic with a ceramic material containing micro- and/or meso-pores has not been explored much, because the resulting component loses the high permeability which is necessary for several applications. However, the ceramic cellular structure offers protection and mechanical support to otherwise very weak materials, such as aerogels, enabling the fabrication of components which could be useful as gas (humidity) adsorbers. Moreover, if the cellular ceramic is conductive, regeneration of the adsorber by heating via Joule effect is possible. In our laboratory (in collaboration with researchers at VITO, B), microcellular SiOC foams containing a silica aerogel were obtained, using vacuum infiltration and a base-catalyzed sol-gel solution, with a SSA of ~220 m^2/g for the component.

e) Use of preceramic polymers

One of the most effective methods for producing high SSA ceramics is to perform a well controlled heat treatment cycle to preceramic polymers. This approach takes advantage of the transient porosity generated upon heat treating a precursor in the temperature range at which the polymer-to-ceramic conversion occurs.[42] The transformation generally seen in the ~400-800°C temperature range, and is accompanied by shrinkage density change.[3, 21] The build-up of internal pressure in the component, provoked mainly by the decomposition of the organic moieties of the preceramic polymer (with generation of mainly CH_4 or C_6H_6), leads to the formation of porosity (with pore size typically below 50-100 nm). This porosity is transient, because it is eliminated when the pyrolysis temperature leading to the completion of the ceramization process is increased, according to a densification mechanism based on surface reaction/pyrolysis accommodated by viscous flow.[21] However, by employing a well controlled heat treatment cycle and limiting the pyrolysis temperature to 500-700°C, it is

possible to stabilize and maintain this porosity, and therefore achieve components with very high SSA values (up to ~650m^2/g).[44, 47-49] This approach has been successfully applied to foams made from silicones,[166] producing components with hierarchical porosity in which the amount of specific surface area was stable up to the pyrolysis temperature reached, even after prolonged heating at the same temperature, see **Figure 2.3-18 (a)** for the generally morphology of siloxane/PU derived foams and **(b)** for the Nitrogen adsorption–desorption isotherms versus pyrolysis temperature including SSA values.[166]

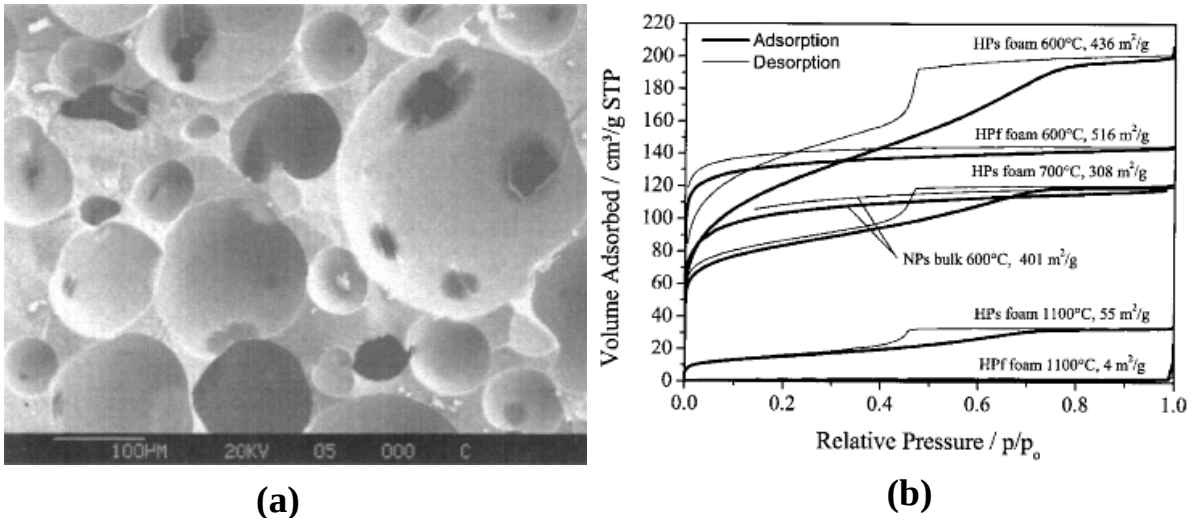

(a) **(b)**

Figure 2.3-18. a) SEM image of the foam derived from silicone resin/PU (1:1 weight ratio) upon pyrolysis in between 800-1200°C, and b) Nitrogen adsorption–desorption isotherms for foams (HP: silicone resin/PU in 1:1 weight ratio) and bulk samples (NP: polymethylsiloxane derived bulk samples, warm pressed powders followed by pyrolysis) after pyrolysis treatment at different temperatures. The measured surface area is also reported for each sample.[166]

f) Direct synthesis without the use of template

A sol-gel method accompanied by phase separation is well established technique to produce silica (SiO_2)-based monolithic gels with multiscale porous structures.[364] This approach can be called as direct foaming and polymerization reaction produces a wet gel with a bicontinuous structure, in which each of gel-rich and solvent-rich phases is interconnected, i.e. the formation of spinodal decomposition type phase separation concurrently with gelation.

Following solvent exchange and thermal treatment, thus aging treatment in hydrothermal conditions, mesopores in the SiO_2-rich phase via dissolution/reprecipitation (Ostwald ripening) and macropores from the solvent-rich phase is generated.[364-367] Although, sol-gel processing is well established and fairly straightforward to produce bimodal porous silica monoliths, requirements for relatively high concentration of precursors, and so their reactivity significantly affects the feasibility of producing uniform, crack-free monoliths.[367] Due to these limitations roughly speaking, the method is limited to silica based materials since the control of hydrolysis and polycondensation reactions for silicon alkoxides is relatively easy compared to the other alkoxides such as titanium and zirconium alkoxides.[365] Apart from the studies dealt with silica materials ; very recently with a careful control of the hydrolysis and condensation rates of the inorganic sources, hierarchical porous components of titania,[368] titanium phosphate,[199] aluminosilicate,[369], zirconium phosphate[370], hafnia and zirconia[371] have been produced without the need of template. However, these irregular micron size particles with a meso-macro pore structure cannot be thought as monoliths. Some very recent strategies have been developed to overcome this problem; showing the possibility to manufacture high SSA titania [365, 366, 372] and zirconia monoliths[367] having meso-macro pore size hierarchy without the use of any structure directing agents. Konishi et al. described a method for the fabrication of TiO_2 monoliths with multiscale porous structure from titanium "alkoxy-derived" sol-gel systems under template-free conditions. [365, 366] The authors have shown that after calcination (between 60-400°C) of the gels, high SSA titania monoliths ($150 m^2/g$) with controllable meso-pores in 5-15nm range and macropores less than 2µm is obtained. Backlund et al.[372] has lately demonstrated a comparable sol-gel approach for a direct, fully reproducible, template-free synthesis route of hierarchically porous titania monoliths (SSA<$180 m^2/g$, macropores<4µm and mesopores 3-4nm). In a parallel study while highly dependent on the thermal treatment temperature, high SSA <$200 m^2/g$ meso-macro porous zirconia monoliths have also been formed.[367] Although these very recent studies have shown the possibility to obtain porous ceramic monoliths without the use of templates, the exact mechanism underlying these hierarchical porosity remains elusive.[199]

g) "Hard" monolithic templating

Utilization of macro-porous hard templates to form hierarchical porous ceramics, which can be though as "nano-macrocasting", has been explored only after Nakanishi and co-workers who developed a sol-gel method for the easy preparation of meso-macroporous silica monoliths.[364] It is shown that by controlled phase separation (i.e. sol-gel transition of the inorganic precursors or well-controlling the hydrodynamic conditions[200]) in a confined space bimodal (meso/macro) pore silica forms (SSA reaching ~500m^2/g) can be prepared.[314] Porous silica monoliths produced in this way has proven to be an excellent starting (hard template) material in nanocasting procedures to form carbon monoliths,[221, and references therein] several other metal oxides having multi-modal pore hierarchy,[204] and zeolites as explained before in detail.[314] Among these studies; monolithic forms of ceramic monoliths in a well/preserved shape including hierarchical porosity is scarcely documented; Smatt et al.[221, 373] have shown the formation of hierarchically porous (medium SSA <40m^2/g) monoliths of cobalt oxide (Co_3O_4), tin oxide (SnO_2), and manganese oxide (MnO_2 or Mn_2O_3) by nanocasting route starting from the silica monoliths with macropores (0.5-30 μm) as well as mesopores which can be altered between 3 and 30 nm, see **Figure 2.3-19**. First, formed silica monolith is impregnated with a metal salt solution, which is subsequently decomposed to a metal oxide by heat treatments to form a SiO_2/MeO_x composite. Finally, the silica part can be removed by leaching in either NaOH or HF acid.[221] This processing strategy although simple it is rather time consuming and so far limited only to the some metal oxide forms.

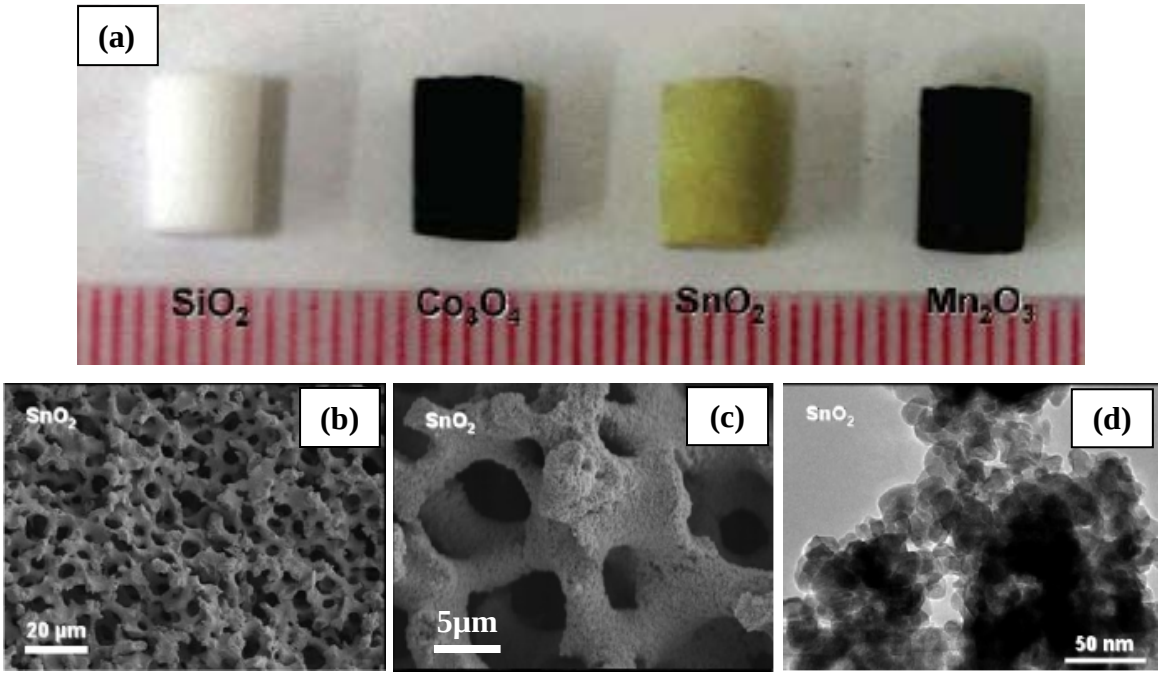

Figure 2.3-19. a) Photograph of the parent SiO_2 monolith together with Co_3O_4, SnO_2, and Mn_2O_3 replicas (scale bar in millimeters), b&c) SEM images, and d) TEM image of the SnO_2 foam.

2.4. References

[1]M.N. Rahaman, "Ceramic processing and sintering," pp. 770, Dekker M., New York, 1995.

[2]P. Greil, "Polymer Derived Engineering Ceramics," *Advanced Engineering Materials*, 2 [6] 339-48 (2000).

[3]E. Kroke, Y.-L. Li, C. Konetschny, E. Lecomte, C. Fasel, and R. Riedel, "Silazane derived ceramics and related materials," *Materials Science and Engineering: R: Reports*, 26 [4-6] 97-199 (2000).

[4]G.D. Soraru, Q. Liu, L.V. Interrante, and T. Apple, "Role of Precursor Molecular Structure on the Microstructure and High Temperature Stability of Silicon Oxycarbide Glasses Derived from Methylene-Bridged Polycarbosilanes," *Chemistry of Materials*, 10 [12] 4047-54 (1998).

[5]P. Dibandjo, S. Diré, F. Babonneau, and G.D. Soraru, "Influence of the polymer architecture on the high temperature behavior of SiCO glasses: A comparison between linear- and cyclic-derived precursors," *Journal of Non-Crystalline Solids*, 356 132–40 (2010).

[6]E. Radovanovic, M.F. Gozzi, M.C. Gonçalves, and I.V.P. Yoshida, "Silicon oxycarbide glasses from silicone networks," *Journal of Non-Crystalline Solids*, 248 [1] 37-48 (1999).

[7]R. Riedel and W. Dressler, "Chemical formation of ceramics," *Ceramics International*, 22 [3] 233-9 (1996).

[8]C. Moysan, R. Riedel, R. Harshe, T. Rouxel, and F. Augereau, "Mechanical characterization of a polysiloxane-derived SiOC glass," *Journal of the European Ceramic Society*, 27 [1] 397-403 (2007).

[9]S. Yajima, K. Okamura, J. Hayashi, and M. Omori, "Synthesis of Continuous SiC Fibers with High Tensile Strength," *Journal of the American Ceramic Society*, 59 [7-8] 324-7 (1976).

[10]T.L. Cottrell, "The Strengths of Chemical Bonds," pp. 317, Butterworths Scientific Publications, London, 1958.

[11]M. Grandbois, M. Beyer, M. Rief, H. Clausen-Schaumann, and H.E. Gaub, "How Strong Is a Covalent Bond?," *Science*, 283 [5408] 1727-30 (1999).

[12]R. Riedel, E. Ionescu, and I.-W. Chen, "Modern Trends in Advanced Ceramics," pp. 3-38 in Ceramics Science and Technology, Volume 1: Structures. Edited by R. Riedel and I.-W. Chen. WILEY-VCH Verlag GmbH & Co. KGaA Weinheim, 2008.

[13]Y. Abe and T. Gunji, "Oligo- and polysiloxanes," *Progress in Polymer Science*, 29 [3] 149-82 (2004).

[14]R. Riedel, G. Mera, R. Hauser, and A. Klonczynski, "Silicon-Based Polymer-Derived Ceramics: Synthesis Properties and Applications-A Review," *Journal of the Ceramic Society of Japan*, 114 [1330] 425-44 (2006).

[15]D. Seyferth, "Birth, Death and Transfiguration: The Synthesis of Preceramic Polymers, Their Pyrolysis and Their Conversion to Ceramics," pp. 567-99 in The Proceedings of the Second European Ceramic Society Conference (Ecers'91), Vol. 1, *Euroceramic II.* Edited by G.Z.a.H. Hausner. Deutsche Keramische Gesellschaft, Köln, 1991.

[16]P. Colombo, G.D. Soraru, R. Riedel, and H.J. Kleebe, "Polymer Derived Ceramics. From Nano-Structure to Applications," pp. 489, DESTech Publications, Lancaster, PA, 2009.

[17]763C. Lassen, C. Libak Hansen, S. Hagen Mikkelsen, and J. Maag, "Siloxanes - Consumption, Toxicity and Alternatives," COWI A/S Environmental Project No. 1031 2005, 2005.

[18]J. Torrey, R. Bordia, C. Henager, Y. Blum, Y. Shin, and W. Samuels, "Composite polymer derived ceramic system for oxidizing environments," *Journal of Materials Science*, 41 [14] 4617-22 (2006).

[19]M. Scheffler, T. Gambaryan-Roisman, T. Takahashi, J. Kaschta, H. Muenstedt, P. Buhler, and P. Greil, "Pyrolytic decomposition of preceramic organo polysiloxanes," pp. 239–50 in Proceedings of Innovative Processing and Synthesis of Ceramics, Glasses, and Composites IV (St. Louis, Missouri), Vol. 115, *Ceramic Transactions.* Edited by N. Bansal and J.P. Singhe. The American Ceramic Society, Westerville, Ohio, 2000.

[20]R. Melcher, P. Cromme, M. Scheffler, and P. Greil, "Centrifugal Casting of Thin-Walled Ceramic Tubes from Preceramic Polymers," *Journal of the American Ceramic Society*, 86 [7] 1211-3 (2003).

[21]J. Wan, M.J. Gasch, and A.K. Mukherjee, "In Situ Densification Behavior in the Pyrolysis Consolidation of Amorphous Si-N-C Bulk Ceramics from Polymer Precursors," *Journal of the American Ceramic Society*, 84 [10] 2165-9 (2001).

[22]J. Wan, M.J. Gasch, and A.K. Mukherjee, "Consolidation and crystallization of Si3N4/SiC nanocomposites from a poly(urea-silazane) ceramic precursor," *Journal of Materials Research*, 16 [11] 3274-86 (2001).

[23]Y.D. Blum, D.B. MacQueen, and H.-J. Kleebe, "Synthesis and characterization of carbon-enriched silicon oxycarbides," *Journal of the European Ceramic Society*, 25 [2-3] 143-9 (2005).

[24]M.A. Schiavon, C. Gervais, F. Babonneau, and G.D. Soraru, "Crystallization Behavior of Novel Silicon Boron Oxycarbide Glasses," *Journal of the American Ceramic Society*, 87 [2] 203-8 (2004).

[25]R. Harshe, C. Balan, and R. Riedel, "Amorphous Si(Al)OC ceramic from polysiloxanes: bulk ceramic processing, crystallization behavior and applications," *Journal of the European Ceramic Society*, 24 [12] 3471-82 (2004).

[26]S. Yajima, J. Hayashi, and K. Okamura, "Pyrolysis of a polyborodiphenylsiloxane," *Nature*, 266 [5602] 521-2 (1977).

[27]G.D. Soraru, F. Babonneau, S. Maurina, and J. Vicens, "Sol-gel synthesis of SiBOC glasses," *Journal of Non-Crystalline Solids*, 224 [2] 173-83 (1998).

[28]G. Ambadas, S. Packirisamy, and K.N. Ninan, "Synthesis, characterization and thermal properties of boron and silicon containing preceramic oligomers," *Journal of Materials Science Letters*, 21 [13] 1003-5 (2002).

[29]M. Fukushima, E. Yasuda, Y. Nakamura, and Y. Tanabe, "Pyrolysis Behavior of Organic-Inorganic Hybrids with Si-O-Nb/Si-O-Ta Oxygen Bridged Heterometallic Bonds," *Journal of the Ceramic Society of Japan*, 111 [1299] 857-9 (2003).

[30]S. Dirè, R. Ceccato, and F. Babonneau, "Structural and Microstructural Evolution During Pyrolysis of Hybrid Polydimethylsiloxane-Titania Nanocomposites," *Journal of Sol-Gel Science and Technology*, 34 [1] 53-62 (2005).

[31]V. Ischenko, R. Harshe, R. Riedel, and J. Woltersdorf, "Cross-linking of functionalised siloxanes with alumatrane: Reaction mechanisms and kinetics," *Journal of Organometallic Chemistry*, 691 [19] 4086-91 (2006).

[32]S.H. Yu, R.E. Riman, S.C. Danforth, and R.Y. Leung, "Pyrolysis of Titanium-Metal-Filled Poly(siloxane) Preceramic Polymers: Effect of Atmosphere on Pyrolysis Product Chemistry," *Journal of the American Ceramic Society*, 78 [7] 1818-24 (1995).

[33]R.G. Jones, W. Andō, and J. Chojnowski, "Silicon-containing polymers: the science and technology of their synthesis applications," Kluwer Academic Publishers, 2000.

[34]S. Trassl, D. Suttor, G. Motz, E. Rossler, and G. Ziegler, "Structural characterisation of silicon carbonitride ceramics derived from polymeric precursors," *Journal of the European Ceramic Society*, 20 [2] 215-25 (2000).

[35]Y.-L. Li, E. Kroke, R. Riedelm, C. Fasel, C. Gervais, and F. Babonneau, "Thermal cross-linking and pyrolytic conversion of poly(ureamethylvinyl)silazanes to silicon-based ceramics," *Applied Organometallic Chemistry*, 15 [10] 820-32 (2001).

[36]V. Liebau-Kunzmann, C. Fasel, R. Kolb, and R. Riedel, "Lithium containing silazanes as precursors for SiCN:Li ceramics--A potential material for electrochemical applications," *Journal of the European Ceramic Society*, 26 [16] 3897-901 (2006).

[37]J. Lücke, J. Hacker, D. Suttor, and G. Ziegler, "Synthesis and Characterization of Silazane-Based Polymers as Precursors for Ceramic Matrix Composites," *Applied Organometallic Chemistry*, 11 [2] 181-94 (1997).

[38]J. Zeschky, T. Höfner, C. Arnold, R. Weißmann, D. Bahloul-Hourlier, M. Scheffler, and P. Greil, "Polysilsesquioxane derived ceramic foams with gradient porosity," *Acta Materialia*, 53 [4] 927-37 (2005).

[39]A. Saha, S.R. Shah, and R. Raj, "Amorphous Silicon Carbonitride Fibers Drawn from Alkoxide Modified Ceraset&#x2122," *Journal of the American Ceramic Society*, 86 [8] 1443-5 (2003).

[40]M. Weinmann, J. Schuhmacher, H. Kummer, S. Prinz, J. Peng, H.J. Seifert, M. Christ, K. Muller, J. Bill, and F. Aldinger, "Synthesis and Thermal Behavior of Novel S-B-C-N Ceramic Precursors," *Chemistry of Materials*, 12 [3] 623-32 (2000).

[41]N.V. Ravi Kumar, R. Mager, Y. Cai, A. Zimmermann, and F. Aldinger, "High temperature deformation behaviour of crystallized Si-B-C-N ceramics obtained from a boron modified poly(vinyl)silazane polymeric precursor," *Scripta Materialia*, 51 [1] 65-9 (2004).

[42]P. Colombo, "Engineering porosity in polymer-derived ceramics," *Journal of the European Ceramic Society*, 28 [7] 1389-95 (2008).

[43]J. Cordelair and P. Greil, "Electrical conductivity measurements as a microprobe for structure transitions in polysiloxane derived Si-O-C ceramics," *Journal of the European Ceramic Society*, 20 [12] 1947-57 (2000).

[44]A.V. Belyakov, N.N. Fomin, and D. Koch, "Nanoporous Ceramics Based on Organosilicon Polymers," *Glass and Ceramics*, 59 [1] 54-7 (2002).

[45]J. Ma, L. Shi, Y. Shi, S. Luo, and J. Xu, "Pyrolysis of polymethylsilsesquioxane," *Journal of Applied Polymer Science*, 85 [5] 1077-86 (2002).

[46]M. Scheffler, P. Greil, A. Berger, E. Pippel, and J. Woltersdorf, "Nickel-catalyzed in situ formation of carbon nanotubes and turbostratic carbon in polymer-derived ceramics," *Materials Chemistry and Physics*, 84 [1] 131-9 (2004).

[47]A.V. Belyakov, N.N. Fomin, and D. Kokh, "Formation of Open Micropores in Nanoporous Ceramics Based on Organosilicon Polymers," *Glass and Ceramics*, 59 [5] 171-3 (2002).

[48]A.V. Belyakov, N.N. Fomin, and D. Koch, "Effect of Granule Size on the Structure of Nanoporous Ceramics Based on Organosilicon Polymer," *Glass and Ceramics*, 60 [1] 14-6 (2003).

[49]M. Wilhelm, C. Soltmann, D. Koch, and G. Grathwohl, "Ceramers--functional materials for adsorption techniques," *Journal of the European Ceramic Society*, 25 [2-3] 271-6 (2005).

[50]M. Monthioux and O. Delverdier, "Thermal behavior of (organosilicon) polymer-derived ceramics. V: Main facts and trends," *Journal of the European Ceramic Society*, 16 [7] 721-37 (1996).

[51]R. Raj, R. Riedel, and G.D. Soraru, "Introduction to the Special Topical Issue on Ultrahigh-Temperature Polymer-Derived Ceramics," *Journal of the American Ceramic Society*, 84 [10] 2158-9 (2001).

[52]P.H. Mutin, "Control of the Composition and Structure of Silicon Oxycarbide and Oxynitride Glasses Derived from Polysiloxane Precursors," *Journal of Sol-Gel Science and Technology*, 14 [1] 27-38 (1999).

[53]E. Bernardo, P. Colombo, E. Pippel, and J. Woltersdorf, "Novel Mullite Synthesis Based on Alumina Nanoparticles and a Preceramic Polymer," *Journal of the American Ceramic Society*, 89 [5] 1577-83 (2006).

[54]G.D. Soraru, S. Modena, E. Guadagnino, P. Colombo, J. Egan, and C. Pantano, "Chemical Durability of Silicon Oxycarbide Glasses," *Journal of the American Ceramic Society*, 85 [6] 1529-36 (2002).

[55]C.G. Pantano, A.K. Singh, and H. Zhang, "Silicon Oxycarbide Glasses," *Journal of Sol-Gel Science and Technology*, 14 [1] 7-25 (1999).

[56]H.-J. Kleebe and Y.D. Blum, "SiOC ceramic with high excess free carbon," *Journal of the European Ceramic Society*, 28 [5] 1037-42 (2008).

[57]E. Breval, M. Hammond, and C. Pantano, "Nanostructural Characterization of Silicon Oxycarbide Glasses and Glass-Ceramics," *Journal of the American Ceramic Society*, 77 [11] 3012-8 (1994).

[58]Q. Wei, E. Pippel, J. Woltersdorf, M. Scheffler, and P. Greil, "Interfacial SiC formation in polysiloxane-derived Si-O-C ceramics," *Materials Chemistry and Physics*, 73 [2-3] 281-9 (2002).

[59]M. Scheffler, E. Pippel, J. Woltersdorf, and P. Greil, "In situ formation of SiC-Si_2ON_2 micro-composite materials from preceramic polymers," *Materials Chemistry and Physics*, 80 [2] 565-72 (2003).

[60]M.G. Segatelli, E. Radovanovic, M.d.C. Gonçalves, and I.V.P. Yoshida, "Investigation of the morphological changes promoted by heating of Si-C-O ceramics derived from a phenyl-rich hybrid polymer. Effect of Ni in the polymeric precursor," *Journal of the European Ceramic Society*, 29 [15] 3279-87 (2009).

[61]M.G. Segatelli, A.T.N. Pires, and I.V.P. Yoshida, "Synthesis and structural characterization of carbon-rich SiCxOy derived from a Ni-containing hybrid polymer," *Journal of the European Ceramic Society*, 28 [11] 2247-57 (2008).

[62]A. Saha and R. Raj, "Crystallization Maps for SiCO Amorphous Ceramics," *Journal of the American Ceramic Society*, 90 578-83 (2007).

[63]H.J. Kleebe, C. Turquat, and G.D. Soraru, "Phase Separation in an SiCO Glass Studied by Transmission Electron Microscopy and Electron Energy-Loss Spectroscopy," *Journal of the American Ceramic Society*, 84 [5] 1073-80 (2001).

[64]G. Gregori, H.J. Kleebe, H. Brequel, S. Enzo, and G. Ziegler, "Microstructure evolution of precursors-derived SiCN ceramics upon thermal treatment between 1000 and 1400 °C," *Journal of Non-Crystalline Solids*, 351 [16-17] 1393-402 (2005).

[65]A. Saha, R. Raj, and D.L. Williamson, "A Model for the Nanodomains in Polymer-Derived SiCO," *Journal of the American Ceramic Society*, 89 2188-95 (2006).

[66]A. Scarmi, G.D. Sorarù, and R. Raj, "The role of carbon in unexpected visco(an)elastic behavior of amorphous silicon oxycarbide above 1273 K," *Journal of Non-Crystalline Solids*, 351 [27-29] 2238-43 (2005).

[67]L. Biasetto, R. Peña-Alonso, G.D. Soraru, and P. Colombo, "Etching of SiOC ceramic foams," *Advances in Applied Ceramics*, 107 106-10 (2008).

[68]G. Gregori, H.J. Kleebe, Y.D. Blum, and F. Babonneau, "Evolution of C-rich SiOC ceramics Part II. Characterization by high lateral resolution techniques: Electron energy-loss spectroscopy, high-resolution TEM and energy-filtered TEM," *International Journal of Materials Research*, 97 [6] 710-20 (2006).

[69]R. Pena-Alonso, G. Mariotto, C. Gervais, F. Babonneau, and G.D. Soraru, "New Insights on the High-Temperature Nanostructure Evolution of SiOC and B-Doped SiBOC Polymer-Derived Glasses," *Chemistry of Materials*, 19 [23] 5694-702 (2007).

[70]P. Dibandjo, Dir, Sandra, F. Babonneau, and G.D. Soraru, "New insights into the nanostructure of high-C SiOC glasses obtained via polymer pyrolysis," *Glass Technology - European Journal of Glass Science and Technology Part A*, 49 175-8 (2008).

[71]H.J. Kleebe, G. Gregori, F. Babonneau, Y.D. Blum, D. Brent MacQueen, and S. Masse, "Evolution of C-rich SiOC ceramics Part I. Characterization by integral spectroscopic techniques: Solid-state NMR and Raman spectroscopy," *International Journal of Materials Research*, 97 [6] 699-709 (2006).

[72]D.H. Filsinger and D.B. Bourrie, "Silica to Silicon: Key Carbothermic Reactions and Kinetics," *Journal of the American Ceramic Society*, 73 [6] 1726-32 (1990).

[73]T. Plachky, Z. Lences, L. Hric, P. Sajgalík, P. Balaz, R. Riedel, and H.J. Kleebe, "Processing and mechanical properties of Si3N4 composites employing polymer-derived SiAlOC as sintering aid," *Journal of the European Ceramic Society*, 30 [3] 759-67 (In press).

[74]M. Esfehanian, R. Oberacker, T. Fett , and M.J. Hoffmann, "Development of Dense Filler-Free Polymer-Derived SiOC Ceramics by Field-Assisted Sintering," *Journal of the American Ceramic Society*, 91 [11] 3803-5 (2008).

[75]A.W. Weimer, K.J. Nilsen, G.A. Cochran, and R.P. Roach, "Kinetics of carbothermal reduction synthesis of beta silicon carbide," *AIChE Journal*, 39 [3] 493-503 (1993).

[76]J. Zheng, M.J. Kramer, and M. Akinc, "In Situ Growth of SiC Whisker in Pyrolyzed Monolithic Mixture of AHPCS and SiC," *Journal of the American Ceramic Society*, 83 [12] 2961-6 (2000).

[77]H.-J. Kleebe, D. Suttor, H. Muller, and G. Ziegler, "Decomposition-Crystallization of Polymer-Derived Si-C-N Ceramics," *Journal of the American Ceramic Society*, 81 [11] 2971-7 (1998).

[78]G. Ziegler, H.J. Kleebe, G. Motz, H. Müller, S. Traßl, and W. Weibelzahl, "Synthesis, microstructure and properties of SiCN ceramics prepared from tailored polymers," *Materials Chemistry and Physics*, 61 [1] 55-63 (1999).

[79]E. Ionescu, C. Linck, C. Fasel, M. Müller, H.-J. Kleebe, and R. Riedel, "Polymer-Derived SiOC/ZrO₂ Ceramic Nanocomposites with Excellent High-Temperature Stability," *Journal of the American Ceramic Society*, 9999 [9999] (2009).

[80]V. Liebau, R. Hauser, and R. Riedel, "Amorphous SiBCO ceramics derived from novel polymeric precursors," *Comptes Rendus Chimie*, 7 [5] 463-9 (2004).

[81]H.M. Williams, E.A. Dawson, P.A. Barnes, B. Rand, and R.M.D. Brydson, "The development and stability of porosity formed during the pyrolysis of polyborodiphenylsiloxane," *Microporous and Mesoporous Materials*, 99 [3] 261-7 (2007).

[82]A. Klonczynski, G. Schneider, R. Riedel, and R. Theissmann, "Influence of Boron on the Microstructure of Polymer Derived SiCO Ceramics," *Advanced Engineering Materials*, 6 [1-2] 64-8 (2004).

[83]M.A. Schiavon, N.A. Armelin, and I.V.P. Yoshida, "Novel poly(borosiloxane) precursors to amorphous SiBCO ceramics," *Materials Chemistry and Physics*, 112 [3] 1047-54 (2008).

[84]R.L. Siqueira, I.V.P. Yoshida, L.C. Pardini, and M.A. Schiavon, "Poly(borosiloxanes) as precursors for carbon fiber ceramic matrix composites," *Materials Research*, 10 147-51 (2007).

[85]S. Dirè, R. Ceccato, S. Gialanella, and F. Babonneau, "Thermal evolution and crystallisation of polydimethylsiloxane-zirconia nanocomposites prepared by the sol-gel method," *Journal of the European Ceramic Society*, 19 [16] 2849-58 (1999).

[86]M. Fukushima, E. Yasuda, Y. Teranishi, K. Nakamura, and Y. Tanabe, "Raman Characterization of Oxidation Behavior of Free Carbon in Silicon Oxycarbide Ceramics," *Journal of the Ceramic Society of Japan*, 112 [1311] 612-4 (2004).

[87]G. Mera, R. Riedel, F. Poli, and K. Müller, "Carbon-rich SiCN ceramics derived from phenyl-containing poly(silylcarbodiimides)," *Journal of the European Ceramic Society*, 29 [13] 2873-83 (2009).

[88]C. Haluschka, H.-J. Kleebe, R. Franke, and R. Riedel, "Silicon carbonitride ceramics derived from polysilazanes Part I. Investigation of compositional and structural properties," *Journal of the European Ceramic Society*, 20 [9] 1355-64 (2000).

[89]H.J. Kleebe, "Microstructure and Stability of Polymer-Derived Ceramics; the Si-C-N System," *Physica status solidi. A. Applied research*, 166 [1] 297-313 (1998).

[90]N. Janakiraman and F. Aldinger, "Fabrication and characterization of fully dense Si-C-N ceramics from a poly(ureamethylvinyl)silazane precursor," *Journal of the European Ceramic Society*, 29 [1] 163-73 (2009).

[91]H.J. Seifert, J. Peng, H.L. Lukas, and F. Aldinger, "Phase equilibria and thermal analysis of Si-C-N ceramics," *Journal of Alloys and Compounds*, 320 [2] 251-61 (2001).

[92]D. Bahloul, M. Pereira, P. Goursat, N. Choong Kwet Yive, and R. Corriu, "Preparation of Silicon Carbonitrides from an Organosilicon Polymer: I, Thermal Decomposition of the Cross-linked Polysilazane," *Journal of the American Ceramic Society*, 76 [5] 1156-62 (1993).

[93]H. Störmer, H.-J. Kleebe, and G. Ziegler, "Metastable SiCN glass matrices studied by energy-filtered electron diffraction pattern analysis," *Journal of Non-Crystalline Solids*, 353 [30-31] 2867-77 (2007).

[94]H.J. Kleebe, H. Störmer, S. Trassl, and G. Ziegler, "Thermal stability of SiCN ceramics studied by spectroscopy and electron microscopy," *Applied Organometallic Chemistry*, 15 [10] 858-66 (2001).

[95]D. Bahloul, M. Pereira, and C. Gerardin, "Pyrolysis chemistry of polysilazane precursors to silicon carbonitride Part 1.-Thermal degradation of the polymers," *Journal of Material Chemistry*, 7 [1] 109-16 (1997).

[96]S. Trassl, H.-J. Kleebe, H. Stormer, G. Motz, E. Rossler, and G. Ziegler, "Characterization of the Free-Carbon Phase in Si-C-N Ceramics: Part II, Comparison of Different Polysilazane Precursors," *Journal of the American Ceramic Society*, 85 [5] 1268-74 (2002).

[97]S. Trassl, G. Motz, E. Rossler, and G. Ziegler, "Characterization of the Free-Carbon Phase in Precursor-Derived Si-C-N Ceramics: I, Spectroscopic Methods," *Journal of the American Ceramic Society*, 85 [1] 239-44 (2002).

[98]T. Cross, R. Raj, S.V. Prasad, T.E. Buchheit, and D.R. Tallant, "Mechanical and Tribological Behavior of Polymer-Derived Ceramics Constituted from $SiC_xO_yN_z$," *Journal of the American Ceramic Society*, 89 [12] 3706-14 (2006).

[99]Y. Iwamoto, W. Volger, E. Kroke, R. Riedel, T. Saitou, and K. Matsunaga, "Crystallization Behavior of Amorphous Silicon Carbonitride Ceramics Derived from Organometallic Precursors," *Journal of the American Ceramic Society*, 84 [10] 2170-8 (2001).

[100]R.M. Morcos, G. Mera, A. Navrotsky, T. Varga, R. Riedel, P. Fabrizia., and K. Müller, "Enthalpy of Formation of Carbon-Rich Polymer-Derived Amorphous SiCN Ceramics," *Journal of the American Ceramic Society*, 91 [10] 3349-54 (2008).

[101]A.H. Tavakoli, J.A. Golczewski, and J. Bill, "Thermal Stability: Decomposition and Crystallization," in Polymer Derived Ceramics. From Nano-Structure to Applications. Edited by P. Colombo, et al. DESTech Publications, Lancaster, PA, 2009.

[102]S.R. Shah and R. Raj, "Mechanical properties of a fully dense polymer derived ceramic made by a novel pressure casting process," *Acta Materialia*, 50 [16] 4093-103 (2002).

[103]T. Nishimura, R. Haug, J. Bill, G. Thurn, and F. Aldinger, "Mechanical and thermal properties of Si–C–N material from polyvinylsilazane," *Journal of Materials Science*, 33 [21] 5237-41 (1998).

[104]S. Walter, G.D. Soraru, H. Bréquel, and S. Enzo, "Microstructural and mechanical characterization of sol gel-derived Si-O-C glasses," *Journal of the European Ceramic Society*, 22 [13] 2389-400 (2002).

[105]G.M. Renlund, S. Prochazka, and R.H. Doremus, "Silicon oxycarbide glasses: Part II. Structure and properties," *Journal of Materials Research*, 6 [12] 2723-34 (1991).

[106]R. Brückner, "Properties and structure of vitreous silica. I," *Journal of Non-Crystalline Solids*, 5 [2] 123-75 (1970).

[107]R. Raj, "Fundamental Research in Structural Ceramics for Service Near 2000C," *Journal of the American Ceramic Society*, 76 [9] 2147-74 (1993).

[108]A. Bauer, M. Christ, A. Zimmermann, and F. Aldinger, "Fracture Toughness of Amorphous Precursor-Derived Ceramics in the Silicon-Carbon-Nitrogen System," *Journal of the American Ceramic Society*, 84 [10] 2203-7 (2001).

[109]L. Bharadwaj, Y. Fan, L. Zhang, D. Jiang, and L. An, "Oxidation Behavior of a Fully Dense Polymer-Derived Amorphous Silicon Carbonitride Ceramic," *Journal of the American Ceramic Society*, 87 [3] 483-6 (2004).

[110]S. Modena, G.D. Soraru, Y. Blum, and R. Raj, "Passive Oxidation of an Effluent System: The Case of Polymer-Derived SiCO," *Journal of the American Ceramic Society*, 88 [2] 339-45 (2005).

[111]A. Müller, P. Gerstel, E. Butchereit, K.G. Nickel, and F. Aldinger, "Si/B/C/N/Al precursor-derived ceramics: Synthesis, high temperature behaviour and oxidation resistance," *Journal of the European Ceramic Society*, 24 [12] 3409-17 (2004).

[112]C. Haluschka, C. Engel, and R. Riedel, "Silicon carbonitride ceramics derived from polysilazanes Part II. Investigation of electrical properties," *Journal of the European Ceramic Society*, 20 [9] 1365-74 (2000).

[113]P. Colombo, T. Gambaryan-Roisman, M. Scheffler, P. Buhler, and P. Greil, "Conductive Ceramic Foams from Preceramic Polymers," *Journal of the American Ceramic Society*, 84 [10] 2265-8 (2001).

[114]L. Zhang, Y. Wang, Y. Wei, W. Xu, D. Fang, L. Zhai, ., K.-C. Lin, and L. An, "A Silicon Carbonitride Ceramic with Anomalously High Piezoresistivity," *Journal of the American Ceramic Society*, 91 [4] 1346-9 (2008).

[115]K. Terauds, P.E. Jimenez-Sanchez, R. Raj, C. Vakifahmetoglu, and P. Colombo, "Giant Piezoresistivity of Polymer-Derived Ceramics at High Temperatures," *manuscript in preparation.*

[116]R. Riedel, L. Toma, E. Janssen, J. Nuffer, T. Melz, and H. Hanselka, "Piezoresistive Effect in SiOC Ceramics for Integrated Pressure Sensors," *Journal of the American Ceramic Society*, (in press 2009).

[117]A. Karakuscu, R. Guider, L. Pavesi, and G.D. Soraru, "White Luminescence from Sol–Gel-Derived SiOC Thin Films," *Journal of the American Chemical Society*, (in press 2009).

[118]I. Menapace, G. Mera, R. Riedel, E. Erdem, R.-A. Eichel, A. Pauletti, and G. Appleby, "Luminescence of heat-treated silicon-based polymers: promising materials for LED applications," *Journal of Materials Science*, 43 [17] 5790-6 (2008).

[119]L. Biasetto, A. Francis, P. Palade, G. Principi, and P. Colombo, "Polymer-derived microcellular SiOC foams with magnetic functionality," *Journal of Materials Science*, 43 [12] 4119-26 (2008).

[120]A. Saha, S.R. Shah, R. Raj, and S.E. Russek, "Polymer-derived SiCN composites with magnetic properties," *Journal of Materials Research*, 18 [11] 2549-51 (2003).

[121]X.H. Yan, X.N. Cheng, C.S. Li, R. Hauser, and R. Riedel, "Synthesis and Low Temperature Magnetic Properties of Metal Elements Filled Polymer-Derived SiCN Ceramic Composites," *Materials Science Forum*, 546 - 549 2269-72 (2007).

[122]R. Hauser, A. Francis, R. Theismann, and R. Riedel, "Processing and magnetic properties of metal-containing SiCN ceramic micro- and nano-composites," *Journal of Materials Science*, 43 [12] 4042-9 (2008).

[123]P. Greil, "Active-Filler-Controlled Pyrolysis of Preceramic Polymers," *Journal of the American Ceramic Society*, 78 [4] 835-48 (1995).

[124]P. Greil and M. Seibold, "Modelling of dimensional changes during polymer-ceramic conversion for bulk component fabrication," *Journal of Materials Science*, 27 [4] 1053-60 (1992).

[125]E. Bernardo, E. Tomasella, and P. Colombo, "Development of multiphase bioceramics from a filler-containing preceramic polymer," *Ceramics International*, 35 [4] 1415-21 (2009).

[126]R. Riedel, M. Seher, J. Mayer, and D.V. Szabó, "Polymer-derived Si-based bulk ceramics, part I: Preparation, processing and properties," *Journal of the European Ceramic Society*, 15 [8] 703-15 (1995).

[127]M. Zemanová, E. Lecomte, P. Sajgalík, and R. Riedel, "Polysilazane derived micro/nano Si3N4/SiC composites," *Journal of the European Ceramic Society*, 22 [16] 2963-8 (2002).

[128]J. Anggono and B. Derby, "Mullite formation from the pyrolysis of aluminium-loaded polymethylsiloxanes: The influence of aluminium powder characteristics," *Journal of the European Ceramic Society*, 26 [7] 1107-19 (2006).

[129]T. Michalet, M. Parlier, F. Beclin, R. Duclos, and J. Crampon, "Elaboration of low shrinkage mullite by active filler controlled pyrolysis of siloxanes," *Journal of the European Ceramic Society*, 22 143-52 (2002).

[130]E. Bernardo and P. Colombo, "Advanced Oxide Ceramics from a Preceramic Polymer and Fillers," *Soft Materials*, 4 [2] 175 - 85 (2006).

[131]T. Gumula, J. Podporska, C. Paluszkiewicz, and M. Blazewicz, "New Bioactive Ceramics Obtained by Heat Treatment of Modified Polymeric Precursors," *Macromolecular Symposia*, 253 [1] 109-14 (2007).

[132]S. Brahmandam and R. Raj, "Novel Composites Constituted from Hafnia and a Polymer-Derived Ceramic as an Interface: Phase for Severe Ultrahigh Temperature Applications," *Journal of the American Ceramic Society*, 90 [10] 3171-6 (2007).

[133]E. Bernardo, P. Colombo, and S. Hampshire, "SiAlON-Based Ceramics from Filled Preceramic Polymers," *Journal of the American Ceramic Society*, 89 [12] 3839-42 (2006).

[134]C. Paluszkiewicz, T. Gumula, J. Podporska, and M. Blazewicz, "Structure and bioactivity studies of new polysiloxane-derived materials for orthopedic applications," *Journal of Molecular Structure*, 792-793 176-81 (2006).

[135]J. Bill and F. Aldinger, "Precursor-derived Covalent Ceramics," *Advanced Materials*, 7 [9] 775-87 (1995).

[136]A.R. Studart, U.T. Gonzenbach, E. Tervoort, and L.J. Gauckler, "Processing Routes to Macroporous Ceramics: A Review," *Journal of the American Ceramic Society*, 89 [6] 1771-89 (2006).

[137]M. Scheffler and P. Colombo, "Cellular ceramics: structure, manufacturing, properties and applications," WILEY-VCH Verlag GmbH, Weinheim, Germany, 2005.

[138]P. Colombo, "In Praise of Pores," *Science*, 322 [5900] 381-3 (2008).

[139]L.J. Gibson and M.F. Ashby, "Cellular solids, structure and properties," pp. 510, Cambridge University Press, Cambridge, UK, 1999.

[140]P. Colombo, "Conventional and novel processing methods for cellular ceramics," *Philosophical Transactions of the Royal Society A: Mathematical, Physical and Engineering Sciences*, 364 [1838] 109-24 (2006).

[141]E. Maire, P. Colombo, J. Adrien, L. Babout, and L. Biasetto, "Characterization of the morphology of cellular ceramics by 3D image processing of X-ray tomography," *Journal of the European Ceramic Society*, 27 [4] 1973-81 (2007).

[142]J. Haber, "Manual on catalyst characterization," *Pure and Applied Chemistry*, 63 [9] 1227-46 (1991).

[143]J.E. Martini-vvedensky, N.P. Suh, and F.A. Waldman, *Microcellular closed cell foams and their method of manufacture*. 1984, US Patent 4,473,665.

[144]P. Colombo, E. Bernardo, and L. Biasetto, "Novel Microcellular Ceramics from a Silicone Resin," *Journal of the American Ceramic Society*, 87 [1] 152-4 (2004).

[145]F.C. Patcas, G.I. Garrido, and B. Kraushaar-Czarnetzki, "CO oxidation over structured carriers: A comparison of ceramic foams, honeycombs and beads," *Chemical Engineering Science*, 62 [15] 3984-90 (2007).

[146]T.A. Nijhuis, A.E.W. Beers, T. Vergunst, I. Hoek, F. Kapteijn, and J.A. Moulijn, "Preparation of monolithic catalysts," *Catalysis Reviews: Science and Engineering*, 43 [4] 345 - 80 (2001).

[147]Y.-J. Lee and K.B. Yoon, "Effect of composition of polyurethane foam template on the morphology of silicalite foam," *Microporous and Mesoporous Materials*, 88 [1-3] 176-86 (2006).

[148]D.J. Green and P. Colombo, "Theme Article - Cellular Ceramics: Intriguing Structures, Novel Properties, and Innovative Applications," *Materials Research Society Bulletin*, 28 [4] 296–300 (2003).

[149]M. Scheffler and P. Colombo, "Cellular ceramics: structure, manufacturing, properties and applications," pp. 670, WILEY-VCH Verlag GmbH, Weinheim, Germany, 2005.

[150]R. Brezny and D.J. Green, "Mechanical Behavior of Cellular Ceramics," pp. 463-516 in Materials Science and Technology-A Comprehensive Treatment; Structure and Properties of Ceramics, Vol. 11. Edited by R.W. Cahn, P. Haasen, and E.J. Kramer. VCH, Weinheim, Germany, 1994.

[151]G.M. Renlund, W.P. Minnear, and A.A. Bracco, *Cellular silicon-oxycarbide glass from foamed silicone resins*. 1991, US Patent 4,981,820.

[152]L.L. Whinnery, M.C. Nichols, D.R. Wheeler, and D.A. Loy, *Process for preparing silicon carbide foam*. 1997, US Patent 5,668,188.

[153]X. Bao, M.R. Nangrejo, and M.J. Edirisinghe, "Synthesis of silicon carbide foams from polymeric precursors and their blends," *Journal of Materials Science*, 34 2495-505 (1999).

[154]F. Berndt, Jahn, P., Rendtel, A., Motz, G., Ziegler, G, "Monolithic SiOC Ceramics with Tailored Porosity," *Key Engineering Materials*, 206-213 1927-30 (2002).

[155]C. Vakifahmetoglu and P. Colombo, "A Direct Method for the Fabrication of Macro-Porous SiOC Ceramics from Preceramic Polymers," *Advanced Engineering Materials*, 10 [3] 256-9 (2008).

[156]T.J. Fitzgerald and A. Mortensen, "Processing of microcellular SiC foams, Part I Curing kinetics of polycarbosilane in air " *Journal of Materials Science*, 30 [4] 1025-32 (1995).

[157]T.J. Fitzgerald, V.J. Michaud, and A. Mortensen, "Processing of microcellular SiC foams, Part II Ceramic foam production," *Journal of Materials Science*, 30 [4] 1037-45 (1995).

[158]M.R. Nangrejo, X. Bao, and M.J. Edirisinghe, "The structure of ceramic foams produced using polymeric precursors," *Journal of Materials Science Letters*, 19 [9] 787-9 (2000).

[159]M.R. Nangrejo, X. Bao, and M.J. Edirisinghe, "Preparation of silicon carbide-silicon nitride composite foams from pre-ceramic polymers," *Journal of the European Ceramic Society*, 20 [11] 1777-85 (2000).

[160]B.H. Jones and T.P. Lodge, "High-Temperature Nanoporous Ceramic Monolith Prepared from a Polymeric Bicontinuous Microemulsion Template," *Journal of the American Chemical Society*, 131 [5] 1676-7 (2009).

[161]P. Colombo and J. Hellmann, "Ceramic foams from preceramic polymers," *Materials Research Innovations*, 6 [5] 260-72 (2002).

[162]P. Colombo, J.R. Hellmann, and D.L. Shelleman, "Thermal Shock Behavior of Silicon Oxycarbide Foams," *Journal of the American Ceramic Society*, 85 [9] 2306-12 (2002).

[163]P. Colombo, J.R. Hellmann, and D.L. Shelleman, "Mechanical Properties of Silicon Oxycarbide Ceramic Foams," *Journal of the American Ceramic Society*, 84 [10] 2245-51 (2001).

[164]T. Takahashi, H. Münstedt, M. Modesti, and P. Colombo, "Oxidation resistant ceramic foam from a silicone preceramic polymer/polyurethane blend," *Journal of the European Ceramic Society*, 21 [16] 2821-8 (2001).

[165]P. Colombo and M. Modesti, "Silicon Oxycarbide Ceramic Foams from a Preceramic Polymer," *Journal of the American Ceramic Society*, 82 [3] 573-8 (1999).

[166]H. Schmidt, D. Koch, G. Grathwohl, and P. Colombo, "Micro-/Macroporous Ceramics from Preceramic Precursors," *Journal of the American Ceramic Society*, 84 [10] 2252-5 (2001).

[167]J. Zeschky, F. Goetz-Neunhoeffer, J. Neubauer, S.H. Jason Lo, B. Kummer, M. Scheffler, and P. Greil, "Preceramic polymer derived cellular ceramics," *Composites Science and Technology*, 63 [16] 2361-70 (2003).

[168]M. Scheffler, T. Gambaryan-Roisman, J. Zeschky, F. Scheffler, and P. Greil, "Self-Foamed Cellular Ceramics from Silicone Resins with a Zeolite Surface," pp. 203-10 in Ceramic Engineering and Science Proceedings, Vol. 23. Edited by M.S. Hau-Tay Lin, 2002.

[169]F. Scheffler, A. Zampieri, W. Schwieger, J. Zeschky, M. Scheffler, and P. Greil, "Zeolite covered polymer derived ceramic foams: novel hierarchical pore systems for sorption and catalysis," *Advances in Applied Ceramics*, 104 43-8 (2005).

[170]G.A. Danko, R. Silberglitt, P. Colombo, E. Pippel, and J. Woltersdorf, "Comparison of Microwave Hybrid and Conventional Heating of Preceramic Polymers to Form Silicon Carbide and Silicon Oxycarbide Ceramics," *Journal of the American Ceramic Society*, 83 [7] 1617-25 (2000).

[171]R. Rocha, E. Moura, A. Bressiani, and J. Bressiani, "SiOC ceramic foams synthesized from electron beam irradiated methylsilicone resin," *Journal of Materials Science*, 43 [13] 4466-74 (2008).

[172]B.-H. Yoon, C.-S. Park, H.-E. Kim, and Y.-H. Koh, "In Situ Synthesis of Porous Silicon Carbide (SiC) Ceramics Decorated with SiC Nanowires," *Journal of the American Ceramic Society*, 90 [12] 3759-66 (2007).

[173]B.-H. Yoon, E.-J. Lee, H.-E. Kim, and Y.-H. Koh, "Highly Aligned Porous Silicon Carbide Ceramics by Freezing Polycarbosilane/Camphene Solution," *Journal of the American Ceramic Society*, 90 [6] 1753-9 (2007).

[174]T. Takahashi and P. Colombo, "SiOC Ceramic Foams through Melt Foaming of a Methylsilicone Preceramic Polymer," *Journal of Porous Materials*, 10 113-21 (2003).

[175]C. Vakifahmetoglu, I. Menapace, A. Hirsch, L. Biasetto, R. Hauser, R. Riedel, and P. Colombo, "Highly porous macro- and micro-cellular ceramics from a polysilazane precursor," *Ceramics International*, 35 [8] 3281-90 (2009).

[176]Y.-W. Kim, S.-H. Kim, X. Xu, C.-H. Choi, C.B. Park, and H.-D. Kim, "Fabrication of porous preceramic polymers using carbon dioxide," *Journal of Materials Science Letters*, 21 [21] 1667-9 (2002).

[177]Y.-W. Kim and C.B. Park, "Processing of microcellular preceramics using carbon dioxide," *Composites Science and Technology*, 63 [16] 2371-7 (2003).

[178]Y.-W. Kim, S.-H. Kim, C. Wang, and C. Park, B., "Fabrication of Microcellular Ceramics Using Gaseous Carbon Dioxide," *Journal of the American Ceramic Society*, 86 [12] 2231-3 (2003).

[179]C. Wang, J. Wang, C.B. Park, and Y.W. Kim, "Cross-linking behavior of a polysiloxane in preceramic foam processing," *Journal of Materials Science*, 39 [15] 4913-5 (2004).

[180]C. Wang, J. Wang, C. Park, and Y.-W. Kim, "Fabrication of cellular and microcellular ceramics with controllable open-cell content from polysiloxane-LDPE blends: I. Compounding and Foaming," *Journal of Materials Science*, 42 [8] 2854-61 (2007).

[181]H. Wang, S.-Y. Zheng, X.-D. Li, and D.-P. Kim, "Preparation of three-dimensional ordered macroporous SiCN ceramic using sacrificing template method," *Microporous and Mesoporous Materials*, 80 [1-3] 357-62 (2005).

[182]H. Wang, X.-d. Li, J.-s. Yu, and D.-p. Kim, "Fabrication and characterization of ordered macroporous PMS-derived SiC from a sacrificial template method," *Journal of Materials Chemistry*, 14 [9] 1383-6 (2004).

[183]I.-K. Sung, S.-B. Yoon, J.-S. Yu, and D.-P. Kim, "Fabrication of macroporous SiC from templated preceramic polymers," *Chemical Communications*, [14] 1480-1 (2002).

[184]I.-K. Sung, M.M. Christian, D.-P. Kim, and P.J.A. Kenis, "Tailored Macroporous SiCN and SiC Structures for High-Temperature Fuel Reforming," *Advanced Functional Materials*, 15 [8] 1336-42 (2005).

[185]C. Zollfrank, R. Kladny, H. Sieber, and P. Greil, "Biomorphous SiOC/C-ceramic composites from chemically modified wood templates," *Journal of the European Ceramic Society*, 24 [2] 479-87 (2004).

[186]V. Bakumov, M. Schwarz, and E. Kroke, "Emulsion processing of polymer-derived porous Si/C/(O) ceramic bodies," *Journal of the European Ceramic Society*, 29 [13] 2857-65 (2009).

[187]D.-H. Jang, Y.-W. Kim, I.-H. Song, H.-D. Kim, and C.B. Park, "Processing of Highly Porous, Open-Cell, Microcellular Silicon Carbide Ceramics by Expansion Method Using Expandable Microspheres," *Journal of the Ceramic Society of Japan*, 114 [1330] 549-53 (2006).

[188]P. Colombo and E. Bernardo, "Macro- and micro-cellular porous ceramics from preceramic polymers," *Composites Science and Technology*, 63 [16] 2353-9 (2003).

[189]S. Costacurta, L. Biasetto, E. Pippel, J. Woltersdorf, and P. Colombo, "Hierarchical Porosity Components by Infiltration of a Ceramic Foam," *Journal of the American Ceramic Society*, 90 [7] 2172-7 (2007).

[190]M. Shibuya, T. Takahashi, and K. Koyama, "Microcellular ceramics by using silicone preceramic polymer and PMMA polymer sacrificial microbeads," *Composites Science and Technology*, 67 [1] 119-24 (2007).

[191]S. Vaucher, J. Kuebler, O. Beffort, L. Biasetto, F. Zordan, and P. Colombo, "Ceramic foam-reinforced Al-based micro-composites," *Composites Science and Technology*, 68 [15-16] 3202-7 (2008).

[192]L. Biasetto, P. Colombo, M.D.M. Innocentini, and S. Mullens, "Gas Permeability of Microcellular Ceramic Foams," *Industrial & Engineering Chemistry Research*, 46 [10] 3366-72 (2007).

[193]E. Bernardo, P. Colombo, and E. Manias, "SiOC glass modified by montmorillonite clay," *Ceramics International*, 32 [6] 679-86 (2006).

[194]I.-H. Song, M.-J. Kim, H.-D. Kim, and Y.-W. Kim, "Processing of microcellular cordierite ceramics from a preceramic polymer," *Scripta Materialia*, 54 [8] 1521-5 (2006).

[195]S.-H. Chae, Y.-W. Kim, I.-H. Song, H.-D. Kim, and M. Narisawa, "Porosity control of porous silicon carbide ceramics," *Journal of the European Ceramic Society*, 29 [13] 2867-72 (2009).

[196]F. Schüth, K.S.W. Sing, and J. Weitkamp, "Handbook of porous solids," pp. 3191, Wiley-VCH Verlag GmbH, Weinheim, Germany, 2002.

[197]J.-H. Smatt, S. Schunk, and M. Linden, "Versatile Double-Templating Synthesis Route to Silica Monoliths Exhibiting a Multimodal Hierarchical Porosity," *Chemistry of Materials*, 15 [12] 2354-61 (2003).

[198]P.O. Vasiliev, Z. Shen, R.P. Hodgkins, and L. Bergstrom, "Meso/Macroporous, Mechanically Stable Silica Monoliths of Complex Shape by Controlled Fusion of Mesoporous Spherical Particles," *Chemistry of Materials*, 18 [20] 4933-8 (2006).

[199]T.-Z. Ren, Z.-Y. Yuan, A. Azioune, J.-J. Pireaux, and B.-L. Su, "Tailoring the Porous Hierarchy of Titanium Phosphates," *Langmuir*, 22 [8] 3886-94 (2006).

[200]Z.-Y. Yuan and B.-L. Su, "Insights into hierarchically meso-macroporous structured materials," *Journal of Materials Chemistry*, 16 [7] 663-77 (2006).

[201]F. Mizukami, G.P.-B.J.B.N. I. Kiricsi, and H.G. Karge, "Application of zeolite membranes, films and coatings," pp. 1-12 in Studies in Surface Science and Catalysis, Vol. Volume 125. Edited. Elsevier, 1999.

[202]F. Schuth, "Engineered Porous Catalytic Materials," *Annual Review of Materials Research*, 35 [1] 209-38 (2005).

[203]F. Schüth, "Endo- and Exotemplating to Create High-Surface-Area Inorganic Materials," *Angewandte Chemie International Edition*, 42 [31] 3604-22 (2003).

[204]M. Tiemann, "Repeated Templating," *Chemistry of Materials*, 20 [3] 961-71 (2007).

[205]A.H. Lu and F. Schüth, "Nanocasting: A Versatile Strategy for Creating Nanostructured Porous Materials," *Advanced Materials*, 18 [14] 1793-805 (2006).

[206]V. Meille, "Review on methods to deposit catalysts on structured surfaces," *Applied Catalysis A: General*, 315 1-17 (2006).

[207]P. Yang, T. Deng, D. Zhao, P. Feng, D. Pine, B.F. Chmelka, G.M. Whitesides, and G.D. Stucky, "Hierarchically Ordered Oxides," *Science*, 282 [5397] 2244-6 (1998).

[208]B.T. Holland, C.F. Blanford, and A. Stein, "Synthesis of Macroporous Minerals with Highly Ordered Three-Dimensional Arrays of Spheroidal Voids," *Science*, 281 [5376] 538-40 (1998).

[209]B.T. Holland, C.F. Blanford, T. Do, and A. Stein, "Synthesis of Highly Ordered, Three-Dimensional, Macroporous Structures of Amorphous or Crystalline Inorganic Oxides, Phosphates, and Hybrid Composites," *Chemistry of Materials*, 11 [3] 795-805 (1999).

[210]T. Sen, G.J.T. Tiddy, J.L. Casci, and M.W. Anderson, "Synthesis and Characterization of Hierarchically Ordered Porous Silica Materials," *Chemistry of Materials*, 16 [11] 2044-54 (2004).

[211]J.-P. Dacquin, J.r.m. Dhainaut, D. Duprez, S.b. Royer, A.F. Lee, and K. Wilson, "An Efficient Route to Highly Organized, Tunable Macroporousâˆ'Mesoporous Alumina," *Journal of the American Chemical Society*, 131 [36] 12896-7 (2009).

[212]Y. Kim, C. Kim, and J. Yi, "Synthesis of tailored porous alumina with a bimodal pore size distribution," *Materials Research Bulletin*, 39 [13] 2103-12 (2004).

[213]G. Gundiah, "Macroporous silica-alumina composites with mesoporous walls," *Bulletin of Materials Science*, 24 [2] 211-4 (2001).

[214]M. Antonietti, B. Berton, C. Goltner, and H.-P. Hentze, "Synthesis of Mesoporous Silica with Large Pores and Bimodal Pore Size Distribution by Templating of Polymer Latices," *Advanced Materials*, 10 [2] 154-9 (1998).

[215]Q. Luo, L. Li, B. Yang, and D. Zhao, "Three-Dimensional Ordered Macroporous Structures With Mesoporous Silica Walls," *Chemistry Letters*, 29 [4] 378-9 (2000).

[216]D. Kuang, T. Brezesinski, and B. Smarsly, "Hierarchical Porous Silica Materials with a Trimodal Pore System Using Surfactant Templates," *Journal of the American Ceramic Society*, 126 [34] 10534-5 (2004).

[217]K.R. Seddon, A. Stark, and M.-J. Torres, "Influence of chloride, water, and organic solvents on the physical properties of ionic liquids," *Pure and Applied Chemistry*, 72 [12] 2275-87 (2000).

[218]Y. Zhou and M. Antonietti, "A novel tailored bimodal porous silica with well-defined inverse opal microstructure and super-microporous lamellar nanostructure," *Chemical Communications*, [20] 2564-5 (2003).

[219]T. Sen, G.J.T. Tiddy, J.L. Casci, and M.W. Anderson, "One-Pot Synthesis of Hierarchically Ordered Porous-Silica Materials with Three Orders of Length Scale," *Angewandte Chemie International Edition*, 42 [38] 4649-53 (2003).

[220]N. Suzuki, Y. Sakka, and Y. Yamauchi, "Simple preparation of silica and alumina with a hierarchical pore system via the dual-templating method," *Science and Technology of Advanced Materials*, 10 [2] 025002 (2009).

[221]J.-H. Smatt, C. Weidenthaler, J.B. Rosenholm, and M. Linden, "Hierarchically Porous Metal Oxide Monoliths Prepared by the Nanocasting Route," *Chemistry of Materials*, 18 [6] 1443-50 (2006).

[222]H. Maekawa, J. Esquena, S. Bishop, C. Solans, and B.F. Chmelka, "Meso/Macroporous Inorganic Oxide Monoliths from Polymer Foams," *Advanced Materials*, 15 [7-8] 591-6 (2003).

[223]L. Huerta, C. Guillem, J. Latorre, A. Beltran, D. Beltran, and P. Amoros, "Large monolithic silica-based macrocellular foams with trimodal pore system," *Chemical Communications*, [12] 1448-9 (2003).

[224]L. Huerta, C. Guillem, J. Latorre, A. Beltrán, D. Beltrán, and P. Amorós, "Silica-based macrocellular foam monoliths with hierarchical trimodal pore systems," *Solid State Sciences*, 7 [4] 405-14 (2005).

[225]S. Álvarez and A.B. Fuertes, "Synthesis of macro-mesoporous silica and carbon monoliths by using a commercial polyurethane foam as sacrificial template," *Materials Letters*, 61 [11-12] 2378-81 (2007).

[226]Y. Deng, C. Liu, T. Yu, F. Liu, F. Zhang, Y. Wan, L. Zhang, C. Wang, B. Tu, P.A. Webley, H. Wang, and D. Zhao, "Facile Synthesis of Hierarchically Porous Carbons from Dual Colloidal Crystal/Block Copolymer Template Approach," *Chemistry of Materials*, 19 [13] 3271-7 (2007).

[227]Y. Tong, T. Zhao, F. Li, and Y. Wang, "Synthesis of Monolithic Zeolite Beta with Hierarchical Porosity Using Carbon as a Transitional Template," *Chemistry of Materials*, 18 [18] 4218-20 (2006).

[228]L.-L. Li, W.-T. Duan, Q. Yuan, Z.-X. Li, H.-H. Duan, and C.-H. Yan, "Hierarchical y-Al2O3 monoliths with highly ordered 2D hexagonal mesopores in macroporous walls," *Chemical Communications*, [41] 6174-6 (2009).

[229]Z.-G. Shi, L.-Y. Xu, and Y.-Q. Feng, "A new template for the synthesis of porous inorganic oxide monoliths," *Journal of Non-Crystalline Solids*, 352 [38-39] 4003-7 (2006).

[230]L.-Y. Xu, Z.-G. Shi, and Y.-Q. Feng, "A facile route to a silica monolith with ordered mesopores and tunable through pores by using hydrophilic urea formaldehyde resin as a template," *Microporous and Mesoporous Materials*, 98 [1-3] 303-8 (2007).

[231]F. Ocampo, H.S. Yun, M.M. Pereira, J.P. Tessonnier, and B. Louis, "Design of MFI Zeolite-Based Composites with Hierarchical Pore Structure: A New Generation of Structured Catalysts," *Crystal Growth & Design*, 9 [8] 3721-9 (2009).

[232]H.S. Yun, S.-e. Kim, Y.-t. Hyun, S.-j. Heo, and J.-w. Shin, "Hierarchically mesoporous-macroporous bioactive glasses scaffolds for bone tissue regeneration," *Journal of Biomedical Materials Research Part B: Applied Biomaterials*, 87B [2] 374-80 (2008).

[233]Y.J. Lee, J.S. Lee, Y.S. Park, and K.B. Yoon, "Synthesis of Large Monolithic Zeolite Foams with Variable Macropore Architectures," *Advanced Materials*, 13 [16] 1259-63 (2001).

[234]Y.-J. Lee, Y.-W. Kim, K.-W. Jun, N. Viswanadham, J. Bae, and H.-S. Park, "Textural Properties and Catalytic Applications of ZSM-5 Monolith Foam for Methanol Conversion," *Catalysis Letters*, 129 [3] 408-15 (2009).

[235]W.J. Kim, T.J. Kim, W.S. Ahn, Y.J. Lee, and K.B. Yoon, "Synthesis, Characterization and Catalytic Properties of TS-1 Monoliths," *Catalysis Letters*, 91 [1] 123-7 (2003).

[236]B.T. Holland, L. Abrams, and A. Stein, "Dual Templating of Macroporous Silicates with Zeolitic Microporous Frameworks," *Journal of the American Chemical Society*, 121 [17] 4308-9 (1999).

[237]P. Greil, "Biomorphous ceramics from lignocellulosics," *Journal of the European Ceramic Society*, 21 [2] 105-18 (2001).

[238]H. Sieber, "Biomimetic synthesis of ceramics and ceramic composites," *Materials Science and Engineering: A*, 412 [1-2] 43-7 (2005).

[239]B. Zhang, S.A. Davis, and S. Mann, "Starch Gel Templating of Spongelike Macroporous Silicalite Monoliths and Mesoporous Films," *Chemistry of Materials*, 14 [3] 1369-75 (2002).

[240]J. Li, Q. Xu, J. Wang, J. Jiao, and Z. Zhang, "Controlled Synthesis of Monolithic Hierarchical Porous Materials Using Wood as a Template with Assistance of Supercritical Carbon Dioxide," *Industrial & Engineering Chemistry Research*, 47 [20] 7680-5 (2008).

[241]A. Dong, Y. Wang, Y. Tang, N. Ren, Y. Zhang, Y. Yue, and Z. Gao, "Zeolitic Tissue Through Wood Cell Templating," *Advanced Materials*, 14 [12] 926-9 (2002).

[242]A. Zampieri, S. Kullmann, T. Selvam, J. Bauer, W. Schwieger, H. Sieber, T. Fey, and P. Greil, "Bioinspired Rattan-Derived SiSiC/Zeolite Monoliths: Preparation and Characterisation," *Microporous and Mesoporous Materials*, 90 [1-3] 162-74 (2006).

[243]V. Valtchev, M. Smaihi, A.-C. Faust, and L. Vidal, "Biomineral-Silica-Induced Zeolitization of Equisetum Arvense," *Angewandte Chemie International Edition*, 42 [24] 2782-5 (2003).

[244]V.P. Valtchev, M. Smaihi, A.-C. Faust, and L. Vidal, "Equisetum arvense Templating of Zeolite Beta Macrostructures with Hierarchical Porosity," *Chemistry of Materials*, 16 [7] 1350-5 (2004).

[245]Y. Wang, Y. Tang, A. Dong, X. Wang, N. Ren, W. Shan, and Z. Gao, "Self-Supporting Porous Zeolite Membranes with Sponge-like Architecture and Zeolitic Microtubes," *Advanced Materials*, 14 [13-14] 994-7 (2002).

[246]J. Xu, J. Yao, C. Zeng, L. Zhang, and N. Xu, "Preparation of binderless honeycomb silicalite-1 monolith by using bundled palm fibers as template," *Journal of Porous Materials*, 1-6 (2009).

[247]W. Liu, L. Zhang, H. Wang, N. Xu, Z.G.J.C. Ruren Xu, and Y. Wenfu, "Preparation of silicalite-1 microtube arrays supported on cordierite honeycomb by using palm fibers as templates," pp. 408-13 in Studies in Surface Science and Catalysis, Vol. Volume 170, Part 1. Edited. Elsevier, 2007.

[248]G. Li, R. Singh, D. Li, C. Zhao, L. Liu, and P.A. Webley, "Synthesis of biomorphic zeolite honeycomb monoliths with 16000 cells per square inch," *Journal of Materials Chemistry*, 19 [44] 8372-7 (2009).

[249]M. Anderson, W., S. Holmes, M., N. Hanif, and C. Cundy, S., "Hierarchical Pore Structures through Diatom Zeolitization," *Angewandte Chemie International Edition*, 39 [15] 2707-10 (2000).

[250]Y. Wang, Y. Tang, A. Dong, X. Wang, N. Ren, and Z. Gao, "Zeolitization of diatomite to prepare hierarchical porous zeolite materials through a vapor-phase transport process," *Journal of Materials Chemistry*, 12 [6] 1812-8 (2002).

[251]D. Losic, J. Mitchell, G., and N. Voelcker, H., "Diatomaceous Lessons in Nanotechnology and Advanced Materials," *Advanced Materials*, 21 [29] 2947-58 (2009).

[252]K.L. Vyshnyakova, G. Yushin, L.N. Pereselentseva, and Y. Gogotsi, "Formation of Porous SiC Ceramics by Pyrolysis of Wood Impregnated with Silica," *International Journal of Applied Ceramic Technology*, 3 [6] 485-90 (2006).

[253]M. Iwasaki, S.A. Davis, and S. Mann, "Spongelike Macroporous TiO2 Monoliths Prepared from Starch Gel Template," *Journal of Sol-Gel Science and Technology*, 32 [1] 99-105 (2004).

[254]H. Sieber, C. Hoffmann, A. Kaindl, and P. Greil, "Biomorphic Cellular Ceramics," *Advanced Engineering Materials*, 2 [3] 105-9 (2000).

[255]Y. Shin, C. Wang, and G.J. Exarhos, "Synthesis of SiC Ceramics by the Carbothermal Reduction of Mineralized Wood with Silica," *Advanced Materials*, 17 [1] 73-7 (2005).

[256]Y. Shin, J. Liu, J.H. Chang, Z. Nie, and G.J. Exarhos, "Hierarchically Ordered Ceramics Through Surfactant-Templated Sol-Gel Mineralization of Biological Cellular Structures," *Advanced Materials*, 13 [10] 728-32 (2001).

[257]L.-Q. Wang, Y. Shin, W.D. Samuels, G.J. Exarhos, I.L. Moudrakovski, V.V. Terskikh, and J.A. Ripmeester, "Magnetic Resonance Studies of Hierarchically Ordered Replicas of Wood Cellular Structures Prepared by Surfactant-Mediated Mineralization," *The Journal of Physical Chemistry B*, 107 [50] 13793-802 (2003).

[258]F. Carn, H. Saadaoui, P. Masse, S. Ravaine, B. Julian-Lopez, C. Sanchez, H. Deleuze, D.R. Talham, and R. Backov, "Three-Dimensional Opal-Like Silica Foams," *Langmuir*, 22 [12] 5469-75 (2006).

[259]D. Zhao, P. Yang, B.F. Chmelka, and G.D. Stucky, "Multiphase Assembly of Mesoporousâˆ'Macroporous Membranes," *Chemistry of Materials*, 11 [5] 1174-8 (1999).

[260]H. Nishihara, S.R. Mukai, D. Yamashita, and H. Tamon, "Ordered Macroporous Silica by Ice Templating," *Chemistry of Materials*, 17 [3] 683-9 (2005).

[261]A. Farid, O.V. Petr, and B. Lennart, "Hierarchically Porous Ceramics from Diatomite Powders by Pulsed Current Processing," *Journal of the American Ceramic Society*, 92 [2] 338-43 (2009).

[262]P.O. Vasiliev (2009). Functionalization and processing of porous powders into hierarchically porous monoliths. Department of Physical, Inorganic and Structural Chemistry. Stockholm, Stockholm University. **PhD.:** 68.

[263]K. Li, "Ceramic Membranes for Separation and Reaction," pp. 316, Wiley, Chichester, England 2007.

[264]P. Avila, M. Montes, and E.E. Miró, "Monolithic reactors for environmental applications: A review on preparation technologies," *Chemical Engineering Journal*, 109 [1-3] 11-36 (2005).

[265]B. Mitra and D. Kunzru, "Washcoating of Different Zeolites on Cordierite Monoliths," *Journal of the American Ceramic Society*, 91 [1] 64-70 (2008).

[266]F.-C. Buciuman and B. Kraushaar-Czarnetzki, "Preparation and characterization of ceramic foam supported nanocrystalline zeolite catalysts," *Catalysis Today*, 69 [1-4] 337-42 (2001).

[267]C. Agrafiotis and A. Tsetsekou, "Deposition of meso-porous γ-alumina coatings on ceramic honeycombs by sol-gel methods," *Journal of the European Ceramic Society*, 22 [4] 423-34 (2002).

[268]M.V. Twigg and J.T. Richardson, "Fundamentals and Applications of Structured Ceramic Foam Catalysts," *Industrial & Engineering Chemistry Research*, 46 [12] 4166-77 (2007).

[269]C.K. Narula, J.E. Allison, D.R. Bauer, and H.S. Gandhi, "Materials Chemistry Issues Related to Advanced Materials Applications in the Automotive Industry," *Chemistry of Materials*, 8 [5] 984-1003 (1996).

[270]C. Agrafiotis and A. Tsetsekou, "The effect of processing parameters on the properties of γ-alumina washcoats deposited on ceramic honeycombs," *Journal of Materials Science*, 35 [4] 951-60 (2000).

[271]L. Villegas, F. Masset, and N. Guilhaume, "Wet impregnation of alumina-washcoated monoliths: Effect of the drying procedure on Ni distribution and on autothermal reforming activity," *Applied Catalysis A: General*, 320 43-55 (2007).

[272]N.A. Jarrah, J.G. van Ommen, and L. Lefferts, "Growing a carbon nano-fiber layer on a monolith support; effect of nickel loading and growth conditions," *Journal of Materials Chemistry*, 14 [10] 1590-7 (2004).

[273]N. Jarrah, J.G. van Ommen, and L. Lefferts, "Development of monolith with a carbon-nanofiber-washcoat as a structured catalyst support in liquid phase," *Catalysis Today*, 79-80 29-33 (2003).

[274]J.T. Richardson, M. Garrait, and J.K. Hung, "Carbon dioxide reforming with Rh and Pt-Re catalysts dispersed on ceramic foam supports," *Applied Catalysis A: General*, 255 [1] 69-82 (2003).

[275]S. Deng and Y. Lin, "Microwave synthesis of mesoporous and microporous alumina powders," *Journal of Materials Science Letters*, 16 [15] 1291-4 (1997).

[276]C. Agrafiotis, A. Tsetsekou, and A. Ekonomakou, "The effect of particle size on the adhesion properties of oxide washcoats on cordierite honeycombs," *Journal of Materials Science Letters*, 18 [17] 1421-4 (1999).

[277]C. Agrafiotis and A. Tsetsekou, "The effect of powder characteristics on washcoat quality. Part I: Alumina washcoats," *Journal of the European Ceramic Society*, 20 [7] 815-24 (2000).

[278]C. Agrafiotis and A. Tsetsekou, "The effect of powder characteristics on washcoat quality. Part II: Zirconia, titania washcoats -- multilayered structures," *Journal of the European Ceramic Society*, 20 [7] 825-34 (2000).

[279]M.E. Davis, "Zeolite-based catalysts for chemicals synthesis," *Microporous and Mesoporous Materials*, 21 [4-6] 173-82 (1998).

[280]T. Bein, "Synthesis and Applications of Molecular Sieve Layers and Membranesâ€ " *Chemistry of Materials*, 8 [8] 1636-53 (1996).

[281]A. Tavolaro and E. Drioli, "Zeolite Membranes," *Advanced Materials*, 11 [12] 975-96 (1999).

[282]L. Li, B. Xue, J. Chen, N. Guan, F. Zhang, D. Liu, and H. Feng, "Direct synthesis of zeolite coatings on cordierite supports by in situ hydrothermal method," *Applied Catalysis A: General*, 292 312-21 (2005).

[283]C.D. Madhusoodana, R.N. Das, Y. Kameshima, A. Yasumori, and K. Okada, "Characterization and Adsorption Behavior of ZSM-5 Zeolite Film on Cordierite Honeycombs Prepared by a Novel in situ Crystallization Method," *Journal of Porous Materials*, 8 [4] 265-71 (2001).

[284]J.C. Jansen, J.H. Koegler, H. van Bekkum, H.P.A. Calis, C.M. van den Bleek, F. Kapteijn, J.A. Moulijn, E.R. Geus, and N. van der Puil, "Zeolitic coatings and their potential use in catalysis," *Microporous and Mesoporous Materials*, 21 [4-6] 213-26 (1998).

[285]E.R. Silva, J.M. Silva, M.F. Vaz, F.A.C. Oliveira, and F. Ribeiro, "Cationic polymer surface treatment for zeolite washcoating deposited over cordierite foam," *Materials Letters*, 63 [5] 572-4 (2009).

[286]O. Öhrman, J. Hedlund, and J. Sterte, "Synthesis and evaluation of ZSM-5 films on cordierite monoliths," *Applied Catalysis A: General*, 270 [1-2] 193-9 (2004).

[287]K. Okada, Y. Kameshima, C.D. Madhusoodana, and R.N. Das, "Preparation of zeolite-coated cordierite honeycombs prepared by an in situ crystallization method," *Science and Technology of Advanced Materials*, 5 [4] 479 (2004).

[288]M.A. Ulla, R. Mallada, J. Coronas, L. Gutierrez, E. Miró, and J. Santamaría, "Synthesis and characterization of ZSM-5 coatings onto cordierite honeycomb supports," *Applied Catalysis A: General*, 253 [1] 257-69 (2003).

[289]E.I. Basaldella, A. Kikot, J.F. Bengoa, and J.C. Tara, "ZSM-5 zeolite films on cordierite modules. Effect of dilution on the synthesis medium," *Materials Letters*, 52 [4-5] 350-4 (2002).

[290]R. Aiello, F. Crea, F. Testa, A. SpantiGattuso, G.P.-B.J.B.N. I. Kiricsi, and H.G. Karge, "In situ crystallization of MFI-type zeolites over cordierite support," pp. 29-36 in Studies in Surface Science and Catalysis, Vol. Volume 125. Edited. Elsevier, 1999.

[291]X. Lin, E. Kikuchi, and M. Matsukata, "Growth of oriented mordenite membranes on porous [alpha]-Al2O3 supports," pp. 162- in Studies in Surface Science and Catalysis, Vol. Volume 135. Edited. Elsevier, 2001.

[292]G.B.F. Seijger, O.L. Oudshoorn, W.E.J. van Kooten, J.C. Jansen, H. van Bekkum, C.M. van den Bleek, and H.P.A. Calis, "In situ synthesis of binderless ZSM-5 zeolitic coatings on ceramic foam supports," *Microporous and Mesoporous Materials*, 39 [1-2] 195-204 (2000).

[293]G.B.F. Seijger, O.L. Oudshoorn, A. Boekhorst, H. van Bekkum, C.M. van den Bleek, and H.P.A. Calis, "Selective catalytic reduction of NOx over zeolite-coated structured catalyst packings," *Chemical Engineering Science*, 56 [3] 849-57 (2001).

[294]J. Sterte, J. Hedlund, D. Creaser, O. Öhrman, W. Zheng, M. Lassinantti, Q. Li, and F. Jareman, "Application of the seed-film method for the preparation of structured molecular sieve catalysts," *Catalysis Today*, 69 [1-4] 323-9 (2001).

[295]C. Falamaki, M.S. Afarani, and A. Aghaie, "In Situ Crystallization of Highly Oriented Silicalite Films on Porous Zircon Supports," *Journal of the American Ceramic Society*, 89 [2] 408-14 (2006).

[296]Y. Yan, M.E. Davis, and G.R. Gavalas, "Preparation of Zeolite ZSM-5 Membranes by In-Situ Crystallization on Porous a-Al2O3," *Industrial & Engineering Chemistry Research*, 34 [5] 1652-61 (1995).

[297]Y. Yan, M. Tsapatsis, G.R. Gavalas, and M.E. Davis, "Zeolite ZSM-5 membranes grown on porous a-Al2O3," *Journal of the Chemical Society, Chemical Communications*, 227-8 (1995).

[298]H.P. Calis, A.W. Gerritsen, C.M.V.D. Bleek, C.H. Legein, J.C. Jansen, and H.V. Bekkum, "Zeolites grown on wire gauze: A new structured catalyst packing for dustproof, low pressure drop denox processes," *The Canadian Journal of Chemical Engineering*, 73 [1] 120-8 (1995).

[299]E.R. Geus, M.J. den Exter, and H. van Bekkum, "Synthesis and characterization of zeolite (MFI) membranes on porous ceramic supports," *Journal of the Chemical Society, Faraday Transactions*, 88 [20] 3101-9 (1992).

[300]Y. Yan, M.E. Davis, and G.R. Gavalas, "Preparation of highly selective zeolite ZSM-5 membranes by a post-synthetic coking treatment," *Journal of Membrane Science*, 123 [1] 95-103 (1997).

[301]L. Zhang and H. Wang, "Preparation of ZnAPO-34 films on alumina substrates," *Journal of Materials Science*, 38 [7] 1439-45 (2003).

[302]H. Katsuki, S. Furuta, and S. Komarneni, "Formation of Novel ZSM-5/Porous Mullite Composite from Sintered Kaolin Honeycomb by Hydrothermal Reaction," *Journal of the American Ceramic Society*, 83 [5] 1093-7 (2000).

[303]A.E.W. Beers, T.A. Nijhuis, F. Kapteijn, and J.A. Moulijn, "Zeolite coated structures for the acylation of aromatics," *Microporous and Mesoporous Materials*, 48 [1-3] 279-84 (2001).

[304]A.E.W. Beers, T.A. Nijhuis, N. Aalders, F. Kapteijn, and J.A. Moulijn, "BEA coating of structured supports--performance in acylation," *Applied Catalysis A: General*, 243 [2] 237-50 (2003).

[305]J.M. Zamaro, M.A. Ulla, and E.E. Miró, "Zeolite washcoating onto cordierite honeycomb reactors for environmental applications," *Chemical Engineering Journal*, 106 [1] 25-33 (2005).

[306]J.M. Zamaro, M.A. Ulla, and E.E. Miró, "The effect of different slurry compositions and solvents upon the properties of ZSM5-washcoated cordierite honeycombs for the SCR of NOx with methane," *Catalysis Today*, 107-108 86-93 (2005).

[307]F.C. Patcas, "The methanol-to-olefins conversion over zeolite-coated ceramic foams," *Journal of Catalysis*, 231 [1] 194-200 (2005).

[308]S. Ivanova, B. Louis, B. Madani, J.P. Tessonnier, M.J. Ledoux, and C. Pham-Huu, "ZSM-5 Coatings on b-SiC Monoliths: Possible New Structured Catalyst for the Methanol-to-Olefins Process," *The Journal of Physical Chemistry C*, 111 [11] 4368-74 (2007).

[309]B. Louis, C. Tezel, L. Kiwi-Minsker, and A. Renken, "Synthesis of structured filamentous zeolite materials via ZSM-5 coatings of glass fibrous supports," *Catalysis Today*, 69 [1-4] 365-70 (2001).

[310]W. Schwieger, M. Rauscher, R. Mönnig, F. Scheffler, D. Freude, S. Abdelhamid, and J. Mietek, "Supported Crystallization of MFI- and FER-type Molecular Sieves on Porous Glasses," pp. 121-30 in Studies in Surface Science and Catalysis, Vol. Volume 129. Edited. Elsevier, 2000.

[311]A. Zampieri, P. Colombo, G.T.P. Mabande, T. Selvam, W. Schwieger, and F. Scheffler, "Zeolite Coatings on Microcellular Ceramic Foams: A Novel Route to Microreactor and Microseparator Devices," *Advanced Materials*, 16 [9-10] 819-23 (2004).

[312]Y.-Y. Wang, G.-Q. Jin, and X.-Y. Guo, "Growth of ZSM-5 coating on biomorphic porous silicon carbide derived from durra," *Microporous and Mesoporous Materials*, 118 [1-3] 302-6 (2009).

[313]Q. Lei, T. Zhao, F. Li, Y. Wang, and M. Zheng, "Fabrication of Hierarchically Structured Monolithic Silicalite-1 through Steam-assisted Conversion of Macroporous Silica Gel," *Chemistry Letters*, 35 [5] 490-1 (2006).

[314]Q. Lei, T. Zhao, F. Li, Y. Wang, and L. Hou, "Zeolite beta monoliths with hierarchical porosity by the transformation of bimodal pore silica gel," *Journal of Porous Materials*, 15 [6] 643-6 (2008).

[315]L. Huerta, J. El Haskouri, D. Vie, M. Comes, J. Latorre, C. Guillem, M.D. Marcos, R. Martinez-Manez, A. Beltran, D. Beltran, and P. Amoros, "Nanosized Mesoporous Silica Coatings on Ceramic Foams: New Hierarchical Rigid Monoliths," *Chemistry of Materials*, 19 [5] 1082-8 (2007).

[316]T. Vergunst, M.J.G. Linders, F. Kapteijn, and J.A. Moulijn, "Carbon-based monolithic structures," *Catalysis Reviews: Science and Engineering*, 43 [3] 291 - 314 (2001).

[317]J.A. Alcañiz-Monge, D. Cazorla-Amorós, A. Linares-Solano, E. Morallón, and J. Vázquez, "Preparation of conductive carbon-ceramic composites from coal tar pitch and ceramic monoliths," *Carbon*, 36 [7-8] 1003-9 (1998).

[318]T. Vergunst, F. Kapteijn, and J.A. Moulijn, "Preparation of carbon-coated monolithic supports," *Carbon*, 40 [11] 1891-902 (2002).

[319]T. Valdés-Solís, G. Marbán, and A.B. Fuertes, "Preparation of microporous carbon-ceramic cellular monoliths," *Microporous and Mesoporous Materials*, 43 [1] 113-26 (2001).

[320]A.F. Pérez-Cadenas, F. Kapteijn, J.A. Moulijn, F.J. Maldonado-Hódar, F. Carrasco-Marín, and C. Moreno-Castilla, "Pd and Pt catalysts supported on carbon-coated monoliths for low-temperature combustion of xylenes," *Carbon*, 44 [12] 2463-8 (2006).

[321]A.F. Pérez-Cadenas, M.M.P. Zieverink, F. Kapteijn, and J.A. Moulijn, "Selective hydrogenation of fatty acid methyl esters on palladium catalysts supported on carbon-coated monoliths," *Carbon*, 44 [1] 173-6 (2006).

[322]E. Garcia-Bordeje, M.J. Lazaro, R. Moliner, J.F. Galindo, J. Sotres, and A.M. Baro, "Structure of vanadium oxide supported on mesoporous carbon-coated monoliths and relationship with its catalytic performance in the SCR of NO at low temperatures," *Journal of Catalysis*, 223 [2] 395-403 (2004).

[323]A.F. Pérez-Cadenas, S. Morales-Torres, F. Kapteijn, F.J. Maldonado-Hódar, F. Carrasco-Marín, C. Moreno-Castilla, and J.A. Moulijn, "Carbon-based monolithic supports for palladium catalysts: The role of the porosity in the gas-phase total combustion of m-xylene," *Applied Catalysis B: Environmental*, 77 [3-4] 272-7 (2008).

[324]E. Garcia-Bordeje, F. Kapteijn, and J.A. Moulijn, "Preparation and characterisation of carbon-coated monoliths for catalyst supports," *Carbon*, 40 [7] 1079-88 (2002).

[325]K.P. Gadkaree, "Carbon honeycomb structures for adsorption applications," *Carbon*, 36 [7-8] 981-9 (1998).

[326]K.M. de Lathouder, T. Marques Fló, F. Kapteijn, and J.A. Moulijn, "A novel structured bioreactor: Development of a monolithic stirrer reactor with immobilized lipase," *Catalysis Today*, 105 [3-4] 443-7 (2005).

[327]K.M. de Lathouder, D. Lozano-Castelló, A. Linares-Solano, F. Kapteijn, and J.A. Moulijn, "Carbon coated monoliths as support material for a lactase from Aspergillus oryzae: Characterization and design of the carbon carriers," *Carbon*, 44 [14] 3053-63 (2006).

[328]K.M. de Lathouder, J. Bakker, M.T. Kreutzer, F. Kapteijn, J.A. Moulijn, and S.A. Wallin, "Structured reactors for enzyme immobilization: advantages of tuning the wall morphology," *Chemical Engineering Science*, 59 [22-23] 5027-33 (2004).

[329]E.A. Dawson, P.A. Barnes, and M.J. Chinn, "Preparation and characterisation of carbon-coated ceramic foams for organic vapour adsorption," *Carbon*, 44 [7] 1189-97 (2006).

[330]F.J. Maldonado-Hodar, S. Morales-Torres, F. Ribeiro, E.R. Silva, A.F. Perez-Cadenas, F. Carrasco-Marin, and F.A.C. Oliveira, "Development of Carbon Coatings for Cordierite Foams: An Alternative to Cordierite Honeycombs," *Langmuir*, 24 [7] 3267-73 (2008).

[331]B. Schimmoeller, H. Schulz, S.E. Pratsinis, A. Bareiss, A. Reitzmann, and B. Kraushaar-Czarnetzki, "Ceramic foams directly-coated with flame-made V2O5/TiO2 for synthesis of phthalic anhydride," *Journal of Catalysis*, 243 [1] 82-92 (2006).

[332]E. Garcia-Bordeje, I. Kvande, D. Chen, and M. Ronning, "Carbon Nanofibers Uniformly Grown on γ-Alumina Washcoated Cordierite Monoliths," *Advanced Materials*, 18 [12] 1589-92 (2006).

[333]E. Garcia-Bordeje, I. Kvande, D. Chen, and M. Ronning, "Synthesis of composite materials of carbon nanofibres and ceramic monoliths with uniform and tuneable nanofibre layer thickness," *Carbon*, 45 [9] 1828-38 (2007).

[334]M.A. Ulla, A. Valera, T. Ubieto, N. Latorre, E. Romeo, V.G. Milt, and A. Monzón, "Carbon nanofiber growth onto a cordierite monolith coated with Co-mordenite," *Catalysis Today*, 133-135 7-12 (2008).

[335]B. Gong, R. Wang, B. Lin, F. Xie, X. Yu, and K. Wei, "Preparation of Carbon Nanotubes (CNTs)-Cordierite Monoliths by Catalytic Chemical Vapor Deposition as Catalyst Supports for Ammonia Synthesis," *Catalysis Letters*, 122 [3] 287-94 (2008).

[336]J. Wang, R. Wang, X. Yu, J. Lin, F. Xie, and K. Wei, "Preparation and Characterization of Carbon Nanotubes-Coated Cordierite for Catalyst Supports," *Journal of Natural Gas Chemistry*, 15 [3] 211-6 (2006).

[337]D.D. Jayaseelan, W.E. Lee, D. Amutharani, S. Zhang, K. Yoshida, and H. Kita, "In Situ Formation of Silicon Carbide Nanofibers on Cordierite Substrates," *Journal of the American Ceramic Society*, 90 [5] 1603-6 (2007).

[338]S. Rul, C. Laurent, A. Peigney, and A. Rousset, "Carbon nanotubes prepared in situ in a cellular ceramic by the gelcasting-foam method," *Journal of the European Ceramic Society*, 23 [8] 1233-41 (2003).

[339]A. Cordier, F. Rossignol, C. Laurent, T. Chartier, and A. Peigney, "A new fast method for ceramic foam impregnation: Application to the CCVD synthesis of carbon nanotubes," *Appl. Catal. A: General*, 319 7-13 (2007).

[340]V.G. de Resende, E. De Grave, A. Cordier, A. Weibel, A. Peigney, and C. Laurent, "Catalytic chemical vapor deposition synthesis of single- and double-walled carbon nanotubes from α-(Al1-xFex)2O3 powders and self-supported foams," *Carbon*, 47 [2] 482-92 (2009).

[341]A. Cordier, E. Flahaut, C. Viazzi, C. Laurent, and A. Peigney, "In situ CCVD synthesis of carbon nanotubes within a commercial ceramic foam," *Journal of Materials Chemistry*, 15 [37] 4041-50 (2005).

[342]P.W.A.M. Wenmakers, J.v.d. Schaaf, B.F.M. Kuster, and J.C. Schouten, ""Hairy Foam": carbon nanofibers grown on solid carbon foam. A fully accessible, high surface area, graphitic catalyst support," *Journal of Materials Chemistry*, 18 [21] 2426-36 (2008).

[343]S. Mukhopadhyay, M., A. Karumuri, and I.T. Barney, "Hierarchical nanostructures by nanotube grafting on porous cellular surfaces," *Journal of Physics D: Applied Physics*, 42 [19] 195503, 9pp (2009).

[344]E. Vanhaecke, S. Ivanova, A. Deneuve, O. Ersen, D. Edouard, G. Wine, P. Nguyen, C. Pham, and C. Pham-Huu, "1D SiC decoration of SiC macroscopic shapes for filtration devices," *Journal of Materials Chemistry*, 18 [39] 4654-62 (2008).

[345]D. Edouard, S. Ivanova, M. Lacroix, E. Vanhaecke, C. Pham, and C. Pham-Huu, "Pressure drop measurements and hydrodynamic model description of SiC foam composites decorated with SiC nanofiber," *Catalysis Today*, 141 [3-4] 403-8 (2009).

[346]A. Berger, E. Pippel, J. Woltersdorf, M. Scheffler, P. Cromme, and P. Greil, "Nanoprocesses in polymer-derived Si-O-C ceramics: Electronmicroscopic observations and reaction kinetics," *Physica Status Solidi A*, 202 [12] 2277-86 (2005).

[347]S. Zhu, H.-A. Xi, Q. Li, and R. Wang, "In Situ Growth of b-SiC Nanowires in Porous SiC Ceramics," *Journal of the American Ceramic Society*, 88 [9] 2619-21 (2005).

[348]X. Yao, S. Tan, Z. Huang, S. Dong, and D. Jiang, "Growth mechanism of b-SiC nanowires in SiC reticulated porous ceramics," *Ceramics International*, 33 [6] 901-4 (2007).

[349]C. Vakifahmetoglu and P. Colombo, "Porous Polymer Derived Ceramics Decorated with In-situ Grown Nano-structures," in Proceedings of Pac-Rim 8, *Ceramic Transactions.* Edited, Vancouver, Canada, in press, 2009.

[350]C. Vakifahmetoglu, E. Pippel, J. Woltersdorf, and P. Colombo, "Growth of 1D-Nanostructures in Porous Polymer Derived Ceramics by Catalyst-Assisted-Pyrolysis. Part I: Iron Catalyst," *Journal of the American Ceramic Society*, (In press, 2009).

[351]C. Vakifahmetoglu, S. Carturan, E. Pippel, J. Woltersdorf, and P. Colombo, "Growth of 1D-Nanostructures in Porous Polymer Derived Ceramics by Catalyst-Assisted-Pyrolysis. Part II: Cobalt Catalyst," (manuscript in preparation).

[352]H. Moawad, M. M. and H. Jain, "Creation of Nano-Macro-Interconnected Porosity in a Bioactive Glass-Ceramic by the Melt-Quench-Heat-Etch Method," *Journal of the American Ceramic Society*, 90 [6] 1934-6 (2007).

[353]H. Moawad and H. Jain, "Development of nano-macroporous soda-lime phosphofluorosilicate bioactive glass and glass-ceramics," *Journal of Materials Science: Materials in Medicine*, 20 [7] 1409-18 (2009).

[354]A.M. Wilson, G. Zank, K. Eguchi, W. Xing, B. Yates, and J.R. Dahn, "Pore Creation in Silicon Oxycarbides by Rinsing in Dilute Hydrofluoric Acid," *Chemistry of Materials*, 9 [10] 2139-44 (1997).

[355]R. Pena-Alonso, G.D. Soraru, and R. Raj, "Preparation of Ultrathin-Walled Carbon-Based Nanoporous Structures by Etching Pseudo-Amorphous Silicon Oxycarbide Ceramics," *Journal of the American Ceramic Society*, 89 2473-80 (2006).

[356]H.E. Thomas, "Selective Leaching of Extruded Cordierite Honeycomb Structures," pp. 40-51 in Applications of Refractories: Ceramic Engineering and Science Proceedings. Edited by S. William, 1986.

[357]Y. Gogotsi, A. Nikitin, H. Ye, W. Zhou, J.E. Fischer, B. Yi, H.C. Foley, and M.W. Barsoum, "Nanoporous carbide-derived carbon with tunable pore size," *Nature Materials*, 2 [9] 591-4 (2003).

[358]S.-H. Yeon, P. Reddington, Y. Gogotsi, J.E. Fischer, C. Vakifahmetoglu, and P. Colombo, "Carbide-Derived-Carbons with Hierarchical Porosity from a Preceramic Polymer," *Carbon*, 48 [1] 201-10 (2010).

[359]P. Krawiec, C. Schrage, E. Kockrick, and S. Kaskel, "Tubular and Rodlike Ordered Mesoporous Silicon (Oxy)carbide Ceramics and their Structural Transformations," *Chemistry of Materials*, 20 [16] 5421-33 (2008).

[360]P. Krawiec, E. Kockrick, L. Borchardt, D. Geiger, A. Corma, and S. Kaskel, "Ordered Mesoporous Carbide Derived Carbons: Novel Materials for Catalysis and Adsorption," *The Journal of Physical Chemistry C*, 113 [18] 7755-61 (2009).

[361]A. Taguchi, J.H. Smått, and M. Lindén, "Carbon Monoliths Possessing a Hierarchical, Fully Interconnected Porosity," *Advanced Materials*, 15 [14] 1209-11 (2003).

[362]Z.-G. Shi, Y.-Q. Feng, L. Xu, S.-L. Da, and M. Zhang, "Synthesis of a carbon monolith with trimodal pores," *Carbon*, 41 [13] 2677-9 (2003).

[363]L.-Y. Xu, Z.-G. Shi, and Y.-Q. Feng, "Preparation of a carbon monolith with bimodal perfusion pores," *Microporous and Mesoporous Materials*, 115 [3] 618-23 (2008).

[364]K. Nakanishi, "Pore Structure Control of Silica Gels Based on Phase Separation," *Journal of Porous Materials*, 4 [2] 67-112 (1997).

[365]J. Konishi, K. Fujita, K. Nakanishi, and K. Hirao, "Monolithic TiO2 with Controlled Multiscale Porosity via a Template-Free Sol-Gel Process Accompanied by Phase Separation," *Chemistry of Materials*, 18 [25] 6069-74 (2006).

[366]J. Konishi, K. Fujita, K. Nakanishi, K. Hirao, K. Morisato, S. Miyazaki, and M. Ohira, "Sol-gel synthesis of macro-mesoporous titania monoliths and their applications to chromatographic separation media for organophosphate compounds," *Journal of Chromatography A*, 1216 [44] 7375-83 (2009).

[367]J. Konishi, K. Fujita, S. Oiwa, K. Nakanishi, and K. Hirao, "Crystalline ZrO2 Monoliths with Well-Defined Macropores and Mesostructured Skeletons Prepared by Combining the Alkoxy-Derived Sol-Gel Process Accompanied by Phase Separation and the Solvothermal Process," *Chemistry of Materials*, 20 [6] 2165-73 (2008).

[368]A. Collins, D. Carriazo, S.A. Davis, and S. Mann, "Spontaneous template-free assembly of ordered macroporous titania," *Chemical Communications*, [5] 568-9 (2004).

[369]A. Leonard and B.-L. Su, "A novel and template-free method for the spontaneous formation of aluminosilicate macro-channels with mesoporous walls," *Chemical Communications*, [14] 1674-5 (2004).

[370]T.-Z. Ren, Z.-Y. Yuan, and B.-L. Su, "Thermally stable macroporous zirconium phosphates with supermicroporous walls: a self-formation phenomenon of hierarchy," *Chemical Communications*, [23] 2730-1 (2004).

[371]D.C. Hoth, J.G. Rivera, and L.A. Colón, "Metal oxide monolithic columns," *Journal of Chromatography A*, 1079 [1-2] 392-6 (2005).

[372]S. Backlund, J.-H. Smatt, J.B. Rosenholm, and M. Linden, "Template-Free Sol-Gel Synthesis of Hierarchically Macro- and Mesoporous Monolithic TiO2," *Journal of Dispersion Science and Technology*, 28 [1] 115 - 9 (2007).

[373]J.-H. Smatt, B. Spliethoff, J.B. Rosenholm, and M. Linden, "Hierachically porous nanocrystalline cobalt oxide monoliths through nanocasting," *Chemical Communications*, [19] 2188-9 (2004).

CHAPTER III

PRODUCTION AND PROPERTIES OF POLYMER DERIVED CELLULAR CERAMICS

The main aim of the present chapter is to investigate new processing techniques for the fabrication of porous polymer derived ceramics (PDCs), especially the ones having more than 60vol% of total porosity; i.e. cellular ceramics. For that initially, macro-porous SiOC ceramics were produced by using commercial polysiloxanes having different characteristics. Then, in order to improve those ceramics (in particular with respect to the mechanical strength and pore characteristics), particle based processes utilizing the same or different types of precursors were explored to form porous SiOC(N) ceramics. Successive experiments have been applied to produce porous SiCN ceramics. For this, both templates and blowing agent have been used in order to introduce porosity. While templating resulted in micro-cellular Si(O)CN ceramic foams, blowing agent let to obtain macro-cellular SiCN with a negligible oxygen contamination. In a similar fashion, in the last part of this chapter porous SiOBC and microcellular SiBCN ceramics have been produced by polymer blending and templating approach, respectively. In the following subsections; the results of the pyrolysis experiments are provided in a sequential order.

3.1. Direct Fabrication of Macro-Porous SiOC Ceramics

Published in part in: C. Vakifahmetoglu and P. Colombo, "A Direct Method for the Fabrication of Macro-Porous SiOC Ceramics from Preceramic Polymers," Adv. Eng. Mater., 10[3] 256-259 (2008).

3.1.1. Introduction

Cellular ceramics, possessing both open or closed porosity, find use in several demanding engineering applications because of their favorable set of properties.[1] Several processing methods have been proposed for their fabrication, including the replication of the structure of polymeric foams, direct blowing, the use of sacrificial fillers, extrusion through special dies (for honeycombs), solid freeform techniques, the mimicking of natural templates (e.g. wood) or the assemblage of fibers or hollow bodies, see Chapter 2.3.1 for more details on cellular ceramcs.

Preceramic polymers, in particular silicones, have been successfully used for obtaining ceramic components (such as foams and membranes) possessing a large amount of porosity, in the micro-, meso- and macro-size scale.[2, and references therein] However, some of the fabrication methods have some limitations: for instance, direct foaming techniques often lead to a gradient in the porosity amount and pore size along the main expansion axis;[3, 4] the infiltration of a silicone resin within organic sacrificial fillers requires a burn out step that has to be carried out in a very controlled fashion in order to produce components without defects (besides often requiring warm pressing – depending on the rheological characteristics of the preceramic polymer – to obtain a well controlled morphology), thus limiting the size and shape of the component that can be produced;[5] the use of supercritical CO_2 is regulated by the diffusion within the solid polymer, and works well only for components of limited thickness.[6] In recent years, it has been shown that blending preceramic polymers with different characteristics (molecular weight, molecular architecture, ceramic yield) allows to produce cellular ceramics.[7, 8] In the present study we further explore this possibility, with the specific aim of directly developing a large amount of porosity within the resulting ceramic body during a one-pot pyrolysis treatment.

3.1.2. Experimental Details

As precursors for the production of macro-porous ceramics, three types of commercially available silicone polymers were used; a liquid silicone elastomer comprising component A, poly(methyl-vinyl-siloxane) together with ~8mg/kg platinum and component B, poly(methyl-hydrogenosiloxane) (RTV 141A and RTV 141B, respectively, Rhone-Poulenc, Lyon, France),

and two solid polysiloxanes: a poly(methyl-siloxane) (PMS), and a poly(methyl-phenyl-siloxane) (PMPS), (respectively MK and H44, Wacker AG, Germany). Pure poly(dimethyl-siloxane) samples (PDMS) were obtained by mixing the two components in a ratio suggested by the manufacturer (10/1 wt% RTV 141A / RTV 141B). Component A contains Si-vinyl groups, while component B has Si-H groups, so the crosslinking is carried out through a catalyzed (due to platinum) hydrosilylation reaction, see Chapter 2.1.1.2 for more details on silicone elastomers. Other samples were produced by separately adding to the pure PDMS either one of the two silicone resins (PMS-MK or PMPS-H44) in varying amount (see **Table 3.1-1** for the sample compositions and legenda). After pouring oil A (10 parts) in a Pyrex dish, finely ground PMS or PMPS was added at room temperature followed by the addition of oil B (1 part). After that, the blend was thoroughly mixed for 20 min by hand and then put into an oven at 90ºC for 4 hours for curing. Samples with a diameter of 4 cm and a thickness of about 1 cm were produced. Then, the crosslinked specimens were removed from the Pyrex dish (aluminum foil or Teflon based molds can also be used) and cut into desired pieces for pyrolysis, which was carried out for 2h at 1200°C in an alumina tube furnace in the presence of flowing N_2 gas (1 atm; heating rate 2°C/min). For some additional experiments azodicarbonamide (ADA) (Merck, Germany) a physical blowing agent was also incorporated to enhance the total porosity via following curing at ~200°C/4h in air and pyrolysis at 1200°C/2h in N_2 (Carbolite 1200 tube furnace with alumina tube is used for all experiments).

Table 3.1-1. Compositions (wt%) of the green (not pyrolyzed) samples prepared by blending the different silicone precursors (PDMS, PMS and PMPS).

Sample Label	PDMS (RTV 141)	PMS (MK)	PMPS (H44)	ADA
PS0	100	-	-	-
PM1	40	60	-	-
PM2	50	50	-	-
PM3	60	40	-	-
PM4	70	30	-	-

PM5	80	20	-	-
PH1	40	-	60	-
PH2	50	-	50	-
PH3	60	-	40	-
PH4	70	-	30	-
PH5	80	-	20	-
PSA1	99	-	-	1
PSA2	57.5	37.5	-	5
PSA3	57.5	-	37.5	5

Crosslinked samples were subjected to thermogravimetric analysis to 1500ºC (TGA, STA 409, Netzsch GmbH, Selb, Germany; 5ºC/min, flowing N_2). The microstructural features were evaluated from fracture surfaces by scanning electron microscope (SEM, Stereoscan 250, Cambridge Inst., Cambridge, UK). SEM images were subsequently analyzed with the ImageTool software (UTHSCSA, University of Texas, USA) to determine the size of the cells. Bulk densities were calculated as the mass of dry weight divided by the sample volume, and the true density of the SiOC ceramic material, was measured using a pycnometer. The amount of open/closed porosity was assessed using the data obtained by the Archimedes method, using xylene as the infiltrating medium, coupled with the bulk and true density values for the ceramic components.

3.1.3. Results and Discussion

The conversion process from the crosslinked polymeric state to a monolithic porous amorphous ceramic body occurred mainly in two distinct temperature stages (< 450°C, low temperature zone, and > 450°C, high temperature zone). This is apparent from **Figure 3.1-1** (a) and (b), which includes the weight loss data for the samples of pure PDMS, PMS and PMPS. As already shown by Scheffler et al.[9], between 100°C and 420°C only crosslinking products (water, alcohols) and oligomers are released from the PMS (MK) and PMPS (H44) polymers, and this is

in a good agreement with our results. In this temperature range, pure PDMS did not lose any of its weight up to roughly 350°C, where it started to decompose by releasing cyclic silicone oligomers as gaseous volatiles (mainly hexamethylcyclotrisiloxane).[10, 11] As seen in **Figure 3.1-1** (a) that the pyrolytic decomposition of PDMS was completed at ~450°C. Therefore, it can be concluded that during the first stage of pyrolysis of the blends (T < 450°C) only decomposition of PDMS and dehydrogenation and evaporation of the low molecular weight species from PMS or PDMS took place.[9, 12, 13] In the second stage of pyrolysis, variations were chiefly due to the polymer-to-ceramic transformation of PMS and PMPS (starting temperature for PMS ~550°C; for PMPS ~450°C) corresponding to the mineralization process. It was demonstrated previously by several authors that during organic to inorganic conversion between 500°C and 900°C, cleavage and reorganization of various bonds (Si-CH_3, Si-C_6H_5, Si-H, Si-CH_2-Si, etc.), leading to dehydrogenation occur.[12-16] As it can be seen from **Figure 3.1-1**, increasing the PDMS amount in the blends led to an increase in the total weight loss in comparison to the pure silicone resin, which is proportional to the amount of PDMS present and can of course be attributed to the lower ceramic yield of the PDMS. The large difference in weight loss between PDMS and PMS (or PMPS) is mainly due to the molecular architecture of the silicone precursors (not to the starting molecular weight, as the components were crosslinked before pyrolysis), which strongly affects their decomposition and thus the ceramic yield.[17-20] PDMS has a linear structure, while PMS and PMPS possess a much more complex, cage-like or partial ladder structure (hence the latter are properly termed poly(silsesquioxanes) or silicone resins, see Chapter 2.1.1.3 for more details of silicone resins).[21] The same trend was also observed in the PDMS-PMPS system (see **Figure 3.1-1**(b)), however with a higher total weight loss for samples with the same concentration of PMDS. Interestingly, there seems to be an effect of the mixing of the PDMS with the PMS or PMPS, as shown by the fact that the weight loss in blends starts only above ~400°C, suggesting an influence on the crosslinking behavior of the silicone resins. Detailed FT-IR studies need to be conducted to further elucidate this point but this is out of the scope of this thesis study.

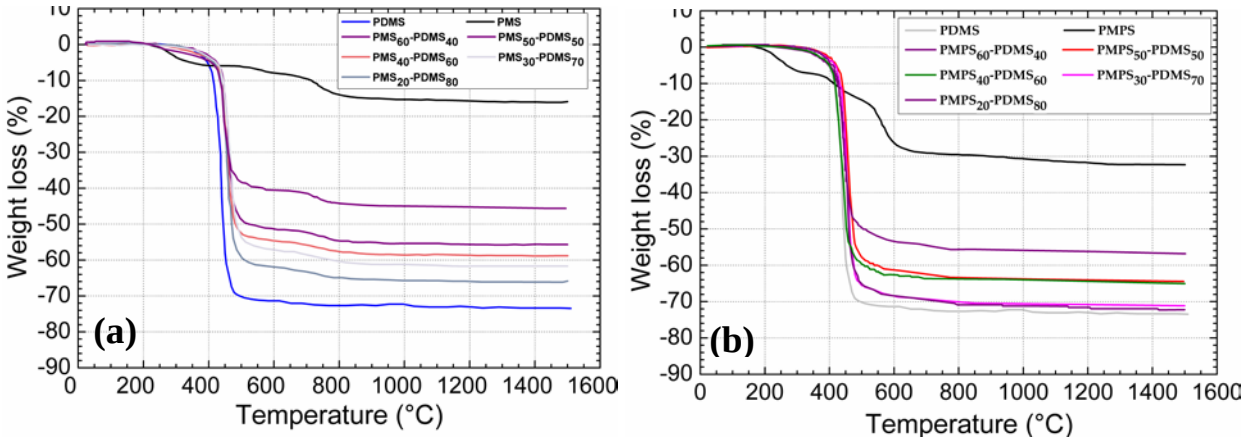

Figure 3.1-1. Weight loss for the a) PDMS-PMS (RTV-MK) system, and b) PDMS-PMPS (RTV-H44) system. Analyses performed in N_2.

Obviously, associated with the weight loss at T> ~500°C is the simultaneous release of gases, as well as three-dimensional shrinkage. The gases are mainly comprised of methane or benzene, depending on the composition of the starting precursor, with C_6H_6 and CH_4 release peaking respectively at ~600°C and ~750°C.[9, 12] It is these concurrent factors (different ceramic yield, release of gases and differential shrinkage), that lead to the development of a large amount of (macro-)porosity in the ceramized samples. All these factors occur more strongly in the polysiloxane with a linear structure than for the silicone resins, and we can therefore state that PDMS can be used as a sort of "sacrificial filler"[5, 22] for the creation of a network of pores when mixed with silicone resins. The amount of total (open and closed) porosity in the samples indeed depends directly on the amount of PDMS in the blend (see **Figure 3.1-2**), evidently more linearly for PMPS (correlation coefficient for linear fitting = 0.9539) than for PMS (correlation coefficient for linear fitting = 0.8684). The observed difference in total porosity among components containing one or the other polysilsesquioxane is certainly related to their different ceramic yield, although we cannot exclude for the PMPS resin a contribution deriving from its tendency to form porous bodies by self-foaming during curing or pyrolysis.[23]

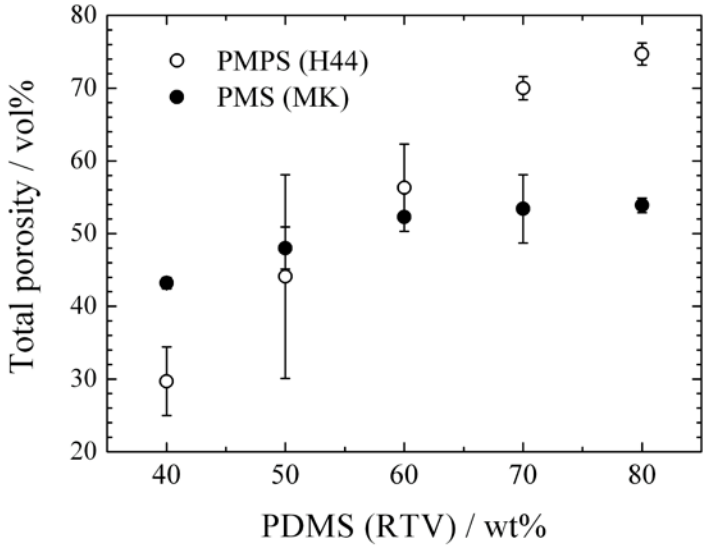

Figure 3.1-2. Total porosity vs. amount of PDMS for both system (PMS and PMPS). Samples pyrolyzed at 1200°C in N_2.

The data for the closed and open porosity are shown in **Figure 3.1-3**. The wide standard deviation in the measured values indicates a limited microstructural homogeneity within the produced components (various pieces coming from the same sample were measured to give each data point in the plots). There does not seem to be a significant influence of the type of polysilsesquioxane precursor used on the amount of closed or open porosity present in the final porous ceramic.

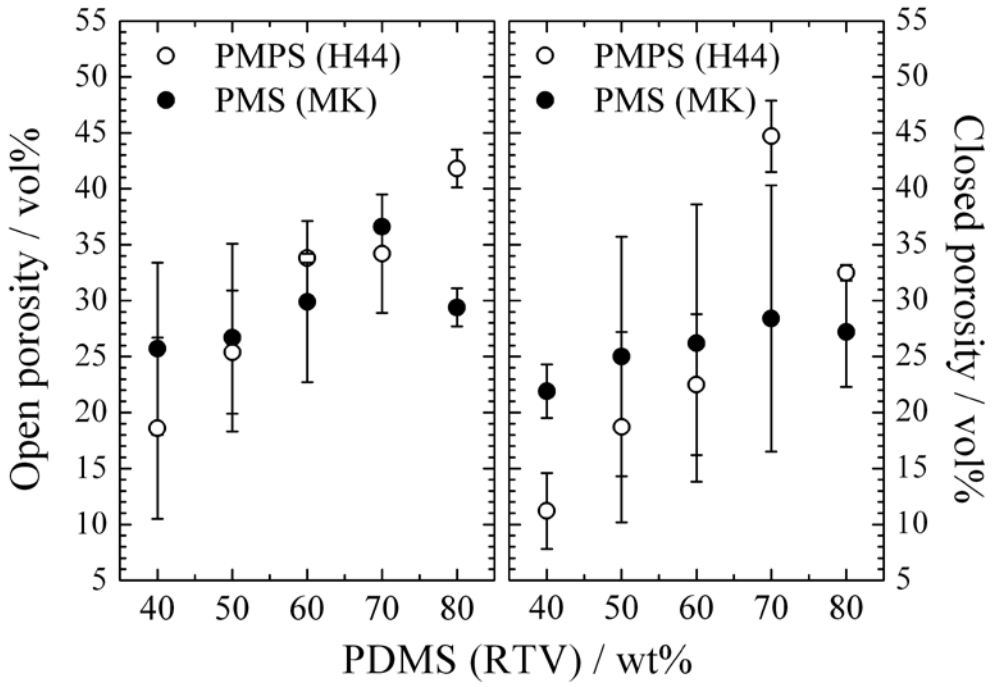

Figure 3.1-3. Open and closed porosity vs. amount of PDMS for both system (PMS and PMPS). Samples pyrolyzed at 1200°C in N_2.

SEM investigations applied on the green samples (see **Figure 3.1-4** (a&b)) show the presence of two separate polymeric phases, seemingly with the PDMS constituting a continuous matrix and the PMS (or PMPS) phase contained within discrete particles (see later slightly higher amount of carbon observed in the EDS data taken over the particle). EDS data taken from both matrix and particulates showed almost the same composition including only Si, O, and C (see **Figure 3.1-4** (c&d), Au peaks are due to gold coating applied on the samples for SEM observations).

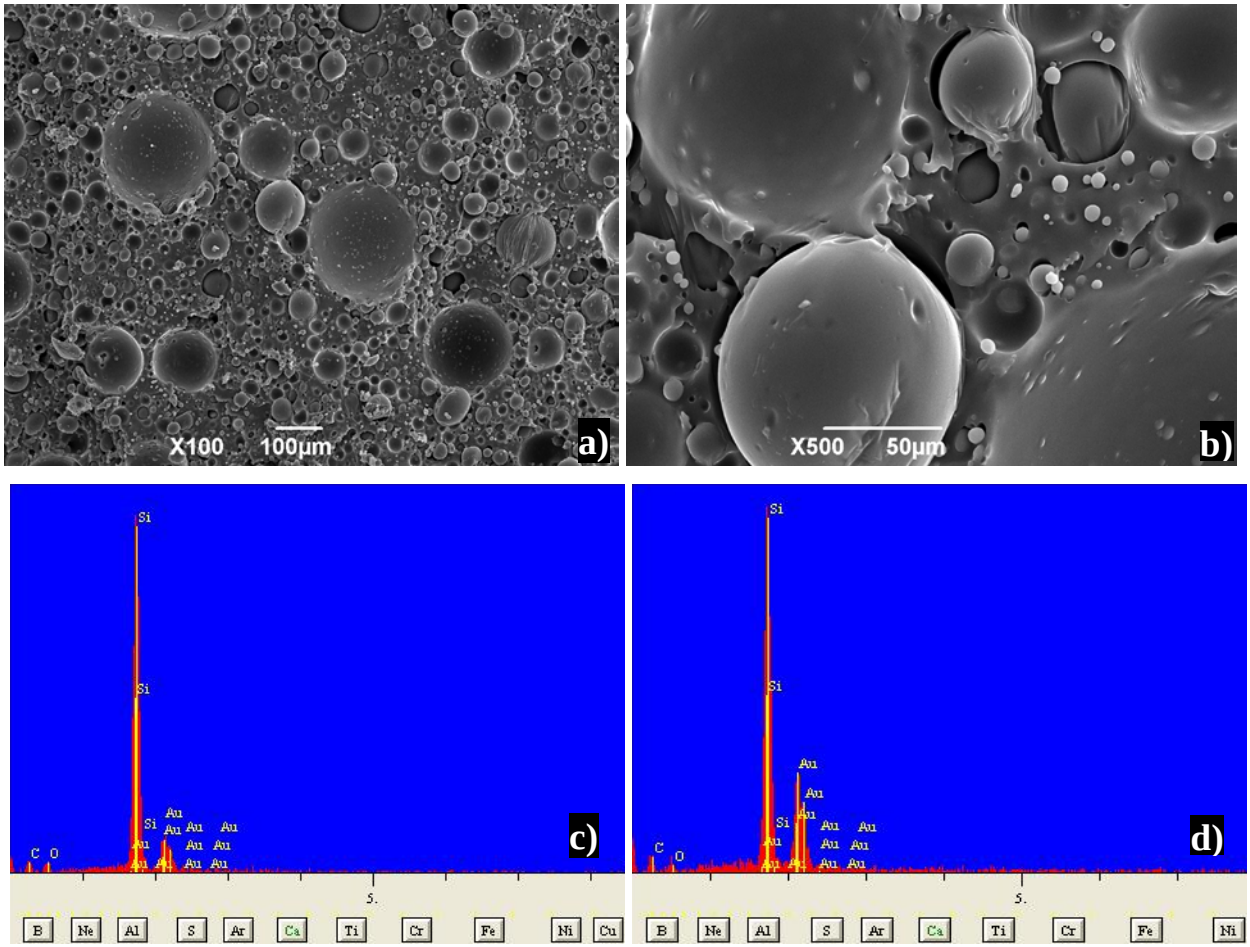

Figure 3.1-4. a&b) SEM images taken from the fracture surfaces of green samples, 90°C/12h cured thermoset of representative sample (PH2). EDX analyses given in c) taken from the continuous phase (matrix), and d) from the particles.

Micrographs showing the morphology of the fracture surface of different samples are reported in **Figure 3.1-5** (a-d) and **Figure 3.1-6** (a-b). A large amount of porosity was formed in all the samples, mostly of it apparently interconnected, with pores homogeneously distributed in the entire volume of the pyrolyzed ceramic monoliths. The specimens possessed a quite complex morphology, as was the case for samples obtained using a similar fabrication procedure which were investigated in previous studies.[7, 8] In addition to large cells of a few hundred microns in size (up to about 600 µm), a large amount of smaller, micron sized pores (~5 µm) and cavities were present. Interestingly, the increase in the PDMS amount in the blends did not seem to significantly affect the mean pore size for both systems (PMS and PMPS).

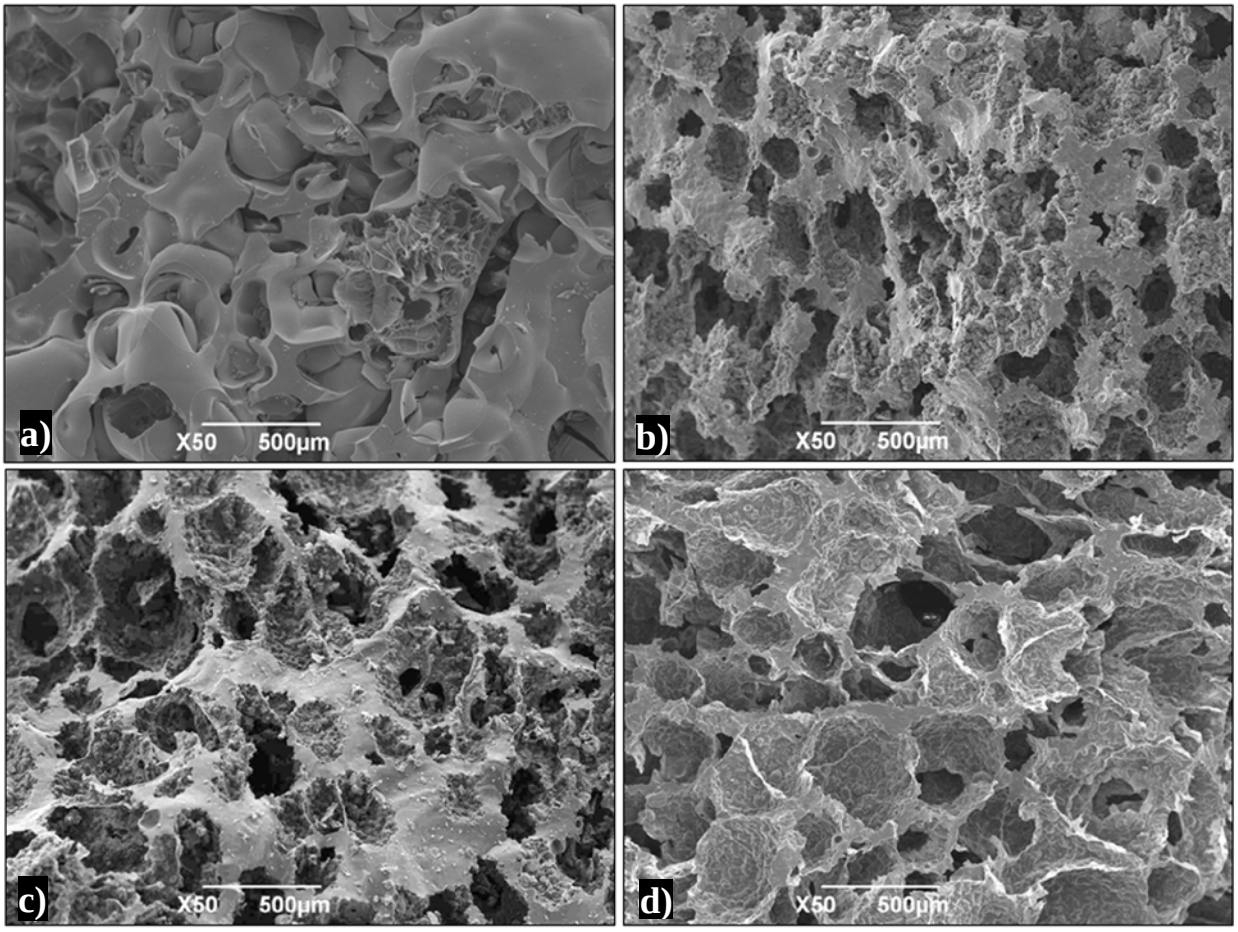

Figure 3.1-5. SEM micrographs taken from the fracture surfaces of samples: a) PS0 (90°C cured, 100wt% PDMS), b) PM2 (50wt% PDMS-50wt% PMS), c) PM3 (60wt% PDMS-40wt% PMS), and d) PM4 (70wt% PDMS-30wt% PMS). Samples pyrolyzed at 1200°C in N_2.

Furthermore, no specific influence of the silicone resin precursor (PMS or PMPS) on the general morphology of the macro-porosity was observed. It has to be noted that the presence in cellular ceramics of porosity with a non homogeneous size distribution does not particularly represent a problem, as several important properties (in particular mechanical properties) are linked to the relative density of the component (i.e. the total amount of porosity) and not to the cell size.[24]

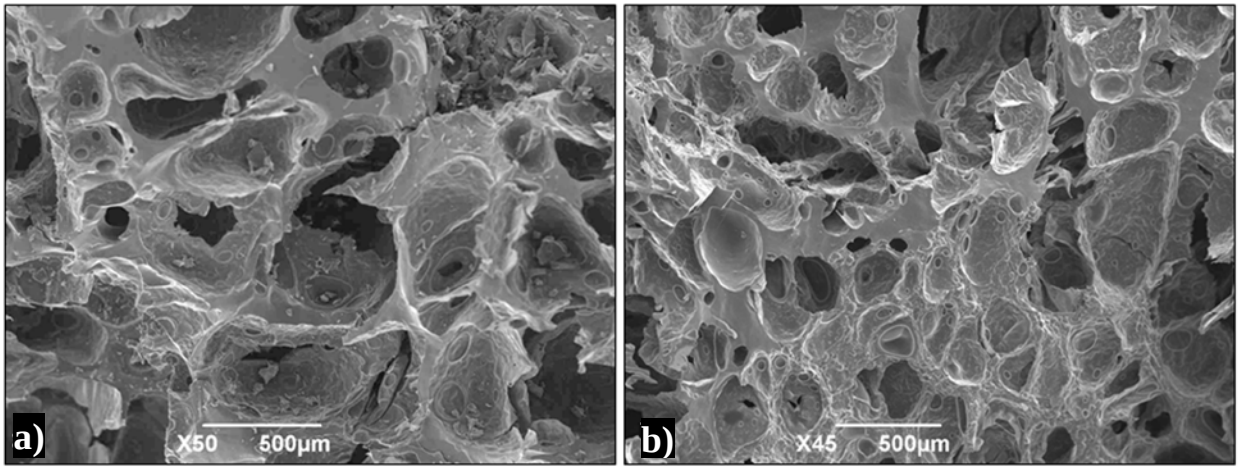

Figure 3.1-6. SEM micrographs taken from the fracture surfaces of samples: a) PH2 (50wt% PDMS-50wt% PMPS), and b) PH3 (60% PDMS-40% PMPS). Samples pyrolyzed at 1200°C in N_2.

While the transient porosity which forms upon pyrolysis in the polymer-to-ceramic conversion temperature interval (roughly 600 to 800°C) is in the micro- and meso- range (< 2 nm and between 2 and 50 nm, respectively), and tends to be removed upon further heating (due to pore shrinkage aided by the formation of active radicals and viscous flow),[25] the macro-porosity generated by this process cannot be eliminated, due to its much larger length scale, and thus remains within the resulting ceramic body. Occasionally, some cracks were observed in the structure of some of the produced porous ceramic monoliths, caused by stresses originating from several factors, including the large volume of gas released and a possible non homogeneous distribution of the two silicone precursors (PDMS and polysilsesquioxane) within the unfired, dense body.

Further investigations have been followed by introducing a physical blowing agent, ADA into this blend system while simultaneously increasing the curing temperature to 200°C. ADA is a powdered yellow compound that decomposes between 210°C[26] and 260°C[27]. The gas yield is about 200-220 mL/min and consists of N_2, CO, CO_2, and some ammonia, (see Chapter 3.3. for more details about the decomposition of ADA). Although it is recommended that a basic ADA should be processed ≥210°C, actual decomposition is thought to begin at lower temperatures.[26]

Moreover, when the decomposition has been initiated, the reaction is exothermic and so self-catalyzing.[26] While ADA is yellow in its basic form, after decomposition the color becomes more neutral. If curing occurs with complete decomposition of ADA, then the color of the cured polysiloxane body generally turns back to white from yellow. However, this is a bit tricky issue since during curing of preceramic polymers a color change is a common phenomena.

Sample compositions and labels made by using ADA are previously given in **Table 3.1-1**. The sample PSA1 (99wt% PDMS-1wt% ADA) after pyrolysis was very weak and as can be seen in **Figure 3.1-7** (a) microstructurally non-homogeneous. This can be attributed to the very low ceramic yield governed by the pyrolysis of PDMS polymer itself.[10, 28] The incorporation of ADA into pure PDMS together with curing at 200°C resulted in a different morphology than that of the pure PDMS (see **Figure 3.1-7** (b)); including higher amount of open porosity throughout matrix. The change in morphology should be related more to the change in crosslinking degree of the precursor than to the decomposition of ADA.

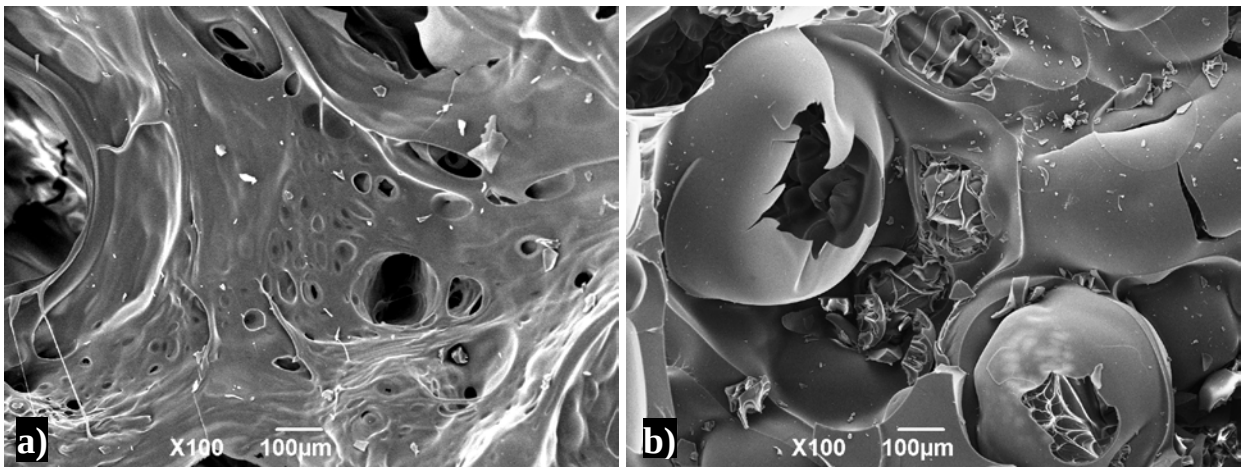

Figure 3.1-7. SEM micrographs taken from the fracture surfaces of samples; a) PSA1 (99wt% PDMS-1wt%ADA, cured at 200°C), b) made from PS0 (100wt% PDMS, cured at 90°C). Samples pyrolyzed at 1200°C in N_2.

The mixed systems (PDMS+PMS+ADA or PDMS+PMPS+ADA) were better resulting in a good structural integrity after pyrolysis at 1200°C. Ceramics made by using PDMS+PMS+ADA

mixtures, see **Figure 3.1-8** (a-b), had almost the same microstructure; open and closed pores distributed in SiOC matrix with some micron size cracks. The sample made by using PDMS-PMS and ADA resulted in a macrocellular component including both open and closed porosity, while the effect of (5wt%) ADA addition does not seem to be profound compared to the SEM images of the samples made without the use of ADA. On the other hand ceramics made from PMPS resulted in flawless structures, see **Figure 3.1-8** (c-d). This could be attributed to the differences in the weight loss, the viscosity during curing and the amount of shrinkage occurred during pyrolysis between these materials since the only parameter changed was the precursor type. In order to select a suitable porogen; time, temperature and the condition of the polymer matrix must all be considered. It is known that if the blowing agent decomposes too fast, the polymer may not be processed to maintain the gas within the matrix. The gas will escape, but the material cannot be foamed in that condition. At the other extreme, the polymer viscosity may be so high that when the blowing agent decomposes, the gas pressure will not be sufficient to cause the polymer to expand even though decomposition has occurred. Therefore, cracks seen in the sample having PMS+PDMS+ADA could be related to the high viscosity of PMS polymer during decomposition of ADA. Additionally, as could be seen from the microstructural differences between **Figure 3.1-8** (b) and (d), blend system including PMPS always showed higher %P compared to PMS made ones which might be explained considering the self-blowing property of PMPS upon curing, i.e. higher volatile release during curing and thermolysis.[4]

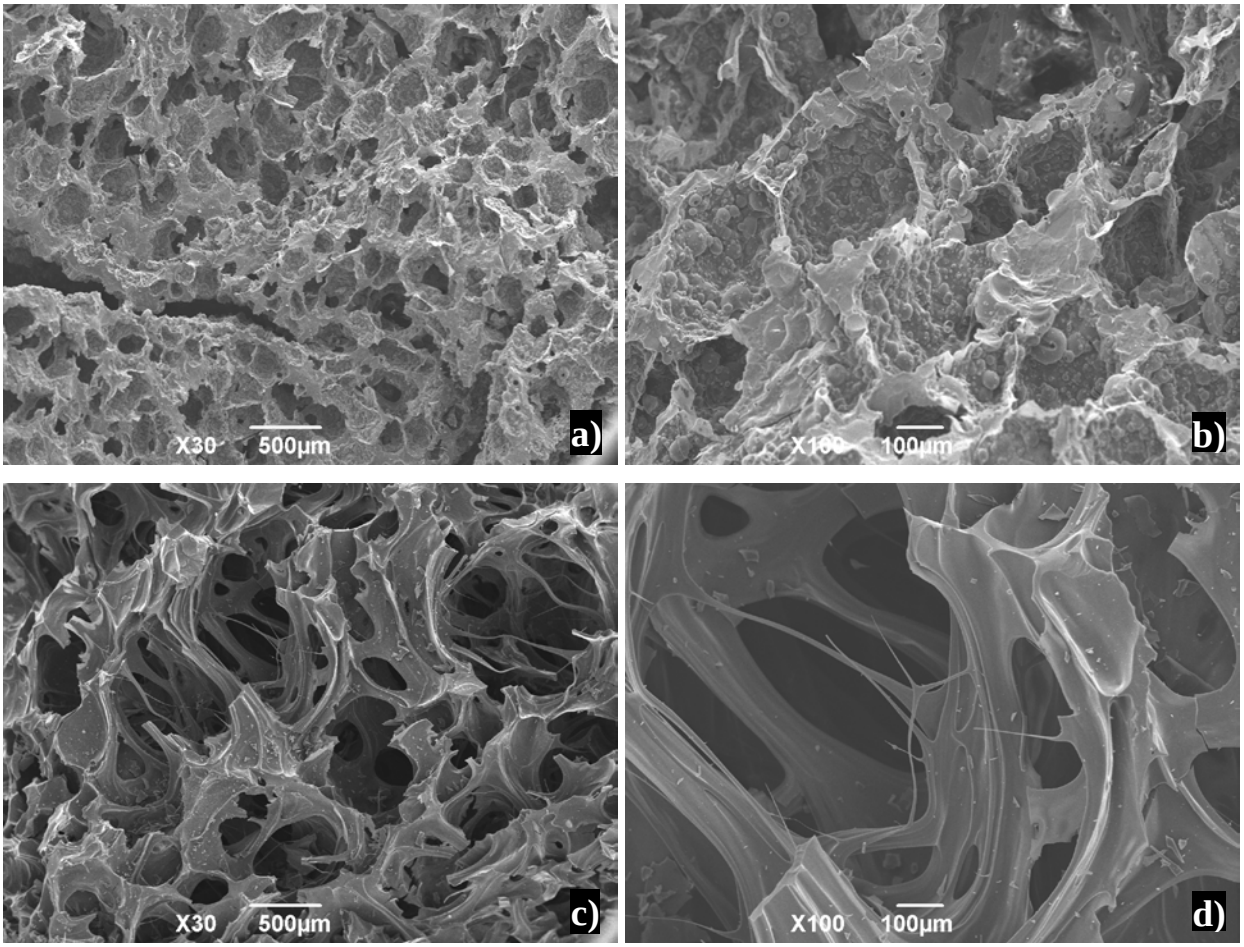

Figure 3.1-8. SEM micrographs taken from the fracture surfaces of samples; a&b) PSA2, c&d) PSA3. Samples pyrolyzed at 1200°C in N_2.

As can be seen from the images, generally speaking, it is possible to say that increasing the ADA amount leads to an increase of the total porosity (%P) and cell size after thermal treatment comparing to the previous samples made without using ADA. However, the increase in curing temperature from 90°C to 200°C might be another possible reason causing the obtained pore characteristic of the pyrolyzed bodies. Therefore, some controlling experiments have been conducted on the samples made by; 50wt%-50wt% PDMS-PMS (or PMPS); with no ADA addition but curing at 200°C and following the remaining procedure similar to previous samples. The results obtained from the SEM analyses are given in **Figure 3.1-9** (a&b) for the sample PM2 (50wt% PDMS-50wt% PMS, 200°C cured), and in **Figure 3.1-9**(c&d) for the sample PH2 (50wt% PDMS-50wt% PMPS, 200°C cured). Comparing the SEM images of the same samples

made with 5wt% ADA addition, it is possible to comment that the samples with no ADA addition are even more homogenous than ones produced with ADA. Flawless samples having high amount of porosity has been obtained. It seems that PMS made blends were not affected from the increase in curing temperature (See **Figure 3.1-5** (b) for the SEM image of the samples prepared at 90°C and **Figure 3.1-9** (a) that of the one cured at 200°C), instead PMPS made system was highly effected from the increase in curing temperature. Interestingly the resulted ceramics showed similar foam like character with 3D interconnected pores compared with the previous samples made from the mixtures of PDMS-PMPS and ADA. Implying that, in the present experimental circumstances the effect of ADA incorporation into precursor mixtures on the pore characteristics of the final components was very limited. That is; foam like character of PMPS made samples are due to both self blowing property of the used precursor and high release of gaseous species coming from the decomposition of PDMS precursor. It seems that ADA decomposes (mostly) during pyrolysis causing some micron size cracks unless the structure has sufficient enough integrity and 3D interconnected porosity which will let the resulted gas coming from ADA decomposition evolve with no harm. Most probably, even the highest curing temperature (200°C) applied in the present part of the studies was not enough to decompose ADA completely. Suggesting that the polysiloxane components did not “kicked” the decomposition of ADA (see Chapter 3.3. for more details about the decomposition of ADA).

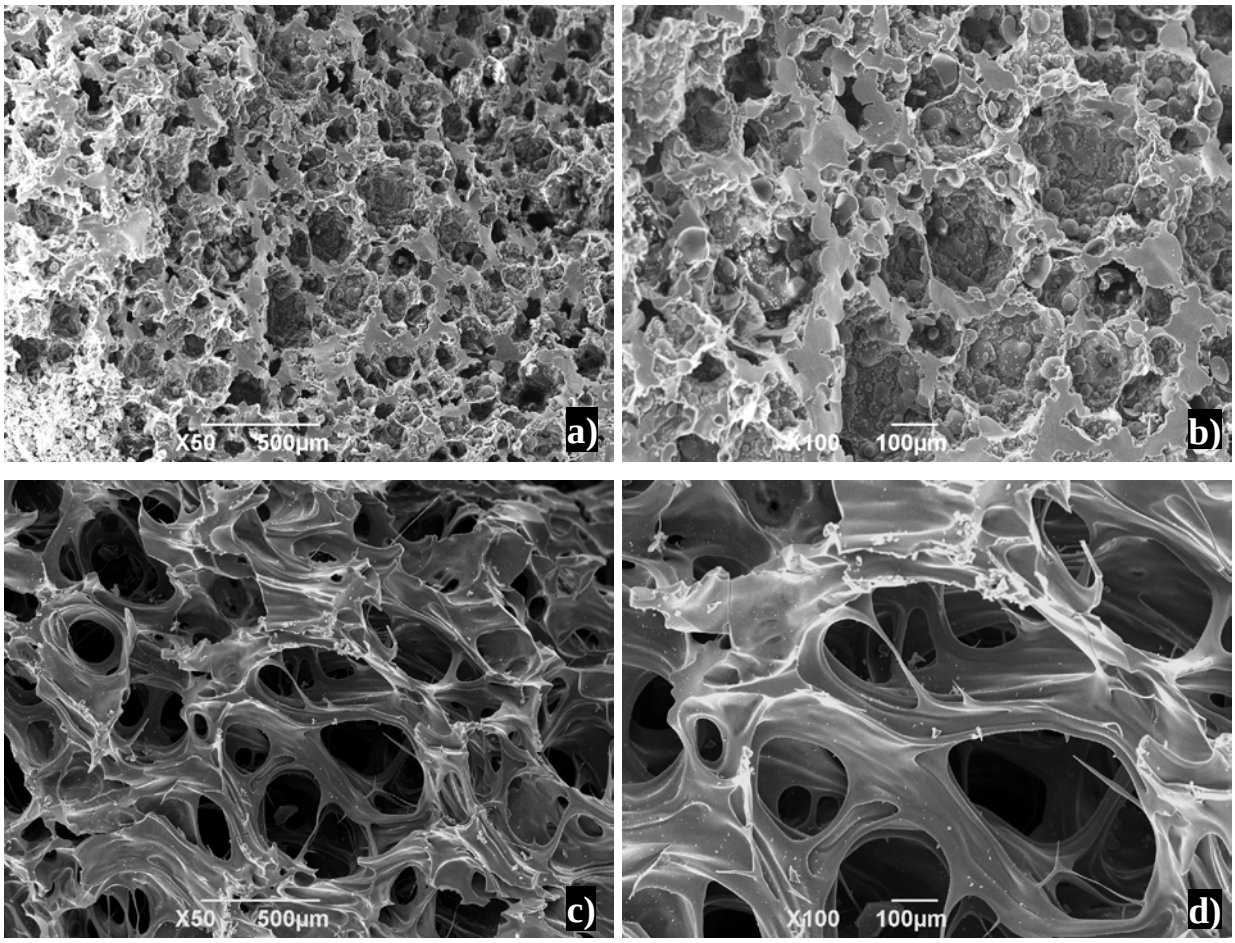

Figure 3.1-9. SEM micrographs taken from the fracture surfaces of samples: a&b) PM2 (50wt% PDMS-50wt% PMPS); c&d) PH2 (50% PDMS-50% PMPS). All cured at 200°C and pyrolyzed at 1200°C in N_2.

3.1.4. Conclusions

The mixing of silicone precursors having different characteristics, in particular a different molecular architecture, led to the fabrication of samples possessing a large amount of porosity after pyrolysis. This process is simple and allows for the direct (one step pyrolysis) fabrication of cellular SiOC ceramic components. The morphology of the produced porosity was rather complex, and comprised pores with a size ranging from a few microns to a few hundred microns. An influence of the amount of linear silicone and of the type of polysilsesquioxane (resin) used

on the total porosity was observed, while this effect was much less evident when considering the content of open and closed pores present in the various samples. Further experiments showed also that in order to obtain flawless ceramics with controlled pore characteristics (amount, cell size, strut density, etc), the viscosity of used precursor during porogen decomposition should be defined carefully. Moreover, it was found in particular that the crosslinking step plays a very important role in the determination of the general properties of the pyrolyzed components.

3.1.5. References

[1]M. Scheffler and P. Colombo, "Cellular ceramics: structure, manufacturing, properties and applications," pp. 670, WILEY-VCH Verlag GmbH, Weinheim, Germany, 2005.

[2]P. Colombo, "Engineering porosity in polymer-derived ceramics," *Journal of the European Ceramic Society*, 28 [7] 1389-95 (2008).

[3]P. Colombo and J. Hellmann, "Ceramic foams from preceramic polymers," *Materials Research Innovations*, 6 [5] 260-72 (2002).

[4]J. Zeschky, T. Höfner, C. Arnold, R. Weißmann, D. Bahloul-Hourlier, M. Scheffler, and P. Greil, "Polysilsesquioxane derived ceramic foams with gradient porosity," *Acta Materialia*, 53 [4] 927-37 (2005).

[5]P. Colombo, E. Bernardo, and L. Biasetto, "Novel Microcellular Ceramics from a Silicone Resin," *Journal of the American Ceramic Society*, 87 [1] 152-4 (2004).

[6]Y.-W. Kim and C.B. Park, "Processing of microcellular preceramics using carbon dioxide," *Composites Science and Technology*, 63 [16] 2371-7 (2003).

[7]X. Bao, M.R. Nangrejo, and M.J. Edirisinghe, "Synthesis of silicon carbide foams from polymeric precursors and their blends," *Journal of Materials Science*, 34 2495-505 (1999).

[8]F. Berndt, Jahn, P., Rendtel, A., Motz, G., Ziegler, G, "Monolithic SiOC Ceramics with Tailored Porosity," *Key Engineering Materials*, 206-213 1927-30 (2002).

[9]M. Scheffler, T. Gambaryan-Roisman, T. Takahashi, J. Kaschta, H. Muenstedt, P. Buhler, and P. Greil, "Pyrolytic decomposition of preceramic organo polysiloxanes," pp. 239–50 in Proceedings of Innovative Processing and Synthesis of Ceramics, Glasses, and Composites IV (St. Louis, Missouri), Vol. 115, *Ceramic Transactions.* Edited by N. Bansal and J.P. Singhe. The American Ceramic Society, Westerville, Ohio, 2000.

[10]G. Camino, S.M. Lomakin, and M. Lazzari, "Polydimethylsiloxane thermal degradation Part 1. Kinetic aspects," *Polymer*, 42 [6] 2395-402 (2001).

[11]G. Camino, S.M. Lomakin, and M. Lageard, "Thermal polydimethylsiloxane degradation. Part 2. The degradation mechanisms," *Polymer*, 43 [7] 2011-5 (2002).

[12]R. Harshe, C. Balan, and R. Riedel, "Amorphous Si(Al)OC ceramic from polysiloxanes: bulk ceramic processing, crystallization behavior and applications," *Journal of the European Ceramic Society*, 24 [12] 3471-82 (2004).

[13]J. Ma, L. Shi, Y. Shi, S. Luo, and J. Xu, "Pyrolysis of polymethylsilsesquioxane," *Journal of Applied Polymer Science*, 85 [5] 1077-86 (2002).

[14]V. Gualandris, D. Hourlier-Bahloul, and F. Babonneau, "Structural Investigation of the First Stages of Pyrolysis of Si-C-O Preceramic Polymers Containing Si-H Bonds," *Journal of Sol-Gel Science and Technology*, 14 39-48 (1999).

[15]R. Corriu, D. Leclercq, P. Mutin, and A. Vioux, "Preparation and structure of silicon oxycarbide glasses derived from polysiloxane precursors," *Journal of Sol-Gel Science and Technology*, 8 [1] 327-30 (1997).

[16]E. Radovanovic, M.F. Gozzi, M.C. Gonçalves, and I.V.P. Yoshida, "Silicon oxycarbide glasses from silicone networks," *Journal of Non-Crystalline Solids*, 248 [1] 37-48 (1999).

[17]E. Kroke, Y.-L. Li, C. Konetschny, E. Lecomte, C. Fasel, and R. Riedel, "Silazane derived ceramics and related materials," *Materials Science and Engineering: R: Reports*, 26 [4-6] 97-199 (2000).

[18]M. Birot, J.-P. Pillot, and J. Dunogues, "Comprehensive Chemistry of Polycarbosilanes, Polysilazanes, and Polycarbosilazanes as Precursors of Ceramics," *Chemical Reviews*, 95 [5] 1443-77 (1995).

[19]P. Dibandjo, S. Diré, F. Babonneau, and G.D. Soraru, "Influence of the polymer architecture on the high temperature behavior of SiCO glasses: A comparison between linear- and cyclic-derived precursors," *Journal of Non-Crystalline Solids*, 356 132–40 (2010).

[20]D. Seyferth, "Birth, Death and Transfiguration: The Synthesis of Preceramic Polymers, Their Pyrolysis and Their Conversion to Ceramics," pp. 567-99 in The Proceedings of the Second European Ceramic Society Conference (Ecers'91), Vol. 1, *Euroceramic II.* Edited by G.Z.a.H. Hausner. Deutsche Keramische Gesellschaft, Köln, 1991.

[21]T. Takahashi, J. Kaschta, and H. Münstedt, "Melt rheology and structure of silicone resins," *Rheologica Acta*, 40 [5] 490-8 (2001).

[22]P. Colombo, "Conventional and novel processing methods for cellular ceramics," *Philosophical Transactions of the Royal Society A: Mathematical, Physical and Engineering Sciences*, 364 [1838] 109-24 (2006).

[23]J. Zeschky, F. Goetz-Neunhoeffer, J. Neubauer, S.H. Jason Lo, B. Kummer, M. Scheffler, and P. Greil, "Preceramic polymer derived cellular ceramics," *Composites Science and Technology*, 63 [16] 2361-70 (2003).

[24]L.J. Gibson and M.F. Ashby, "Cellular solids, structure and properties," pp. 510, Cambridge University Press, Cambridge, UK, 1999.

[25]J. Wan, M.J. Gasch, and A.K. Mukherjee, "In Situ Densification Behavior in the Pyrolysis Consolidation of Amorphous Si-N-C Bulk Ceramics from Polymer Precursors," *Journal of the American Ceramic Society*, 84 [10] 2165-9 (2001).

[26]S. Quinn, "Chemical blowing agents: providing production, economic and physical improvements to a wide range of polymers," *Plastics, Additives and Compounding*, 3 16-21 (2001).

[27]A.S.P. Lin, T.H. Barrows, S.H. Cartmell, and R.E. Guldberg, "Microarchitectural and mechanical characterization of oriented porous polymer scaffolds," *Biomaterials*, 24 [3] 481-9 (2003).

[28]C. Vakifahmetoglu and P. Colombo, "A Direct Method for the Fabrication of Macro-Porous SiOC Ceramics from Preceramic Polymers," *Advanced Engineering Materials*, 10 [3] 256-9 (2008).

3.2. Fabrication of Particle-Based Macro-Porous SiOC Ceramics

To be Published in part in: K. Terauds, P.E. Jimenez-Sanchez, R. Raj, C. Vakifahmetoglu, and P. Colombo, "Giant Piezoresistivity of Polymer-Derived Ceramics at High Temperatures," submitted manuscript, 2009.

3.2.1. Introduction

In this part of the study, a particle based methodology analogous to the powder metallurgy techniques has been explored. Commercial polysiloxane precursors were crosslinked, crushed, and then sieved to different particle sized powders. The selected sized powder was compacted in a various proportions together with binder being the same or different type of partially cured or non cured polysiloxane, by cold pressing at 55 MPa. The shaped green bodies were pyrolyzed at 1200°C under nitrogen atmosphere. Highly porous SiOC monoliths (with around 50 vol% of total porosity (mostly open)) were obtained. The resulted ceramic bodies showed compressive strength values reaching to 37.4MPa with ~53vol% porosity. In step part of the study, samples were rendered to be conductive by heat treating for 45h in a hot-isostatic-press (HIP) under N_2 atmosphere with a peak temperature of 1400°C and a maximum pressure of ~26MPa, conducing to the formation of SiOC(N) tablets having extremely high piezoresistivity in between 100-1700 at high temperatures (700-1000°C).

3.2.2. Experimental Procedure

Initially, a pure MK (PMS) polymer was cured at either 250°C or 350°C for 5h in air. The resulted thermoset was crushed, ball milled (350rpm/3h) and sieved to two main mesh sizes; namely; 170-200mesh (88-74µm) and <400mesh (<37 µm). These homogenous powders have been utilized to produce ceramic monoliths by mixing with a secondary phase comprising either pure (MK) or different commercial polysiloxanes (H44, Silres 601 (both Wacker, Germany, see Chapter 2.1.1.3 for the precursor details). Several different samples have been investigated which were made from the varying ratios of pre-cured MK (>50wt%) and second phase polysiloxane

(<50wt%). The powder mixture was blended in a porcelain mortar and pestle for 10 minutes, then blend was pressed into 20 mm diameter cylindrical tablets with 55MPa, for a tablet ~4g of mixture was used. The obtained green tablets were placed in an alumina tube furnace (Carbolite 1200) and pyrolyzed under N_2 atmosphere at 1200°C for 2h with a 2°C/min heating and cooling rate. The true density was measured from finely ground ceramic powder using a He-Pycnometer ((Micromeritics AccuPyc 1330, Norcross, GA)). Open and closed porosity of the sintered ceramics were determined by the Archimedes principle (ASTM C373-72), using xylene as buoyant medium. Compression testing was performed at room temperature on selected pyrolyzed samples, which were cut before pyrolysis to avoid shape distortions to find out the cold crushing strength. Instron type machine (1121 UTM, Instron, Norwood, MA) using steel loading rams at a strain rate of 0.5 mm/min was used for testing. Specimens with a nominal dimension of (0.5 cm*0.5 cm*0.5 cm) were cut from larger samples and all the cube surfaces were polished down to 1 μm with a resin bonded diamond wheel. 10 samples per data point were tested.

3.2.3. Results and Discussion

After curing and sieving, homogenous particles having different sizes were obtained depending on the sieve (see **Figure 3.2-1** (a-d)). Particle size is measured by image analysis software from at least 100points to obtain a reliable data. MK cured at 250°C for 5h and sieved in between 170-250mesh (88-74μm) yielded with 93.01 ± 27.33 μm particle size, and as expected MK cured at 250°C for 5h and sieved below 400mesh (37μm) resulted in much smaller particle size; 40.54 ± 20.10 μm. Unsurprisingly, the data for 350°C cured samples were almost similar.

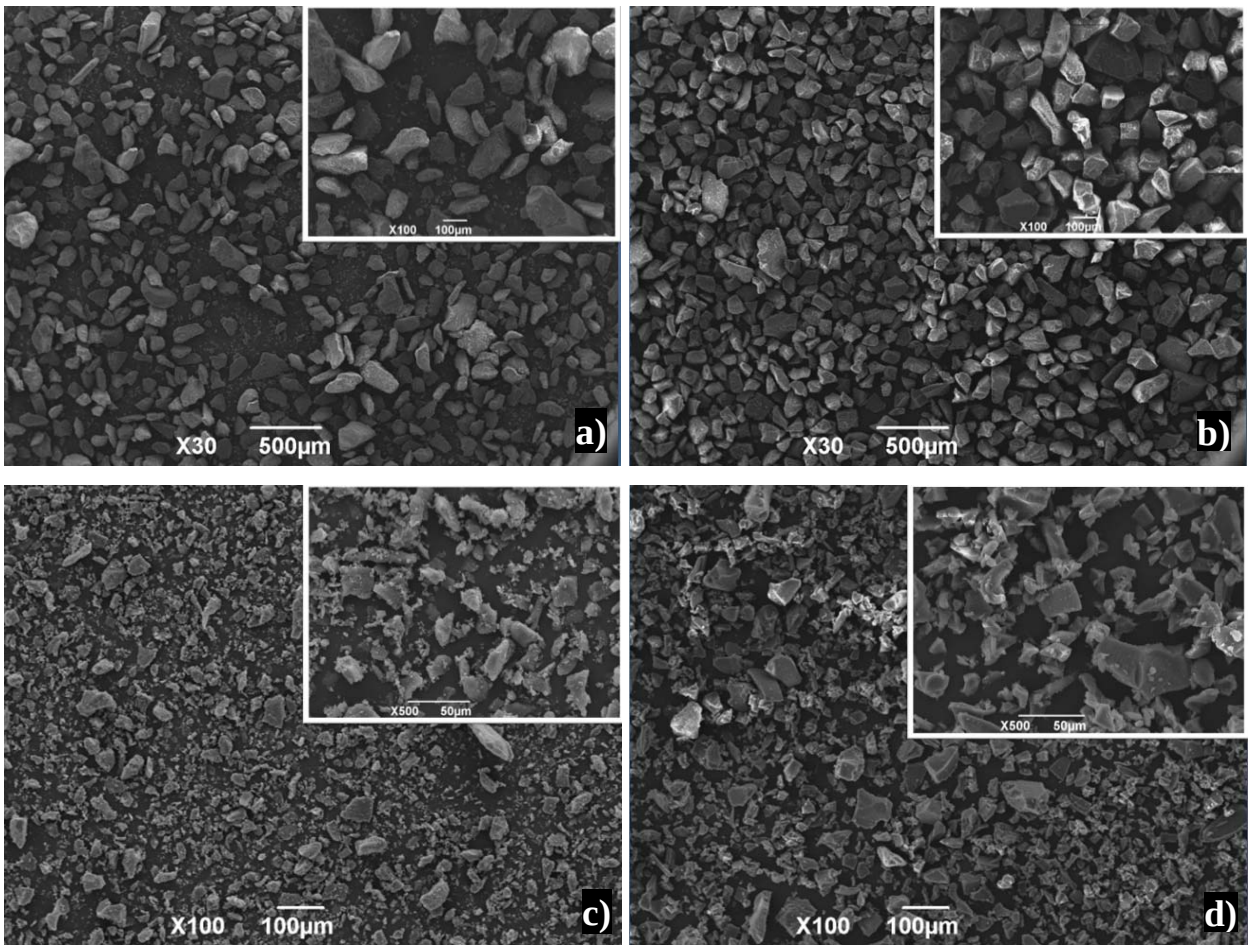

Figure 3.2-1 SEM images of; a) MK 250°C/5h cured, 170-250mesh, b) MK 350°C/5h cured, 170-250mesh, c) MK 250°C/5h cured, <400mesh, and d) MK 350°C/5h cured <400mesh.

Since the central objective was to come up with a precursor mixture leading to a ceramic with a highly porous microstructural assembly together with good mechanical strength, all the samples primarily investigated by Archimedes to understand the amount of porosity then SEM has been applied on selected samples and depending on the resulted microstructural arrangement other characterizations have been applied. Concerning the pure MK system; samples prepared from 30wt% of bare MK and 70wt% of pre-cured MK generally gave the best results. Different size powders yielded with different pore amounts and pore dimensions. **Table 3.2-1** summarizes the data obtained from these monoliths.

As could be seen, the highest porosity was obtained from the samples prepared by using 70wt%

of MK cured at 250°C/5h; it was found that increasing the curing temperature of MK, decreased the total porosity. Similarly, increasing the particle size decreased the total porosity. Moreover, It was not possible to obtain a green sample by using 70wt% of 350°C/5h cured MK having small particle size (<400mesh). Thus the binder amount was increased to 50wt% to obtain a green tablet which decreased the total porosity (mostly closed pores) considerably. Under the light of present results during the following experimental part, the binder amount was always kept less than 30 wt% in order to enlarge both total porosity and the ratio of open/closed porosity.

Table 3.2-1. Sample composition and %P data for pure MK system.

#	Binder (wt%)	Cured MK (wt%)	δ(bulk)	Total P. (vol%)	Closed P. (vol%)	Open P. (vol%)
HS1	As received 30%	250°C/5h (170-200mesh) 70%	1.3172	43.6398	1.5974	42.04
HS2	As received 30%	350°C/5h (170-200mesh) 70%	1.3654	41.5790	10.2380	31.34
HS3	As received 30%	250°C/5h (<400mesh) 70%	1.1029	52.8091	1.5986	51.21
HS4	As received 50%	350°C/5h (<400mesh) 50%	1.7179	26.4961	25.6485	0.85

SEM images given in **Figure 3.2-2** (a-d) show the general morphology of samples given in **Table 3.2-1**, inset figures are the taken from the higher magnifications. Consistently with porosity measurements when the amount of binder increased, total (and also open) porosity decreases, see **Figure 3.2-2**(d). Although pre-cured precursors were sieved to the same particle size, it is clear from the images that the sample prepared by using 350°C/5h cured MK has bigger grains and higher amount of closed porosity compared to that of the one prepared from 250°C/5h cured MK. This implies that higher amount of crosslinking obtained at higher curing temperature (350°C), did not let these solid particles melt during pyrolysis, instead seemingly they were covered by un-cured MK binder powder which melts during heating and forms particle this type of microstructure, see **Figure 3.2-2**(b). Moreover, it is clear from these images that the

particle size is also effective on altering the pore cell size. Logically, while smaller particles give smaller pores, bigger particles yields with bigger pores, see **Figure 3.2-2**(a) and (c).

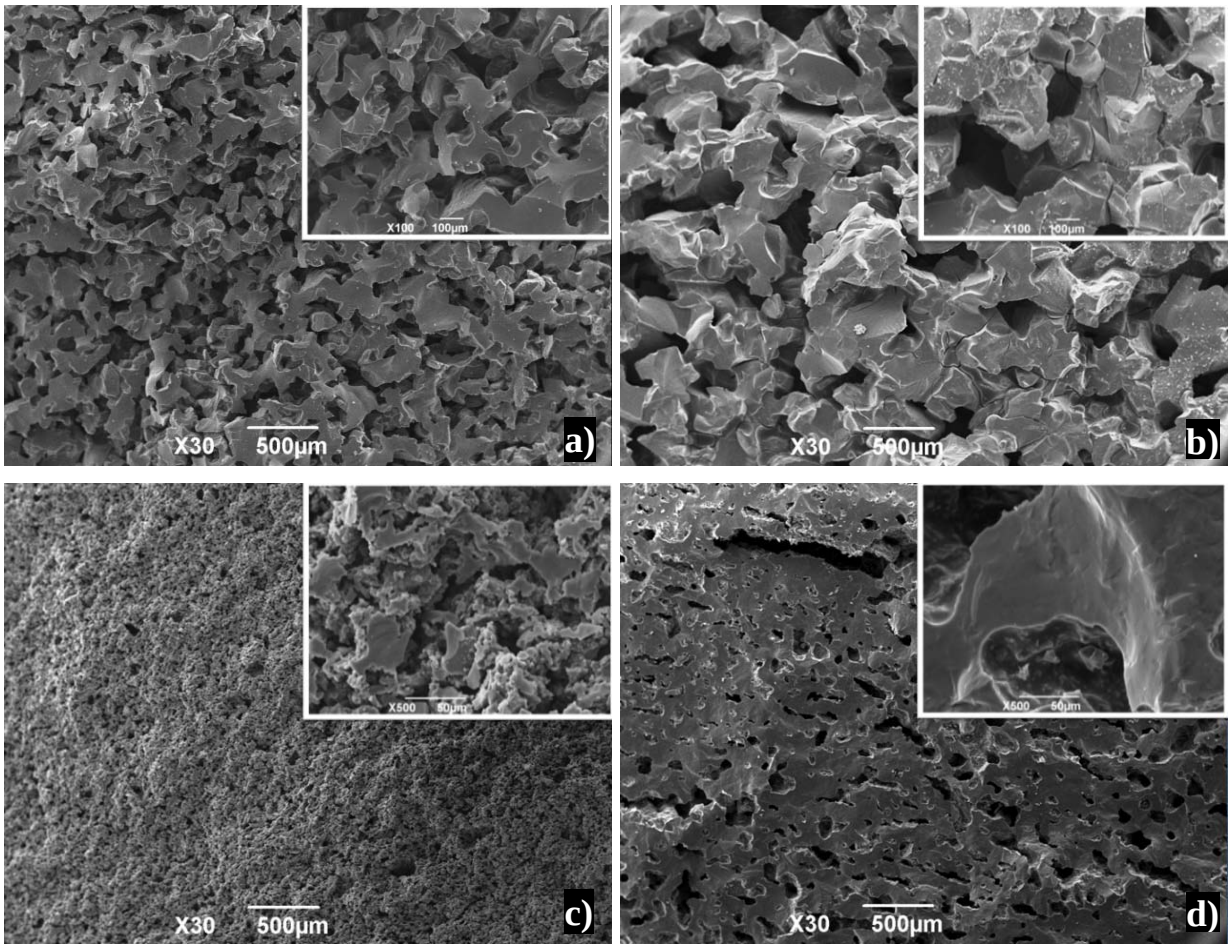

Figure 3.2-2. SEM images of the pyrolyzed (1200°C/2h) sample fracture surfaces; a) HS1, b) HS2, c) HS3, and d) HS4

In further experiments modification have been applied in order to enhance the total porosity namely; with less amount of as received MK (5wt%) or partially cured (either 100°C/30min or 100°C/3h) MK has been used as binder together with MK cured at lower temperatures ≤250°C as a main SiOC phase. It seems that when less binder is used, the effect of particle size on the total porosity diminishes, see **Table 3.2-2**. However, this effect cannot be controlled on the samples prepared by using 200°C/5h or 350°C/5h cured powders; it was not possible to prepare green tablets due to limited amount of binder which was not sufficient for lubrication. As seen from the

results, there is a clear increase in the totally porosity with the decrease in binder amount. When curing temperature of the main phase decreased to 200°C, total porosity decreased considerably; implying that temperatures <250°C are not sufficient enough to supply adequate crosslinking in order to keep structural integrity so the green sample melts (partially or totally depending on the amount of binder phase) during pyrolysis causing a limited amount of total porosity with high fraction of closed porosity. For the samples prepared by using partially cured MK as a binder, the same trend on porosity was observed; i.e. increasing the particle size or curing temperature of main phase, decreased the total porosity and increased the amount of closed porosity. However, a slight increase in total porosity compared to the samples made by using as received MK can be observed, see **Table 3.2-2**.

Table 3.2-2. The sample composition and %Porosity data for pure MK system.

#	Binder (MK) (wt%)	Cured MK (wt%)	δ(bulk)	Total P. (vol%)	Closed P. (vol%)	Open P. (vol%)
HS5	As received 5%	200°C/5h (170-200mesh), 95%	2.0179	13.6562	6.3117	7.34
HS6	As received 5%	250°C/5h (170-200mesh), 95%	1.0121	56.6950	1.5628	55.13
HS7	As received 5%	250°C/5h (<400mesh), 95%	1.0144	56.5966	0.3046	56.29
HS8	100°C/180min 30%	250°C/5h (170-200mesh), 70%	1.2811	45.1839	3.0178	42.17
HS9	100°C/180min 30%	350°C/5h (170-400mesh), 70%	1.3866	40.6716	11.6570	29.01
HS10	100°C/30min 30%	250°C/5h <400mesh, 70%	1.1008	52.9008	6.1435	46.76
HS11	100°C/180min 30%	250°C/5h <400mesh, 70%	1.0775	53.8976	4.6174	49.28
HS12	100°C/180min 50%	350°C/5h <400mesh, 50%	1.6360	30.0006	18.7645	11.24

SEM images further corroborated the porosity data, sample (HS5) made with 200C cured MK, showed very limited porosity with a high fraction of closed porosity, see **Figure 3.2-3** (a). On the other hand utilization of 5wt% binder caused samples having microstructures resembling particle compacts rather than foams or monoliths, see **Figure 3.2-3** (b) and (c). The samples showed different morphology depending on the particle size, but it was clear from the images that the binder phase used was not enough to create clear defined cells and so most probably only bonded the particles in a limited way.

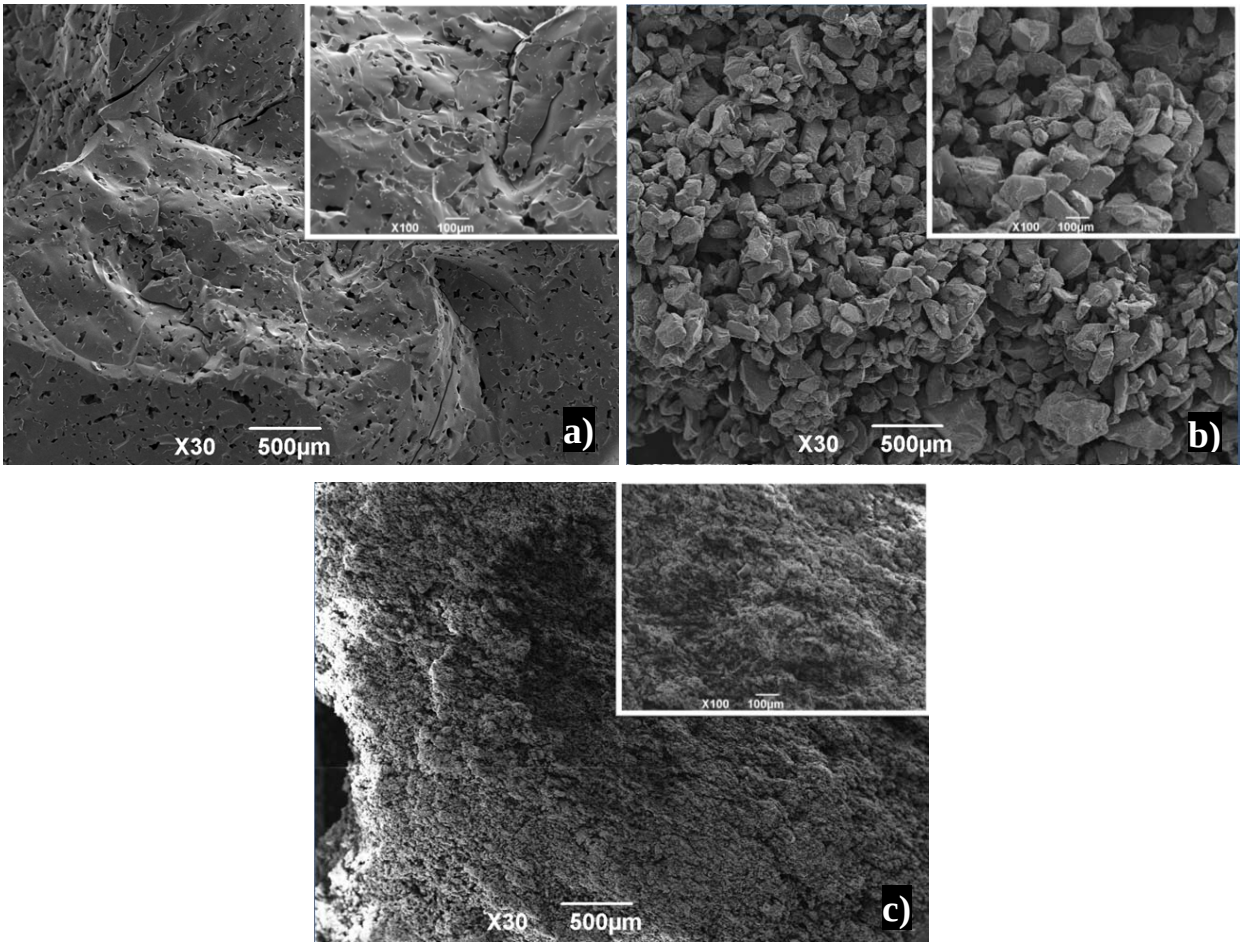

Figure 3.2-3. SEM images of the pyrolyzed (1200°C/2h) sample fracture surfaces; a) HS5, b) HS6, and c) HS7

Generally inhomogeneous microstructures were observed from the samples made by using partially cured MK as a binder, see **Figure 3.2-4** (a) and (b) for the representative microstructures of the samples prepared by using 100°C/0.5h and 100°C/3h cured MK as a binder and having the highest amount of total porosity (mostly open), respectively. It should be noted that increasing the time of mixing step before pressing the tablets did not yield with homogenous microstructures; this suggested that the formed liquid or viscosity phase during pyrolysis was not sufficient enough to cause homogenous segregation media.

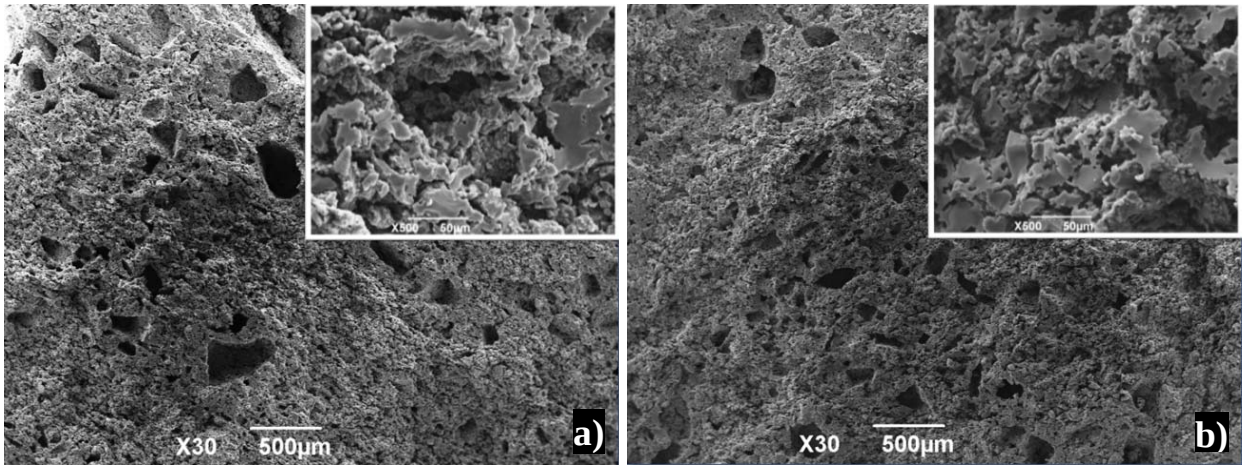

Figure 3.2-4. SEM images of the pyrolyzed (1200°C/2h) sample fracture surfaces**;** a) HS10, and b) HS11.

Some limited experiments have been applied by using different precursors namely; H44 (PMPS) and Silres 601 (PPS) as a binder phase while aiming to enhance the porosity. Utilization of both of these precursors as a binder resulted in microstructurally inhomogeneous and very weak powder like samples, see **Figure 3.2-5** (a) and (b). Implying that the amount and the type of binder has a vital impact on the integrity of the formed body. Samples made from as recieved MK with even very limited amount (5wt%) yielded with materials having better structural integrity. Therefore, these samples are excluded from further characterization. The reason for this behavior is still elusive but certainly related with the polymer characteristics.

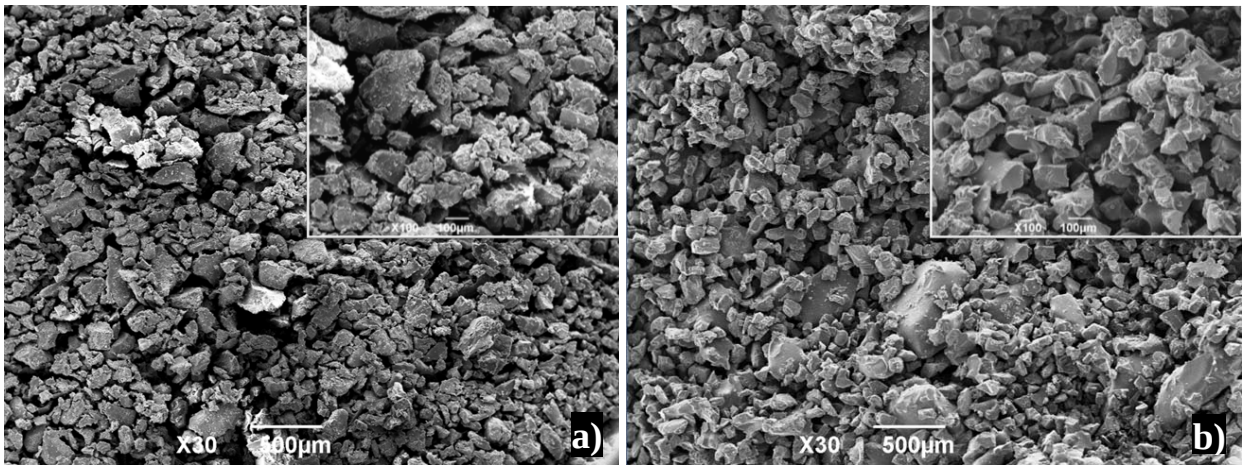

Figure 3.2-5. SEM images of the selected samples a) 10wt%H44-90wt%MK (250°C/5h <170-200mesh), and b) 10wt%Silres 601-90wt%MK (250°C/5h <170-200mesh).

Cold crushing test was performed at room temperature on selected pyrolyzed samples, the criteria of selection was based on the highest porosity and best microstructural assembly, i.e. samples prepared by using 250°C cured MK together with either 5wt% or 30wt% as received MK as a binder. The results given in **Table 3.2-3**, are well consistent with those of SEM investigations; meaning that when limited amount of binder was used, powder compacts where the particles were hardly in contact with each other without a clear strut formation, have been obtained and the data on compression strength for these samples was very low. Instead samples made by using 30% of binder yielded with porous (43-52 vol%) SiOC samples having a strength of 26-37 MPa.

Table 3.2-3. Compression strength (MPa) together with standard deviation values of some selected samples.

Sample	As Recevied MK (wt%)	MK cured at 250°C (wt%)	Cured MK Sieve numbers	Total Porosity (vol%)	Open Porosity (vol%)	Compression Strength (MPa.)
HS6	5%	95%	170-200	56.7%	55.1%	n.p.
HS7	5%	95%	<400	56.6%	56.3%	0.3 ± 0.18
HS1	30%	70%	170-200	43.6%	42.0%	26.1 ± 6.02
HS3	30%	70%	<400	52.8%	51.2%	37.4 ± 13.55

n.p. Tablets after pyrolysis were not though enough to prepare regular mechanical test samples.

The sample HS3 is selected for further characterization due to its high cold crushing strength and high amount of porosity. The green tablet of HS3 was first pyrolyzed at 1200°C/2h with 2°C/min heating and cooling rate. In step two, the sample was rendered to be conductive by heat treating for 45h in a hot-isostatic-press (HIP) under N_2 atmosphere with a peak temperature of 1400°C and a maximum pressure of ~26MPa. After heat treatment, the sample was 3.0mm thick with a 3.4mm x 4.2mm cross-section and had a room temperature conductivity of 2.0 x 10^{-4} $\Omega^{-1}cm^{-1}$. The piezoresistive properties of the formed ceramic having the composition of $Si_{0.32}O_{0.48}C_{0.17}N_{0.03}$, was measured in the temperature range of 700°C to 1000°C at stresses ranging from 1 to 10 MPa. The gauge factor (piezoresistive coefficient (k) is defined as the fractional change in resistance due to an applied strain) was found strongly stress and temperature dependent. In this full range of stress and temperature the gauge factor varied between 100 and 1700, with the lowest value relating to the highest stress and temperature, and the highest value to the lowest stress and temperature. The room temperature piezoresistive behavior of SiOC[1] and SiCN[2] ceramics were previously measured and demonstrated high values 145 and 1000-4000 respectively. It should be noted that commercially available strain gauges typically had values of k ~2.[1] It appears that PDC materials have a high potential for sensor

applications. The results of our experiments provided, for the first time, high temperature piezoresistivity data for SiOC(N) ceramics for which the gauge factor far exceeds the performance of any known materials in this temperature range (see **Table 3.2-4**)[3] making them ideal candidates for sensor materials in extreme environments. It should be noted that the cost of SiOC(N) ceramics are much lower than that of SiCN due to more cheaper precursor utilization that is polysiloxane, thus offering an economic way of producing both low and high temperature sensor materials.

Table 3.2-4. Gauge factor of various piezoresistive materials, including SiOC.

Material	Gauge Factor	Temperature Limit (°C)
SiOC(N)	~1000	>1000
Germanium	10	135
Silicon	180	200
Diamond	100	300
SiC	40	500

3.2.4. Conclusions

By mixing of pre-cured, sieved polysiloxane precursors with bare un-cured precursors of the same type, macroporous (%P could be as high as 56.7vol%) SiOC components having high compressive strength values reaching to ~37.4MPa were obtained. Hot isostatically pressing of these formed bodies under N_2 atmosphere at high temperature ~1400°C yielded with SiOC(N) tablets having extremely high piezoresistivity in between 100-1700 at high temperatures (700-1000°C).

3.2.5. References

[1]R. Riedel, L. Toma, E. Janssen, J. Nuffer, T. Melz, and H. Hanselka, "Piezoresistive Effect in SiOC Ceramics for Integrated Pressure Sensors," *Journal of the American Ceramic Society*, (in press 2009).

[2]L. Zhang, Y. Wang, Y. Wei, W. Xu, D. Fang, L. Zhai, ., K.-C. Lin, and L. An, "A Silicon Carbonitride Ceramic with Anomalously High Piezoresistivity," *Journal of the American Ceramic Society*, 91 [4] 1346-9 (2008).

[3]K. Terauds, P.E. Jimenez-Sanchez, R. Raj, C. Vakifahmetoglu, and P. Colombo, "Giant Piezoresistivity of Polymer-Derived Ceramics at High Temperatures," *submitted manuscript, 2009*.

3.3. Fabrication of Cellular SiCN/SiOCN Ceramics

*Published in part in: C. Vakifahmetoglu, I. Menapace, A. Hirsch, L. Biasetto, R. Hauser, R. Riedel, and P. Colombo, "Highly porous macro- and micro-cellular ceramics from a polysilazane precursor," Ceramics International, **35[8]** 3281-3290.2009.*

3.3.1. Introduction

Ceramic foams are a specific group of cellular materials possessing a very favorable combination of properties, such as low density, low thermal conductivity and low dielectric constant, high permeability, high thermal shock resistance, high chemical stability and high specific strength.[1, 2] As a result, these materials are used in different engineering applications ranging from metallurgy (removal of impurities from liquid metals) or high-temperature processing (thermal insulation) to the automotive (control of gas and diesel emissions), petrochemical (catalyst support), combustion technology (porous-medium burners), or biomedical (biological implants) fields[3-7]. The properties of cellular materials are affected by their relative density (amount of porosity), morphological characteristics (cell size and shape), distribution of the pores (pore interconnectivity and cell wall/strut porosity), and finally the material type.[8]

It has been recently demonstrated that preceramic polymers can be used to produce highly porous structures (foams, membranes, components with hierarchical porosity) of various compositions (SiC, Si_3N_4, SiOC, SiOCN, SiCN and Si(E)CN (E=B, Al, Ti, etc.) and morphologies.[3, 5, 9] In particular, polysiloxane and polysilazane precursors, used for the production of silicon oxycarbide (SiOC) and silicon carbonitride (SiCN) ceramics respectively, have significant potential for the fabrication of advanced components. Preceramic polymer derived SiOC foams have been manufactured by following many different processing strategies.[3, 10-13] Among these routes, foaming has been achieved by using sacrificial processing aids such as polyurethane (PU),[2, 10, 14, 15] poly(methylmetacrylate) (PMMA) microbeads[1, 3, 5, 11, 16-18] and foaming agents such as azodicarbonamide (ADA).[19] Each of these decomposing agents has its own benefits and drawbacks as regards to manufacturing. The use of sacrificial

microspheres has been shown to give better microstructural control (homogeneous pore distribution) on the resulting ceramic foam. Particularly, it was shown that foams produced with PMMA microbeads[17] display better mechanical properties than those of macro-cellular foams of the same density, because of smaller struts (hence smaller critical flaws) and the presence of a smaller amount of processing defects (micro-cracks) in micro-cellular ceramics. It should be noted that the low mechanical properties of ceramic foams produced by using ADA were attributed both to the inhomogeneity of the microstructure and the defects therein.[19] Direct blowing of pure polysiloxanes, without any aid of other additives, has also been employed to fabricate SiOC macro-cellular foams[20, 21] and micro-cellular foams,[22] while supercritical CO_2 enabled to obtain micro-cellular foams[12] (see also references given in Chapter 2.3.2).

Although foaming in SiOC system has been intensively studied in the past, only few papers have been published so far concerning highly porous SiCN ceramics. It is already known that non-oxide SiCN ceramics have higher chemical, thermal (roughly speaking, onset of Tg for SiOC is 1300°C[23] and for SiCN is 1400°C[24]) and microstructural (higher crystallization temperature[25] and higher temperature of carbothermal decomposition) stability in comparison to SiOC ceramics. Moreover, SiCN ceramics possess additional properties such as tailorable electro-magnetic behavior [26-28], luminescence[29, 30], high temperature oxidation and creep resistance[31] which make the manufacture of cellular SiCN ceramics of interest in particular for advanced filtering and sorption applications.

Recently, highly porous ceramic monoliths possessing pore diameters ranging from 50 nm to 10 µm were obtained by the pyrolysis of polysilazane-filled packed beds of polystyrene (PS) or silica (SiO_2) spheres[32]. Wang et al.[33] manufactured porous SiCN ceramic having 455 m^2/g specific surface area (SSA), with a cell (macropore) size of about 0.1–0.6 µm, by templating the polysilazane precursor with colloidal SiO_2 particles. Likewise, Song et al.[34] produced two-dimensional (2D) ordered macroporous SiCN ceramics by solution dipping method based on the 2D SiO_2 monolayers. However, the removal of hard templates such as silica can damage or contaminate the resulting material[35]. As an alternative to SiO_2 etching, Yan et al.[35] used PS spheres and obtained the SiCN foams with a cell size of 0.5-1 µm, having a SSA of 184.5 and 71 m^2/g, respectively. The authors claimed that the foams produced by PS templating have higher

thermal stability comparing with that of those produced by SiO_2 particles due to the lack of damages created during acid etching[35]. Very recently nano-porous PE was used as a template for the synthesis of SiCN ceramic monolith with bi-continuous pore structure having 60-100 nm pores[36]. However, none of these studies reported any data concerning the mechanical properties of the SiCN foams produced, and the above processing procedures are more suitable to the production of components with small dimensions, because of the difficulty in packing very small beads on a large, three-dimensional scale. Moreover, large cell sizes (e.g., in the range 10 to 1000 μm) were never obtained.

The aim of the present study was to produce highly porous micro- and macro-cellular SiCN foams possessing interconnected cells with a dimension ranging from a few microns to a few hundred microns. Two different processing routes were employed: I) templating with sacrificial polymeric beads, and II) direct blowing using a physical blowing agent.

3.3.2. Experimental Procedure

Ceramic foams were produced by using a commercially available poly(methylvinyl)silazane (Ceraset™ VL20, KiON Corporation, Clariant, USA), as SiCN precursor, mixed, in partially crosslinked state, with poly(methylmetacrylate) (PMMA) microbeads of 20 μm nominal size (Aldrich Chemical Company Inc., USA), acting as sacrificial filler, and, as received, with azodicarbonamide (ADA, Sigma–Aldrich, USA) as physical blowing agent.

It should be underlined here that that this work lies within a PolyCerNet collaboration between our lab and the group of *Prof. Ralf Riedel,* in the Institute of Materials Science, Darmstadt University of Technology, Germany. Different processing routes were followed to prepare the green bodies. In processing route I (PMMA sacrificial microbeads), liquid polysilazane was first partially cross-linked by heating in a vertical tube furnace under Ar flow with heating rate of 1°C/min up to 300°C (dwelling time 8 h). The heating schedule was chosen in order to achieve a suitable compromise between the polymer meltability, required during the warm pressing step, and its capability of retaining the original shape, necessary during the sacrificial filler burn-out. The pre-crosslinked polymer (abbreviated as PCVL20 in the following) was ground in a

planetary ball mill at 180 rpm for 2 h, followed by sieving. The pre-crosslinked precursor powder was dry mixed with PMMA microbeads in two different PCVL20/PMMA weight ratios, 20/80 and 30/70. The powders were homogenized by planetary ball-milling at 180 rpm for 2 h, and the mixture was then warm pressed in air for 2 h at 165°C (the actual temperature inside the mold was measured by a calibrated K type thermocouple) in a metallic die with a uniaxial hydraulic press equipped with heating plates (warm press Type 123, Collin Technology, Aichach, Germany), by applying a pressure of 13 MPa. Prior to each pressing, the rectangular mold (40 mm x 30 mm) was sprayed with silicone oil to reduce the friction between the green body and the pressing form. The green bodies were subsequently pyrolyzed in a quartz tube furnace (Gero, Germany) in the presence of flowing Ar (99.999% pure). Samples were heated to 450°C with a rate of 0.5ºC/min, held for 3h in order to guarantee the complete decomposition of the sacrificial beads, and then pyrolyzed at 1100ºC (heating rate 2°C/min) for 2h, followed by cooling in the furnace.

In processing route II (physical blowing agent), ADA powder was mixed with liquid polysilazane under Ar atmosphere, using standard *Schlenk* techniques. ADA was added to the liquid precursor at concentrations of 1, 3 and 6 wt% under magnetic stirring at room temperature. The homogenous mixtures, after 12h of stirring, were poured separately in aluminum trays and cured at 300°C for 4h (with 2°C/min heating and cooling rate) under N_2 atmosphere (99.999% pure). During this treatment curing and blowing was accomplished (ADA decomposes completely in the 200 to 300°C range – see later), and the foamed polymer monoliths were then pyrolyzed under nitrogen at 1100ºC for 2h (2ºC/min heating and cooling rate) in an alumina tube furnace (Carbolite 1200). In **Table 3.3-1** the compositions of the prepared samples, using either processing procedure I or II, are reported.

Table 3.3-1. Sample labels and composition (wt%)

Sample	Polysilazane (VL20)	PMMA	ADA
P-SiCN-1	30 (Pre-cured)	70	0
P-SiCN-2	20 (Pre-cured)	80	0
A-SiCN-1	99	0	1
A-SiCN-2	97	0	3
A-SiCN-3	94	0	6

TGA – DTA measurements were carried out with a 2°C/min heating rate up to 1200 °C under Ar (Netzsch STA 429, Selb, Germany) for the samples prepared with PMMA, and under N_2 for the samples obtained using the blowing agent. The true density was measured from finely ground ceramic powder using a He-Pycnometer (Pycnomatic ATC, Porotec). Bulk densities, open and closed porosity of the sintered ceramics were determined by the Archimedes principle (ASTM C373-72), using xylene as buoyant medium.

The crushing strength of the foams was measured at room temperature by compression, using (Instron 5569 UTM, Norwood, MA, USA; cross-head speed of 0.5 mm/min), on samples of nominal size ~ 5 x 5 x 10 mm^3, cut from larger specimens. Each data point represents the average value of five to 5 individual tests. The C, N and O content of the ceramics were analyzed by hot gas extraction using a C-Analyzer Leco C-200 and NO-Analyzer Leco TC-436, respectively (LECO Instrumente GmbH, Mönchengladbach, Germany) and Si amount is related to the difference from 100 wt%. The morphological features of the PDC foams were analyzed from fresh fracture surfaces using a scanning electron microscope (JSM-6300F SEM, JEOL, Tokyo, Japan). SEM images were subsequently analyzed with the ImageTool software (UTHSCSA, University of Texas, USA) to quantify the cell size and cell size distribution. The raw data obtained by image analysis were converted to 3D values to obtain the effective cell dimension through the well-known stereological equation: $D_{sphere}=D_{circle}/0.785$.[37]

3.3.3. Results and Discussion

Ceramics in the Si-C-N ternary system are usually obtained by the pyrolysis of poly(silazane) polymers. These precursors are characterized by repeating units of silicon and nitrogen atoms in their backbone, and one of the most popular commercial precursor in this category is polyurea(methylvinyl)silazane (PUMVS) of Kion corporation (Ceraset™).[26] The only difference between the specific polysilazane precursor used in this study (Ceraset™ VL20), and PUMVS (Ceraset™), is that the latter contains urea functionality and more low molecular weight silazane components.[38] Therefore, the literature data regarding PUMVS could be used as a reference for comparison purposes.

PUMVS cures thermally between 250-480°C in inert atmosphere, by hydrosilylation and addition of vinyl groups, without the need of any peroxide radical initiator and catalyst.[39] The ceramization of the polymer takes place predominately between 500 and 800°C. Thermolysis at 1100°C in inert atmosphere results in an amorphous material with ceramic yield of 70-80%.[39] Further increases in temperature induce the crystallization of nano-sized silicon carbide and silicon nitride.[40] Rigorously speaking, it was shown that amorphous SiCN ceramic derived from PUMVS at 1100°C is located in the Si_3N_4, SiC and carbon tri-phase equilibrium area (p=1 bar N_2) and is stable up to ~1450°C,[39] when the carbothermal reduction of Si_3N_4 starts to form SiC.[41] X-ray diffraction analysis confirmed that both the micro- and macro-cellular ceramics obtained by pyrolysis at 1100°C were X-ray amorphous.[39]

3.3.3.1. Micro-cellular foams (sacrificial microbeads fillers)

A schematic overview of the process is reported in **Figure 3.3-1**.

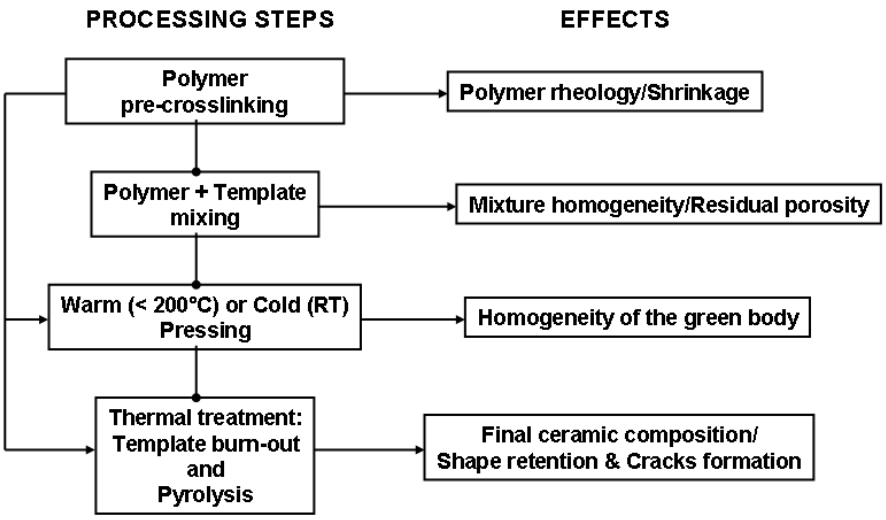

Figure 3.3-1. A schematic overview of the process employing sacrificial templates.

The following key points should be emphasized: (I) the viscosity of the preceramic polymer has to be kept sufficiently low to ensure that the sacrificial beads will be covered completely and homogenously during the warm pressing step; (II) the polymer should be able to retain the shape and the integrity of the morphology in order to avoid collapsing during the template burn-out in pyrolysis; (III) the polymer should not be excessively pre-crosslinked, in order to avoid cracking during the PMMA burn-out. Depending on the characteristics of the preceramic polymer (directly related to its synthesis process), the forming step can significantly vary; for instance the mixture of the preceramic polymer and template can be compacted by either warm[16, 17, 42] or cold pressing.[1, 11] For warm pressing, besides the degree of crosslinking of the precursor, processing parameters such as forming time, temperature and pressure are very important. Pressing at 165°C for 60 min of the pre-crosslinked powders yielded flawless samples before and after pyrolysis (see **Figure 3.3-2** (a-c)).

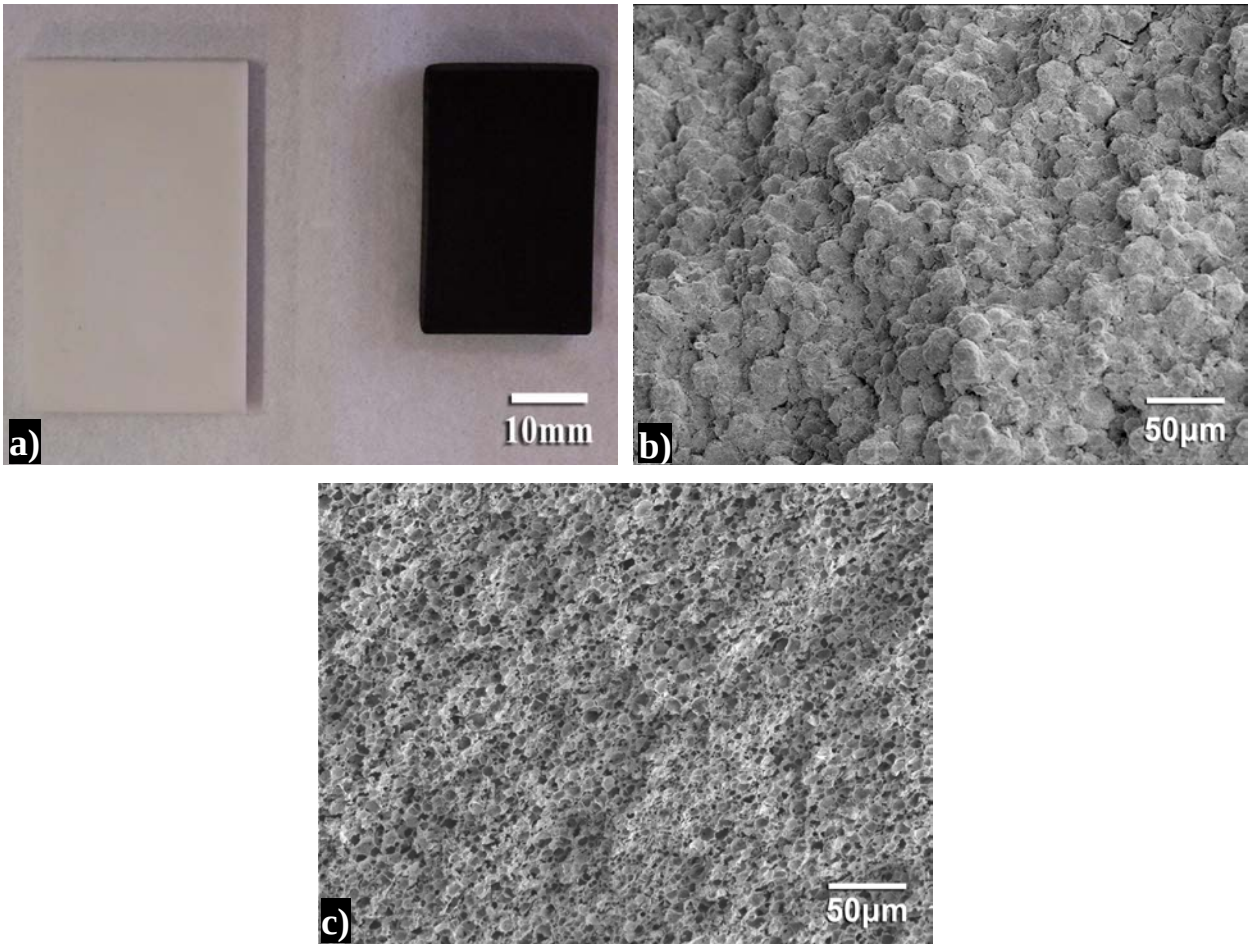

Figure 3.3-2. Sample P-SiCN-2 (80/20): a) after warm pressing (left) and pyrolysis (right); b) after warm pressing (165°C, 1h); and c) after pyrolysis (1100°C, 2h).

As it can be seen from **Figure 3.3-3**, the main decomposition step of pure precured VL20 occurs between 400-800°C, corresponding to a weight loss of 19%. These data are in accordance with those reported by Li et al.[39] for PUMVS, and are directly related to the initial degree of crosslinking of the preceramic polymer. The degradation of the pure PMMA beads starts at 220°C and completes at around 420°C. The TGA curve of sample P-SiCN-1 shows a shift of the decomposition to lower temperatures in comparison to that of pure PMMA, while for sample P-SiCN-2 the degradation starts at higher temperatures. Since it is not possible to extrapolate a linear behavior in accordance with the rule of mixtures, it can be inferred that the PMMA beads and the crosslinked silicon polymer have a mutual influence on their thermal stability. After the complete decomposition of PMMA at T > 400°C, the further mass loss is due to the degradation

of the PCVL20 fraction, exclusively. This finding is in accordance with the TGA of the pure PCVL20. A slow heating rate (1°C /min) and a dwelling time of 3 hours at 450°C were therefore chosen in order to burn-out the PMMA beads and at the same time allowing the pyrolysis gases to escape through the interconnected porosity without causing cracking. Between 800-1200°C the weight loss of PCVL20 was almost negligible, indicating the complete ceramization of the preceramic precursor.

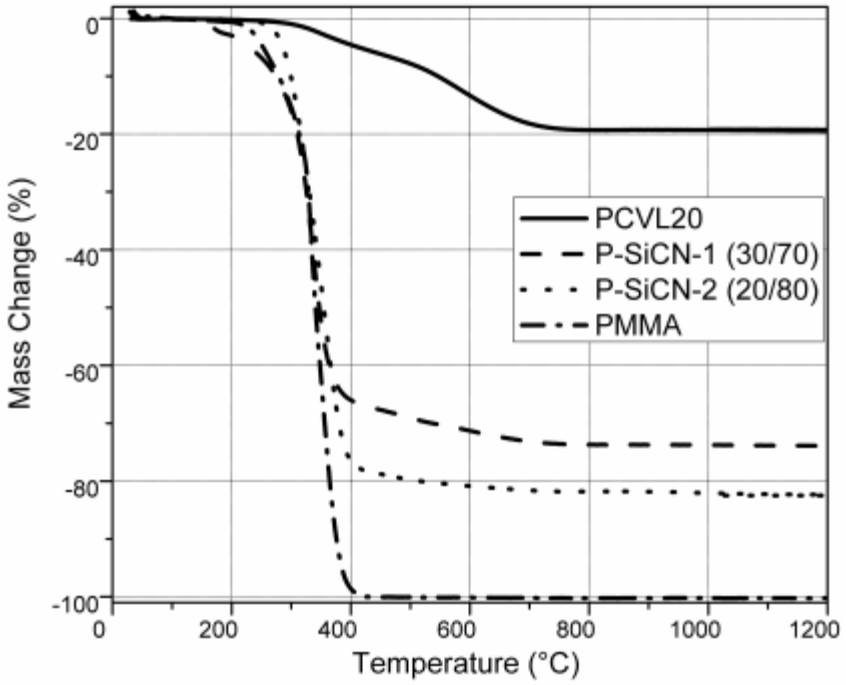

Figure 3.3-3. TGA analysis (Ar) of PCVL20, PMMA microbeads and samples P-SiCN-1 (30/70) and P-SiCN-2 (20/80).

The measured total mass loss data for samples P-SiCN-1 (30/70) and P-SiCN-2 (20/80) at 1100°C were 73.8% and 82.3%, respectively. These values are comparable with the theoretical calculation data (considering a ceramic yield of 81% for the PCVL20) namely; 75.7% and 83.8%. The mass loss difference could be attributed to the presence of oxygen in the final ceramic. In fact, elemental analysis (EA) revealed that the amount of oxygen in sample P-SiCN-2 (20/80) was 24 wt%, and it was 33 wt% in sample P-SiCN-1 (30/70) (see Table II). Cross et al.[43] recently reported that the amount of C, O and N in the $SiO_xC_yN_z$ system has a profound

effect on the tribological properties of resulted ceramic. Nevertheless, none of the studies mentioned before concerning the SiCN ceramic foams had given information about the final chemical composition. Although highly depending on the processing method employed, it is known that SiCN ceramics produced from preceramic polymers often contain significant amounts of oxygen, due to the high sensitivity of the precursor polymer to moisture.[43] For example, it was shown that the oxygen level could be kept under 1 wt%[39] or could be as high as 27 wt%,[43] for coupons of PUMVS precursor pyrolyzed at 1000°C in N_2 overpressure. The oxygen intake, in the present study, could be attributed to the combined effects of (a) accumulation of oxygen due to the evaporation of volatile C containing components,[44] (b) presence of residual humidity on the PMMA beads, and (c) relatively high sensitivity of the preceramic polymer to moisture (during ball milling and warm pressing)[43], (d) presence of silicone oil used for the lubrication of the mold. The bulk density and the total and open porosity values are reported in **Table 3.3-2**, including the data from compression tests measurements.

Table 3.3-2. Density, porosity, compression strength and approximate empirical formula of Si(O)CN foams produced using sacrificial fillers along with the standard deviation values.

Sample	ρ_{bulk} (g/cm^{-3})	Relative density	P_{total} vol%	P_{open} vol%	P_{closed} vol%	σ (MPa)	$SiO_xC_yN_z$
P-SiCN-1 (30/70)	0.885 ±0.01	0.387 ±0.01	61.1 ±1.38	50.0 ±1.07	11.1 ±0.29	11.6 ±1.1	$SiO_{1.61}C_{1.85}N_{0.17}$
P-SiCN-2 (20/80)	0.520 ±0.01	0.227 ±0.01	77.24 ±0.57	73.94 ±1.28	3.3 ±0.71	5.6 ±0.7	$SiO_{0.78}C_{0.59}N_{0.36}$

It is not easy to speculate on these results since the mechanical properties of cellular SiCN ceramics have not been yet covered in the literature. The model proposed by Gibson and Ashby[45] for brittle materials could be applicable only to the sample made by using 80 wt% of PMMA microbeads, since the relative density for the sample made by using 70 wt% PMMA was higher than 0.3, for which the validity of the model is exceeded. Therefore, sample SiCN-1 (70/30) should be considered to be a highly porous component rather than a true foam. In Gibson and Ashby`s[45] micromechanical bending model for cellular materials, the morphology of closed-cell

foams is considered one in which the cell walls are completely retained and do not contain any openings (cell windows). In the same model, the morphology of open-cell foams are idealized as interconnected ligaments without any cell walls (typical microstructure of “reticulated foams” produced by the replica method). Even if the samples prepared by sacrificial templating in the present study can be considered as open cell foams due to their mostly interconnected porosity, the morphology of the foams, as shown in **Figure 3.3-4** (a) and (b), is much more similar to that of the closed foams in which the cell walls are mostly retained. Therefore, it is reasonable that the strength data for our samples are more descriptive to what the model predicts for closed-cell foams. Similar behavior was previously observed by Colombo et al.[2] for SiOC foams. Due to the limited amount of data available, it was not possible to ascertain the value for the exponent for the logarithmic correlation function linking relative density and relative strength. However, the increase in compression strength values with the increase of bulk density is here confirmed, and the strength values measured were rather high, and comparable to what observed for SiOC micro-cellular foams.[11]

SEM micrographs (**Figure 3.3-4** (a) and (b)) show that a great amount of porosity, mostly interconnected, was formed in both samples, with pores ranging from about 5 μm to 15 μm in size. Roughly spherical shaped cells were homogeneously distributed throughout the entire volume of the pyrolyzed ceramic monoliths. Cell size and shape were not precisely similar to those of the PMMA templating beads, because of the large amount of volumetric shrinkage occurring during the ceramization step (~70 vol%). However, the distribution in cell sizes resembles that of the original PMMA microbeads.

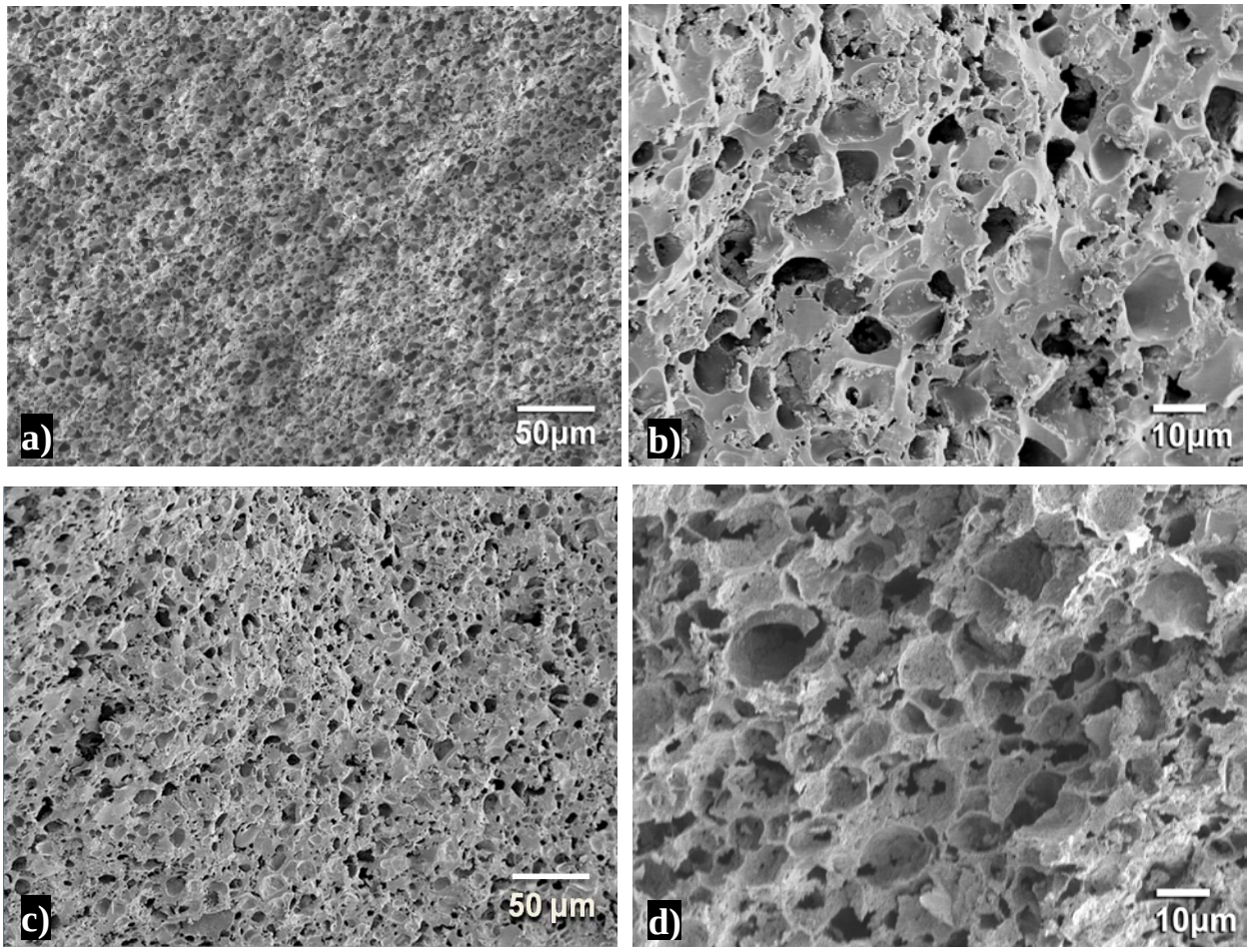

Figure 3.3-4. SEM micrographs of the fracture surface of pyrolyzed (1100°C, 2h) samples: a&b) SiCN-1 (70/30) and c&d) P-SiCN-2 (80/20).

The amount of the total porosity increased with the increased amount of sacrificial templates, while closed porosity showed the opposite trend. It should be noticed that a small amount of porosity may be attributed to other factors than the presence of the sacrificial microbeads. In fact, it was reported that warm pressed pre-crosslinked polysilazane powders possessed ~3 vol% porosity after pyrolysis at 1100°C[46]. The increased amount of closed porosity in samples SiCN-1 (70/30) could be attributed to the higher amount of preceramic polymer in the starting mixture and to the lower amount of PMMA beads that could cause a partial non-contact among the same beads, consequently giving rise to thicker struts and cell walls.

3.3.3.2. Macro-cellular foams (physical blowing agent)

For in-situ foaming with a physical blowing agent, ADA was selected since its gas yield during decomposition is very high (200-220 mL/g), which makes it the most cost efficient among all commercially available foaming agents.[47] In order to examine the effects of the porogen amount on the morphology and other characteristics, ADA was inserted into the liquid polysilazane precursor in increasing amounts (see **Table 3.3-1**). The decomposition onset temperature for pure ADA is between 210°C[47] and 260°C[48] and the gas released consists mostly of nitrogen (65 vol%) and a mixture of carbon monoxide, carbon dioxide, and ammonia.[19, 48] The solid residue after decomposition consists of urazol, biurea, cyamelide, and cyanuric acid, see **Figure 3.3-5**.[49] Depending on the processing conditions, different compositions in the end-product may be favored; however it was shown that there is always some amount of solid residue acting as a nucleating agent for the blowing process during decomposition. The decomposition reaction was found to be autocatalytic, resulting in a color change from yellow to a more neutral one.[50, 51]

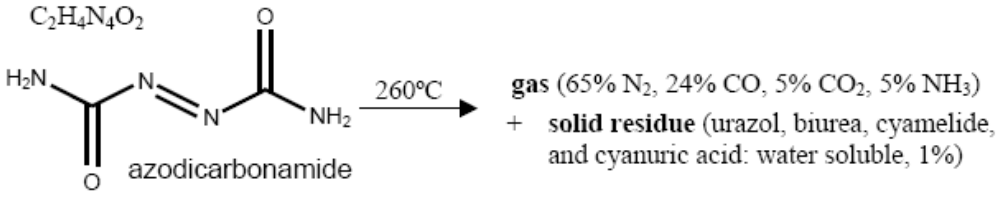

Figure 3.3-5. A chemical depiction of ADA with its decomposition products.[47, 48]

In the literature, many studies can be found concerning foaming of various polymeric systems using ADA.[19, 48, 50, 52] In situ foaming with porogens necessitates a careful control between the activation (rate, temperature) of the blowing agent and the melt viscosity of the precursor polymer. If the blowing agent decomposes before the polymeric precursor possesses sufficient enough melt viscosity to maintain the gas within the matrix, there will not be foaming. On the contrary, the polymer viscosity could be too high during the decomposition of the porogen so that insufficient gas pressure cannot initiate blowing, even though decomposition has occurred. For that reason, various parameters such as the decomposition temperature and rate of the blowing agent and the processing conditions of the precursor matrix must all be considered

before a polymeric material is selected.[47] Moreover, the decomposition process of porogens can be controlled by varying its particle size, heating rate and processing temperature, activator type and concentration, etc.[47, 50] Commonly, some transition metal compounds, polyols, urea, alcohol, amines, and some organic acids such as stearic acid[50] are used as "activators" or "kickers" to reduce the already mentioned decomposition temperature of ADA to the values as low as 150°C.[47] For example, it was recently shown that the addition of only 0.1wt% of ZnO accelerated the thermal decomposition of ADA and decreased the onset temperature[50].

As one can see from **Figure 3.3-6**(a), the thermo-gravimetric curve of pure ADA used in these experiments showed a decomposition onset at around 210°C, and off-set at around 320°C, with a large weight loss reaching 88 wt%; a clear exothermic peak can be observed at 210°C (**Figure 3.3-6**(b)). The solid residue contamination as a result of ADA decomposition within the foamed ceramic was therefore very limited ($\leq$ 1.1 wt% , using the highest amount of ADA (6wt%) and taking the ceramic yield of VL20 ~70% and solid residue of ADA ~12% at 1100°C).

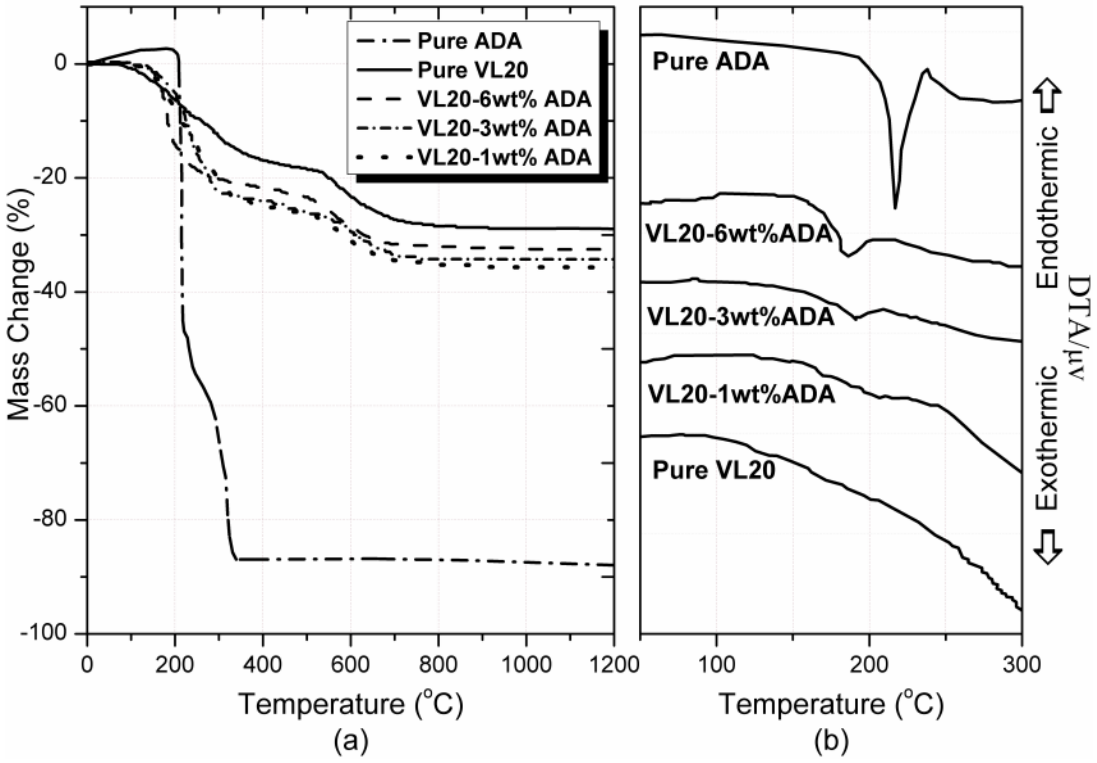

Figure 3.3-6. TG/DTA results for pure ADA, pure VL20 and all other samples made by using VL20 and ADA (under N_2 flow).

At 300°C, the mass loss for pure VL20 was around 10 wt%, and around 20 wt% for the samples containing ADA. The increased mass loss values for the porogen including samples are certainly attributable to the presence of ADA. It appeared that increasing the amount of ADA in the ADA-containing samples decreased the mass loss during the second stage of curing (300-500°C); all the foamed samples displayed the same behavior during ceramization (in the 500-800°C range) and no further significant mass loss was detectable between 800 and 1200°C. However, unexpectedly, at the end of the pyrolysis the measured ceramic yield was lower than the one computed on the basis of the rule of mixture (theoretical) especially for the samples fabricated from 1 wt% and 3 wt% of ADA. The effect attributable to the higher mass losses (compared to theoretical calculations) for the ADA including samples could arise due to enhanced release of gaseous by-products due both to the curing reactions and especially to the evaporation of low molecular weight components (Si-containing oligomers) occurring before such reactions link all the polymeric chains into a three-dimensional network.

For the samples made by using ADA there was an increase in the ceramic yield (lower total weight loss) with increasing incorporation of ADA. This implies that there was an interaction between VL20 and ADA which presumably altered the branching or crosslinking sequence of the polymer depending on the amount of ADA. The use of peroxide or azo compounds as free radical initiators is indeed recommended to promote vinyl crosslinking of silazane precursor.[38] These groups may facilitate curing when energy is provided even at relatively low temperatures. The exothermic reaction with free radicals decreases the cross linking temperature and increases the degree of polymer cross linking. This results in the reduction of evaporable oligomers and an increase of the ceramic yield. For example, the addition of dicumyl peroxide to PUVMS or VL20 leads to a decrease of the cross-linking temperature from 180-250°C to 90-190°C.[39] Furthermore, the degree of transamination might be reduced by the increase in ADA amount. Transamination is also important because it involves cleavage of Si-N bonds, and this may cause the formation of oligomeric units from the cross-linked polymer network.[39] Results from the elemental analyses agreed with the above observation; the increase in the ADA amount led to higher nitrogen content in final ceramics. More specific investigations (e.g. solid state NMR analysis) will have to be performed to ascertain the mechanism leading to an increased ceramic

yield with increasing incorporation of ADA in the foamed samples, but this is beyond the scope of the present thesis study. Another possibility is that the interaction between VL20 and ADA activated ADA so that it decomposed at lower temperatures than expected (note that the decrease in the particle size of ADA while dispersing in liquid precursor has a parallel effect). In fact, the occurrence of the latter is very clear from the shift to lower temperatures of the exothermic peak linked to ADA decomposition (see **Figure 3.3-6** (b)). The sample with 6 wt% ADA showed an exothermic effect around 170°C, temperature lower than the actual decomposition temperature of pure ADA.

Li et al.[39] have shown that PUMVS can be thermally set into a solid product without any catalyst, and that the transformation from liquid to a solid product is completed in 35 min at 150°C and in less than 5 min at 280°C. The authors explained that below 250°C, the viscosity of the liquid precursor increases to form a gel-like product, and a stable solid can be obtained at 300°C with a high crosslinking yield. Likewise, Lucke et al.[53] have demonstrated that after passing a minimum around 120°C, the melt viscosity values increased rapidly due to hydrosilylation reactions and above 200°C synthesized poly(methylvinylsilazane) precursor became solid-like. At temperatures higher than 250°C hydrosilylation reactions came to an end,[53] and thereafter vinyl polymerization occurred to form a thermoset.[39] Therefore, considering the literature data and with reference to TGA results, the curing schedule was selected. Specifically, heating to 300°C with a 2°C/min heating rate was found optimal for the sample with 1 wt% of ADA (A-SiCN-1), enabling the complete decomposition of the porogen, while at the same time the melt viscosity of the precursor was suitable to retain the morphological integrity. A further indication for the complete decomposition of ADA could be found from the final color of the thermoset; the yellowish color of the blend turned to an opaque material after processing at 300°C. Holding at this temperature for 4h resulted in a foamed polymeric thermoset (see **Figure 3.3-7**(a)).

SEM investigations given in **Figure 3.3-7**(b-d)) revealed that the samples possessed a regular morphology comprised of homogenously distributed spheroidal cells with a diameter up to 1.5 mm, with circular interconnecting windows having 100-300 µm diameter, and dense struts. Quite a few number of these cell windows were closed by a very thin layer of precursor material (see

white arrows). There were no observable cracks in the polymeric cellular matrix. The microstructure of the pyrolyzed monolith, **Figure 3.3-7**(b), closely resembled the one for the thermoset, except that most of the cell windows were open and the cell size was smaller, due to the shrinkage occurring during ceramization (average cell size 735 ± 225 µm). The shrinkage did not cause crack formation, and monoliths having dense struts and homogenously distributed interconnected cells were obtained (see **Figure 3.3-7**(d)).

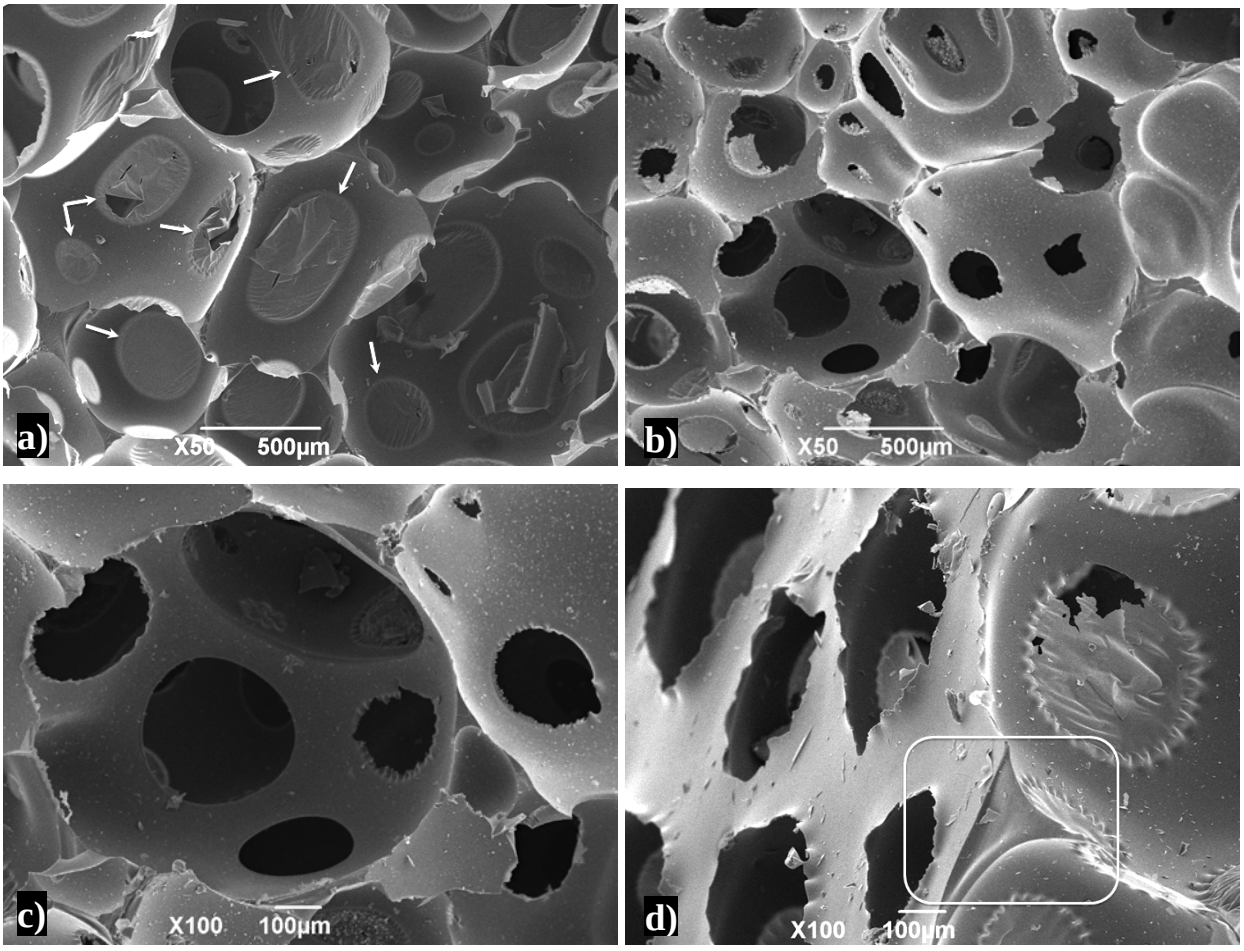

Figure 3.3-7. SEM micrographs of the fracture surface of sample A-SiCN-1; a) foamed thermoset (at 300°C; white arrows indicate membranes on cell windows); b) pyrolyzed monolith (at 1100°C); and detailed view of pyrolyzed monolith c) from the cross section and d) from the edge (white rectangle indicates a representative dense strut).

The samples with 3 wt % ADA (see **Figure 3.3-7** (a-c)) and more evidently the one with 6 wt% ADA contained a gradient in porosity (see **Figure 3.3-7** (d-f)). SiOC foams with graded porosity were obtained by other researchers using direct blowing.[21, 54] It should be noted that, in general, inclusion of porogens lowers the melt viscosity due to a plasticizing effect of the microbubbles.[55] For instance, the reduction in the melt viscosity of the PE/ADA system was found to be dependent on the concentration of ADA and increasing the amount of ADA decreased the viscosity, due to enhanced plasticizing effect.[55] These findings suggest that the amount of ADA incorporation in our experiments affected the melt viscosity of the preceramic polymer, and therefore the pore morphology and porosity distribution within the component.

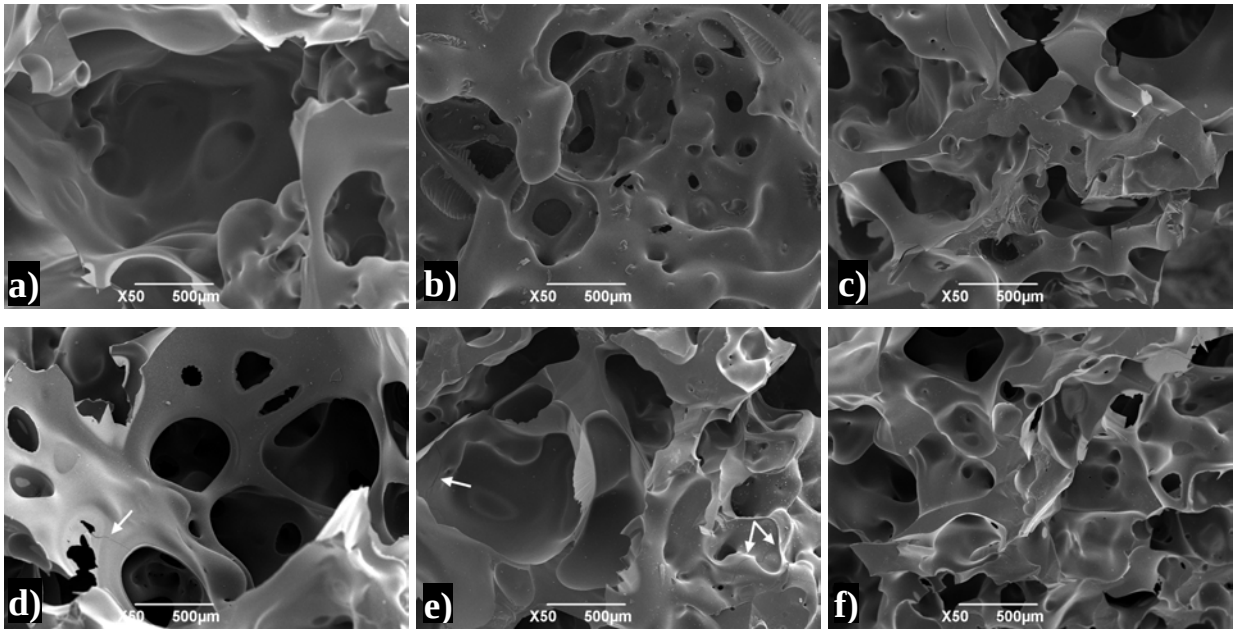

Figure 3.3-8. SEM micrographs of the fracture surface of samples after pyrolysis at 1100°C; a) A-SiCN-2 (3 wt% ADA) taken from the bottom; b) from the sample taken from the middle; c) taken from the top, and d) A-SiCN-3 (6 wt% ADA) taken from the bottom; e) taken from the middle (white arrows indicate cracks); f) taken from the top.

The influence of the melt viscosity of the precursor on the foam morphology was not intentionally investigated here, since it was beyond the scope of the present work, but the study of Takahashi and Colombo[19] on SiOC foams showed that there is a relation between the

morphology of a foam produced by direct blowing of a preceramic polymer, and the melt viscosity. Zeschky et al.[21] linked the formation of graded porosity related to a non-linear increase in viscosity, and showed that bubbles three times larger formed at the bottom of the sample compared to the ones at the top. The same behavior was observed in the present study for the samples containing 3 wt% ADA and more visibly 6 wt% ADA (**Figure 3.3-7** (d-f)). In fact, an increased amount of ADA particles enhanced the microbubble nucleation during its decomposition, so that the melt viscosity of the mix decreased due to plasticizing effect. At this stage, the bubble rise occurred easily, due to low viscosity or the polymer, leading to an accumulation of pores at the foam surface. Continuation of heating yielded a pronounced increase of viscosity due to concurrent curing reactions taking place during bubble formation and bubble rise, analogous to the observations of Zeschky et al.[21] Moreover, it should be noted that the decomposition of ADA is exothermic. Most probably, homogenously distributed ADA particles acted also as a heat source and locally enhanced the curing reactions. When the viscosity reached a certain minimum level, the ratio of bubble rise velocity to bubble growth rate became less than unity. Hence, the bubbles still could grow at the bottom of the sample due to Ostwald ripening arising from interbubble gas diffusion.[20] Coalescence by film (cell wall) rupture was not observed at that stage, due to the thickness of the lamella and high viscosity of the polymer (preventing liquid drainage), therefore resulting in smaller cells at the top (< 500 µm, see **Figure 3.3-7** (f)) and bigger cells at the bottom of the sample (>1 mm, see **Figure 3.3-7** (d)). Further increase in viscosity reduced the molecular gas diffusion through the system, thus preventing the possibility of further coarsening and finally yielding a thermoset containing graded porosity along the expansion axis. The produced ceramics with graded pores exhibited differences in structure; while the one with 3 wt% ADA was flawless, the one with 6 wt% ADA had some internal micron-sized cracks (see white arrows in **Figure 3.3-7** (d) and (f)).

All the samples possessed a large amount of porosity after pyrolysis, which was mostly open. Increasing the amount of ADA in the blends led to an increase in the cell size and affected the pore morphology, interconnectivity and amount of porosity. The presence of cells with a non homogeneous size distribution does not particularly represent a problem since several important properties are not linked to the cell size but rather to the relative density of the component.[45] Correspondingly, compression strength was found to be dependent on relative density and to the

presence of internal defects. The mechanical properties and porosity values of the samples are reported in **Table 3.3-3**. They are lower than the values obtained for micro-cellular SiOCN foams, in accordance with what already observed for SiOC samples.[11]

Table 3.3-3. Density, porosity, compression strength and approximate empirical formula of SiCN foams produced using a physical blowing agent along with the standard deviation values.

Sample	ρ_{bulk} (g/cm^{-3})	Relative Density	P_{total} vol%	P_{open} vol%	P_{closed} vol%	σ (MPa)	$SiO_xC_yN_z$
A-SiCN-1 (1wt% ADA)	0.687 ±0.18	0.293 ±0.08	70.68 ±8.07	49.45 ±10.91	21.22 ±9.74	2.89 ±1.04	$SiO_{0.03}C_{0.66}N_{0.60}$
A-SiCN-2 (3wt% ADA)	0.811 ±0.09	0.344 ±0.04	64.74 ±3.90	45.58 ±5.29	20.16 ±5.04	3.31 ±1.38	$SiO_{0.10}C_{0.66}N_{0.70}$
A-SiCN-3 (6wt% ADA)	0.830 ±0.21	0.352 ±0.09	63.92 ±9.32	47.14 ±9.02	16.78 ±8.97	1.08 ±0.56	$SiO_{0.10}C_{0.66}N_{0.74}$

The level of oxygen contamination was found to be very limited when ADA was used as a physical blowing agent. For instance the concentration of oxygen impurity was 0.87 wt% for the sample made by using 1wt% ADA. This is a very low value and almost the same as that of the ceramic made by using pure VL20 precursor (0.60 wt% of oxygen with an approximate empirical formula of $SiO_{0.02}C_{0.66}N_{0.58}$). The results given in **Table 3.3-3** indicated that even with the highest amount of ADA usage, ceramic foams with substantially low amount of oxygen contamination (<3.32 wt%) could be obtained by the method described in the present study.

3.3.4. Conclusions

Two different processing routes have been proposed to fabricate SiCN and SiOCN ceramic foams from a polysilazane preceramic polymer. Pyrolysis of the warm pressed mixture of partially crosslinked polysilazane and PMMA microspheres resulted in microcellular SiOCN ceramics having cell size up to 15 μm. Pre-curing of silazane precursor, PMMA/silazane ratio

and warm pressing parameters were found to be important factors in determining the amount of porosity, pore morphology and the degree of interconnections of the cells. In the second route, liquid polysilazane was mixed with a physical blowing agent and the blend was cured and pyrolyzed, leading to the formation of macro-cellular ceramics with ~70 vol% porosity in a one-step process. With a low amount of blowing agent addition (1 wt%) ceramic foams with regular morphology comprised of homogenously distributed spheroidal cells with a diameter~700 μm were produced. Increasing the amount of blowing agent in the precursor led to a porous component with graded porosity with small cells at the top (< 500 μm) and large cells at the bottom of the sample (>1 mm). The oxygen contamination in the pyrolyzed ceramic was very limited. The compression strength of macro-cellular foams was lower than those of the micro-cellular samples. It was shown that the Polymer Derived Ceramic (PDC) route is an efficient and versatile way to produce Si(O)CN foams possessing tailored pore architecture and properties suitable for high temperature applications.

3.3.5. References

[1]P. Colombo, E. Bernardo, and L. Biasetto, "Novel Microcellular Ceramics from a Silicone Resin," *Journal of the American Ceramic Society*, 87 [1] 152-4 (2004).

[2]P. Colombo, J.R. Hellmann, and D.L. Shelleman, "Mechanical Properties of Silicon Oxycarbide Ceramic Foams," *Journal of the American Ceramic Society*, 84 [10] 2245-51 (2001).

[3]P. Colombo, "Engineering porosity in polymer-derived ceramics," *Journal of the European Ceramic Society*, 28 [7] 1389-95 (2008).

[4]R. Zhuo, P. Colombo, C. Pantano, and E.A. Vogler, "Silicon oxycarbide glasses for blood-contact applications," *Acta Biomaterialia*, 1 [5] 583-9 (2005).

[5]L. Biasetto, A. Francis, P. Palade, G. Principi, and P. Colombo, "Polymer-derived microcellular SiOC foams with magnetic functionality," *Journal of Materials Science*, 43 [12] 4119-26 (2008).

[6]P. Colombo, T. Gambaryan-Roisman, M. Scheffler, P. Buhler, and P. Greil, "Conductive Ceramic Foams from Preceramic Polymers," *Journal of the American Ceramic Society*, 84 [10] 2265-8 (2001).

[7]P. Colombo, J.R. Hellmann, and D.L. Shelleman, "Thermal Shock Behavior of Silicon Oxycarbide Foams," *Journal of the American Ceramic Society*, 85 [9] 2306-12 (2002).

[8]P. Colombo, "Conventional and novel processing methods for cellular ceramics," *Philosophical Transactions of the Royal Society A: Mathematical, Physical and Engineering Sciences*, 364 [1838] 109-24 (2006).

[9]P. Colombo and M. Scheffler, "Highly Porous Components," in Polymer-Derived-Ceramics. Edited by P. Colombo, et al. DESTech Publications, Lancaster, PA, 2009.

[10]P. Colombo and M. Modesti, "Silicon Oxycarbide Ceramic Foams from a Preceramic Polymer," *Journal of the American Ceramic Society*, 82 [3] 573-8 (1999).

[11]P. Colombo and E. Bernardo, "Macro- and micro-cellular porous ceramics from preceramic polymers," *Composites Science and Technology*, 63 [16] 2353-9 (2003).

[12]Y.-W. Kim and C.B. Park, "Processing of microcellular preceramics using carbon dioxide," *Composites Science and Technology*, 63 [16] 2371-7 (2003).

[13]C. Vakifahmetoglu and P. Colombo, "A Direct Method for the Fabrication of Macro-Porous SiOC Ceramics from Preceramic Polymers," *Advanced Engineering Materials*, 10 [3] 256-9 (2008).

[14]T. Takahashi, H. Münstedt, M. Modesti, and P. Colombo, "Oxidation resistant ceramic foam from a silicone preceramic polymer/polyurethane blend," *Journal of the European Ceramic Society*, 21 [16] 2821-8 (2001).

[15]H. Schmidt, D. Koch, G. Grathwohl, and P. Colombo, "Micro-/Macroporous Ceramics from Preceramic Precursors," *Journal of the American Ceramic Society*, 84 [10] 2252-5 (2001).

[16]S. Costacurta, L. Biasetto, E. Pippel, J. Woltersdorf, and P. Colombo, "Hierarchical Porosity Components by Infiltration of a Ceramic Foam," *Journal of the American Ceramic Society*, 90 [7] 2172-7 (2007).

[17]M. Shibuya, T. Takahashi, and K. Koyama, "Microcellular ceramics by using silicone preceramic polymer and PMMA polymer sacrificial microbeads," *Composites Science and Technology*, 67 [1] 119-24 (2007).

[18]Y.-W. Kim, S.-H. Kim, H.-D. Kim, and C.B. Park, "Processing of closed-cell silicon oxycarbide foams from a preceramic polymer," *Journal of Materials Science*, 39 [18] 5647-52 (2004).

[19]T. Takahashi and P. Colombo, "SiOC Ceramic Foams through Melt Foaming of a Methylsilicone Preceramic Polymer," *Journal of Porous Materials*, 10 113-21 (2003).

[20]T. Fujiu, G.L. Messing, and W. Huebner, "Processing and Properties of Cellular Silica Synthesized by Foaming Sol-Gels," *Journal of the American Ceramic Society*, 73 [1] 85-90 (1990).

[21]J. Zeschky, T. Höfner, C. Arnold, R. Weißmann, D. Bahloul-Hourlier, M. Scheffler, and P. Greil, "Polysilsesquioxane derived ceramic foams with gradient porosity," *Acta Materialia*, 53 [4] 927-37 (2005).

[22]R. Rocha, E. Moura, A. Bressiani, and J. Bressiani, "SiOC ceramic foams synthesized from electron beam irradiated methylsilicone resin," *Journal of Materials Science*, 43 [13] 4466-74 (2008).

[23]A. Saha and R. Raj, "Crystallization Maps for SiCO Amorphous Ceramics," *Journal of the American Ceramic Society*, 90 578-83 (2007).

[24]H.J. Seifert, J. Peng, H.L. Lukas, and F. Aldinger, "Phase equilibria and thermal analysis of Si-C-N ceramics," *Journal of Alloys and Compounds*, 320 [2] 251-61 (2001).

[25]M. Friess, J. Bill, J. Golczewski, A. Zimmermann, F. Aldinger, R. Riedel, and R. Raj, "Crystallization of Polymer-Derived Silicon Carbonitride at 1873 K under Nitrogen Overpressure," *Journal of the American Ceramic Society*, 85 [10] 2587-9 (2002).

[26]E. Kroke, Y.-L. Li, C. Konetschny, E. Lecomte, C. Fasel, and R. Riedel, "Silazane derived ceramics and related materials," *Materials Science and Engineering: R: Reports*, 26 [4-6] 97-199 (2000).

[27]A. Saha, S.R. Shah, R. Raj, and S.E. Russek, "Polymer-derived SiCN composites with magnetic properties," *Journal of Materials Research*, 18 [11] 2549-51 (2003).

[28]C. Haluschka, C. Engel, and R. Riedel, "Silicon carbonitride ceramics derived from polysilazanes Part II. Investigation of electrical properties," *Journal of the European Ceramic Society*, 20 [9] 1365-74 (2000).

[29]I. Menapace, G. Mera, R. Riedel, E. Erdem, R.-A. Eichel, A. Pauletti, and G. Appleby, "Luminescence of heat-treated silicon-based polymers: promising materials for LED applications," *Journal of Materials Science*, 43 [17] 5790-6 (2008).

[30]X.-W. Du, Y. Fu, J. Sun, and P. Yao, "The evolution of microstructure and photoluminescence of SiCN films with annealing temperature," *Journal of Applied Physics*, 99 [9] 093503-4 (2006).

[31]G. Thurn, J. Canel, J. Bill, and F. Aldinger, "Compression creep behaviour of precursor-derived Si-C-N Ceramics," *Journal of the European Ceramic Society*, 19 [13-14] 2317-23 (1999).

[32]I.-K. Sung, M.M. Christian, D.-P. Kim, and P.J.A. Kenis, "Tailored Macroporous SiCN and SiC Structures for High-Temperature Fuel Reforming," *Advanced Functional Materials*, 15 [8] 1336-42 (2005).

[33]H. Wang, S.-y. Zheng, X.-d. Li, and D.-p. Kim, "Preparation of three-dimensional ordered macroporous SiCN ceramic using sacrificing template method," *Microporous and Mesoporous Materials*, 80 [1-3] 357-62 (2005).

[34]I.-H. Song, Y.-J. Kim, H.-D. Kim, and D.-P. Kim, "Colloidal Crystal Templating of Two-Dimensional Ordered Macroporous SiCN Ceramics," *Solid State Phenomena*, 135 27-30 (2008).

[35]J. Yan, L.-Y. Hong, A. Wang, and D.-P. Kim, "Facile Synthesis of SiCN Ceramic Foam Via Self-sacrificial Template Method," *Solid State Phenomena*, 124-126 727-30 (2007).

[36]B.H. Jones and T.P. Lodge, "High-Temperature Nanoporous Ceramic Monolith Prepared from a Polymeric Bicontinuous Microemulsion Template," *Journal of the American Chemical Society*, 131 [5] 1676-7 (2009).

[37]ASTM D 3576, "Standard test method for cell size of rigid cellular plastics," in Annual Book of ASTM Standards, Vol. 08.02. Edited, West Conshohocken, PA., 1997.

[38]Technical Bulletin 1, KiON Ceraset polyureasilazane and KiON ceraset polysilazane 20 heat-curable resins of KiON Corporation, http://www.kioncorp.com/bulletins.html (Last accessed 01.2010).

[39]Y.-L. Li, E. Kroke, R. Riedelm, C. Fasel, C. Gervais, and F. Babonneau, "Thermal cross-linking and pyrolytic conversion of poly(ureamethylvinyl)silazanes to silicon-based ceramics," *Applied Organometallic Chemistry*, 15 [10] 820-32 (2001).

[40]H. Schmidt, G. Borchardt, A. Müller, and J. Bill, "Formation kinetics of crystalline Si3N4/SiC composites from amorphous Si-C-N ceramics," *Journal of Non-Crystalline Solids*, 341 [1-3] 133-40 (2004).

[41]D. Seyferth, C. Strohmann, N.R. Dando, and A.J. Perrotta, "Poly(ureidosilazanes): Preceramic Polymeric Precursors for Silicon Carbonitride and Silicon Nitride. Synthesis, Characterization, and Pyrolytic Conversion to Si3N4/SiC Ceramics," *Chemistry of Materials*, 7 [11] 2058-66 (1995).

[42]L. Biasetto (2007). Functional Ceramic Foams from Preceramic Polymers. Dipartimento di Chimica Applicata e Scienza dei Materiali. Bologna, Università di Bologna. **PhD.:** 149.

[43]T. Cross, R. Raj, S.V. Prasad, T.E. Buchheit, and D.R. Tallant, "Mechanical and Tribological Behavior of Polymer-Derived Ceramics Constituted from $SiC_xO_yN_z$," *Journal of the American Ceramic Society*, 89 [12] 3706-14 (2006).

[44]S. Gumann, N. Nestle, V. Liebau-Kunzmann, and R. Riedel, "Investigations of Li-containing SiCN(O) ceramics via 7Li MAS NMR," *Solid State Nuclear Magnetic Resonance*, 31 [2] 82-90 (2007).

[45]L.J. Gibson and M.F. Ashby, "Cellular solids, structure and properties," pp. 510, Cambridge University Press, Cambridge, UK, 1999.

[46]C. Konetschny, D. Galusek, S. Reschke, C. Fasel, and R. Riedel, "Dense silicon carbonitride ceramics by pyrolysis of cross-linked and warm pressed polysilazane powders," *Journal of the European Ceramic Society*, 19 [16] 2789-96 (1999).

[47]S. Quinn, "Chemical blowing agents: providing production, economic and physical improvements to a wide range of polymers," *Plastics, Additives and Compounding*, 3 16-21 (2001).

[48]A.S.P. Lin, T.H. Barrows, S.H. Cartmell, and R.E. Guldberg, "Microarchitectural and mechanical characterization of oriented porous polymer scaffolds," *Biomaterials*, 24 [3] 481-9 (2003).

[49]A.S. Prakash, W.A. Swam, and A.N. Strachan, "The thermal decomposition of azodicarbonamide (1,1-azobisformamide)," *J. Chem. Soc., Perkin Trans. 2,*, 46-50 (1975).

[50]J.R. Robledo-Ortiz, C. Zepeda, C. Gomez, D. Rodrigue, and R. González-Núñez, "Non-isothermal decomposition kinetics of azodicarbonamide in high density polyethylene using a capillary rheometer," *Polymer Testing*, 27 [6] 730-5 (2008).

[51]L. Rychlá, J. Rychlý, J. Svoboda, and J. Šimonik, "DSC study of the decomposition of azodicarbonamide in different media," *Journal of Thermal Analysis and Calorimetry*, 29 [1] 77-85 (1984).

[52]Q. Huang, R. Klotzer, B. Seibig, and D. Paul, "Extrusion of microcellular polysulfone using chemical blowing agents," *Journal of Applied Polymer Science*, 69 [9] 1753-60 (1998).

[53]J. Lücke, J. Hacker, D. Suttor, and G. Ziegler, "Synthesis and Characterization of Silazane-Based Polymers as Precursors for Ceramic Matrix Composites," *Applied Organometallic Chemistry*, 11 [2] 181-94 (1997).

[54]P. Colombo and J. Hellmann, "Ceramic foams from preceramic polymers," *Materials Research Innovations*, 6 [5] 260-72 (2002).

[55]X. Qin, M. R. Thompson, A. N. Hrymak, and A. Torres, "Rheology studies of polyethylene/chemical blowing agent solutions within an injection molding machine," *Polymer Engineering & Science*, 45 [8] 1108-18 (2005).

3.4. Fabrication of Boron Including Polymer Derived Cellular Ceramics

3.4.1. Introduction

In the last decade a number of lab-scale polymeric precursors have been developed to produce ceramics in Si-O-B-C system with different Si/B ratios.[1-16] Since, in most of these studies the main interest was to describe a synthesis route and define the chemical and thermal stability of the product, generally ceramic powders have been obtained. Apart from powder forms, the possibility of fiber processing in this quaternary system has also been documented.[9, 17] The most important result that can be drawn from these aforementioned literature is that the incorporation of boron generally enhances the thermal stability of SiOC ceramics at least up to 1400°C. In particular, the presence of B in the SiOC network has been found to (i) increase the decomposition temperature of amorphous matrix around 1500°C (ii) reduce the tendency of SiO_2 crystallization, (iii) increase the crystallization rate of SiC,[2, 18] and (iv) promote the graphitization.[12]

A recent study done by Pena-Alonso et al.[12] on sol-gel derived SiOC and SiOBC ceramic, have documented that below 1200°C where bare SiOC already started to phase separate, SiOBC remains amorphous and the nanostructure is built up by mixed silicon and boron oxycarbide units. The degree of disorder is higher for the SiOBC glasses as revealed by the fact that they cannot be etched as like bare SiOC by Hydrofluoric acid (HF). However, above this temperature (1400 and 1500°C), the presence of B in the silicon oxycarbide glass favors the consumption of the mixed Si (and mixed B in SiOBC) units with a phase separation into SiC_4 and borosilicate glass clusters together with the precipitation of graphite. The authors compared the SSA results of etched B-free SiOC and SiOBC glasses and documented that upon high temperature pyrolysis (>1400°C) SiOBC is more easily etched and developed higher porosity with larger pore size.[12] Boron incorporation into SiOC structure has also been followed by the pyrolysis of commercial silicon resin (MK, 75wt%) and amorphous $9SiO_2/1B_2O_3$ (25wt%, as an active filler) powder mixtures.[18] The mixed powder was warm pressed to obtain green tablets which further pyrolyzed to obtain SiOBC bodies. No information was given concerning the dense monolithic structure

and the properties especially on porosity and mechanical strength. Yet, similar effect causing enhanced high temperature stability is shown for the samples including boron compared to that of bare SiOC. In another study to obtain ceramic tablets, hot pressing the SiO(B)CN powder which were previously obtained from the synthesized precursors[8] resulted in a monolithic structure having a high bending strength (150 MPa measured by 3p-bending) and fracture toughness (2.10 $MPa.m^{1/2}$, measured by the single edge notched beam (SENB) method).[7]

Although the first publication on polyborodiphenylsiloxane (abbreviated as PBPS) related with its synthesis and high temperature stability was in 1977,[19] the pyrolysis of this, the only commercial boron including polysiloxane, precursor itself has received little attention and virtually no studies have been used PBPS to form ceramic components.[20] This is in fact PBPS does not include any crosslinking active sites causing relatively low ceramic yield upon pyrolysis. It melts during pyrolysis and since it cannot be obtained as a thermoset body, it is generally thought as unsuitable for monolith production.[20] The published TGA data shows that on pyrolysis, PBPS precursor gave a low ceramic yield <50%,[19] and the majority of the weight loss occurs in the initial stages of the pyrolysis process, i.e. between 300-600°C.[20] Due to low ceramic yield PBPS is rather preferred as an initiator in the production of polycarbosilane (PCS) from polydimethylsilane and has been used as a binder in the sintering of SiC and Si_3N_4 powders.[20]. While as a pyrolysis product, black colored powder was obtained, monolithic structures could not be produced due most probably to the high gas release through thermolysis. During thermolysis of PBPS (in both Ar and N_2 atmospheres) around 1200°C, nanodomains of SiC become noticeable, and the domain size increases with the increase in thermolysis temperature from ~3nm up to 16nm at 1600°C.[20] Originally Yajima et al.[19] and lately Williams et al.[20] reported that up to the temperatures ~1575°C, the pyrolysis product includes boron in its structure. The first authors found that the pyrolysis of PBPS at 1700°C/2h in Ar atmosphere, yields with β-SiC, a glassy carbon and a slight amount of B_4C. Subsequently heating of this material in air at 1400°C, converted B_4C into an amorphous B_2O_3 and proved the presence of boron in the structure even after high temperature pyrolysis. This is further corroborated by the Electron Energy Loss Spectroscopy (EELS) studies of Williams et al.[20] documenting that B_4C forms ≥1200°C in N_2 and remains in the structure till to the temperatures of ~1575°C. No other study could be found focusing mainly to produce boron including SiOC bodies via utilizing

PBPS. Here in the first part of this study, we will try to produce porous SiO(B)C ceramic monoliths from the mixtures of commercial precursors; i.e. PBPS and PMS (MK).

The preparation of SiBCN ceramics derived from polymeric precursor has been intensively studied[21-40] due to its extraordinary high temperature stability; i.e. amorphous at temperatures up to 1700°C and does not decompose significantly up to 1800-2000°C.[21, 24, 32] By starting from polymeric precursors complex shaped SiBCN structures such as fibers,[38, 39, 41] fiber composites,[26] microtubes,[34] films,[37] and very recently continuous, ordered 2D hexagonal mesoporous components by nanocasting[35] have been obtained. Nevertheless, no study has been found specifically focusing on to produce cellular SiBCN monoliths which possibly be used in effective catalyst supports or filtration devices where the material has to give a service under severe conditions; i.e. high temperature >1500°C or highly oxidative. Technically the production of SiBCN is far difficult and expensive compared to SiOBC ceramics, since latter material can easily be obtained by starting from highly accessible polysiloxanes while SiBCN has to be produced from more expensive polysilazanes which are difficult to handle in ambient conditions due to high volatilization. In the second part of this section, we will give some preliminary results obtained from the experiments in order to produce microcellular SiBCN ceramics.

3.4.2. Experimental Procedure

For SiO(B)C monoliths; as received poly(boro)diphenylsiloxane (PBPS (Gelest), crushed in a porcelain mortar with pestle) was mixed with either as received MK (PMS) or pre-cured MK depending on the ratios and conditions given in **Table 3.4-1**. The powder mixture was blended in a mortar with pestle for 10 min, and the blend was pressed into 20 mm diameter cylindrical tablets with 15MPa, for a tablet ~4g of mixture is used. The obtained green tablets were placed in an alumina tube furnace (Carbolite 1200) and pyrolyzed under N_2 atmosphere at 1200°C for 2h with a 2°C/min heating and cooling rate. No additional curing step is followed and upon pyrolysis ceramic tablet ~1.5cm in diameter and ~1cm thickness were obtained.

For SiBCN monoliths; polymers were synthesized in the laboratory conditions according to the published procedure.[42] It should be underlined here that that this work lies within a PolyCerNet

collaboration between our lab and the group of *Prof. Philippe Miele* in Laboratoire des Multimatériaux et Interfaces - Université Claude Bernard LYON 1 where the polymer synthesis, green sample preparation and pyrolysis of the formed tablets have been applied. First of all; commercial PMMA micro beads of (25 μm of diameters, Altugas BS-Italy) were dried in vacuum at 60°C overnight and were mixed with polymer precursor using an agate mortar inside an Ar-filled glove box to prevent polymer oxidation (all the green sample preparation is followed in globe box due to high volatilization of boron modified silazane precursor). Two different types of precursors; $(B[C_2H_4SiCH_3NCH_3]_3)n$ C_2H_4=$CHCH_3$, CH_2CH_2 (abbreviated as PBPSZ-1), and $[B(C_2H_4SiCH_3NH)_3]n$ C_2H_4=$CHCH_3$, CH_2CH_2 (abbreviated as PBPSZ-2) have been mixed with varying amounts of PMMA (70-80wt%). Then, the blend was warm pressed at 74 MPa within the temperature range of 80-130°C using a steel mold of uniaxial press set-up in a N_2-filled glove-box. The obtained green samples were pyrolyzed in different temperatures ranging from 1000°C to 1600°C for 2h under N_2 atmosphere using graphite chamber furnace (Gero,. Neuhausen, Germany, HTK8). For all samples prepared the true density was measured from finely ground ceramic powder using a He-Pycnometer ((Micromeritics AccuPyc 1330, Norcross, GA)). Open and closed porosity of the sintered ceramics were determined by the Archimedes principle (ASTM C373-72), using xylene as buoyant medium. Compression tests were done using Galdabini SUN2500 load cell 24000N, with a cross head speed of 0.5mm/min on as pyrolyzed cylindrical SiBCN samples having ~6mm diameter and ~2.5mm thickness.

3.4.3. Results and Discussion

3.4.3.1. Porous SiO(B)C monoliths.

The tablets prepared from the mixtures of as received MK and PBPS does not need curing and the pyrolysis results in a flawless monolithic structure. **Table 3.4-1** summarizes the obtained data after pyrolysis of the polymer mixture samples. Ceramic having up to 72vol% of total porosity was formed. Yet, high fraction of closed porosity was always present for all samples. Samples prepared by using pre-cured MK (curing temperatures is given parenthesis in **Table 3.4-1**) generally yielded with lower amount of total porosity (18-55 vol%) compared to the mixtures

including as received (not cured) MK powders; 40-72 vol% total porosity. It seems from the porosity data that the latter system is more favorable since it does not necessitate also pre-curing step.

Table 3.4-1. The sample composition and %Porosity data for preceramic polymer blend systems.

#	PBPS (wt%)	PMS (wt%)	δ(bulk)	Total P. (vol%)	Closed P. (vol%)	Open P. (vol%)
HSB1	5%	As received 95%	0.7969	65.9010	18.2971	47.60
HSB2	30%	As received 70%	0.6649	71.5500	31.1200	40.43
HSB3	50%	As received 50%	0.9996	57.2294	44.5295	12.70
HSB4	70%	As received 30%	1.4062	39.8308	31.0967	8.73
HSB5	5%	200°C/<400mesh 95%	1.3719	41.2990	26.6441	14.65
HSB6	5%	200°C/170-200mesh 95%	1.9147	18.0745	8.9836	9.09
HSB7	30%	200°C/<400mesh 70%	1.3850	40.7385	14.5343	26.20
HSB8	30%	250°C/<400mesh 70%	1.0439	55.3340	3.7218	51.61
HSB9	30%	350°C/<400mesh 70%	1.4478	38.0519	7.0146	31.04

While more detailed characterization is still highly demanded concerning the phase stability especially for boron including phases, it is important to note that the microstructures obtained from the mixtures of PBPS and PMS precursors are comprised of spherical pores with dense struts, resembling typical foam like formations with defined cells, see **Figure 3.4-1** (a). On one hand, this type of microstructure may supply high strength, on the other hand, pore analysis measurements documented high fraction of closed porosity for all the samples when both polymers were used as received, i.e. with no curing. Instead when pre-cured MK is used, samples had partially lost microstructural homogeneity and defined cell structure. Pores are formed between necked grains of pre-cured PMS particles, see **Figure 3.4-1** (b-d) and depending on the blending ratio less extend of closed porosity is obtained.

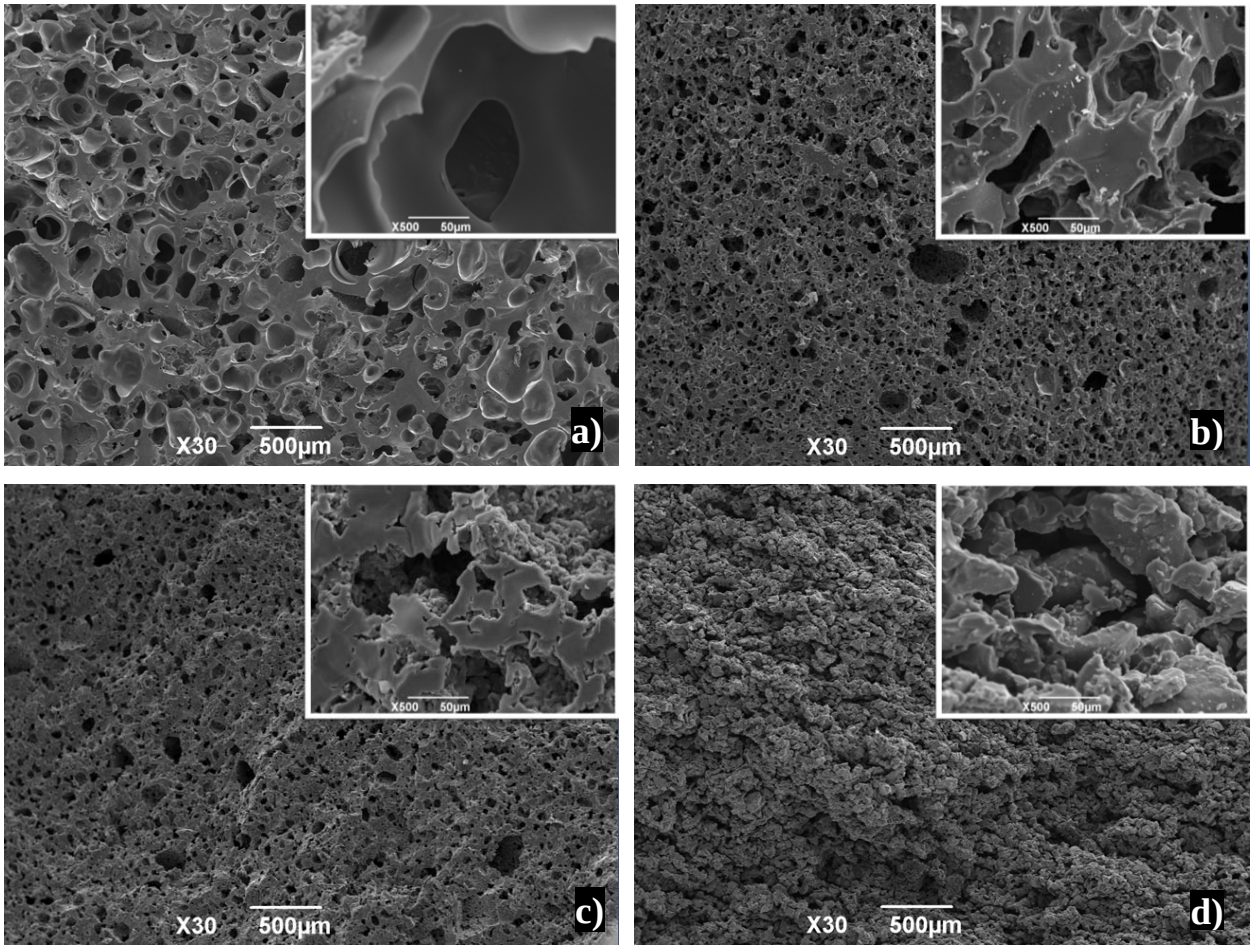

Figure 3.4-1. SEM images of samples a) HSB3, b) HSB5, c) HSB7, and d) HSB8, all treated at 1200°C for 2h in N_2.

3.4.3.2. Microcellular Si(B)CN monoliths.

During the preliminary tests it was observed that a poor reactivity of PBPSZ-1 due to the presence of Si- and N- bonded methyl groups did not allow to reach a sufficient level of cross-linking upon warm-pressing. The resulted ceramic had irregular shape with high amount of inhomogeneity and a high fraction of closed porosity (see **Figure 3.4-2**). Changing the warm pressing parameters (i.e. temperature (80 or 100°C) and the ratio of powder mixture (PMMA 80- or 70 wt%) resulted in a same type of microstructure. Although, incorporation of pre-cured (a bare precursor is cured under ammonia at 200°C which resulted in an infusible product with a

ceramic yield of ~80% measured in by TGA done in N_2) powder in 20-50 wt% relative to the bare precursor, enhanced the structural integrity and a foam like structure is obtained, the material especially with the increase in relative amount of pre-cured polymer addition, showed considerable amount of closed porosity and some micro size cracks ($T_{warm\ pressing}$=120°C with 80wt% of PMMA). Cracking problem might be partially due to high heating rate which was 60°C/h, thus for the following samples the rate was decreased to 30°C/h. It is worth mentioning that when a green sample is made only from the mixtures of PMMA and pre-cured polymer, no integrity remained.

In order to enhance the cross-linking (so integrity), a different type of polymer, PBPSZ-2 which includes higher proportion of thermally reactive units, have been used. By warm pressing at 130°C, either with 70 or 80 wt% of PMMA addition; highly porous SiBCN foams were obtained, see **Figure 3.4-2**(c-e). It was observed during warm pressing; PBPSZ-2 precursor became viscous and covered the microbeads` surfaces. Cross-linking degree throughout this process increased and resulted in a solid thermoset body which kept de-polymerization of the precursor at a sufficiently low level during pyrolysis, i.e. while the mineralization and filler burnout were achieved concurrently (so that a high amount of gas release) a porous monolithic structure was formed. It should be noted that further increase in the cross-linking degree of boron-modified polysilazanes can also be made; for example it was recently documented that a different type precursor with a plausible formula of $B[C_2H_4SiHNCH_3]_3)n$ (C_2H_4=$CHCH_3$, CH_2CH_2) is highly reactive causing higher amount of curing than both PBPSZ-1 and PBPSZ-2 types.[43] This type of precursor also does not necessitates additional curing step like PBPSZ-2, and can still be partially meltable which seems not enough for fiber drawing[42] but might be adequate for foaming.

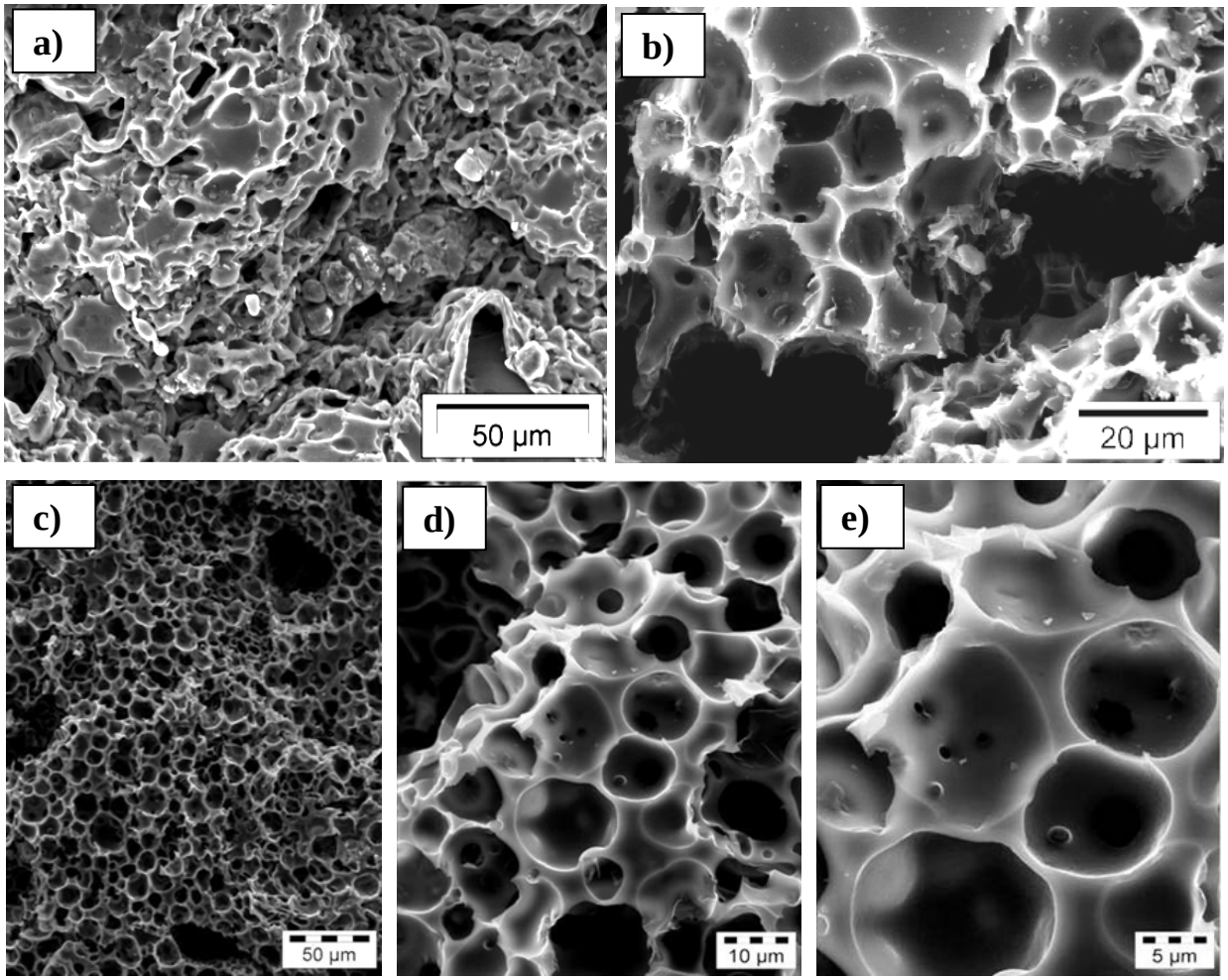

Figure 3.4-2. SEM images taken from the fracture surfaces of the pyrolyzed (1000°C/N_2)samples made from a) 20wt% PBPSZ-1 / 80wt% PMMA, b) 10wt% PBPSZ-1 / 10wt% pre-cured PBPSZ-1 / 80wt% PMMA, and c) 30wt% PBPSZ-2 / 70wt% PMMA mixtures, d) and e) are the high magnification images taken from the same sample.

Porosity measurements by Archimedes method by taking the theoretical density of pyrolyzed bodies as 2.42 g/cm^3 and 2.50 g/cm^3 for 1000°C and 1600°C treatments, respectively, showed that the samples had 64-69 vol% (~45 vol% open porous) porosity produced by 70 wt% PMMA addition when pyrolysis is done at 1000°C while measurement for the same sample pyrolyzed at 1600°C resulted in total porosity of 65-73 vol% but with a higher fraction of (~65 vol%) open porosity which might be partially caused by liquid/viscous sintering mechanism commonly

undergoing for PDC systems,[44] otherwise due to sample compacting problems during green sample preparation.

In order to prepare compression test samples a previous batch amount has been increased from 300mg to 600mg. The compressive stress–strain curves of the composite foams are given in **Figure 3.4-3** (a) for the representative samples treated either at 1000°C or at 1600°C. Taking the first collapse point as a yield point compressive strength lower than 2MPa can be found. Nevertheless, the observed stress-strain graphs did not show a clear, defined plateau which is a typical observation during compressive test of foams[45] and has been previously shown to occur around 5% strain in cellular SiOC ceramics.[46] While there was no clear plateau, increase in the flow stress with increasing strain is documented, i.e. strain hardening phenomenon exhibiting some serrations (stress oscillations in the collapse region). Such effect observed in the present study resembled more like the behavior of what was documented for SiOC foams having gradient porosity.[47] This was unexpected since previous SEM investigations have shown a mono-model pore size distribution of homogenous microcellular structure, see **Figure 3.4-2**(c). As could be seen from the observed stress-strain graphs; throughout loading, the tested samples collapse in a quasi-periodic manner with an approximate period of ~<5% strain (see **Figure 3.4-3** (a)) comparable to that of SiOC foams having pore gradient,[47] see **Figure 3.4-3** (b)) exhibiting a non-catastrophic fracture behavior. One of the reasons that caused strain hardening with no obvious plateau can be the low aspect ratio (height(h)/diameter(D)) of the tested samples ~0.4 (note that all the samples tested under low strain rate ~3×10^{-3}/s; i.e. quasi-static conditions). However, in order to explain periodic stress oscillation behavior, further examinations have been conducted by SEM analysis.

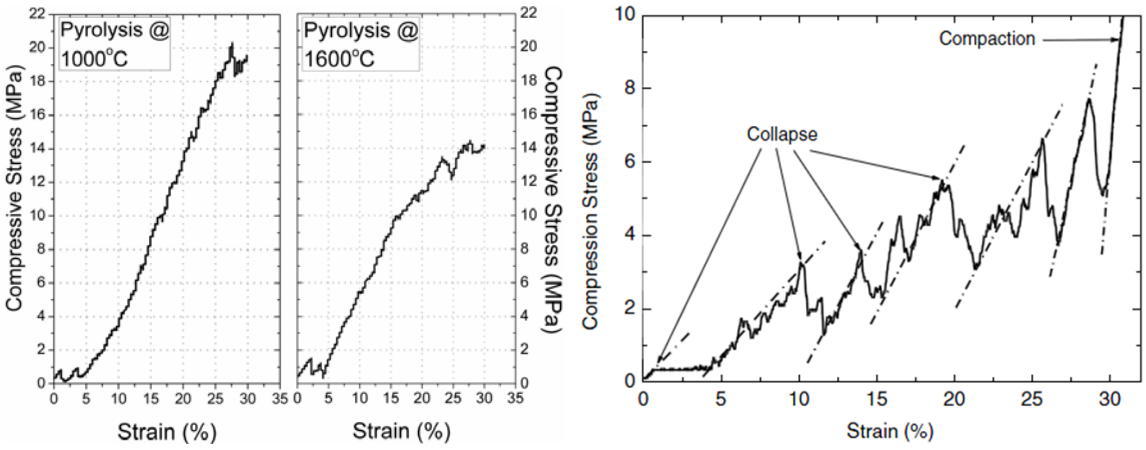

Figure 3.4-3. Plots for Compressive Stress (MPa) versus Strain (%) for a) the representative samples treated both at 1000°C and 1600°C, and b) SiOC foam having gradient porosity.[47]

The results for the SEM investigations conducted on the compression test samples (both crushed and non-crushed samples) pyrolyzed at 1000°C and 1600°C are given in **Figure 3.4-4** (a-d) and **Figure 3.4-5**(a-d), respectively. The obtained microstructures led to a better understanding of the mechanical behavior; meaning that the samples, as could be seen, did not exhibit mono-modal pore size distribution which indeed was expected. Instead, large pores, generally bigger than 200 µm together with small pores around 10-20 µm due to PMMA templating, have been observed. It seems that bigger size pores flattened perpendicular to compression axis during test (see **Figure 3.4-4**(c) and **Figure 3.4-5**(c)). Moreover there is an apparent pore closure after the application of test (more evidently for the samples pyrolyzed at 1000°C) which in fact explains oscillations in stress strain graphs. Therefore, now the question remained is why we obtained bi-modal pore size distribution? The reason lying behind the bi-modal pore size distribution (actually bigger size pores) is related to the increase in batch amount; i.e. in order to obtain bigger size samples batch was doubled which possibility caused; i) an increased amount of released gas during filler burn out, and ii) particle agglomeration of microbeads resulting in bigger size pores due most probably to the inadequate amount of mixing. Note that although tested samples had a low aspect ratio, a probable barreling effect is not considered since the samples are brittle SiBCN ceramics having possibly no ductility. Moreover, these further microstructural analyses have shown that increasing the pyrolysis temperature up to 1600°C did

not affect the structural integrity to a large extent causing only a small amount of volumetric shrinkage.

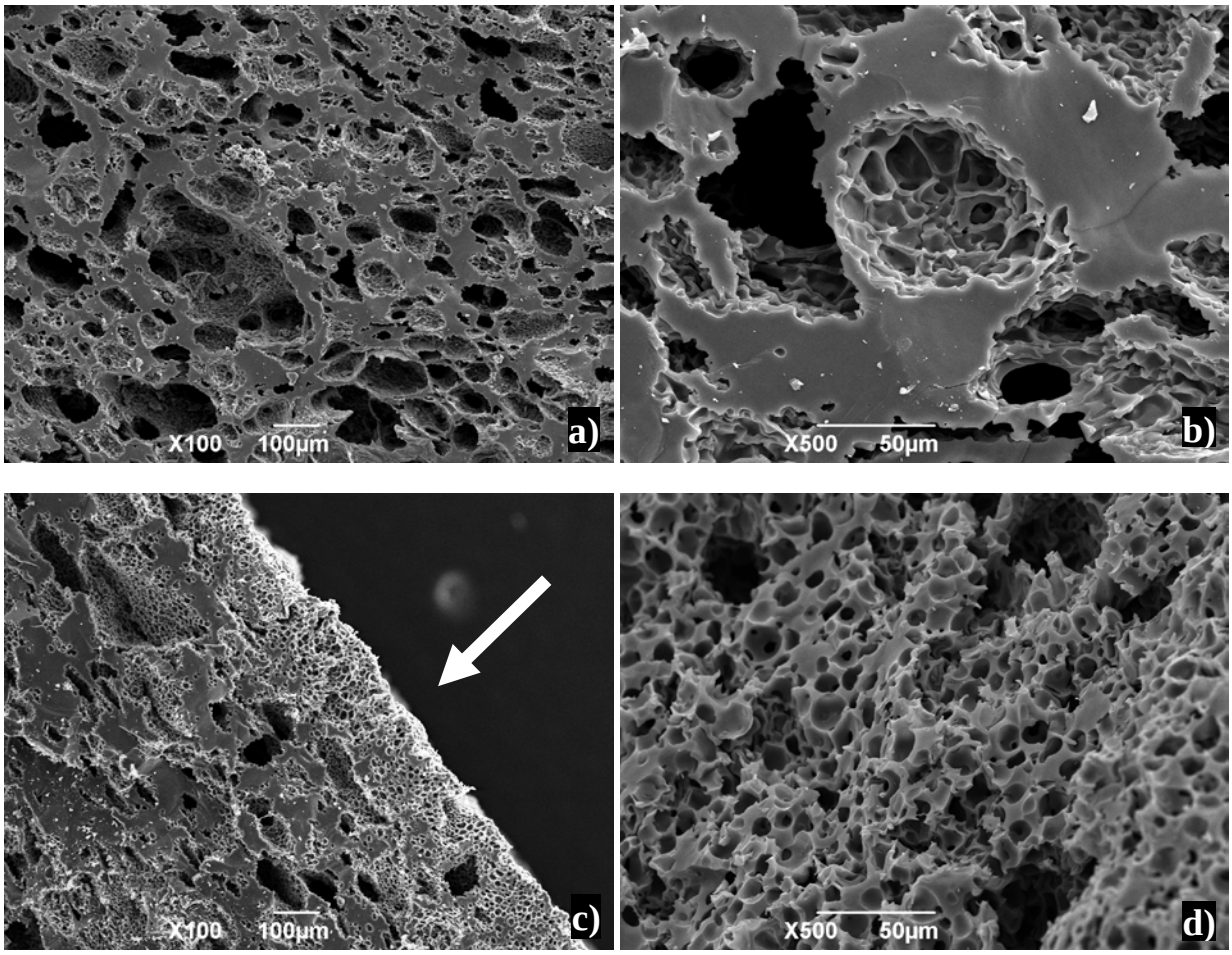

Figure 3.4-4. SEM images of the compression test samples pyrolyzed at 1000°C; a&b) fracture surface of as pyrolyzed non-crushed samples, c&d) after compression test (white arrow showing the compression axis).

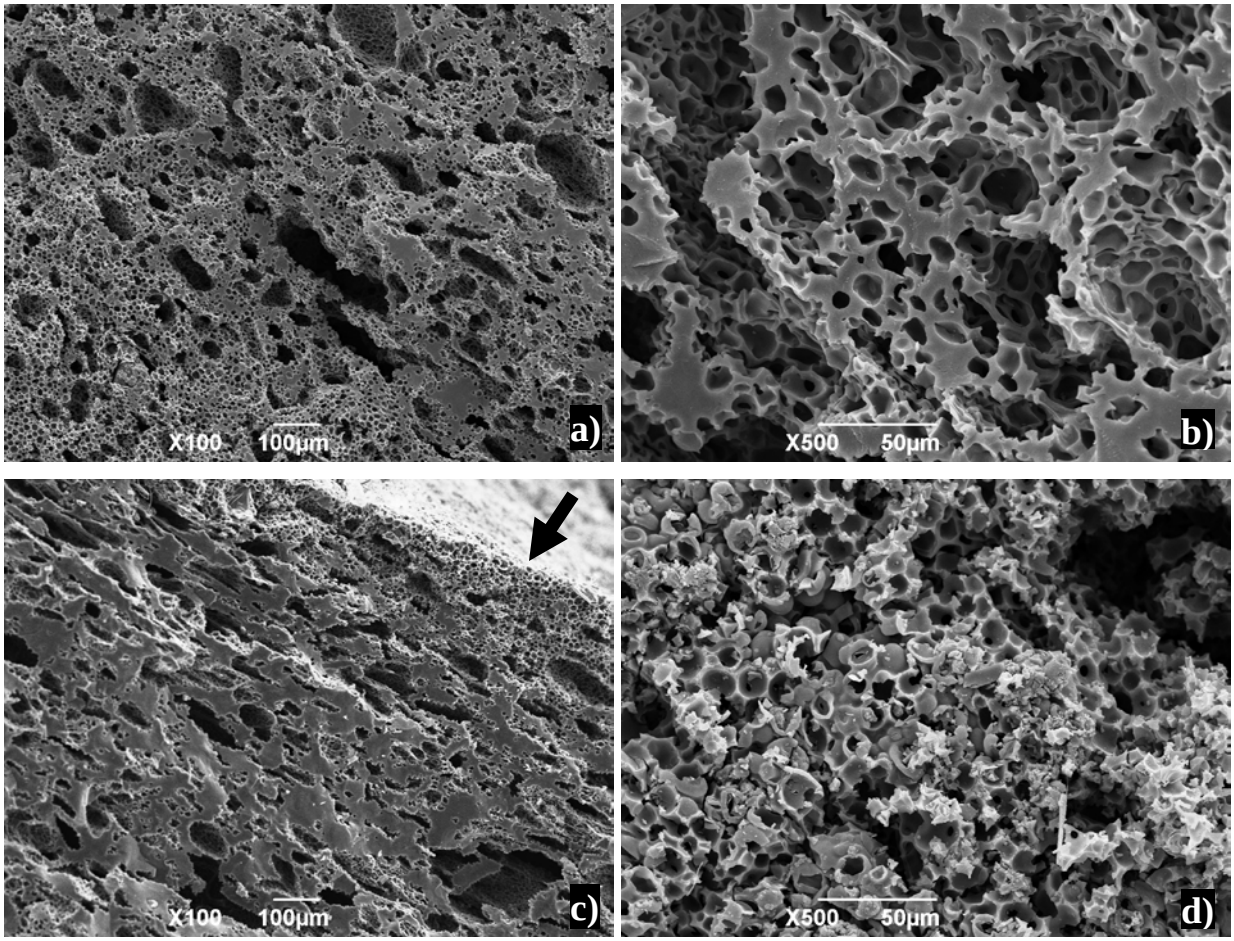

Figure 3.4-5. SEM images of the compression test samples pyrolyzed at 1600°C; a&b) fracture surface of as pyrolyzed, non–crushed samples, c&d) after compression test (black arrow showing the compression axis).

3.4.4. Conclusions

For both SiO(B)C and Si(B)CN systems very encouraging results have been obtained. Highly porous (reaching to ~70vol%) SiOBC bodies have been produced from the mixtures of commercial preceramic polymers with no addition of any other templating or blowing agents. The future study will be focused on to enhance the total porosity especially the fraction of open porosity while characterizing the produced foam in detail. For the SiBCN system, microcellular monoliths (reaching to ~70vol%) have been produced. similarly although these are the preliminary studies, promising results even towards the high temperature resistance, because the

microporous structure is retained even after annealing at 1600°C in N_2, have been obtained via sacrificial templating. It is previously shown that the cross-linking degree of boron-modified polysilazanes can be tuned by the introduction of thermally reactive units in the polymer network.

3.4.5. References

[1]G.D. Soraru, F. Babonneau, S. Maurina, and J. Vicens, "Sol-gel synthesis of SiBOC glasses," *Journal of Non-Crystalline Solids*, 224 [2] 173-83 (1998).

[2]C. Gervais, F. Babonneau, N. Dallabonna, and G.D. Soraru, "Sol-Gel-Derived Silicon-Boron Oxycarbide Glasses Containing Mixed Silicon Oxycarbide (SiCxO4-x>) and Boron Oxycarbide (BCyO3-y) Units," *Journal of the American Ceramic Society*, 84 [10] 2160-4 (2001).

[3]G. Ambadas, S. Packirisamy, and K.N. Ninan, "Synthesis, characterization and thermal properties of boron and silicon containing preceramic oligomers," *Journal of Materials Science Letters*, 21 [13] 1003-5 (2002).

[4]V. Liebau, R. Hauser, and R. Riedel, "Amorphous SiBCO ceramics derived from novel polymeric precursors," *Comptes Rendus Chimie*, 7 [5] 463-9 (2004).

[5]M.A. Schiavon, C. Gervais, F. Babonneau, and G.D. Soraru, "Crystallization Behavior of Novel Silicon Boron Oxycarbide Glasses," *Journal of the American Ceramic Society*, 87 [2] 203-8 (2004).

[6]W. Qian, F. Liying, H. Xiaowen, Z. Zhijie, and X. Zemin, "Preparation and properties of borosiloxane gels," *Journal of Applied Polymer Science*, 99 [3] 719-24 (2006).

[7]G. Wen, F. Li, and L. Song, "Structural characterization and mechanical properties of SiBONC ceramics derived from polymeric precursors," *Materials Science and Engineering: A*, 432 [1-2] 40-6 (2006).

[8]F. Li, G. Wen, H.W. Bai, and L. Song, "Synthesis and structural characterization of amorphous nano-sized SiBONC ceramic powders via polymer pyrolysis," *Journal of Non-Crystalline Solids*, 353 [4] 379-83 (2007).

[9]R. Peña-Alonso and G.D. Sorarù, "Synthesis and characterization of hybrid borosiloxane gels as precursors for Si–B–O–C fibers," *Journal of Sol-Gel Science and Technology*, 43 [3] 313-9 (2007).

[10]V. Ischenko, E. Pippel, J.r. Woltersdorf, B.R.N. Yappi, R. Hauser, C. Fasel, R. Riedel, F. Poli, and K. Muỳˆller, "Influence of the Precursor Cross-Linking Route on the Thermal Stability of Si-B-C-O Ceramics," *Chemistry of Materials*, 20 [22] 7148-56 (2008).

[11]R. Ngoumeni-Yappi, C. Fasel, R. Riedel, V. Ischenko, E. Pippel, J.r. Woltersdorf, and J.r. Clade, "Tuning of the Rheological Properties and Thermal Behavior of Boron-Containing Polysiloxanes," *Chemistry of Materials*, 20 [11] 3601-8 (2008).

[12]R. Pena-Alonso, G. Mariotto, C. Gervais, F. Babonneau, and G.D. Soraru, "New Insights on the High-Temperature Nanostructure Evolution of SiOC and B-Doped SiBOC Polymer-Derived Glasses," *Chemistry of Materials*, 19 [23] 5694-702 (2007).

[13]M. Beckett, M. Rugen-Hankey, and K. Varma, "Formation of borosilicate glasses from silicon alkoxides and metaborate esters in dry non-aqueous solvents," *Journal of Sol-Gel Science and Technology*, 39 [2] 95-101 (2006).

[14]A. Kasgoz, M. Kuramata, and Y. Abe, "Preparation and properties of borosilicate gels by the reaction of tetraacetoxysilane with boron tri-n-butoxide," *Journal of Materials Science*, 34 [24] 6137-41 (1999).

[15]A.M. Wootton, M. Rappensberger, M.H. Lewis, S. Kitchin, A.P. Howes, and R. Dupree, "Structural properties of multi-component silicon oxycarbide glasses derived from metal alkoxide precursors," *Journal of Non-Crystalline Solids*, 204 [3] 217-27 (1996).

[16]R.L. Siqueira, I.V.P. Yoshida, L.C. Pardini, and M.A. Schiavon, "Poly(borosiloxanes) as precursors for carbon fiber ceramic matrix composites," *Materials Research*, 10 147-51 (2007).

[17]A. Kasgöz, T. Misono, and Y. Abe, "Sol-gel preparation of borosilicates," *Journal of Non-Crystalline Solids*, 243 [2-3] 168-74 (1999).

[18]A. Klonczynski, G. Schneider, R. Riedel, and R. Theissmann, "Influence of Boron on the Microstructure of Polymer Derived SiCO Ceramics," *Advanced Engineering Materials*, 6 [1-2] 64-8 (2004).

[19]S. Yajima, J. Hayashi, and K. Okamura, "Pyrolysis of a polyborodiphenylsiloxane," *Nature*, 266 [5602] 521-2 (1977).

[20]H.M. Williams, E.A. Dawson, P.A. Barnes, B. Rand, and R.M.D. Brydson, "The development and stability of porosity formed during the pyrolysis of polyborodiphenylsiloxane," *Microporous and Mesoporous Materials*, 99 [3] 261-7 (2007).

[21]R. Riedel, A. Kienzle, W. Dressler, L. Ruwisch, J. Bill, and F. Aldinger, "A silicoboron carbonitride ceramic stable to 2,000°C," *Nature*, 382 796-8 (1996).

[22]F. Aldinger, M. Weinmann, and J. Bill, "Precursor-derived Si-B-C-N ceramics," *Pure Appl. Chem*, 70 [2] 439-48 (1998).

[23]R. Riedel, L. Ruswisch, M., L. An, and R. Raj, "Amorphous Silicoboron Carbonitride Ceramic with Very High Viscosity at Temperatures above 1500C," *Journal of the American Ceramic Society*, 81 [12] 3341-4 (1998).

[24]B. Baufeld, H. Gu, J. Bill, F. Wakai, and F. Aldinger, "High Temperature Deformation of Precursor-derived Amorphous Si-B-C-N Ceramics," *Journal of the European Ceramic Society*, 19 [16] 2797-814 (1999).

[25]M. Christ, G. Thurn, M. Weinmann, J. Bill, and F. Aldinger, "High-Temperature Mechanical Properties of Si-B-C-N-Precursor-Derived Amorphous Ceramics and the Applicability of Deformation Models Developed for Metallic Glasses," *Journal of the American Ceramic Society*, 83 [12] 3025-32 (2000).

[26]M. Weinmann, T.W. Kamphowe, J. Schuhmacher, K. Muller, and F. Aldinger, "Design of Polymeric Si-B-C-N Ceramic Precursors for Application in Fiber-Reinforced Composite Materials," *Chemistry of Materials*, 12 [8] 2112-22 (2000).

[27]M. Weinmann, J. Schuhmacher, H. Kummer, S. Prinz, J. Peng, H.J. Seifert, M. Christ, K. Muller, J. Bill, and F. Aldinger, "Synthesis and Thermal Behavior of Novel S-B-C-N Ceramic Precursors," *Chemistry of Materials*, 12 [3] 623-32 (2000).

[28]B. Elke, G.N. Klaus, and M. Anita, "Precursor-Derived Si-B-C-N Ceramics: Oxidation Kinetics," *Journal of the American Ceramic Society*, 84 [10] 2184-8 (2001).

[29]H. Seifert and F. Aldinger, "Phase Equilibria in the Si-B-C-N System," pp. 1-58 in High Performance Non-Oxide Ceramics I. Edited, 2002.

[30]A. Zern, J. Mayer, N. Janakiraman, M. Weinmann, J. Bill, and M. Ruhle, "Quantitative EFTEM study of precursor-derived Si-B-C-N ceramics," *Journal of the European Ceramic Society*, 22 1621-9 (2002).

[31]A. Müller, P. Gerstel, E. Butchereit, K.G. Nickel, and F. Aldinger, "Si/B/C/N/Al precursor-derived ceramics: Synthesis, high temperature behaviour and oxidation resistance," *Journal of the European Ceramic Society*, 24 [12] 3409-17 (2004).

[32]N.V. Ravi Kumar, R. Mager, Y. Cai, A. Zimmermann, and F. Aldinger, "High temperature deformation behaviour of crystallized Si-B-C-N ceramics obtained from a boron modified poly(vinyl)silazane polymeric precursor," *Scripta Materialia*, 51 [1] 65-9 (2004).

[33]S. Duperrier, C. Gervais, S. Bernard, D. Cornu, F. Babonneau, C. Balan, and P. Miele, "Design of a Series of Preceramic B-Tri(methylamino)borazine-Based Polymers as Fiber Precursors: Architecture, Thermal Behavior, and Melt-Spinnability," *Macromolecules*, 40 [4] 1018-27 (2007).

[34]L. Gottardo, S. Bernard, M.P. Berthet, and P. Miele, "Preparation of SiBCN Microtubes from Melt-Spinnable Polymers," *Key Engineering Materials*, 368 - 372 926-8 (2008).

[35]X.-B. Yan, L. Gottardo, S. Bernard, P. Dibandjo, A. Brioude, H. Moutaabbid, and P. Miele, "Ordered Mesoporous Silicoboron Carbonitride Materials via Preceramic Polymer Nanocasting," *Chemistry of Materials*, 20 [20] 6325-34 (2008).

[36]Y. Tang, J. Wang, X. Li, W. Li, H. Wang, and X. Wang, "Thermal stability of polymer derived SiBNC ceramics," *Ceramics International*, 35 [7] 2871-6 (2009).

[37]Q.-D. Nghiem and D.-P. Kim, "Highly-resistant SiCBN films prepared by a simple spin-coating process with poly(borosilazane)," *Journal of Materials Chemistry*, 15 [22] 2188-92 (2005).

[38]S. Bernard, M. Weinmann, P. Gerstel, P. Miele, and F. Aldinger, "Boron-modified polysilazane as a novel single-source precursor for SiBCN ceramic fibers: synthesis, melt-spinning, curing and ceramic conversion," *Journal of Materials Chemistry*, 15 [2] 289-99 (2005).

[39]S. Bernard, M. Weinmann, D. Cornu, P. Miele, and F. Aldinger, "Preparation of high-temperature stable SiBCN fibers from tailored single source polyborosilazanes," *Journal of the European Ceramic Society*, 25 [2-3] 251-6 (2005).

[40]A.H. Tavakoli, P. Gerstel, J.A. Golczewski, and J. Bill, "Effect of boron on the crystallization of amorphous Si–(B–)C–N polymer-derived ceramics," *Journal of Non-Crystalline Solids*, 355 2381–9 (2009).

[41]P. Baldus, M. Jansen, and D. Sporn, "Ceramic Fibers for Matrix Composites in High-Temperature Engine Applications," *Science*, 285 [5428] 699-703 (1999).

[42]L. Gottardo (2009). Design, process and properties of polymer derived ceramic SiBCN fibers. Laboratoire des Multimatériaux et Interfaces. Lyon, Université Claude Bernard Lyon 1. **PhD.:** 248.

[43]P.O. Vasiliev (2009). Functionalization and processing of porous powders into hierarchically porous monoliths. Department of Physical, Inorganic and Structural Chemistry. Stockholm, Stockholm University. **PhD.:** 68.

[44]Y.-W. Kim, S.-H. Kim, H.-D. Kim, and C.B. Park, "Processing of closed-cell silicon oxycarbide foams from a preceramic polymer," *Journal of Materials Science*, 39 [18] 5647-52 (2004).

[45]L.J. Gibson and M.F. Ashby, "Cellular solids, structure and properties," pp. 510, Cambridge University Press, Cambridge, UK, 1999.

[46]P. Colombo and M. Modesti, "Silicon Oxycarbide Ceramic Foams from a Preceramic Polymer," *Journal of the American Ceramic Society*, 82 [3] 573-8 (1999).

[47]J. Zeschky, T. Höfner, C. Arnold, R. Weißmann, D. Bahloul-Hourlier, M. Scheffler, and P. Greil, "Polysilsesquioxane derived ceramic foams with gradient porosity," *Acta Materialia*, 53 [4] 927-37 (2005).

CHAPTER IV

PRODUCTION AND PROPERTIES OF HIGH SPECIFIC SURFACE AREA COMPONENTS FROM PRECERAMIC POLYMERS

During the second part of studies we described one-pot processing strategies enabling to produce cellular ceramic components with hierarchical porosity and high specific surface area (SSA). By using Periodic Mesoporous Organosilica (PMO) particles as a mesoporous filler and PDMS as a high temperature binder phase; high SSA, hierarchically porous, permeable SiOC ceramic monoliths have been produced. Subsequently; experiment results are documented where cellular SiOC composite ceramics having a macro-cellular 3D pore network decorated with SiC, Si_2ON_2 or Si_3N_4 nanowires (depending on the experimental conditions) were obtained. The methodology; catalyst assisted pyrolysis, that one can find in the following subsections is very facile, one-pot strategy to produce high SSA, hierarchical porous materials from preceramic polymers. Studies are finalized with the selective etching of different PDCs by halogens in order to produce high specific surface area carbon forms.

4.1. SiOC Ceramic Monoliths with Hierarchical Porosity

4.1.1. Introduction

A porous ceramic component containing pores on two or more length scales is referred to as a material with hierarchical porosity; see Chapter 2.3.3 for more details on hierarchically porous ceramics. Such components are of significant technological interest, and are used in several industrial processes and household products. Applications include catalysis, filtration (of liquids

or gases), extraction, separation, sorption and scaffolds for biological applications.[1] When porous materials are required to perform multiple functions, hierarchical porosity constitutes a means to accomplish these multiple tasks. For example, micro-macro porosity can greatly improve the performance of microporous materials in applications where a material with both catalytic function and high mechanical strength is required. In general, it can be said that a macroporous ceramic framework offers chemical and mechanical stability, as well as high convective heat transfer, high turbulence, low pressure drop and a high external mass transfer rate due to interconnections between the macropores,[2] while the micro/meso-porous system would provide the functionality for a given application. Several routes have been explored to fabricate ceramics with hierarchical porosity, including one-pot or dual-step strategies as previously explained in Chapter 2.3.3.[3-5] Preceramic polymers have also been used for this purpose; hierarchical porosity was achieved by a controlled thermal treatment and/or the addition of suitable fillers,[6] by depositing zeolites onto the cell walls of SiOC microcellular foams,[7] by coating with a meso-porous film [8] or by selective etching.[9]

PMOs have recently experienced a great development in their chemical properties and applications.[10-12] Mesoporosity, with uniform pore size and shape, is typically achieved via surfactant self assembly process followed by further surfactant removal treatments. A large number of variants such as temperature, pH, concentrations, surfactant type (e.g., CTAC, Brij56, F127, etc),[13-15] and the type of organic units of the polysilsesquioxane precursors (R= $-CH_2-$, $-CH_2-CH_2-$, $-CH=CH-$, benzene)[10, 11, 16-19] are responsible for the structural and chemical design of the PMOs family. Recently, mesoporous SiOC glasses have been produced, possessing a diverse structure (cubic, hexagonal) and microstructural stability to high temperatures (800 to 1000°C).[20, 21] Here, a novel production route for SiOC glass monoliths possessing meso- and macro-porosity, obtained by embedding Periodic Mesoporous Organosilica (PMO) particles into a foamed siloxane preceramic polymer is documented.

4.1.2. Experimental Details

Two different types of periodic mesoporous organosilica (PMOs) particles; Type-A (*Cubic Fm3m)* and Type-B (*Cubic Pm3n)* were prepared, according to previously published methods.[13, 21] It should be underlined here that this work lies within a PolyCerNet collaboration between our lab and the group of *Dr. Florence Babonneau*, Chimie de la Matière Condensée, University P. et M. Curie-Paris 6, UMR CNRS 757 where the PMO particles have been synthesized. PMO Type-A is prepared by following the method proposed by Pauletti et al.[21] In a typical synthesis, 0.9g of Pluronic F127 (non-ionic triblock copolymer $(PEO)_{106}$ $(PPO)_{70}$ $(PEO)_{106}$ (MW 12600 provided by BASF) and 5g of K_2SO_4 (Fluka) were carefully added to 40g of 0.7 M HCl solution under continues stirring at 40°C. After complete dissolution, 3.22g of 1,2-bis(triethoxysilyl)ethane (BTEE 97%, Gelest) were added to this mixture and the blend was kept in a closed plastic bottle and mixing was continued for 24h followed by aging in oven at 85°C for another 24h. White precipitate was recovered by filtration, washed several times with distilled water and dried at 37°C for 48h. The surfactant was removed by the procedure reported previously (1g of as-synthesized material was refluxed in 150ml of ethanol with 2.8g of a 36% HCl aqueous solution for 6h and then was dried overnight at 90°C).[13, 17, 19, 22] While, PMO Type-B (*Cubic Pm3n)* is obtained from 1,2-bis(trimethoxysilyl)ethane (BTME) (Gelest, Morrisville, PA) used as precursors and cetyltrimethylammonium chloride (C16TAC) (Aldrich, St. Louis, MO) as surfactant. The molar ratio of the mixture was; BTME: 1; C16TAC: 0.91, NaOH: 1; H_2O: 336, the details of the synthesis procedure can be found elsewhere.[13, 20]

Two different commercially available silicone polymers were used for the production of macro-porous ceramics: a solid poly(methyl-phenyl-silsesquioxane) (PMPS, H44), and a liquid silicone elastomer (RTV 141A and B). As suggested by the manufacturer, mixing the two components of RTV141, A and B, in a ratio of 10:1 (wt%) results in a poly(dimethylsiloxane) (PDMS) polymer. Macroporous SiOC ceramic bodies can be obtained by the pyrolysis of the above mentioned preceramic polymer mixtures, as discussed previously in Chapter 3.1.[23]

To this siloxane precursor mixture, PMO particles were added in order to develop macro-porous ceramic monoliths possessing also hierarchical porosity. Several different compositions were prepared; varying the ratio between the siloxane precursors and the amount of PMO particles

(see **Table 4.1-1**). In a typical experiment, surfactant extracted PMO powder was added to an Al-mold containing silicone oil (component A - vinyl-silicone) or a combination of previously mixed siloxanes (component A - vinyl-silicone and PMPS), and the blend was then mixed with magnetic stirrer for 20 min. Once homogenization was achieved, the other silicone oil (component B – hydrosilyl-silicone) was poured into the mixture, and the blend was mixed with a glass spatula for additional 5 min. After that, it was transferred into an oven operated at 180ºC for 4 h in order to crosslink the blends (PDMS and PMPS), if ADA is incorporated then curing was done at 225ºC. The crosslinked thermoset was removed from the mold, cut into desired pieces and then pyrolyzed at 1000°C holding for 2h at peak temperature in an alumina tube furnace (Carbolite 1200) in flowing Argon gas (1 atm; heating and cooling rate 2°C/min). All the samples were prepared following the same route, except for the sample prepared by using PMPS and PMO (sample PMC1, no PDMS), where two solid powders were mixed by hand and crosslinked at 225°C for 4h, followed by pyrolysis under the same conditions of the previous samples. Surfactant extracted bare PMO powders were also pyrolyzed following the procedure described above, to serve as reference.

Table 4.1-1. Composition (wt%) of the as prepared samples obtained by mixing the different silicone precursors (PDMS, PMPS) and PMO particles.

Sample label	PDMS (RTV 141) (wt%)	PMPS (H44) (wt%)	PMO Type-A *Cubic Fm3m* (wt%)	PMO Type-B *Cubic Pm3n* (wt%)	ADA (wt%)
PMC0	0	80	20	-	-
PMC1	0	80	-	20	-
PMC2	55	35	10	-	-
PMC3	55	35	-	10	-
PMC4	50	35	15	-	-
PMC5	50	35	-	15	-
PMC6	54	34	10	-	2
PMC7	52.5	32.5	10	-	5
PMC8	52.5	32.5	-	10	5
PMC9	85	0	15	-	-
PMC10	85	0	-	15	-

Crosslinked samples were subjected to thermogravimetric analysis to 1500ºC (TGA, STA 409, Netzsch GmbH, Selb, D; 5ºC/min, flowing Ar). The microstructural features were evaluated from fracture surfaces by scanning electron microscope (SEM, Stereoscan 250, Cambridge Instruments, Cambridge, UK, and Zeiss Microscope Ultra 55 type FEG-SEM coupled with EDX). A powder diffractometer in Bragg-Bentano configuration equipped with a graphite monocromator was used for X-Ray Diffraction Analysis (XRD) with data collection ranging from 0.5° to 3° with steps of 0.01° and 1s acquisition time (CuKα radiation, Bruker AXS

Advance Diffractometer, Karlsruhe, D). N_2 adsorption-desorption isotherms were collected at 77 K with relative pressure p/p_0 ranging from 0.05 to 0.99 (Micrometrics ASAP 2010 Surface Analyzer, Norcross GA, USA). Samples were outgassed at 200°C overnight before analysis. The specific surface area was determined by the Brunauer-Emmet-Teller (BET) method in the range $0.05 < p/p_0 < 0.30$. The total pore volume was estimated from the amount of N_2 adsorbed at $p/p_0 = 0.99$.

Compression testing was performed at room temperature on selected pyrolyzed samples which were cut before pyrolysis to avoid shape distortions to find out the cold crushing strength (CCS). Instron type machine (1121 UTM, Norwood, MA, USA) using steel loading rams at a strain rate of 0.5 mm/min was used for testing. Specimens with a nominal dimension of (0.5x0.5x0.5) cm^3 were cut from larger samples; 10 samples per data point were tested. Bulk density and apparent porosity values were determined by Archimedes' technique, employing xylene. Skeletal densities of the pyrolyzed samples were obtained from finely ground powders using helium pycnometry (AccuPyc 1330, Micromeritics, Norcross, GA).

4.1.3. Results and Discussion

We have previously shown that by mixing polysiloxanes with different characteristics (linear or cage-like molecular structure, different ceramic yield) macro-porous SiOC ceramic components can be fabricated. By varying the processing conditions and the relative amount of the different precursor employed, it is possible to produce a high degree of open cells possessing a variable size, and to control the amount of total porosity in the final ceramic body.[23] The samples here discussed always contained some PMO particles that were added to the polysiloxane precursors to produce macro-porous ceramics with a high specific surface area.

PMO Type-A (cubic *Fm3m*) formed an irregular shaped triangle like particles after surfactant removal and retained its cubic structure up to the pyrolysis temperatures ~1000°C.[21] It was already shown by Toury et al.[20] that PMO Type-B (cubic *Pm3n*) synthesized from BTME have a truncated rhombic dodecahedral shape, which is characteristic for cubic symmetry, with a Pm3n

space group and the particular shape is retained after solvent extraction. After pyrolysis at 1000°C in Ar, only a limited modification of the initial well defined shape occurs, which converts the particles into SiOC ceramic interconnected and/or distorted cubes of around 5 μm in size. The analysis of the powders employed in this study, pyrolyzed without mixing with the polysiloxane precursors, confirmed the above findings of Toury et al.[20] (see **Figure 4.1-1** (a) and (b)).

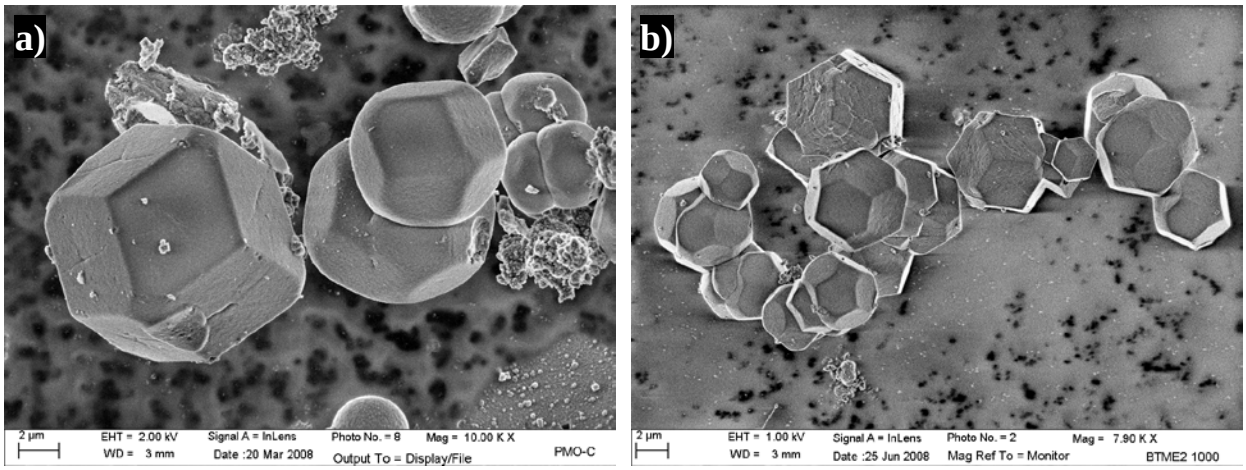

Figure 4.1-1. FEG-SEM images of PMO-Type B particles after: a) solvent extraction; and b) pyrolysis at 1000°C/2h/Ar.

Figure 4.1-2 (a-d) shows the SEM micrographs taken from the fracture surface of samples made by using PMPS and both types of PMO particles after pyrolysis. As seen, the specimens exhibit an inhomogeneous morphology at the macroscopic scale, as well as some cracks due most probably to the stresses originating from several factors, including the large volume of gas released during pyrolysis and the inherent disadvantage of inhomogeneous mixing of solid constituents. It can be seen in **Figure 4.1-2** (b) and more evidently in **Figure 4.1-2** (d) that the SiOC matrix phase deriving from the ceramization of PMPS completely embeds the PMO particles, which are distributed as discrete islands as pointed out by black arrows in the figure.

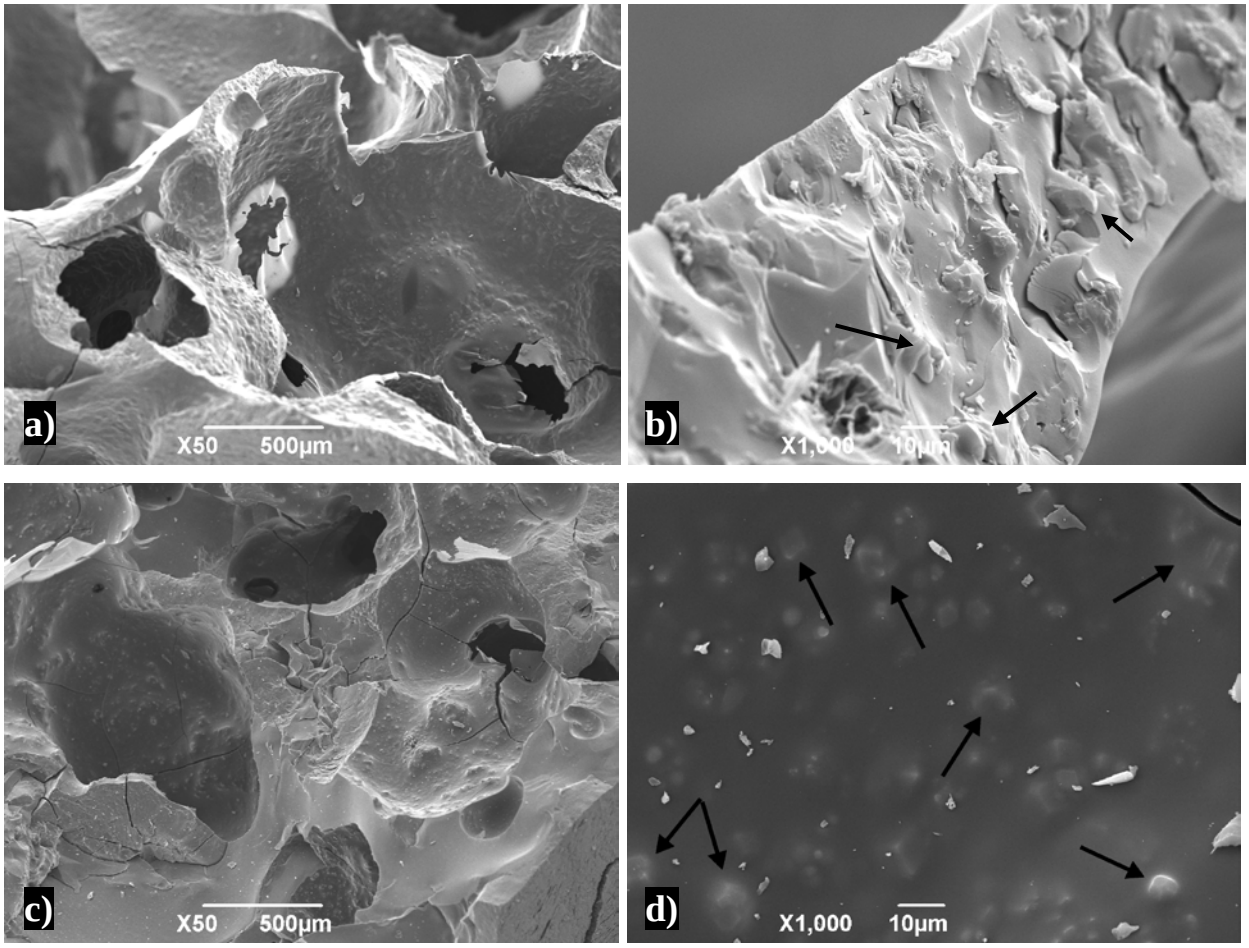

Figure 4.1-2. SEM micrographs taken from the fracture surfaces of the 1000°C pyrolyzed samples; a) PMC0 (80 wt% PMPS - 20 wt% PMO Type A) general morphology; b) detail at higher magnification, c) PMC1 (80 wt% PMPS - 20 wt% PMO Type B); general morphology; d) detail at higher magnification, black arrows indicate embedded PMO particles.

The SEM micrographs for samples PMC2 and PMC3 (55 wt% PDMS - 35 wt% PMPS - 10 wt% PMO) are reported in **Figure 4.1-3** (a) and (b) for PMC2 and **Figure 4.1-3** (c) and (d) for PMC3. It seems that PMO grains are rather well distributed throughout the entire volume of the macro-porous sample, and are present within the struts and at the surface of the cells, retaining also, at least partially, their morphological integrity (see **Figure 4.1-3** (b) and (d)), note that the shape of bare surfactant extracted particles namely; irregular (triangle like) shape of Type-A and dodecahedral shape of Type-B particles. No cracks were observed in the samples.

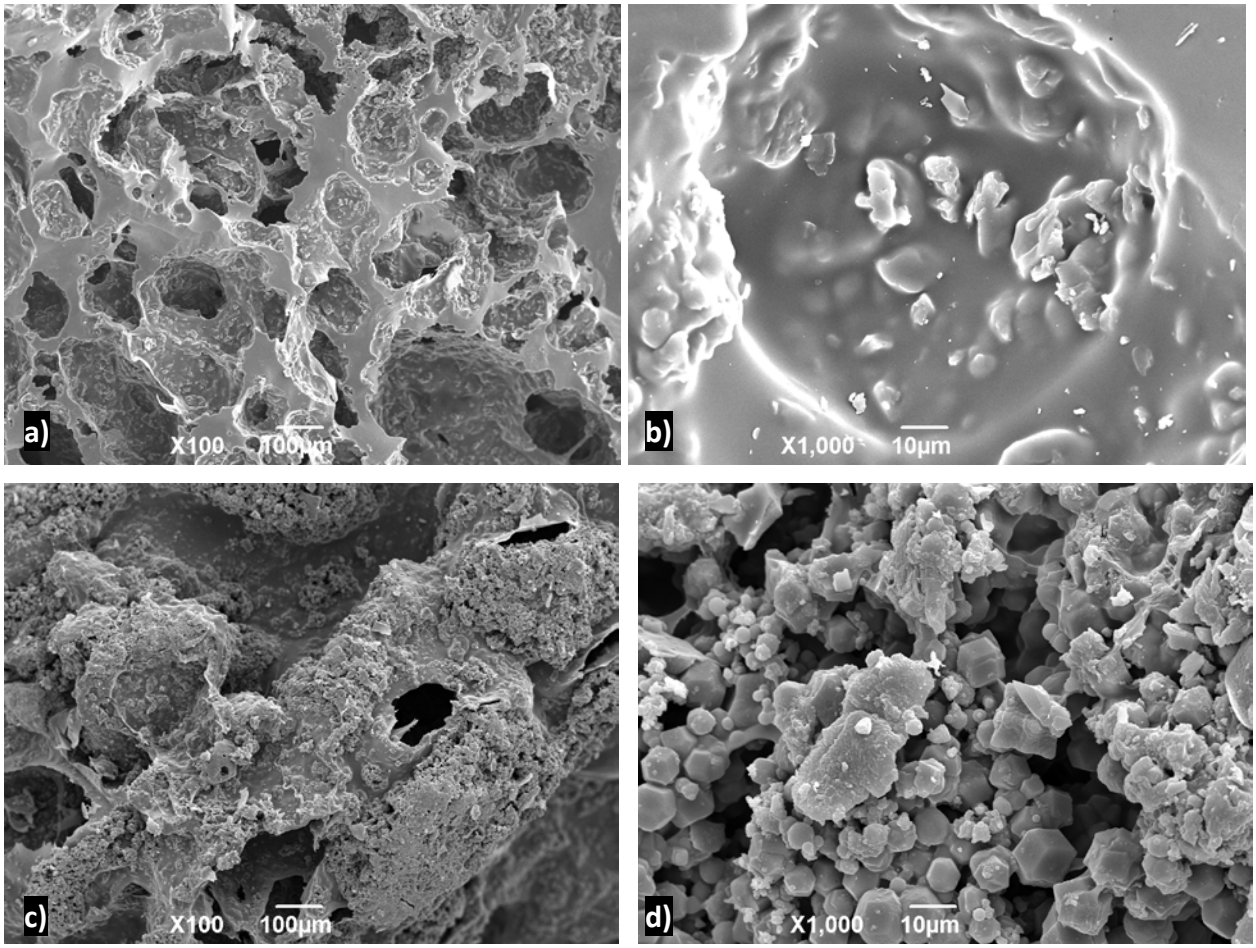

Figure 4.1-3. SEM micrographs taken from the fracture surfaces of the 1000°C pyrolyzed samples; a) PMC2 (55 wt% PDMS - 35 wt% PMPS - 10 wt% PMO Type A, general morphology; b) detail at higher magnification; c) PMC3 (55 wt% PDMS - 35 wt% PMPS - 10 wt% PMO Type B), general morphology; and d) detail at higher magnification.

The microstructure of samples PMC4 and PMC5 (50 wt% PDMS - 35 wt% PMPS - 15 wt% PMO), both are quite similar to the ones prepared with less amount of PMO but instead more liquid polysiloxane. This demonstrates that the presence of the liquid silicone oil assists in the homogeneous distribution of the PMO particles throughout the SiOC matrix, and the much lower ceramic yield of the PDMS with respect to the PMPS (~26 wt% vs ~80 wt% at 1000°C) allows

for the surfacing of the PMO particles on the cell walls. When comparing these two samples with the previously investigated ones (PMC2 and PMC3), the improvement in surface morphology achieved by increasing the PMO/Silicone precursors ratio is evident, showing a more consistent distribution of the particles in the ceramic matrix, especially for the sample made from Type-B PMO particles, unambiguously embedded within the struts and cell walls of the macro-porous SiOC monolith (**Figure 4.1-4** (d)). It has to be noted that both type of particles, seem to have undergone a limited morphological transformation; for example PMO Type-B (sample PMC5) shows a more rounded shape than that reported in **Figure 4.1-1** (a and b). This could be attributable either to a partial reaction/dissolution of the PMO particles within the surrounding SiOC matrix, or to a covering effect produced by the polysiloxane residues.

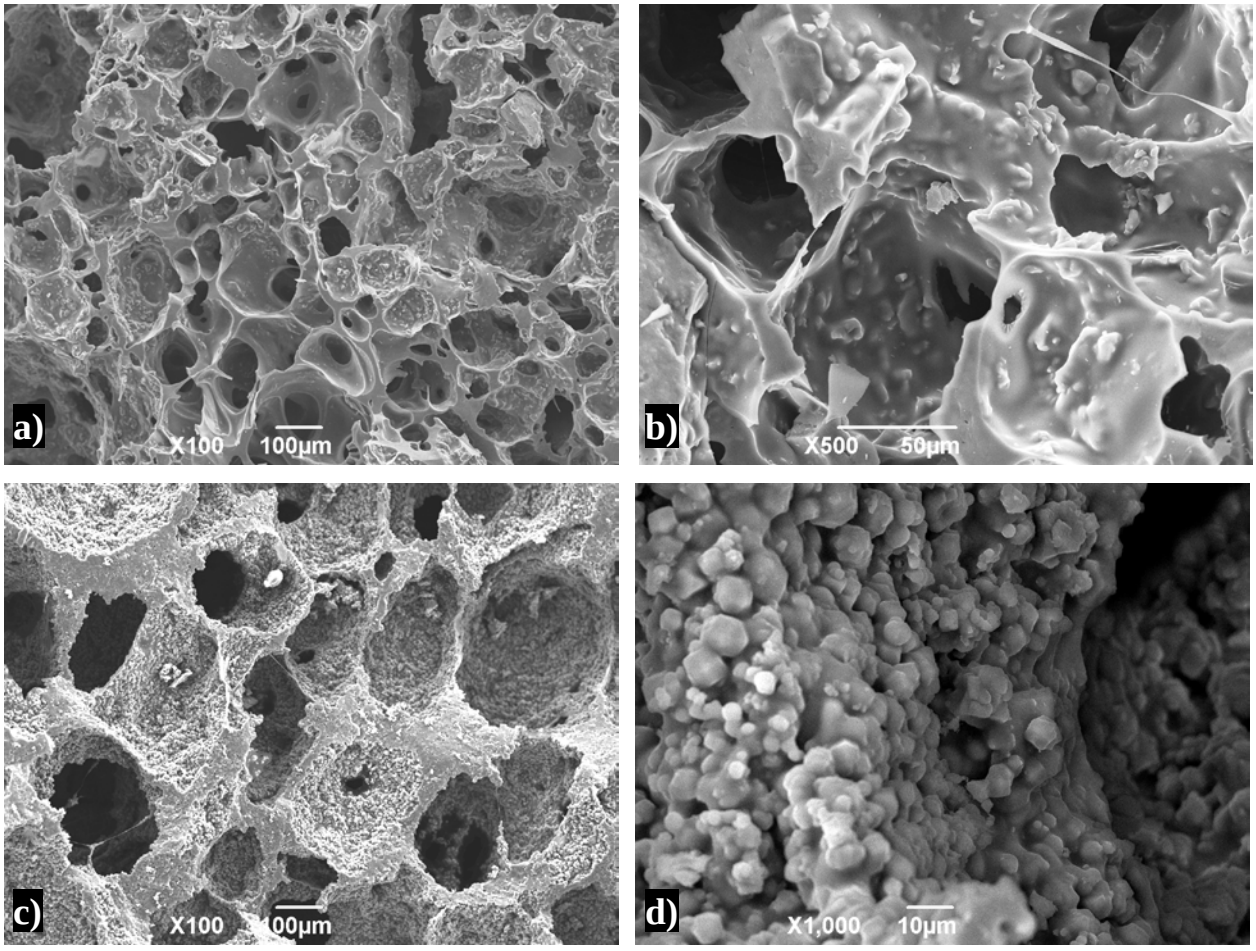

Figure 4.1-4. SEM micrographs taken from the fracture surfaces of the 1000°C pyrolyzed samples; a) PMC4 (50 wt% PDMS - 35 wt% PMPS - 15 wt% PMO Type A), general morphology; b) detail at higher magnification; c) PMC5 (50 wt% PDMS - 35 wt% PMPS - 15 wt% PMO Type B), general morphology; and d) detail at higher magnification.

The microstructures of sample PMC6 (PDMS-PMPS with 2 wt% ADA and 10 wt% PMO-Type A), are shown in **Figure 4.1-5** (a and b). The presence of three-dimensionally interconnected, open macro-porosity is evident. Higher magnification images demonstrate that the PMO particles are homogeneously embedded in the cell walls (**Figure 4.1-5** (b) and inset therein). Increasing the ADA amount caused a profound effect on microstructure resulting in a highly porous component, see SEM images for PMC7 with 5 wt% ADA together with 10 wt% PMO-Type A given in **Figure 4.1-5** (c and d). Similar results are obtained from the sample PMC8 with 5 wt% ADA together with 10 wt% PMO-Type B, see **Figure 4.1-5** (e and f). Although, 3D interconnected porosity and PMO particles distributed on the cell walls and struts of the foam are clear from the images for both of the samples made by using 5 wt% ADA. Complete coverage of the cell surfaces is not obtained due most probably to increases in the geometrical surface area because of the transformation from a porous structure to foam like structure. Moreover, PMO particles (see embedded high magnification images given in Figure 4.1-5 (b, d and f) did not preserve their distinct shapes similarly to what was observed from the previous samples. There is again a kind of “coverage” over the particles coming due to viscous flow during curing.

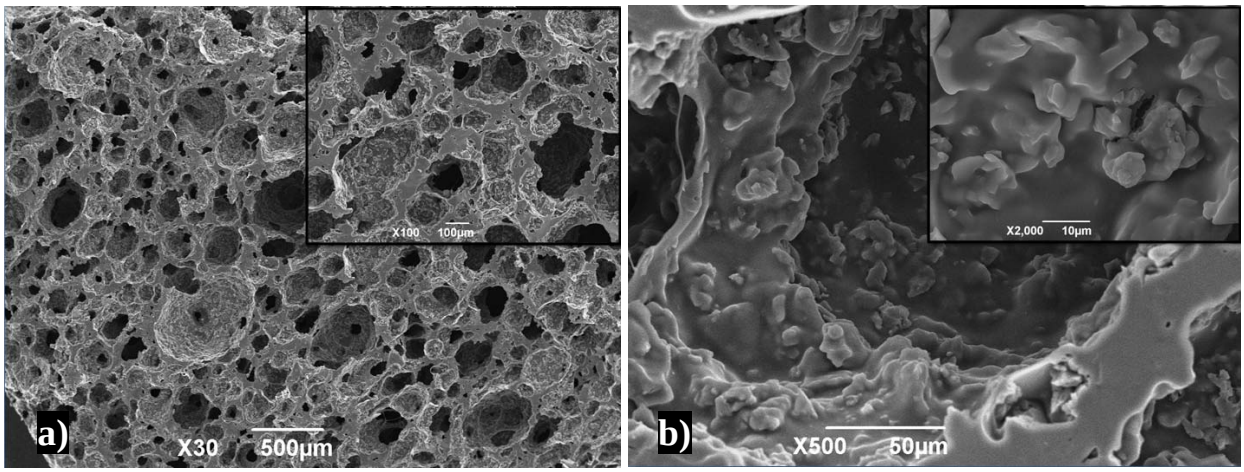

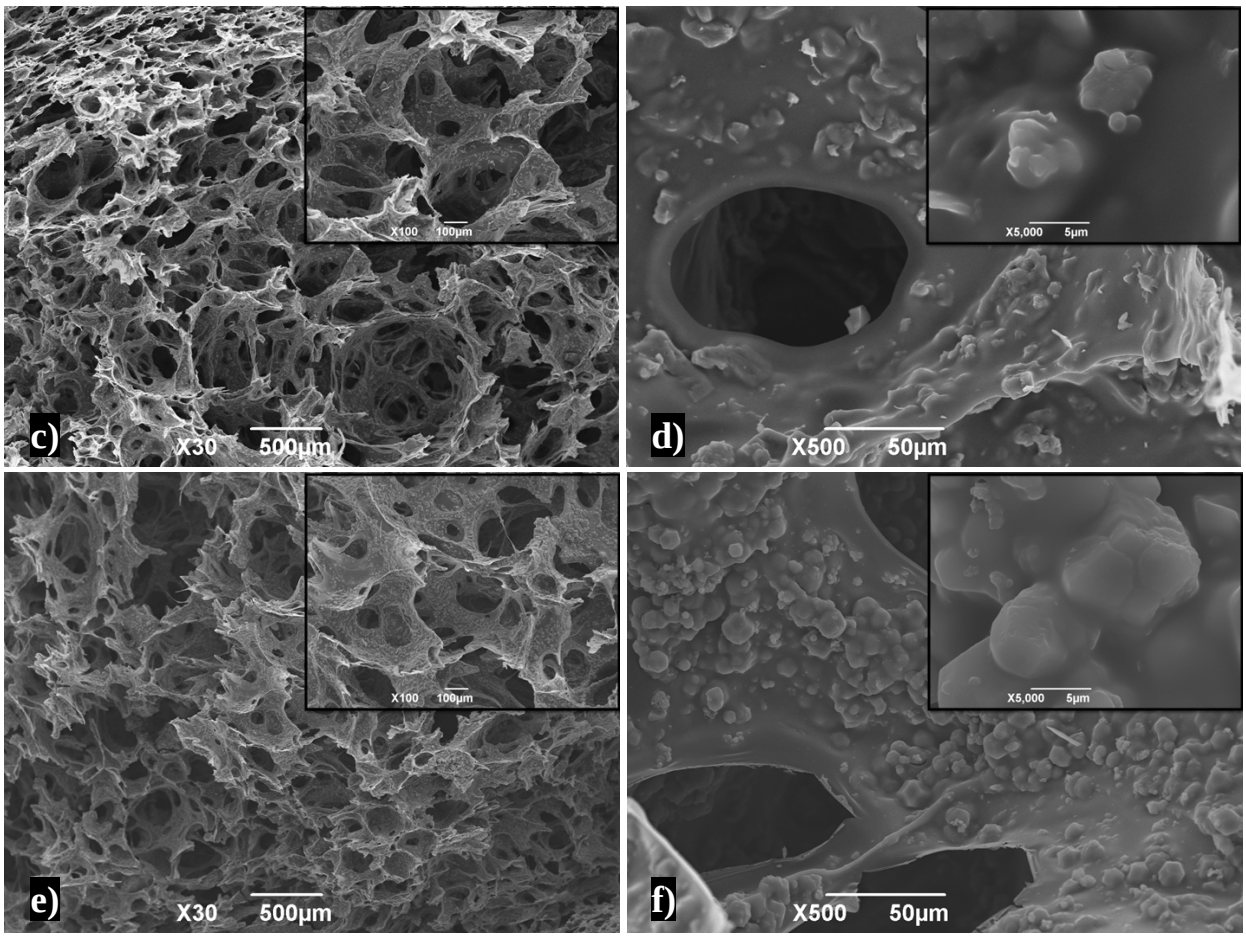

Figure 4.1-5. SEM micrographs taken from the fracture surfaces of the 1000°C pyrolyzed samples; a) PMC6 (with 2 wt% ADA, together with 10 wt% PMO Type A), general morphology; b) detail at higher magnification; c) PMC7 (with 5 wt% ADA, together with 10 wt% PMO Type A), general morphology; d) detail at higher magnification; e) PMC8 (with 5 wt% ADA, together with 10 wt% PMO Type B), general morphology; f) detail at higher magnification.

The SEM micrographs for samples PMC9 and PMC10 (85 wt% PDMS - 15 wt% PMO) are reported in **Figure 4.1-6** (a) and (b), respectively. These images were taken from the cured thermoset samples and it should be underlined that the blends do not include any pore forming precursor like PDMS (note that the self blowing property of the PMPS precursor)[24, 25] or physical

blowing agent. Both samples, as seen, exhibit some amount of closed porosity with cell walls including PMO particles.

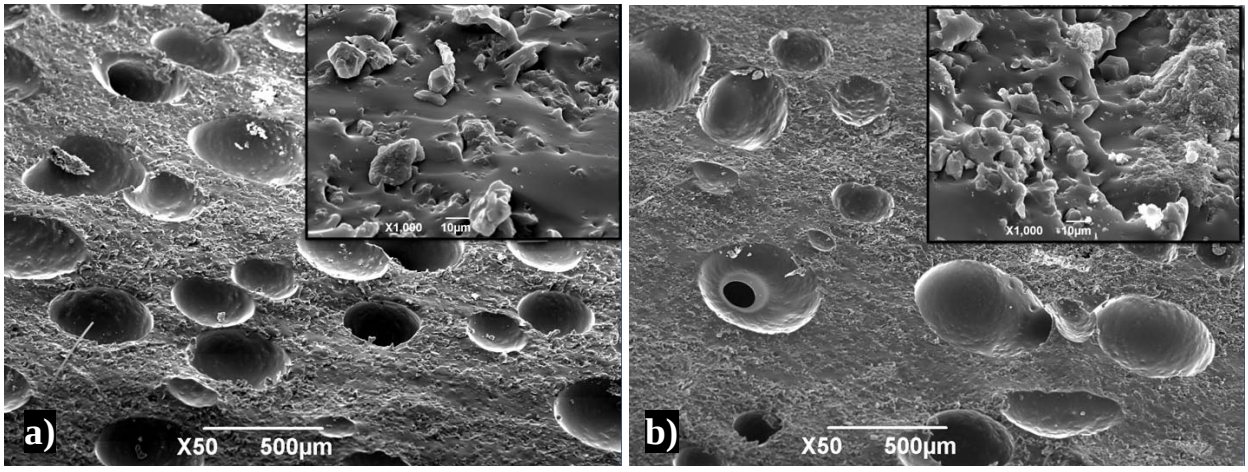

Figure 4.1-6. SEM micrographs taken from the fracture surfaces of the cured sample; a) PMC9 (85 wt% PDMS - 15 wt% PMO Type A) and b) PMC10 (85 wt% PDMS -15 wt% PMO Type B), insets show details at higher magnifications.

The microstructures of the sample PMC9 (85 wt% PDMS - 15 wt% PMO-Type A), is given in **Figure 4.1-7**(a-d). The presence of irregularly shaped, interconnected open macro-porosity is evident. Comparing with the SEM images taken from the cured bodies, it's clear that low ceramic yield of PDMS precursor resulted in a high yield of porosity. In fact, in this system PDMS can be thought as a high temperature binder for PMO particles since it`s known that pure PDMS losses around 70wt% of its starting weight.[23] Higher magnification images show that the PMO particles are homogeneously distributed within the struts of the foam, and covered the cell walls. However, it is not so clear from the images that whether PMO-Type A particles are covered with some kind of residue (or ceramic yield) coming from the PDMS pyrolysis, see **Figure 4.1-7**(d).

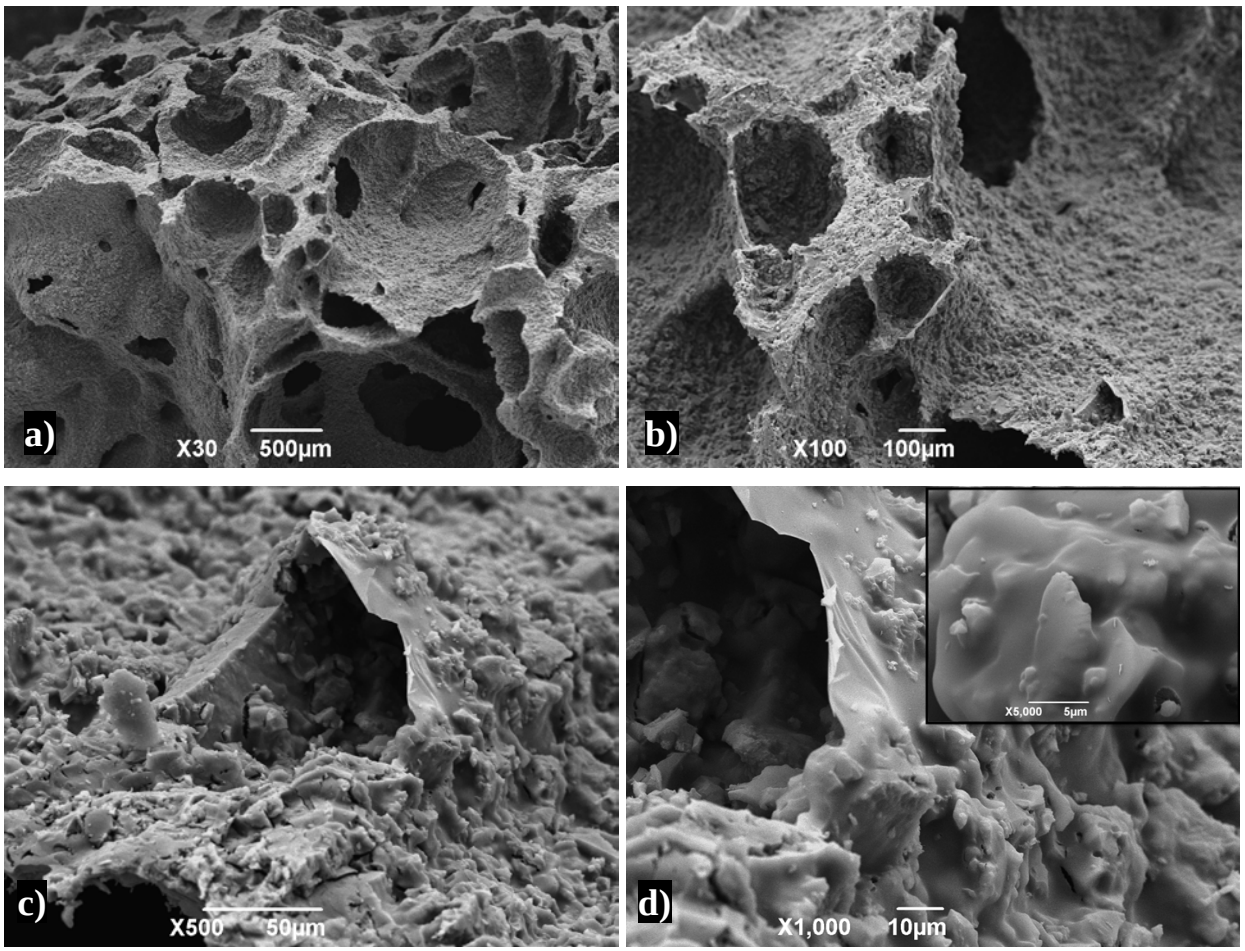

Figure 4.1-7 SEM micrographs taken from the fracture surfaces of the 1000°C pyrolyzed samples; a) PMC9 (85 wt% PDMS - 15 wt% PMO Type-A), general morphology; b) detail at higher magnification; c) cell wall; and d) detail of a cell wall, inset showing higher magnification.

The microstructures of the last sample PMC10 (85 wt% PDMS - 15 wt% PMO-Type B), is shown in **Figure 4.1-8**(a-d). Similar to PMC9, the presence of 3D-interconnected, open macro-porosity is evident. Higher magnification images show that the PMO particles are homogeneously distributed within the struts of the foam, and completely cover the cell walls, see **Figure 4.1-8** (c). Clearly, PMO particles preserved their distinct shapes when compared to the

grains of the bare PMO particles (see **Figure 4.1-1** (a and b)), maintaining their truncated rhombic dodecahedral shape.[13]

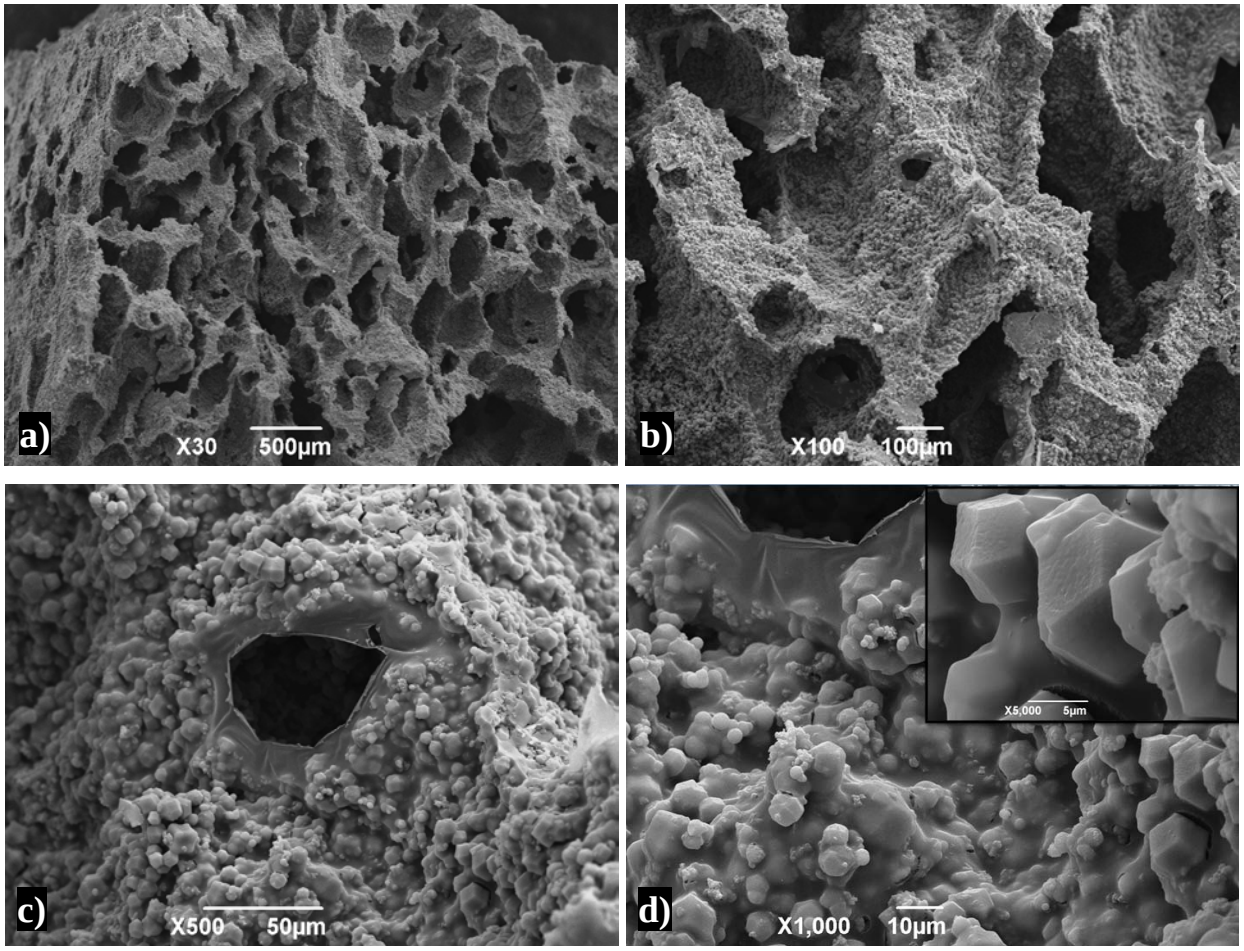

Figure 4.1-8. SEM micrographs taken from the fracture surfaces of the 1000°C pyrolyzed samples; a) PMC10 (85 wt% PDMS – 15 wt% PMO-Type II), general morphology; b) detail at higher magnification; c) cell wall; and d) detail of a cell wall, inset showing higher magnification

The N_2 adsorption-desorption curves for the bare PMO powders pyrolyzed at 1000ºC given in **Figure 4.1-9**, show that both types of powders exhibit Type IV behavior, according to the IUPAC classification,[26] with hysteresis loops showing capillary evaporation at $p/p_0 \sim 0.4$. The measured BET surface area values for the pyrolyzed bare PMO powders were 262 ± 5 m^2/g and

634 ± 5 m^2/g for Type-A and Type-B respectively, in accordance to what previously reported.[20, 21]

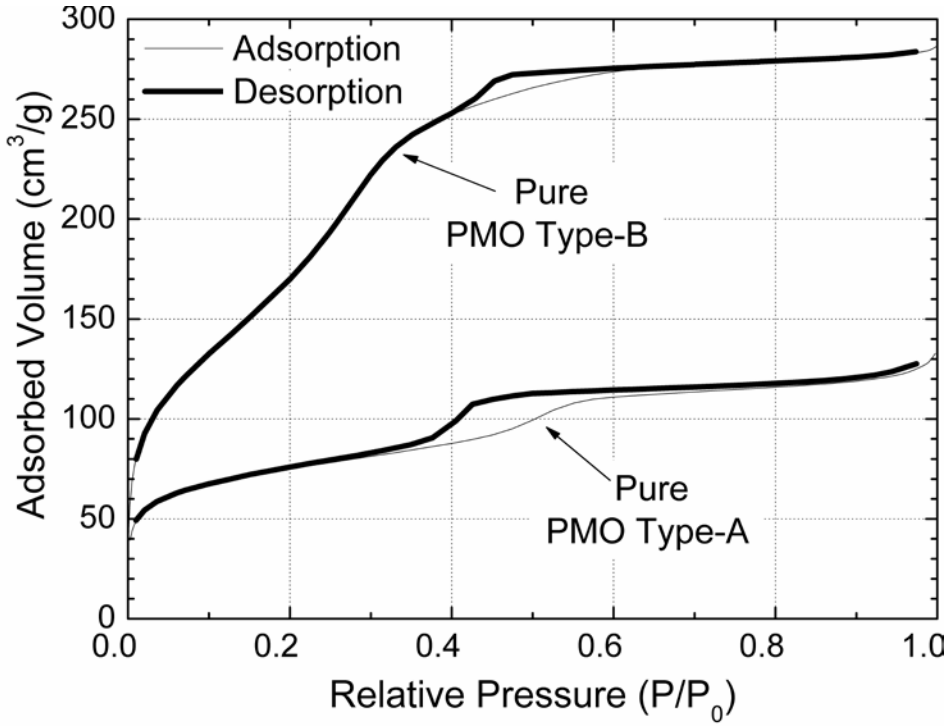

Figure 4.1-9. N_2 adsorption-desorption isotherms for the samples after pyrolysis, including pure PMO powder.

The adsorption-desorption isotherms for the samples prepared by using PMO particles together with PMPS and PDMS precursors were clearly different than the ones prepared by using only PDMS, (see **Figure 4.1-10** (a) and (b)). Specifically; PMC2 (55 wt% PDMS - 35 wt% PMPS - 10 wt% PMO Type A) and PMC7 (the same composition yet including 5wt% ADA), given in **Figure 4.1-10** (a) exhibit typical Type II isotherm (a common observation for macroporous components) with a very low N_2 volume adsorption indicating a poor pore accessibility i.e. pore blockage or collapse. Similarly, the isotherms for samples PMC3, PMC5 and PMC8 are consistent with Type II (almost reversible), with no hysteresis loop, and appear almost identical, thus in **Figure 4.1-10** (b) the curves for the sample PMC8 was excluded but the data for this sample can be seen in **Table 4.1-2**. Besides, compared to the samples prepared by using PMO-

Type-A, these samples (prepared by using PMO Type-B) had higher N_2 volume adsorption indicating relatively higher pore accessibility.

Interestingly, for the samples made by using only PDMS together with either PMO Type-A (PMC9) or Type-B (PMC10), we have observed irreversibility in the curves causing a hysteresis. Sample PMC9 showed a strange behavior; as seen in **Figure 4.1-10**(a) desorption curve crosses the adsorption curve around p/p_0~0.5 where capillary evaporation was expected. This is impossible from a theoretical point of view and although the real reason is still not known, it seems that some residual amount of humidity remained trapped in the pores of PMO Type-A even after degassing at 200°C for 12h. In fact, the sample PMC10 has a clear hysteresis (a non-reversible isotherm, see **Figure 4.1-10**(b)) with no crossing phenomenon suggesting that the reason of curve crossing previously observed is directly related with the type of PMO particles used. For the sample PMC10, while the adsorption branch recalls a Type II isotherm, typical of macroporous solids as a result of the capillary condensation occurring only at high p/p_0 values ($p/p_0 > 0.95$), the desorption branch followed a different path. In the latter case capillary evaporation took place at p/p_0 ~0.4, a value which is typical for mesoporous adsorbents corresponding to pores with diameter of about 4 nm.[27] Thus, the sample displayed a mixed behavior, with a contribution from the macro-pores and one from the meso-pores. The rather large hysteresis loop suggests a wide pore size distribution, possibly spanning from the meso to the macro region. Moreover, the increase in adsorbed volume at very low p/p_0 indicates the presence of micro-pores, suggesting that sample PMC10 indeed possessed a hierarchically porous architecture.

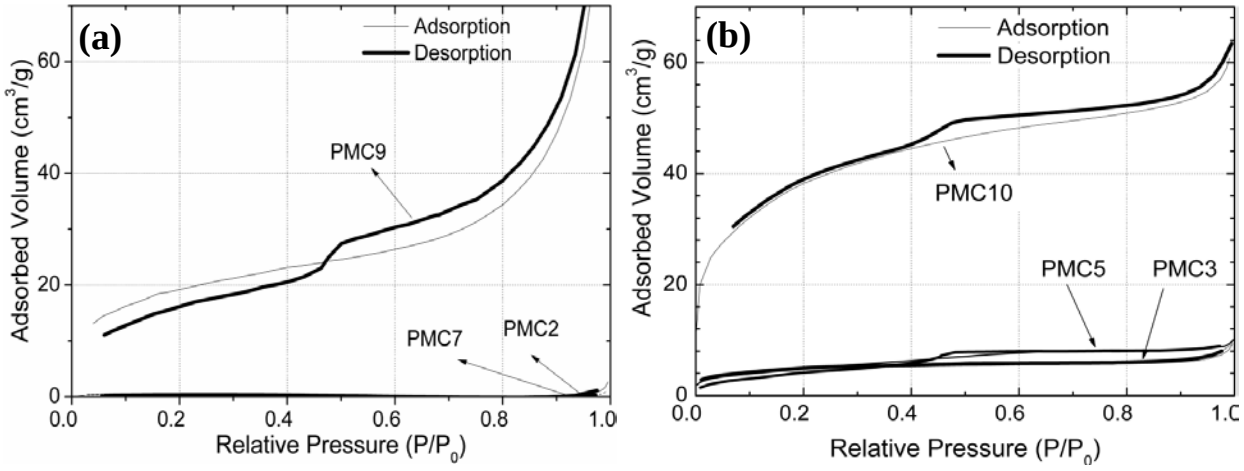

Figure 4.1-10. N_2 adsorption-desorption isotherms for the samples after pyrolysis at 1000°C; a) PMO Type-A made samples; and b) PMO Type-B made samples.

The data extracted from all the isotherms are summarized in **Table 4.1-2**. Since a meso-porous powder having high a SSA value was utilized as filler for the siloxane precursors, it was expected that the macro-porous SiOC matrix would contain meso-porous particles which would afford a high SSA value to the manufactured ceramic. However, the adsorption/desorption results indicated that the situation was different. As could be seen, generally samples made by using PMO Type-B gave much higher results (PMC3, PMC8 and PMC5 yielded with SSA values of ~17, 21 and 24 m^2/g, respectively) than that of PMO-Type-A made ones. Moreover, as a general trend, samples having higher PMO/PMPS ratios possessed higher surface area, as well as displaying a better morphological homogeneity. The highest value of SSA ~137 m^2/g was obtained from sample PMC10. Taking into consideration the fact that 15 wt% of PMO particles in the green sample resulted in a PMO concentration of 34 wt% in the ceramic monolith after pyrolysis, it could be concluded that about 64% of the meso-pores were still accessible to the nitrogen gas. Although, utilization of PMO Type-A gave low SSA values, maximum reaching for PMC9 to ~11 m^2/g, it is of interest to speculate on this value since the observed isotherms crossed each other. It is interesting to note that the "C" values documented in **Table 4.1-2** for all the samples (made with PMO-Type A), were either negative or >250. This suggests that the

validity of the used BET formula is exceeded thus the values corresponding to specific surface area for those samples are probably not the "real" SSA values. It is customary to apply the BET equation in the linear form given in equation (4.1-1).[26]

$$\frac{p}{W((p^0/p)-1)} = \frac{1}{W_m C} + \frac{(C-1)}{W_m C}\left(\frac{p}{p^0}\right) \qquad \textbf{4.1-1}$$

Where W is the weight of gas adsorbed at a relative pressure, P/P^0, and W_m is the weight of adsorbate constituting a monolayer of surface coverage. According to the BET theory C is related exponentially to the enthalpy (heat) of adsorption in the first adsorbed layer. It is now generally recognized, however, that although the value of C may be used to characterize the shape of the isotherm in the BET range it does not provide a quantitative measure of enthalpy of adsorption but merely gives an indication of the magnitude of the adsorbent-adsorbate interaction energy. Thus, in reporting BET data it is recommended that C values are stated, but not converted to enthalpies of adsorption.[26] The BET equation (4.1-1) requires a linear plot of $1/[W(P^0/P)-1]$ vs P/P^0 which for most solids, using nitrogen as the adsorbate, is restricted to a limited region of the adsorption isotherm, usually in the P/P^0 range of 0.05 to 0.35. This linear region is shifted to lower relative pressures for microporous materials. The standard multipoint BET procedure requires a minimum of three points in the appropriate relative pressure range. The weight of a monolayer of adsorbate W_m can then be obtained from the slope and intercept of the BET plot. After having the W_m one can obtain the total surface area S_t via following the formula (4.1-2).

$$S_t = \frac{W_m . N . A_{cs}}{M} \qquad \textbf{4.1-2}$$

where N is Avogadro's number (6.023×10^{23} molecules/mol) and M is the molecular weight of the adsorbate. The specific surface area (SSA) of the solid can then be calculated from the total surface area S_t and the sample weight w, according to equation (4.1-3).[26]

$$SSA = \frac{S_t}{w} \qquad \textbf{4.1-3}$$

Nitrogen is the most widely used gas for surface area determinations since it exhibits intermediate values for the C constant (50-250) on most solid surfaces, precluding either localized adsorption or behavior as a two dimensional gas.[28] Since it has been established that the C constant influences the value of the cross-sectional area of an adsorbate,[29] the acceptable range of C constants (roughly 0-300) for nitrogen makes it possible to calculate its cross sectional area from its bulk liquid properties. For the hexagonal close-packed nitrogen monolayer at 77 K, the cross-sectional area A_{cs} for nitrogen is 16.2 $Å^2$. Sing[30] underlined that usually it can be assumed that the nitrogen molecules are in a close-packed 'liquid' state at 77 K but with an extra caution if the C value is low (say, C<50) or high (C>150). Therefore; the strange C values (negative or >250) observed from the PMO Type-A made samples, causes an uncertainty on the obtained SSA values, i.e. making them unreliable. In fact, if the standard BET procedure is to be used, it should be established that monolayer-multilayer formation is operative and is not accompanied by micropore filling, which is usually associated with an increase in the value of C (> 200). It should be appreciated that the BET analysis does not take into account the possibility of micropore filling or penetration into cavities of molecular size. These effects can thus falsify the BET surface areas.[26] Indeed sample PMC9 had a very high C value (667), but relatively low SSA ($11 m^2/g$), this under the light of aforementioned reason might be read as a large "contraction" of mesoporosity in the PMO Type-A particles causing either inaccessible microporosity or nano-roughness which enhanced the interaction between the adsorbate-adsorbent, i.e. high C value. This phenomenon together with residual humidity resulted in this type of adsorption-desorption behavior, causing a low SSA value. Nevertheless, these issues are still elusive and needs more detailed further work to clarify.

Table 4.1-2. Results obtained from the N_2 adsorption/desorption isotherms.

Sample	BET (m^2/g)	Meso-pore volume (cm^3/g)	Meso-pore size (4V/A) (nm)	External surface area (m^2/g)	C Coefficient	Micro-pore area (m^2/g)
PMC2	2.09	0.001	2.36	nm	-56.93	nm
PMC3	17.12	0.0110	2.6	16	65.64	1.2
PMC5	24.02	0.0100	n.a.	20	96.49	3.8
PMC7	1.74	0.0003	0.80	nm	292.45	nm
PMC8	21.76	0.012	2.29	nm	87.48	nm
PMC9	11.005	0.020	7.35	nm	667.98	nm
PMC10	136.91	0.0880	2.6	123	108.59	14.1

XRD analysis performed on the selected samples made by using PMO particles, revealed that in all of them the particles retained to some extent their ordered porosity after being embedded within the precursors and pyrolysis, as demonstrated by the peak below ~1 degree (2θ) for cubic *Fm3m*[21] (see **Figure 4.1-11** (a), for the data of the samples made by using PMO-Type A) and ~2 degrees (2θ) for cubic *Pm3n*[31](see **Figure 4.1-11** (b) for the data of the samples made by using PMO-Type A). The observed peaks are slightly shifted to greater 2θ values compared to that of the bare PMO powders pyrolyzed under the same conditions; this indicates a contraction of the cell parameter. Moreover, the peaks are also broadened, implying a probable decrease/collapse in the long-range mesoscopic order of the formed samples, as observed by other authors.[31]

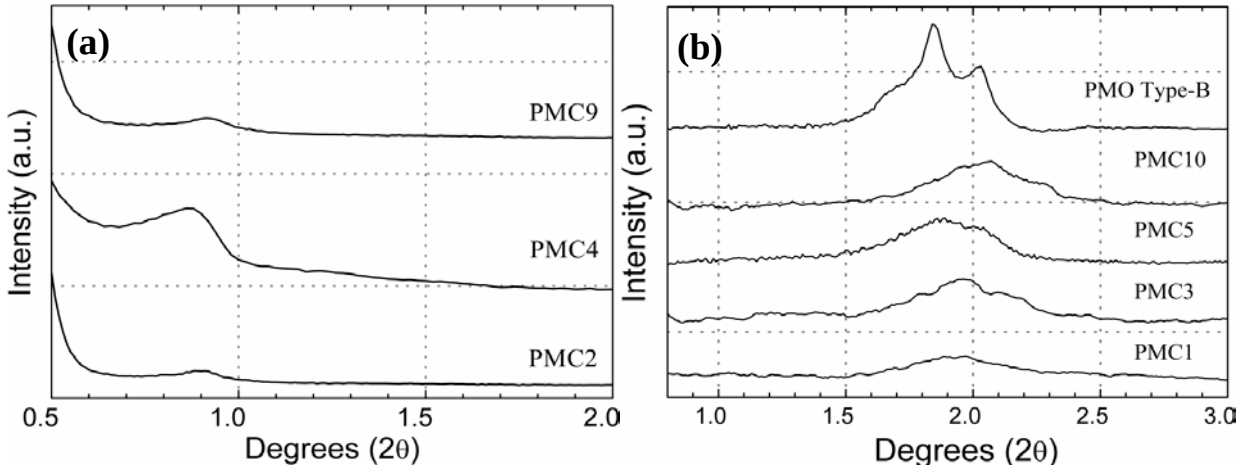

Figure 4.1-11. Small angle XRD data of the samples after pyrolysis, including pure PMO powder.

By combining XRD analysis and BET results for all the samples prepared by using PMO-Type A, it seems that the reason for the low BET surface area values are due to the contraction of the ordered mesoporosity in the cubic *Fm3m* PMO particles which highly limited the accessibility of the pores by N_2 adsorption-desorption measurements. This, partially, might also be caused by the coverage of the PMO surfaces during pyrolysis of the polysiloxane precursors. The sample PMC2 as given previously showed only a very limited amount of SSA (~2m^2/g) and a diffraction peak ~1 (2θ) degree, this sample is further investigated by TEM, in order to explain the observed behavior. TEM images given in **Figure 4.1-12** (a) and (b) belong to the sample PMC2 and a companion image in **Figure 4.1-12** (c) is obtained from the bare PMO Type-A which is used to make sample PMC2.[21] As could be seen, while pure particle includes apparently defined accessible mesostructured order, sample PMC2 contains a possible coating on the surface of the particles for which a noticeable boundary layer is formed (see **Figure 4.1-12** (b)), together with an observable contraction in the pore/cell size. Although the sample also had some degree of order, this coating region jointly with a clear cell contraction is thought to "block" the pore accessibility and caused a low SSA value but a noticeable peak in small angle XRD.

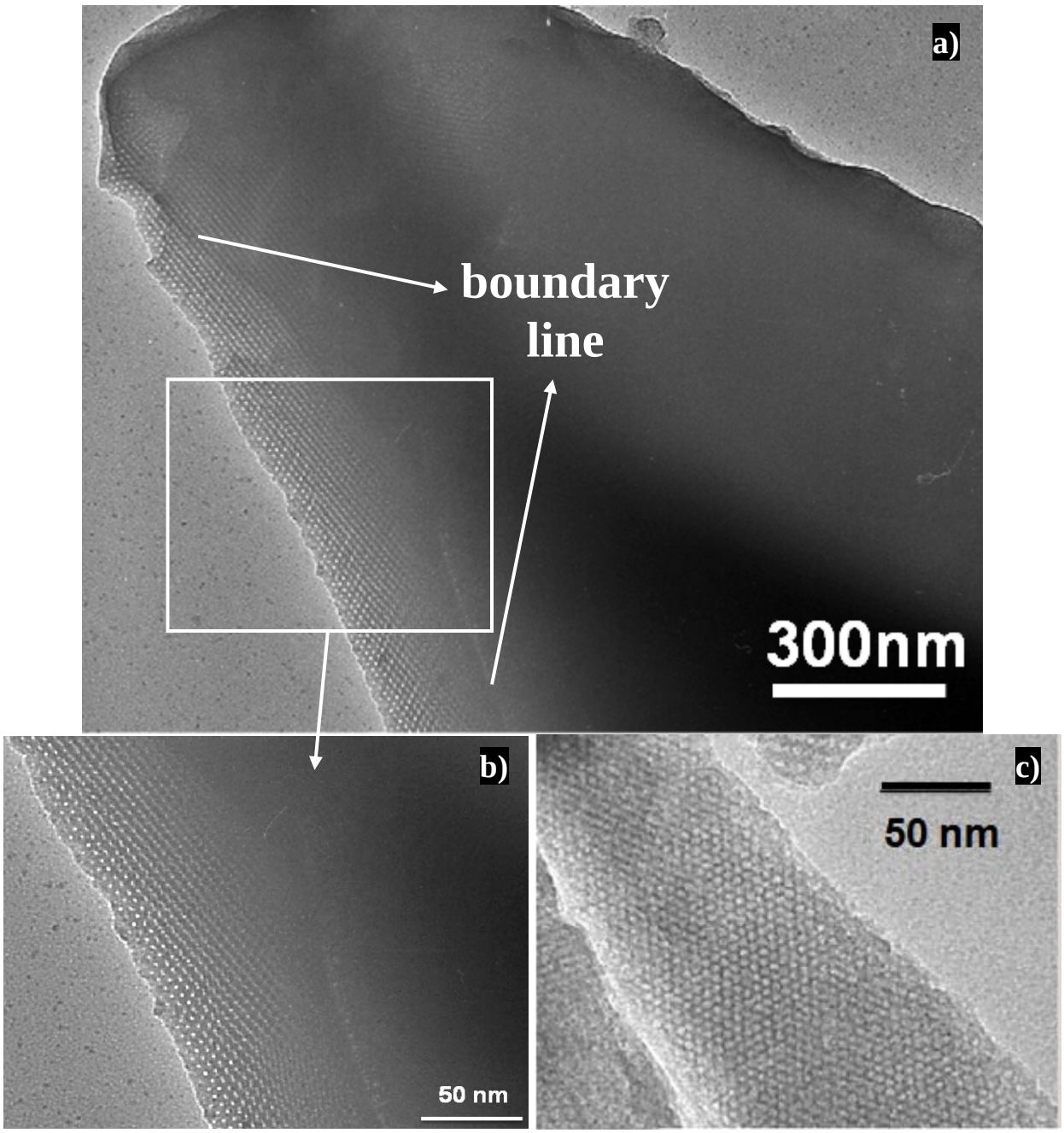

Figure 4.1-12. TEM images of the samples; a) PMC2, overview on the particle showing coating layer; b) higher magnification image from the boundary line detail; and c) for pure PMO Type-B. All pyrolyzed at 1000°C.

The TGA curves for the selected samples are shown in **Figure 4.1-13**. As expected, the sample containing the PMO particles has a lower weight loss due to the substitution of part of the low ceramic yield silicone precursor with a higher yield component. No evidence of any decomposition or reaction of the PMO particles with the surrounding PDMS-derived SiOC matrix can be found.

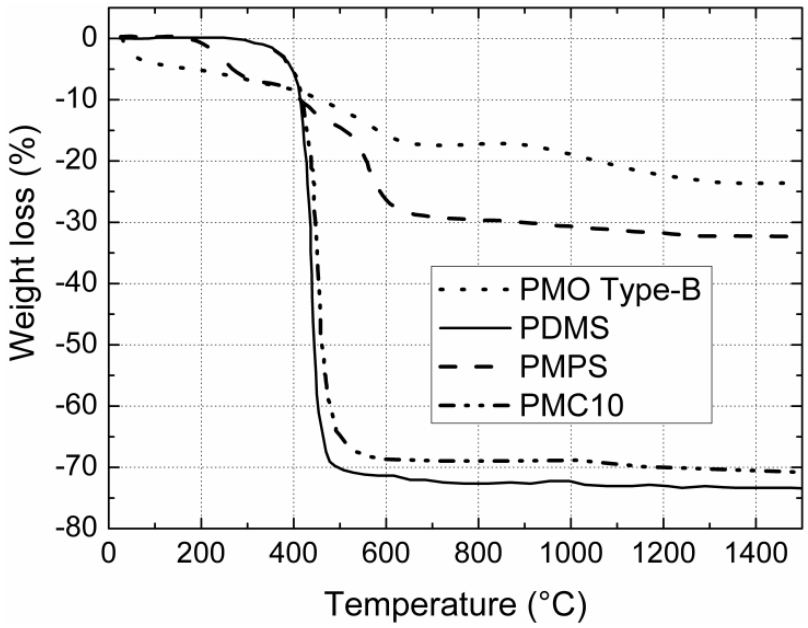

Figure 4.1-13. Weight loss for pure PDMS (RTV), pure PMPS (H44), pure PMO Type-B particles (note that Type-A particles give ~72% of ceramic yield upon 1000°C/Ar pyrolysis, i.e. the processing condition of the present study[21]), and sample PMC10.

Only the sample having highest amount of SSA, that is PMC10, is investigated for mechanical properties. The average cold crushing strength of sample PMC10, which possessed a total porosity of 64.3 vol% (the open porosity was 53.5vol%), was found as 1.72 ± 0.360 MPa. The rather large scattering in the strength values was probably due to the occasional presence of defects (small cracks) in some tested samples. As a last comment it should be noted here that we also tried to produce samples from the PMO particles including surfactants (so no extracted versions) and also from the already pyrolyzed ones. Both of these trial resulted in components

having very high amount of cracking problems therefore these samples are not investigated for further characterizations. However, the problems that we observed might be due to the types of PMO particles we have investigated, other systems might behave differently and since in the literature no studies can be found, a comparison cannot be made.

4.1.4. Conclusions

The pore characteristics and specific surface area values of the ceramic monoliths were strongly dependent on the processing conditions and on the type and amount of precursors (siloxanes and PMO particles) employed. A large amount of open (interconnected) macro-porosity was present for all samples. The microstructural analysis of the pyrolyzed samples demonstrated that, after pyrolysis, the PMO particles homogenously covered all the struts and the surface of the cells. PMO Type-B made samples gave higher SSA maintaining their truncated rhombic dodecahedral shape and retaining most of their ordered mesoporosity. The compression strength of a sample, possessing an elevated specific surface area and a total porosity of 64 vol%, was 1.72 ± 0.360 MPa. The results of the study demonstrate that this novel one-pot processing approach enables to fabricate permeable SiOC ceramic monoliths possessing hierarchical porosity. In fact this processing strategy can be adapted to other polymer derived ceramic systems to produce high SSA components in the family of Si-O-B-C-N.

4.1.5. Acknowledgements

We are very grateful to the “Laboratoire des systems interfaciaux à l’échelle nanometrique, SIEN” at UPMC-Paris 6, France for the N_2 adsorption-desorption measurements.

4.1.6. References

[1]F. Schüth, K.S.W. Sing, and J. Weitkamp, "Handbook of porous solids," pp. 3191, Wiley-VCH Verlag GmbH, Weinheim, Germany, 2002.

[2]M. Twigg and J.T. Richardson, "Fundamentals and Applications of Structured Ceramic Foam Catalysts," *Industrial & Engineering Chemistry Research*, 46 4166-77 (2007).

[3]Z.-Y. Yuan and B.-L. Su, "Insights into hierarchically meso-macroporous structured materials," *Journal of Materials Chemistry*, 16 [7] 663-77 (2006).

[4]C. Danumah, S. Vaudreuil, L. Bonneviot, M. Bousmina, S. Giasson, and S. Kaliaguine, "Synthesis of macrostructured MCM-48 molecular sieves," *Microporous and Mesoporous Materials*, 44-45 241-7 (2001).

[5]T. Sen, G.J.T. Tiddy, J.L. Casci, and M.W. Anderson, "One-Pot Synthesis of Hierarchically Ordered Porous-Silica Materials with Three Orders of Length Scale," *Angewandte Chemie International Edition*, 42 [38] 4649-53 (2003).

[6]H. Schmidt, D. Koch, G. Grathwohl, and P. Colombo, "Micro-/Macroporous Ceramics from Preceramic Precursors," *Journal of the American Ceramic Society*, 84 [10] 2252-5 (2001).

[7]A. Zampieri, P. Colombo, G.T.P. Mabande, T. Selvam, W. Schwieger, and F. Scheffler, "Zeolite Coatings on Microcellular Ceramic Foams: A Novel Route to Microreactor and Microseparator Devices," *Advanced Materials*, 16 [9-10] 819-23 (2004).

[8]S. Costacurta, L. Biasetto, E. Pippel, J. Woltersdorf, and P. Colombo, "Hierarchical Porosity Components by Infiltration of a Ceramic Foam," *Journal of the American Ceramic Society*, 90 [7] 2172-7 (2007).

[9]L. Biasetto, R. Peña-Alonso, G.D. Soraru, and P. Colombo, "Etching of SiOC ceramic foams," *Advances in Applied Ceramics*, 107 106-10 (2008).

[10]T. Asefa, M.J. MacLachan, N. Coombs, and G.A. Ozin, "Periodic mesoporous organosilicas with organic groups inside the channel walls," *Nature*, 402 [6764] 867-71 (1999).

[11]S. Inagaki, S. Guan, Y. Fukushima, T. Ohsuna, and O. Terasaki, "Novel mesoporous materials with a uniform distribution of organic groups and inorganic oxide in their frameworks," *Journal of the American Chemical Society*, 121 [41] 9611-4 (1999).

[12]B.J. Melde, B.T. Holland, C.F. Blanford, and A. Stein, "Mesoporous sieves with unified hybrid inorganic/organic frameworks," *Chemistry of Materials*, 11 [11] 3302-8 (1999).

[13]S. Guan, S. Inagaki, T. Ohsuna, and O. Terasaki, "Cubic hybrid organic-inorganic mesoporous crystal with a decaoctahedral shape," *Journal of the American Chemical Society*, 122 [23] 5660-1 (2000).

[14]W.P. Guo, J.Y. Park, M.O. Oh, H.W. Jeong, W.J. Cho, I. Kim, and C.S. Ha, "Triblock copolymer synthesis of highly ordered large-pore periodic mesoporous organosilicas with the aid of inorganic salts," *Chemistry of Materials*, 15 [12] 2295-+ (2003).

[15]S. Hamoudi and S. Kaliaguine, "Periodic mesoporous organosilica from micellar oligomer template solution," *Chemical Communications*, [18] 2118-9 (2002).

[16]C. Yoshina-Ishii, T. Asefa, N. Coombs, M.J. MacLachlan, and G.A. Ozin, "Periodic mesoporous organosilicas, PMOs: fusion of organic and inorganic chemistry 'inside' the channel walls of hexagonal mesoporous silica," *Chemical Communications*, [24] 2539-40 (1999).

[17]S. Inagaki, S. Guan, T. Ohsuna, and O. Terasaki, "An ordered mesoporous organosilica hybrid material with a crystal-like wall structure," *Nature*, 416 [6878] 304-7 (2002).

[18]T. Asefa, M.J. MacLachlan, H. Grondey, N. Coombs, and G.A. Ozin, "Metamorphic channels in periodic mesoporous methylenesilica," *Angewandte Chemie-International Edition*, 39 [10] 1808-+ (2000).

[19]S.Y. Guan, S. Inagaki, T. Ohsuna, and O. Terasaki, "Hybrid ethane-siloxane mesoporous materials with cubic symmetry," *Microporous and Mesoporous Materials*, 44 165-72 (2001).

[20]B. Toury, R. Blum, G. Valérie., and F. Babonneau, "Thermal Stability of Periodic Mesoporous SiCO Glasses," *Journal of Sol-Gel Science and Technology*, 33 99-102 (2005).

[21]A. Pauletti, S. Handjani, C. Fernandez Martin, C. Gervais, and F. Babonneau, "A new example of periodic mesoporous SiCO glasses with cubic symmetry stable at 1000°C," *Journal of the Ceramic Society of Japan*, 116 [1351] 449-53 (2008).

[22]S. Inagaki, S. Guan, Y. Fukushima, T. Ohsuna, and O. Terasaki, "Novel Mesoporous Materials with a Uniform Distribution of Organic Groups and Inorganic Oxide in Their Frameworks," *Journal of the American Chemical Society*, 121 [41] 9611-4 (1999).

[23]C. Vakifahmetoglu and P. Colombo, "A Direct Method for the Fabrication of Macro-Porous SiOC Ceramics from Preceramic Polymers," *Advanced Engineering Materials*, 10 [3] 256-9 (2008).

[24]M. Scheffler, T. Gambaryan-Roisman, J. Zeschky, F. Scheffler, and P. Greil, "Self-Foamed Cellular Ceramics from Silicone Resins with a Zeolite Surface," pp. 203-10 in Ceramic Engineering and Science Proceedings, Vol. 23. Edited by M.S. Hau-Tay Lin, 2002.

[25]J. Zeschky, F. Goetz-Neunhoeffer, J. Neubauer, S.H. Jason Lo, B. Kummer, M. Scheffler, and P. Greil, "Preceramic polymer derived cellular ceramics," *Composites Science and Technology*, 63 [16] 2361-70 (2003).

[26]K.S.W. Sing, D.H. Everett, R.A.W. Haul, L. Moscou, R.A. Pierotti, J. Rouquerol, and T. Siemieniewska, "Reporting physisorption data for gas/solid systems with special reference to the determination of surface area and porosity," *Pure and Applied Chemistry*, 57 603-19 (1985).

[27]M. Kruk and M. Jaroniec, "Gas Adsorption Characterization of Ordered Organic-Inorganic Nanocomposite Materials," *Chemistry of Materials*, 13 [10] 3169 -83 (2001).

[28]NOVAWin2, V.2.1, Operation Manual, NOVA Series Windows Based Operating and Data Analysis Software, Quantachrome Instruments. 2003: FL, USA.

[29]S. Lowell, J. Shields, G. Charalambous, and J. Manzione, "Adsorbate Cross-Sectional Area as a Function of the BET C Constant," *Journal of Colloid and Interface Science*, 86 [1] 191-5 (1982).

[30]K. Sing, "The use of nitrogen adsorption for the characterisation of porous materials," *Colloids and Surfaces A: Physicochemical and Engineering Aspects*, 187-188 3-9 (2001).

[31]B. Toury and F. Babonneau, "Synthesis of periodic mesoporous organosilica from bis(triethoxysilyl)methane and their pyrolytic conversion into porous SiCO glasses," *Journal of the European Ceramic Society*, 25 [2-3] 265-70 (2005).

4.2. Growth of 1D-Nanostructures in Polymer Derived Cellular Ceramics by Catalyst-Assisted-Pyrolysis.

Published in part in:
C. Vakifahmetoglu, E. Pippel, J. Woltersdorf, and P. Colombo, "Growth of 1D-Nanostructures in Porous Polymer Derived Ceramics by Catalyst-Assisted-Pyrolysis. Part I: Iron Catalyst," J. Am. Ceram. Soc., (in press, 2009).

C. Vakifahmetoglu, S. Carturan, E. Pippel, J. Woltersdorf, and P. Colombo, "Growth of 1D-Nanostructures in Porous Polymer Derived Ceramics by Catalyst-Assisted-Pyrolysis. Part II: Cobalt Catalyst," (Submitted to J. Am. Ceram. Soc (2010)).

C. Vakifahmetoglu and P. Colombo, "Porous Polymer Derived Ceramics Decorated with In-situ Grown Nano-structures," in Proceedings of Pac-Rim 8, Ceramic Transactions. Edited, Vancouver, Canada, (in press, 2009).

4.2.1. Introduction

A porous component containing pores with dimension within two or more length scales is referred to as a material with hierarchical porosity. Different microstructures may exist according to the range of pore sizes that are involved in the porous structure, see Chapter 2.3.3 for more details on hierarchically porous cellular materials. The solid walls surrounding the pores of cellular structure can be modified to provide the functionality for a given application (such as chemical affinity towards specific pollutants, surface roughness, etc.). In particular, the presence of a high specific surface area (SSA) is greatly demanded to accelerate surface reactions due to enhanced interfacial contact area between the substrate and the active phase (gas or liquid phase), i.e. roughly speaking; the higher the SSA is, the higher the reactivity of the material.

The synthesis of one-dimensional nano-structures (nanotubes, nanowires, nanobelts, etc.) has been the subject of a steadily growing interest owing to their unique and often superior properties

compared to their bulk and/or microscale counterparts, and a great number of manufacturing techniques have been developed for the production of these materials.[1] In particular, the use of preceramic polymers is very promising, due to the great tailorability of their structures on a molecular scale and ease of processing. It has been shown that various types of nanostructures, such as whiskers,[2] nano-tubes[3, 4] and nano-cables[5] / wires[6-8] / fibers[9-11] of different compositions can be produced directly from preceramic polymers, without the use of any transition metal additives as catalyst. Recently, great progress has been made in the production of nano-structures from preceramic polymers (mostly polysilazanes or polycarbosilanes) by applying Catalyst-Assisted-Pyrolysis (CAP), leading to improved yield and the formation of varied morphologies. For example, carbon nanotubes (CNTs) were synthesized from a polycarbosilane (PCS) containing iron nano-particles,[12] or from a borazine-based precursor including nickel as catalyst,[13] while SiC/SiO_2 core/shell nanocables were produced using poly(dimethylsiloxane) coupled with ferrocene.[14] Likewise, a polysilazane was used to produce amorphous silicon carbonitride (SiCN) powder with *in situ* grown single-crystal Si_3N_4 nanowires/nanobelts, using $FeCl_2$ as catalyst.[15] A similar methodology was also used to synthesize powders containing SiC nanorods,[16] Si_3N_4 nanobelts,[17-19] single-crystalline Si_3N_4 nanowires with[20] or without[21] aluminum doping, and finally silicon-doped boron nitride (BN) nanotubes having a bamboo structure.[22] Furthermore, pyrolysis of PCS was shown to yield ceramic powders containing SiC whiskers, when nickel ferrite was incorporated in the precursor.[23, 24]

The presence of 1D nanostructures (such as nanofibers/wires) on the surface of a dense material may lead to an increase of its SSA. In fact, their unique morphology (i.e. nanosize diameter, high aspect ratio, presence of bundles and aggregates) provides significant additional geometric surface, and pores of various size (micro-, meso-, macro-) can be found among the fibers and between the fibers and host matrix. This feature has been exploited to transform low SSA cellular ceramics into medium SSA materials, in which nanofibers/wires are obtained on the cell walls of the host ceramic via in-situ formation,[25] therefore enabling it to fulfill similar applications to those of a properly termed hierarchical porosity component. Moreover, this approach enables to add alternative phases to the material, which can further functionalize the system (for example altering its mechanical, magnetic or electrical properties).

The first studies in this field investigated the formation of carbon 1D nanostructures (nanofibers (CNF) or nanotubes (CNT)) on the surface of ceramic honeycombs (cordierite,[26-34] and highly porous acicular mullite[35]). As a general trend, the total porosity of the component decreased with the amount of CNF/CNTs, whereas the specific surface area of the porous monoliths increased reaching values of 63 m^2/g.[27] SiC nanofibers were obtained by Jayaseelan et al.[11] on the surface of cordierite honeycombs via the carbothermal reduction reaction of carbon added to the oxide raw materials; when processing in inert atmosphere, medium SSA values (~36 m^2/g) were obtained. Ceramic foams have also been used as substrate for the growth of nanostructures. A $Mg_{0.9}Co_{0.1}Al_2O_4$ foam was heated in H_2-CH_4 atmosphere, giving rise to large bundles of CNTs on its cell walls.[36] Surface area measurements performed both on the processed foam and the same specimen subsequently oxidized in air (to burn out CNTs), revealed that the difference was ~30 m^2/g, demonstrating the large contribution of 1D nanostructures the SSA. An open cell ceramic foam (containing α-alumina (>80wt%), mullite and cristobalite) was also impregnated by a slurry of α-$Al_{1.8}Fe_{0.2}O_3$ and covered by CNTs via catalytic chemical vapor deposition (CCVD).[37] In a similar way, very recently, an α-$(Al_{1-x}Fe_x)_2O_3$ foam was also used to form CNTs via CCVD.[38] In another study, Cordier et al.[39] impregnated 50 ppi alumina-silicate foams with a slurry of $Mg_{(1-x)}(Co_{0.75}Mo_{0.25})_xO$ (X=0.01-0.2), and subsequently formed CNTs via CCVD. The produced cellular ceramic had a multi-scale pore structure, and the CNTs very well distributed on the cell walls afforded a surface area of ~15 m^2 per each gram of foam.[39] Mukhopadhyay et al.[40] also utilized commercial carbon foams to grow CNTs via two stage CVD, using a ferrocene catalyst.

Apart from CNTs, Pham-Huu and Ledoux[41] and later Wenmakers et al.[42] deposited Ni on reticulated vitreous carbon foams and produced CNFs by reaction with hydrocarbons at temperatures around 500°C. Different types of CNF structures with a large fiber diameter distribution (30 to 1100 nm) were observed with high SSA ranging from 118 to 146 m^2/g. Following a parallel strategy, Vanhaecke et al.[25] produced SiC nanofibers (NFs) in the macropores of a SiC foam by converting the CNFs that had previously formed on the SiC host structure via CCVD, using SiO vapor as a reactant at 1300°C. The final SSA value for SiC-

NFs/SiC foam was 50 m^2/g. The produced samples were tested in a diesel particulate filtration system, and the microstructure of the composite foam, comprising a macroscopic interconnected porosity and walls covered with nanofibers, led to a small pressure drop and high trapping efficiency during the filtration step of fine and ultrafine soot.[25, 43]

However, very few studies have so far investigated the formation of nanostructures during pyrolysis, via Catalyst-Assisted-Pyrolysis, in the pores of preceramic polymer derived monoliths. Scheffler et al.[44] pyrolyzed nickel acetate-containing poly(methyl-phenyl)silsesquioxane (PMPS) and observed the formation of multiwall carbon nanotubes only within the pores that were formed during the polymer-to-ceramic conversion of the polymeric matrix. The authors described these pores as "catalytic microreactors", and afterwards showed the in situ formation of carbon nanotubes, when silicon was added, and of SiC/SiO_2 nanowires when nickel acetate and silicon were incorporated together into the PMPS precursor. The formation of nickel silicide tips was observed for both types of systems, and therefore a well-known Vapor-Liquid-Solid (VLS) process as a possible growth mechanism was proposed.[45] Although, the processing technique used was simple and enabled to produce nanostructures, according to the TEM and SEM images reported in those studies, the produced nanofibers/wires/tubes in the pores of the pyrolyzed monoliths were very few. *In situ* formation of β-SiC nanowires having spherical particles on their tips was also observed in the channels of porous SiC ceramics fabricated from α-SiC powder and PCS precursor as a binder.[46, 47] Catalyst particles for the growth of the nanowires were considered to originate from unwanted iron impurity in the starting SiC powder, suggesting a similar VLS mechanism of growth.[46] In this case also, the amount of nano-structures produced was very limited. Similarly, recent studies of Sagatelli et al. [48, 49] showed that the release of decomposition gases, when pyrolyzing preceramic polymers at high temperature in inert atmosphere including Ni, led to develop 1D-nanostructures in the pores of the formed ceramics via catalyst assisted pyrolysis (CAP). Using emulsion-based processing of a preceramic polymer containing transition metals such as Fe, Co, Ni or Pd, nanofibers consisting of β-SiC/α-SiO_2 were also very recently obtained in the pores of the produced SiOC foam.[50] An application of this processing concept to the growth of nanofibers on the surface of cellular polymer-derived-ceramic has been recently pursued by Yoon et al.[51] and in our laboratory.[52-54]

The authors reported the formation of highly aligned macro-porous SiC ceramics decorated with homogenously distributed SiC nanowires, produced by unidirectional freeze casting of SiC/camphene slurries with different amounts of the PCS precursor. Iron, an unwanted impurity in the starting SiC powder, was the catalyst enabling the growth of the nanowires, which afforded SSA values ranging from 30 to 86 m^2/g, depending on the length of the nanostructures.

The work done in our laboratory has focused on the deliberate one-pot synthesis of foams with hierarchical porosity via catalyst assisted pyrolysis (CAP) using different catalysts (Fe, Co, Pt) and polysiloxanes. Cellular SiOC ceramics, possessing a large amount of interconnected porosity (>70 vol%), were produced by direct foaming, and the addition of a catalyst enabled the formation of 1D-nanostructures (nanowires) in large quantity on the surface of the cell walls. We clearly discussed that, depending on the preceramic polymer (Si:C:O ratio) and pyrolysis conditions (atmosphere and temperature), different 1D nanostructures could be obtained. In particular, when heating in N_2, single crystal Si_3N_4 nanowires were obtained, while pyrolysis in Ar resulted in SiC nanowires. Moreover we also documented, as one can see in the following sentences, the effect of a different catalyst type, and the properties of the porous components, including SSA values as a function of processing conditions. Our main aim is the production of macroporous ceramic components possessing high SSA values, for gas adsorption, catalyst support and pollutant removal applications.

4.2.2. Experimental Procedure

Three different sets of samples have been prepared and the sample compositions are given in **Table 4.2-1**, **Table 4.2-2**, and **Table 4.2-3**. During the preliminary experimenting, we have followed the processing methodologies that we have previously mentioned in detail to produce macroporous cellular components (see Chapter 3) and tried to either “catalyze” these systems to produce 1-D nanostructures in the cells of the pyrolyzed components or embed already formed nanostructural forms. We aimed to vary the chemical composition of the pure preceramic polymer bodies (and so PDCs) in order to affect the important characteristics such as: porosity (size, tortuosity and interconnection), strength, specific surface area and catalytic properties.

In this manner, first of all cellular SiOC ceramic have been prepared by using PMO Type-B (*Cubic Pm3n)* together with either carbon nanohorns (shortened as CNHs) or an iron complex; ferrocene, $Fe(C_5H_5)_2$ (abbreviated as FeCp2). **Table 4.2-1** shows the compositions that are used to form green thermoset bodies. The information on RTV (PDMS), ADA and PMO (Type-B, synthesized in the laboratory of *Dr. Florence Babonneau*, Chimie de la Matière Condensée, University P. et M. Curie-Paris 6, UMR CNRS 757) can be found in Chapter 4.1. Single walled CNHs were kindly supplied by Carbonium srl, (Selvazzano, Padova, Italy (info@carbonium.it) where synthesis of these particles made by a patented method), and FeCp2 (Sigma-Aldrich, Fluka, Germany) was used as received. Similarly what was explained in Chapter 4.1, first liquid silicon oil of component A is poured in mold and then either CNHs or FeCp2 together with PMO particles were added and the blend was then mixed with a glass spatula for 10 minutes. Once homogenization was achieved, the other silicone oil (component B – hydrosilyl-silicone) was poured into the mixture and stirring continued for additional 5 min. After that, the mix was transferred into an oven operated at 250ºC for 4 h for curing. The crosslinked thermoset was removed from the mold, cut into desired pieces and then pyrolyzed at temperatures between 1000-1200°C in 100 steps holding for 2h at peak temperature in an alumina tube furnace in flowing Ar gas (1 atm; heating and cooling rate 2°C/min, Carbolite 1200 furnace is used for all experiments).

Table 4.2-1. The compositions of the ceramic bodies prepared by using PMO particles.

Sample label	PDMS (RTV 141) (wt%)	PMO (Type-B) (wt%)	CNHs (wt%)	ADA (wt%)	Ferrocene [FeCp2] (wt%)
PMO-N1	85.0	13.5	1.5	-	-
PMO-N2	80.0	13.5	1.5	5.0	-
PMO-N3	80.0	12	-	5.0	3

During the following experiments in order to investigate the catalytic effect of FeCp2, macroporous SiOC ceramic bodies were synthesized from the mixtures of preceramic polymers including FeCp2 as well. Typical processing to form green bodies was similar to that was explained in Chapter 3.1. Briefly all three components, including either PMS or PMPS (information on these precursors can be found in Chapter 3) depending on the chemical proportions given in **Table 4.2-2**, were mixed, cured at 90°C/12h in air, followed by 1200°C/1h pyrolysis under flowing Ar or N_2 gas (1 atm; heating and cooling rate 2°C/min, (Carbolite 1200 tube furnace with alumina tube is used for all experiments).

Table 4.2-2. The compositions of the ceramic bodies prepared by using precursor mixtures together with FeCp2.

Sample Label	PDMS (RTV 141) (wt%)	PMS (MK) (wt%)	PMPS (H44) (wt%)	Ferrocene [FeCp2] (wt%)
PM-F	48.5	48.5	-	3.0
PH-F	48.5	-	48.5	3.0

In the final part of the present study, aforementioned blend systems were further simplified and other catalytic metal sources have been introduced together with physical blowing agent. Transition metal halides, better than 98% purity (Sigma–Aldrich, USA), have been used instead of FeCp2. Ingredients given in **Table 4.2-3**, were first ball milled for 12h at 350rpm then the blend put into 2-4cm diameter Al-foil type cooking containers. The batch in Al-foil mold was then transferred to an oven and the temperature was increased to 90°C for 1h, and then curing was obtained at 250°C (2°C/min heating rate). Dwelling at this temperature for 5h enabled to form a porous infusible polymer. As a highly critical parameter is the homogeneity of the viscous blend during foaming and curing (since the addition of transition metals affects the cross-linking characteristics of polysiloxane precursors),[55] mixing with a thin glass spatula was performed just

before the foaming, which occurred between 150-200°C (a mask has to used during mixing for the possible Co volatiles). Porous thermoset monoliths thus obtained were then individually pyrolyzed under N_2 or Ar (both 99.999% pure) in an alumina tube furnace (2h at the required temperature, in the range 1250 to 1400°C; 2ºC/min heating and cooling rate). Different alumina crucibles have been used for different set of samples in order to terminate the possible contamination from different metallic sources.

Table 4.2-3. The compositions of the ceramic bodies prepared by using silicone resins and physical blowing agent together with metal halides.

Sample label	PMS (MK) (wt%)	PMPS (H44) (wt%)	ADA (wt%)	$FeCl_2$ (wt%)	$CoCl_2$ (wt%)	$PtCl_4$ (wt%)
PMA-Fe	86	-	1	3	-	-
PMA-Co	86	-	1	-	3	-
PHA-Fe	-	86	1	3	-	-
PHA-Co	-	86	1	-	3	-

As a furnace Lindberg-Blue with Molybdenum Disilicide ($MoSi_2$) heating elements which can reach up to 1700°C has been used. Heating elements were sidewall mounted to protect integrity of chamber roof so roof penetrations are avoided. 3” outer diameter, USA standard (99.8% pure) alumina tube having 120cm length was mounted in to the furnace and extra sealing was done by porous mullite bricks. The tube ends were closed by aluminum flanges having a water cooling system. Silicon O-Rings were used in between tube and flanges to guarantee safe sealing. Two type "B" thermocouples (in order to control inside tube temperature; one of them was introduced

from the gas-out part of the tube where flange has an opening for thermocouple entrance and a gland was used to ensure high-quality sealing and other one was outside the tube just above the hot zone (~15cm in the center area of the 120cm tube) assure accurate temperature measurements and long thermocouple life. Although, these thermocouples are more expensive and have lower sensitivity; approximately 10 μV/°C, than other thermocouple types, they are the most stable thermocouples having a long cycle life.

For desired samples the following characterizations have been conducted; the true density was measured from finely ground (ball milling the pyrolyzed bodies for 12h at 350rpm and therefore assuming that no closed porosity remains) ceramic powder using a He-Pycnometer ((Micromeritics AccuPyc 1330, Norcross, GA)). Open and closed porosity of the sintered ceramics were determined by the Archimedes principle (ASTM C373-72), using xylene as buoyant medium. After immersion of dried component into xylene including tubes 24h is waited then the measurements were done. Compression testing was performed at room temperature on selected pyrolyzed samples, which were cut before pyrolysis to avoid possible shape distortions. Universal testing machine (1121 UTM, Instron, Norwood, MA) using steel loading rams at a strain rate of 0.5 mm/min was used for testing. Minimum 5 specimens with a nominal dimension of (0.5 cm x 0.5 cm x 0.5 cm) were tested per data point. Combustion (C with Eltra CS-800 analyzer, O with ELTRA ONH-2000 analyzer) and XRF techniques (Co, Fe, Cl with Siemens SRS 303) have been conducted for the elemental analysis made on as pyrolyzed and powdered samples.

Thermal analysis (TG-DTA) measurements were carried out under Ar or N_2 (Netzsch STA 429, Selb, Germany; 2°C/min heating rate) on the already cured samples. The morphological features of the samples were analyzed from fresh fracture surfaces using a scanning electron microscope (SEM, JSM-6300F SEM, JEOL, Tokyo, Japan). SEM images were subsequently analyzed with the ImageTool software (UTHSCSA, University of Texas, USA) to quantify the cell size, cell size distribution, nanowire length and diameter. The raw data obtained by image analysis were converted to 3D values to obtain the effective cell dimension by applying the stereological equation: $D_{sphere}=D_{circle}/0.785$.[56] Specimens appropriate for high resolution transmission electron

microscopy (HRTEM) were prepared using an adapted cross-sectioning technique. Atomically resolved characterization as well as electron energy loss (EELS) and energy dispersive X-ray spectroscopy (EDXS) was performed using an aberration-corrected (C_s probe corrector) FEI TITAN 80-300 analytical scanning transmission electron microscope, allowing a spatial resolution of better than 1 Å in STEM mode and an energy resolution of the EELS measurements of about 0.2 eV, which was of special importance for the recording of the fine structure signals near the ionization edges (ELNES), yielding information on chemical bonding. The microstructures of some selected samples were investigated using a Philips CM 20 FEG (field emission gun) microscope, operating at 200 keV with a point to point resolution of 0.24 nm and equipped with both a Gatan Imaging Filter (GIF 200) and an EDX-detector enabling the detection of light elements (IDFix-system, SAMx-Germany). X-ray diffraction data (XRD, Bruker D8-Advance, Karlsruhe, Germany) were collected using Cu $K_{\alpha 1}$ radiation (40 kV, 40 mA, step scan of 0.05°, counting time of 5 s/step). Raman spectra were recorded with an Invia Renishaw Raman microspectrometer attached to a confocal microscope (50× objective) using the 633 nm line of a He–Ne laser as the excitation wavelength. Samples were ground and the powders were used for analysis, using a low laser power (5%).

Nitrogen adsorption/desorption at 77 K were measured using a Micromeritics ASAP 2020 system. The sample was first degassed under high vacuum ($3x10^{-3}$ mbar) at 400°C for 15h and then was transferred to the analysis system for the free-space measurement with helium. Thereafter, the sample was again degassed under vacuum at 400°C for further 2 hours, prior to sorption analysis. SSA was calculated from N_2 adsorption data at relative pressures below 0.20, by the multipoint Brunauer-Emmett- Teller (BET) method. Data were also analyzed by the t-plot method and by the Barrett-Joyner-Halenda (BJH) method, using the manufacturer's software. The apparent micropore distribution was calculated from N_2 adsorption data by the Horvath-Kawazoe (HK) method.

4.2.3. Results and Discussion

4.2.3.1. PMO including samples

The details for the production of cellular components from the mixtures of PDMS elastomer and PMO particles can be found in Chapter 4.1. Here, the information on CNHs and FeCp2 should be given first. CNHs are a new class of carbon-based nanomaterials derived from carbon nanotubes (CNTs), thus they exhibit high surface area (~300-350m^2/g)[57, 58] and adsorption capability suggesting that they ensure a great affinity with organic compounds making them promising candidates for hydrogen and methane storage as well as drug delivery systems.[59] CNHs are high purity (>95% purity) carbon materials and can be easily prepared in bulk amounts with a very low cost.[59] CNHs, different than CNTs which are generally contaminated with metallic particles of iron, cobalt, nickel and other others, does not include metallic particles. In CNHs, CNTs associate with each other to give rise to round-shaped aggregates (flower-like) of 100 nm in diameter. In **Figure 4.2-1** (a-c), electron microscopy investigations done on as received CNHs are given, these images are well fitting with the published literature data.[60] In **Figure 4.2-1** (b) a single aggregate having 100nm size is given, in **Figure 4.2-1** (c) a higher magnification of the previous image shows the hallow structure of tubes or "horns", and as can be seen each "horn" is ~2 to 3 nm in diameter and 30 to 50 nm in length. The XRD spectra showed only graphite peaks, being hundred intensity peak is ~26° (2θ) related with (002) plane, see **Figure 4.2-1**(d).

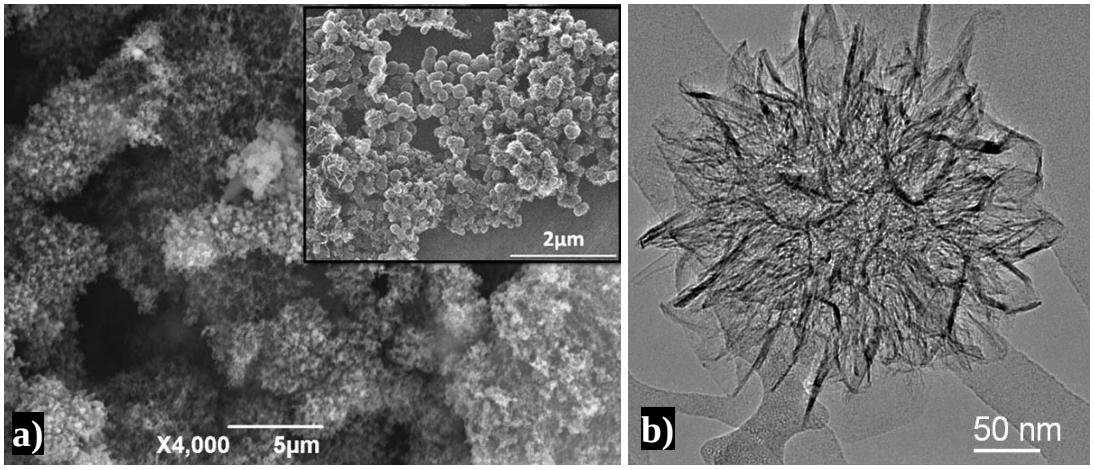

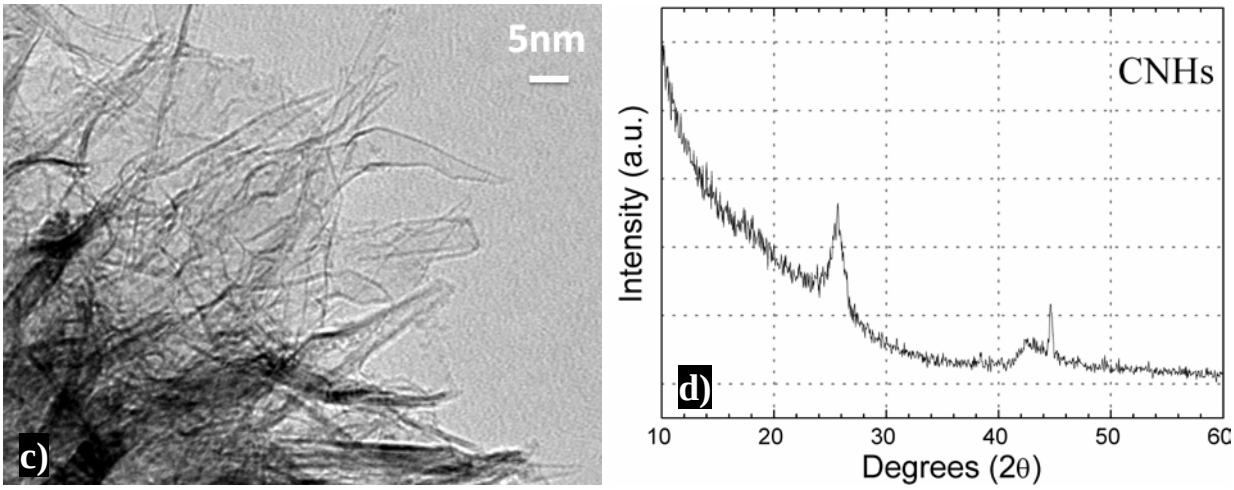

Figure 4.2-1. a) SEM image of as received CNHs (inset shows higher magnification), b) and c) TEM images of the same powder; and d) XRD data of CNHs showing only graphite peaks.

The SEM images of the first sample in **Table 4.2-1**, PMO-N1 (made from the mixtures of PDMS, PMO and CNHs) are given in **Figure 4.2-2** (a) and (b), and **Figure 4.2-2** (c) and (d) obtained from 1000°C and 1200°C pyrolysis, respectively. Samples made from 1000°C pyrolysis exhibit high fraction of macroporosity and PMO particles embedded on the cell walls (see **Figure 4.2-2** (a) and (b)), this was expected concerning the results documented in Chapter 4.1, however, interesting nanowires (NWs) type of formations (seemingly longer than CNHs) are observed in some segregated areas generally over the PMO particles, see inset in **Figure 4.2-2** (b). Increasing the pyrolysis temperature to 1200°C caused a lost in open macropore structure (see, **Figure 4.2-2** (c)), and no PMO particles remained in the cell walls and apparently all the previously empty areas are covered with a high fraction of entangled NWs causing only closed porosity. The randomly entangled 1D nanostructures (see **Figure 4.2-2** (d)) are observed in the cells forming a layer starting from one side the cell wall and arriving to other side (**Figure 4.2-2** (c)), so the length is limited by the pore size of bare SiOC matrix. This implies a probable reaction, occurring inside the pores via reaction of the decomposed gaseous species; i.e. these pores can be regarded as *catalytic microreactors*.[44]

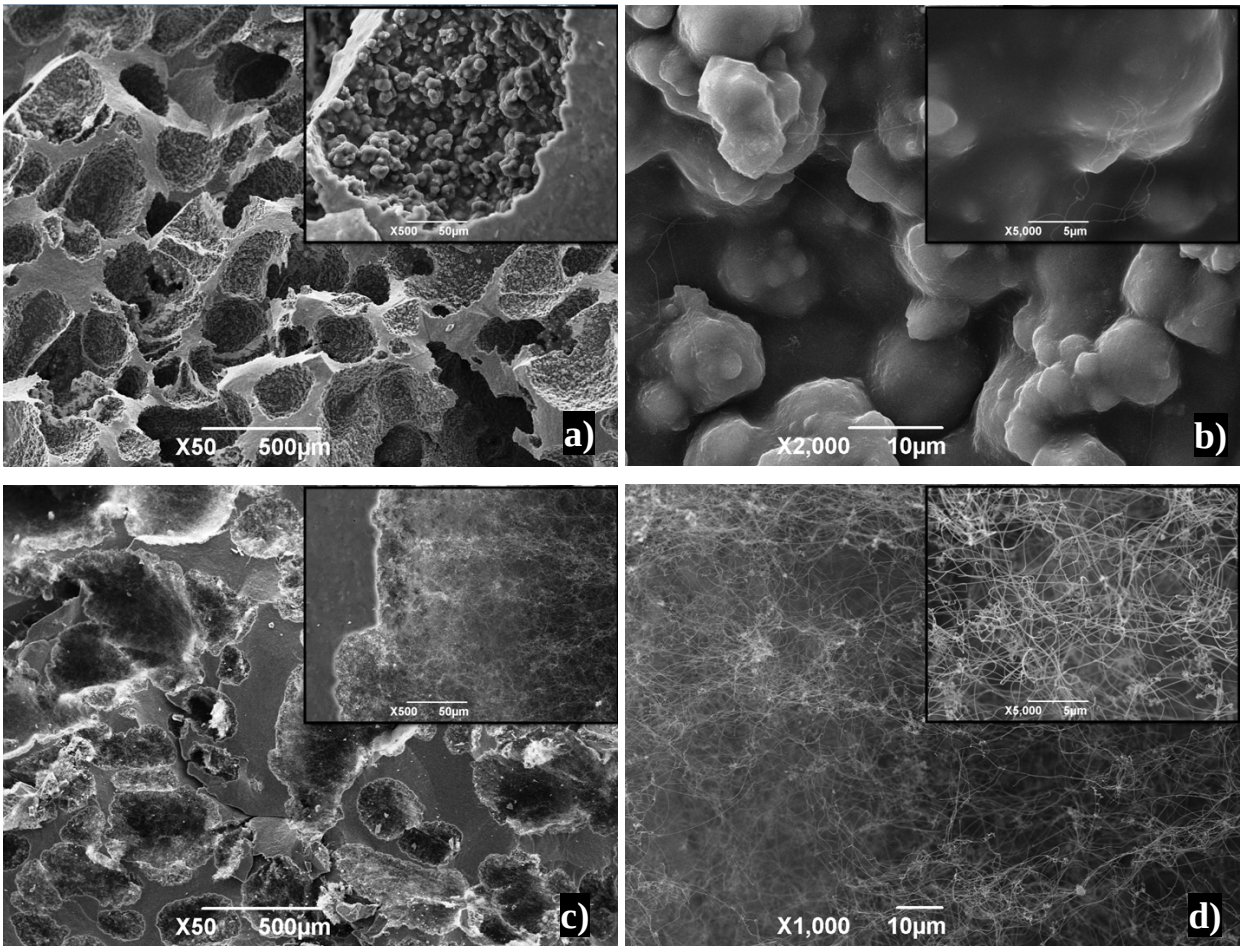

Figure 4.2-2. SEM images taken from the fracture surfaces of the sample PMO-N1 (made from the mixtures of PDMS, PMO and CNHs), obtained from a) 1000°C pyrolysis; b) detail from the cell wall at higher magnification; c) 1200°C pyrolysis; and d) detail from the cell at higher magnification, insets show higher magnification images.

Incorporation of ADA into the PDMS, PMO, and CNHs mixture resulted in a higher fraction of open porosity compared to previous samples even at 1200°C where previous sample contained mostly closed porosity. While the sample shows very few amount of 1D nanostructural formations at 1100°C (see **Figure 4.2-3**(a)), upon 1200°C pyrolysis very interesting flower like nanostructures resembling the original shape of CNHs, have been observed without a complete loss in the shape of PMO particulates. Most probably the high temperature stability of these

particles is governed by the partial pressure of released gases inside the pore, meaning that if its closed cell then a complete decomposition and formation of longer, higher amount of NWs, if not decomposition in a more limited extend causes smaller length NWs protruding from the surface of PMO particles which are embedded on the cell walls of SiOC matrix, see **Figure 4.2-3**(c-d) and inset therein.

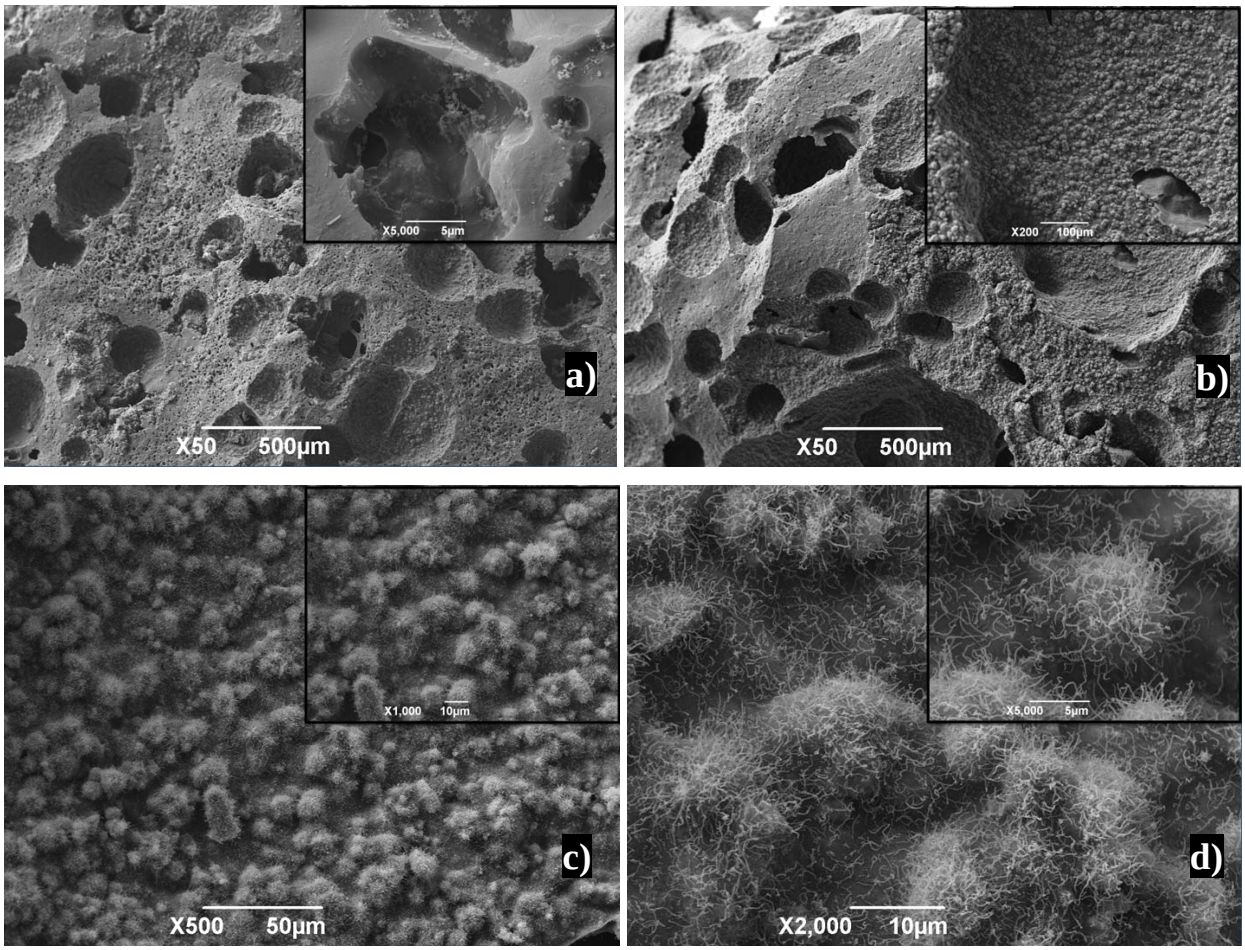

Figure 4.2-3. SEM images taken from the fracture surfaces of sample PMO-N2 (made from the mixtures of PDMS, PMO, CNHs and ADA), obtained at; a) 1100°C, and b) 1200°C pyrolysis; c) cell wall detail; and d) nanowire details, insets show higher magnification images.

Although, investigation done on these two samples have given us an idea of in-situ formation of 1D nanostructure; the procedure to form a ceramic body was a bit cumbersome via this method. Because, it necessitates the synthesis of PMO (which requires at least 2-3 days) and CNHs then mixing of them with PMPS and ADA which needs to be followed by curing and pyrolysis. In fact, it seems that during pyrolysis most probably, PMO particles only acted as a pool for Si elements (probably in the form of SiO gas) and reacted with CNHs which were a pool for C elements. Therefore; in order to simplify this system, we prepared the last sample (PMO-N3) by excluding the CNHs from the batch while preparing the green sample, but including FeCp2 by aiming to catalyze phase evolutions. Macroscopic investigations reveals almost the same type of microstructure (see **Figure 4.2-4** (a), and inset), i.e. irregularly shaped macropores in the defined cells (~100µm-1mm). However, this time some smaller sized pores (generally <50µm) are also observed on the struts, implying a probable interaction between ADA and FeCp2 altering the viscosity of the precursor during ADA decomposition, see **Figure 4.2-4** (b). As can be seen from the high magnification view, some cell walls are covered with long nanowire formations leaving behind an open pore, see **Figure 4.2-4** (c), while in some other areas these pores are all filled up with NWs (or nanofibers with rounded tips, see **Figure 4.2-4** (d)). The reason for such behavior remained elusive yet it was clear from the results that FeCp2 could be used as a catalyst source to form in-situ derived 1D- nanostructures since these samples did not include any already formed 1D nanostructures such as CNHs.

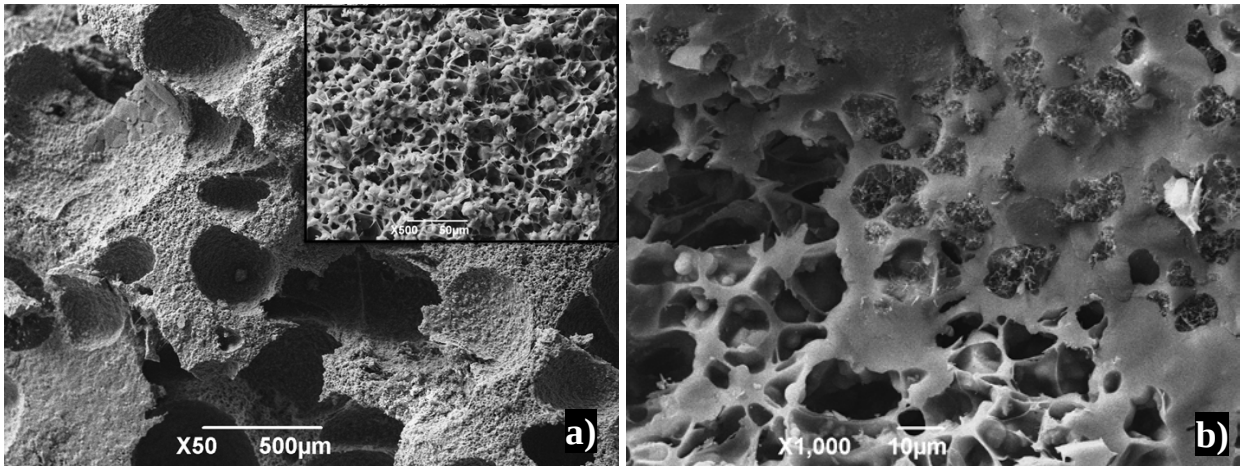

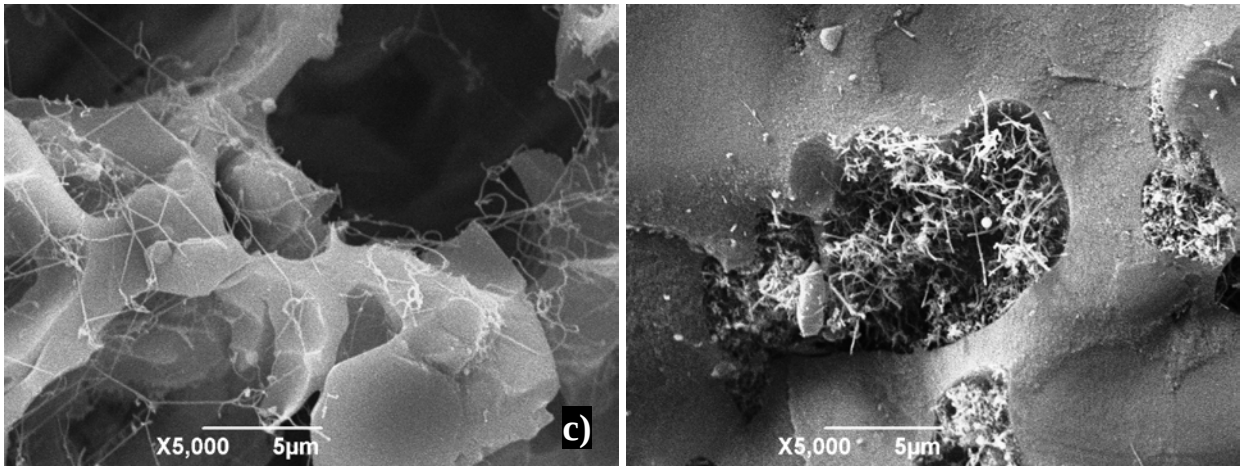

Figure 4.2-4. SEM images taken from the fracture surfaces of sample PMO-N3 (made from the mixtures of PDMS, PMO, ADA and FeCp2), obtained at 1200°C pyrolysis; a) general view; b) strut detail; c) cell wall detail; and d) cell window detail, insets show higher magnification images.

4.2.3.2. Preceramic polymer blends with FeCp2

All the aforementioned results obtained from these experiments motivated us to apply further experiments in the aim of in-situ D nanostructure formation in cell walls of porous component without the need of additionally incorporated particles such as PMO of CNHs. In order to accomplish this, we have prepared some other samples from the mixtures of PDMS and silicon resins which are thought to supply adequate amount of Si and C to a system and previously shown to yield with interconnected open porous cellular SiOC ceramics, see **Table 4.2-2** for the sample compositions prepared from silicone resin and elastomer mixtures including FeCp2. It should be noted that actually several samples have been prepared in this section yet information concerning only these two samples will be given in the following sentences. since they were found to represent the whole set truly. SEM images of the sample PM-F (PDMS-PMS-FeCp2) is given in **Figure 4.2-5**(a) and (b) for the pyrolysis under Ar and N_2 atmosphere at 1200°C/1h, respectively. Similar to our previous observations, the porosity generation was caused by the

differences in terms of weight loss, shrinkage and amount of gas generated for the blends through the pyrolysis step. As seen; the sample both in macro and nanoscale resembles the ones prepared without the use of FeCp2 (see Chapter 3.1), i.e. no catalytic effect of FeCp2 is observed, see embedded inlets in **Figure 4.2-5** (a) and (b) showing no 1D nanostructures in both Ar and N_2 pyrolysis, respectively.

The SEM image taken from the fracture surface of the sample PH-F (PDMS-PMPS-FeCp2) treated under Ar at 1200°C/1h is given in **Figure 4.2-5**(c), as seen it resembles the samples treated with no FeCp2 (see Chapter 3.1) as like the sample made by using PMS precursor. In macro scale the general morphology of the same sample treated under N_2 (see, **Figure 4.2-5**(d)) is similar to the one treated under Ar but with a higher proportion of open porosity. However, when investigations are done in higher magnification, it is clear that some NWs are formed in the cells in an entangled form which is totally different than the situation observed by Ar pyrolysis; compare the inlets given in these figures. In **Figure 4.2-5**(e) high magnification SEM image and **Figure 4.2-5**(f) TEM overview of NWs formed inside the pores shown in **Figure 4.2-5**(d, inlet) and (e) is given.

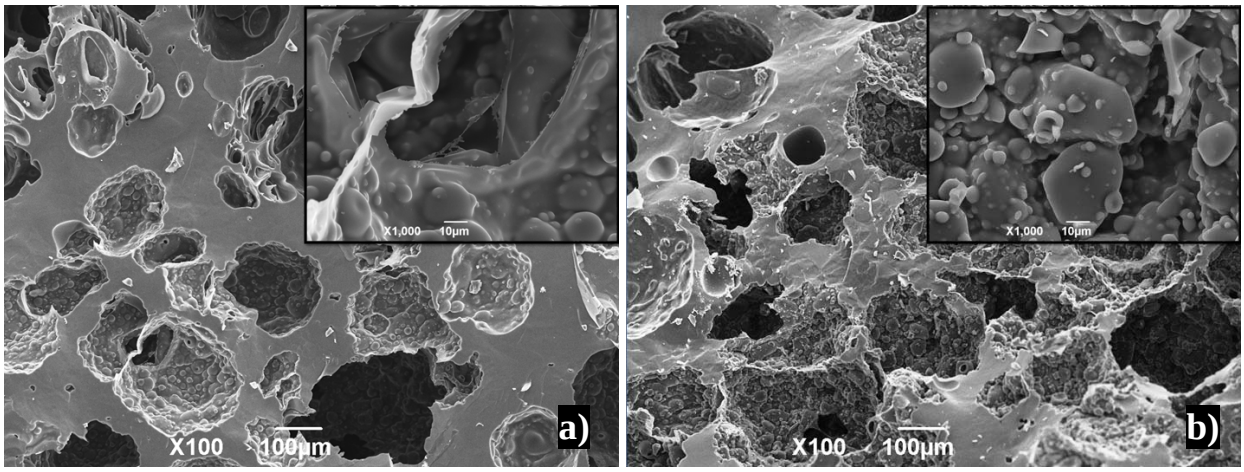

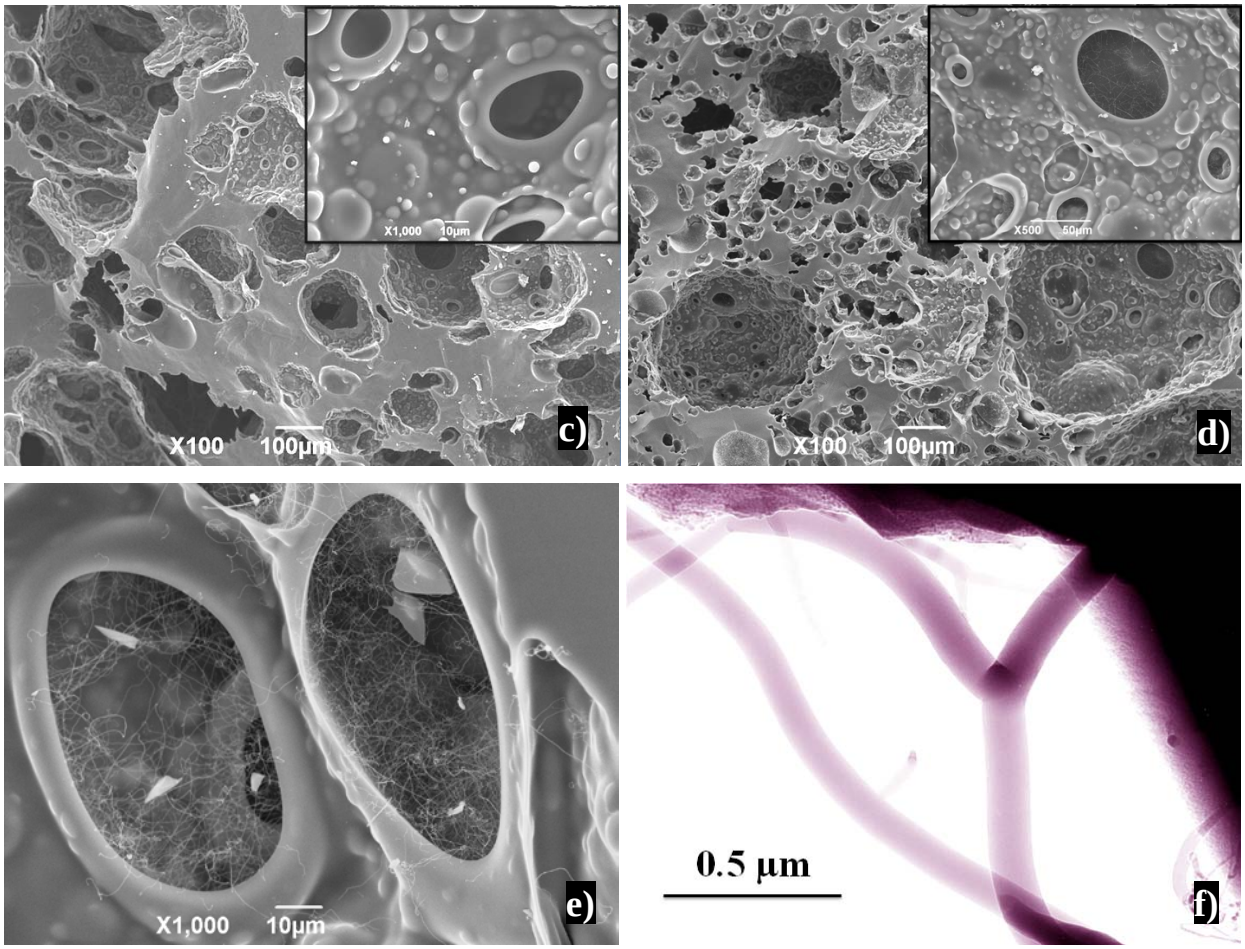

Figure 4.2-5. SEM images taken from the fracture surfaces of the sample PM-F (PDMS-PMS-FeCp2) treated in a) Ar; b) N_2, and SEM images of the sample PH-F (PDMS-PMPS-FeCp2) treated in c) Ar, d) N_2, e) pore details, and f) TEM overview of the same sample. All samples were pyrolyzed at 1200°C/1h.

The XRD data taken from both of the samples showed no clear defined peaks that can be attributable to any crystalline phases, but a halo between 20-30° (2θ) is known to occur due to amorphous SiOC phase, and a peak around 35.5° (2θ) due to SiC, **Figure 4.2-6**.

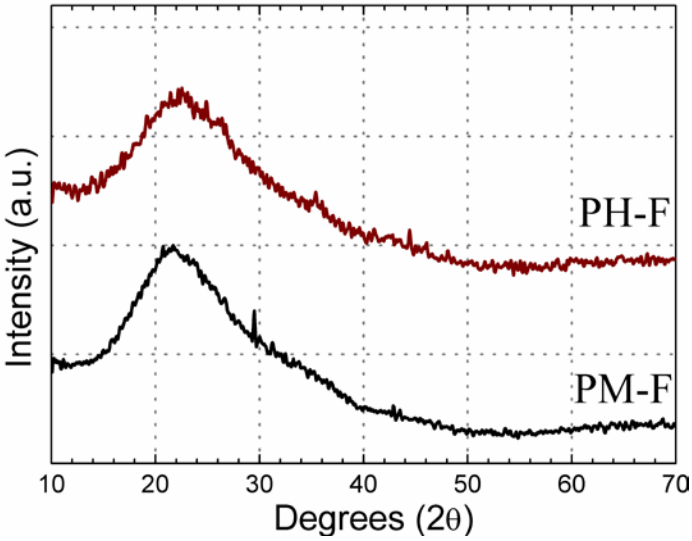

Figure 4.2-6. XRD of samples pyrolyzed at 1200°C/1h/N_2 showing amorphous characters of both of the samples.

In order to speculate on the formation and growth mechanism of these NWs we have conducted further TEM investigations coupled with EELS analyses. The results given in **Figure 4.2-7** (a-d) show that the previously observed NWs by SEM are amorphous (see also Figure 4.2-5(f)) and have caps (tips) which are polycrystalline iron (see **Figure 4.2-7**(b)) rather than a silicide and in the form of a sphere rather than a hemisphere (see **Figure 4.2-7**(a)). According to the finger print of the Si-L_{23} edge, the bonding state of Si is similar to stoichiometric composition of Si_2N_2O, see **Figure 4.2-7**(c). Surface coating layer shown in **Figure 4.2-7**(d) might be due to TEM preparation.

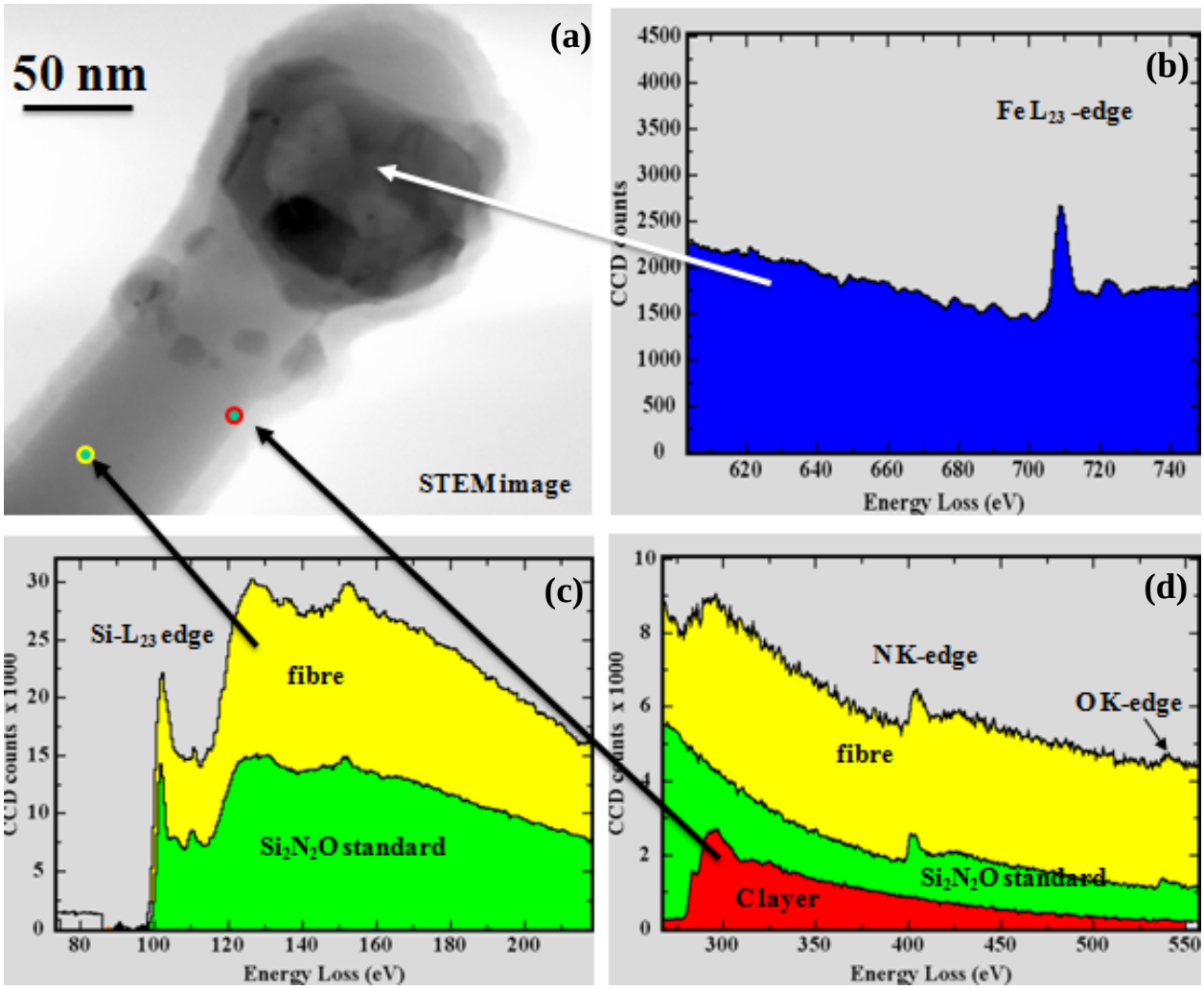

Figure 4.2-7. a) STEM image of formed NWs showing a metallic iron tip of the nanowire. EELS data given in b) taken from the cap; c) taken from the body of nanowire; and d) from the nanowire surface.

The observed presence of the particles connected to the NWs is consistent with the vapor–liquid–solid (VLS) mechanism, originally proposed for the growth of crystalline silicon whiskers by Wagner and Ellis more than 40 years ago.[45] However, the present results described above indicate that the VLS growth mechanism is involved during the growth of the amorphous Si_2N_2O NWs and not crystalline. At first sight, the amorphous nature of the NWs seems to be

inconsistent with the conventional VLS mechanism proposed for crystalline growth (single crystalline). However, recent studies report the generation of amorphous silica NWs by several different methods in which the VLS mechanism is considered to be the explanation for the observation of NWs.[61-72] The growth temperature is generally kept below the crystallization temperature of the silica phase, so amorphous SiO_x NWs were obtained. Although, this hypothesis is consistent with our results since the experiments in the present part of the study were always carried out at temperatures ≤1200°C, the mechanism of the formation and growth of NWs necessitates more attention. In most of these aforementioned reports, no detailed information on the effect of the growth parameters for the amorphous silica NWs has been documented, and thus, very important details regarding the growth mechanisms are usually missing. The reported works refer only to some chemical reactions but no clear mechanism has been postulated.

The only investigation in this manner was done by Aharonovich et al.[63, 64] in which the authors proposed two alternative growth mechanisms for amorphous silica NWs and generally for all type of amorphous NWs having metallic tips, i.e. governed by VLS. The initial stages of the first possibility discussed, follow a common VLS mechanism in which Si (or SiO) vapor diffuses into the metal catalyst and after supersaturation is achieved, it nucleates in the lower hemisphere of the catalyst. After the nucleation and growth of single crystalline silicon (Si) NW with metallic head, ambient oxygen reacts with crystalline Si NW and oxidize it, creating a silica sheath. The oxidation process continues as long as a crystalline silicon core exists or forms. However, the possibility of crystalline Si NW formation and its complete oxidation to yield with an amorphous silica NW was shown unlikely to occur especially for the NWs with diameters larger than 15 nm. Because, the formed silica interface prevents further oxidation thus a core shell structure usually evolves. But, as in our case and in many other cases, it is shown that relatively thick NWs (15-100nm in NW diameters) are formed with no crystalline core (so no core-shell structure).[63, 64] The second possible route proposed by Aharonovich et al.[63, 64] for SiO_x NWs growth does not involve diffusion of Si element (wherever it comes) into the catalyst particulate (probably pseudo-liquid). The mechanism is based on preferential adsorption or formation of SiO_x clusters on the catalyst droplet without penetration into the droplet (note that if this is the case then no

silicide formation should be observed). The SiO_x slips (can be thought as a surface diffusion towards bottom of the sphere) to the lower hemisphere of the catalyst due to the low solubility of SiO_x clusters in the metal catalyst, and begins to form a NW structure there by penetrating to the metal catalyst/SiOx NW interface to grow SiOx NW.[63, 64] Previous reports on gold wettings of different substrates at high temperatures revealed that the contact angle between the liquid droplet and the substrate is about 125-130°. This angle allows relatively easy penetration of SiO_x clusters beneath the droplet particles.[63, 64] For example; Levi and Kaplan[73, 74] showed that an oxygen rich interface forms at the $Al–Al_2O_3$ interface during the wetting of Al on sapphire, leading to a decrease of the Al-sapphire interface energy. Levi and Kaplan's conclusions of the Al-sapphire system indeed demonstrated that the surface diffusion of oxygen/oxide on the sphere does occur and leads to the growth of an oxide in the lower hemisphere of the droplet.

This modified VLS mechanism, can be called as *cluster directed VLS* mechanism, as far as we observed have some distinctive signs which are dissimilar from the conventional VLS-grown, namely; i) in classical VLS the growth direction corresponds to energetically or kinetically favorable configurations, however, a preferred growth in a specific direction should not be expected for amorphous 1D nanostructures for which, there is no template to grow on it; ii) generally split growth may occur; i.e., one nanowire may split into two branches, and the newly formed branch also splits into two subbranches, and so on. Interestingly the branches or the sub-branches have diameter and growth direction similar to the parent one. This ramification phenomenon has been observed by Zhu et al.[75] in their cobalt-catalyzed amorphous silica nanofibers, and more recently by Pan et al.[70] in their gallium-catalyzed amorphous silica nanofibers; iii) metal catalyst particles observed on the tips of crystalline NWs generally have a shape of half sphere with a straight/smooth interface between the catalyst particle and the formed NW this is documented by thousands of papers after Wagner and Ellis[45] (see also later), while in the form of amorphous NWs spherical/oval shape tips are observed and these particles are covered with a thin layer.[61, 63, 64, 75] Certainly these issues are not more than our hypothesis/obervatios and need very careful, detailed work which may be the interest of a new thesis study to verify and for sure out of the scope of the present one. However, all the results that we have obtained throughout this thesis study are in support of these hypotheses.

The metallocene family has a “sandwich structure” of two parallel cyclopentadienyl rings with a metal in the center between these rings ($M(C_5H_5)_2$ with M= Fe, Co, Ni), is solid at room temperature, and dissolvable in various organic solvents, but also shows suitable decomposition behavior in the temperature range 600-1150°C.[76] The pyrolysis of metallocenes shows a complex decomposition process of consecutive, parallel, and catalytic reaction series. At a temperature ≥ 500°C, FeCp2 decomposes as given in Equation 4.2-1.[76]

$$Fe(C_5H_5)_2 \rightarrow Fe + H_2 + CH_4 + C_5H_6 + ... \qquad 4.2\text{-}1$$

This means, at a temperature of >700°C, solid or liquid-like Fe particles and different kinds of hydrocarbons exist in the reaction zone coming both from the FeCp2 and preceramic polymer decomposition. In the light of the previously explained theories for the formation of amorphous NWs; 2 probable mechanisms can be postulated; i) first, iron droplets are formed on the SiOC matrix substrate, then continuous supply of Si, O (in the form of SiO coming from preceramic polymer decomposition) resulted in silica clusters which diffused to the lower hemisphere of the catalyst particle (without penetration into the droplet so iron did not give any reaction to form silicide, see **Figure 4.2-7** (b)) and entered to the bottom of the particle detaching it from the substrate, forming an amorphous silica NW[63, 64] with a quasi spherical metallic particle (see **Figure 4.2-7**(a)) which is then reacted with copious flow N_2 to form amorphous silicon oxynitride (a-SiO*x*N*y*) NWs[77] (note that the spitted growth shown in **Figure 4.2-5** (f)); otherwise ii) SiO*x*N*y* clusters were formed directly on the surface of the iron particle from where they diffused (surface) to the bottom of the particle, detached it by forming a-SiO*x*N*y* interface which grew due to continues supply of Si, O and N. Logically the latter seems more probable since the formation of SiO_2 has a higher demand of oxygen saturation compared to that of silicon oxynitride. Our results are different that what was published recently by Peng et al.[62] where the authors investigated the N_2 thermolysis of perhydropolysilazane precursor on alumina wafers coated with $FeCl_2$ catalyst, and obtained only amorphous SiOx NWs. Not excluding the possibility to have SiOx NWs in some local parts; the difference between our results; i.e. obtaining a-SiOxNy and not a-SiOx NWs, might arise due the differences in preceramic polymer

types (backbone architecture) and gas flow rate which both can affect the local partial pressures of SiO, O_2 and N_2. In fact a recent study of Zheng et al.[72] have shown the formation of a-SiOxNy NWs through thermal treatment of nickel coated silicon wafers in NH_3 plasma. The authors underlined that in plasma process both reactive nitrogen and oxygen species were present causing a competitive formation of Si-N and Si-O bonds resulted in the formation of a-SiOxNy NWs. When the position which was 20 cm away from the plasma coil investigated, it was understood that the plasma activation effect was weak to create active nitrite species thus; oxygen species exhibited higher reactivity than nitrogen ones and were advantageous in competing silicon to form a-SiOx instead of oxynitride. Thus, it is highly possible to assume a similar phenomenon; i.e. a high and similar activity of both nitrite and oxide species; resulting in a-SiOxNy and not silica, occurred in the present experimental conditions.

4.2.3.3. Preceramic polymers with metal halides

From the previous studies where Fe(Cp2) has been used, it was understood that iron is an effective catalytic source in producing 1D nanostructured formations on the pore surface of the macroporous ceramic bodies via pyrolysis of polysiloxane precursors (≤1200°C). In the light of previous experiences, in the last part of this section, we have prepared some other samples for which the compositions are already given in **Table 4.2-3**. These samples are prepared in order to have a better control on the pore characteristics (size, shape, amount, open/closed pore ratio, etc.) and to increase the NW yield with the aim of enhancing the specific surface area and functionalize the cellular components produced from preceramic polymers.

For these last samples, we have used metal halides as a catalyst source and either PMS (MK) or PMPS (H44) as an only preceramic precursor which can be cured thermally at temperatures >100°C without the need of any peroxide radical initiator and curing agent.[10, 78, 79] The color of the polymeric samples, after cross-linking, was affected by type of transition metal halide; $FeCl_2$ gave red-brown color, while $CoCl_2$ resulted in a purple color, as expected. The mineralization of these precursors takes place predominately between 400 and 800°C[80] (where the reduction of

metal halide occurs causing metallic particles in a series of steps) and a Si-O-C material forms which remains amorphous at least up to pyrolysis temperatures of 1400°C.[81] Increases in the pyrolysis temperature results in phase separation/decomposition/crystallization of the metastable matrix, all these issues are explained previously in detail in Chapter 2.

Many studies can be found in the literature concerning foaming of various polymeric systems using ADA.[78, 82-84] ADA has also been used to produce macrocellular SiOC[78] and as we have explained previously to produce SiCN[85] ceramics from preceramic polymers. It is also known that activators, such as transition metal compounds, may reduce the decomposition temperature of ADA to the values as low as 150°C.[86] ADA is used either with PMS or with PMPS preceramic polymer and different amount of total porosity and especially different ratios in open/closed porosity were obtained in these two systems.

4.2.3.3.1. PMS based samples

a) Foaming, Crosslinking and Thermal Analysis

TG-DTA analyses measurements, displayed in **Figure 4.2-8** (a) for N_2 and (b) for Ar, are in good agreement with the literature data. The final ceramic yield was slightly affected by the incorporation of the metal catalyst and values of ~90% were obtained whatever the used atmosphere (Ar or N_2) and catalyst (Fe or Co) was (see **Figure 4.2-8** (a) and (b), left)). There was also no clear difference in DTA plots given in **Figure 4.2-8** (a, right) and (b, right) when Fe or Co is added or not and whatever the working atmosphere was (the specimens were already cross-linked before analysis).

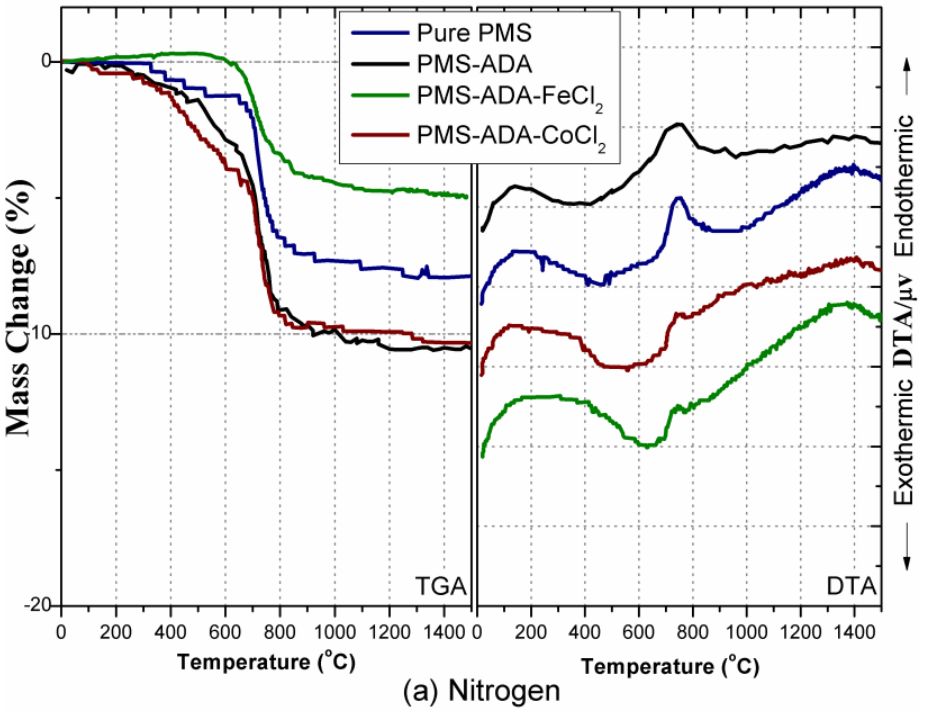

(a) Nitrogen

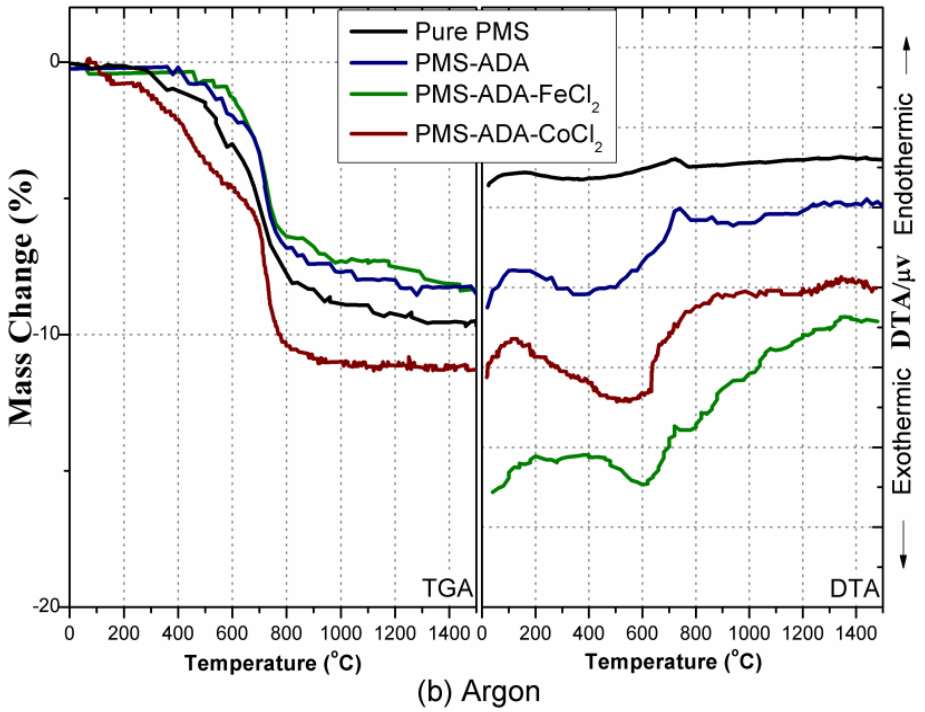

(b) Argon

Figure 4.2-8. TG/DTA results for PMS samples including pure PMS, PMS-ADA, PMS-ADA-$FeCl_2$ and PMS-ADA-$CoCl_2$ pyrolyzed under a) N_2, and b) Ar atmosphere.

In **Figure 4.2-10** (a) SEM image taken from the cured polymer including Fe is given (green sample of PMA-Fe). As could be seen the microstructure has cellular structure yet the fraction of closed porosity is very high. The presence of high amount of closed porosity can be attributed both to the limited amount of gas release (volatiles/oligomers) during the PMS curing[80] and to the poor match between the decomposition temperature of the blowing agent and the polymer viscosity at this temperature.[78, 79] Inset given in the figure shows the high magnification SEM image of the cell wall which includes metallic iron chloride particles (confirmed by EDS, see **Figure 4.2-9** (b) and inset therein) generally <5µm in diameter. This confirms the incorporation of halide into polysiloxane matrix.

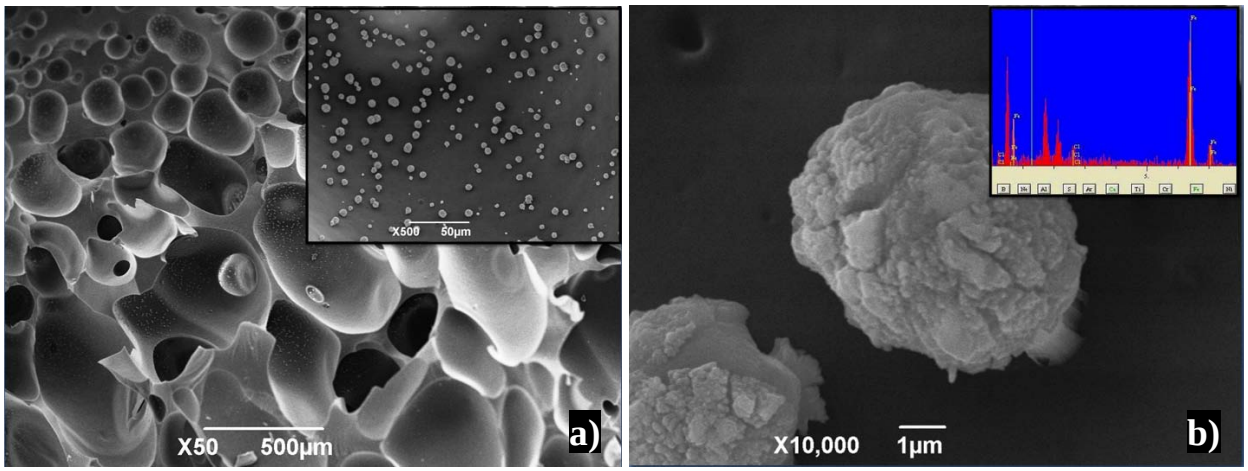

Figure 4.2-9 a) SEM image taken from the fracture surface of cured PMS-ADA-$FeCl_2$ mixture, inset shows higher magnification images taken from the cell wall, b) SEM images showing the detail of cell wall, inset demonstrate EDS analysis taken over the spherical particle showing Fe and Cl elements (Au peaks were due to gold sputtering over the sample surface).

a) Structural Characterization

In **Figure 4.2-10** (a) SEM image of the same sample treated under Ar at 1300°C is given. Although, slightly higher amount of open porosity is observed, no distinctive changes occurred during pyrolysis and the resulted material did not include any 1D-nanostructure. The crack in the figure most probably aroused while preparing the sample for SEM investigation. In higher magnification, some particle agglomeraties are observed generally <3µm (see **Figure 4.2-10** (b)) and EDS analysis taken of these parts proved the permanency of iron (see inset in **Figure 4.2-10** (b)). While increases the thermolysis temperature under Ar atmosphere did not caused much difference, upon N_2 pyrolysis we have observed much different morphologies, especially in nanoscale. The SEM image of the sample treated at 1300°C is given in **Figure 4.2-10** (c), and the image for the same sample treated in at 1400°C is in **Figure 4.2-10** (d). As seen N_2 caused a reactive ambient, causing the formation and growth of NWs. Increases in pyrolysis temperature resulted in longer and higher amount of NWs formation protruding from the cell walls and forming a layer closing the entire pore openings in the cells walls. No SEM observable metallic tips are found on the heads of these NWs, differently than what we have observed previously.

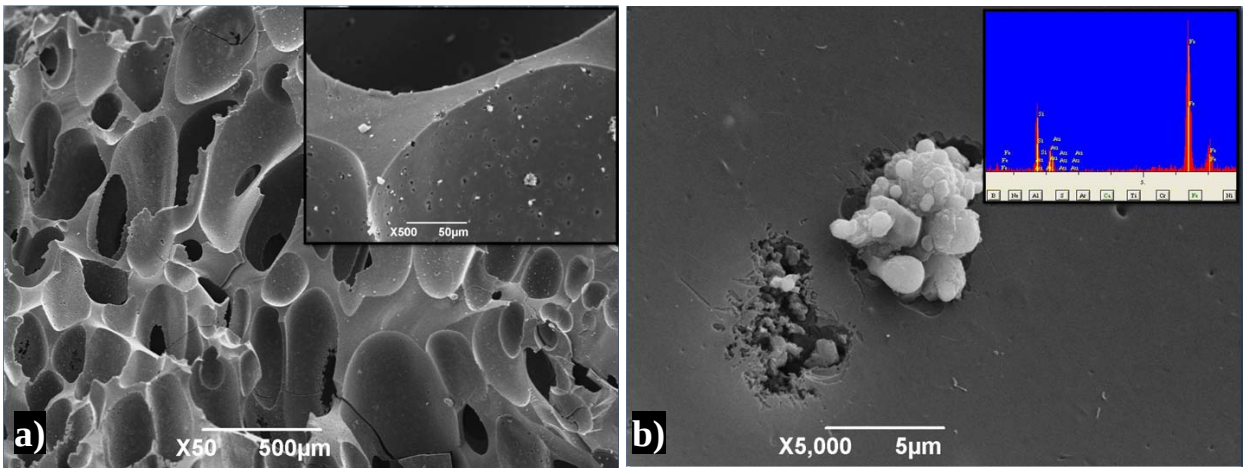

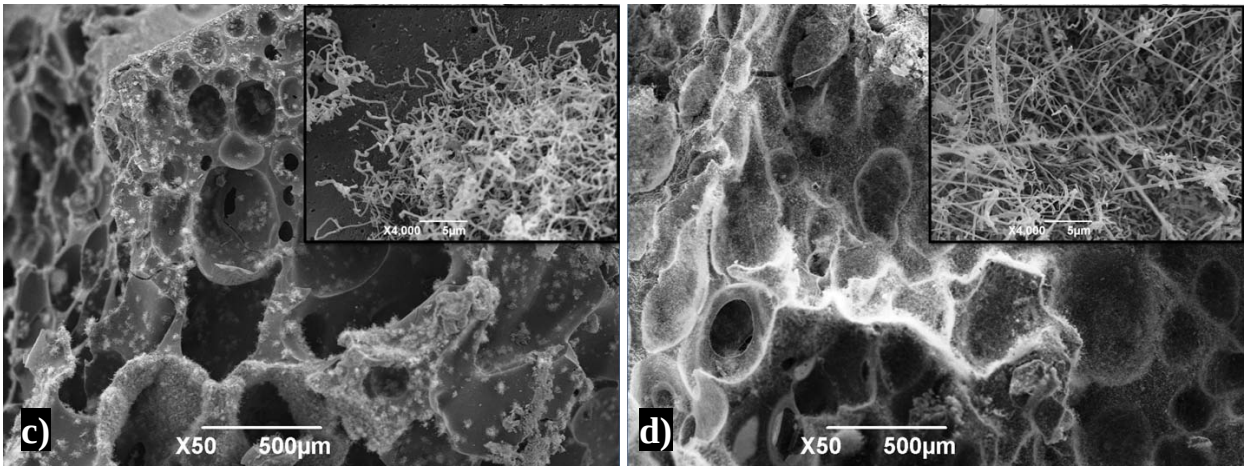

Figure 4.2-10. SEM micrographs taken from the fracture surfaces of PMS-$FeCl_2$-ADA samples treated at: a) Cured polymer, b) pyrolyzed at 1300°C (under Ar), inset gives EDS taken over the white colored agglomerate (Au peaks were due to gold sputtering over the sample surface), and c) 1300°C (under N_2), d) 1400°C (under N_2).

Similar to the observations obtained from PMS-Fe system, a porous structure with some amount closed porosity is observed when Co was used instead of Fe, see SEM images given in **Figure 4.2-11** (a-d). In fact, the morphology of the ceramic foam (PMS-$CoCl_2$-ADA) closely resembled, in macroscale, that of the polymeric thermosets not containing the catalyst, namely showing both open and closed porosity with dense struts, similarly to the previous investigations.[78] Pyrolysis at 1250°C under Ar atmosphere resulted in a porous monolith (see **Figure 4.2-11**(a)) with large cells (>500 µm), having small size pores within the cell wall and the struts, see embedded image in **Figure 4.2-11**(a)) for strut detail. With increasing the pyrolysis temperature to 1400°C, several cavities (around 20 µm) containing micron size pores appeared on the walls and struts of the ceramic foam. No formation of 1D nanostructures was observed in samples pyrolyzed in Ar. However, the change in pyrolysis atmosphere caused differences in the final products at the nanoscale. Upon 1250°C heating under N_2, entanglements of NWs were created, as shown in **Figure 4.2-11** (c) and inset (higher magnification SEM image therein). Increases in pyrolysis temperature to 1400°C caused the formation of a large amount of NWs on the cell wall surface,

as reported in **Figure 4.2-11** (d). The inset given in **Figure 4.2-11** (d) shows the details of NWs with metallic tips implying a different mechanism (most VLS) is governed the formation of NWs than in Fe containing samples where no metallic tips were observed.

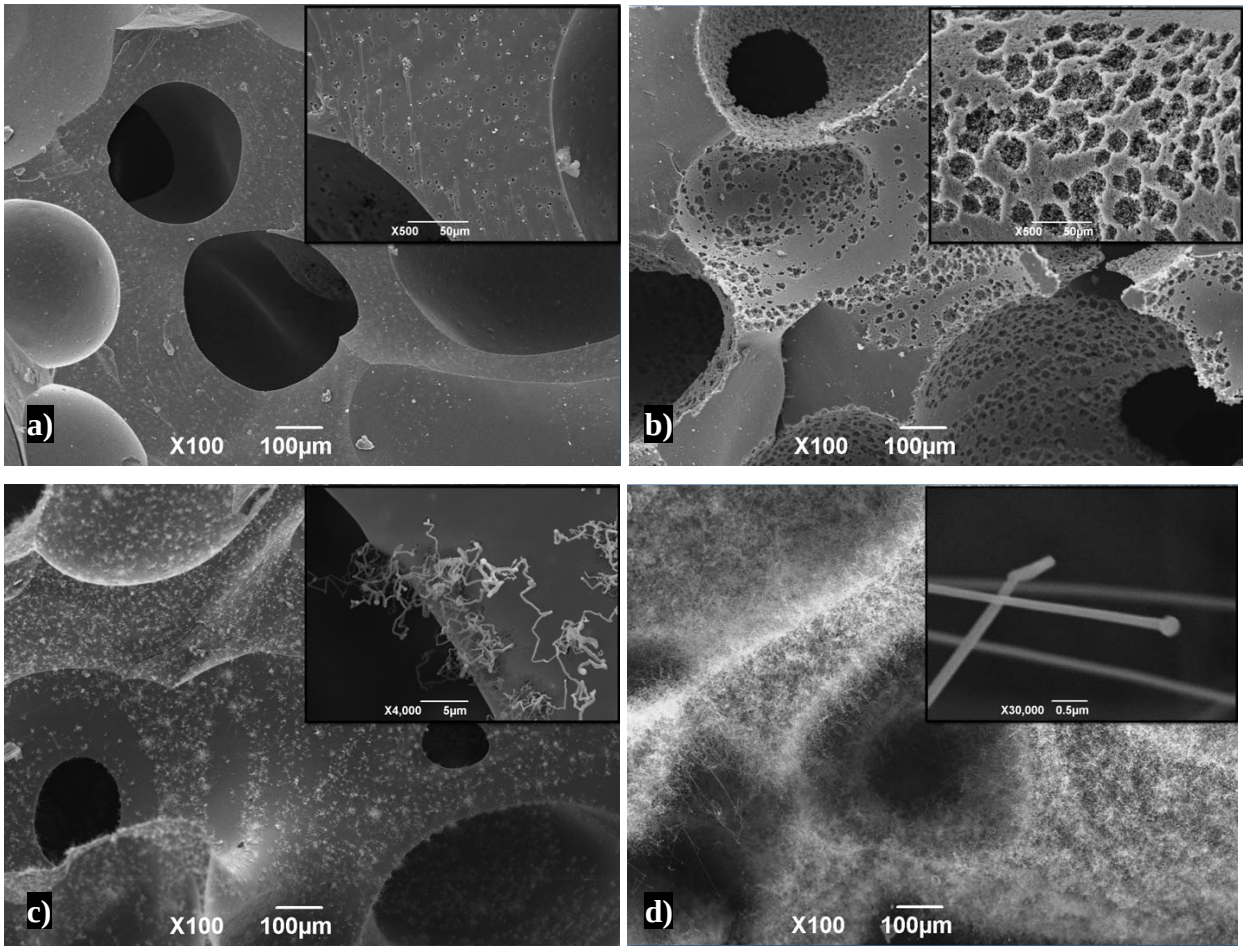

Figure 4.2-11. SEM micrographs taken from the fracture surfaces of sample PMS-$CoCl_2$-ADA samples treated at; a) 1250°C, b) 1400°C (under Ar), and c) 1250°C, d) 1400°C (under N_2).

XRD spectroscopy was performed in order to identify the phase evolution, and the results for the samples pyrolyzed both under N_2 and Ar atmosphere between 1250 to 1400°C (by 50°C steps)

are shown in **Figure 4.2-12**(I) and (II), respectively. The samples obtained at 1250°C displayed a characteristic diffraction pattern of amorphous SiC*x*O*y*, with a broad hump in the 20-30 degrees range (2θ) and the peak at ~26 (2θ) which could be related to free carbon (labeled C in the graphs).[87] In Ar atmosphere at low temperature iron silicide (Fe-Si) phase mixture is observed, and with the increase in pyrolysis temperature silicidation occurred with a phase change in Fe-Si yielding with FeSi and Fe_5Si_3 silicides at 1400°C. Instead under N_2 atmosphere at low temperatures some peak combinations have been observed around 45° (2θ) which could be attributed to the different silicides (Fe_3Si, Fe_5Si_3 and FeSi). Increasing the thermolysis temperature, and so enhancing the crystallization of the amorphous matrix caused a depression in the iron-silicide related peaks, assigned in the **Figure 4.2-12**(I-d) as "*", and even upon 1400°C pyrolysis no phase pure FeSi is obtained; i.e. although the reaction with the silicon-based matrix occurred resulting in an iron silicide phase with an increased silicon content, the process (silicidation) was not complete to yield with FeSi. In both atmospheres, the formation of iron carbide or iron silicate compounds was not observed by XRD analysis. Moreover, Increasing the thermolysis temperature decreased the intensity of amorphous silica and carbon related peaks, and improved crystallization, similarly to what reported for a Ni-containing polysiloxane.[48] While the sample treated under Ar at 1400°C shows only broad features for β-SiC (JCPDS # 29-1129), the one treated under N_2 contained well defined crystalline features of Si_2N_2O (JCPDS # 47-1627). This sample can be thought as a composite ceramic including amorphous SiOC matrix where high amount of Si_2N_2O NWs were formed.

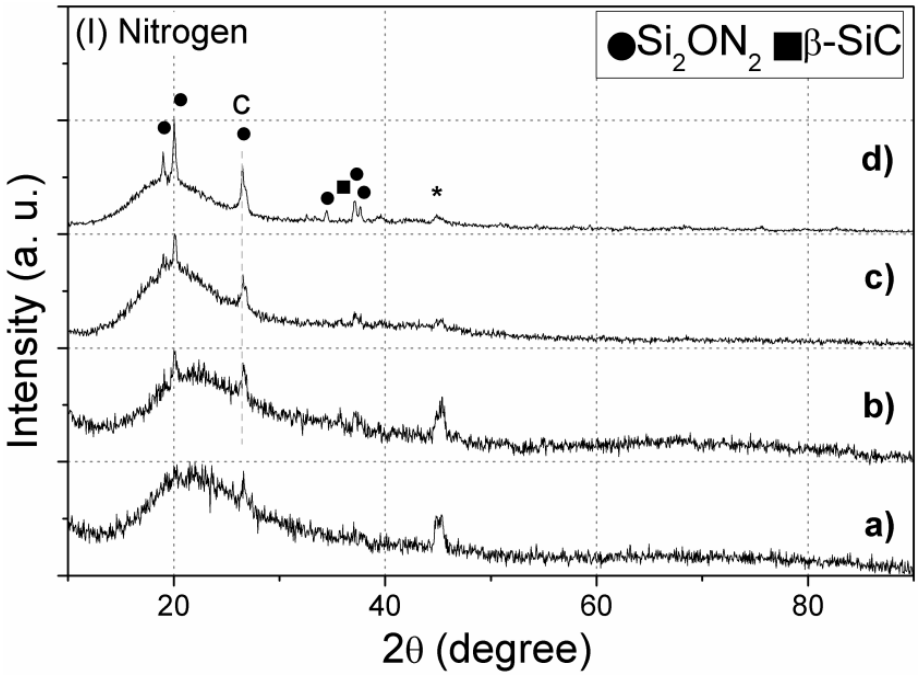
(I) Nitrogen
●Si2ON2 ■β-SiC
c
*
d)
c)
b)
a)
Intensity (a. u.)
20
40
60
80
2θ (degree)

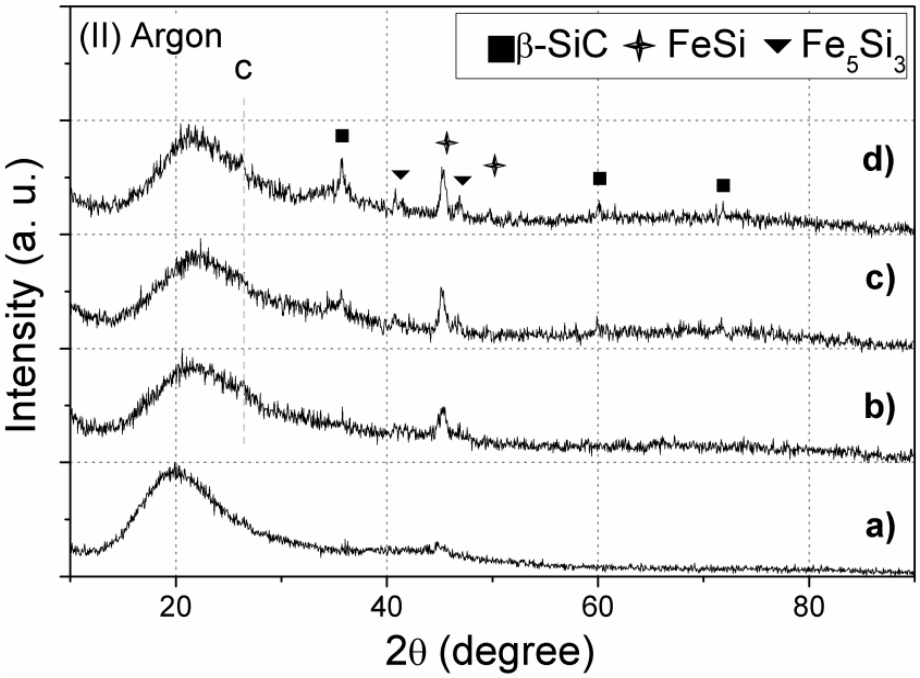
(II) Argon
■β-SiC ✦ FeSi ▼ Fe5Si3
c
d)
c)
b)
a)
Intensity (a. u.)
20
40
60
80
2θ (degree)

Figure 4.2-12. XRD plots for PMS-ADA-$FeCl_2$ samples pyrolyzed under I) N_2, and II) Ar, at a) 1250°C; b) 1300°C; c) 1350°C; and d) 1400°C.

XRD results for the Co including samples which were pyrolyzed either N_2 or Ar atmospheres between 1250-1400°C are shown in **Figure 4.2-13** (I) and (II), respectively. Similar to the previous observations, the samples obtained at 1250°C displays a characteristic diffraction pattern of amorphous SiC*x*O*y*, with a broad hump in the 20-30 degrees range (2θ) and the peak at ~26° (2θ) which is related to free carbon (labeled C in the graphs).[87] Experiments performed at lower temperatures showed that cubic Co (JCPDS #15-0826) was the primary cobalt phase (see later). It seems that when the thermolysis temperature increased, reaction with the silicon-based matrix occurred resulting in a cobalt silicide phase mixture. While thermolysis at 1250°C yielded Co_2Si (JCPDS #04-0847) as the main silicide phase, at 1400°C under both pyrolysis atmosphere CoSi (JCPDS #50-1337) was observed, indicating that the silicidation reaction occurred through the phase sequence: cubic Co→ Co $_2$Si → CoSi, in agreement with previous studies.[88, 89] The formation of cobalt carbide or cobalt silicate compound was not observed by XRD analysis. In a similar way to iron including samples; increasing the thermolysis temperature decreased the intensity of amorphous silica (SiOC) and carbon related peaks, and improved crystallization. While the sample treated under Ar at 1400°C shows only broad features for β-SiC (JCPDS # 29-1129), the one treated under N_2 contained well defined crystalline features of Si_2N_2O (JCPDS # 47-1627), together with small amount of β-SiC.

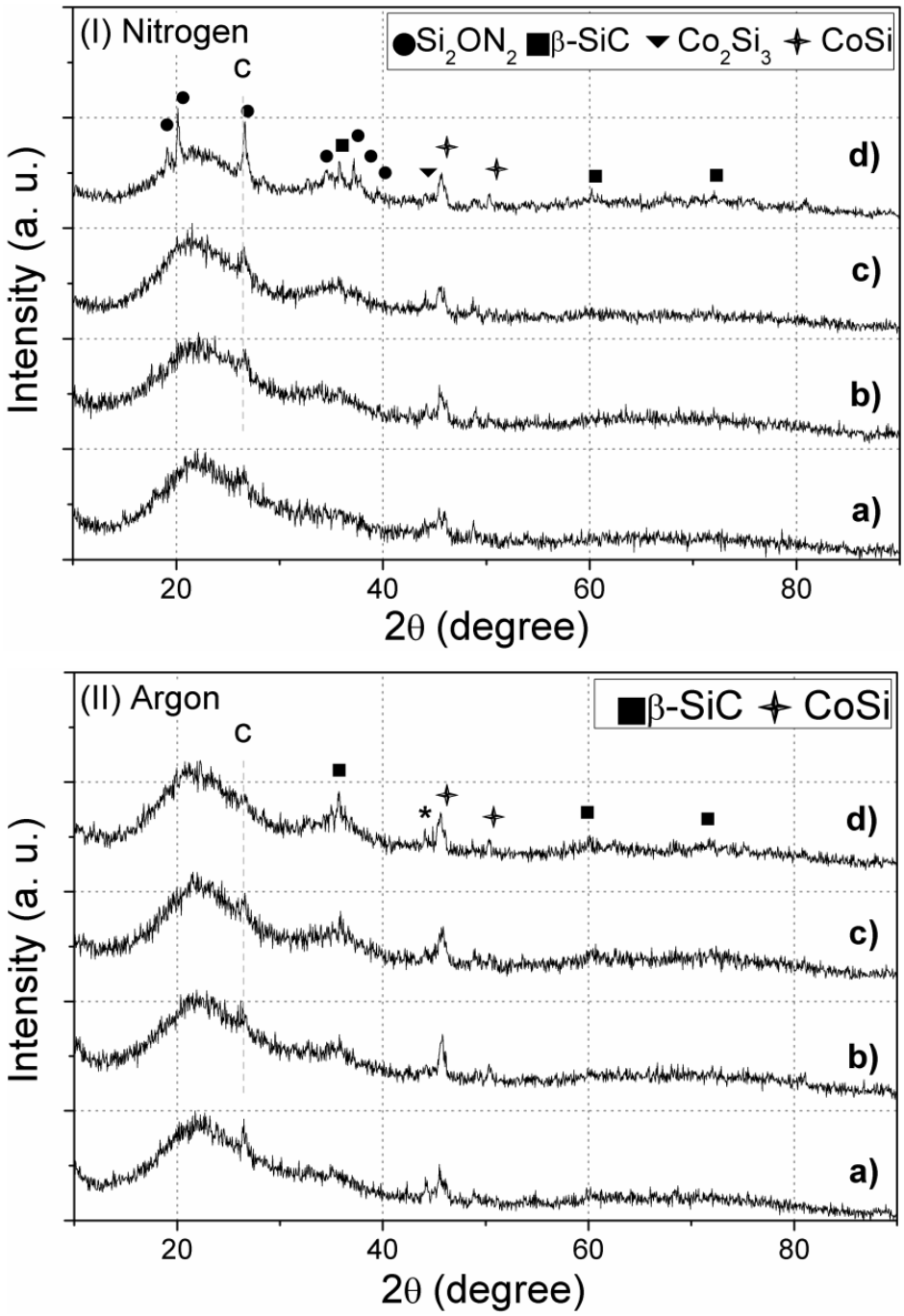
(I) Nitrogen
●Si2ON2 ■β-SiC ▼Co2Si3 ✦CoSi
c
d)
c)
b)
a)
Intensity (a. u.)
20
40
60
80
2θ (degree)
(II) Argon
■β-SiC ✦CoSi
c
*
d)
c)
b)
a)
Intensity (a. u.)
20
40
60
80
2θ (degree)

Figure 4.2-13. XRD plots for PMS-ADA-$CoCl_2$ samples pyrolyzed under I) N_2, and II) Ar, at a) 1250°C; b) 1300°C; c) 1350°C; and d) 1400°C.

The formation of a Si_2N_2O (silicon oxynitride) phase has been shown to occur after pyrolysis of the same polysiloxane including silicon (Si) as a reactive filler under N_2.[10, 90] The authors showed that the reaction of SiO gas (released from the precursor during pyrolysis) and N_2 (the heating atmosphere) formed Si_2N_2O, and that a further increase in the temperature resulted in a continuous increase in the absorption of nitrogen up to the melting point of Si ($Tm_{(Si)}$~ 1414°C). It should be noticed that in these studies only a small amount of Si_2N_2O was detected after pyrolysis in N_2 at temperatures lower than the melting temperature of the silicon powder additive. In the present study, we have demonstrated that the addition of both Fe and Co catalysts particles allow the formation of a well defined Si_2N_2O crystalline phase without the need of any other reactive filler, such as Si. Porous monoliths pyrolyzed at 1400°C under Ar were comprised of an amorphous SiOC matrix containing some amount of nano-crystalline β-SiC, whereas the samples heat treated under N_2 were comprised of amorphous SiOC and rather well defined crystalline silicon oxynitride phase (in the NWs).

It was shown that SiO and CO are the main gaseous species that form during the pyrolysis of a similar polysiloxane precursor at temperatures higher than 1000°C, and that the partial pressure of both of the gases increases with increasing pyrolysis temperature up to 1400°C.[91] In the present study, while the reaction of SiO and N_2 governed the formation of Si_2N_2O under N_2 pyrolysis, no 1D nanostructure formed during heating under Ar atmosphere. This could be attributable to the differences in nucleation and growth mechanisms of these NWs; in fact, whereas Si_2N_2O does not necessitate carbon for its formation, a specific level of carbon saturation is needed to precipitate SiC crystals from metal silicides, in another words carbon is crucial for SiC nucleation and growth [92] (note that the precursor, PMS, used in the present study contains a very limited amount of carbon compared to that of other types of polysiloxane precursors commonly used to produce SiOC materials, see later also).[80] Similarly the explanation

for the absence of SiO_2 1D nanostructures could be a high demand of oxygen saturation; implying that the partial pressure of oxygen (or SiO) was never in required level in the reaction bed due most probably to the continues flow of Ar inhibiting the formation of silica NWs. Consequently, we believe that the lack of SiC or SiO_2 NWs formation is simply due to the low degree of carbon and oxygen saturation in the formed silicide phases (Fe or Co silicides) which did not let a supersaturated Si-C-(O) liquid droplet for precipitation. It should be noted that when a PMPS was used as a precursor, SiC NWs formed under the same experimental conditions (see later).

Under N_2 atmosphere, similarly, the released SiO gas from PMS precursor reacted with the atmosphere (N_2 which may also include also ~100ppm O_2) and yielded Si_2N_2O NWs with metallic tips upon heating when the samples made from Co catalyst source, instead for the samples made by using Fe catalyst source, Si_2N_2O NWs were obtained with no SEM detectable metallic tips. For both types of catalyst particles the explanation for the absence of SiO_2 1D nanostructures is the higher demand of oxygen saturation compared to that of silicon oxynitride and also occurrence of adequate enough amount of active oxide and nitride species as explained previously for a-SixONy NWs.[72] A metal-containing cap in the tip of the Si_2N_2O NWs implies that the NWs formed by the well-established vapor–liquid–solid (VLS) mechanism when Co was used. It was demonstrated that the amorphous Si_2N_2O residue (produced by the pyrolysis of copolymer precursor at 1000°C in N_2) can be crystallized at different temperatures to produce Si_2N_2O or α-Si_3N_4-Si_2N_2O mixtures.[93] A high C:O ratio in the residue resulted in the consumption of the oxygen during crystallization, and Si_3N_4 was produced. A low C:O ratio (as in the case of the present study) led to the formation of Si_2N_2O. Indeed, similar experiments, performed using a polysiloxane with higher C:O, yielded Si_3N_4 without any silicon oxynitride (see later) phase (for pyrolysis at 1400°C in N_2, see later). We previously documented on the cluster assisted VLS formation of amorphous-SixONy NWs formed when polysiloxane blends (PDMS-PMPS) have been treated at 1200°C in N_2 atmosphere. Although this experimental finding suggests that there is a crystallization possibility of already formed (via VLS) a-Si_2N_2O NWs with the increase in temperature (1250-1400°C in the present part of the study), observations by SEM conducted on samples treated at different temperatures, partially rules out

this possibility since at low temperatures we only observed limited amount of NWs (see **Figure 4.2-10** (c) and **Figure 4.2-11** (c)), while with the increase in pyrolysis temperature large amount of NHs have been formed (**Figure 4.2-10**(d) and **Figure 4.2-11** (d)). Therefore we believe that the crystalline Si_2N_2O NWs are mostly formed via conventional VLS mechanism when Co is incorporated into the system which forms silicon rich silicide phase. The growth mechanism of Fe including samples seems to be governed by a different procedure. Although in order to postulate a defined growth mechanism, a high magnification electron microscopy investigations done on the tips/roots of the NWs together with nanochemical analyses are highly demanded, it seems that vapor-solid then solid-gas (VS-SG) mechanism can be active in this system, see later for the details of VS-SG mechanism.

As a last worth to note that crystalline silicon oxynitride has been shown to exhibit enhanced excellent refractory properties, compared to silicon nitride.[94] Moreover, it possesses high strength, low thermal expansion, high thermal shock and abrasion resistance, and excellent chemical stability in acid, molten non-ferrous metals and air at high temperature.[95, 96] Therefore a synergic effect is expected from the samples produced in this part of the study with N_2 pyrolysis since they are indeed amorphous SiOC ceramics including a large amount of Si_2N_2O NWs. The monoliths pyrolyzed at 1400°C under N_2 had a total porosity of 59.4 vol% (34.0 vol% open porosity). Clearly; while the system investigated has given us many clues about the catalyst assisted pyrolysis, the aim of controlling the pore characteristics again failed. Therefore we prepared the last samples investigated in this part of the study by using PMPS precursor, instead of PMS and treated the samples in an exactly the same way in order to be comparative, i.e. although PMPS has self blowing property we did not exclude ADA from the blends.

4.2.3.3.2. PMPS based samples

a) Foaming, Crosslinking and Thermal Analysis

TGA analysis measurements (see **Figure 4.2-14** (a, left) and (b, left)) were in good agreement with literature data, confirming that the ceramization of cured bodies occurred between 400-

600°C,[80] with a ceramic yield ~70% at 1200°C. We observed that the incorporation of both metallic (Fe and Co) ions affected the stability of the resulting ceramics at high temperatures (T >1000°C), in particular leading to a decrease in ceramic yield at high temperatures. This enhanced decomposition (decrease in thermal stability) occurs with release of gas (SiO and CO) and crystallization, similarly to what reported for a Ni-containing polysiloxane.[48] In particular, while pure PMPS heated in N_2 did not show any significant weight loss above 1000°C, and no peaks were evident in the DTA curve up to 1500°C (**Figure 4.2-14** (a, right)), the data for the sample containing $FeCl_2$ and $CoCl_2$ showed the presence of an endothermic peak around 1450°C, associated with a large weight loss. This was attributed to the occurrence of a carbothermal reduction reaction between Si_3N_4 and C, to form SiC (see later).[16, 97, 98] Data shows that samples containing Co ions had a higher weight loss than those with Fe ions (e.g. ~30 wt% and ~22 wt%, respectively, at 1200°C in N_2), and that the weight loss depended on the heating atmosphere (was higher when heating in Ar). A more detailed investigation of the effect of different metal ions on the weight loss of the polysiloxane precursor was however outside the scope of the present study.[55]

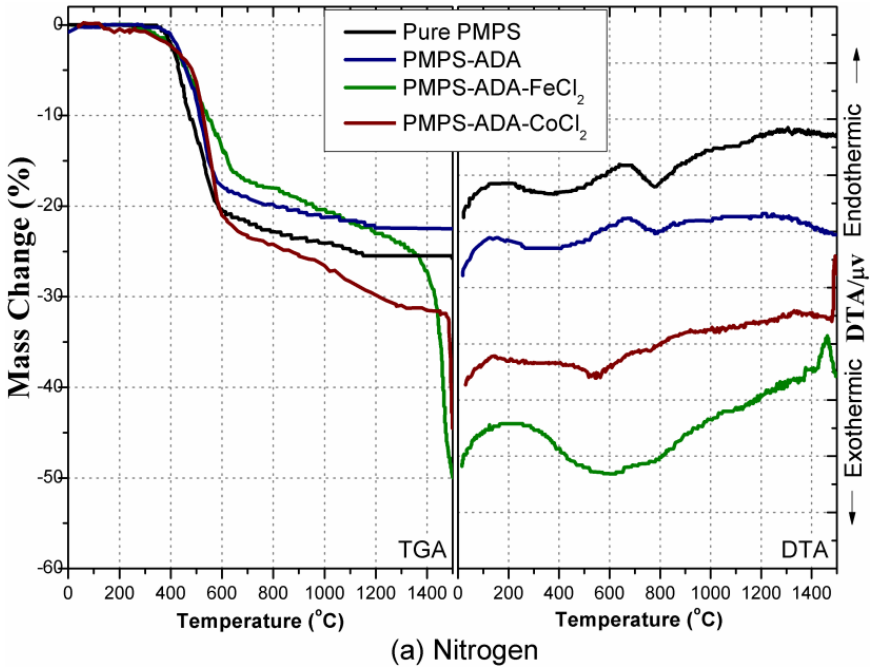

(a) Nitrogen

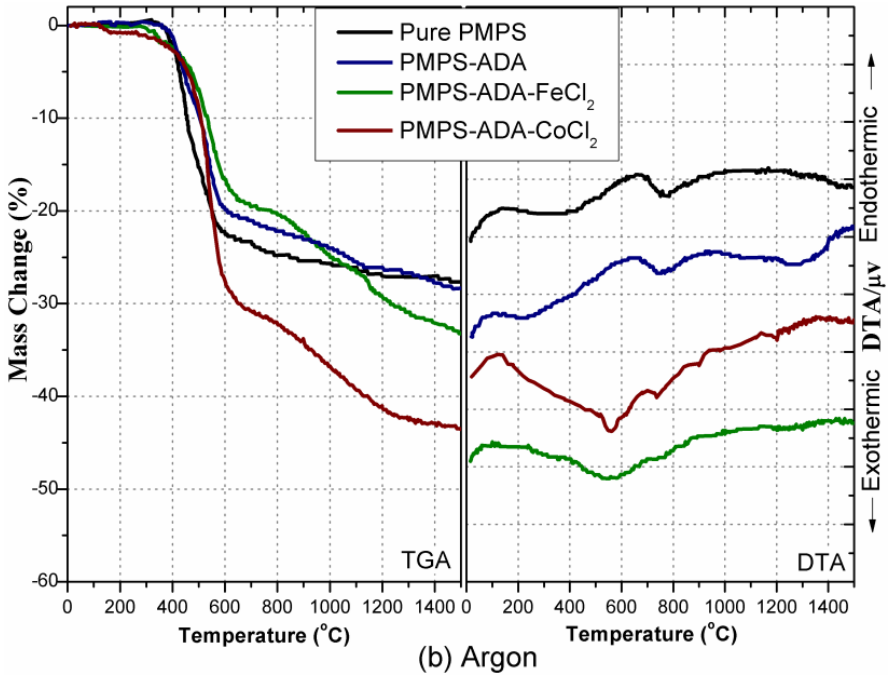

Figure 4.2-14. TG/DTA results for PMPS samples including pure PMS, PMS-ADA, PMS-ADA-$FeCl_2$ and PMS-ADA-$CoCl_2$ pyrolyzed under a) N_2, and b) Ar atmosphere.

After heating at 250°C, cellular thermosets with a high amount of porosity were obtained different than what was observed in PMS system. The presence of higher amount of open porosity (some having thin semi transparent membrane windows which seem highly probable to diminish during pyrolysis, see **Figure 4.2-15** (a, inset)) is attributed both to the continued release of volatiles/oligomers during the PMPS curing[80] and to the good match between the decomposition temperature of the blowing agent and the polymer viscosity at this temperature.[78, 79] **Figure 4.2-15** (b) shows a cell wall detail including white colored particles, inset given therein confirms the incorporation of halide into polysiloxane mixture, similar to the previous observations done for PMS precursor. All the foams retained their morphology during pyrolysis (see later), with no evident signs of melting or formation of cracks, indicating that the amount of cross-linking achieved during foaming was sufficient to prevent thermoplastic flow of the polysiloxane, and that the open-pore structure of the material allowed the release of the decomposition gases.

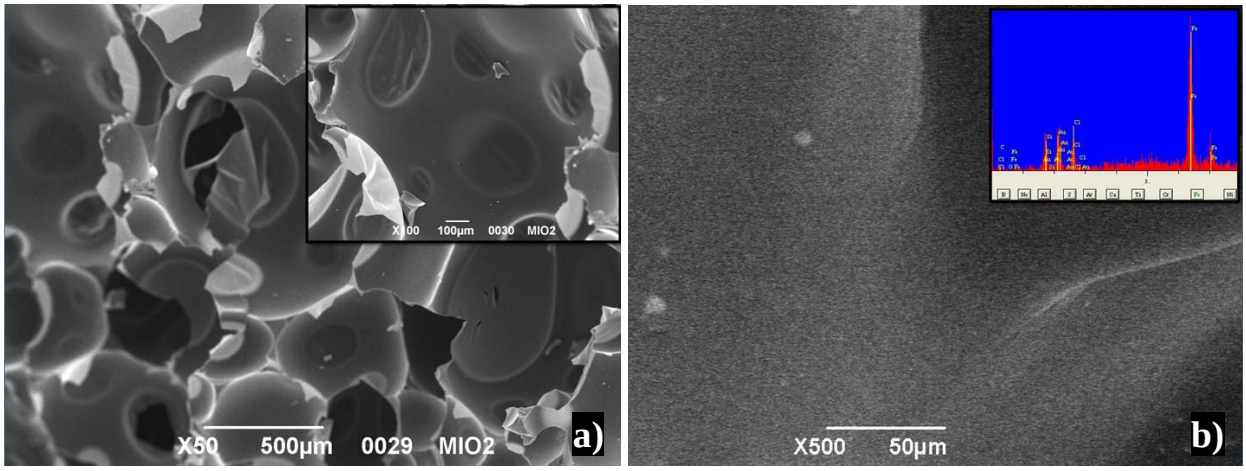

Figure 4.2-15. SEM image taken from the fracture surface of cured PMPS-ADA-$FeCl_2$ mixture, inset shows high magnification image taken from the cell indicating membranes on the cell windows; and b) Higher magnification SEM image showing the detail of cell wall, inset demonstrates EDS analysis taken over the white (or light) colored particle showing Fe and Cl elements (Au peaks were due to gold sputtering over the sample surface).

b) Structural and Nanochemical Characterization

Sample PHA-Fe (PMPS-ADA-$FeCl_2$) under N_2 pyrolysis

The pyrolysis of the PMPS-$FeCl_2$-ADA sample under N_2 atmosphere at 1250°C yielded a macrocellular ceramic decorated with bundles of NWs of different length (see **Figure 4.2-16**(a) and (b) for the general and for the detailed view, respectively). No significant change was observed in the general morphology of the samples heated in the 1250 to 1400°C temperature range (**Figure 4.2-16**(a)-(f)), and the foams had spherical cells (~ 300 ± 150 µm in diameter) with connecting cell windows (135 ± 87 µm in diameter). At all pyrolysis temperatures, a large amount of NWs were homogeneously distributed on the surface of the macro-porous components. No tips (or particles) were observed to be present at the end of the NWs (see

embedded high magnification images in **Figure 4.2-16**(b), (d) and (f)), and the length of the NWs was as high as 500 µm.

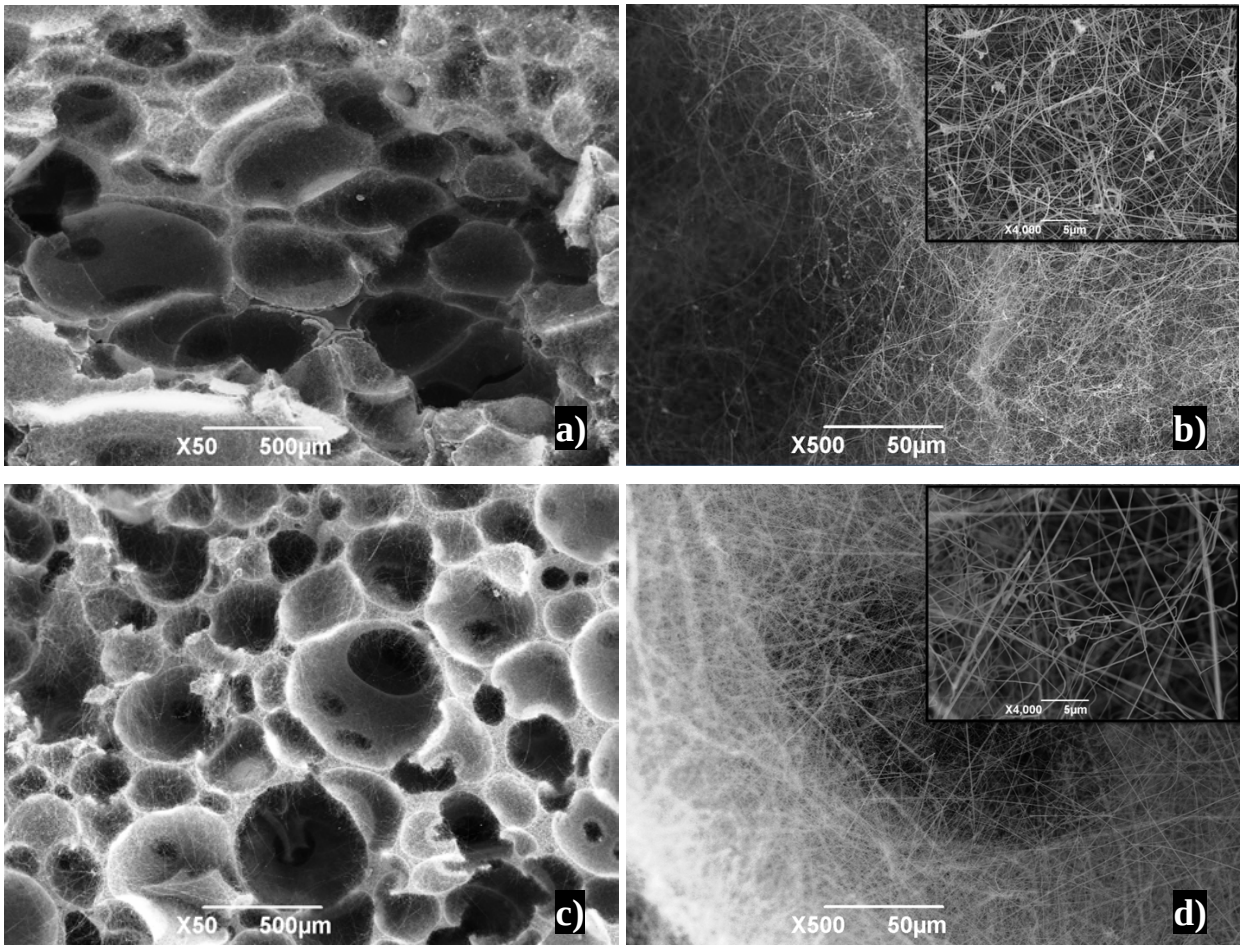

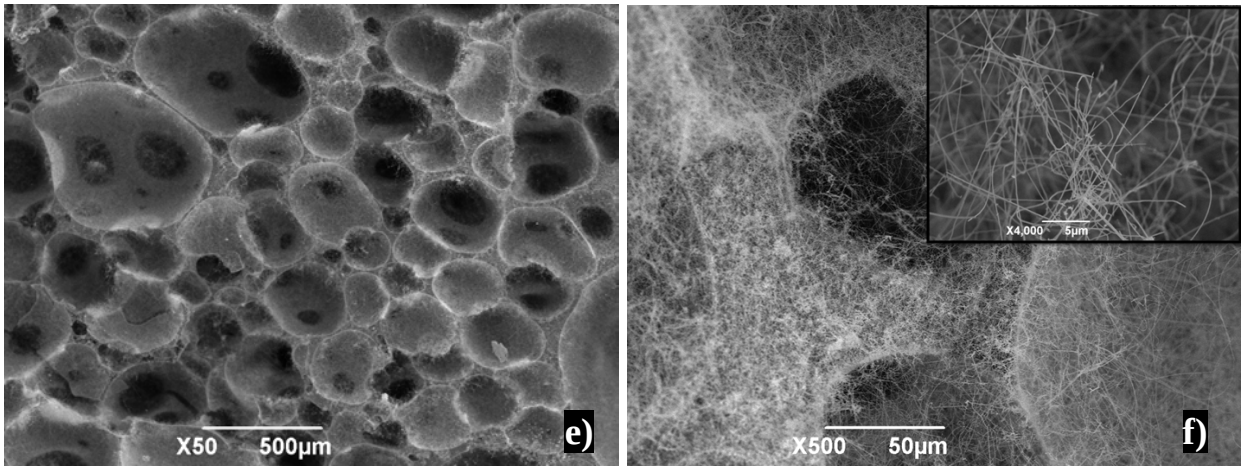

Figure 4.2-16. SEM micrographs taken from the fracture surfaces of sample PMPS–$FeCl_2$–ADA pyrolyzed under N_2; a) at 1250°C, b) cell wall detail; c) at 1350°C, d) cell wall detail; and e) at 1400°C, f) cell wall detail. Insets show high-magnification images of the NWs.

XRD and Raman spectroscopy were performed to understand the phase evolution in dependence on the pyrolysis temperature. **Figure 4.2-17** shows XRD patterns for PMPS-$FeCl_2$-ADA samples pyrolyzed at different temperatures under N_2 atmosphere. Although the sample obtained at 1250°C displayed a typical diffraction pattern of amorphous SiC*x*O*y*, with a broad hump in the 20-30 degrees range (2θ),[87] it also contained well defined crystalline features, attributable to β-SiC (JCPDS #29-1129), α-Si_3N_4 (JCPDS #41-0360) and Fe_3Si (JCPDS #45-1207), together with a small amount of Si_2N_2O (JCPDS #47-1627) phase. The formation of Si_2N_2O (sinoite: silicon oxynitride) phase has been shown to occur after the pyrolysis of polysiloxane precursors in N_2/NH_3 atmosphere at low processing temperatures (<1400°C).[10, 93, 99, 100] A small peak at 33.7° (2θ) (marked with * in **Figure 4.2-17**(a)) is usually attributed to planar defects (stacking faults and rotational twins) in the β-SiC crystalline structure.[101] With an increase in the pyrolysis temperature, the crystalline peaks of β-SiC and α-Si_3N_4 became more intense. At 1350°C, the broad hump completely disappeared, the peaks relative to Si_2N_2O decreased in intensity, while the ones for β-Si_3N_4 became noticeable (2θ = 27.1° and 33.7°). Previous studies revealed that the thermolysis of a polysiloxane and silicon (Si) mixture under N_2 yielded Si_2N_2O, due to the

reaction of released SiO gas from the precursor with the pyrolysis atmosphere (N_2), and a further increase of the temperature resulted in a continuous increase in the absorption of nitrogen up to the melting point of Si ($Tm_{(Si)}$~ 1414°C).[10, 102] Siddiqi et al.[98] showed that the equilibrium stable phases formed on nitriding SiO_2:C mixtures in the temperature range between 1300 and 1500°C are either β-Si_3N_4 + C or Si_2N_2O + C, depending on the oxygen partial pressure. Though the stability of phases depends strongly on impurities such as iron, increase in O_2 partial pressure clearly promotes the Si_2N_2O formation, and with the decrease in O_2 partial pressure Si_3N_4 is stabilized over Si_2N_2O.[98, 103] α-Si_3N_4 is known to be the low temperature polymorph of Si_3N_4, yet if the SiO partial pressure in the reaction bed is high, it remains stable up to the temperature where carbothermal reduction of Si_3N_4 with C occurs, giving SiC.[98] In this study, as deduced from DTA (see DTA in **Figure 4.2-14**(a)), the reaction of Si_3N_4 NWs with carbon occurred only at around 1450°C under N_2; therefore SiC did not form due to the carbothermal reduction of Si_3N_4 but through a different mechanism (see later), and the Si_2N_2O phase transformed to Si_3N_4 when the pyrolysis temperature increased. Indeed, the phase transformation from Si_2N_2O to Si_3N_4 has been shown to be facilitated with increased annealing temperature, especially above 1300°C [104] or with the extension of the heat treatment time in N_2 atmosphere.[77, 102] This is in good agreement with the XRD results of the present study. For the sample pyrolyzed at 1400°C, a composite ceramic containing β-SiC, a mixture of iron silicide phases (predominantly Fe_3Si) and Si_3N_4 (both α (JCPDS #41-0360) and β (JCPDS #33-1160) polymorphs), without any Si_2N_2O, were obtained.

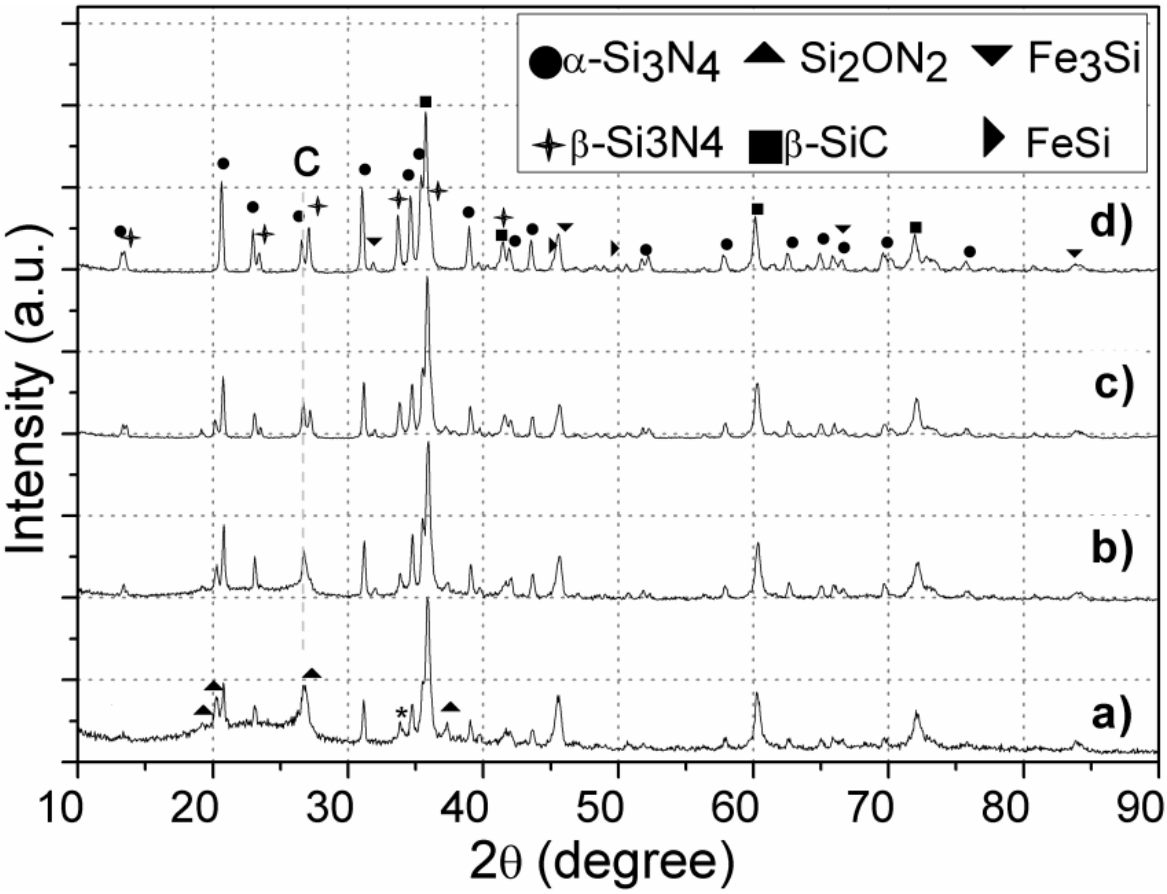

Figure 4.2-17. XRD patterns of the samples pyrolyzed in N_2, a) 1250°C, b) 1300°C, c) 1350°C and d) 1400°C treatment.

XRD analysis performed on samples prepared at lower temperatures (900-1100°C in 100°C steps, **Figure 4.2-18** (a-c)) demonstrate that under N_2 atmosphere at temperatures around 900°C Fe is in metallic form, while strangely no peaks are observed at 1000°C (might be due to experimental errors), starting from 1100°C iron silicide (Fe-Si) phase mixtures (the observed peaks can be resolved for some iron silicide phases, dominantly Fe_2Si (JCPDS #83-1259)) can be found. Most probably metallic iron gives a reaction with the released gases or directly with the matrix and yields with Fe-Si. The reaction giving iron silicide from metallic iron seems to occur

just above 1000°C (see also same data for Ar treatment). This data together with XRD data obtained from the high temperature pyrolyzed samples show that transformation of iron occurs to form iron silicide yet silicidation never reaches to sufficient level (due to depletion of Si) to form silicon rich silicide and even upon pyrolysis at the highest temperature (1400°C) iron silicide phase mixtures are obtained under N_2 atmosphere.

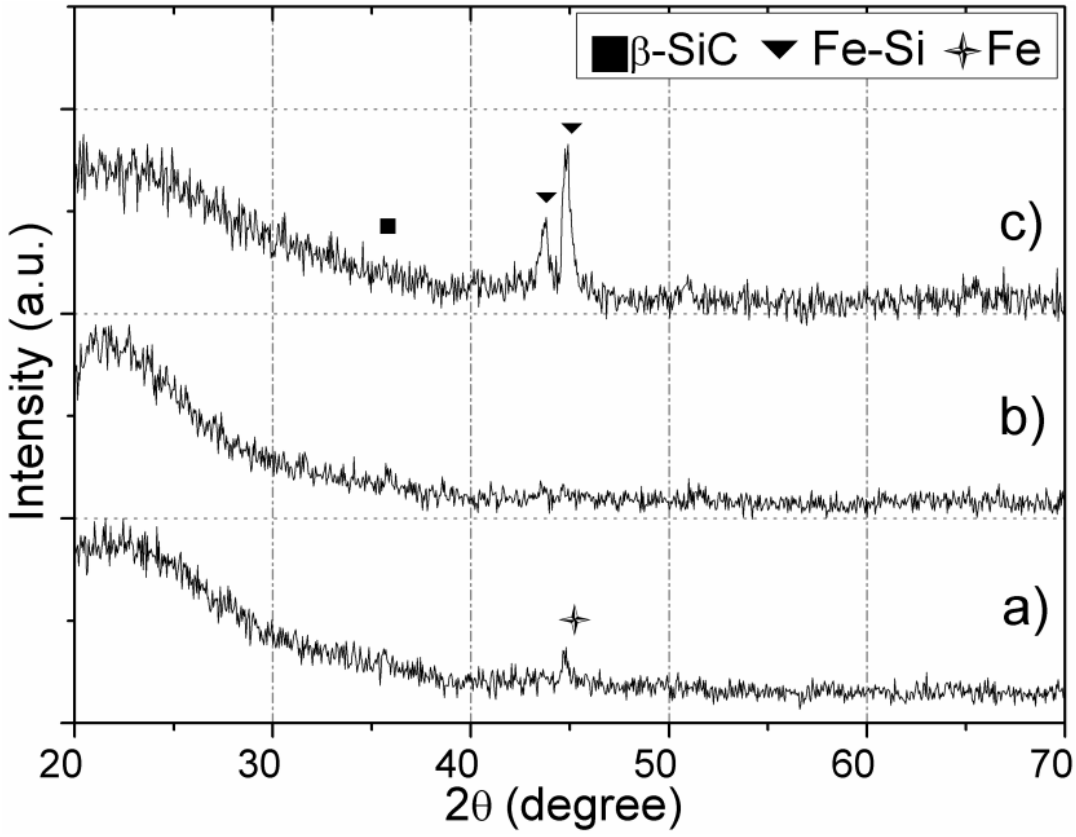

Figure 4.2-18. XRD patterns of the samples pyrolyzed in N_2, a) 900°C, b) 1000°C, and c) 1100°C treatment.

Raman spectroscopy (**Figure 4.2-19**(a-d)) was used to acquire information about the structural evolution, in particular, of the free carbon phase dispersed in the resulted matrix obtained at different pyrolysis temperatures. The ceramic foam obtained at 1250°C pyrolysis under N_2

atmosphere exhibited features typical of amorphous carbon, with a broad D band (~1330 cm^{-1}), more intense than the G band (~1580 cm^{-1}), and a small 2D band centered around 2660 cm^{-1}, see **Figure 4.2-19**(a). As the pyrolysis temperature increased, besides a separation of the G-peak into two separate maxima at 1580 cm^{-1} (actual G-band) and 1620 cm^{-1} (D'-band), all the peaks narrowed. While the intensity of G band increased continuously, the intensity of D band decreased. This indicates an enhancement in the ordering of carbon towards graphite, with increasing pyrolysis temperature.[105, 106] Raman data demonstrate the permanence of carbon in the structure at high pyrolysis temperature, in accordance with EELS. Furthermore, in addition to the bands related to carbon, some other bands located at between 700 and 1000 cm^{-1} became visible above 1300°C pyrolysis. According to the reported SiC Raman data,[107] the bands arising from transverse optical (TO) modes are recorded in the region from 750 to 810 cm^{-1} (~795 cm^{-1} for β-SiC)[108], while bands originating from longitudinal optical (LO) modes are observed in the region from 900 to 1000 cm^{-1} (~970 cm^{-1}1 for β-SiC). In a similar way peaks around 920-950cm^{-1} are generally attributed to Si-N vibration.[109] Therefore without going into details these bands observed in the study are attributed to both to the Si-C and Si-N vibrations for which their crystalline phases are already characterized by XRD and TEM. This observation supports that above 1300°C, high amount of crystallization is obtained in the system meaning that higher long range ordered phases are formed for which Raman is effective to define band vibrations (i.e. in contrast to IR spectra).[109]

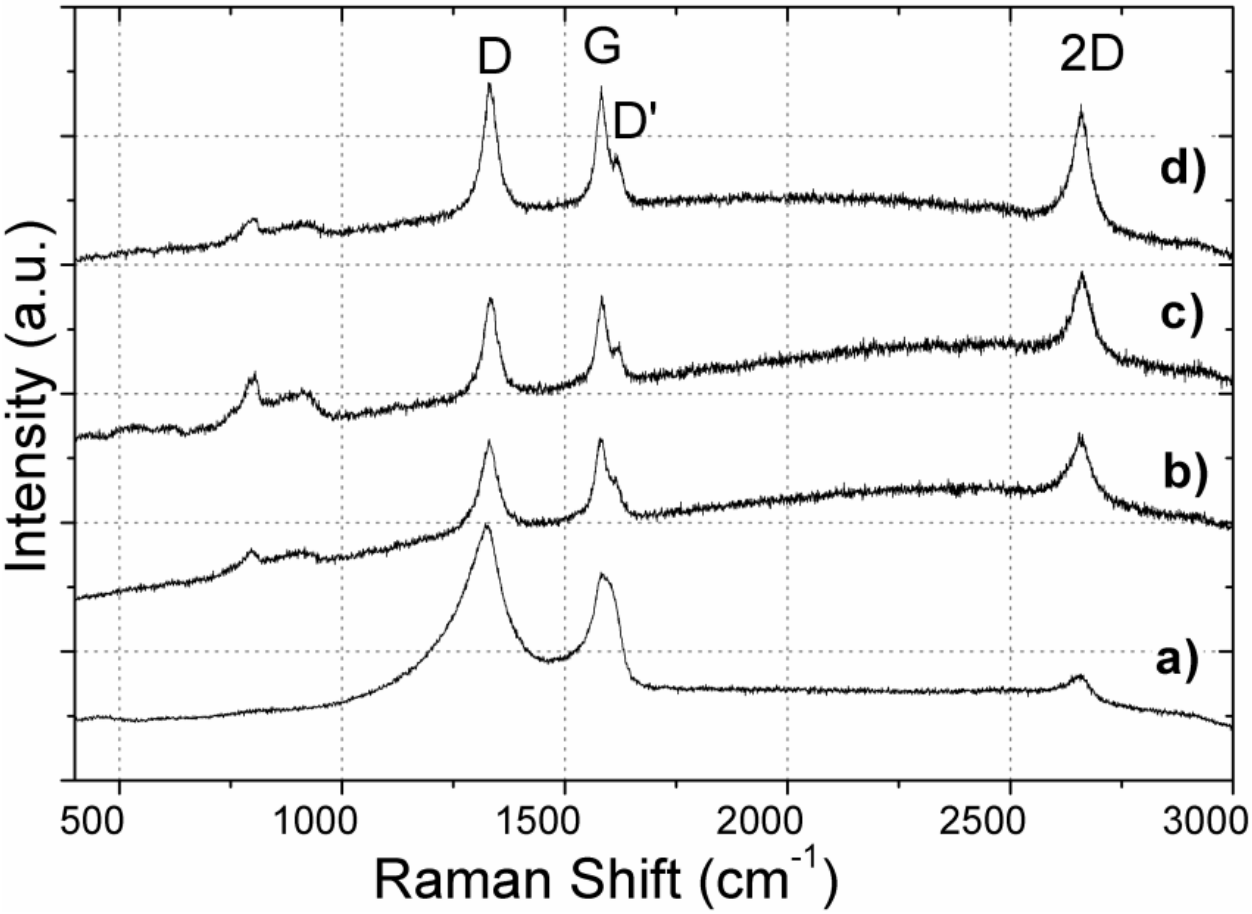

Figure 4.2-19. Raman spectroscopy of the samples pyrolyzed in N_2, a) 1250°C, b) 1300°C, c) 1350°C and d) 1400°C treatment.

In **Figure 4.2-20**, the results of the HRTEM, EDXS, and EELS analyses are reported. Figure **4.2-20**(a) shows a TEM overview of the sample pyrolyzed at 1400°C in N_2. The EELS (top right) reveals that the matrix phase surrounding the NWs consisted of silicon carbide, containing some percent oxygen, and of graphitic carbon (hence, it was a not completely crystallized SiOC material). The EELS (middle right) and the EDX profile (bottom right) were taken from the NWs, both indicating that the NWs contained only silicon and nitrogen. The quantification of the spectra evidenced that the NWs consisted of pure Si_3N_4. Obviously, the nitrogen originated from the flowing N_2 gas present in the pyrolysis tube, as confirmed by the fact that no Si_3N_4 phase was observed when Ar was used as pyrolysis atmosphere (see later). Similar investigations on samples heat treated at lower temperature indicated that nitrogen was always present only in the

NWs. The HRTEM image of the silicon nitride NWs, shown in **Figure 4.2-20**(b), reveals that they had a perfect single crystalline silicon nitride structure, without defects (as confirmed also by the selected area electron diffraction pattern – see insert), which was identical over the entire nanowire. Both the HRTEM image and the SAED pattern suggest that the NWs grew along the [$\underline{1}$11] direction. **Figure 4.2-20**(c) shows a lattice plane imaging of an agglomeration of nanoparticles in the vicinity of NWs, revealing that these particles contain graphitic regions (together with amorphous carbon distributed in the sample, as supported by Raman investigations) and silicon carbide, in accordance with EELS data.

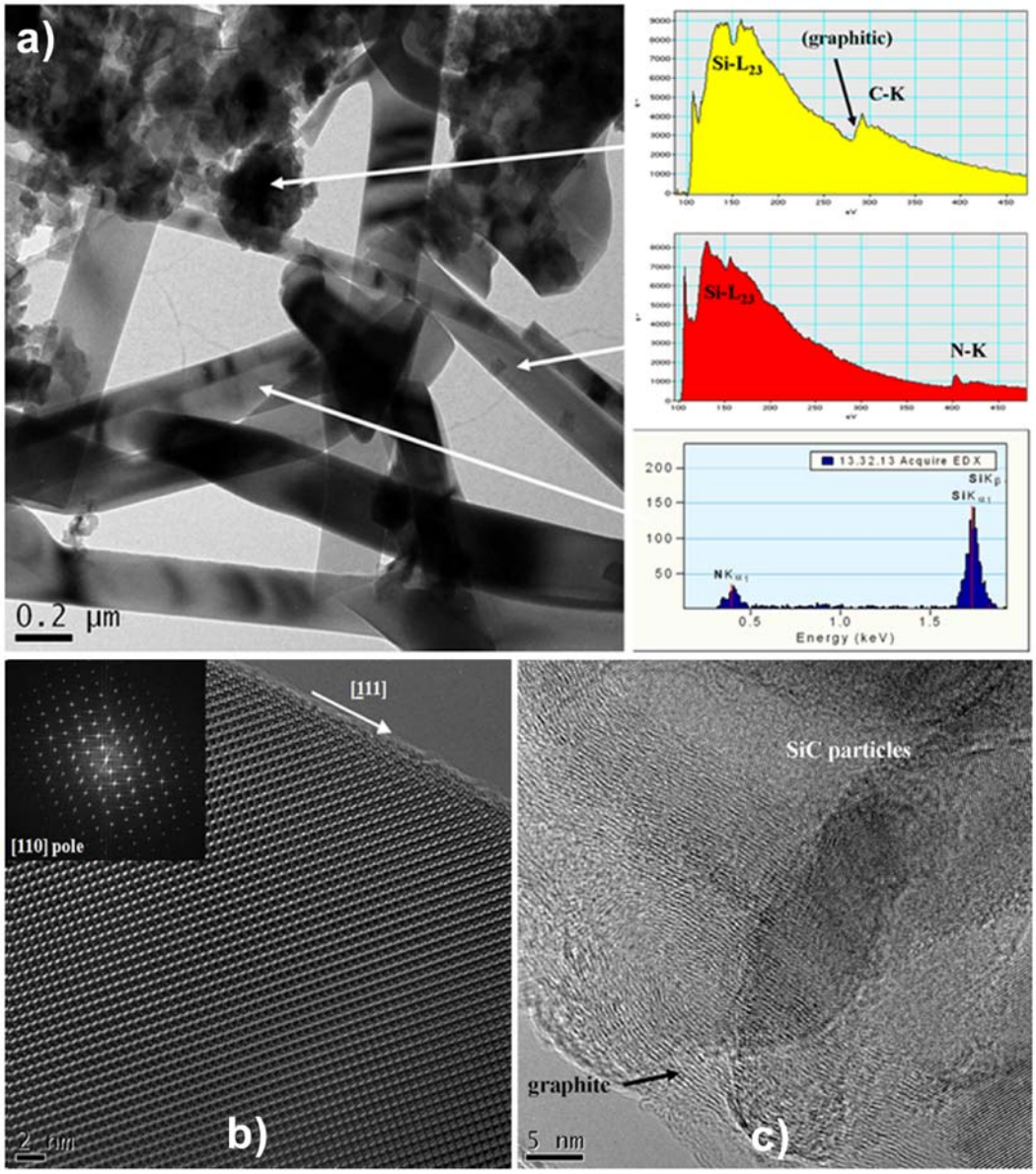

Figure 4.2-20. HRTEM/EELS/EDXS analyses of sample PMPS-$FeCl_2$-ADA pyrolyzed at 1400°C under N_2 atmosphere; a) TEM-overview with corresponding nanochemical measurements: EELS of matrix phase (top), EELS of NWs (middle), and EDX of NWs (bottom), b) HRTEM image of the atomic regularity of NWs, with diffraction pattern, c) HRTEM image of matrix phase directly surrounding the Si_3N_4 NWs, showing SiC with graphitic regions.

As mentioned before, XRD results indicated that the β-Si_3N_4 phase became more visible with increasing pyrolysis temperature, while the Si_2N_2O phase gradually disappeared. This result, in combination with TEM data, implies that β-Si_3N_4 formed via a phase transformation of the oxynitride phase. Weimer et al.[110] have in fact shown that the control of the intermediate phase, being either carbon-rich (Si-O-C) or nitrogen-rich (Si-O-N), dictates the formation of α-Si_3N_4 or β-Si_3N_4 phase, respectively, although the factors controlling the β-Si_3N_4 formation are very complex.[111] In order to understand the growth mechanism of the NWs, microstructural investigations were carried out both by SEM and HRTEM, but attempts to identify transition metal-containing compounds on the tips and roots of the NWs were not successful. Consequently, the iron silicide phase, whose presence is evident from XRD data, is believed to be randomly distributed within the matrix phase. It was shown that SiO and CO are the main gaseous species that form during the pyrolysis of a similar polysiloxane precursor at temperatures higher than 1000°C, and that the partial pressure of both of the gases increases with increasing pyrolysis temperature up to 1400°C.[91] Therefore, it can be assumed, that SiO gas reacted with N_2, together with the free carbon, to nucleate Si_3N_4 crystallites according to the proposed reaction (4.2-2):[110]

$$3SiO(g) + 3C(s) + 2N_2(g) \rightarrow Si_3N_4(s) + 3CO(g) \qquad \textit{4.2-2}$$

The nucleation thus occurred via a Vapor-Solid (VS) mechanism, following reaction (4.2-2), when the concentration of SiO and N_2 near the carbon clusters was high.[110] However, this reaction by itself is not sufficient to explain the growth mechanism of the NWs, due to increased CO partial pressure, resulting from the precursor decomposition and from the byproduct of the reactions, which would make reaction (4.2-2) difficult to proceed.[110] Accordingly, the growth of the formed Si_3N_4 nuclei should rather progress via a gas-phase process following reaction (4.2-3), as observed in other studies.[77, 103, 110, 112, 113]

$$3SiO(g) + 3CO(g) + 2N_2(g) \rightarrow Si_3N_4(s) + 3CO_2(g) \qquad \textit{4.2-3}$$

The SiO and CO gases could also react with each other to form SiC via gas-gas reaction, as shown below in equation (4.2-4*)*. However, previous investigations showed that this reaction is not thermodynamically favored over the entire pyrolysis temperature range of the present study (1250-1400°C).[114] Therefore, formation of SiC proceeds rather via a solid–gas process, according to reaction (4.2-5).[2, 112, 114] Further evidences for reaction (4.2-5) being active in the system are provided by (i) the fact that SiC was almost always found in close proximity to the graphitic regions (see **Figure 4.2-20**(c)), and (ii) the existence of stacking faults, implying that SiC was formed through a solid-gas reaction with carbon.[115]

$$SiO(g) + 3CO(g) \rightarrow SiC(s) + 2CO_2(g) \qquad 4.2\text{-}4$$

$$SiO(g) + 2C(s) \rightarrow SiC(s) + CO(g) \qquad 4.2\text{-}5$$

The effect of the metal catalyst on the phase evolution can be described as follows. In the reaction zone, firstly $FeCl_2$ was reduced to metallic Fe nanoparticles, subsequently the reaction between the silicon-containing matrix and Fe particles yielded iron silicide[116, 117] without any other forms of iron (such as Fe_3C, Fe_4N, etc.), the driving force being primarily the negative enthalpy of the metal silicides formation.[118] Concerning the catalytic activity of Fe in silicon-containing systems, when iron silicide phase is found on the tips or roots of 1D nanostructures, the VLS or SLS growth mechanism is proposed, respectively.[119-121] Nevertheless, for the samples heated under N_2 in this study, as mentioned before, it was not possible to identify by HRTEM any iron-containing areas either on the tips or in the roots of the NWs. XRD data suggested the presence of only a limited amount of FeSi (JCPDS #38-1397) phase, at 1400°C, and Fe_3Si was the predominant silicide phase. It may be assumed that the depletion of Si (due to its requirement to form Si based compounds such as SiC, Si_2N_2O, α and β-Si_3N_4) caused the formation of an iron-rich silicide phase mixture rather than pure FeSi. It was shown that the solubility of carbon is the critical parameter for the precipitation of crystals in iron silicide fluxes, in dependence also on the Fe/Si ratio.[92, 121, 122] While saturated carbon dissolution in iron rich silicide melts (such as Fe_3Si) leads to a precipitation of carbon, silicides with Fe to Si ratio around 1:1 produce SiC precipitation, exactly as we observed for Ar treated samples (see next section). When carbon

rather than SiC precipitates from Fe_3Si, a phase change causing Fe-Si richer in silicon should be observed, while precipitation of SiC from FeSi flux does not cause any phase transformation in the iron silicide phase.[122] This is indeed in agreement with our observation in this study (see later also). Additionally, it is known that iron particles might facilitate the dissociation of N_2 [77] and the removal of oxygen from silica.[108] The iron oxide formed in such a reaction would readily get reduced back to iron[108] and then forms iron silicide in a reducing atmosphere. We can therefore summarize in two main points the role played by iron in samples pyrolyzed under N_2: (i) it increases the carbon solubility in the molten droplets, which leads to a precipitation of graphitic carbon,[121] and (ii) it affects the stability of the resulting ceramics at high temperatures, leading to an increased crystallization of the corresponding ceramic, analogous to the role played by Ni in a hybrid polysiloxane precursor.[48]

Sample PHA-Fe (PMPS-ADA-$FeCl_2$) under Ar pyrolysis

Pyrolysis in Ar did not change the macroscopic morphology of the highly porous ceramics, as expected. The chemical composition and details of the microstructure, however, were rather different. SEM images of the fracture surface of samples heat treated at temperatures ranging from 1250 to 1400°C in Ar are shown in **Figure 4.2-21**. For the PMPS-$FeCl_2$-ADA sample pyrolyzed at 1250°C, the micrographs reveal the presence of some degree of porosity in the cell walls and struts, implying the evolution of gaseous products during pyrolysis (in agreement with TGA results), but no 1D nanostructures were observed. While the 1300°C pyrolyzed sample had features similar to the 1250°C treated one, the microstructures of the pyrolyzed monoliths treated at 1350°C and 1400°C were different from the previous ones, particularly at a nanoscale level. The samples pyrolyzed at the higher temperatures maintained the macrocellular structure (see **Figure 4.2-21**(c) and (e)), but showed the presence of NWs (see **Figure 4.2-21**(d) and (f)) having spherical tips (see embedded high magnification images in these figures) protruding from the cell walls. SEM investigations revealed that NWs started to form at temperatures≥1350°C, and that the nanowire length was affected by the pyrolysis temperature.

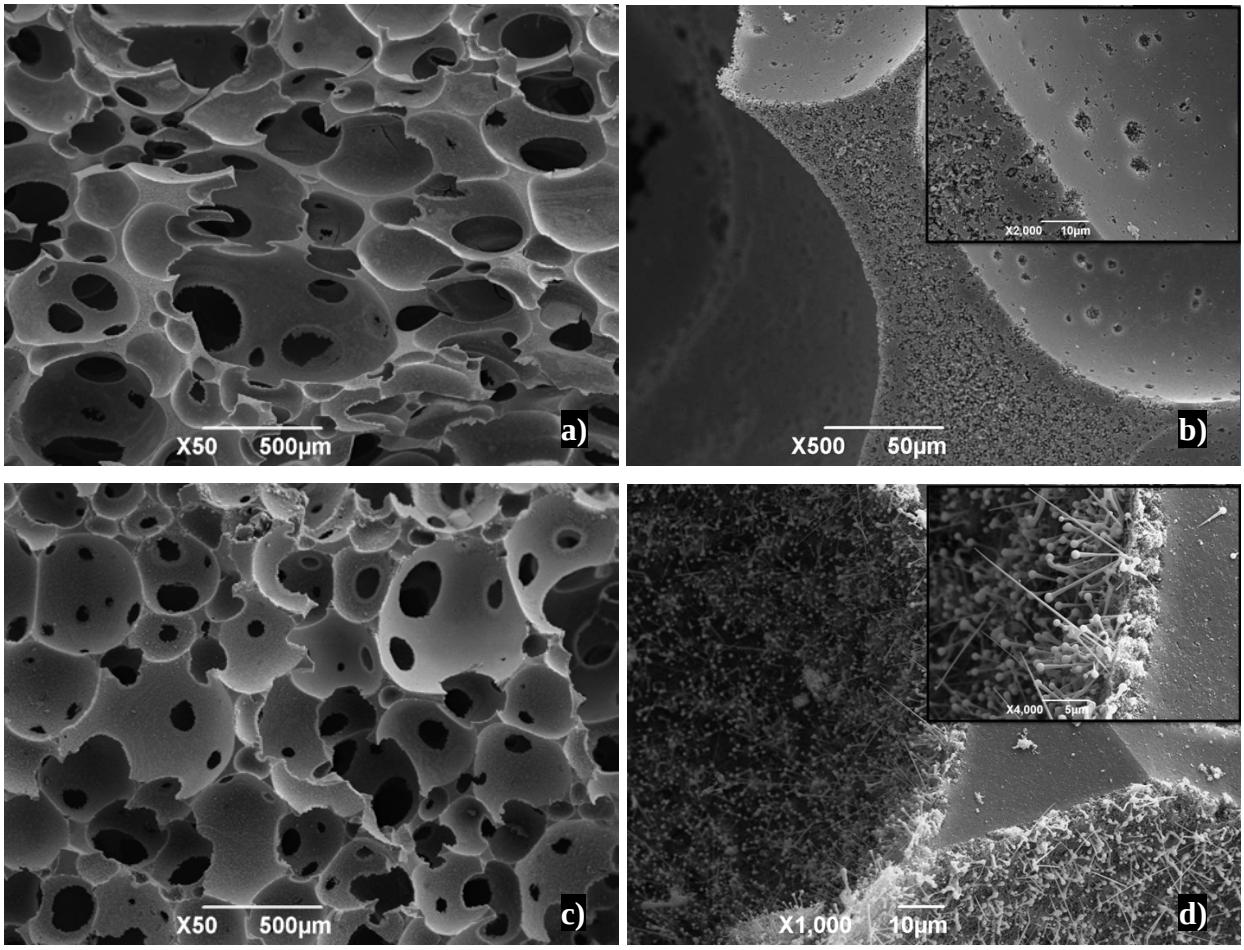
X50 500µm
a)
X500 50µm
X2,000 10µm
b)
X50 500µm
c)
X1,000 10µm
X4,000 5µm
d)

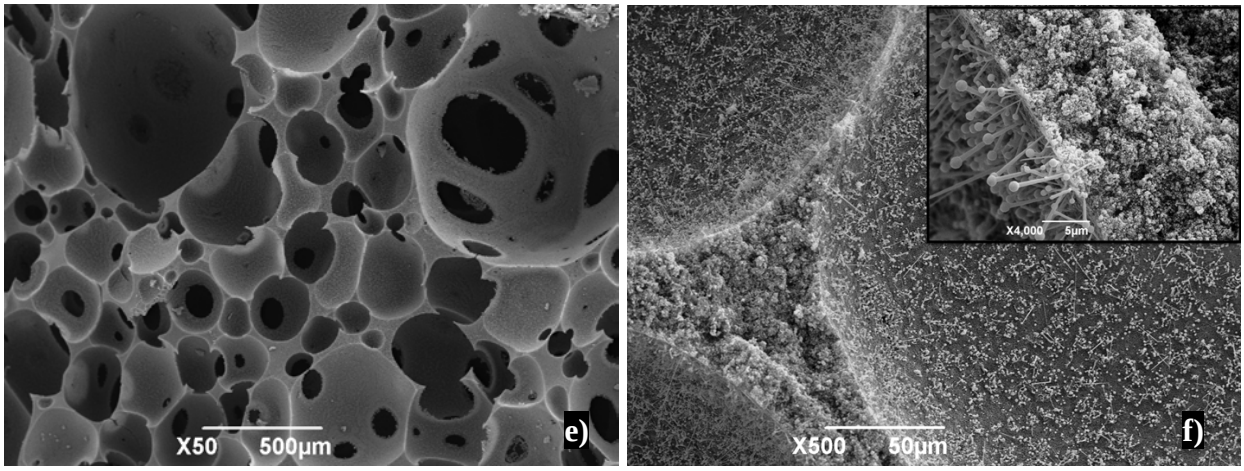

Figure 4.2-21. SEM micrographs taken from the fracture surfaces of sample PMPS-$FeCl_2$-ADA pyrolyzed under Argon: a) at 1250°C; b) strut detail; c) at 1350°C; d) strut detail; and e) at 1400°C; f) strut detail. Insets show high resolution images.

Figure 4.2-22 shows the XRD data for PMPS-$FeCl_2$-ADA samples pyrolyzed at different temperatures in Ar. The samples obtained at 1250°C and 1300°C displays similar diffraction patterns, namely an amorphous SiC_xO_y phase, with a broad hump centered 21° (2θ),[87] clearly defined crystalline peaks for β-SiC (JCPDS #29-1129) and iron silicide phases (Fe_5Si_3 (JCPDS #38-0438) and Fe_3Si (JCPDS #45-1207)) and a broad peak of amorphous carbon at ~26°. Increases in pyrolysis temperature promoted a depression of the amorphous halo, a better β-SiC crystallization and the transformation of the iron silicide phases to FeSi (JCPDS #38-1397), above 1300°C. NWs became visible by SEM, indicating the formation of SiC at the expense of the amorphous carbon and silica-rich phase (giving SiO gas).[112] Pyrolysis at 1400°C resulted in a ceramic including only β-SiC and minor amount of FeSi. The peak marked with * at 33.7° (2θ) was assigned to defects in the β-SiC crystalline structure, as explained previously.[101] XRD observations are further supported by elemental analysis results; while the sample treated at 1250°C had 28.0 ± 0.4 wt% of C, 26.0 ± 0.5 wt% of O, 0.5wt% Cl, and 1wt% of Fe, the one treated at 1400°C had 29.9 ± 0.3 wt% of C, 4.7 ± 0.4 wt% of O, and 1wt% of Fe. This together with XRD data implies that oxide based gases are released from the system while carbon and

silicon is kept in the SiC structure. Note that XRF in principle, is not a quantitative technique of analysis, but it can be used for semi-quantitative analysis with the typical range of error is at least ±5%. Concerning that it is possible to comment that Fe remains in the system with most probably less than 3wt%, and Cl leaves the system most probably in the form of HCl gas with the increase in pyrolysis temperature.

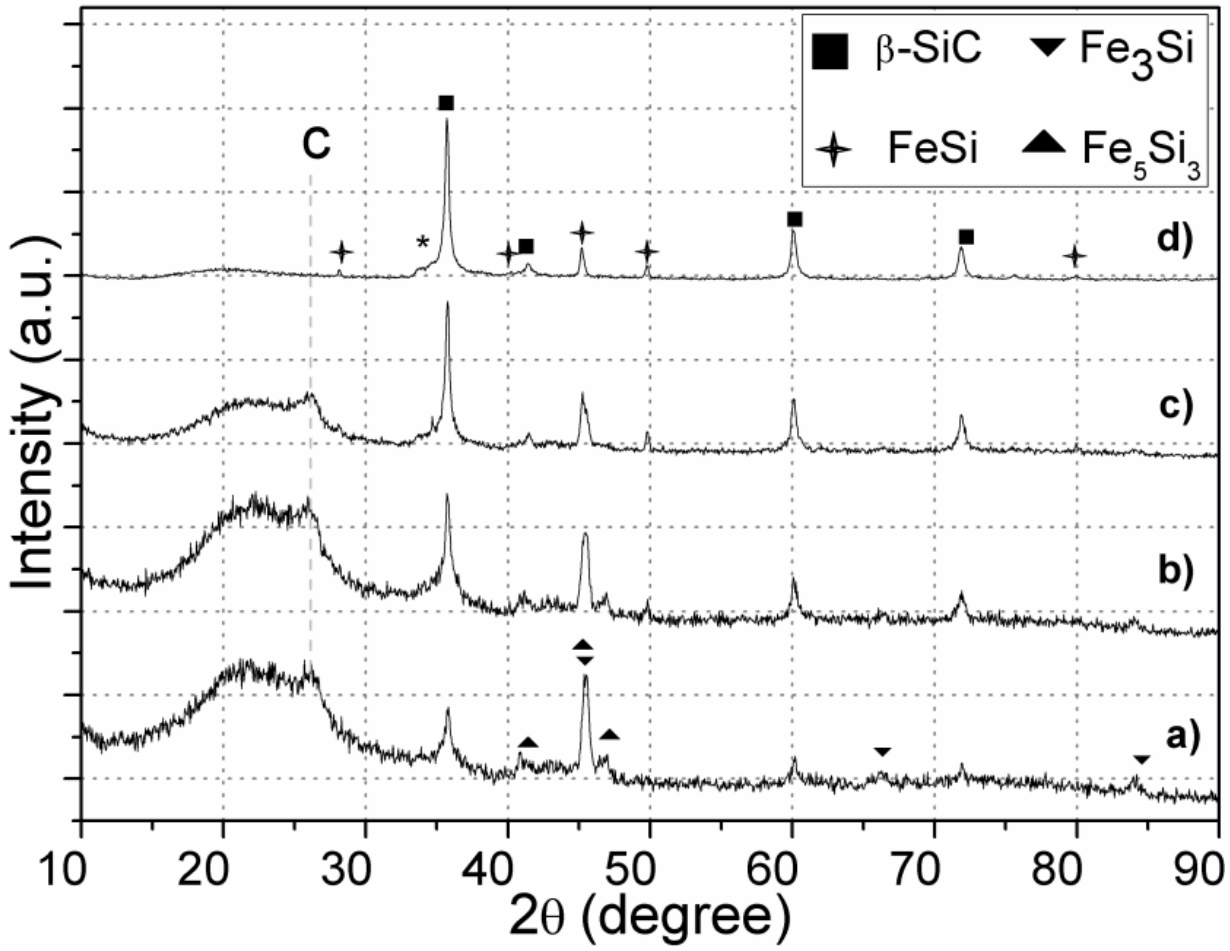

Figure 4.2-22. XRD patterns of the samples pyrolyzed in Ar at, a) 1250°C, b) 1300°C, c) 1350°C and d) 1400°C.

XRD analysis performed on samples prepared at lower temperatures (900-1200°C in 100°C steps, see **Figure 4.2-23**) demonstrated that under Ar atmosphere ~900°C the formation of

metallic iron is noticeable, and with the increases in pyrolysis temperature iron silicide (Fe_2Si) forms around 1100°C, as like in N_2 treatment. Comparing these results with the ones obtained from the samples similarly treated at low temperatures (900-1100°C) but under N_2, it can be inferred that pyrolysis atmosphere was not much effective on the phase transformation of Fe; meaning that the system undergoes similar changes in both pyrolysis atmospheres up to ~1100°C where after the effects of each thermolysis atmospheres differentiate. XRD data obtained previously on high temperatures (1250-1400°C) implies that Fe transforms from metallic state to iron silicide phase mixture (Fe_2Si, Fe_5Si_3, and FeSi) ~1250°C above which silicidation continues forming Fe-Si ~1:1 at temperatures higher than 1300°C under Ar atmosphere, differently from the N_2 treatment.

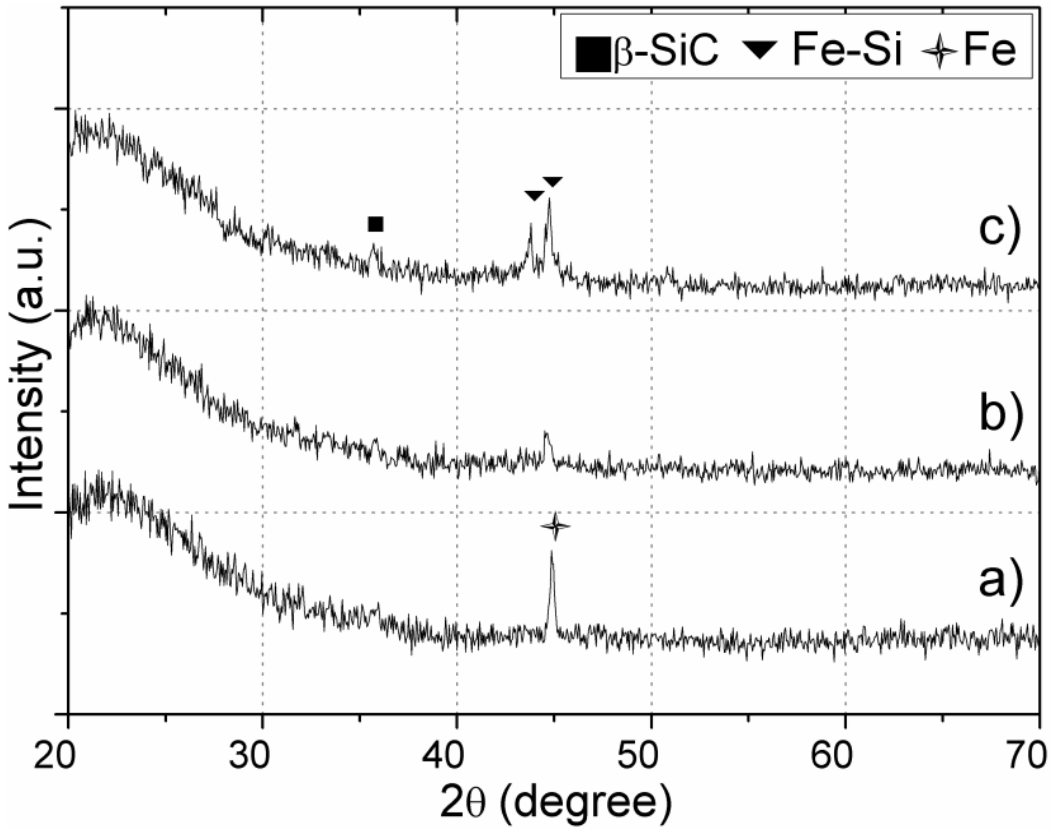

Figure 4.2-23. XRD patterns of the samples pyrolyzed in Ar at, a) 900°C, b) at 1000°C, and c) 1100°C.

Raman spectra of the samples treated at different temperatures are shown in **Figure 4.2-24**. Although peak narrowing and a small shift of G band towards lower frequencies was observed, implying the ordering of carbon with the increase in pyrolysis temperature, such an intense D band together with a broad and less intense G band indicates that highly disordered amorphous carbon nano-domains were present in all samples. The peaks which can be characterized for SiC ($780cm^{-1}$ (TO) and $970cm^{-1}$ (LO)) are not observed in Ar treated samples in spite of being clearly identified by XRD patterns. The absence of these bands in this part of the study is due to both relatively high Raman efficiency of C–C bonds, about ten times that of SiC,[107, 123] and to relatively small SiC grains.[48, 107, 124] These results are similar to the recent observations of Segatelli et al.[48] where the authors showed Raman data for Ni containing polysiloxane pyrolyzed

up to 1500°C and showed only D and G bands related with carbon while with XRD clear SiC was observed.

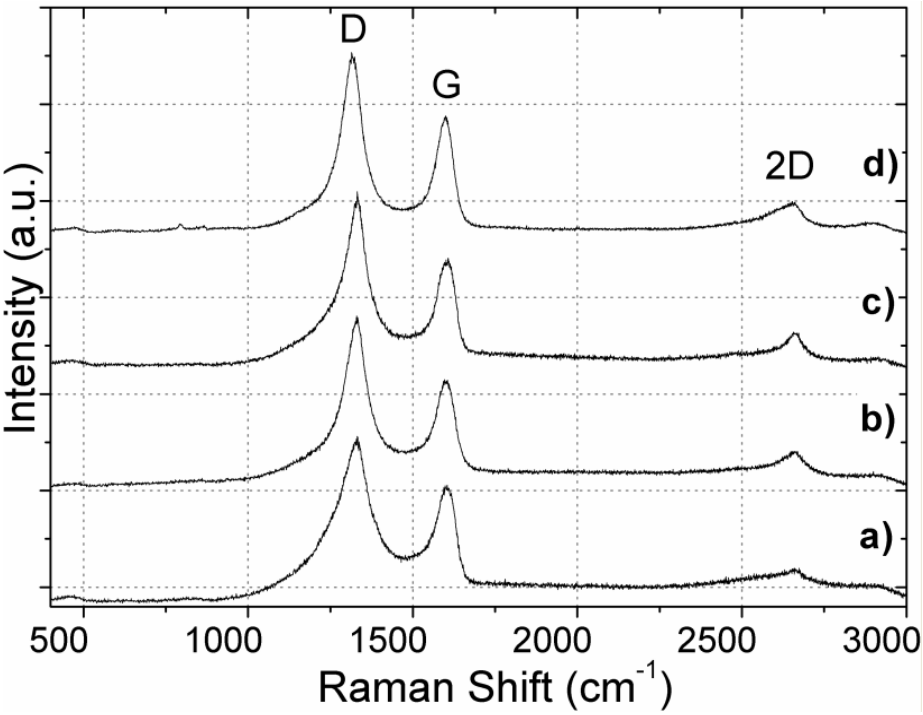

Figure 4.2-24. Raman spectroscopy of the samples pyrolyzed in Ar, a) 1250°C, b) 1300°C, c) 1350°C and d) 1400°C treatment.

HRTEM observations combined with EDX and EELS measurements enabled to determine the nanochemical composition of the NWs and to ascertain their growth mechanism. **Figure 4.2-25**(a) shows a STEM/HAADF (high angle annular dark field) image of the PMPS-$FeCl_2$-ADA sample pyrolyzed at 1400°C under Ar. The different components of the pyrolyzed material have the following compositions: (i) the *caps* of the NWs consist of iron silicide of varying stoichiometry (around 1:1), as revealed by their typical EDX spectrum, **Figure 4.2-25**((a), right middle), in good agreement with the XRD result, (ii) the *NWs* were formed by β-SiC (corresponding to their EDX spectrum in **Figure 4.2-25**((a), right above), (iii) the *matrix*

particles consisted likewise of β-SiC, but with a few percent oxygen, as indicated by **Figure 4.2-25**((a), right below). The compositions of the NWs and matrix phase were further confirmed as silicon carbide by EELS measurements near the ionisation edge (ELNES) (data not shown here for brevity). The arrangement of the atomic planes of the SiC NWs observed by HRTEM (cf. **Figure 4.2-25**(b)) reveals that the interface between cap and fiber was atomically smooth, and that the growth direction of the fiber was precisely orthogonal to the {111} planes of the silicon carbide NWs. This observed growth direction is typical for SiC NWs grown by a solution–precipitation mechanism.[11, 16, 46] In some cases, the SiC NWs contained arrays of typical planar defects, also resulting in characteristic multiple reflexes in the diffraction pattern, both evidenced in **Figure 4.2-25**(c), in agreement with the XRD results and previous investigations.[46, 125]

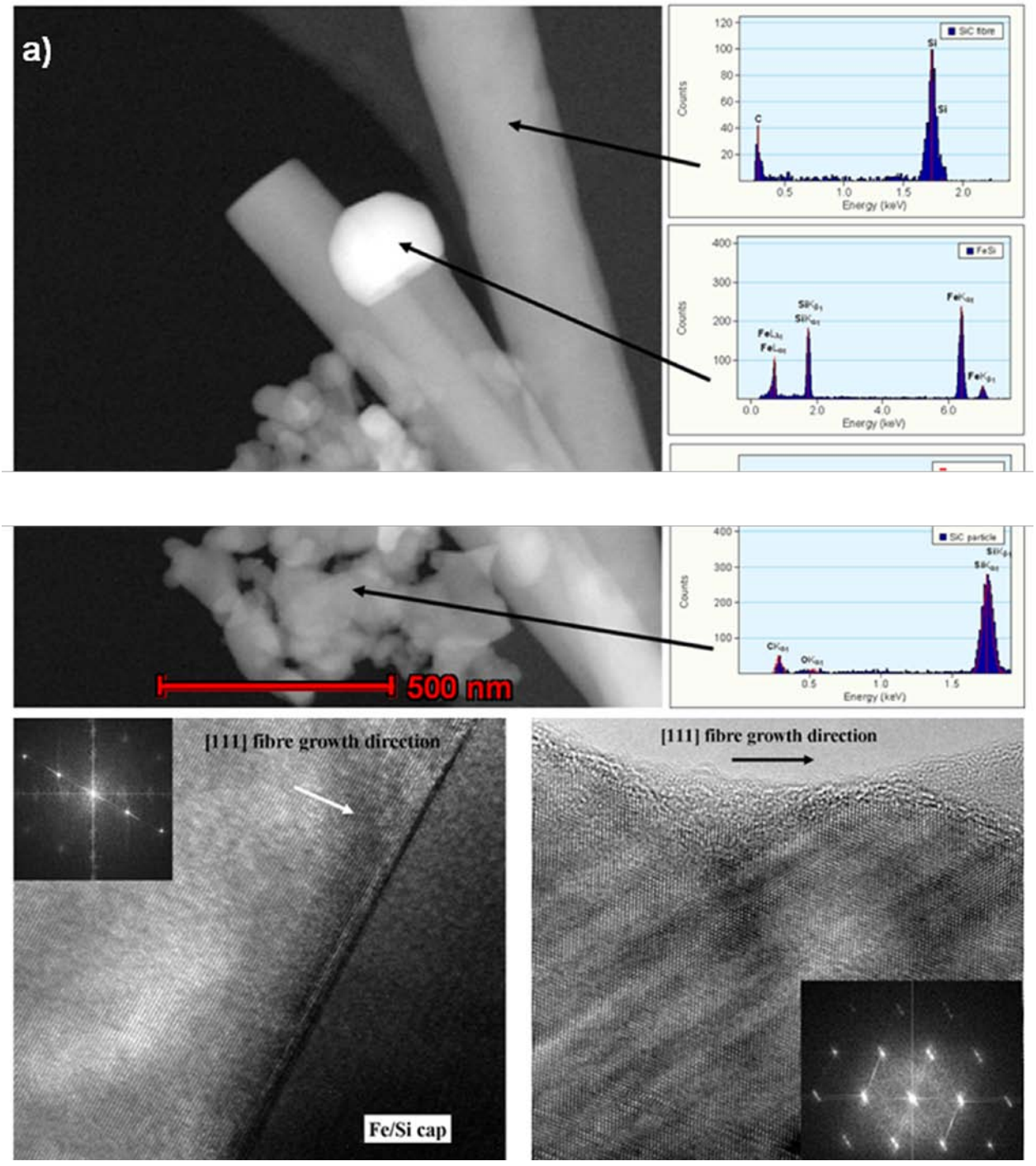

Figure 4.2-25. HRTEM/EDXS analyses of sample PMPS-$FeCl_2$-ADA pyrolyzed at 1400°C under Ar; a) overview and related EDX spectra taken from selected areas (top: nanowire; middle: spherical tip; bottom: matrix phase); b) atomically smooth interface between cap and nanowire;

growth direction orthogonal to {111} SiC planes; c) arrays of typical planar defects in the NWs due to the polytypism of SiC, with characteristic multiple reflexes in the diffraction pattern.

The presence of catalyst droplets at the tips of the SiC NWs (**Figure 4.2-25**(a)), together with the fact that NWs were obtained only when $FeCl_2$ was present, indicates that the growth proceeded through a solution–precipitation (VLS) mechanism.[45] As in the case of pyrolysis under N_2, during the heat treatment $FeCl_2$ was reduced and fine particles of metallic Fe formed a Fe-Si solution, in analogy also to previous observations.[120-122] Since the Fe-Si binary phase diagram shows eutectic points around 1200°C,[126] and the melting points of nanoclusters are lower than that of corresponding bulk solids,[46] the formation of liquid iron-silicide (Fe-Si) alloys at all temperatures studied here is highly probable ($Tm_{(Fe3Si)}$=1200°C, $Tm_{(FeSi)}$=1409°C [126]). It is known that the surface of these liquid droplets has a large accommodation coefficient, and therefore they are a preferred deposition site for the incoming SiO and CO gases,[46] which formed during pyrolysis of the polysiloxane preceramic polymer.[91] As evidenced by XRD data, at 1250°C an iron rich Fe-Si phase mixture (Fe_5Si_3+Fe_3Si) was observed, and SEM images showed that no NWs formed. The increase in pyrolysis temperature led to the formation of the FeSi (presumably in a pseudo-liquid state) due to the abundance of Si. Carbon then dissolved in this FeSi flux to form a supersaturated solution (with respect to Si and C atoms) from which solid-phase SiC crystals nucleated via precipitation, and grew along the thermodynamically more favorable direction, i.e., the <111>.

At pyrolysis temperatures of 1350 and 1400°C, a highly porous SiC ceramic decorated with SiC NWs, having FeSi tips, was obtained. These NWs were homogeneously distributed on the cell walls, but they were shorter than those produced when heating in N_2 and appeared not to be amassed in bundles. The reason for this is attributable to the difference in the growth mechanisms between SiC and Si_3N_4-based NWs observed in the present study. A schematic formation mechanism of NWs, derived from the above discussion is shown in **Figure 4.2-26**.

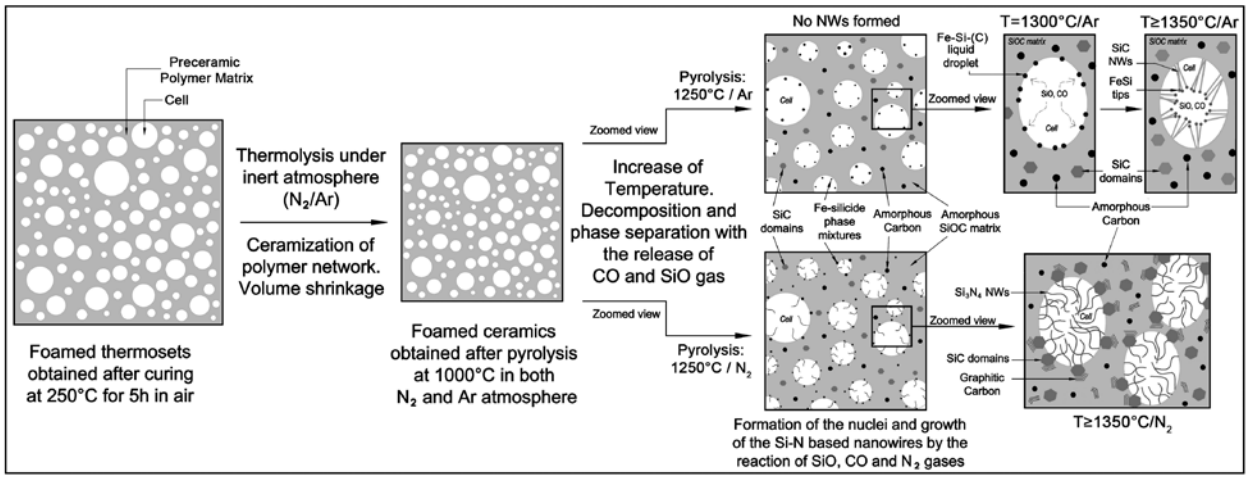

Figure 4.2-26. Schematic representation for the formation of NWs in the pores of polymer-derived ceramic foams.

Sample PHA-Co (PMPS-ADA-$CoCl_2$) under N_2 pyrolysis

The general morphology of the ceramic samples produced using $CoCl_2$ as a catalyst was very similar to that of samples containing $FeCl_2$, indicating that these metal ions had a similar effect, if any, on the decomposition of the physical blowing agent and the low-temperature rheology of the polysiloxane precursor. Yet, this particular issue necessitates more detailed investigations, which are outside the scope of this study. As expected, no significant change could be observed in the morphology at the macro-scale for samples heated between 1300 and 1400°C (see **Figure 4.2-27**(a)-(d)). A decrease in the cell size and cell window diameter with increasing pyrolysis temperature was observed, due to the shrinkage which preceramic polymers undergo during heating, and at 1400°C under N_2 foams having spherical cells (483.4 ± 225.6 μm in diameter) with connecting cell windows (128.6 ± 105.6 μm in diameter) were obtained. These results are comparable with those for the samples produced by using Fe as a catalyst source. All the samples contained a large amount of NWs (see embedded high magnification images in **Figure**

4.2-27(b)-(d) protruding from the cell walls upon pyrolysis at temperatures≥1300°C, and the nanowire length was affected by the pyrolysis temperature (as high as 300 µm NWs were obtained by 1400°C pyrolysis). The diameter of the NWs was computed by image analysis from an average of 200 measurements per each sample. Upon pyrolysis at 1400°C under N_2, NWs with an average diameter of 100.13 ± 33.38 nm were produced. As could be seen, pyrolysis under N_2 at 1300°C caused nanowire bundles originating from scattered locations on the cell walls (see **Figure 4.2-27**(a) and (b)). Bundle like formation of NWs has already been observed by other researchers,[127, 128] and it has recently been proposed that the controlling parameter for the development of this nanostructural morphology is dictated by the growth mechanism, i.e. VLS (see later).[127] Increasing the temperature caused an increase in the number of these bundles, resulting in a full coverage of the cell wall surfaces at 1350°C (**Figure 4.2-27**(c) and (d)), followed by the formation of long, straight NWs connecting the different bundles (see **Figure 4.2-27**(e) and (f) and inset therein).

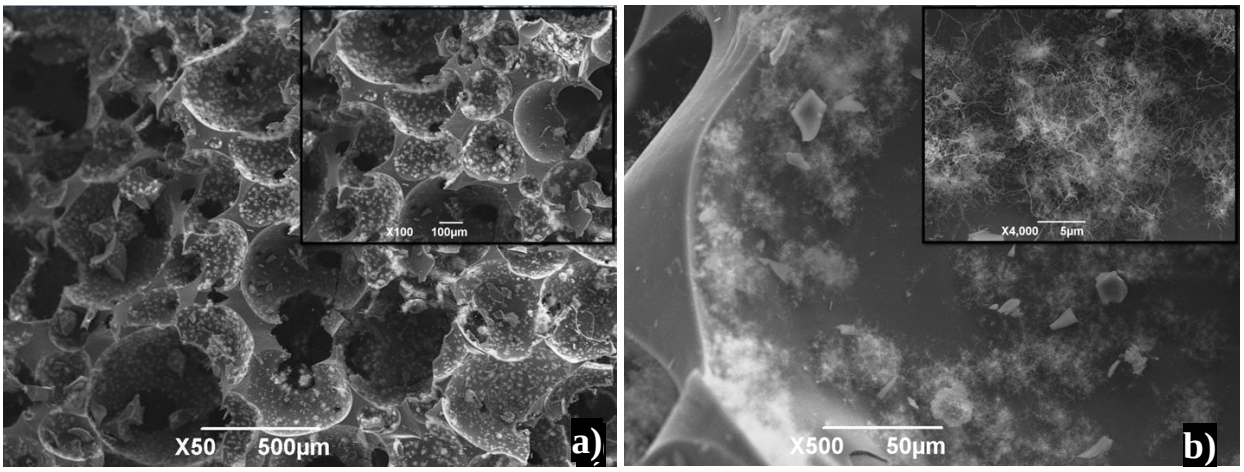

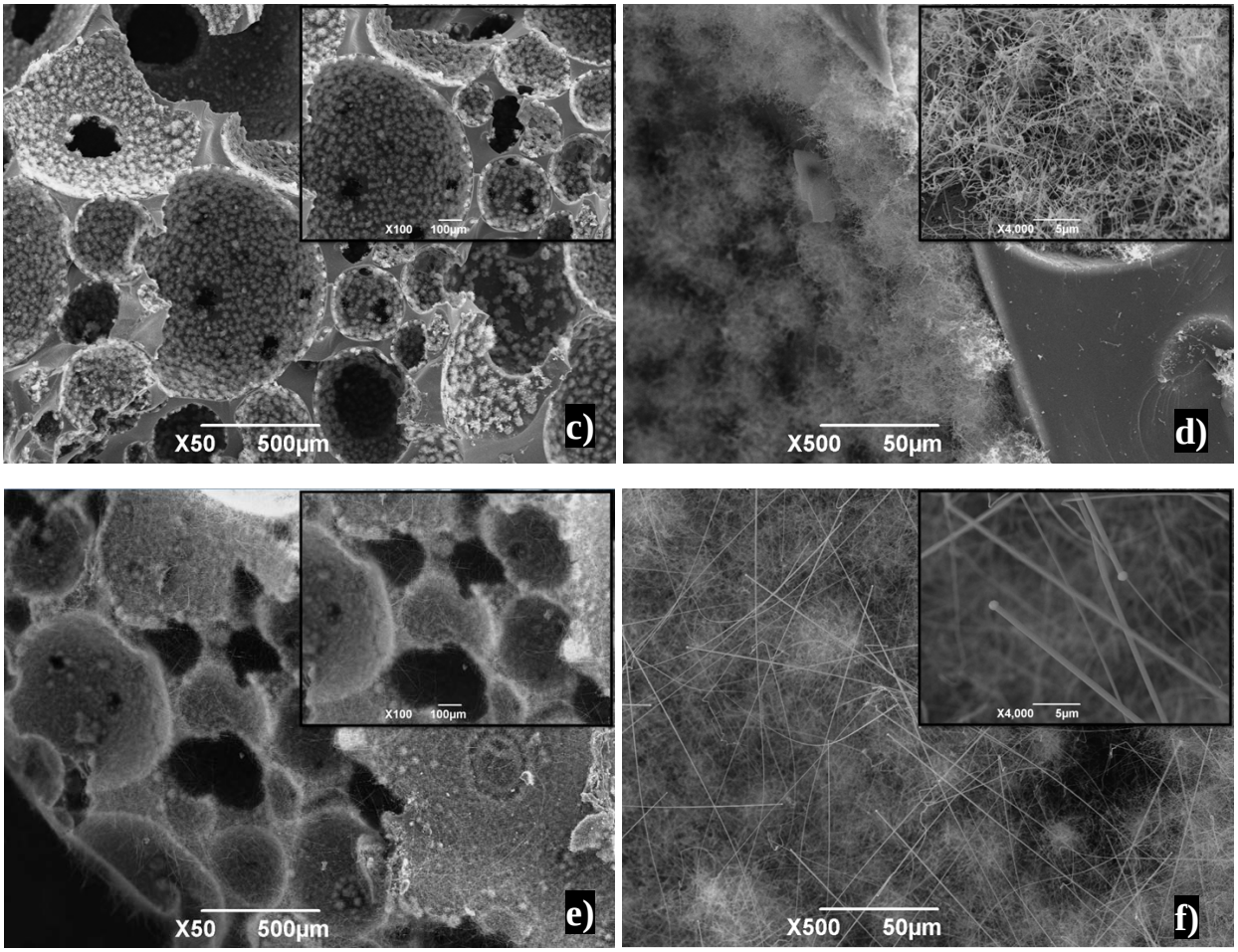

Figure 4.2-27. SEM micrographs taken from the fracture surface of pyrolyzed samples of PMPS-$CoCl_2$-ADA at a) 1300°C, b) detail from the cell at higher magnification showing dense strut and few nanowires; c) 1350°C, d) detail from the cell at higher magnification showing dense strut and a bunch of nanowires; e) 1400°C, and f) detail from the cell at higher magnification showing straight NWs with tips; insets included show higher magnification images, all samples were treated in N_2 atmosphere.

The XRD patterns of the samples pyrolyzed at different temperature in N_2 are reported in **Figure 4.2-28**. The samples produced at 1250-1350°C showed the presence of a significant amount of SiCxOy amorphous phase (broad hump in the 20-30° region)[87] and clearly defined crystalline

peaks attributable to β-SiC (JCPDS # 29-1129) and cobalt silicide CoSi (JCPDS #72-1328). Whilst the sample pyrolyzed at 1250°C had a distinct peak at 2θ~26° corresponding to the (002) plane of graphite, this peak (labeled as "C" in graphs) decreased considerably with increasing the thermolysis temperature, concurrently promoting β-SiC crystallization. This is further corroborated by Raman analysis (see later) showing the widening of both D and G peaks, seemingly with the increase in pyrolysis temperature graphitic carbon is consumed. Peaks attributable to Si_3N_4 phases became more noticeable above 1300°C, and pyrolysis at 1400°C resulted in a ceramic containing β-SiC, Si_3N_4 (both α (JCPDS #41-0360) and β (JCPDS #33-1160) polymorphs) and CoSi. The peak located at ~33.7° could be assigned both to the stacking faults in the β-SiC crystalline structure[129] and to the (101) plane of β-Si_3N_4. No oxynitride phase was observed, and clearly carbon and amorphous silica (or SiOC) were consumed with increasing in the pyrolysis temperature. Supporting the findings of Siddiqi and Hendry,[98] it was observed by Yu et al.[93] that the crystallization of preceramic polymer derived amorphous Si_2N_2O residue results in different products, namely either Si_2N_2O or α-Si_3N_4-Si_2N_2O mixture depending on the C:O ratio. While a high C:O ratio involves the consumption of oxygen during crystallization, and therefore Si_3N_4 is produced, a low C:O ratio enables the formation of Si_2N_2O. Indeed, parallel experiments performed using a low carbon containing polysiloxane (MK by Wacker, carbon ~13wt%[80]) and a similar catalyst source yielded Si_2N_2O.[54] This implies that in the present experimental conditions (i.e. the use of a high carbon containing precursor, H44, carbon ~40wt%[80]), the partial pressure of oxygen was always kept lower than that required to form Si_2N_2O.

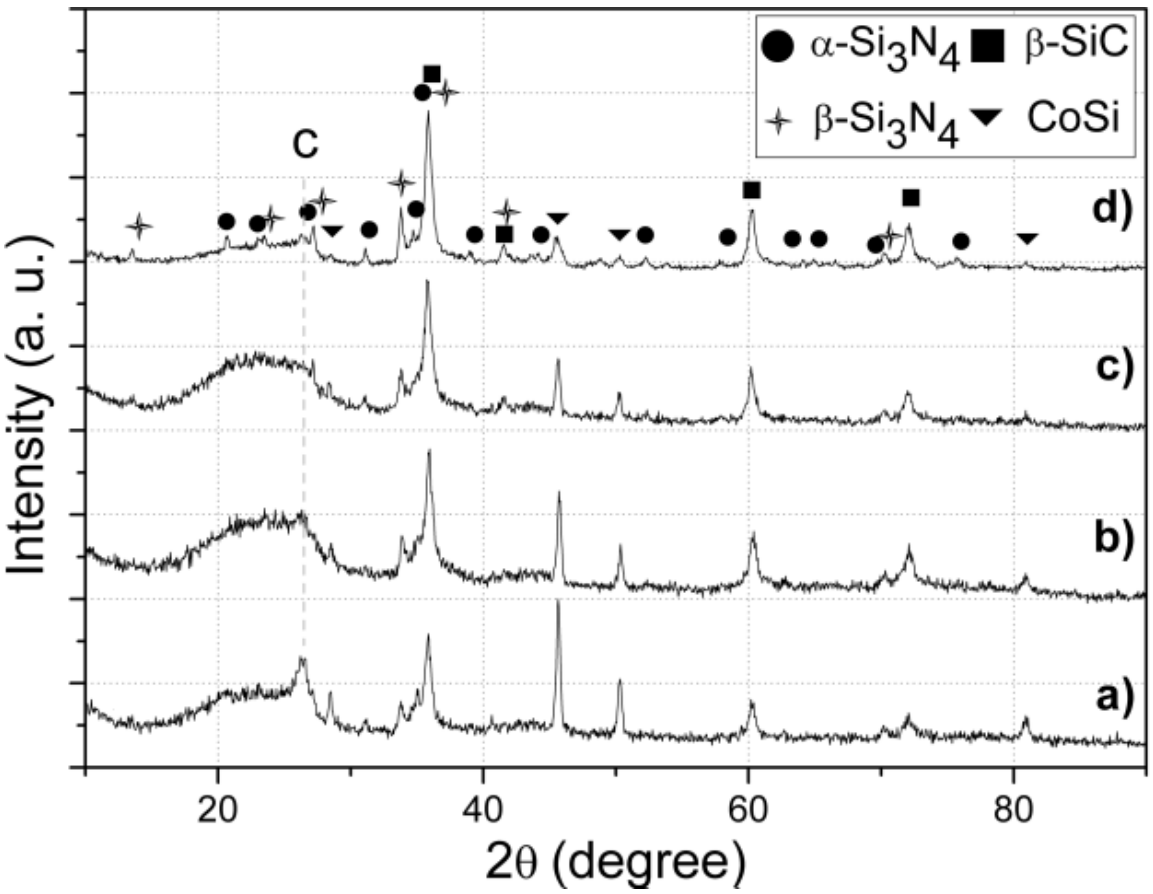

Figure 4.2-28. XRD patterns of the samples pyrolyzed in N_2, a) 1250°C; b) 1300°C; c) 1350°C; and d) 1400°C treatment, label "C" in XRD plots with a vertical line ~26° shows graphite peak.

CoSi formed at all pyrolysis temperatures in both pyrolysis atmospheres, similarly to what observed for the samples containing Fe, in which iron silicide phases were obtained, because of the good affinity between the two elements, as found also when joining Si-containing ceramics to cobalt or its alloys by solid-state bonding.[89] The reduction of $CoCl_2$ to micron-sized metallic Co particles during heating in inert atmosphere and their interaction with the silicon containing matrix was responsible for the formation of CoSi.[130, 131] XRD analysis performed on samples prepared at lower temperatures (900-1200°C in 100°C steps, see **Figure 4.2-29**) demonstrates that under N_2 atmosphere metallic Co (JCPDS #15-0806) forms at 900°C and with the increase

in pyrolysis temperature, silicidation proceeds resulting in CoSi ~1200°C. Most probably the observed oxide at ~1000°C (Co_3O_4 (JCPDS #42-1467), assigned with "*" in **Figure 4.2-29** (b)), was due to the carrier gas since under Ar pyrolysis no oxide was observed (see later), i.e. a probable contamination (note that oxide can easily be reduced back to its metallic state since the reaction tube includes highly reducing atmosphere at around this temperature).

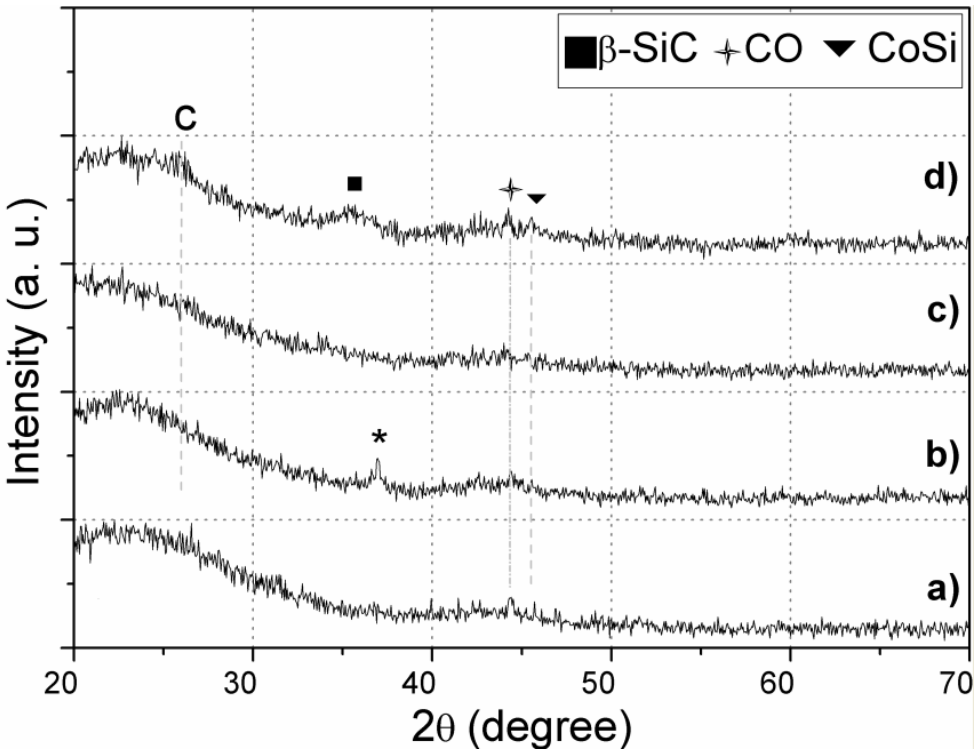

Figure 4.2-29. XRD patterns of the samples pyrolyzed in N_2, a) 900°C, b) 1000°C, c) 1100°C and d) 1200°C treatment, label "C" in XRD plots ~26° shows graphite peak, and "*" belongs to Co_3O_4.

Raman spectra of the samples treated at different temperatures are shown in **Figure 4.2-30** (a-d). Both D and G bands, resolved for carbon are present implying highly disordered carbon forms in the samples. It seems that with the increase in pyrolysis temperature ordering in carbon phase is partially lost, so peaks widen. This together with XRD results implies that with the increase in

temperature graphitic carbon is consumed. No other clear peaks are observed that can be characterized for SiC (780cm^{-1} (TO) and 970cm^{-1} (LO)) or Si_3N_4, this implies that high amount of C–C bonds were always present in the system, for which the Raman efficiency is about ten times stronger than that of SiC.[107, 123] Raman data proves that at all temperatures carbon is present in the system

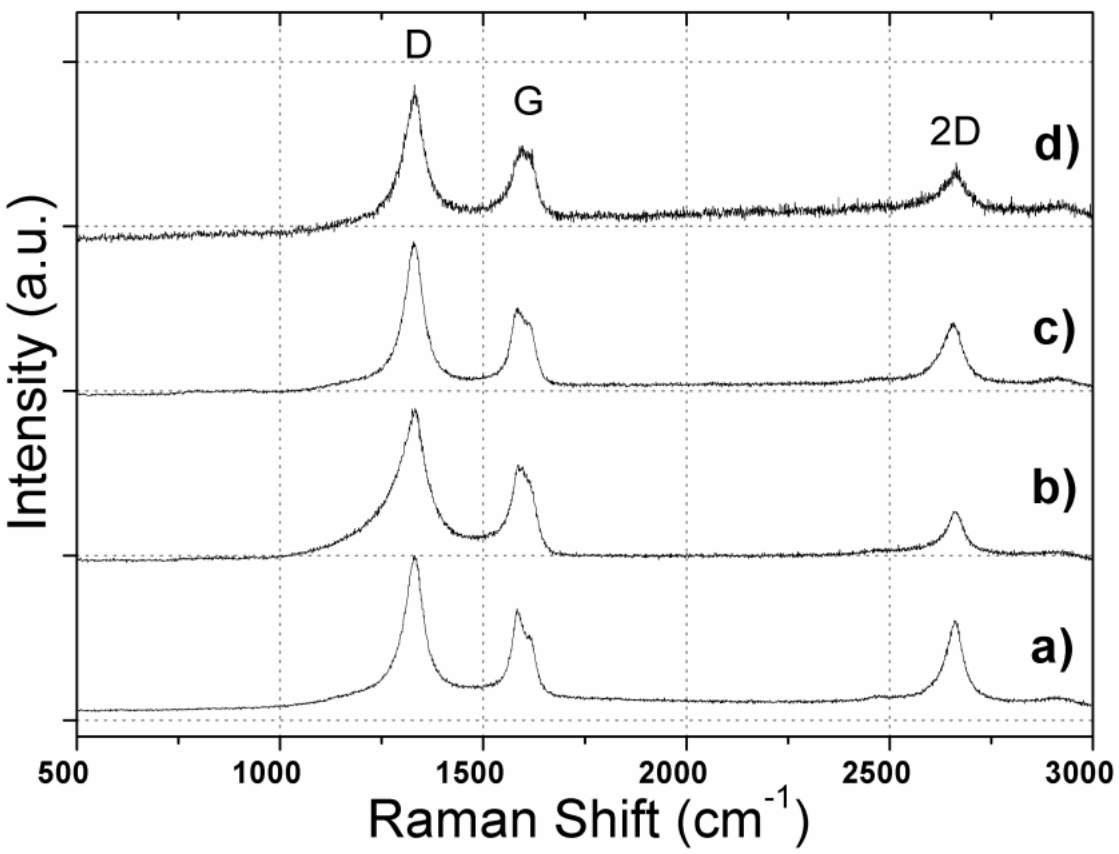

Figure 4.2-30. Raman spectroscopy of the samples pyrolyzed in N_2, a) 1250°C; b) 1300°C; c) 1350°C; and d) 1400°C treatment.

HRTEM investigations combined with EDX measurements enabled to determine the nanochemical composition of the NWs and to ascertain their growth mechanism. An HRTEM image of a Si_3N_4 nanowire formed on a cell wall of a sample pyrolyzed at 1400°C in N_2 is reported in **Figure 4.2-31**(a). The EDX profile taken from the body of the nanowire (**Figure 4.2-31**, bottom left), indicated that the nanowire contained only silicon and nitrogen. Obviously, the nitrogen derived from the flowing N_2 gas present in the pyrolysis tube, as confirmed by the fact that no Si_3N_4 phase was observed when Ar was used as pyrolysis atmosphere (see later). The caps of the NWs consisted of cobalt silicide of varying stoichiometry (around 1:1), as revealed by their typical EDX spectrum (**Figure 4.2-31**, bottom right), in good agreement with the XRD result. A higher magnification HRTEM image, reported in **Figure 4.2-31**(b), shows that the nanowire had a perfect single crystal α-Si_3N_4 structure, without defects (as confirmed also by the selected area electron diffraction pattern (SAED) – see inset), which was identical over the entire wire length. This observation is consistent with the recent results obtained from polysilazane samples containing Fe.[127, 132] The HRTEM image together with the SAED pattern (the pole orientation is [110]) suggests that the nanowire grew along the [1-10] direction (see arrow). The factors controlling the transformation between Si_3N_4 polymorphs (α to β) are very complex,[110, 111] especially for complex multiphase systems like those of the present study, and their detailed investigation was outside the scope of this work. We can briefly comment, however, that generally this transformation occurs at temperatures ≥1300°C, unless the local SiO partial pressure within the reacting material is high, in which case the alpha polymorph is stable over the beta one up to the nitride decomposition temperature, leading to the formation of SiC.[110] Therefore, we posit that the beta polymorph (high temperature polymorph) observed by XRD formed in some local areas in which the SiO partial pressure was not high enough to stabilize α-Si_3N_4. Although the transformation from Si_2N_2O phase to Si_3N_4 is a common phenomenon,[110] we can exclude that this occurred in the present system, since XRD data for samples pyrolyzed at lower temperatures (800-1200°C in 100°C steps) did not show the presence of Si_2ON_2, unless of course such phase was amorphous.

Since the melting point of nanoclusters are lower than that of the corresponding bulk solids,[133, 134] it is plausible to assume that in these experiments CoSi (T_m=1480°C) was in pseudo-liquid state above 1250°C (note that nanowires were obtained only when heating at temperatures

~≥1300°C which is also high enough to cause SiO volatilization from the SiOC matrix[135,91]). It is known that the surface of these liquid droplets has a large accommodation coefficient, and therefore they are a preferred deposition site for the incoming SiO and CO gases,[133] which forms during pyrolysis of the polysiloxane preceramic polymer,[91] and for nitrogen from the heating atmosphere. The incorporation of these gases may lead to a supersaturation of the liquid phase in the elements forming the crystals (SiC, Si_3N_4).[121, 136, 137] The presence of catalyst droplets at the tips of the Si_3N_4 nanowires (Fig. 4(a)), together with the fact that nanowires were obtained only when Co was present, indicate that the growth proceeded through a solution-precipitation (VLS) mechanism.[45, 127] The growth mechanism for the Si_3N_4 nanowires therefore differed from what observed when $FeCl_2$ was used as a catalyst source under the same experimental conditions. This is most probably due to the different silicide phase, i.e. different content of silicon in the silicide phase. Generally, similar results, but different conclusions, have been reported for catalyst systems in which Ni, Co and Fe react on Si substrates forming metal silicides.[138, and references therein] Various parameters can affect the catalytic activity; for example Esconjauregui et al.[138] have very recently shown the importance of particle topography on the catalytic activity of metal silicides (silicon-rich Ni or Co silicides) to produce CNTs. Yang et al.[121] reported that while metal-rich silicides (such as Fe_3Si) are not suitable for the precipitation of SiC, silicon-rich melts (such as CoSi) can be successfully used to produce SiC crystals. In this manner, Li et al.[136] obtained α-Si_3N_4 nanowires from high-energy ball milled Si powder via thermolysis under N_2. The produced nanowires had silicon rich ($FeSi_2$) metallic tips, and the common VLS mechanism was proposed for their formation. Together with previously published results on the catalytic activity of different metal silicide phases, our results illustrate that the stoichiometry of the metal (Fe or Co) silicide compound (i.e. metal-rich or silicon-rich) is a key controlling parameter for the precipitation of SiC and Si_3N_4 crystals via VLS.[53, 121, 136] In fact, when Fe-containing samples were treated under N_2, the formed silicide phase was always rich in metal (predominantly Fe_3Si), and precipitation from this phase was hindered due to inability of carrying the liquid to saturation with respect to Si, C and N.[53, 121] On the other side, the use of Co catalyst resulted in a Si-rich (CoSi) silicide phase, which is a suitable medium for the saturation with Si, C, N. In the next stage, then, Si_3N_4 nanowires precipitated from this supersaturated liquid droplet. The reason why only Si_3N_4 (and not SiC) nanowires formed is simply because (i) Si_3N_4 is thermodynamically

more stable over SiC up to ~1450°C in the presence of 0.1 MPa N_2 (i.e. the present experimental conditions)[16, 139], and (ii) a copious flow of N_2 gas.

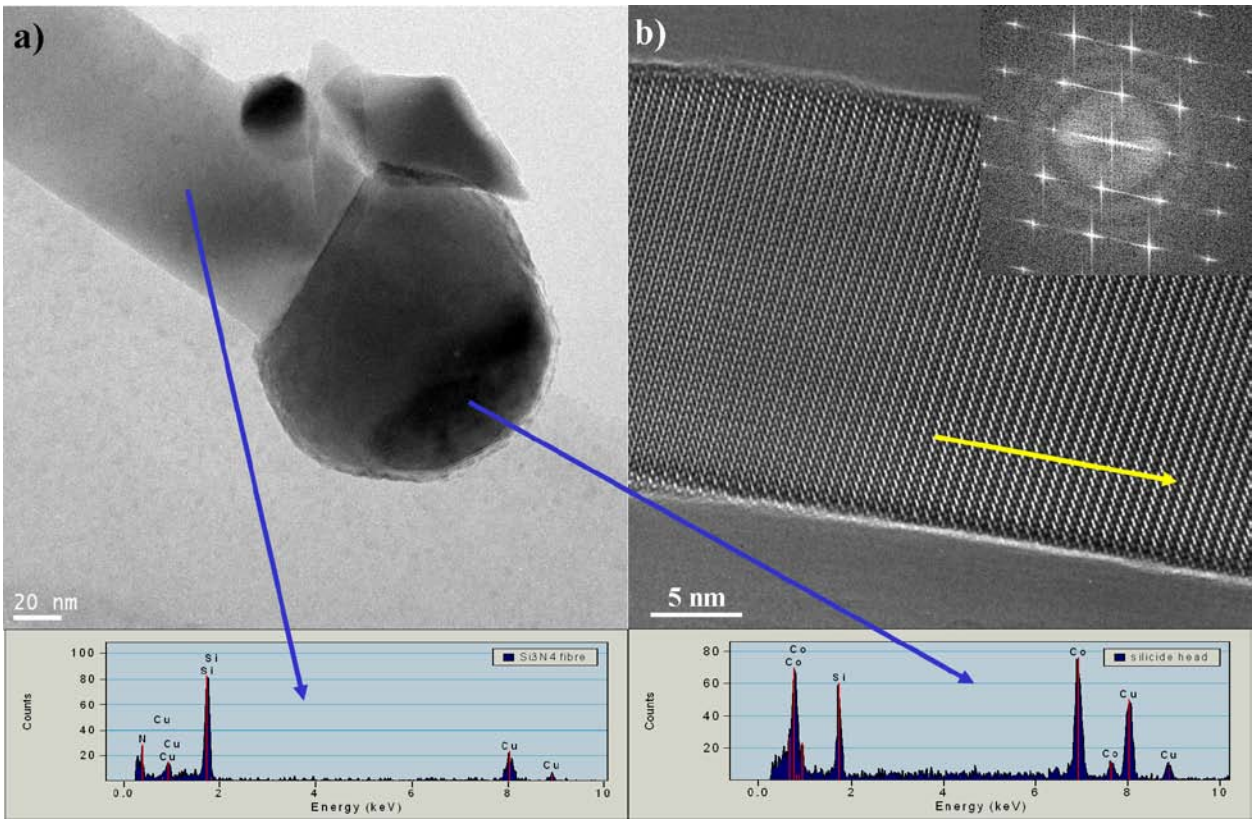

Figure 4.2-31. HRTEM/EDX analyses of a sample pyrolyzed at 1400°C under N_2; a) overview with corresponding nanochemical data: EDX (bottom left) of nanowire, and EDX (bottom right) of nanowire tip (Cu comes from TEM grid)**,** b) HRTEM image showing the regularity at the atomic scale of the nanowire body, with diffraction pattern (inset).

FEG-TEM analyses were also performed on the cell wall surfaces, in order to investigate their nanochemical and microstructural features. In **Figure 4.2-32** is reported a FEG-TEM image taken from the cell wall surface of a sample heated at 1400°C in N_2, in the vicinity of a nanowire. It reveals that the amorphous matrix phase contained small (~5 nm) crystalline SiC regions, and a few areas of graphitic carbon (as indicated also by Raman investigations), while

no micro- (< 2 nm) and meso- (between 2 and 50 nm) pores were found. These results corroborate the well known phenomenon of phase separation which occurs in SiOC ceramics at high temperatures.[140] The EDX spectrum (right) shows that the matrix phase consisted only of silicon, carbon and oxygen atoms thereby confirming, together with previous HRTEM analyses, that nitrogen was always present only in the NWs. Also, no Co was found in the ceramic foam, but always only at the tip of the NWs. EDX analysis show a lower carbon amount compared to the samples prepared under Ar atmosphere; this, together with TGA and RAMAN data, implies a probable carbothermal reduction occurring during pyrolysis in N_2 (at ~1400°C), but not in Ar.

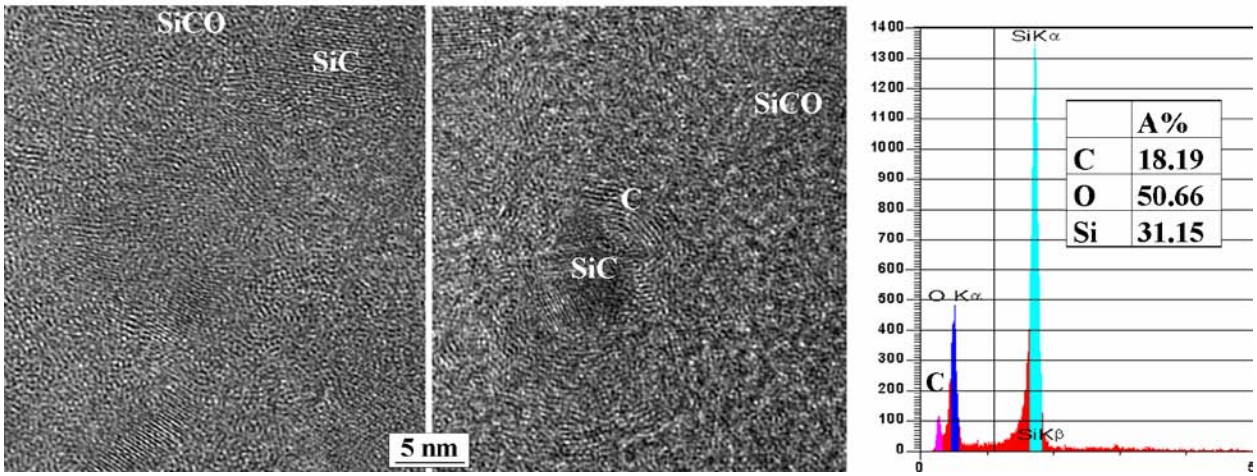

Figure 4.2-32. FEG-TEM image taken from the cell wall surface of a sample pyrolyzed 1400°C under N_2 (left), and EDX spectrum (recorded from the whole area at an average, right).

Sample PHA-Co (PMPS-ADA-$CoCl_2$) under Ar pyrolysis

The samples pyrolyzed under Ar had the cell walls uniformly coated with NWs too (see **Figure 4.2-33**(a) and (b) for SEM micrographs of samples pyrolyzed at 1350°C and 1400°C, respectively), but their morphology and composition was different from those produced when heating in N_2. In fact, these nanofibers appeared to be 128.68 ± 33.06 in diameter and less than 50 µm in length (shorter than those produced when heating in N_2) and were not amassed in

bundles but formed some small entanglements, differently to what observed for Fe-containing samples.[53]

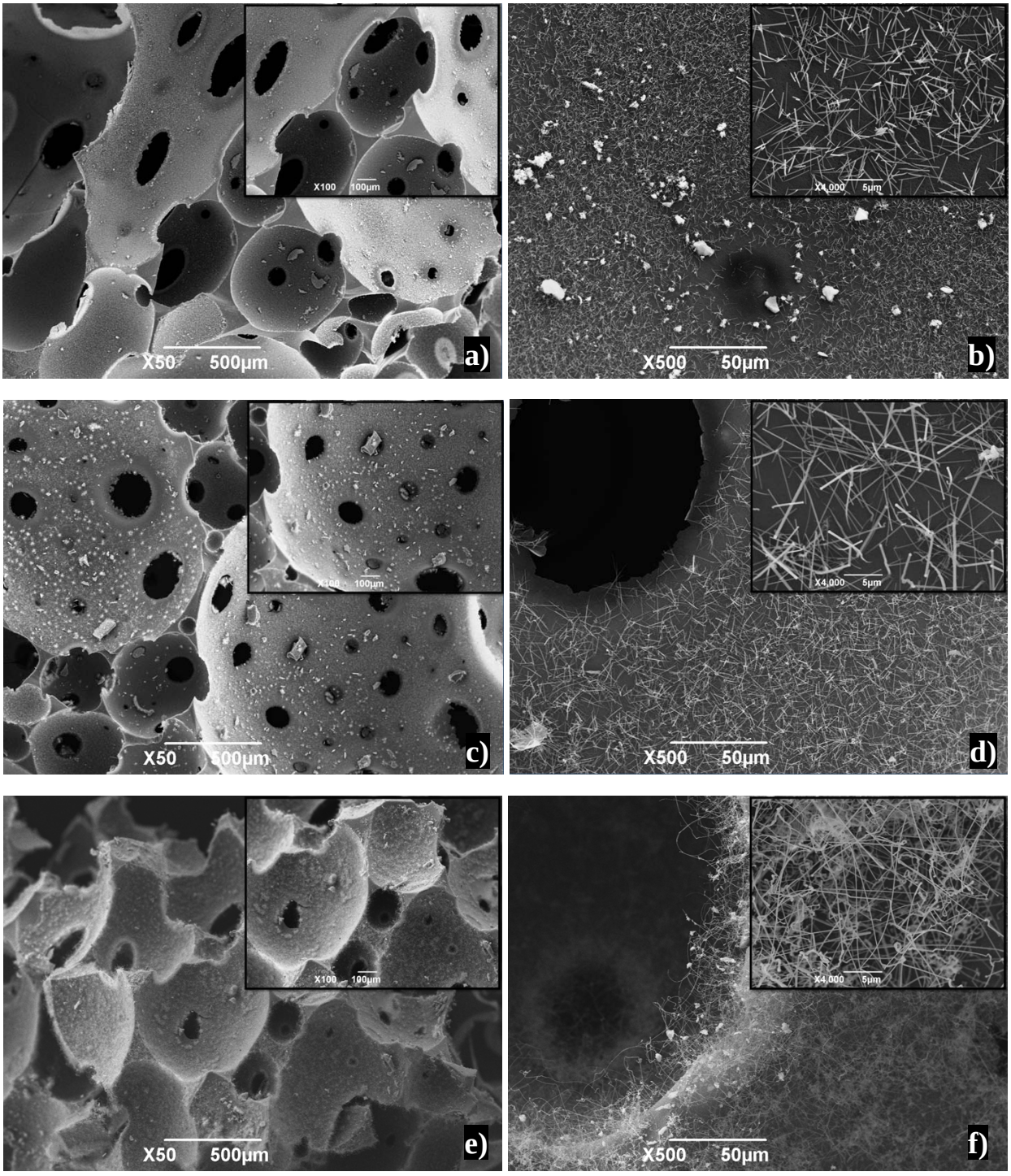

Figure 4.2-33. SEM micrographs taken from the fracture surface of pyrolyzed samples of PMPS-$CoCl_2$-ADA at a) 1300°C, inset shows dense struts; b) detail from the cell at higher

magnification; c) 1350°C, d) detail from the cell at higher magnification showing high amount of protruded nanowires; e) 1400°C, and f) detail from the cell at higher magnification showing longer NWs; insets included demonstrate higher magnification images, all samples were treated in Ar atmosphere.

Figure 4.2-34 reports the XRD patterns of samples heated at different temperatures in Ar. Samples pyrolyzed at 1250 to 1350°C showed again the presence of an amorphous SiCxOy phase, together with well defined peaks of β-SiC and cobalt silicide (CoSi), while the graphite peak was less evident. As observed for all other samples, an increase in pyrolysis temperature promoted better SiC crystallization. The depression of the amorphous silica (SiOC) hump suggests again that SiC formed at the expense of amorphous silica (or SiOC). Pyrolysis at 1400°C in Ar atmosphere resulted in a well crystallized ceramic containing only β-SiC and CoSi crystals. Similar results compared to Fe made samples were obtained from the elemental analysis, which further supports the XRD results; while the sample treated at 1250°C had 40.8 ± 0.4 wt% of C, 19.0 ± 0.5 wt% of O, 0.2wt% Cl, and 1wt% of Co, the one treated at 1400°C had 34.5 ± 0.6 wt% of C, 9.2 ± 0.2 wt% of O, and 1wt% of Co. This together with XRD data implies that oxide based gases are released (note that the decrease in O with temperature) from the system while carbon and silicon is kept in the SiC structure. It is also possible to comment here that Co remains in the system with most probably less than 3wt% (due to possible XRF inaccuracy in quantitative elemental analysis, as explained previously for Fe including samples) and Cl leaves the system most probably in the form of HCl gas with the increase in pyrolysis temperature.

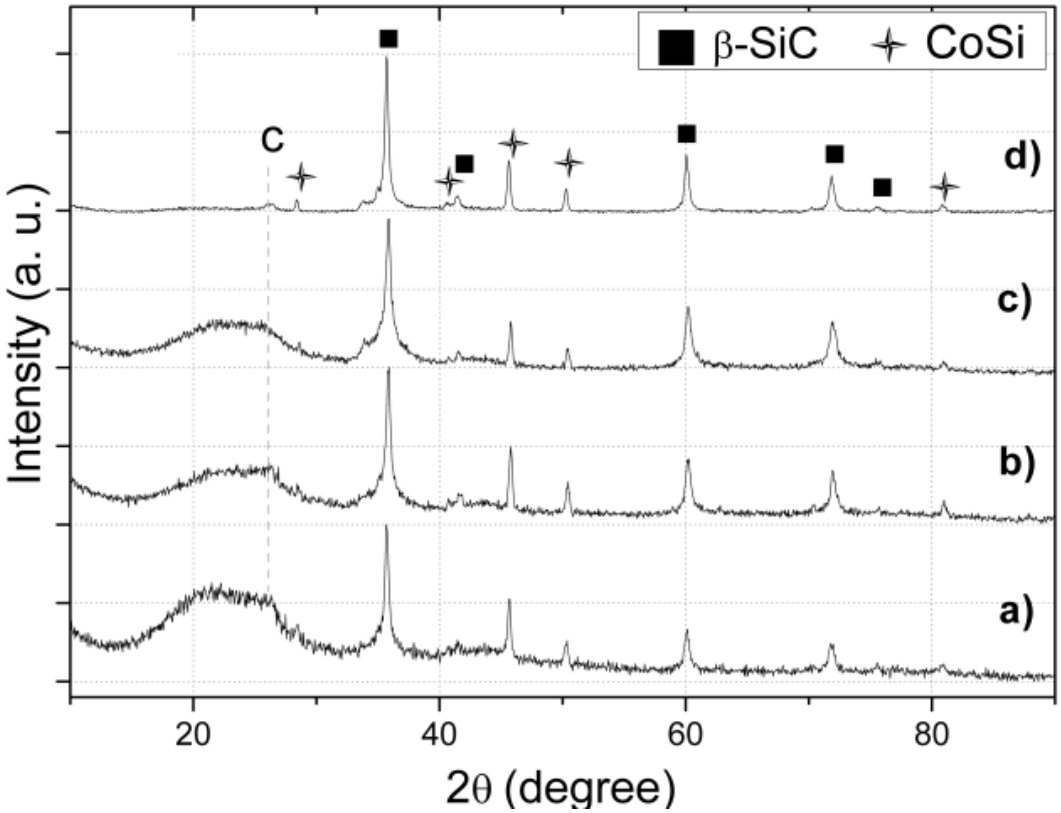

Figure 4.2-34. XRD patterns of the samples pyrolyzed in Ar, a) 1250°C; b) 1300°C; c) 1350°C and d) 1400°C treatment, label "C" in XRD plots with a vertical line ~26° shows graphite peak.

XRD analysis performed on samples prepared at lower temperatures; 500-1200°C in 100°C steps, including the data for cured polymer as well are given in **Figure 4.2-35**. Data demonstrates that under Ar atmosphere, CoSi starts to form around 1200°C, similar to the previous observations done by N_2 treatment and also well corresponds to the findings of Bourg et al.[131] Moreover, under Ar no oxide is observed and metallic Co is noticeable above 600°C and it is possible to resolve peaks related with it even up to ~1200°C where silicidation forms cobalt silicide. These results are well corresponding with the ones obtained from the samples treated under N_2 at low temperature (900-1200°C). Therefore; under the light of all XRD data; we can comment that the pyrolysis atmosphere (both Ar and N_2) is not a critical parameter defining the

phase transformation of metallic particles (Co or Fe) at temperatures seemingly up to 1200°C where above it affects the transformation.

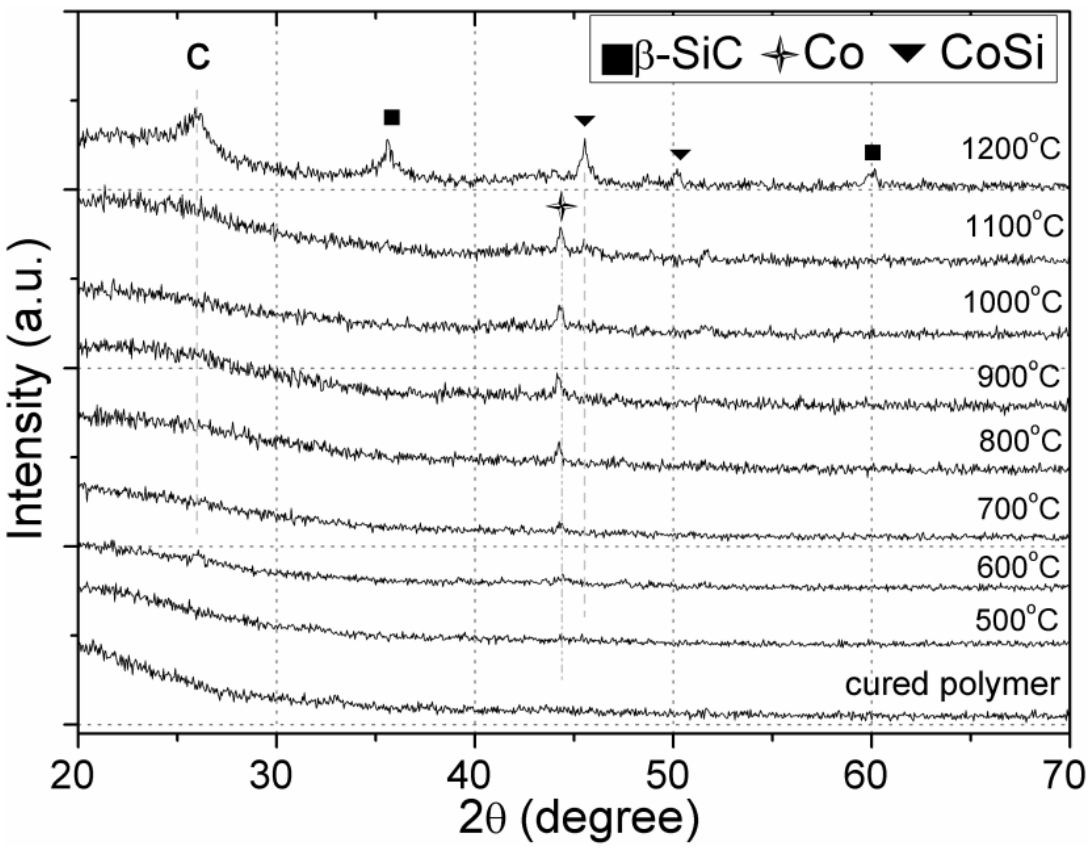

Figure 4.2-35. XRD patterns of the samples pyrolyzed in Ar at different temperatures from 500-1200°C, including the data for cured polymer as well, label "C" in XRD plots ~26° shows graphite peak.

Raman spectroscopy was used to acquire information about the free carbon phase dispersed in the matrix, at different pyrolysis temperatures. The data given in **Figure 4.2-36** (a-d) demonstrates the permanence of carbon in the materials at all pyrolysis temperature under Ar like Fe-containing samples and further corroborated by HRTEM (see later). Similar to the N_2

pyrolysis both D and G peaks are widened and 2D peak is almost diminished suggesting the distortion in the ordering of carbon with the increase of treatment temperature. Another reason can be the consumption of graphite; meaning that while graphite is consumed, amorphous carbon still remained in the system in some proportion which is also consistent with the XRD data (see depression of peak signed with "C" in XRD plots given in **Figure 4.2-34**). A very weak peak appeared ~450 cm^{-1} can be attributable to SiC formation similarly what was observed by Segatelli et al.[48]

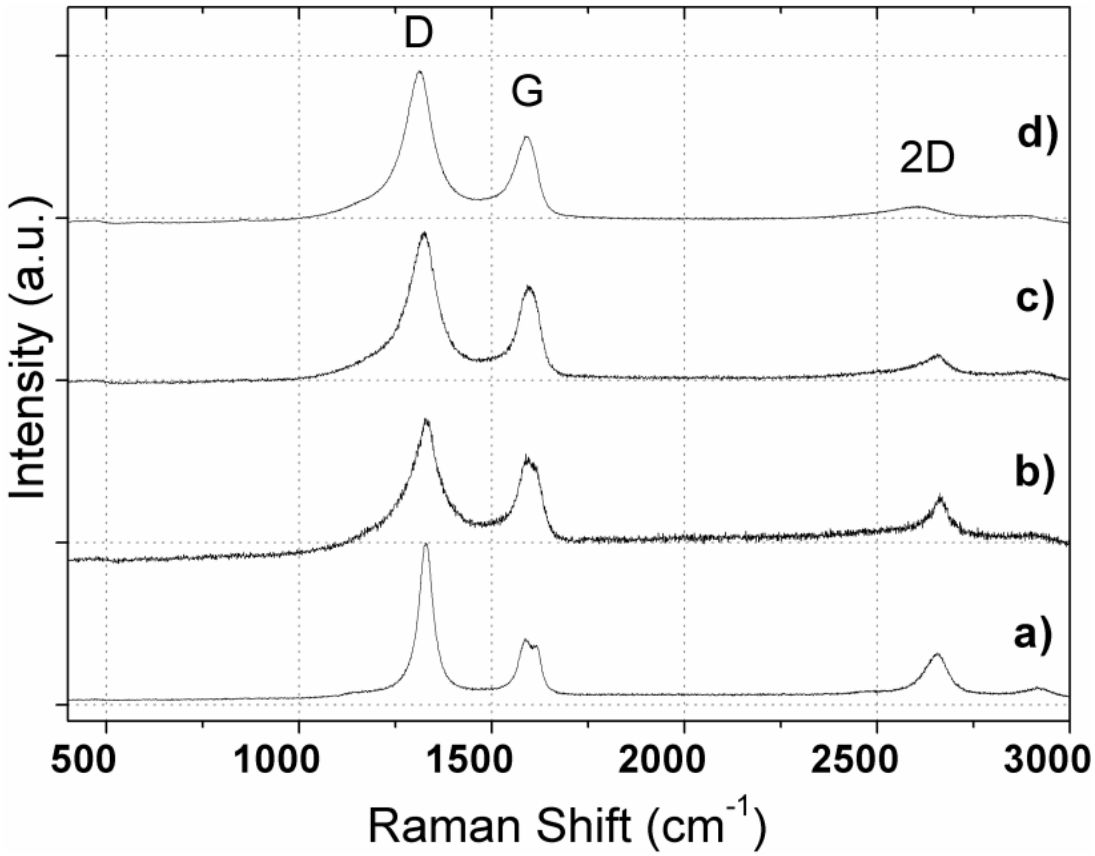

Figure 4.2-36. Raman spectroscopy of the samples pyrolyzed in Ar, a) 1250°C, b) 1300°C, c) 1350°C and d) 1400°C treatment.

TEM investigations enabled also to ascertain the nanochemical composition of the NWs and their growth mechanism when the sample was pyrolyzed in Ar at 1400°C (see **Figure 4.2-37**(a) and (b)). The caps of the NWs consisted again of cobalt silicide of varying stoichiometry (around 1:1 as revealed by their EDX spectrum, data not shown) in agreement with the XRD data. The NWs contained only Si and C (see EDX spectra in **Figure 4.2-37**(a), bottom left) and the electron diffraction pattern (**Figure 4.2-37**(b), top right) together with the XRD data revealed that they were comprised of β-SiC. The arrangement of the atomic planes of the SiC NWs observed by HRTEM (**Figure 4.2-37**(b), top right) indicated that the growth direction of the nanofiber was orthogonal to the {111} planes of the SiC nanowire (the arrow in **Figure**

4.2-37(b) shows the growth direction of the nanowire). This observed growth direction is indeed typical of SiC NWs grown by a solution–precipitation mechanism.[11, 16, 46, 141] In some cases, the SiC NWs contained arrays of planar defects, also resulting in characteristic multiple reflexes in the diffraction pattern (see SAED pattern in **Figure 4.2-37**(b), top right, with the [112] pole parallel to the electron beam), as highlighted by the XRD results and previous investigations.[46, 53, 125]

It has been shown that the formation of a Co-Si liquid phase is essential for the nucleation and growth of SiC, because of a high carbon solubility in it at high temperatures.[92, 120] As in the case for N_2 pyrolysis, due to quantum effect for the nanoparticle catalysts,[46, 134] pseudo-liquid CoSi droplets formed during pyrolysis. The formation of a supersaturated solution with respect to Si and C atoms then occurred, from which solid-phase SiC crystals nucleated via precipitation, followed by growth along the more thermodynamically favorable direction (i.e. <111>). Therefore, combining XRD, SEM (coupled with EDS analysis and HRTEM (coupled with EDX analysis), we can conclude that the SiC nanofibers grew via the well known VLS mechanism,[45] with Co acting as the metal catalyst,[120] similarly to what found for the Fe-containing samples pyrolyzed under Ar.[53] Narciso-Romero et al.[120] compared the syntheses of SiC whiskers from rice hulks using different catalyst sources (Fe, Co, and Ni), and showed an increasing order of catalytic activity, in terms of reaction rate, according to Ni > Co > Fe. Comparing the images of the fracture surfaces of samples produced using the two different catalysts (assuming that the distribution of NWs were homogenous on both surfaces upon fracture) we can confirm that the catalytic effect of Co was higher than that of Fe,[120] leading to the formation of a larger amount of SiC NWs during pyrolysis under Ar atmosphere.

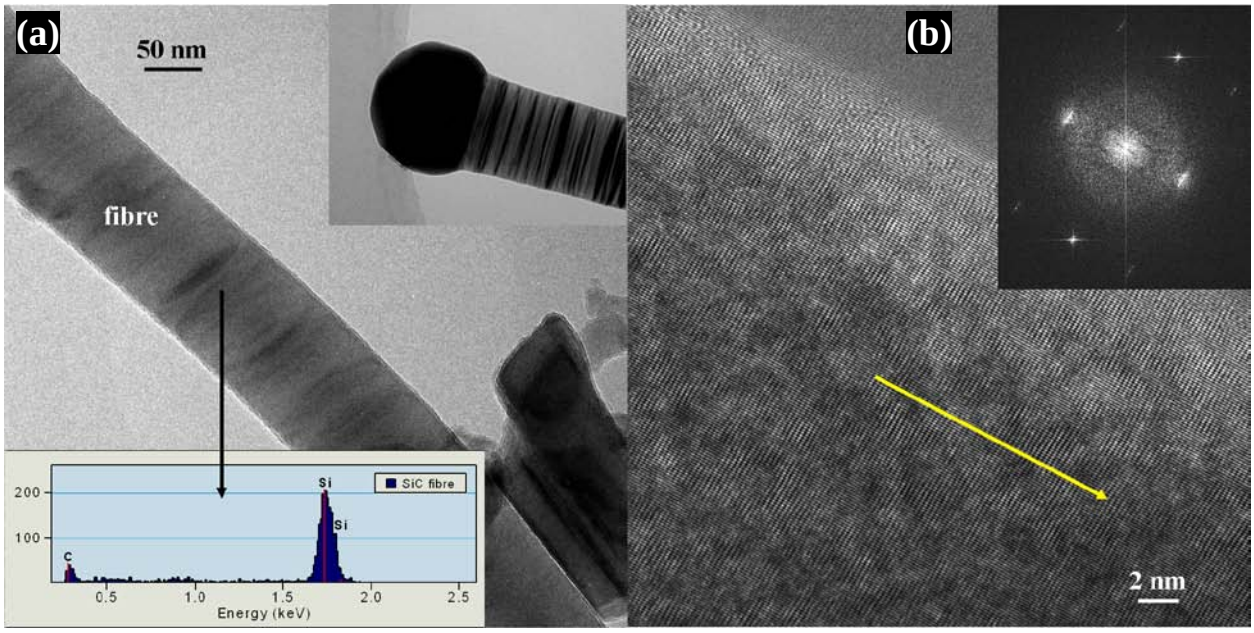

Figure 4.2-37. HRTEM/EDX analyses of a sample pyrolyzed at 1400°C under Ar; a) Fiber overview and related EDX spectra (bottom left) taken from body of the nanowire. Top right inset shows the smooth interface between metallic cap and nanowire; b) Magnification showing the growth direction (arrow) orthogonal to {111} SiC planes; inset reports the SAED pattern showing characteristic multiple reflexes caused by planar defects in the nanowire due to SiC polytypism.

Similarly, no porosity was found in the ceramic cell wall of a sample heated at 1400°C in Ar (see **Figure 4.2-38**). Compared to pyrolysis in N_2, larger (10-20 nm) and more frequent crystalline SiC regions together with larger graphitic carbon areas (~5nm) could be observed. As expected, EDX analysis gave only silicon, carbon and oxygen.

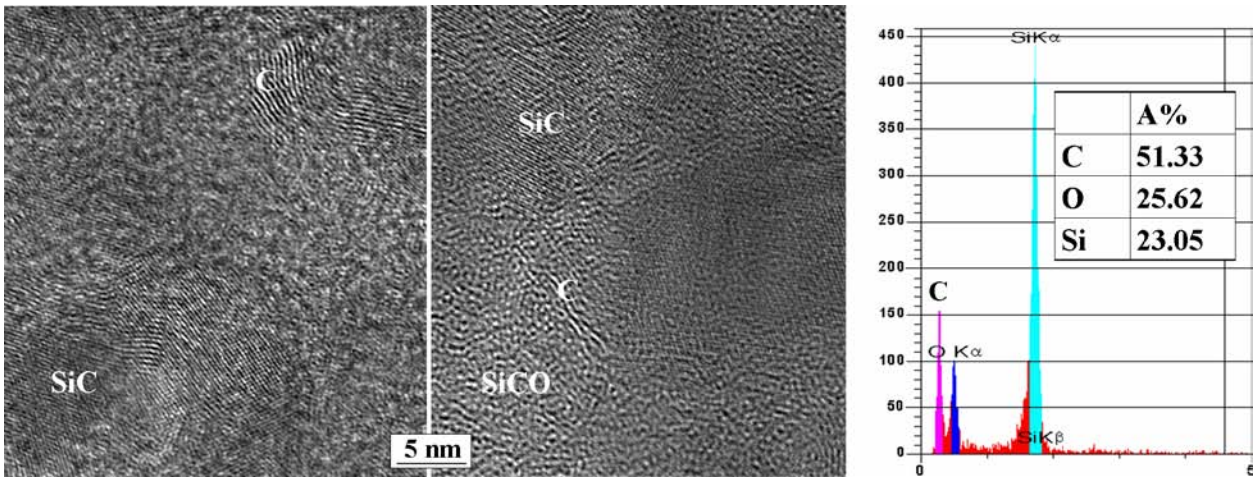

Figure 4.2-38. FEG-TEM image taken from the cell wall surface of a sample pyrolyzed 1400°C under Ar (left), and EDX spectrum (recorded from the whole area at an average, right).

In **Table 4.2-4** all the results obtained from the samples including PMS or PMPS and with Fe or Co catalyst and under N_2 or Ar atmosphere are summarized.

Table 4.2-4. Collection of previously given data for the observed NWs depending on reaction conditions, precursor and catalyst type.

Sample	Gas atm.	Temp. (°C)	Catalyst Source / NW info (amount, form, assembly and tip)	
			$FeCl_2$	$CoCl_2$
PMA: (PMS-ADA)	N_2	1250	No	Few, small bundles, with tips.
		1300	Few, small bundles & entanglements, no clear tip by SEM.	Many, long & straight ones with tips.
		1350	Many, entanglements, long & straight ones no clear tip by SEM.	Many, long & straight ones with tips.
		1400	Many, long & straight, no clear tip by SEM.	Many, long & straight ones with Co-Si tips (EDS) (XRD gives: Co, Co_2Si and CoSi -dominantly-peaks).
PMA: (PMS-ADA)	Ar	1250	No	No
		1300	No	No (in some experiments very few fibers are observed with tips)
		1350	No	No (in some experiments very few fibers are observed with tips)
		1400	No	No
PHA: (PMPS-ADA)	N_2	1250	Many, long & straight, No tips	No
		1300	Many, long & straight, No tips	Many, entanglements in bundles with tips.
		1350	Many, long & straight, No tips	Many, entanglements in bundles with tips.
		1400	Many, long & straight, No tips	Many, entanglements in bundles with CoSi tips.
PHA: (PMPS-ADA)	Ar	1250	No	No
		1300	Very few, with tips.	Many, with tips.
		1350	Many, with tips	Many, with tips
		1400	Many, with tips (XRD, EDX gives FeSi)	Many, with tips (XRD, EDX gives CoSi)

4.2.3.3.3. Porosity and Specific Surface Area

While the total porosity of the samples prepared by using PMS precursor was always less than 60 vol% (~50% of it is open porosity), samples with PMPS precursor showed higher than 70 vol%

of total porosity (open porosity was always at least 80% of the total porosity). Although by using both of the precursors we observed NWs formation from the cell walls, utilization of PMPS precursor let us to obtain open cell, permeable ceramic composite foams. As detailed in the experimental section, in order to perform accurate physisorption measurements, a second outgassing step was conducted after the determination of the free space with helium. This procedure is usually adopted in the case of microporous materials to assure that the sample adsorption sites are completely free from entrapped gases. In a standard procedure for mesoporous materials (2 nm < pore size < 50 nm) analysis, the adsorption of helium is considered negligible. But in the case of the samples produced in the present study, the presence of micropores (pore size < 2 nm) could be envisaged, as a result of nanowire growth and assemblage. The need for a second out-gassing step after free space measurement with Helium is demonstrated by the data reported in **Figure 4.2-39**, where N_2 adsorption isotherms are given for the same sample for two different condition; i) only after free spacing with Helium, and ii) two times degassing after free spacing with Helium. The consequence is clear; if the second time degassing is not applied, the BET data is no more reliable. This is also concurrent with our previous N_2 adsorption-desorption measurements and implies that when a sample includes hierarchical porosity and high SSA, degassing should be done very carefully to obtain truthful data.

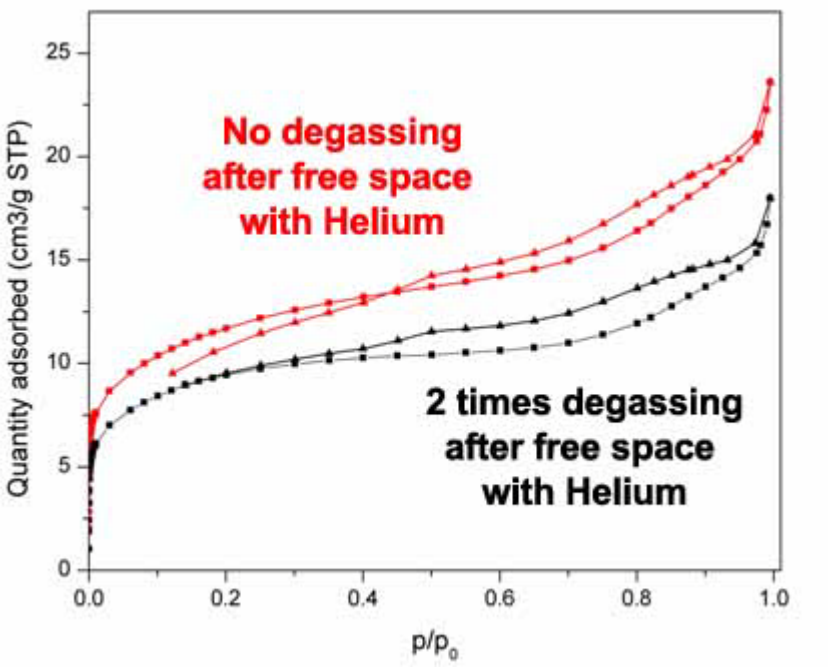

Figure 4.2-39. Nitrogen adsorption isotherms for the representative sample collected through a standard physisorption measurement and by applying a second degassing after free space with Helium.

The nitrogen adsorption-desorption isotherms (77 K) of samples containing Co or Fe, heated under Ar or N_2 at 1400°C, are reported in **Figure 4.2-40**(a) and (b). For the sake of comparison, the isotherm for the pure matrix H44 (1400°C, Ar) was also included in the plot, while the data obtained from PMS precursor is excluded from the plots (see later). The curves for the pure samples without metallic catalytic particles pyrolyzed at 1400ºC exhibited an isotherm close to Type II (IUPAC classification), with no hysteresis loop and almost negligible N_2 adsorption up to very high relative pressure, where a slight N_2 uptake is visible, owing to multilayer adsorption on macropores. The curves for samples including catalytic metal ions indicated a different behavior. Interestingly, the N_2 adsorption isotherms for Co including samples are close in shape to Type IV, with hysteresis loops that can be assigned to type H1 in the case of samples heated in Ar, and H3 in the case of samples heated in N_2. Type H1 loops are often indication of both high

pore size uniformity and high pore connectivity. In this case, the mesopores result from interstices between close packed, regularly arranged ceramic NWs. In the case of Co samples treated in N_2, nanowire bundles were produced together with longer and straight single NWs, as shown in the SEM images previously, which protrude from the cell walls for hundreds of microns and arrange on the cell surface in a highly disordered fashion. This is reflected by the isotherm shape, where the hysteresis loop starts at lower relative pressures ($p/p_0 \approx 0.43$) and does not close until the saturation vapor pressure is reached. It is well known that type H3 loops have been generally obtained with plate-like particles or slit-shaped pores.[142, 143] Here, we can consider the spaces between the NWs as wedge- and slit-shaped pores, where the high packing density hampers the meso-channels connectivity. The size distribution of the mesopores of Co samples heated in Ar or N_2 at 1400°C was obtained through the BJH method, and are reported in the inset of **Figure 4.2-40**(a). As it can be observed, pyrolysis in N_2 gave narrower mesopores with respect to Ar treatment, thus confirming a tighter packing of the NWs. In both cases, N_2 or Ar treatment, the isotherms of samples containing Co displayed a moderate N_2 uptake in the low pressure range, as highlighted in **Figure 4.2-40** (b), associated with the presence of microporosity, as can be also derived from the data of Table I, where the pore structure parameters of the entire set of prepared samples are reported. Hence, it can be inferred that the Co samples possessed hierarchically porous (tri-modal) architecture, with the coexistence of micro- meso- and macropores. The N_2 adsorption-desorption curves for samples containing Fe exhibited mainly a Type II behavior, with gradual N_2 uptake at moderate pressure (p/p_0) and a predominant N_2 adsorption at high p/p_0, associated with the presence of macropores. The hysteresis loop (type H3) is very narrow, the adsorption and desorption branches being almost vertical and nearly parallel above 0.8 of the relative pressure, confirming the presence of a significant external surface. The peak pore size estimated from the adsorption and desorption are listed in **Table 4.2-5**. In both pyrolysis atmospheres, Fe containing samples heated at 1400°C presented broad pore size distributions, as derived via the BJH model applied to the desorption branches of the isotherms (**Table 4.2-5**). In the table, the results obtained from PMS precursor at 1400°C upon only N_2 atmosphere treatments (where the samples had highest amount of NWs) are also given. The samples have SSA values of 11.70 m^2/g and 6.43 m^2/g for Fe and Co, respectively. However, it should be underlined that these data were obtained in a separate

investigation, where no free space and second degassing was applied and only after degassing for 12h at 200°C, BET measurements have been applied. As one can see, while the “C” values for PMPS treated samples are generally in 0-300 range (i.e. SSA values are highly reliable), the ones for PMS made samples are negative. Although an increase due to NWs formation is also documented in these PMS made samples (even if they had high fraction of closed porosity), as explained previously in detail in Chapter 4.1, negative “C” values imply a probable unreliability of the obtained SSA data for PMS treated samples; supporting the theories in the importance of second out-gassing step before the application of test. However, the very limited amount of tested sample mass can also be another parameter.

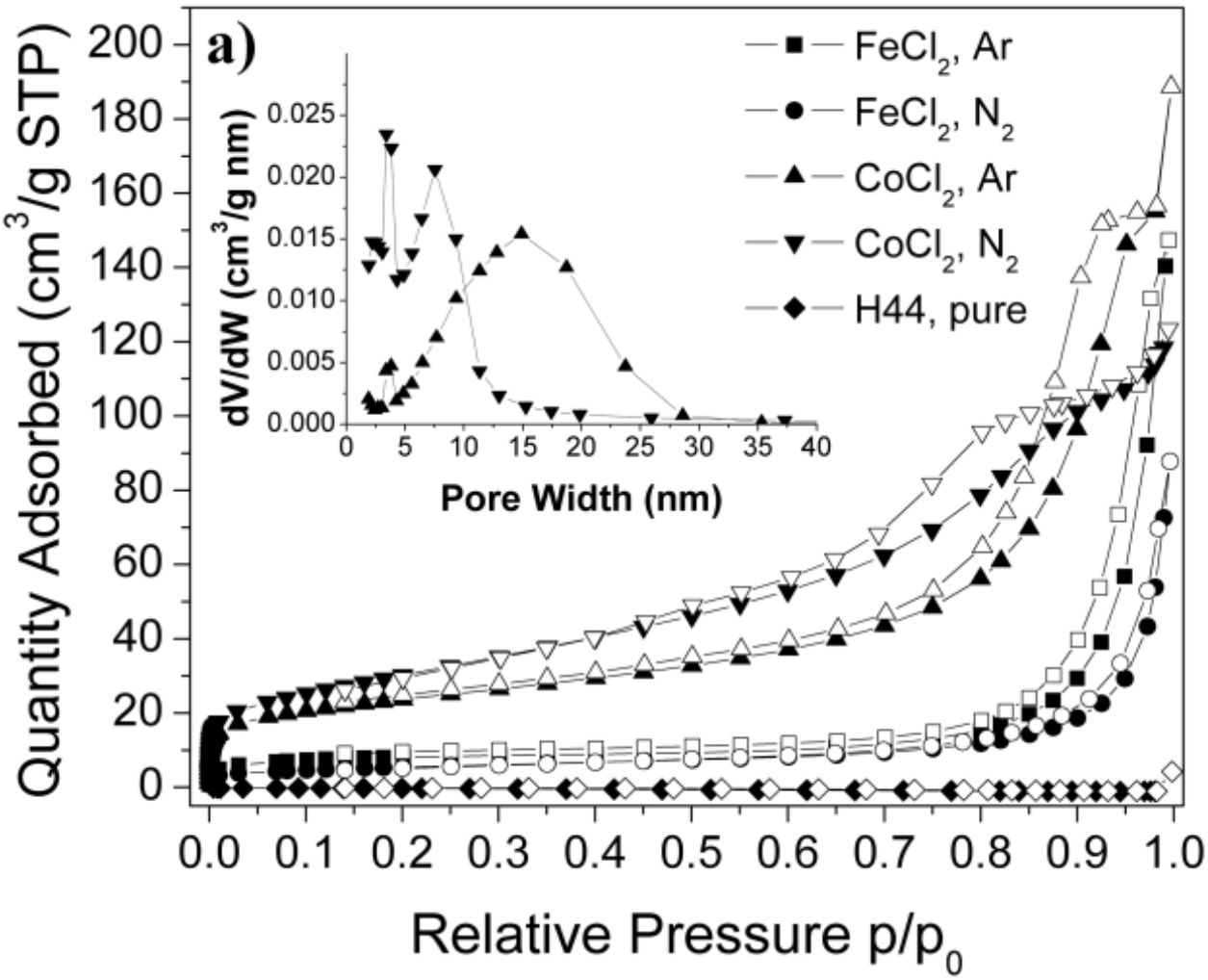

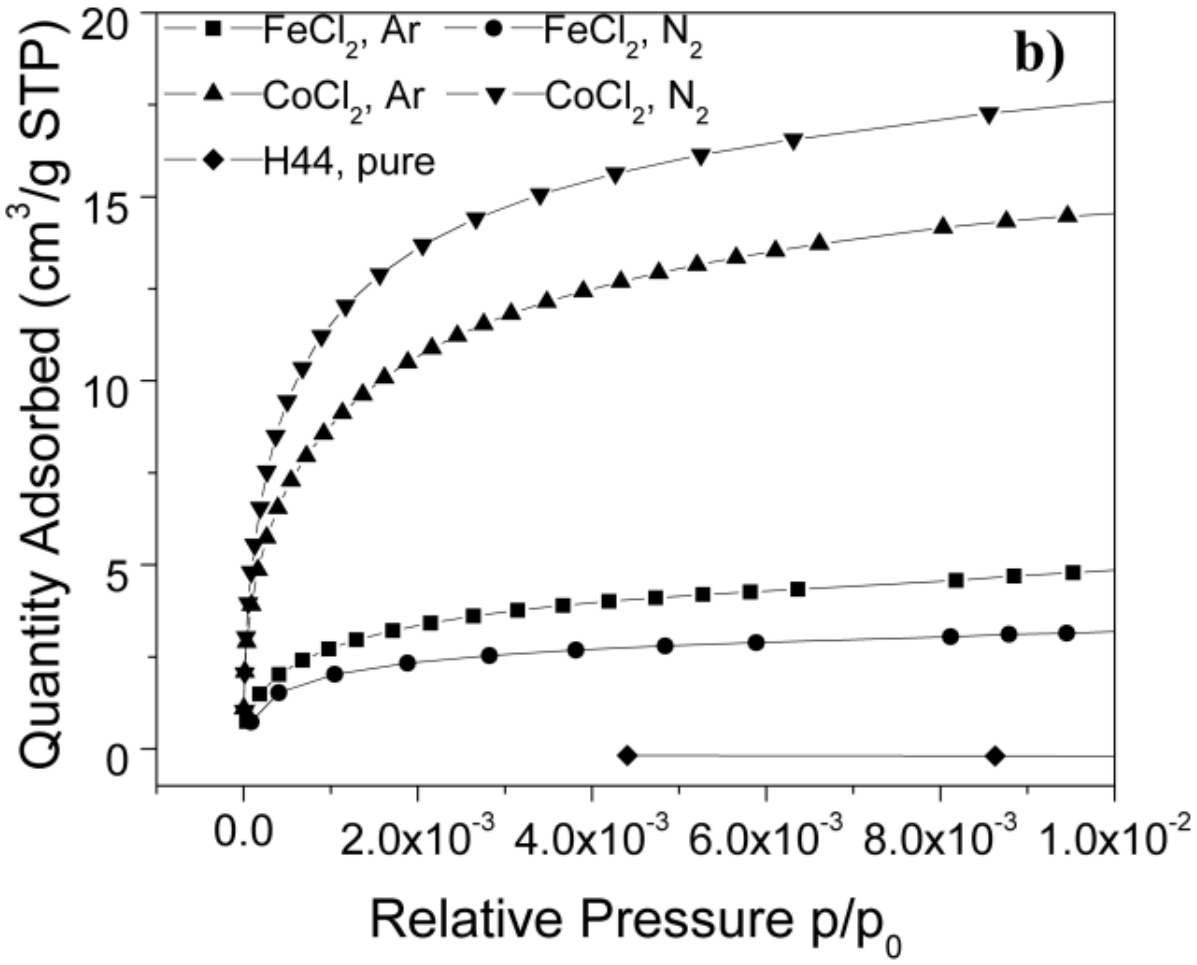

Figure 4.2-40. Nitrogen adsorption isotherms (77 K) of samples containing Co or Fe, heated under Ar or N_2 at 1400°C. For the sake of comparison, the isotherm for the pure matrix H44 (1400°C, Ar) is included in the graph. The solid and open symbols indicate adsorption and desorption branches, respectively. a) Full isotherm and PSD (pore size distribution) of Co samples (inset); b) expanded view of low pressure region.

Table 4.2-5. Specific surface area, external surface area, pore volume and pore size distribution values obtained from the adsorption/desorption isotherms.

Sample	Mass[a] (g)	C value	BET SSA[b] (m^2/g)	Total pore volume[c] (cm^3/g)	Microporosity			Mesoporosity		
					Pore volume[d] (cm^3/g)	Pore Area[d] (m^2/g)	Pore size[e] (nm)	Pore volume (cm^3/g)	External surface area (m^2/g)	Pore size[f] (nm)
H44-1400-Ar no ADA	0.1928	n.d.	<1	0.0066	n.d.	n.d.	n.d.	n.d.	n.d.	n.d.
H44-1400-Ar-ADA	0.3299	n.d.	<1	n.d.	n.d.	n.d.	n.d.	n.d.	n.d.	n.d.
H44-Co/ 1250°C N_2	0.0938	311	9.3	0.0331	0.0030	7.3	0.7	0.0301	2.0	n.d.
H44-Co/ 1300°C N_2	0.0836	188	10.6	0.0081	0.0040	9.1	0.7	0.0041	1.5	n.d.
H44-Co/ 1350°C N_2	0.0580	230	34.1	0.0278	0.0090	21.5	0.7	0.0130	12.6	3.7-7.8(*)
H44-Co/ 1400°C N_2	0.1106	86	109.5	0.1909	0.0001	3.6	0.7	0.1908	105.9	3.7-7.8(*)
H44-Co/ 1250°C Ar	0.1166	270	6.2	0.0386	0.0020	4.7	0.8	0.0366	1.5	n.d.
H44-Co/ 1300°C Ar	0.0630	219	43.7	0.1343	0.0067	15.2	0.7	0.1276	28.5	3.7-10.0(*)
H44-Co/ 1350°C Ar	0.0360	115	51.7	0.0856	0.0091	21.5	0.7	0.0765	30.2	3.7-13.2(*)
H44-Co/ 1400°C Ar	0.0337	194	84.2	0.2918	0.0069	16.5	0.7	0.2849	67.7	3.7-15.0(*)
H44-Fe/ 1250°C N_2	0.0311	n.d.	<1	0.0101	n.d.	n.d.	n.d.	n.d.	n.d	n.d.
H44-Fe/ 1300°C N_2	0.0512	247	10.8	0.0262	0.0030	7.6	0.7; 1.0	0.0232	3.2	n.d.
H44-Fe/ 1350°C N_2	0.0801	337	14.2	0.0384	0.0042	9.8	0.7	0.0342	4.4	n.d.
H44-Fe/ 1400°C N_2	0.0682	105	19.6	0.0669	0.0018	4.5	0.7	0.0651	15.1	4.0-11.6(*)
H44-Fe/ 1250°C Ar	0.0683	n.d.	<1	n.d.	n.d.	n.d.	n.d.	n.d.	n.d.	n.d.
H44-Fe/ 1300°C Ar	0.0270	n.d.	<1	n.d.	n.d.	n.d.	n.d.	n.d.	n.d.	n.d.
H44-Fe/ 1350°C Ar	0.0412	22	15.6	0.0623	n.d.	n.d.	0.7; 1.0	0.0044	n.d.	4.1-18.2(*)
H44-Fe/ 1400°C Ar	0.0322	257	29.5	0.1426	0.0087	20.5	0.7; 1.0	0.1339	9.0	22.6
MK-Co/ 1400°C N_2	0.0165	-52.69	6.42	n.d.	n.d.	n.d.	n.d.	n.d.	n.d.	n.d.
MK-Fe/ 1400°C N_2	0.0180	-87.86	11.70	n.d.	n.d.	n.d.	n.d.	n.d.	n.d.	n.d.

a) Sample weight measured after outgassing; *b*) SSA specific surface area, determined using the BET equation; *c*) Maximum uptake observed at 77 K and p/p_0 0.99; *d)* Thickness curve type Harkins and Jura: t-plot = $[13.99/(0.034- \log(P/P_0))]^{0.5}$; *e)* Determined from HK model; *f)* Determined from the BJH model applied to the desorption branch, (*) bi-modal pore size distribution in mesopore range. H44: PMPS, and MK: PMS precursors.

The SSA value for the foam substrate (containing no catalyst and in the expanded - with ADA- and non expanded form), heated in Ar at 1400°C, was less than 1 m^2/g. As a general trend, the samples containing Co gave higher SSA values compared to those containing Fe (see **Figure 4.2-41**). Moreover, while the samples heated below 1300°C had always low SSA values (<~10m^2/g), the ones produced at higher temperatures resulted in a high SSA samples (10-110m^2/g). The highest value of SSA, 109.5 m^2/g, was obtained for a sample containing Co and pyrolyzed at 1400°C under N_2.

Our results are in accordance with the literature. Jarrah et al.[27, 28] deposited CNFs on the cell walls of γ-alumina washcoated cordierite honeycombs, and showed that the SSA could be increased from 45 to 63 m^2/g, because of the presence of a ~1 μm thick layer of CNFs (diameter of 10-30 nm). The fiber diameter was controlled by the size of the deposited Ni particle, the reactivity of the gas in contact with the particle, and the duration of thermal treatment, and this parameter, together with the total amount of fibers formed, affected the final SSA of the component.[28] BET analysis showed the presence of micropores, which were attributed to the space between the fibers and the pore walls of the washcoat layer, which contained only mesopores (5-20 nm).[28] de Lathouder et al.[30, 31, 35] followed a similar strategy and demonstrated that CNF-containing cordierite monoliths possessed ~8 nm mesopores, which were again attributed to the space among the fibers and therefore not to the presence of pores in the substrate. It was also shown that a correlation between fiber diameter and the SSA values existed (assuming a constant carbon yield), according to which an increase in the fiber diameter caused a decrease in the surface area.[31] Other researchers also underlined the significant influence of the diameter and degree of entanglement of the CNFs on the resulting SSA of the macro-porous ceramics on which they were deposited.[29] Vanhaecke et al.[25] showed that the conversion of such a CNF layer into SiC (via reaction with gaseous SiO) resulted in a decrease of the SSA value, because of the increase of the nanofibers diameter after reaction.

We can therefore attribute the observed differences in the SSA values with the heating temperature, the type of catalyst and the type of pyrolysis atmosphere to the variation in the amount and morphology (diameter, length, degree of entanglement) of the formed nanowires. In fact, Co catalyst produced thinner nanowires (100.13 ± 33.38 nm in N_2; 128.68 ± 33.06 nm in

Ar; samples heated at 1400°C) than those obtained from Fe (154.47 ± 43.04 nm in N_2; 280.23 ± 120.3 nm in Ar; samples heated at 1400°C). This confirms that SSA increases with decreasing the diameter of the nanofibers. Moreover, the pyrolysis in N_2 of Co-containing samples formed bundles of Si_3N_4 nanowires (see **Figure 4.2-27**(a-f)). This particular morphology was caused most probably by multiple nucleation on a same large Co particle, as observed for Si_3N_4 nanowire bundles produced using Fe particles in the pyrolysis polysilazane precursor,[127] while straight nanowires formed starting from smaller droplets (see **Figure 4.2-27**(e) and (f)). Taking also into consideration that no micro/meso-porosity was found by FEG-TEM in the cell walls of the foams heated in both atmospheres (**Figure 4.2-32** and **Figure 4.2-38**) and the BET data, we can therefore state that high SSA values can be attributed to the presence of additional surface (that of the nanowires) and/or the finite spaces among the nanowires and between the nanowires and cell walls. We envision that the ceramic components with hierarchical porosity that we produced in this work could be used for several applications, including trapping of (nano)particles, gas adsorption or catalysis (e.g. Fischer Tropsch synthesis or N_2O decomposition).

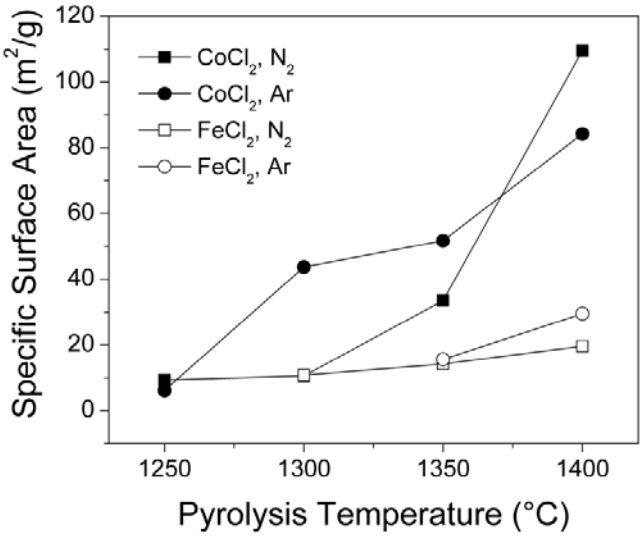

Figure 4.2-41. Plot of Specific Surface Area (from BET regression analysis) vs. pyrolysis temperature for samples PMPS(H44)-ADA-$CoCl_2$ and PMPS(H44)-ADA-$FeCl_2$, heated either in N_2 or Ar at 1400°C.

4.2.4. Conclusions

By means of different preceramic polymers, a blowing agent and a catalyst, macro-porous ceramics with the cell wall surfaces decorated with 1D nanostructures (nanowires, NWs) were produced via catalyst-assisted-pyrolysis. Differences were found depending on the pyrolysis temperature, atmosphere, and precursor and catalyst type. Utilization of low carbon containing PMS precursor under Ar, no NWs formed, due to its low carbon content, while they developed on the surface of a SiOC porous ceramic produced from high carbon containing polysiloxane (PMPS). When PMS precursor is used, thermolysis in N_2 led to the growth of a significant amount of Si_2N_2O NWs on the surface of the SiOC ceramic, and their amount increased with increasing temperature, while utilization of PMPS precursor led to the growth of Si_3N_4 NWs under N_2 pyrolysis. The growth mechanism of the nanostructures are described in detail showing that if there is no metallic tip then the mechanism is based on a gas-phase reaction, while in the case of processing under Ar the only observed mechanism was the solution-precipitation (VLS) forming single crystalline SiC NWs.

The presence of these nanostructures on the surface of the porous ceramics increased considerably the specific surface area of the materials (up to ~110m^2/g), including those produced with $FeCl_2$ as a catalyst, and the observed differences were attributed to the varied nanowire morphology (diameter and assemblage), which depended on the processing conditions and the catalyst type. In particular, increasing the pyrolysis temperature led to the formation a larger amount of NWs, and the Co catalyst produced thinner NWs than the Fe catalyst. The proposed manufacturing strategy for the production of cellular ceramic composite is a simple and effective one-pot method to obtain hierarchical porosity and high specific surface area materials.

4.2.5. References

[1]Y. Xia, P. Yang, Y. Sun, Y. Wu, B. Mayers, B. Gates, Y. Yin, F. Kim, and H. Yan, "One-Dimensional Nanostructures: Synthesis, Characterization, and Applications," *Advanced Materials*, 15 [5] 353-89 (2003).

[2]J. Zheng, M.J. Kramer, and M. Akinc, "In Situ Growth of SiC Whisker in Pyrolyzed Monolithic Mixture of AHPCS and SiC," *Journal of the American Ceramic Society*, 83 [12] 2961-6 (2000).

[3]C. Wan, G. Guo, and Q. Zhang, "SiOC ceramic nanotubes of ultrahigh surface area," *Materials Letters*, 62 [17-18] 2776-8 (2008).

[4]H.-M. Yen, S. Jou, and C.-J. Chu, "Si-O-C nanotubes from pyrolyzing polycarbosilane in a mesoporous template," *Materials Science & Engineering, B*, 122 [3] 240-5 (2005).

[5]K.F. Cai, Q. Lei, and L.C. Zhang, "Ultra long SiC/SiO2 core-shell nanocables from organic precursor," *Journal of Nanoscience and Nanotechnology*, 5 [11] 1925-8 (2005).

[6]F. Li, G. Wen, and L. Song, "Growth of nanowires from annealing SiBONC nanopowders," *Journal of Crystal Growth*, 290 [2] 466-72 (2006).

[7]K.F. Cai, Q. Lei, and A.X. Zhang, "A Simple Route to Ultra Long SiC Nanowires," *Journal of Nanoscience and Nanotechnology*, 7 580–3 (2007).

[8]G.-Y. Li, X.-D. Li, H. Wang, and Z.-Q. Li, "Long silicon nitride nanowires synthesized in a simple route," *Applied Physics A: Materials Science & Processing*, 93 [2] 471-5 (2008).

[9]Y. Xu, A. Zangvil, J. Lipowitz, J.A. Rabe, and G.A. Zank, "Microstructure and Microchemistry of Polymer-Derived Crystalline SiC Fibers," *Journal of the American Ceramic Society*, 76 [12] 3034-40 (1993).

[10]M. Scheffler, E. Pippel, J. Woltersdorf, and P. Greil, "In situ formation of SiC-Si2ON2 micro-composite materials from preceramic polymers," *Materials Chemistry and Physics*, 80 [2] 565-72 (2003).

[11]D.D. Jayaseelan, W.E. Lee, D. Amutharani, S. Zhang, K. Yoshida, and H. Kita, "In Situ Formation of Silicon Carbide Nanofibers on Cordierite Substrates," *Journal of the American Ceramic Society*, 90 [5] 1603-6 (2007).

[12]S. Jou and C.K. Hsu, "Preparation of carbon nanotubes from vacuum pyrolysis of polycarbosilane," *Materials Science & Engineering B*, 106 [3] 275-81 (2004).

[13]J. Haberecht, F. Krumeich, M. Stalder, and R. Nesper, "Carbon nanostructures on high-temperature ceramics - a novel composite material and its functionalization," *Catalysis Today*, 102-103 40-4 (2005).

[14]K.F. Cai, A.X. Zhang, and J.L. Yin, "Ultra thin and ultra long SiC/SiO2 nanocables from catalytic pyrolysis of poly(dimethyl siloxane)," *Nanotechnology*, 18 [48] 485601 (2007).

[15]W. Yang, F. Gao, H. Wang, X. Zheng, Z. Xie, and L. An, "Synthesis of Ceramic Nanocomposite Powders with in situ Formation of Nanowires/Nanobelts," *Journal of the American Ceramic Society*, 91 [4] 1312-5 (2008).

[16]W. Yang, H. Miao, Z. Xie, L. Zhang, and L. An, "Synthesis of silicon carbide nanorods by catalyst-assisted pyrolysis of polymeric precursor," *Chemical Physics Letters*, 383 [5-6] 441-4 (2004).

[17]F. Gao, W. Yang, Y. Fan, and L. An, "Mass production of very thin single-crystal silicon nitride nanobelts," *Journal of Solid State Chemistry*, 181 [1] 211-5 (2008).

[18]W. Yang, L. Zhang, Z. Xie, J. Li, H. Miao, and L. An, "Growth and optical properties of ultra-long single-crystalline α-Si3N4 nanobelts," *Applied Physics A: Materials Science & Processing*, 80 [7] 1419-23 (2005).

[19]W. Yang, Z. Xie, H. Miao, L. Zhang, H. Ji, and L. An, "Synthesis of Single-Crystalline Silicon Nitride Nanobelts Via Catalyst-Assisted Pyrolysis of a Polysilazane," *Journal of the American Ceramic Society*, 88 [2] 466-9 (2005).

[20]W. Yang, H. Wang, S. Liu, Z. Xie, and L. An, "Controlled Al-Doped Single-Crystalline Silicon Nitride Nanowires Synthesized via Pyrolysis of Polymer Precursors," *Journal of Physical Chemistry B*, 111 [16] 4156-60 (2007).

[21]W. Yang, Z. Xie, J. Li, H. Miao, L. Zhang, and L. An, "Ultra-Long Single-Crystalline a-Si3N4 Nanowires: Derived from a Polymeric Precursor," *Journal of the American Ceramic Society*, 88 [6] 1647-50 (2005).

[22]Y. Fan, Y. Wang, J. Lou, S. Xu, L. Zhang, L. An, and H. Heinrich, "Formation of Silicon-Doped Boron Nitride Bamboo Structures Via Pyrolysis of a Polymeric Precursor," *Journal of the American Ceramic Society*, 89 [2] 740-2 (2006).

[23]S. Otoishi and Y. Tange, "Effect of a Catalyst on the Formation of SiC Whiskers from Polycarbosilane. Nickel Ferrite as a Catalyst," *Bulletin of the Chemical Society of Japan*, 72 [7] 1607-13 (1999).

[24]S. Otoishi and Y. Tange, "Growth rate and morphology of silicon carbide whiskers from polycarbosilane," *Journal of Crystal Growth*, 200 [3-4] 467-71 (1999).

[25]E. Vanhaecke, S. Ivanova, A. Deneuve, O. Ersen, D. Edouard, G. Wine, P. Nguyen, C. Pham, and C. Pham-Huu, "1D SiC decoration of SiC macroscopic shapes for filtration devices," *Journal of Materials Chemistry*, 18 [39] 4654-62 (2008).

[26]E. Garcia-Bordeje, I. Kvande, D. Chen, and M. Ronning, "Carbon Nanofibers Uniformly Grown on y-Alumina Washcoated Cordierite Monoliths," *Advanced Materials*, 18 [12] 1589-92 (2006).

[27]N. Jarrah, J.G. van Ommen, and L. Lefferts, "Development of monolith with a carbon-nanofiber-washcoat as a structured catalyst support in liquid phase," *Catalysis Today*, 79-80 29-33 (2003).

[28]N.A. Jarrah, J.G. van Ommen, and L. Lefferts, "Growing a carbon nano-fiber layer on a monolith support; effect of nickel loading and growth conditions," *Journal of Materials Chemistry*, 14 [10] 1590-7 (2004).

[29]E. Garcia-Bordeje, I. Kvande, D. Chen, and M. Ronning, "Synthesis of composite materials of carbon nanofibres and ceramic monoliths with uniform and tuneable nanofibre layer thickness," *Carbon*, 45 [9] 1828-38 (2007).

[30]K.M. de Lathouder, T. Marques Fló, F. Kapteijn, and J.A. Moulijn, "A novel structured bioreactor: Development of a monolithic stirrer reactor with immobilized lipase," *Catalysis Today*, 105 [3-4] 443-7 (2005).

[31]K.M. de Lathouder, D. Lozano-Castelló, A. Linares-Solano, F. Kapteijn, and J.A. Moulijn, "Carbon coated monoliths as support material for a lactase from Aspergillus oryzae: Characterization and design of the carbon carriers," *Carbon*, 44 [14] 3053-63 (2006).

[32]M.A. Ulla, A. Valera, T. Ubieto, N. Latorre, E. Romeo, V.G. Milt, and A. Monzón, "Carbon nanofiber growth onto a cordierite monolith coated with Co-mordenite," *Catalysis Today*, 133-135 7-12 (2008).

[33]B. Gong, R. Wang, B. Lin, F. Xie, X. Yu, and K. Wei, "Preparation of Carbon Nanotubes (CNTs)-Cordierite Monoliths by Catalytic Chemical Vapor Deposition as Catalyst Supports for Ammonia Synthesis," *Catalysis Letters*, 122 [3] 287-94 (2008).

[34]J. Wang, R. Wang, X. Yu, J. Lin, F. Xie, and K. Wei, "Preparation and Characterization of Carbon Nanotubes-Coated Cordierite for Catalyst Supports," *Journal of Natural Gas Chemistry*, 15 [3] 211-6 (2006).

[35]K.M. de Lathouder, J. Bakker, M.T. Kreutzer, F. Kapteijn, J.A. Moulijn, and S.A. Wallin, "Structured reactors for enzyme immobilization: advantages of tuning the wall morphology," *Chemical Engineering Science*, 59 [22-23] 5027-33 (2004).

[36]S. Rul, C. Laurent, A. Peigney, and A. Rousset, "Carbon nanotubes prepared in situ in a cellular ceramic by the gelcasting-foam method," *Journal of the European Ceramic Society*, 23 [8] 1233-41 (2003).

[37]A. Cordier, F. Rossignol, C. Laurent, T. Chartier, and A. Peigney, "A new fast method for ceramic foam impregnation: Application to the CCVD synthesis of carbon nanotubes," *Applied Catalysis A: General*, 319 7-13 (2007).

[38]V.G. de Resende, E. De Grave, A. Cordier, A. Weibel, A. Peigney, and C. Laurent, "Catalytic chemical vapor deposition synthesis of single- and double-walled carbon nanotubes from α-(Al1-xFex)2O3 powders and self-supported foams," *Carbon*, 47 [2] 482-92 (2009).

[39]A. Cordier, E. Flahaut, C. Viazzi, C. Laurent, and A. Peigney, "In situ CCVD synthesis of carbon nanotubes within a commercial ceramic foam," *Journal of Materials Chemistry*, 15 [37] 4041-50 (2005).

[40]S. Mukhopadhyay, M., A. Karumuri, and I.T. Barney, "Hierarchical nanostructures by nanotube grafting on porous cellular surfaces," *Journal of Physics D: Applied Physics*, 42 [19] 195503, 9pp (2009).

[41]C. Pham-Huu and M.-J. Ledoux, "Carbon nanomaterials with controlled macroscopic shapes as new catalytic materials," *Topics in Catalysis*, 40 [1] 49-63 (2006).

[42]P.W.A.M. Wenmakers, J.v.d. Schaaf, B.F.M. Kuster, and J.C. Schouten, ""Hairy Foam": carbon nanofibers grown on solid carbon foam. A fully accessible, high surface area, graphitic catalyst support," *Journal of Materials Chemistry*, 18 [21] 2426-36 (2008).

[43]D. Edouard, S. Ivanova, M. Lacroix, E. Vanhaecke, C. Pham, and C. Pham-Huu, "Pressure drop measurements and hydrodynamic model description of SiC foam composites decorated with SiC nanofiber," *Catalysis Today*, 141 [3-4] 403-8 (2009).

[44]M. Scheffler, P. Greil, A. Berger, E. Pippel, and J. Woltersdorf, "Nickel-catalyzed in situ formation of carbon nanotubes and turbostratic carbon in polymer-derived ceramics," *Materials Chemistry and Physics*, 84 [1] 131-9 (2004).

[45]R.S. Wagner and W.C. Ellis, "Vapor-Liquid-Solid Mechanism of Single Crystal Growth," *Applied Physics Letters*, 4 [5] 89-90 (1964).

[46]S. Zhu, H.-A. Xi, Q. Li, and R. Wang, "In Situ Growth of b-SiC Nanowires in Porous SiC Ceramics," *Journal of the American Ceramic Society*, 88 [9] 2619-21 (2005).

[47]X. Yao, S. Tan, Z. Huang, S. Dong, and D. Jiang, "Growth mechanism of b-SiC nanowires in SiC reticulated porous ceramics," *Ceramics International*, 33 [6] 901-4 (2007).

[48]M.G. Segatelli, A.T.N. Pires, and I.V.P. Yoshida, "Synthesis and structural characterization of carbon-rich SiCxOy derived from a Ni-containing hybrid polymer," *Journal of the European Ceramic Society*, 28 [11] 2247-57 (2008).

[49]M.G. Segatelli, E. Radovanovic, M.d.C. Gonçalves, and I.V.P. Yoshida, "Investigation of the morphological changes promoted by heating of Si-C-O ceramics derived from a phenyl-rich hybrid polymer. Effect of Ni in the polymeric precursor," *Journal of the European Ceramic Society*, 29 [15] 3279-87 (2009).

[50]V. Bakumov, M. Schwarz, and E. Kroke, "Emulsion processing of polymer-derived porous Si/C/(O) ceramic bodies," *Journal of the European Ceramic Society*, 29 [13] 2857-65 (2009).

[51]B.-H. Yoon, C.-S. Park, H.-E. Kim, and Y.-H. Koh, "In Situ Synthesis of Porous Silicon Carbide (SiC) Ceramics Decorated with SiC Nanowires," *Journal of the American Ceramic Society*, 90 [12] 3759-66 (2007).

[52]C. Vakifahmetoglu, S. Carturan, E. Pippel, J. Woltersdorf, and P. Colombo, "Growth of 1D-Nanostructures in Porous Polymer Derived Ceramics by Catalyst-Assisted-Pyrolysis. Part II: Cobalt Catalyst," (Submitted to J. Am. Ceram. Soc (2010)).

[53]C. Vakifahmetoglu, E. Pippel, J. Woltersdorf, and P. Colombo, "Growth of 1D-Nanostructures in Porous Polymer Derived Ceramics by Catalyst-Assisted-Pyrolysis. Part I: Iron Catalyst," *Journal of the American Ceramic Society*, (In press, 2009).

[54]C. Vakifahmetoglu and P. Colombo, "Porous Polymer Derived Ceramics Decorated with In-situ Grown Nano-structures," in Proceedings of Pac-Rim 8, *Ceramic Transactions.* Edited, Vancouver, Canada, in press, 2009.

[55]F. Kolár, V. Machovic, and J. Svítilová, "Cobalt-containing silicon oxycarbide glasses derived from poly[methyl(phenyl)]siloxane and cobalt phthalate," *Journal of Non-Crystalline Solids*, 352 [26-27] 2892-6 (2006).

[56]ASTM D 3576, "Standard test method for cell size of rigid cellular plastics," in Annual Book of ASTM Standards, Vol. 08.02. Edited, West Conshohocken, PA., 1997.

[57]Y. Tao, D. Noguchi, C.M. Yang, H. Kanoh, H. Tanaka, M. Yudasaka, S. Iijima, and K. Kaneko, "Conductive and Mesoporous Single-Wall Carbon Nanohorn/Organic Aerogel Composites," *Langmuir*, 23 [18] 9155-7 (2007).

[58]K. Murata, K. Kaneko, F. Kokai, K. Takahashi, M. Yudasaka, and S. Iijima, "Pore structure of single-wall carbon nanohorn aggregates," *Chemical Physics Letters*, 331 [1] 14-20 (2000).

[59]N. Sano, J. Nakano, and T. Kanki, "Synthesis of single-walled carbon nanotubes with nanohorns by arc in liquid nitrogen," *Carbon*, 42 [3] 686-8 (2004).

[60]C. Cioffi, S. Campidelli, C. Sooambar, M. Marcaccio, G. Marcolongo, M. Meneghetti, D. Paolucci, F. Paolucci, C. Ehli, G.M.A. Rahman, V. Sgobba, D.M. Guldi, and M. Prato, "Synthesis, Characterization, and Photoinduced Electron Transfer in Functionalized Single Wall Carbon Nanohorns," *Journal of the American Chemical Society*, 129 [13] 3938-45 (2007).

[61]D.H. Shin, K. Sung, H.H. Seung, S.-H. Choi., and K. Kyung Joong, "Control of amorphous silica nanowire growth by oxygen content of Si-rich oxide," *Nanotechnology*, 21 [4] 045604, 4pp (2010).

[62]Z. Peng, X. Fu, N. Zhu, X. Guo, C. Wang, and Z. Fu, "Preparation and growth mechanism of clustered one-dimensional SiOx amorphous nanowires by catalytic pyrolysis of a polymer precursor," *Journal of Non-Crystalline Solids*, 355 [43-44] 2156-9 (2009).

[63]I. Aharonovich, Y. Lifshitz, and S. Tamir, "Growth mechanisms of amorphous SiOx nanowires," *Applied Physics Letters*, 90 [26] 263109, 3pp (2007).

[64]I. Aharonovich, S. Tamir, and Y. Lifshitz, "Growth of SiOx nanowires by laser ablation," *Nanotechnology*, 19 [6] 065608, 8pp (2008).

[65]Z. Yang, Z. Yu, H. Chen, Z. Jiao, Y. Jin, Y. He, M. Gong, and X. Sun, "Growth of amorphous SiO2 nano-wires on pre-oxidized silicon substrate via chemical vapor deposition," *Journal of Non-Crystalline Solids*, 354 [15-16] 1731-5 (2008).

[66]D.P. Yu, Q.L. Hang, Y. Ding, H.Z. Zhang, Z.G. Bai, J.J. Wang, Y.H. Zou, W. Qian, G.C. Xiong, and S.Q. Feng, "Amorphous silica nanowires: Intensive blue light emitters," *Applied Physics Letters*, 73 [21] 3076-8 (1998).

[67]C.H. Liang, L.D. Zhang, G.W. Meng, Y.W. Wang, and Z.Q. Chu, "Preparation and characterization of amorphous SiOx nanowires," *Journal of Non-Crystalline Solids*, 277 [1] 63-7 (2000).

[68]X.C. Wu, W.H. Song, K.Y. Wang, T. Hu, B. Zhao, Y.P. Sun, and J.J. Du, "Preparation and photoluminescence properties of amorphous silica nanowires," *Chemical Physics Letters*, 336 [1-2] 53-6 (2001).

[69]Y.J. Chen, J.B. Li, Y.S. Han, Q.M. Wei, and J.H. Dai, "A novel morphology of SiOx nanowires with a modified diameter," *Applied Physics A: Materials Science & Processing*, 74 [3] 433-5 (2002).

[70]Z.W. Pan, Z.R. Dai, C. Ma, and Z.L. Wang, "Molten Gallium as a Catalyst for the Large-Scale Growth of Highly Aligned Silica Nanowires," *Journal of the American Chemical Society*, 124 [8] 1817-22 (2002).

[71]F. Quintero, J. Pou, F. Lusquiños, M. Boutinguiza, R. Soto, and M. Pérez-Amor, "Laser synthesis of amorphous Si-Al oxide nanowires under atmospheric conditions," *Applied Surface Science*, 247 [1-4] 631-5 (2005).

[72]J. Zheng, X. Song, X. Li, and Y. Pu, "Large-Scale Production of Amorphous Silicon Oxynitride Nanowires by Nickel-Catalyzed Transformation of Silicon Wafers in NH3 Plasma," *Journal of Physical Chemistry C*, 112 [1] 27-34 (2008).

[73]G. Levi and W. Kaplan, D., "Iron as an Oxygen Tracer at the Aluminum-Alumina Interface," *Journal of the American Ceramic Society*, 85 [6] 1601-6 (2002).

[74]G. Levi and W.D. Kaplan, "Oxygen induced interfacial phenomena during wetting of alumina by liquid aluminium," *Acta Materialia*, 50 [1] 75-88 (2002).

[75]Y.Q. Zhu, W.K. Hsu, M. Terrones, N. Grobert, H. Terrones, J.P. Hare, H.W. Kroto, and D.R.M. Walton, "3D silicon oxide nanostructures from nanoflowers to radiolaria," *Journal of Materials Chemistry*, 8 [8] 1859 - 64 (1998).

[76]A. Leonhardt, S. Hampel, C. Müller, I. Mönch, R. Koseva, M. Ritschel, D. Elefant, K. Biedermann, and B. Büchner, "Synthesis, Properties, and Applications of Ferromagnetic-Filled Carbon Nanotubes," *Chemical Vapor Deposition*, 12 [6] 380-7 (2006).

[77]F. Wang, G.-Q. Jin, and X.-Y. Guo, "Formation Mechanism of Si3N4 Nanowires via Carbothermal Reduction of Carbonaceous Silica Xerogels," *Journal of Physical Chemistry B*, 110 [30] 14546-9 (2006).

[78]T. Takahashi and P. Colombo, "SiOC Ceramic Foams through Melt Foaming of a Methylsilicone Preceramic Polymer," *Journal of Porous Materials*, 10 113-21 (2003).

[79]C. Vakifahmetoglu and P. Colombo, "A Direct Method for the Fabrication of Macro-Porous SiOC Ceramics from Preceramic Polymers," *Advanced Engineering Materials*, 10 [3] 256-9 (2008).

[80]M. Scheffler, T. Gambaryan-Roisman, T. Takahashi, J. Kaschta, H. Muenstedt, P. Buhler, and P. Greil, "Pyrolytic decomposition of preceramic organo polysiloxanes," pp. 239–50 in Proceedings of Innovative Processing and Synthesis of Ceramics, Glasses, and Composites IV (St. Louis, Missouri), Vol. 115, *Ceramic Transactions.* Edited by N. Bansal and J.P. Singhe. The American Ceramic Society, Westerville, Ohio, 2000.

[81]C.G. Pantano, A.K. Singh, and H. Zhang, "Silicon Oxycarbide Glasses," *Journal of Sol-Gel Science and Technology*, 14 [1] 7-25 (1999).

[82]J.R. Robledo-Ortiz, C. Zepeda, C. Gomez, D. Rodrigue, and R. González-Núñez, "Non-isothermal decomposition kinetics of azodicarbonamide in high density polyethylene using a capillary rheometer," *Polymer Testing*, 27 [6] 730-5 (2008).

[83]A.S.P. Lin, T.H. Barrows, S.H. Cartmell, and R.E. Guldberg, "Microarchitectural and mechanical characterization of oriented porous polymer scaffolds," *Biomaterials*, 24 [3] 481-9 (2003).

[84]Q. Huang, R. Klotzer, B. Seibig, and D. Paul, "Extrusion of microcellular polysulfone using chemical blowing agents," *Journal of Applied Polymer Science*, 69 [9] 1753-60 (1998).

[85]C. Vakifahmetoglu, I. Menapace, A. Hirsch, L. Biasetto, R. Hauser, R. Riedel, and P. Colombo, "Highly porous macro- and micro-cellular ceramics from a polysilazane precursor," *Ceramics International*, 35 [8] 3281-90 (2009).

[86]S. Quinn, "Chemical blowing agents: providing production, economic and physical improvements to a wide range of polymers," *Plastics, Additives and Compounding*, 3 16-21 (2001).

[87]G.D. Soraru, S. Modena, E. Guadagnino, P. Colombo, J. Egan, and C. Pantano, "Chemical Durability of Silicon Oxycarbide Glasses," *Journal of the American Ceramic Society*, 85 [6] 1529-36 (2002).

[88]D. Walter and I.W. Karyasa, "Synthesis and Characterization of Cobalt Monosilicide (CoSi) with CsCl Structure Stabilized by a beta-SiC Matrix," *Zeitschrift für anorganische und allgemeine Chemie*, 631 [6-7] 1285-8 (2005).

[89]H.J. Whitlow, Y. Zhang, C.M. Wang, D.E. McCready, T. Zhang, and Y. Wu, "Formation of cobalt silicide from filter metal vacuum arc deposited films," *Nuclear Instruments and Methods in Physics Research Section B: Beam Interactions with Materials and Atoms*, 247 [2] 271-8 (2006).

[90]P. Colombo, M.O. Abdirashid, M. Guglielmi, L. Mancinelli Degli Esposti, and A. Luca, "Preparation of Ceramic composites by active-filler-controlled-polymer-pyrolysis," *Materials Research Society Symposia Proceedings*, 346 403-8 (1994).

[91]Q. Wei, E. Pippel, J. Woltersdorf, M. Scheffler, and P. Greil, "Interfacial SiC formation in polysiloxane-derived Si-O-C ceramics," *Materials Chemistry and Physics*, 73 [2-3] 281-9 (2002).

[92]G. Yang, R. Wu, M. Gao, J. Chen, and Y. Pan, "SiC crystal growth from transition metal silicide fluxes," *Crystal Research and Technology*, 42 [5] 445-50 (2007).

[93]G.-E. Yu, J. Parrick, M. Edirisinghe, D. Finch, and B. Ralph, "Synthesis of silicon oxynitride from a polymeric precursor," *Journal of Materials Science*, 28 [15] 4250-4 (1993).

[94]V. Weeren, E.A. Leone, S. Curran, L.C. Klein, and S.C. Danforth, "Synthesis and Characterization of Amorphous Si_2N_2O," *Journal of the American Ceramic Society*, 77 [10] 2699-702 (1994).

[95]G. Chollon, U. Vogt, and K. Berroth, "Processing and characterization of an amorphous Si–N–(O) fibre," *Journal of Materials Science*, 33 [6] 1529-40 (1998).

[96]M.E. Washburn, "Silicon oxynitride refractories," *American Ceramic Society Bulletin*, 46 667-71 (1967).

[97]H. Wang and G.S. Fischman, "In Situ Synthesis of Silicon Carbide Whiskers from Silicon Nitride Powders," *Journal of the American Ceramic Society*, 74 [7] 1519-22 (1991).

[98]S. Siddiqi and A. Hendry, "The influence of iron on the preparation of silicon nitride from silica," *Journal of Materials Science*, 20 [9] 3230-8 (1985).

[99]P.H. Mutin, "Control of the Composition and Structure of Silicon Oxycarbide and Oxynitride Glasses Derived from Polysiloxane Precursors," *Journal of Sol-Gel Science and Technology*, 14 [1] 27-38 (1999).

[100]T. Gunji, Y. Taniguchi, and Y. Abe, "Preparation of Polysiloxazanes and Their Transformation to Silicon Oxynitride," *Journal of the Ceramic Society of Japan*, 114 [1330] 492-6 (2006).

[101]V.V. Pujar and J.D. Cawley, "Computer Simulations of Diffraction Effects due to Stacking Faults in b-SiC: II, Experimental Verification," *Journal of the American Ceramic Society*, 84 [11] 2645-51 (2001).

[102]P. Colombo, M.O. Abdirashid, M. Guglielmi, L. Mancinelli Degli Esposti, and A. Luca, "Preparation of Ceramic composites by active-filler-controlled-polymer-pyrolysis," *Mat. Res. Soc. Symp. Proc.*, 346 403-8 (1994).

[103]S.J.P. Durham, K. Shanker, and R.A.L. Drew, "Carbothermal Synthesis of Silicon Nitride: Effect of Reaction Conditions," *Journal of the American Ceramic Society*, 74 [1] 31-7 (1991).

[104]T.N. Zabruskova, I.Y. Guzman, and I.A. Dmitriev, "Stability of silicon oxynitride at high temperatures," *Refractories and Industrial Ceramics*, 13 [1] 118-21 (1972).

[105]L.G. Cançado, K. Takai, T. Enoki, M. Endo, Y.A. Kim, H. Mizusaki, N.L. Speziali, A. Jorio, and M.A. Pimenta, "Measuring the degree of stacking order in graphite by Raman spectroscopy," *Carbon*, 46 [2] 272-5 (2008).

[106]A.C. Ferrari, J.C. Meyer, V. Scardaci, C. Casiraghi, M. Lazzeri, F. Mauri, S. Piscanec, D. Jiang, K.S. Novoselov, S. Roth, and A.K. Geim, "Raman Spectrum of Graphene and Graphene Layers," *Physical Review Letters*, 97 [18] 187401, 4pp (2006).

[107]X. Li and M.J. Edirisinghe, "Structural evaluation of polysilane-derived products: from amorphous to thermodynamically stable phases," *Philosophical Magazine*, 84 [7] 647 - 71 (2004).

[108]G. Gundiah, G.V. Madhav, A. Govindaraj, M.M. Seikh, and C.N.R. Rao, "Synthesis and characterization of silicon carbide, silicon oxynitride and silicon nitride nanowires," *Journal of Materials Chemistry*, 12 [5] 1606-11 (2002).

[109]A. Takase and E. Tani, "Infrared and Raman spectroscopic studies of Si3N4-SiC composites," *Journal of Materials Science Letters*, 8 [6] 684-6 (1989).

[110]A.W. Weimer, G.A. Eisman, D.W. Susnitzky, D.R. Beaman, and J.W. McCoy, "Mechanism and Kinetics of the Carbothermal Nitridation Synthesis of α-Silicon Nitride," *Journal of the American Ceramic Society*, 80 [11] 2853-63 (1997).

[111]C.R. Blanchard and S.T. Schwab, "X-ray diffraction analysis of the pyrolytic conversion of perhydropolysilazane into silicon nitride," *Journal of the American Ceramic Society*, 77 [7] 1729-39 (1994).

[112]J. Li and R. Riedel, "Carbothermal Reaction of Silica-Phenol Resin Hybrid Gels to Produce Silicon Nitride/Silicon Carbide Nanocomposite Powders," *Journal of the American Ceramic Society*, 90 [12] 3786-92 (2007).

[113]S.-C. Zhang and W.R. Cannon, "Preparation of Silicon Nitride from Silica," *Journal of the American Ceramic Society*, 67 [10] 691-5 (1984).

[114]A.W. Weimer, K.J. Nilsen, G.A. Cochran, and R.P. Roach, "Kinetics of carbothermal reduction synthesis of beta silicon carbide," *AIChE Journal*, 39 [3] 493-503 (1993).

[115]W.-S. Seo and K. Koumoto, "Stacking Faults in b-SiC Formed during Carbothermal Reduction of SiO_2," *Journal of the American Ceramic Society*, 79 [7] 1777-82 (1996).

[116]X.H. Yan, X.N. Cheng, G.C. Han, R. Hauser, and R. Riedel, "Synthesis and Magnetic Properties of Polymer Derived Metal/SiCN Ceramic Composites," *Key Engineering Materials*, 353-358 1485-8 (2007).

[117]Y. Zhang and D.G. Ivey, "Fe3Si formation in Fe–Si diffusion couples," *Journal of Materials Science*, 33 [12] 3131-5 (1998).

[118]W.M. Tang, Z.X. Zheng, H.F. Ding, and Z.H. Jin, "A study of the solid state reaction between silicon carbide and iron," *Materials Chemistry and Physics*, 74 [3] 258-64 (2002).

[119]K.F. Cai, L.Y. Huang, A.X. Zhang, J.L. Yin, and H. Liu, "Ultra Long SiCN Nanowires and SiCN/SiO2 Nanocables: Synthesis, Characterization, and Electrical Property," *Journal of Nanoscience and Nanotechnology*, 8 6338-43 (2008).

[120]F.J. Narciso-Romero and F. Rodríguez-Reinoso, "Synthesis of SiC from rice husks catalysed by iron, cobalt or nickel," *Journal of Materials Science*, 31 [3] 779-84 (1996).

[121]G. Yang, R. Wu, J. Chen, Y. Pan, R. Zhai, L. Wu, and L. Jing, "Growth of SiC nanowires/nanorods using a Fe-Si solution method," *Nanotechnology*, 18 [15] 155601, 5pp (2007).

[122]Y. Pan, M.X. Gao, F.J. Oliveira, J.M. Vieira, and J.L. Baptista, "Infiltration of SiC preforms with iron silicide melts: microstructures and properties," *Materials Science & Engineering, A*, 359 [1-2] 343-9 (2003).

[123]Y. Sasaki, Y. Nishina, M. Sato, and K. Okamura, "Raman study of SiC fibres made from polycarbosilane," *Journal of Materials Science*, 22 [2] 443-8 (1987).

[124]M.F. Gozzi and I.V.P. Yoshida, "Structural evolution of a poly(methylsilane)/tetra-allylsilane mixture into silicon carbide," *European Polymer Journal*, 33 [8] 1301-6 (1997).

[125]W. Zhou, Y. Zhang, X. Niu, and G. Min, "One-Dimensional SiC Nanostructures: Synthesis and Properties," pp. 17-59 in One-Dimensional Nanostructures, Lecture Notes in Nanoscale Science and Technology, Vol. 3. Edited by Z.M. Wang. Springer, London, 2008.

[126]G. Neuer, "3.3.1.7 Fe-based alloys," pp. 220-9 in Thermal Conductivity of Pure Metals and Alloys. Edited, 1991.

[127]N. Zhu, Z. Peng, C. Wang, Z. Fu, and H. Miao, "Preparation and characterization of bundled one-dimensional Si3N4 single-crystalline nanowires by catalytic pyrolysis of a polymer precursor," *Solid State Sciences*, 11 [6] 1094-7 (2009).

[128]W. Yang, X. Cheng, H. Wang, Z. Xie, F. Xing, and L. An, "Bundled Silicon Nitride Nanorings," *Crystal Growth & Design*, 8 [11] 3921-3 (2008).

[129]V.V. Pujar and J.D. Cawley, "Computer Simulations of Diffraction Effects due to Stacking Faults in β-SiC: II, Experimental Verification," *Journal of the American Ceramic Society*, 84 [11] 2645-51 (2001).

[130]K. Seo, K.S.K. Varadwaj, P. Mohanty, S. Lee, Y. Jo, M.-H. Jung, J. Kim, and B. Kim, "Magnetic Properties of Single-Crystalline CoSi Nanowires," *Nano Letters*, 7 [5] 1240-5 (2007).

[131]S. Bourg, B. Boury, and R.J.P. Corriu, "Mixed Si/C/M/O ceramics from 2,5-disilahexane/metal carbonyl," *Journal of Materials Chemistry*, 8 [4] 1001-6 (1998).

[132]W. Yang, Z. Xie, J. Li, H. Miao, L. Zhang, and L. An, "Ultra-Long Single-Crystalline α-Si3N4 Nanowires: Derived from a Polymeric Precursor," *Journal of the American Ceramic Society*, 88 [6] 1647-50 (2005).

[133]S. Zhu, H.-A. Xi, Q. Li, and R. Wang, "In Situ Growth of β-SiC Nanowires in Porous SiC Ceramics," *Journal of the American Ceramic Society*, 88 [9] 2619-21 (2005).

[134]Y. Qu, J.D. Carter, and T. Guo, "Silica Nanocoils," *Journal of Physical Chemistry B*, 110 [16] 8296-301 (2006).

[135]G.D. Soraru and D. Suttor, "High Temperature Stability of Sol-Gel-Derived SiOC Glasses," *Journal of Sol-Gel Science and Technology*, 14 69-74 (1999).

[136]B.C.P. Li, J.F. Gerald, and Y. Chen, "Synthesis of Silicon Nitride Nanowires by Ball Milling and Annealing," in Proceedings of 30th Annual Condensed Matter and Materials Meeting. Edited by M. Avdeev, Wagga Wagga, 2006, ISBN 1-920791-09-4.

[137]P.C. Silva and J.L. Figueiredo, "Production of SiC and Si3N4 whiskers in C+SiO2 solid mixtures," *Materials Chemistry and Physics*, 72 [3] 326-31 (2001).

[138]S. Esconjauregui, C.M. Whelan, and K. Maex, "Carbon nanotube catalysis by metal silicide: resolving inhibition versus growth," *Nanotechnology*, 18 015602, 11pp (2007).

[139]H.J. Seifert, J. Peng, H.L. Lukas, and F. Aldinger, "Phase equilibria and thermal analysis of Si-C-N ceramics," *Journal of Alloys and Compounds*, 320 [2] 251-61 (2001).

[140]P. Colombo, G.D. Soraru, R. Riedel, and H.J. Kleebe, "Polymer Derived Ceramics. From Nano-Structure to Applications," pp. 489, DESTech Publications, Lancaster, PA, 2009.

[141]A. Berger, E. Pippel, J. Woltersdorf, M. Scheffler, P. Cromme, and P. Greil, "Nanoprocesses in polymer-derived Si-O-C ceramics: Electronmicroscopic observations and reaction kinetics," *Physica Status Solidi A: Applications and Materials Science*, 202 [12] 2277-86 (2005).

[142]M. Kruk and M. Jaroniec, "Gas Adsorption Characterization of Ordered Organic-Inorganic Nanocomposite Materials," *Chemistry of Materials*, 13 [10] 3169 -83 (2001).

[143]S.J. Gregg and K.S.W. Sing, "Adsorption, Surface area and Porosity," pp. 303, Academic Press, London, 1982.

4.3. Selective Etching of PDCs by Halogens.

Published in part: S.-H. Yeon, P. Reddington, Y. Gogotsi, J.E. Fischer, C. Vakifahmetoglu, and P. Colombo, "Carbide-Derived-Carbons with Hierarchical Porosity from a Preceramic Polymer," Carbon, 48 [1] 201-10 (2010).

4.3.1. Introduction

Porous carbon materials are of interest in many applications such as electrodes for batteries or supercapacitors, adsorbents for separation processes or gas storage, and supports for metal nanoparticles. Conventional activated carbon or carbon molecular sieves synthesized by pyrolysis followed by physical or chemical activation of organic precursors at elevated temperatures normally have pore diameters in the sub-nanometer range, or mesopores of several nanometers in size. However, these materials have a relatively broad pore-size distribution in both the micropore and the mesopore range.[1-3] Mesoporous carbons are manufactured using pre-synthesized organic or inorganic templates,[4] in particular, porous silica.[5, 6] But, this technique is expensive and provides low BET surface areas (700-840 m^2/g), albeit with controllable pore sizes in the range 2-20 nm.[5]

Carbide-derived carbons (CDCs) possess tunable pore structures and narrow pore size distributions in the 0.5-2 nm range that can be formed through selective etching of crystalline metal carbides. This chemical etching method generates microporosity which affords high specific surface areas, large pore volumes, and large adsorption capacities. It also allows pore size matching to different molecules.[7-9] Binary or ternary carbides such as TiC, SiC, ZrC, Mo_2C, and Ti_3SiC_2 are important precursors because the CDC porosities obtained can be tuned over a wide range with sub-Å accuracy by varying the chlorine etching temperature from 200-1200 °C. It is recently shown that BET surface areas up to 3300 m^2/g can be obtained by post-synthesis physical or chemical activation, with concomitant improvements for energy storage applications.[10, 11] CDC production and properties are well documented in the literature,[7, 12-18] therefore here it will not be reviewed in detail. Briefly, however; a crystalline structure of metal

carbide M_xC_y is processed by a halogen gas in the temperature range of 200-1200°C to form an amorphous carbon while by product metal halide leaves the system as a gas, see equation (4.3-1) for the chlorination etching reaction, where M denotes metal. A schematic representation for this process is given in **Figure 4.3-1**.[7]

$$M_xC_y(s) + (z/2)Cl_2(g) \rightarrow xMCl_z(g) + yC(s) \qquad 4.3\text{-}1$$

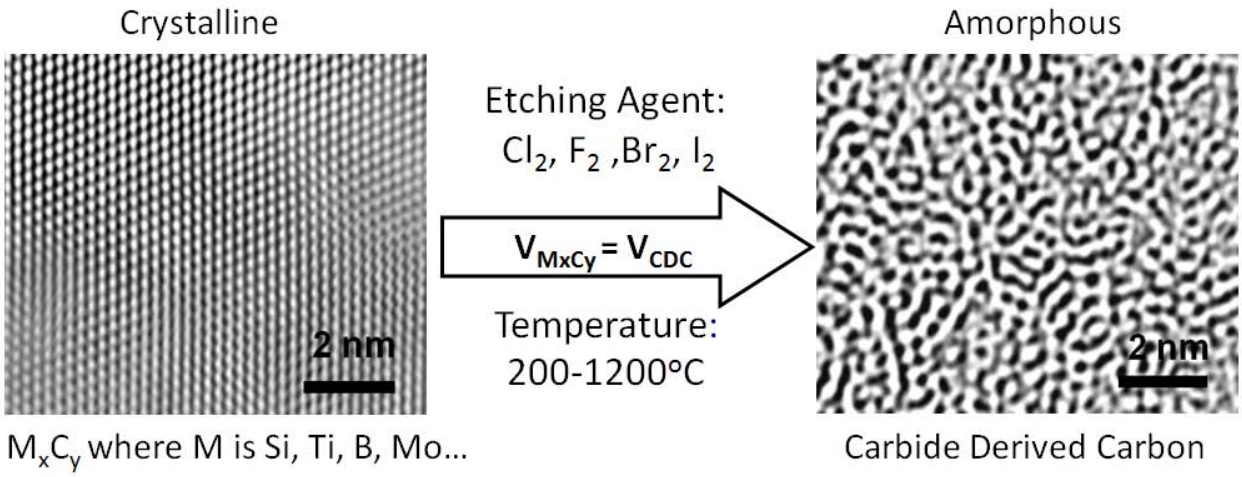

Figure 4.3-1. Etching of metal carbide at high temperature by using chlorine gas.[7]

In this manner, polymer-derived ceramics (PDCs) provide another degree of freedom for optimizing CDC porosity and performance, by controlling the pyrolysis conditions (e.g. temperature) of the preceramic polymer. This results in a precursor with tunable nanostructure, which in turn controls chemical reactions and porosity development during the etching step. Unlike metal carbides, PDCs can be produced by pyrolytic decomposition of a polymeric macromolecular network. These materials, then, can be treated at higher temperature which yield with a phase separation/crystallize (partially/completely) into nano/micro scale phases such as SiC, Si_3N_4, BN, B_4C, etc. depending on the type of the precursor and processing conditions. Etching of this amorphous or phase separated or partially crystallized material may provide different pore sized, high surface area carbon materials. An application of this processing concept to remove silicon from the PDC body has been recently pursued by two different groups

almost in the same time. The first group used polycarbosilane (PCS) precursor to synthesize ordered mesoporous SiC which were obtained by templating the PCS with mesoporous silica (then etching of the silica template) for the production of high SSA carbon forms by high temperature chlorine extraction.[19] The same authors have recently produced ultrathin SiC fibers from PCS precursor as well via electrospinning, then showed that it is possible to obtain high SSA carbon fibers resembling the structure of bare SiC fibers by high temperature Cl_2 etching.[20] Instead during the collaboration between our laboratory and the group of *Prof. Dr. Yury Gogotsi, in* Materials Science and Engineering department of Drexel University, Philadelphia, PA 19104 USA, we have produced several different PDCs from various preceramic precursors such as polysiloxane, polysilazane and boron modified polysilazanes, and then etched these materials at high temperatures by chlorine gas as one can see in the following sub-sections, all the chlorination experiment have been done in the laboratory of *Prof. Dr. Yury Gogotsi* in Drexel University. In this collaboration we aimed to; i) produce high SSA CDCs by two independent strategies: selection and pyrolysis of the PDCs followed by the control of chlorine etching conditions, and ii) get more insights about the nano/micro structural phase evolution of formed PDC materials.

4.3.2. Experimental Procedure

SiCN Ceramic powders were produced by using a commercially available liquid poly(methylvinyl)silazane (PMVSZ, Ceraset™ VL20, KiON Corporation, Clariant, USA). As received polysilazane precursor was poured in aluminum trays and cured at 300 °C for 5 h (with 2°C min^{-1} heating and cooling rate) in inert atmosphere. During this treatment, cross-linking was accomplished thermally without the need of any catalyst or peroxide additions. Infusible polymers were then pyrolyzed under nitrogen (99.999% pure) at temperatures between 600-1550°C holding isothermally for 2h at the peak temperature (2 °C/min heating and cooling rate) in an alumina tube furnace (Lindberg Blue). In a similar way, SiBCN samples prepared from boron modified polysilazane precursor which was synthesized by following the previously published method,[21] and treated at different temperatures in the range from 1100 to 1600°C to vary the phase evolution. It should be underlined here that SiBCN samples are supplied by *Amir*

Tavakoli (University of Stuttgart and Max-Planck-Institute for Metals Research, Heisenbergstr. 3, D-70569 Stuttgart, Germany) within a PolyCerNet collaboration.

Although not only carbide is etched in the present system, we call these materials as Polymer derived ceramic-carbide derived carbons; i.e. PDC-CDC and when a specific PDC is used its abbreviation is replaced instead of using a general PDC term, such as SiCN-CDC to mean carbon obtained from SiCN material via high temperature halogen etching. PDC-CDC powders were produced by chlorination of preceramic polymer-derived SiCN or SiBCN powders (10-50 μm particle size). Ceramic powder was placed in a horizontal tube furnace, purged in Ar flow and rapidly heated at 50 °C min^{-1} to 800/900 or 1200°C, while under the flow of chlorine gas (10-15 cm^3/min) for 3 hours. After chlorination, PDC-CDC powders were annealed at 600°C for 2h under flowing hydrogen, to remove residual chlorine and chlorides trapped in pores. Sample transfer from the furnace to measurement apparatus involved brief exposure to air. Therefore, all measurements were conducted by a degassing consisting of at least 20h at 300°C in 0.2 torr vacuum, sufficient for removing, in our experience, adsorbed water and CO_2.

TGA was performed using a SDT 2960 DTA-TGA from TA instruments and a Perkin Elmer TGA 7. A minimal ambient air flow of 40 mL/min in the temperature range between 25 and 800°C was applied. A heating rate of 2°C/min was chosen for all experiments. Gas adsorption analysis was performed using Quantachrome Instruments Quadrasorb with N_2 adsorbate at 77 K, which is sensitive to pore sizes in the range 1.5-50 nm. Pore size distributions (PSDs) and pore volumes were determined using the non-local density functional theory (NLDFT) method provided by Quantachrome's data reduction software for N_2 isotherms collected at 77 K.[22] For more exact analysis of pores smaller than 1.5 nm, CO_2 adsorbate was used at 273 K. The NLDFT model assumes slit-shaped pores with uniformly dense carbon walls; the adsorbate is considered as a fluid of hard spheres.[22]

Samples were analyzed by micro-Raman spectroscopy (Renishaw 1000) using an Ar ion laser (514 nm) at 20x magnification (~2 μm spot size), 30% defocus, and 10% power. Deconvolution of the Raman spectra was done by using two bands: the D band and the G band of graphite with

the peak fitting by Lorentzian function. *X-ray* diffraction: XRD analysis was done using a Rigaku diffractometer with CuK_α radiation ($\lambda = 0.154$ nm) operated at 30 mA and 40 kV. XRD patterns were collected using step scans, with a step size of 0.01° (2θ) and a count time of 2s per step between 5 (2θ) and 80 (2θ). TEM samples were prepared by dispersing the sample in ethanol and placing the solution over a copper grid with a carbon film, TEM study was performed using the JEOL 2010F microscope at 200 kV. SEM was performed using a Zeiss Supra 50VP Scanning Electron Microscope equipped wtih EDS.

4.3.3. Results and Discussions

4.3.3.1. Etching of polymer derived SiCN ceramics

The changes during processing polysilazane precursors to process SiCN ceramics have been previously explained in detail in Chapter 2. Briefly; polymer-to-ceramic conversion at temperature above 600°C involves decomposition of cross-linked PMVSZ with intermediate moieties such as Si-CH_3, N-H and Si-H. Methane and hydrogen are the major volatile by-products of mineralization. Pyrolysis in the 800 to 1200°C range produces a ternary amorphous Si-C-N material (a-SiCN) consisting mainly of tetrahedral SiC_xN_y (x+y=4) units, and significant volume reduction. Further heat treatments under flowing N_2 promotes structural rearrangements in the amorphous phase leading to the formation of ordered Si-N and Si-C rich regions, in addition to the turbostratic carbon.[23, 24] Crystallization is promoted when these regions exceed the critical nucleation radius.[25] The composition of the amorphous material obtained from similar polysilazane precursor at 1000°C locates on the right-hand side of the N-SiC tie line. Therefore, according to the phase equilibrium in the ternary Si-C-N, at T <1450°C; Si_3N_4, SiC and carbon are thermodynamically stable, while at lower temperatures, N_2 stabilizes Si_3N_4 relative to SiC.[26] Above 1450°C, only Si_3N_4 and SiC are stable (under N_2) and excess carbon reacts with Si_3N_4 to form SiC (note that if the pyrolysis atmosphere is Ar then SiC will be the only stable phase above 1450°C). Si_3N_4 decomposes into liquid silicon and nitrogen at 1876°C,[27] more details about the SiCN phase evolution can be found in Chapter 2.

4.3.3.1.1. Low Temperature (600-1400°C) Pyrolyzed SiCN ceramics.

The pyrolyzed products first characterized in detail to understand their structural and chemical background, in **Figure 4.3-2** XRD plots of the as pyrolyzed SiCN samples are given. As seen crystallization, or phase separation into amorphous Si-C and Si-N domains, begins at 1200°C with further development at 1400°C. At this temperature some peaks that can be resolved to graphitic carbon ~26° (2θ) assigned with "C" in the graphs, β-SiC and Si_3N_4 (both α and β polymorphs) ~35° (2θ) became noticeable.

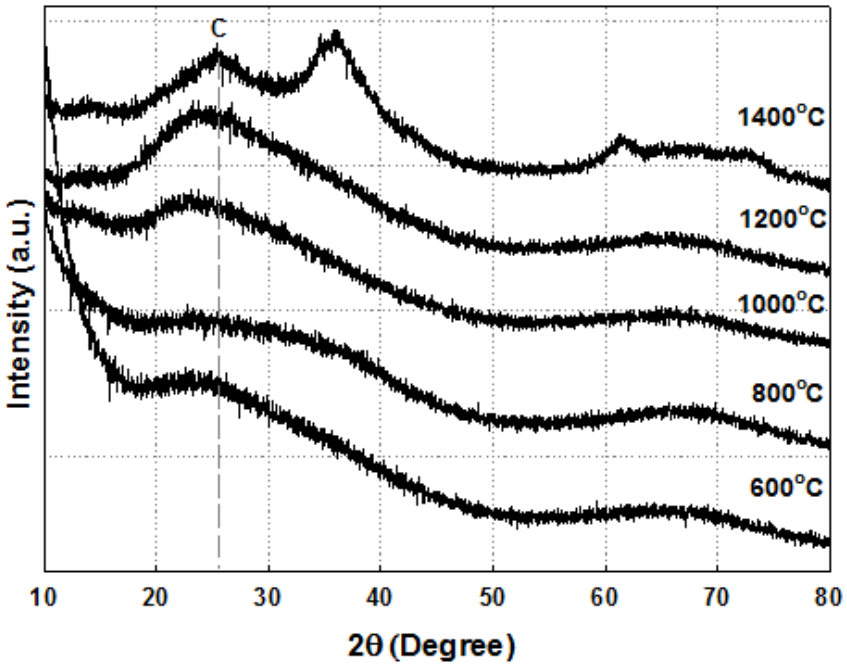

Figure 4.3-2. a) XRD plots of as pyrolyzed samples at different temperatures, "C" marks the (002) plane of graphite.

Raman spectra of the samples are given in **Figure 4.3-3**(a). Seemingly "free carbon" precipitates above around 1000°C, and the sample exhibits very weak D (~1350 cm^{-1}, breathing mode) and G (~1582 cm^{-1}, in-plane vibrational mode) bands,[28, 29] indicating traces of turbostratic carbon. The carbon becomes more ordered with increasing pyrolysis temperature up to 1400°C, ultimately exhibiting narrow G and D peaks. The 1400°C spectrum reveals two distinct components. One is

attributable to disordered amorphous carbon, while the other shows anomalously narrow G and D bands, along with a very intense D band originating from a double resonance effect by defects.[30] In this spectrum, a distinct shoulder at 1620 cm^{-1}, close to the G band, is attributed to the D´ band which corresponds to the highest wavenumber feature in the density of states indicating forbidden structure under defect-free conditions [30, 31]. In the second-order region, three combination modes 2689 (2D), 2938 (D+G), and 3219 cm^{-1} (D´) were observed. These distinct Raman spectra at SiCN pyrolyzed at 1400 °C are fairly consistent with the features of carbon nanowalls (CNWs). From Lorentzian fits, the intensity ratio of D and G bands (I_D/I_G) and the G bandwidth (FWHM) was found as ~3 and ~40 cm^{-1}, respectively (depending on the spot values can change roughly). Typical CNWs grown by plasma-enhanced chemical vapor deposition have I_D/I_G ratios of 2.5-3.5 and narrow G-band FWHM (30-40 cm^{-1}) of G band.[32] FTIR spectra of precursor powders pyrolyzed at different temperatures are shown in **Figure 4.3-3** (b). As the pyrolysis temperature increases, major peaks of C-H (2965-2893 cm^{-1}), Si-H (2140 cm^{-1}), and C-N (1266 cm^{-1}) depresses, disappearing completely at 1400 °C pyrolysis.

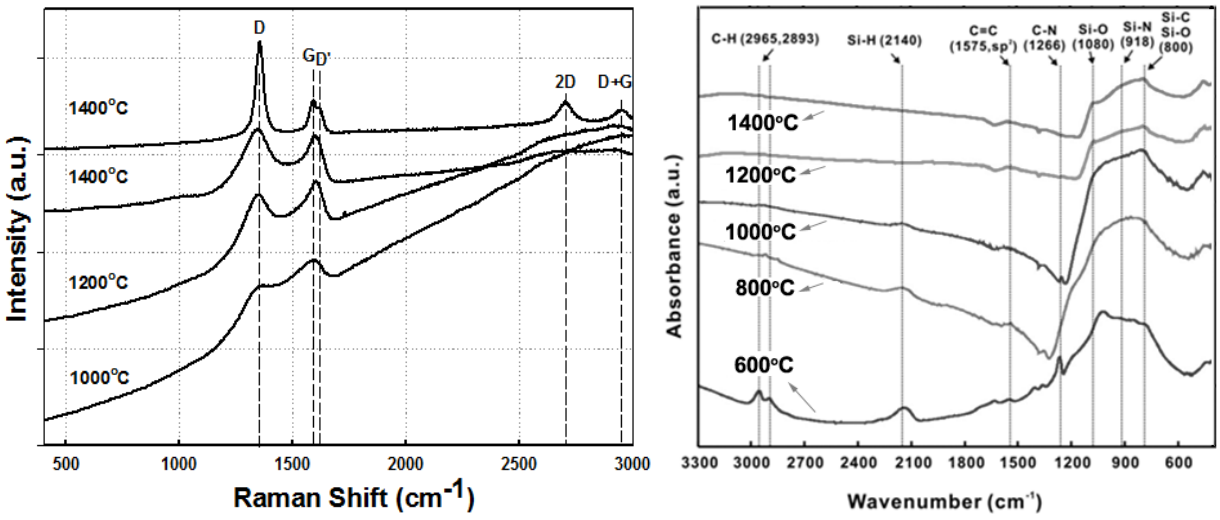

(a) (b)

Figure 4.3-3. a) RAMAN and b) FTIR spectra of SiCN ceramics pyrolyzed at 600-1400°C/N_2.

In **Figure 4.3-4** (a) and (b) SEM images are given for as-pyrolyzed SiCN ceramics treated at 1000°C and 1400°C, respectively. Samples are homogeneous and dense with no SEM observable

macroporosity. The roughness of the fracture surfaces increases with the increase in thermal treatment temperature, implying the evolution of the crystalline phases. TEM investigations applied to the samples treated at 1000°C and 1400°C are given in **Figure 4.3-5** (a) and (b), respectively. While 1000°C pyrolyzed sample shows completely amorphous nature, 1400°C treated samples demonstrates both crystalline domains (marked with white circles in the figure) and turbostratic carbon regions (marked with irregularly shaped white borders in the figure), supporting both XRD and Raman data. Most of the observed crystalline regions are SiC with interplanar distance 0.204-0.225 nm corresponding to the (111) lattice spacing of β-SiC.

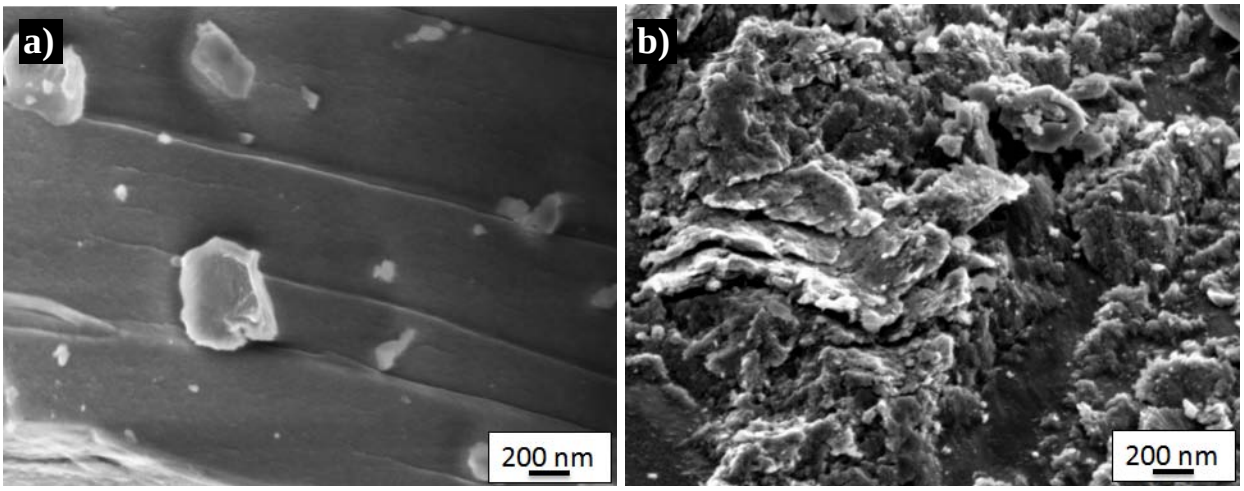

Figure 4.3-4. SEM images taken from the fracture surfaces of the samples treated at a) 1000°C and b) 1400°C both in N_2.

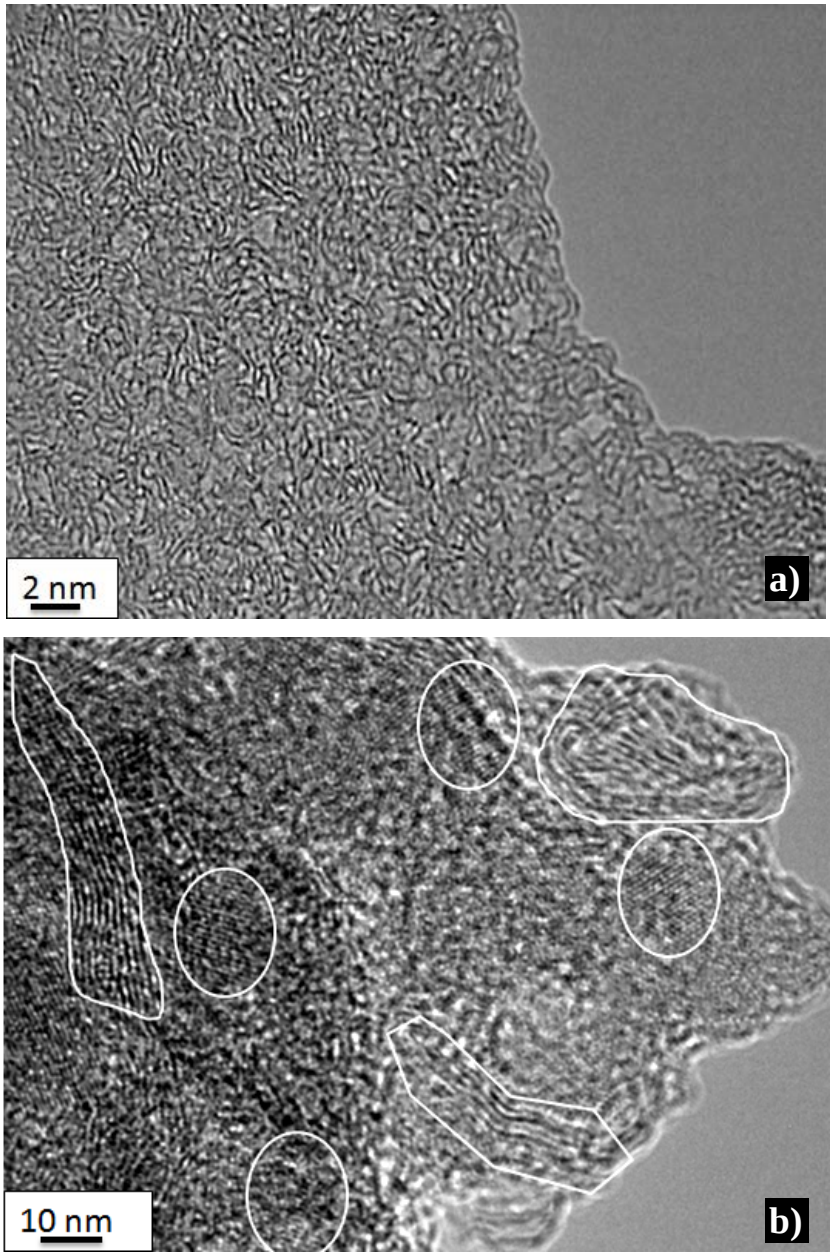

Figure 4.3-5. TEM overview of the samples treated at a) 1000°C and b) 1400°C, in the figure white circles shows crystalline domains, while irregular white borders marks turbostratic carbon regions.

Therefore as one can see the characteristics of the porosity that will be obtained after etching at high temperature, can be controlled by varying the pyrolysis temperature, as this affects the

structure of the ceramic material at nanoscale, see a schematic illustration of the microstructural development of PMVS derived SiCN ceramic in the temperature range between 1000 and ~1400°C given in **Figure 4.3-6**.

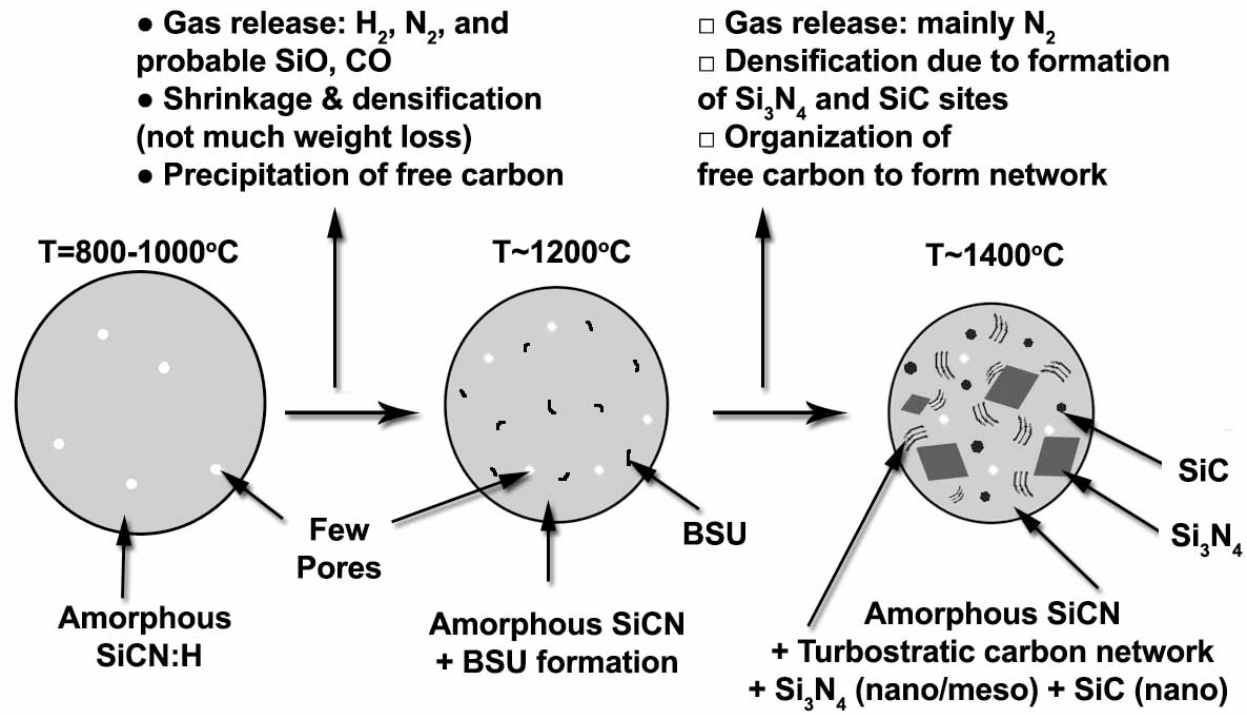

Figure 4.3-6. Schematic illustration of the microstructural development of PMVSZ derived SiCN ceramic in the temperature range between 800-1400°C.

Chlorination temperature is an important parameter and as could be seen from the TGA data obtained under air (given in **Figure 4.3-7**), an incomplete chlorination occurs when chlorination is done at 600 and 800°C with a mass residue > 80%. The particle sizes of all SiCN ceramics were between 10 and 50 μm. More effective chlorination depends on the chlorination kinetic determined by the diverse effects of the precursor particle size, reaction temperature, time, chlorine flow rate, and so on. Therefore, in the following experiments, chlorination temperature is selected > 800°C to ensure high amount of leaching.

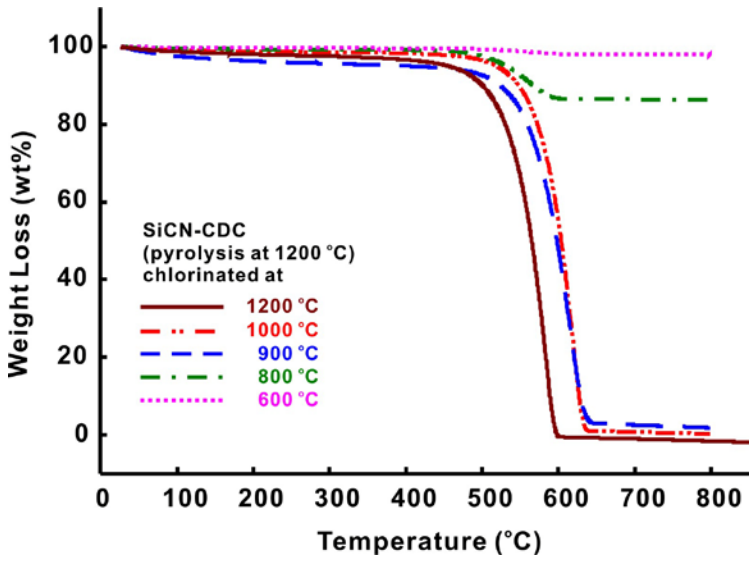

Figure 4.3-7. TGA results (oxidation in air) of SiCN ceramic pyrolyzed at 1200 °C as a function of the chlorination temperature (from 600 °C to 1200 °C).

CDCs from SiCN ceramics (SiCN-CDCs) were produced by chlorination at 900°C or 1200°C, Si and N were eliminated as $SiCl_4$ and N_2, leaving behind a nanoporous network of >98% carbon. Two types of etching reactions occurred, depending on the structural evolution of the SiCN ceramics, which in turn is controlled by pyrolysis conditions. Up to 1200°C, CDC forms from the amorphous SiCN *via* the decomposition reaction given in equation (4.3-2), while for the material obtained upon 1400°C additional reactions may occur as given in equation (4.3-3) and (4.3-4):

$$2SiCxNy + 4Cl_2(g) \rightarrow 2SiCl_4(g) + yN_2(g) + 2xC(s) \qquad 4.3\text{-}2$$

$$SiC + 2Cl_2(g) \rightarrow SiCl_4(g) + C(s) \qquad 4.3\text{-}3$$

$$Si_3N_4 + 6Cl_2(g) \rightarrow 3SiCl_4(g) + 2N_2(g) \qquad 4.3\text{-}4$$

The XRD patterns of SiCN-CDC materials after chlorination at 900°C and 1200°C are given in Figure 4.3-8 (a) and (b). As seen, chlorination was complete as indicated by the disappearance of the diffraction peaks resolved previously for the Si_3N_4 and SiC phases. A very broad peak at 2θ ~26 ° corresponds to the diffraction from the (002) planes of graphite. It seems that, both Si and N has been probably leached out, and C atoms self-organized into an amorphous or disordered, mainly sp^2-bonded, structure. In the etching conditions of the PDC nanocomposite products; concerning the reactions given in equation (4.3-3) and (4.3-4), it seem that SiC leaves behind carbon atoms and so microporosity forms, but instead Si_3N_4 completely disappears, giving rise to the formation of larger pores (probably mesopores, i.e. >2nm) and higher pore volumes.

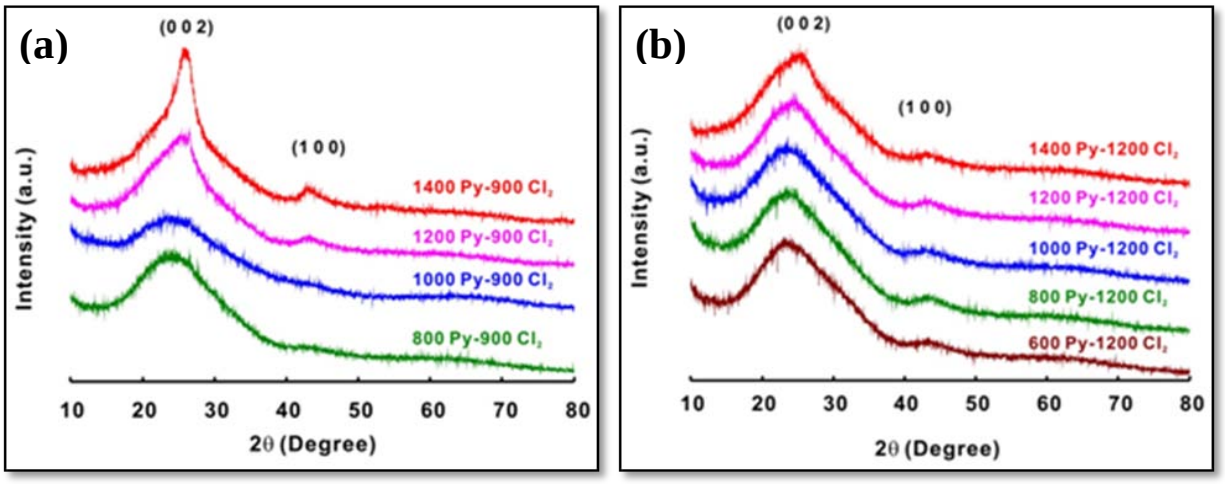

Figure 4.3-8. The XRD patterns of SiCN-CDC after chlorination at a) 900°C, and b) 1200°C.

While the CDC from SiCN pyrolyzed at temperatures <1200°C showed a homogenous carbon matrix (see **Figure 4.3-9** (a) and (b) for the SEM images of the 1000°C pyrolyzed and 900°C chlorinated sample), CDC from SiCN pyrolyzed at 1400°C revealed the presence of micro-voids with a diameters of about 0.3 to 2.6 µm, evolution of these pores are still elusive but might be originate from the PDC system inherently, see **Figure 4.3-9** (c) and (d) for the SEM images of the 1400°C pyrolyzed 900°C chlorinated sample.

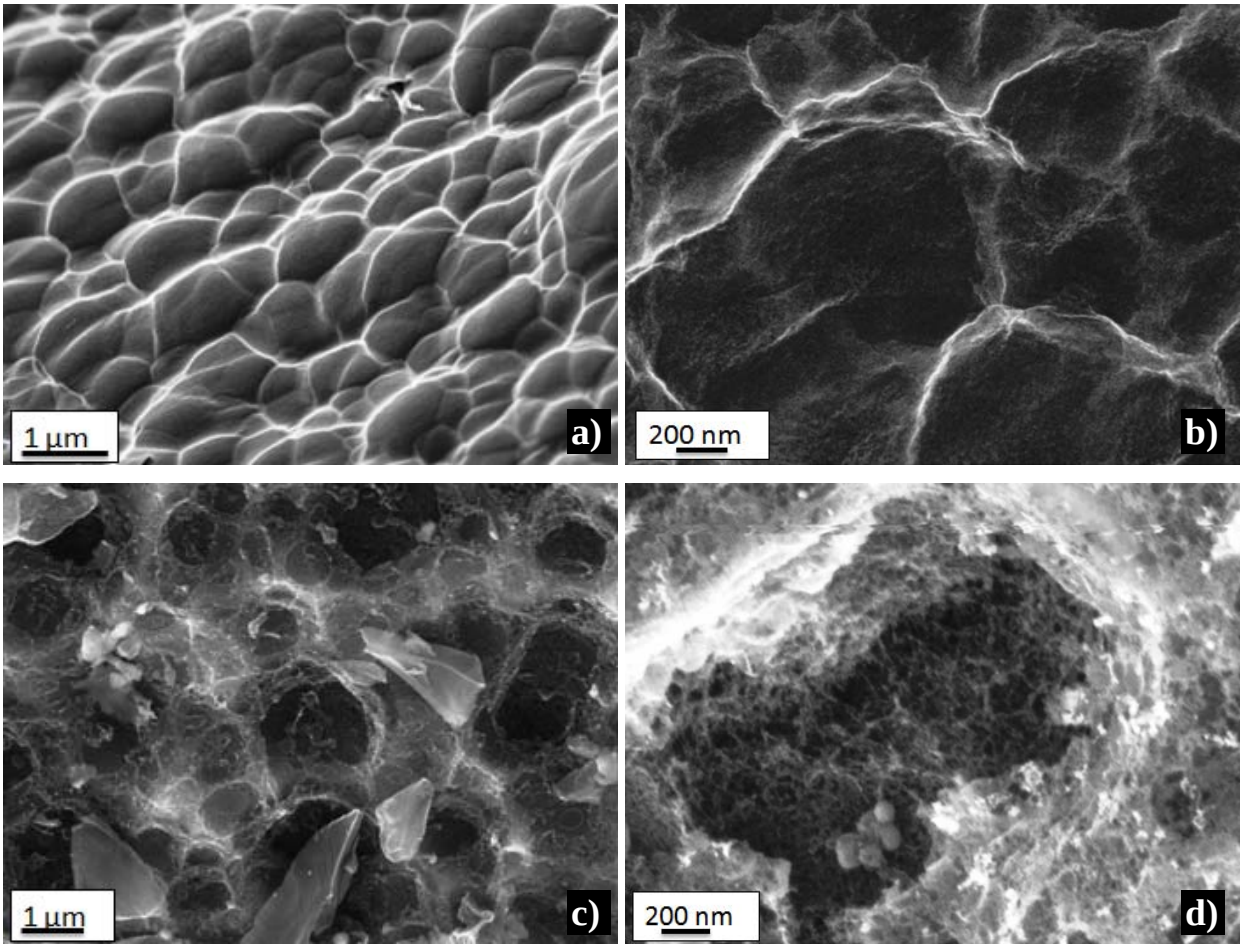

Figure 4.3-9. SEM images of the 900°C chlorinated SiCN samples; a) 1000°C pyrolyzed sample, b) higher magnification image of the same sample, c) 1400°C pyrolyzed sample, d higher magnification image of the same sample.

The composition of the SiCN-CDCs was evaluated by energy dispersive spectroscopy (EDS) **Table 4.3-1**) Unreacted Si element was detected below 10 at% profoundly in 900°C chlorinated samples together with un-removed Cl atom. No nitrogen atom was found by EDS in all SiCN-CDC samples.

Table 4.3-1. EDS analysis of SiCN-CDCs.

Pyrolysis temperature [°C]	**800**	**1000**	**1400**	**600**	**800**	**1200**	**1400**
Chlorination temperature [°C]	**900**			**1200**			
C (at%)	92.85	91.58	91.58	94.87	96.23	98.25	99.57
Si (at%)	6.63	5.33	5.33	4.65	6.63	-	-
Cl (at%)	0.53	3.29	3.29	0.47	0.53	1.75	0.43

Raman spectra of the SiCN-CDC materials produced by 900°C chlorination of precursors pyrolyzed between 800-1400°C are given in **Figure 4.3-10**. As seen, after etching in between 800°C to 1200°C, most SiCN-CDCs show G and D band of amorphous graphite, while SiCN-CDC obtained from SiCN pyrolyzed at 1400°C retains its inherit carbon structure, i.e. already precipitated turbostratic carbon domains as already demonstrated by TEM analysis in Figure 4.3-5 (b).

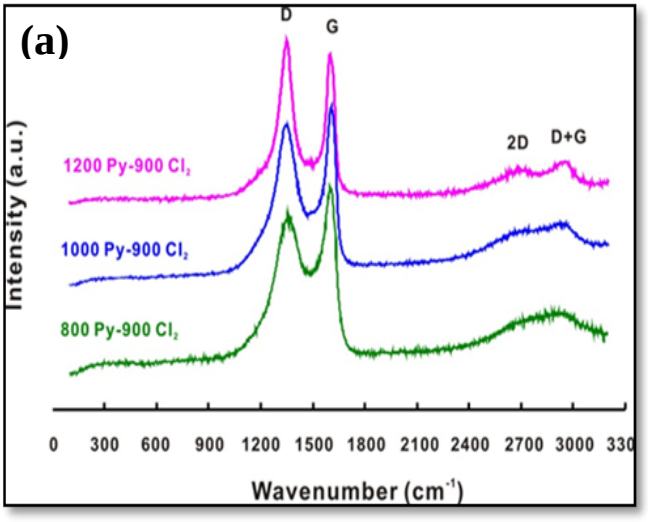

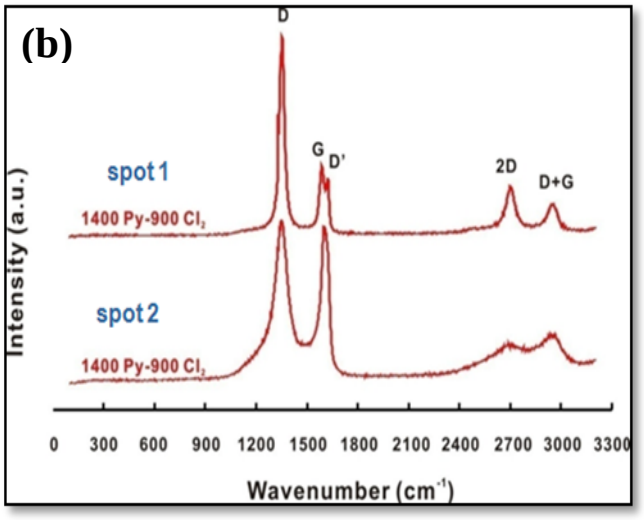

Figure 4.3-10. Raman spectra of SiCN-CDC materials produced by 900°C chlorination of precursors pyrolyzed a) between 800-1200°C, b) 1400°C.

TEM of SiCN-CDC material produced by 1200°C chlorination of SiCN pyrolyzed at 1400°C is given in Figure 4.3-11 (a), likewise 900°C chlorinated SiCN (pyrolyzed at 1400°C) is given in Figure 4.3-11 (b), and similarly TEM image of SiCN (pyrolyzed at 1000°C) and chlorinated at 900C is shown in Figure 4.3-11 (c). As seen, after etching, the SiCN-CDC formed mesopores ~5–20 nm in diameter, as well as ordered curved sheets of graphite (see **Figure 4.3-11**(a)) with interplanar spacing 0.36 nm (see **Figure 4.3-11**(b)), which is slightly higher than the interplanar spacing of graphite (002) planes; 0.335 nm, produced from the crystalline SiC material by chlorine etching method.[25] These ordered sheets result primarily from the high pyrolysis temperature and are insensitive to chlorination conditions; in contrast, pyrolysis at lower temperature invariably leads to amorphous carbon and mesopores in the 2–5 nm range (see **Figure 4.3-11** (c)).

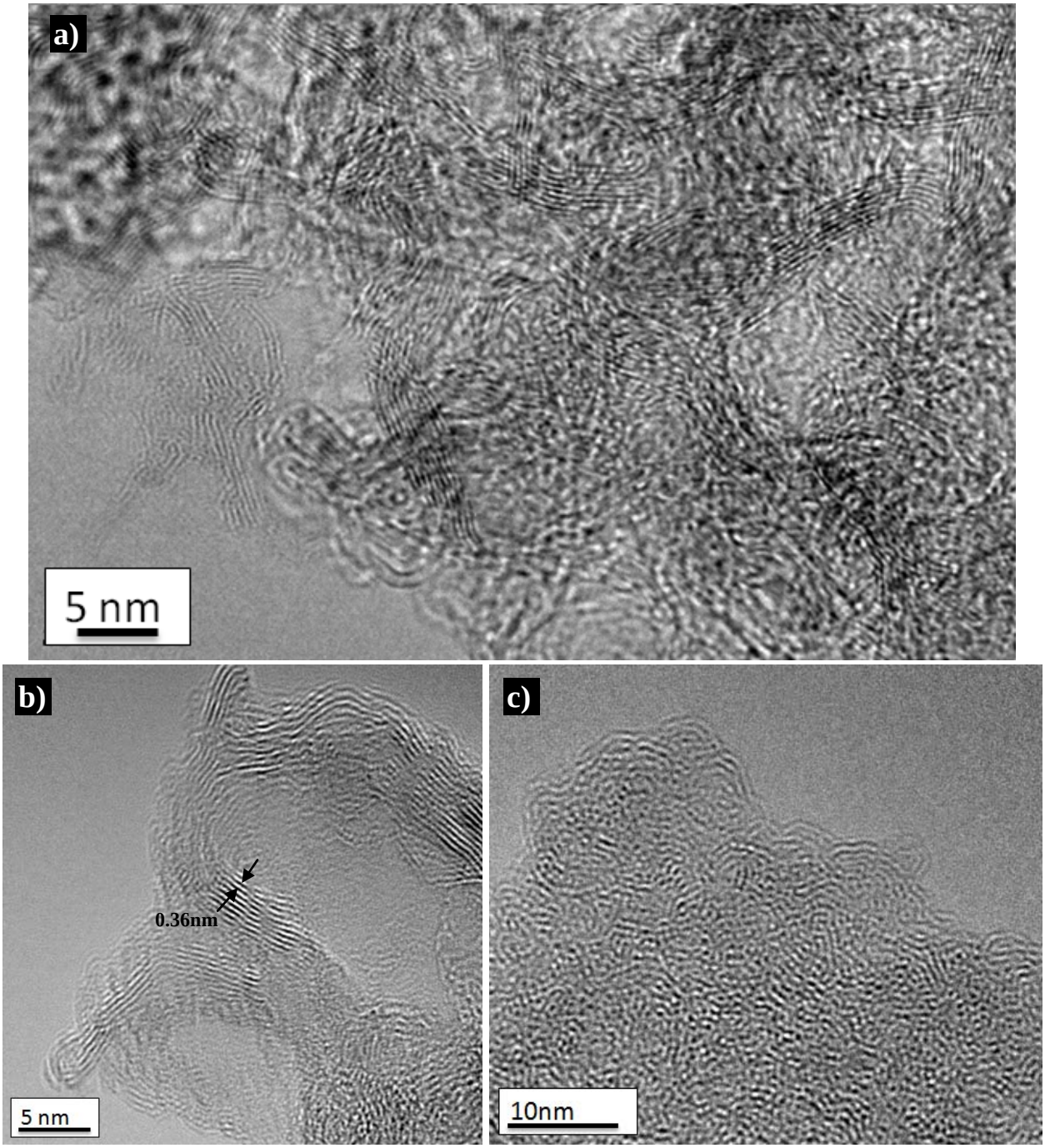

Figure 4.3-11. TEM of SiCN-CDC materials produced by a) 1200°C chlorination of PDC pyrolyzed at 1400°C, b) 900°C chlorination of PDC pyrolyzed at 1400°C, and c) the same chlorination condition for 1000°C pyrolyzed powder.

Figure 4.3-12 shows the N_2 adsorption-desorption isotherms and the estimated pore-size distributions (PSD) of SiCN-CDCs obtained from SiCN precursors pyrolyzed between 600 to 1400°C, determined from CO_2 and N_2 sorption isotherms using NLDFT model assuming slit shaped pores. The marked hysteresis observed in the nitrogen adsorption (**Figure 4.3-12** (a) and (d)) confirms the presence of mesoporosity. All SiCN-CDCs possessed some portion (< 20%) of microporosity (< 1.5 nm), which decreases with increasing pyrolysis temperature as shown in **Table 4.3-2**. The PSDs are quite narrow and bimodal, with peaks centered around 3.5-5.0 nm (mesopores) and 0.6 nm (micropores). In the mesopore range above 1.5 nm, PSDs shift to larger pore size with increasing pyrolysis temperature. Etching at 900°C (**Figure 4.3-12** (b)) led to larger mesopores, which can be tuned in a range from 3 to 10 nm, depending on the pyrolysis temperature (**Figure 4.3-14**(d)). This is not observable in samples etched at 1200°C. The formation of porosity after etching evidently depends directly on the mesostructure of the polymer-derived ceramic. SiCN samples pyrolyzed below 1000°C are fully amorphous. While rearrangement of amorphous domains (especially Si-N) appeared in the sample pyrolyzed at 1200°C, nano-sized SiC, Si_3N_4 and graphite are evident after pyrolysis at 1400°C. Etching at 900°C of a-SiCN pyrolyzed below 1000°C formed 2-4 nm mesopores due to the removal of Si and N atoms homogeneously distributed throughout the amorphous SiCN phase. An increase in mesopore size (4-8 nm) was observed after etching of SiCN pyrolyzed at 1200°C, which indicates the initiation of structural rearrangements (phase separation) and/or chemical degradation (N_2 release) of the formed PDC.[33] The fact that 1200°C chlorination following pyrolysis below 1200°C gives the same pore size distribution indicates that the microstructure has enough time, at this high etching temperature, to evolve to an arrangement characteristic of 1200°C pyrolysis. Therefore, in order to take full advantage of the controllable microstructural development in the PDC, from homogenous and amorphous, to phase separated and amorphous, to nano-crystalline, the etching temperature should not exceed the pyrolysis temperature. In particular, the removal of Si_3N_4 and atomic Si by etching a nano-crystalline SiCN sample pyrolyzed at 1400°C leads to larger pores than those derived from etching an amorphous SiCN phase. It seems that observed mesopores originate from etching Si_3N_4 nanocrystals and/or amorphous Si-N domains, while etched SiC leaves behind a microporous carbon phase. It should be noted that carbon derived from conventional polycrystalline SiC ceramics under the same

conditions has only micropores, with an average size of about 0.8 nm and a narrow PSD.[7] A broader distribution of micropores can be attributed to the disordered structure of amorphous SiC, while larger pores are due to the presence of Si-N species in the SiCN ceramic.

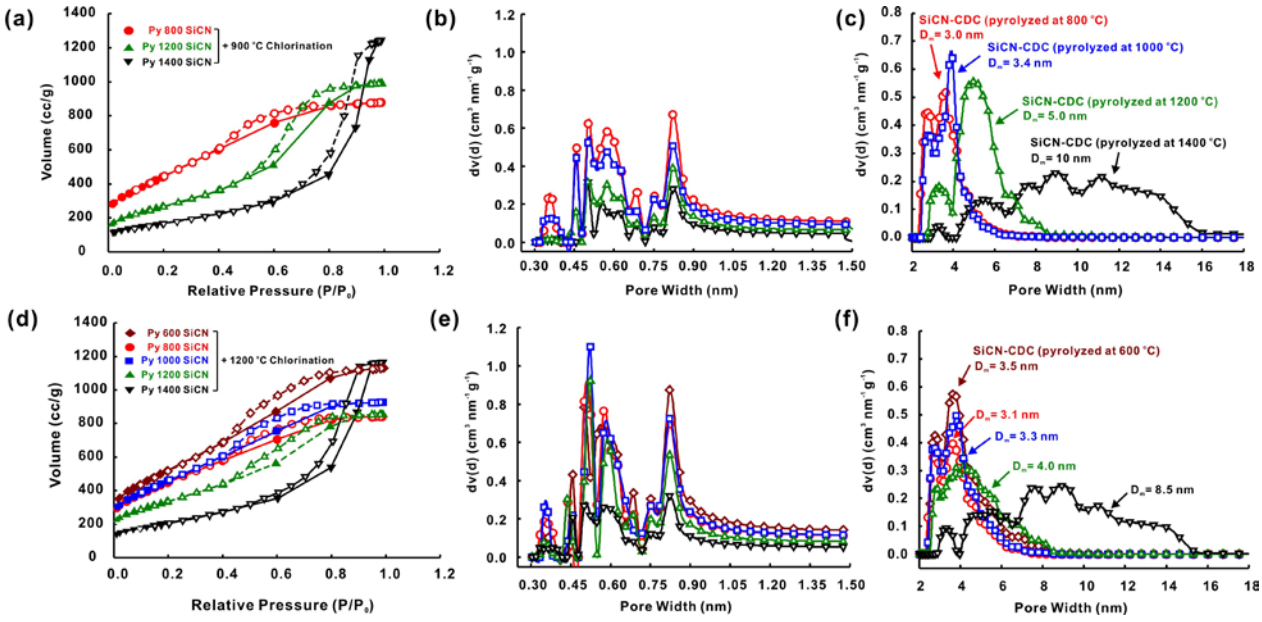

Figure 4.3-12. N_2 adsorption-desorption isotherms for SiCN (Py: pyrolyzed temperature)-CDCs; a) etched at 900°C, b) PSD in micropore range, c) PSD in mesopore range; d) etched at 1200°C , e) PSD in micropore range, f) PSD in mesopore range. Solid symbols correspond to adsorption and empty symbols to desorption of nitrogen. PSD is estimated by NLDFT method using CO_2 and N_2 adsorption after chlorination. The mean pore size (D_m) is also indicated.

Table 4.3-2. Porosity characteristics of SiCN-CDCs, obtained by N_2 and CO_2 gas adsorption technique.

Pyrolysis temperature [°C]	**800**	**1000**	**1200**	**1400**	**600**	**800**	**1000**	**1200**	**1400**
Chlorination temperature [°C]	**900**				**1200**				
Pore volume (ccg^{-1})	1.26	1.16	1.45	1.86	1.6	1.2	1.33	1.24	1.75
Micropore volume (ccg^{-1}) (<1.5 nm) [a]	0.25	0.20	0.13	0.086	0.3	0.27	0.27	0.195	0.12
Mesopore volume(ccg^{-1}) (>1.5 nm) [a]	0.99	0.96	1.36	1.82	1.3	0.87	1.02	1.02	1.67
Meso/Micropore volume ratio	3.96	4.8	10.46	21.2	4.3	3.2	3.8	5.23	13.9
Mean pore size, D_m, (nm)	3	3.4	5	10	3.5	3.1	3.3	4.0	8.5
BET SSA (m^2/g)	**1628**	**1800**	**1245**	**780**	**2433**	**2116**	**2147**	**1559**	**956**

[a]while IUPAC classification designates pores < 2 nm as micropores, we compared pore volumes measured by CO_2 (<1.5 nm) and N_2 (> 1.5 nm).

It is clear that as the pyrolysis temperature decreases, the specific surface area (SSA), especially etching at 1200°C, increases leading to a value as high as 2400 m^2/g for the sample pyrolyzed at 600°C (temperature at which the material is not yet fully ceramized), as reported in **Table 4.3-2** and also in **Figure 4.3-13**. This can be explained considering that a PDC material, when it is pyrolyzed at low temperatures, contains micro- and meso- porosity which gives rise to BET SSA values of a few hundred m^2/g, here we observed SSA of ~400 m^2/g for the sample treated at 600°C. This porosity develops from the release of decomposition gases during the polymer to ceramic transition (typically 600 to 800°C), and is usually eliminated when the material reaches higher temperatures (> 800°C), see **Figure 4.3-13**.[34] The etching process is evidently affected by

the previous presence of this transient porosity in the samples. Therefore, in addition to pore size, we have shown here that pyrolysis temperature affects the total pore volume and SSA as well. Increasing the etching temperature leads to higher SSA because of the more efficient removal of Si and N atoms, while it does not have a significant effect on the mean pore size which is largely controlled by the microstructure of the precursor.

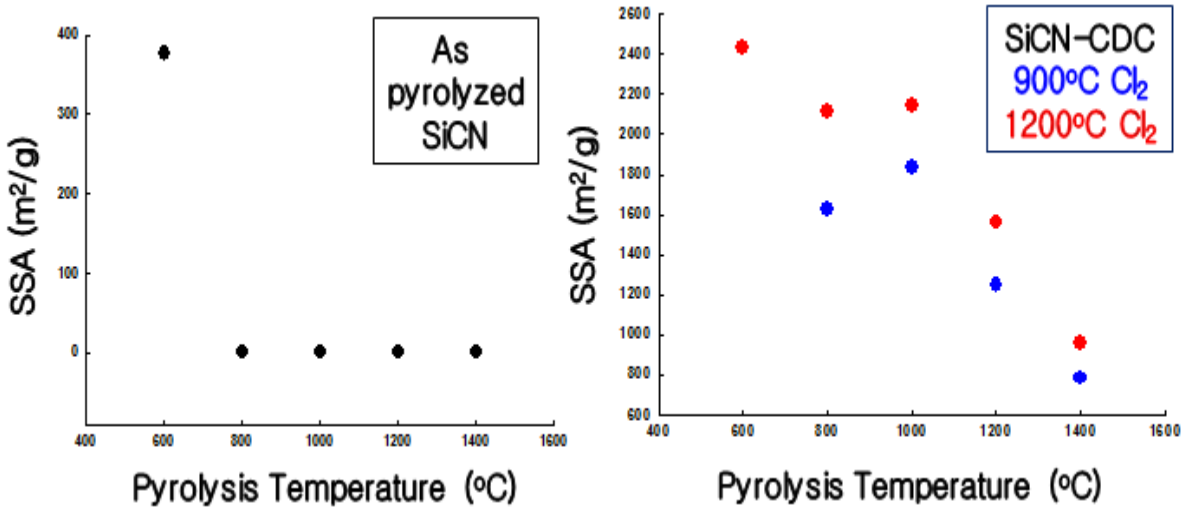

(a) (b)

Figure 4.3-13. Pyrolysis temperature versus SSA values for; a) as pyrolyzed SiCN powders, and b) after chlorination at either 900°C or 1200°C.

A schematic formation mechanism of hierarchical micro and meso-pore structure, derived from the above discussion is postulated in **Figure 4.3-14**. It is envisioned that this novel approach, which takes advantage of the complex precursor microstructure, tailorable at the nano-scale level, could be applied to other systems derived from preceramic polymers, such as SiC from polycarbosilanes, SiBNC from boron-modified polysilazanes.

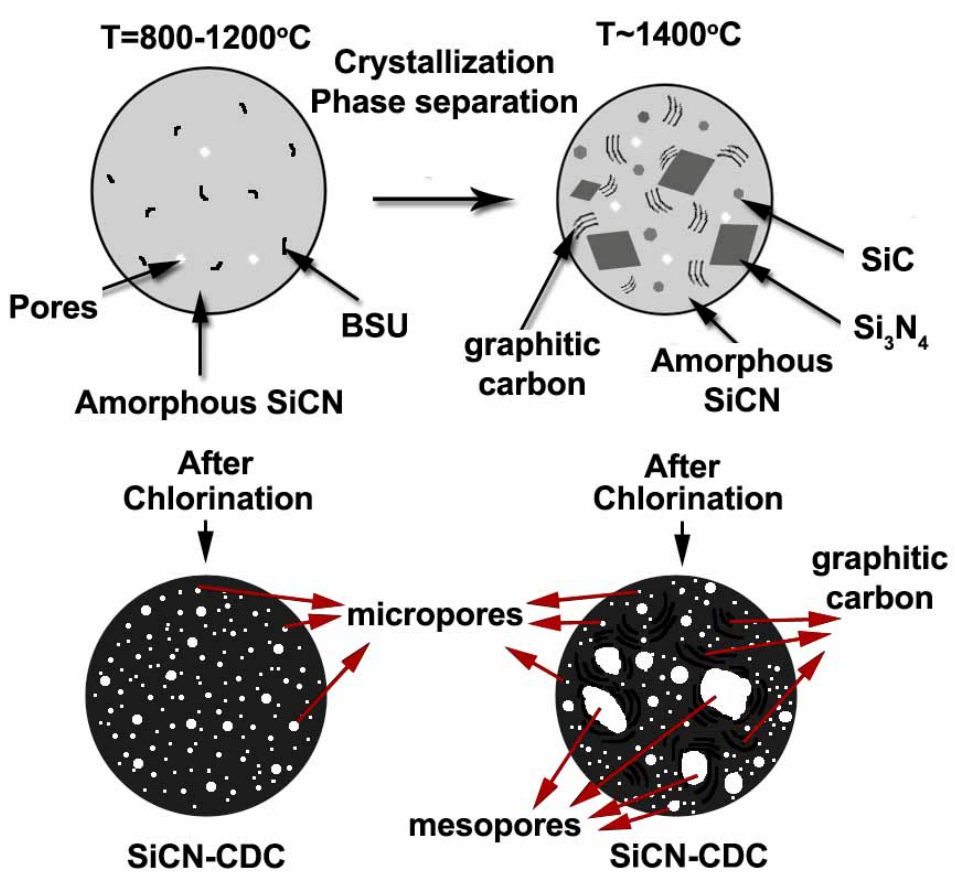

Figure 4.3-14. Schematic representation for the formation of CDCs with hierarchical pore structure from etching of a polymer-derived SiCN ceramic. A silicon-based polymer precursor is ceramized by pyrolysis. The pyrolysis temperature determines the microstructure at the nano-scale of the SiCN material and controls the porosity characteristics in SiCN-CDCs.

In the following experiments, etching of shaped components (e.g. SiCN foams rather than powders) has been carried out. In **Figure 4.3-15**), digital photo images of as pyrolyzed and chlorinated (see insets therein) foam monoliths are given, images show that it is possible to retain the macroscopic morphology of the PCDs after etching, this may supply significant advantages for the development of engineered components for various applications.

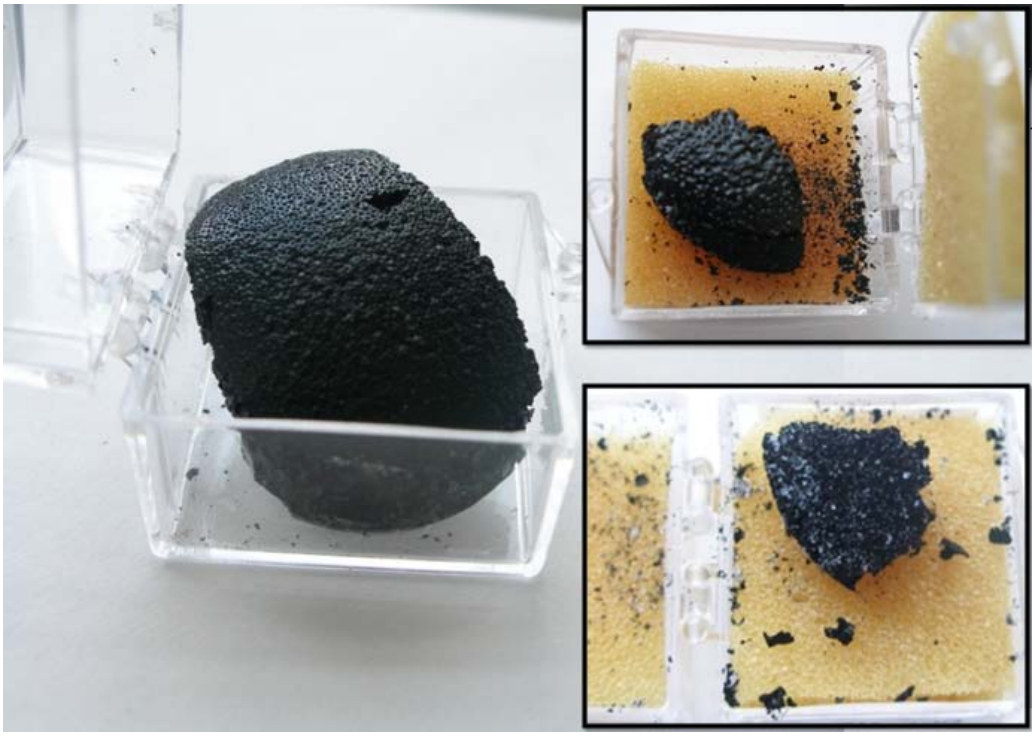

Figure 4.3-15. Digital photo images of the as pyrolyzed (1200°C) SiCN foam, top-right inset) SiCN-CDC chlorinated at 900°C, and bottom-right inset) chlorinated at 1200°C.

4.3.3.1.2. High Temperature (1450-1550°C) Pyrolyzed SiCN ceramics.

It is envisioned during the previos results that further heat treatments at higher temperature may increase the size of Si-N domains leading to larger pore size in the meso-range. Therefore, we processed some additional samples at temperatures between 1450-1550°C by 50°C steps in N_2 atmosphere (one sample additionally treated at 1550°C under Ar) and followed the same procedure to produce SiCN-CDC materials. In **Figure 4.3-16** (a) and (b) SEM images of the as pyrolyzed samples in N_2 and Ar are shown, respectively. While the one treated under N_2 shows some roughness that we already observed for the samples treated at 1400°C, the one pyrolyzed under Ar atmosphere exhibits visible crystalline flakes which are most probably SiC (see later).

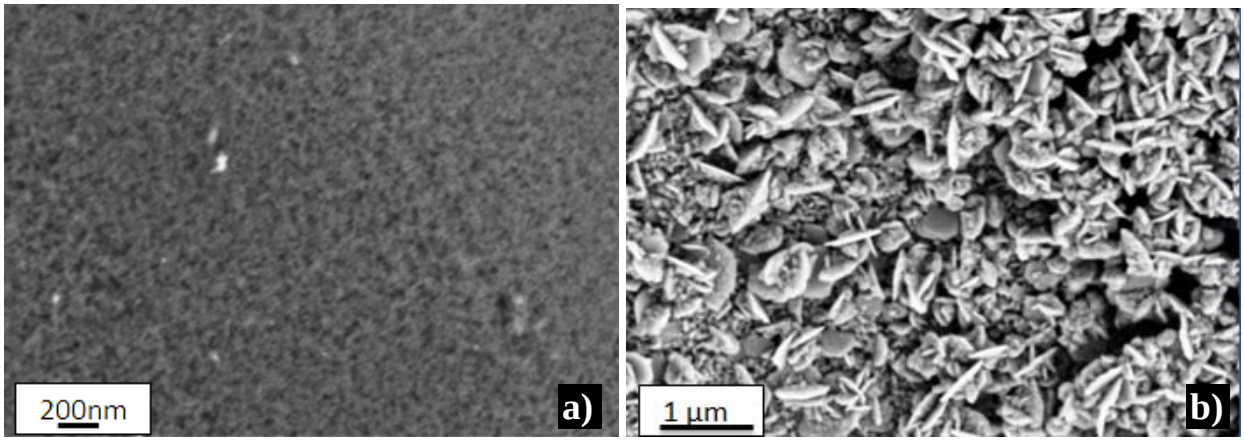

Figure 4.3-16. SEM images of the samples treated at 1550°C; a) in N_2 and b) in Ar.

XRD data obtained from as pyrolyzed (1450-1550°C) and CDC materials chlorinated at different temperatures (800-1200°C) are given in **Figure 4.3-17** (a-d). As seen increasing the pyrolysis temperature (in N_2) clearly induced better crystallization. We previously have shown that the crystallization/phase separation already start below around 1400°C in PMVSZ derived SiCN ceramic when thermolysis is done under N_2. Here, it is clearly shown that further increase from 1400°C to 1550°C yields with an apparent polycrystalline material including graphitic carbon, β-SiC and Si_3N_4 (both α and β polymorphs), see **Figure 4.3-17** (a). As expected, pyrolysis under Ar atmosphere yields with a ceramic including only β-SiC upon pyrolysis at 1550°C, see **Figure 4.3-17** (b).

The effect of chlorination temperature is also documented; see **Figure 4.3-17** (a), while 800°C chlorination was not enough to leach out all phases/domains, above this temperature (≥1000°C) generally high yield of CDC is obtained. Interestingly, 800°C chlorination results with a material that can be though as Si_3N_4-carbon composite, it seems that Si-C is etched out but Si-N remained in the structure, implying that the etching conditions were not sufficient enough to leach out higher bond energy Si-N domains (bond energy ~355 kJ/mol) but instead it was enough to etch Si-C domains (bond energy 318 kjoule/mol).[35, 36] When etching temperature is increased to 1000°C both of these domains are leached out and remaining material became X-ray amorphous

with a halo around 26° (2θ); i.e. most probably pure CDC. Therefore, in the following experiments; either 1000°C or 1200°C is selected as an etching temperature to produce CDC.

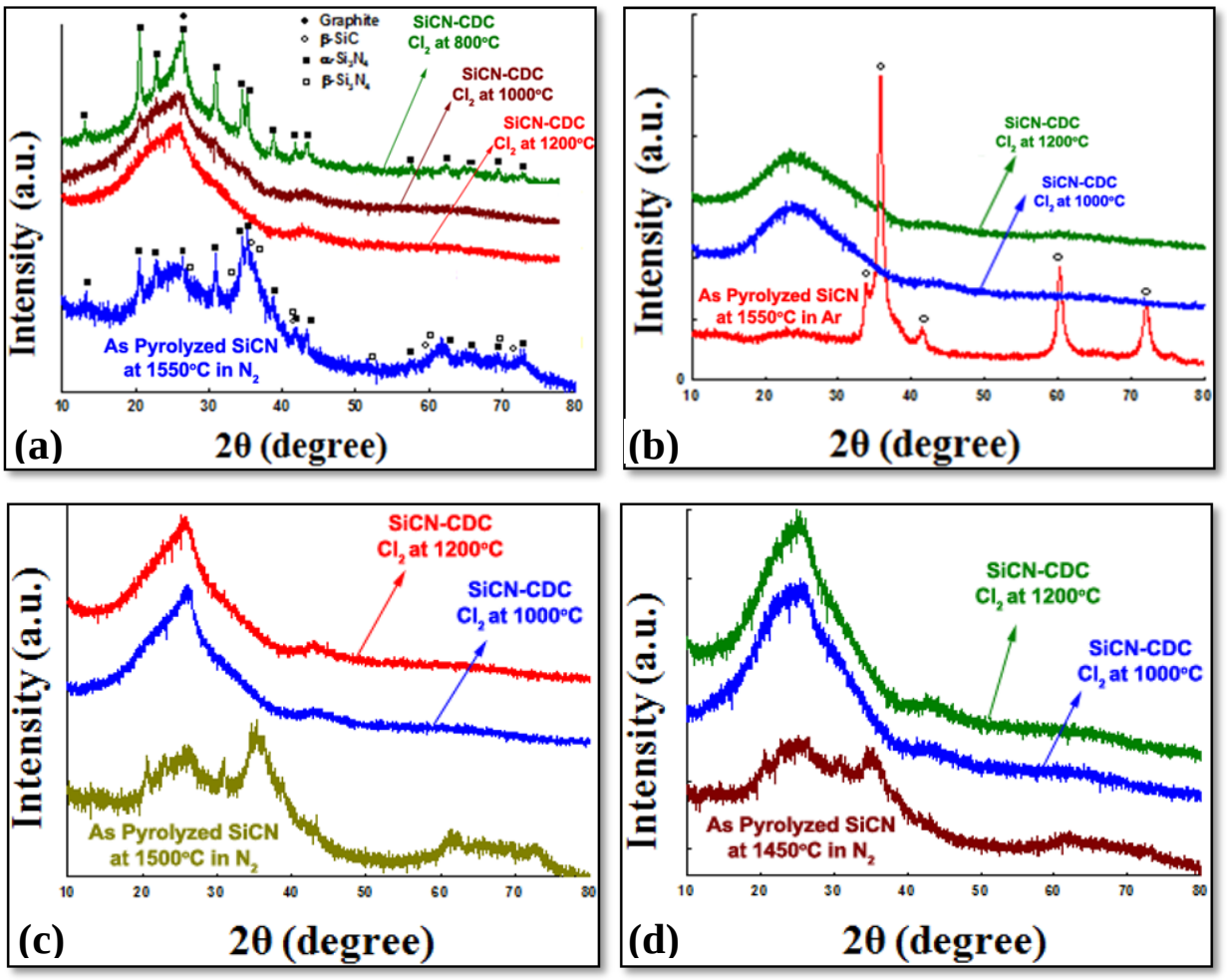

Figure 4.3-17. The XRD patterns of as pyrolyzed SiCN and SiCN-CDC after chlorination at different temperatures; a) sample pyrolyzed at 1550°C in N_2, b) 1500°C in N_2, c) 1450°C in N_2, and d) 1550°C in Ar. All SiCN-CDCs were annealed by H_2 gas at 600 ^{o}C for 2h before XRD test.

Raman data were similar to the previous observations, after etching at 800 and 1200°C, most SiCN-CDCs showed G and D band of amorphous graphite together with graphitic carbon, see **Figure 4.3-18** (a). Similarly, the data for the sample treated under Ar given in **Figure 4.3-18** (b), showed very intense D (implying high amount of disordering in carbon), G, 2D and D+G peaks

together with some peaks in between 700-1000 cm^{-1} which can be attributable to the SiC structure.[37] This implies that relatively (to carbon) higher amount of SiC is formed under Ar treatment since these peaks are not observed for the samples treated under N_2. After chlorination at 1200°C these peaks of SiC completely removed and the remaining material only showed carbon peaks of D and very intense G, a peak marked with "*" could not be assigned and can be due to experimental error or C-H bending.

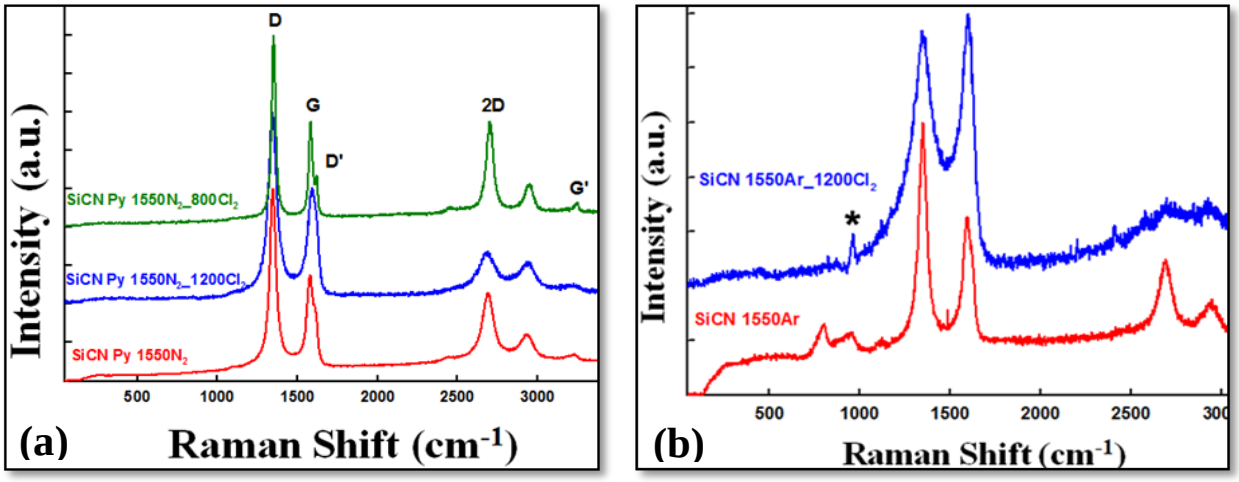

Figure 4.3-18. Raman spectra of as pyrolyzed (at 1550°C) SiCN and SiCN-CDC after chlorination at different temperatures; a) in N_2, and b) in Ar. All SiCN-CDCs were annealed by H_2 gas at 600 ^oC for 2h, before the application of test.

TEM images of SiCN-CDC materials produced from 1200°C chlorination of SiCN materials treated at 1450°C or 1550°C and either in Ar or N_2 are given in Figure 4.3-19. After etching, SiCN-CDC includes mesopores of ~10 nm in diameter, as well as ordered curved sheets of graphite (see **Figure 4.3-19**(a) and (b)). Similar to the previous observations (obtained after etching of 1400°C treated samples) these ordered sheets result from the PDC itself and are insensitive to chlorination conditions; in contrast, pyrolysis under Ar atmosphere yielded with less amount of turbostratic sheets, concurrently with the Raman data, yielding with more amorphous carbon after chlorination, see **Figure 4.3-19** (c) and (d).

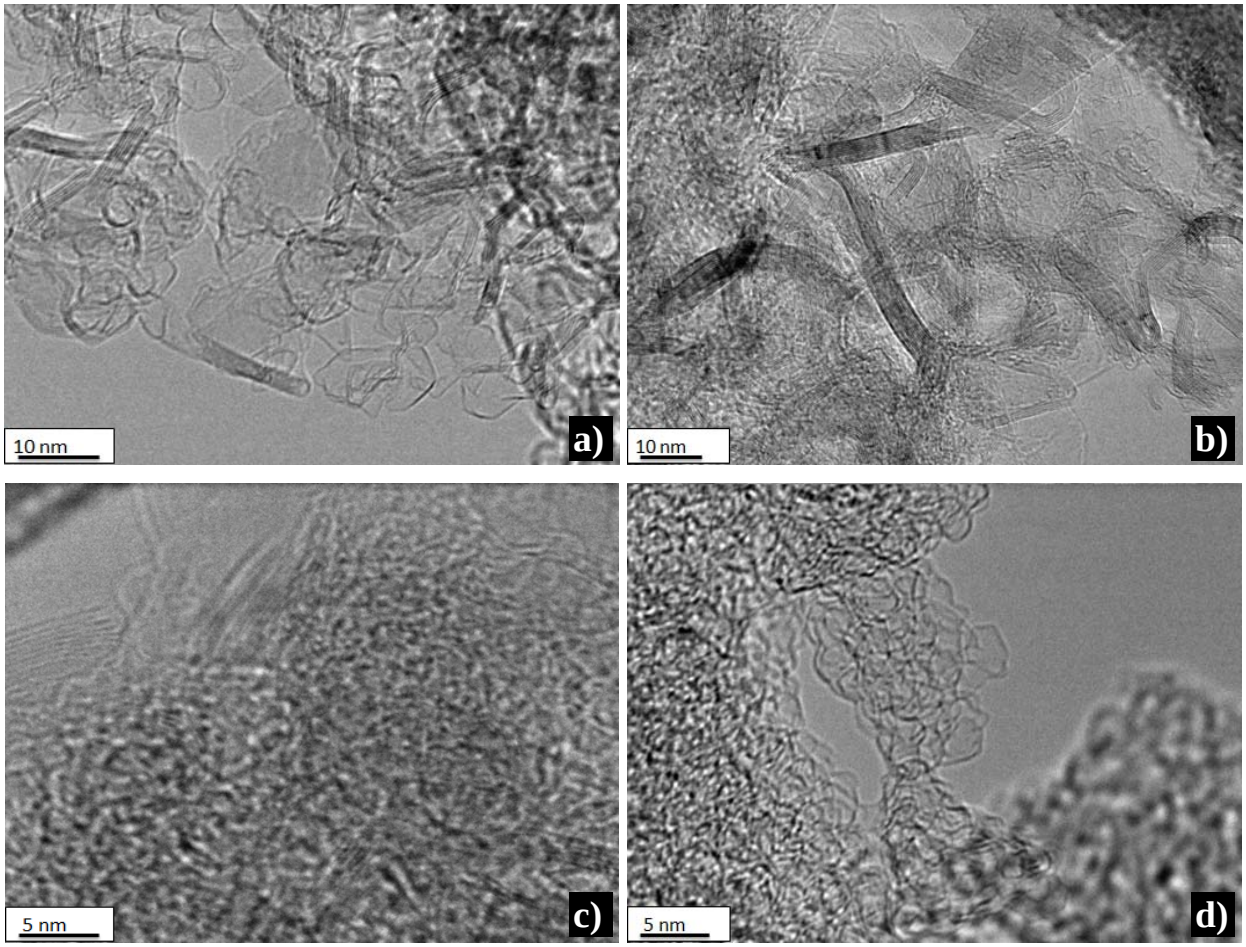

Figure 4.3-19. TEM of SiCN-CDC materials produced from 1200°C chlorination of ceramic powders obtained by the pyrolysis of a) 1450°C in N_2, b) 1550°C in N_2, and c&d) 1550°C in Ar.

Figure 4.3-20 (a) shows the N_2 adsorption-desorption isotherms of SiCN-CDCs obtained from SiCN precursors pyrolyzed in between 1450°C to 1550°C and either in Ar or N_2. Hystereses observed in the isotherms confirm the presence of mesoporosity like the samples pyrolyzed at lower temperatures (≤1400°C). Moreover, Ar treated samples displayed a high N_2 uptake in the low pressure range, associated with the presence of microporosity, as can be seen from the **Figure 4.3-20** (b), where it is shown that all the SiCN-CDCs possess some portion of micropores (< 1.0 nm), which were not affected from the pyrolysis temperature but more by the pyrolysis atmosphere, as shown in **Figure 4.3-20** (b). The PSDs are quite narrow and trimodal, with peaks centered on ~0.4, ~0.6, and ~0.8 nm (micropores) which is more intense in Ar treated samples

than that of N_2 treated ones. In the mesopore range above 1.5 nm, PSDs remains stable with the change in pyrolysis temperature but affected by the pyrolysis atmosphere. Pores are in a wide range but generally located ~10nm, see **Figure 4.3-20** (c). Moreover, for all the samples treated in N_2 between 1450-1550°C slightly bigger size mesopores ~8.5-11.0 nm were obtained compared to the samples pyrolyzed at lower temperature (~1400°C). This implies that although the domain/crystalline size of Si-N structures increased to some extent comparing to that of the samples pyrolyzed at 1400°C, at around 1450°C the maximum phase separation occurred in the ceramics, and therefore the Si-N regions came to their final size. Above that temperature, only crystallization occurred and evidently, the passage from amorphous to crystalline did not change the domain size of the Si-N regions. This is concurrent with the findings showing that the diffusion kinetics is for SiCN ceramics are very slow, and therefore grain growth (crystal growth) of the Si_3N_4 domains (crystals) is generally remains very small.[38] All the data extracted from these isotherms are given in **Table 4.3-3**. Parallel to the previous observations, the formation of porosity after etching was found to depend directly on the nanostructural phase evolution of the PDC. SiCN samples pyrolyzed under Ar had only Si-C domains/crystals which after etching yielded with mostly microporosity, instead the removal of Si-N in the samples treated under N_2 leads to larger pores than those derived from etching an amorphous SiCN phase treated under N_2 and also crystalline ones treated under Ar. Together with the previous results obtained from the samples treated at lower temperatures under N_2 atmospehre, it is here proved that mesopores originate from leaching of Si-N nanocrystals and/or amorphous Si-N domains, while etched SiC leaves behind a microporous carbon phase.

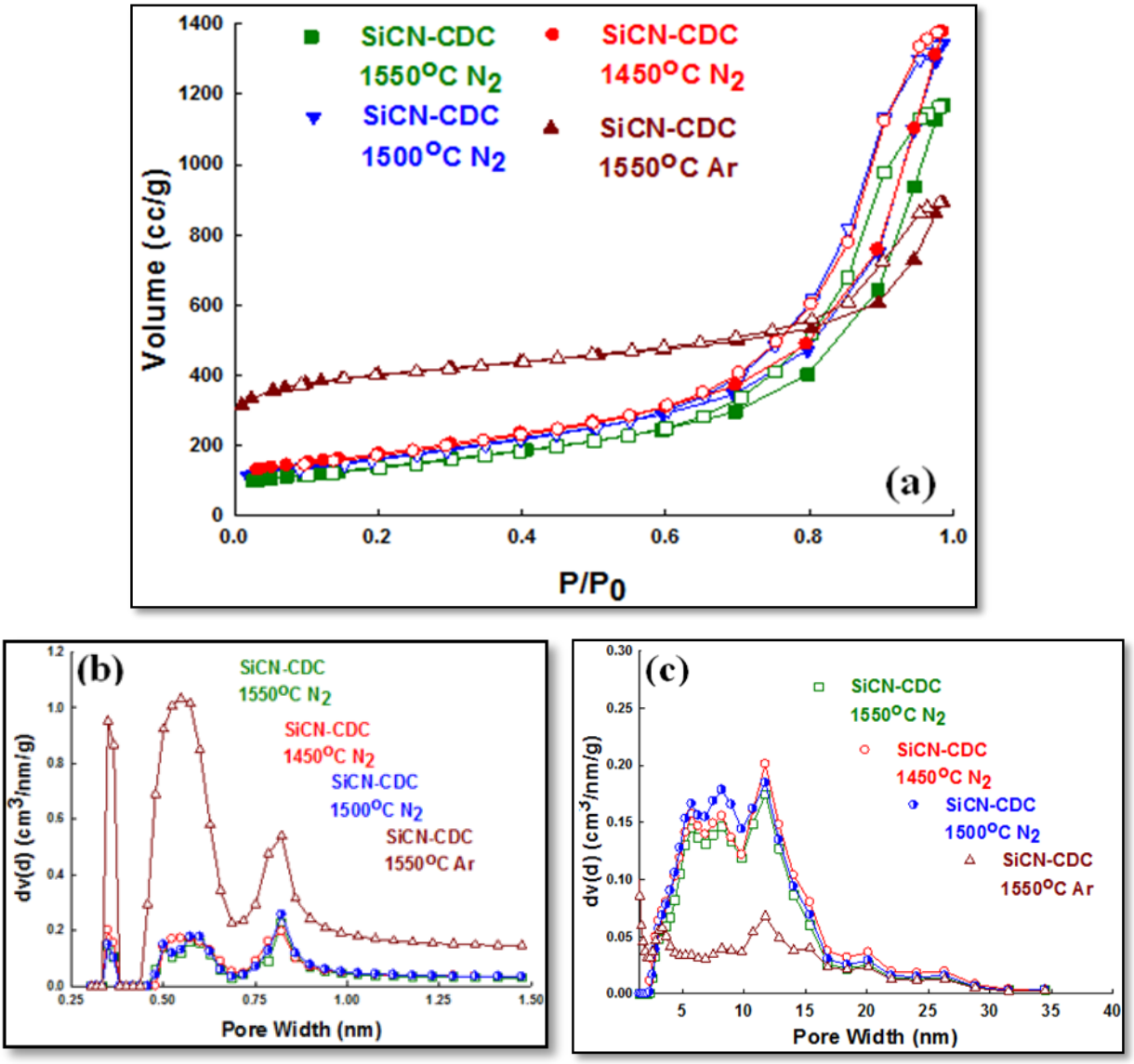

Figure 4.3-20. N_2 sorption isotherms for SiCN-CDCs etched at (a) 1000 °C. Solid symbols correspond to sorption and empty symbols to desorption of nitrogen, b) Estimated (NLDFT method) pore size distributions using CO_2 adsorption after chlorination (all the samples were annealed by H_2 gas at 600 ^oC for 2 h).

Table 4.3-3. Porosity characteristics of SiCN-CDCs, obtained by N_2 and CO_2 gas sorption technique (all the samples were annealed by H_2 gas at 600 ^oC for 2 h).

Pyrolysis Temperature (°C) Atmosphere	Chlorination Temperature (°C)	BET SSA (m^2/g)	Average Pore Size (nm)
1550 / N_2	1200	723	8.8
	1000	498	10.4
1500 / N_2	1200	791	8.7
	1000	593	10.5
1450 / N_2	1200	741	8.5
	1000	631	11.1
1550 / Ar	1200	1166	n.m.
	1000	1268	n.m.

n.m.: not measured

The measured the methane (CH_4) uptake values for the samples treated under Ar or N_2 and chlorinated, are given in **Figure 4.3-21**(a) and (b), respectively. It is known that the storage of CH_4 requires materials with high SSA having micropores close to 1 nm or smaller, this is parallel with our findings; the values obtained from the samples treated under Ar are much higher than that of the N_2 treated ones since the samples treated under Ar and etched by Cl_2 have micropores and higher SSA (see the effect of SSA on the storage capacity for the same sample when it is chlorinated at different temperatures, **Figure 4.3-21** (a)) compared to N_2 treated ones which have micro but mostly meso pores and lower SSA. Similar requirements are needed for H_2 storage, therefore, we only tested Ar treated sample and compared the result with TiC-CDC material which is known with its high SSA and a very narrow micropore size.[13, 15] The result are quite encouraging, see Figure 4.3-21(c), showing ~3wt of H_2 storage at low pressure zone. However, concerning most of the samples produced under N_2, applications of gas storage seems not a feasible process. Catalyst support, battery electrodes, and especially protein sorption which

necessitate pores around ~10nm are possible applications to explore for these N_2 treated and chlorinated SiCN-CDC materials.

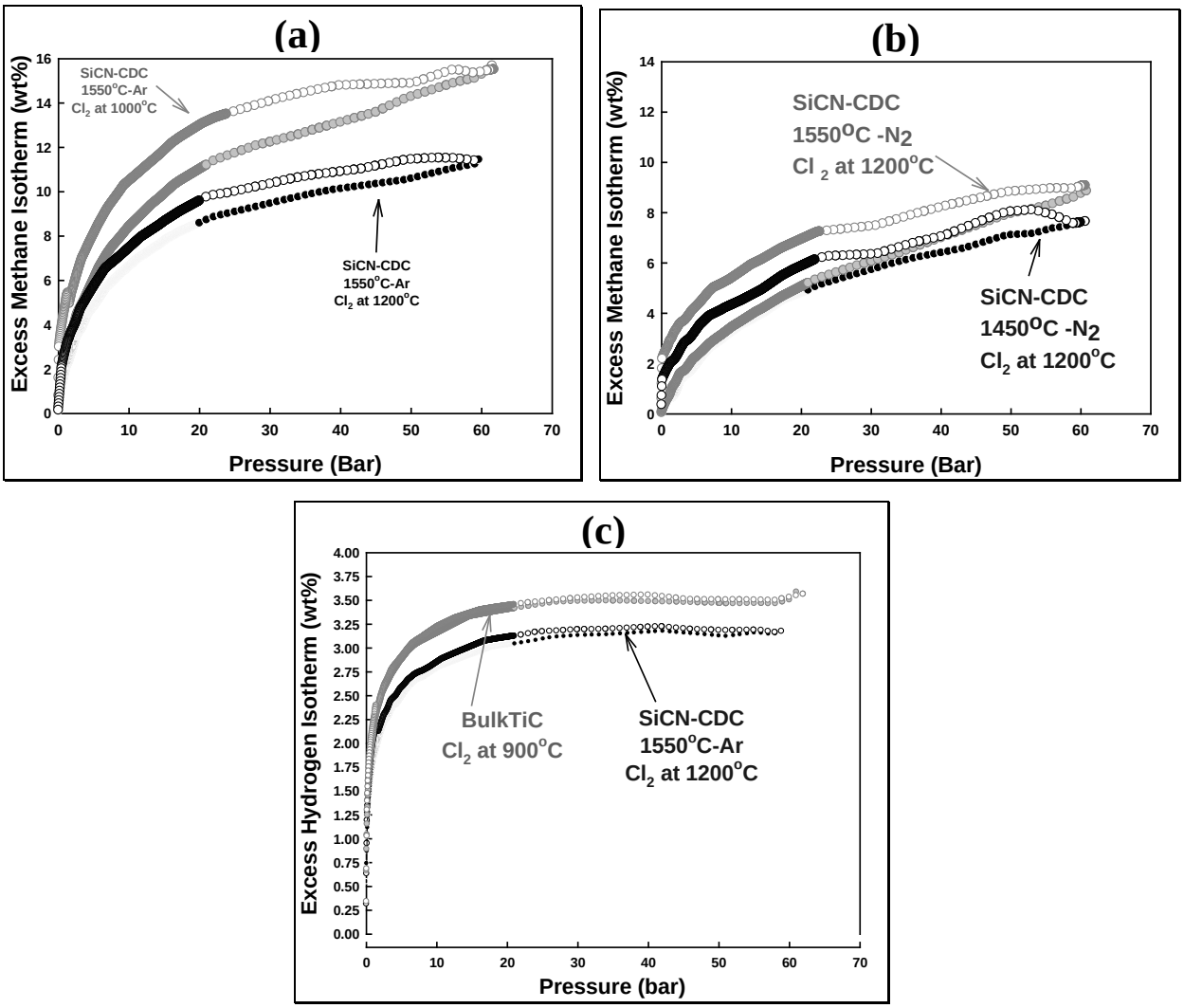

Figure 4.3-21. a) CH_4 uptake at 298K for the SiCN(1550°C/Ar)-CDC samples chlorinated at either 1000°C or 1200°C, b) CH_4 uptake at 298K for the SiCN(1450°C and 1550°C/N_2)-CDC samples both chlorinated at 1200°C, and c) H_2 uptake at 77K for SiCN(1550°C/Ar)-CDC chlorinated at 1200°C. Solid symbols correspond to adsorption and empty ones to desorption of the applied gas (samples were annealed by H_2 gas at 600°C for 2h before the application of test).

Finally it should be mentioned that, by coupling of preceramic polymers with active fillers forming carbides during pyrolysis[39] further possibilities of tailoring the microstructure of the resulting CDCs can be explored. Furthermore, this breakthrough in carbon technology holds significant promise for the detoxification treatments and removal of toxins in the human body, [40] which are sorely needed. This work is currently under way.

4.3.3.2. Etching of polymer-derived SiBCN ceramics

Some preliminary experiments have been applied to produce CDC materials from SiBCN ceramics and compare their results with the ones belonging to the SiCN-CDC. For SiBCN up to now, in reality despite of intensive B and C NMR and HRTEM studies during last 10 years, its still obscure if BCN layer/phase exists or not. From thermodynamic point of view, BN and graphite are two stable phases beside of SiC and Si_3N_4 in these ceramics. Therefore, two theories have been postulated; i) the formation of BCN is possible only in the form of BN-C-BN-C-BN-C layers. However, it is not clear in this theory that whether there is chemical bonding between BN and graphite layers or not, ii) in a less extend some researchers are thinking that there is a layer consisting of B, N and C as a one phase. The study on etching of Si-B-C-N ceramics can take us one step forward about understanding the nature of BNC layers.

The boron modified polysilazane precursor pyrolyzed at 1100°C/4h/Ar and had the chemical composition of Si 46.6wt%, C 28.7wt%, N 19.8wt%, B 3.6wt%, O 0.9wt%, and H 0.6wt% found by elemental analysis. This sample also annealed at 1400°C/4h/Ar and 1800°C/4h/Ar to alter the phase evolution thus three different types of ceramic powders are used in the chlorination experiments in two different chlorination temperatures namely 800°C or 1200°C. It is shown that the same type of modified polysilazane precursor remains X-ray amorphous till to the temperatures of ~1400°C and above phase separation/crystallization occurs resulting only around 1800°C a polycrystalline material. The details on thermal stability of these amorphous Si(B)CN PDC materials can be found elsewhere.[21, 41] Here we will only give some very preliminary BET results obtained after chlorination of these SiBCN materials treated in between 1100-1800°C. The results are documented in **Table 4.3-4**. Although, these results need careful further

characterizations like previously given ones for SiCN-CDC system, it seems that the samples did not yield with SSA values like the ones obtained from the SiCN-CDC materials. The mean pore size is also smaller than that of the SiCN-CDC implying smaller Si-C, Si-N, B-N domain/crystalline sized precipitates. Although the mean pore diameters slightly increased with the increase in annealing temperature, maximum of 4.1nm is obtained from the sample treated at 1800°C. Comparing the BET results obtained from SiCN ceramics, it seems that there is a profound effect of boron on the nano/meso structural phase evolution; it seems that boron inhibits the formation or growth of Si-N domains. In fact, it is recently shown that incorporation of boron promotes the formation of nano SiC as the first crystalline phase within the amorphous matrix whereas the crystallization of nano-sized Si_3N_4 is significantly retarded.[21] If this is the case then by TEM investigations we may see smaller diameter sized pores encapsulated in graphite or possible B-C-N turbostratic layers. Although, these issues will have to be investigated more in detail in order to be sure and certainly here it's just a speculation depending only on BET data and previous observations, initial results are quite encouraging to extend the research effort on etching of boron containing PDC materials.

Table 4.3-4. Porosity characteristics of SiBCN ceramics after chlorine etching (all the samples were annealed by H_2 gas at 600 ^oC for 2h).

Sample	BET SSA (m^2/g)	BJH SSA (m^2/g)	Pore Diam. (nm)	T-Micropore A (m^2/g)	T-External SA (m^2/g)
SiBCN (1100°C) - Cl_2 at 800°C	758	358	3.046	14	743
SiBCN (1100°C) - Cl_2 at 1200°C	920	178	3.027	52	868
SiBCN (1400°C) - Cl_2 at 800°C	70	20	3.037	8	62
SiBCN (1400°C) - Cl_2 at 1200°C	560	nm	nm	nm	nm
SiBCN (1800°C) - Cl_2 at 800°C	173	119	3.033	0	172
SiBCN (1800°C) - Cl_2 at 1200°C	1349	717	4.102	109	1239

4.3.4. Conclusions

An etching process in which amorphous or crystalline polymer-derived SiCN ceramics have been used to form CDCs possessing a hierarchical pore structure (bi-modal: micro and mesopores with mean pore size, 3-10 nm) and large BET surface area, up to 2400 m^2/g. Microstructural investigations show that SiCN remains homogeneous and amorphous up to a pyrolysis temperature of 1200°C, above which nano-crystals of Si_3N_4, SiC and graphite begin to form. Micropores formed by etching Si atoms from the SiC phase, while mesopores derive from the elimination of Si-N moieties. The resulting porosity (pore size, PSD, and SSA) strongly depend on pyrolysis conditions of the preceramic polymer, as well as on etching conditions. The mean pore size increases with increasing pyrolysis temperature. On the other hand, etching temperatures higher than the pyrolysis temperature do not affect the mean pore size, but leads to large BET surface area owing to the high purity. The value of 4-11 nm mean pore size distribution is derived from N_2 adsorption-desorption analysis which is the highest among CDC materials.

In conclusion, the etching of polymer-derived-ceramics has been shown to be an innovative, versatile and effective way to produce porous carbon materials with very high specific surface area and large mesopore volume, potentially suitable for applications such as enterosorbents, absorption of proteins, and catalyst supports for metal particles.

4.3.5. References

[1]R.C. Bansal, J.B. Donnet, and F. Stoeckli, "Active Carbon," pp. 482, *Marcel Dekker*, New York (1988).

[2]C. Liang, Z. Li, and S. Dai, "Mesoporous Carbon Materials: Synthesis and Modification," *Angewandte Chemie International Edition*, 47 [20] 3696-717 (2008).

[3]R.T. Yang, "Adsorbents : Fundamentals and Applications," pp. 410, *Wiley-Interscience, New Yourk*, (2003).

[4]A.-H. Lu and F. Schüth, "Nanocasting: A Versatile Strategy for Creating Nanostructured Porous Materials," *Advanced Materials*, 18 [14] 1793-805 (2006).

[5]J.S. Beck, J.C. Vartuli, W.J. Roth, M.E. Leonowicz, C.T. Kresge, K.D. Schmitt, C.T.W. Chu, D.H. Olson, and E.W. Sheppard, "A new family of mesoporous molecular sieves prepared with liquid crystal templates," *Journal of the American Ceramic Society*, 114 [27] 10834-43 (1992).

[6]M. Kruk, B. Dufour, E.B. Celer, T. Kowalewski, M. Jaroniec, and K. Matyjaszewski, "Synthesis of Mesoporous Carbons Using Ordered and Disordered Mesoporous Silica Templates and Polyacrylonitrile as Carbon Precursor," *Journal of Physical Chemistry. B*, 109 [19] 9216-25 (2005).

[7]Y. Gogotsi, A. Nikitin, H. Ye, W. Zhou, J.E. Fischer, B. Yi, H.C. Foley, and M.W. Barsoum, "Nanoporous carbide-derived carbon with tunable pore size," *Nature Materials*, 2 [9] 591-4 (2003).

[8]J. Chmiola, G. Yushin, R. Dash, and Y. Gogotsi, "Effect of pore size and surface area of carbide derived carbons on specific capacitance," *Journal of Power Sources*, 158 [1] 765-72 (2006).

[9]D.A. Ersoy, M.J. McNallan, and Y. Gogotsi, "Carbon coatings produced by high temperature chlorination of silicon carbide ceramics," *Materials Research Innovations*, 5 [2] 55-62 (2001).

[10]S. Osswald, C. Portet, Y. Gogotsi, G. Laudisio, J.P. Singer, J.E. Fischer, V.V. Sokolov, J.A. Kukushkina, and A.E. Kravchik, "Porosity control in nanoporous carbide-derived carbon by oxidation in air and carbon dioxide," *Journal of Solid State Chemistry*, (in Press, 2009).

[11]S.-H. Yeon, S. Osswald, Y. Gogotsi, J.P. Singer, J.M. Simmons, J.E. Fischer, M.A. Lillo-Rodenas, and A. Linares-Solano, "Enhanced methane storage of chemically and physically activated carbide-derived carbon," *Journal of Power Sources*, 191 [2] 560-7 (2009).

[12]R.K. Dash, G. Yushin, and Y. Gogotsi, "Synthesis, structure and porosity analysis of microporous and mesoporous carbon derived from zirconium carbide," *Microporous and Mesoporous Materials*, 86 [1-3] 50-7 (2005).

[13]R. Dash, J. Chmiola, G. Yushin, Y. Gogotsi, G. Laudisio, J. Singer, J. Fischer, and S. Kucheyev, "Titanium carbide derived nanoporous carbon for energy-related applications," *Carbon*, 44 [12] 2489-97 (2006).

[14]Y. Gogotsi, "Carbon Nanomaterials," pp. 326, Crc Press, 2006.

[15]G.N. Yushin, E.N. Hoffman, A. Nikitin, H. Ye, M.W. Barsoum, and Y. Gogotsi, "Synthesis of nanoporous carbide-derived carbon by chlorination of titanium silicon carbide," *Carbon*, 43 [10] 2075-82 (2005).

[16]K.L. Vyshnyakova, G. Yushin, L.N. Pereselentseva, and Y. Gogotsi, "Formation of Porous SiC Ceramics by Pyrolysis of Wood Impregnated with Silica," *International Journal of Applied Ceramic Technology*, 3 [6] 485-90 (2006).

[17]G. Yushin, Z.G. Cambaz, Y. Gogotsi, K.L. Vyshnyakova, and L.N. Pereselentseva, "Carbothermal Synthesis of β-SiC Micro-Ribbons," *Journal of the American Ceramic Society*, 91 [1] 83-7 (2008).

[18]S.-H. Yeon, P. Reddington, Y. Gogotsi, J.E. Fischer, C. Vakifahmetoglu, and P. Colombo, "Carbide-Derived-Carbons with Hierarchical Porosity from a Preceramic Polymer," *Carbon*, 48 [1] 201-10 (2010).

[19]P. Krawiec, E. Kockrick, L. Borchardt, D. Geiger, A. Corma, and S. Kaskel, "Ordered Mesoporous Carbide Derived Carbons: Novel Materials for Catalysis and Adsorption," *The Journal of Physical Chemistry C*, 113 [18] 7755-61 (2009).

[20]M. Rose, E. Kockrick, I. Senkovska, and S. Kaskel, "High surface area carbide-derived carbon fibers produced by electrospinning of polycarbosilane precursors," *Carbon*, 48 [2] 403-7.

[21]A.H. Tavakoli, P. Gerstel, J.A. Golczewski, and J. Bill, "Effect of boron on the crystallization of amorphous Si–(B–)C–N polymer-derived ceramics," *Journal of Non-Crystalline Solids*, 355 2381–9 (2009).

[22]P.I. Ravikovitch and A.V. Neimark, "Characterization of nanoporous materials from adsorption and desorption isotherms," *Colloids and Surfaces. A*, 187-188 11-21 (2001).

[23]H.-J. Kleebe, D. Suttor, H. MÜler, and G. Ziegler, "Decomposition-Crystallization of Polymer-Derived Si-C-N Ceramics," *Journal of the American Ceramic Society*, 81 [11] 2971-7 (1998).

[24]Y.-L. Li, E. Kroke, R. Riedel, C. Fasel, C. Gervais, and F. Babonneau, "Thermal cross-linking and pyrolytic conversion of poly(ureamethylvinyl)silazanes to silicon-based ceramics," *Applied Organometallic Chemistry*, 15 [10] 820-32 (2001).

[25]C. Haluschka, H.-J. Kleebe, R. Franke, and R. Riedel, "Silicon carbonitride ceramics derived from polysilazanes Part I. Investigation of compositional and structural properties," *Journal of the European Ceramic Society*, 20 [9] 1355-64 (2000).

[26]M. Friess, J. Bill, J. Golczewski, A. Zimmermann, F. Aldinger, R. Riedel, and R. Raj, "Crystallization of Polymer-Derived Silicon Carbonitride at 1873 K under Nitrogen Overpressure," *Journal of the American Ceramic Society*, 85 [10] 2587-9 (2002).

[27]H.J. Seifert, J. Peng, H.L. Lukas, and F. Aldinger, "Phase equilibria and thermal analysis of Si-C-N ceramics," *Journal of Alloys and Compounds*, 320 [2] 251-61 (2001).

[28]C. Thomsen and S. Reich, "Double Resonant Raman Scattering in Graphite," *Physical Review Letters*, 85 [24] 5214 (2000).

[29]F. Tuinstra and J.L. Koenig, "Raman Spectrum of Graphite," *Journal of Chemical Physics*, 53 [3] 1126-30 (1970).

[30]R.J. Nemanich and S.A. Solin, "First- and second-order Raman scattering from finite-size crystals of graphite," *Physical Review B (Condensed Matter)*, 20 [2] 392 (1979).

[31]Z.H. Ni, H.M. Fan, X.F. Fan, H.M. Wang, Z. Zheng, Y.P. Feng, Y.H. Wu, and Z.X. Shen, "High temperature Raman spectroscopy studies of carbon nanowalls," *Journal of Raman Spectroscopy.*, 38 [11] 1449-53 (2007).

[32]S. Kurita, A. Yoshimura, H. Kawamoto, T. Uchida, K. Kojima, M. Tachibana, P. Molina-Morales, and H. Nakai, "Raman spectra of carbon nanowalls grown by plasma-enhanced chemical vapor deposition," *Journal of Applied Physics*, 97 [10] 104320 (2005).

[33]H.-J. Kleebe, "Microstructure and Stability of Polymer-Derived Ceramics; the Si-C-N System," *Physica status solidi. A. Applied research*, 166 [1] 297-313 (1998).

[34]H. Schmidt, D. Koch, G. Grathwohl, and P. Colombo, "Micro-Macroporous Ceramics from Preceramic Precursors," *Journal of the American Ceramic Society*, 84 [10] 2252-5 (2001).

[35]T.L. Cottrell, "The Strengths of Chemical Bonds," pp. 317, Butterworths Scientific Publications, London, 1958.

[36]M. Grandbois, M. Beyer, M. Rief, H. Clausen-Schaumann, and H.E. Gaub, "How Strong Is a Covalent Bond?," *Science*, 283 [5408] 1727-30 (1999).

[37]X. Li and M.J. Edirisinghe, "Structural evaluation of polysilane-derived products: from amorphous to thermodynamically stable phases," *Philosophical Magazine*, 84 [7] 647 - 71 (2004).

[38]H. Schmidt, G. Borchardt, A. Müller, and J. Bill, "Formation kinetics of crystalline Si3N4/SiC composites from amorphous Si-C-N ceramics," *Journal of Non-Crystalline Solids*, 341 [1-3] 133-40 (2004).

[39]P. Greil, "Active-Filler-Controlled Pyrolysis of Preceramic Polymers," *Journal of the American Ceramic Society*, 78 [4] 835-48 (1995).

[40]G. Yushin, E.N. Hoffman, M.W. Barsoum, Y. Gogotsi, C.A. Howell, S.R. Sandeman, G.J. Phillips, A.W. Lloyd, and S.V. Mikhalovsky, "Mesoporous carbide-derived carbon with porosity tuned for efficient adsorption of cytokines," *Biomaterials*, 27 [34] 5755-62 (2006).

[41]A.H. Tavakoli, J.A. Golczewski, and J. Bill, "Thermal Stability: Decomposition and Crystallization," in Polymer Derived Ceramics. From Nano-Structure to Applications. Edited by P. Colombo, et al. DESTech Publications, Lancaster, PA, 2009.

CHAPTER V

SUMMARY & GENERAL CONCLUSIONS

In connection with the main aims and motivations previously described throughout of this work, the primary work was devoted to the production of different cellular PDC components. In this context; first cellular SiOC ceramics were produced by means of three different types of polysiloxane precursors. Linear PDMS and two different polysilsesquioxanes, which contain either methyl or methyl-phenyl side groups), were mixed, crosslinked and pyrolyzed at 1200°C, resulting in the formation of macroporous ceramic components. Pore formation was ascribed to the different behavior of the precursors upon pyrolysis, that is to say much larger weight loss, shrinkage and gas evolution for the linear polysiloxane in comparison to the silicone resins. The amount of porosity depended on the amount of PDMS, of which role can be characterized as a "sacrificial filler" here, brought on the formation of pores ranging from a few microns to a few hundred microns.

In this manner; a particle based methodology analogous to the powder metallurgy techniques has been explored to produce macroporous SiOC bodies. Commercial polysiloxane precursors were crosslinked, crushed, and then sieved to different particle sized powders. The selected sized powder was compacted in a various proportions together with binder being the same or different type of partially cured or non cured polysiloxane, by cold pressing at 55 MPa. The shaped green bodies were pyrolyzed at 1200°C under nitrogen atmosphere. Highly porous SiOC monoliths (with around 50 vol% of total porosity (mostly open) were obtained. The resulted ceramic bodies showed compressive strength values reaching to 37.4MPa with ~53vol% porosity. In step part of the study, samples were rendered to be conductive by heat treating for 45h in a hot-isostatic-press (HIP) under N_2 atmosphere with a peak temperature of 1400°C and a maximum pressure of

~26MPa, conducing to the formation of SiOC(N) tablets having extremely high piezoresistivity in between 100-1700 at high temperatures (700-1000°C).

The production of Microcellular SiOCN and Macrocellular SiCN ceramic foams was accomplished through two different routes by using a polysilazane preceramic polymer. In the adoption of first route, mixture of partially crosslinked polysilazane precursor and polymethylmetacrylate microspheres, used as sacrificial fillers, was warm pressed and pyrolyzed to obtain microcellular SiOCN foams. In the second route, the blend obtained by mixing liquid polysilazane and a physical blowing agent, was cured and pyrolyzed, resulted in the formation of macro-cellular ceramics in a one-step process. According as the former processing method or the latter, ceramic components differed in morphology and characteristics were fabricated. The foams had a mostly interconnected porosity varying from ~60 to 80 vol% and possessed a compressive strength in the range ~1 to 11 MPa. Utilization of sacrificial fillers, conduced to the formation of some oxygen contamination in the foams, due very likely to the adsorbed humidity on their surface.

In the last part related with the production of cellular PDC components; boron including ceramics has been produced. The preparation of these ceramics was acquired through the adoption of two different routes as well as by using two different precursors. That is to say, a particle based methodology enabled to produce SiO(B)C ceramics by using commercial polyborodiphenylsiloxane, while sacrificial micron size bead templating led to the formation of Si(B)CN system from the lab scale synthesized boron-modified polysilazanes. In both cases ceramics displayed high porosity feature reaching to the values of 70 vol%. Preliminary compression test results obtained from Si(B)CN ceramics was generally lower than 2MPa and the reason was attributed to the bi-modal pore size distribution observed in the tested samples.

For the purpose of producing high specific surface area (SSA) cellular PDC monoliths in possession of hierarchical porosity, one-pot processing methods were explored. In this vial,

Periodic Mesoporous Organosilica (PMO) particles were embedded into a foamed polysiloxane polymer. Subsequent to pyrolysis at 1000°C in inert atmosphere, the formation of permeable SiOC ceramic monoliths with high amount of porosity, ranging in size from hundred of microns to a few nanometers, were attained. The components having a particular surface area of 137 m^2/g retained most of the meso-pores after the pyrolytic conversion of the PMO precursor particles. The obtained porous ceramics displayed compression strength of about 1.7 MPa.

By the method; catalyst assisted pyrolysis (CAP), we have demonstrated; how cellular SiOC ceramic composites having 3D interconnected porosity (generally >70vol%) decorated with 1D nanostructures can be produced. It was detected that, the existence of metallic catalyst particles directly contributed to the growth of various nanowire types during the pyrolysis of porous thermosets which was made from a polysiloxane precursor together with a gas-generating porogen. Contingent on the processing atmosphere, silicon oxynitride (Si_2N_2O), silicon nitride (Si_3N_4) or silicon carbide (SiC) nanowires were formed with a length of several microns. In particular heating in N_2 atmosphere led to the growth of significant amount Si_2N_2O nanowires when low carbon including polysiloxane precursor is used, while Si_3N_4 nanowires were obtained from the high carbon containing precursor. Instead, thermolysis under Ar produced SiC nanowires with the high carbon containing precursor. The residual matrix comprised of a partially crystallized SiOC phase which embodied SiC nanocrystals and carbon having both graphitic and amorphous structure depending on the pyrolysis conditions.

It was observed that there is a causal relation between pyrolysis conditions and the morphology and the quantity of nanostructures; namely, an increase in the temperature brought about increase in length and the amount of nanostructures. XRD and HRTEM investigations together with ELS and EDXS methods gave us a chance to verify the growth mechanisms of nanowires, which was dependent on the pyrolysis atmosphere and catalyst type. For N_2 pyrolysis when Fe was used the mechanism was based on gas phase reactions, while when Co was used VLS mechanism was found to be responsible for the growth of nitride based nanowires, for Ar pyrolysis VLS mechanism was observed on both types of metallic sources. Through BET analysis, it was shown

that in the presence of the nanowires, high SSA values were provided to the macro-porous ceramics, ranging from 10 to 110 m^2/g. It was found out that, the SSA values of Co-containing samples were higher than that of the samples containing Fe as a catalyst. The difference in the values was elucidated with reference to the morphological and quantitative dissimilarity of the nanowires as a result of different catalyst usage (Co or Fe). It is envisioned that the ceramic components with hierarchical porosity produced in this work, could be used for several applications, including trapping of (nano)particles, gas adsorption or catalysis (e.g. Fischer Tropsch synthesis or N_2O decomposition).

Studies were finalized with the high temperature selective etching of different PDCs by halogen gases in order to produce high specific surface are carbon; called Carbide Derived Carbon (CDC) in the literature. Commercial polysilazane precursors were first cured and then treated at different temperatures to yield with SiCN materials having amorphous and nanocrystalline domains in different proportions and size. Structural investigations showed that SiCN remained homogeneous and amorphous up to a pyrolysis temperature of 1200°C, above which nano-domains of Si-C, Si-N and graphite begin to form, while above 1400°C predominantly polycrystalline material with SiC, Si_3N_4, and graphite phases were obtained. Chlorine etching of these materials at high temperature (800-1200°C) yielded with micro-meso (bi-modal) porous disordered or graphitic CDC materials with specific surface area in the range 800 to 2400 m^2/g. As a contribution to the understanding of the formation process of micropores and mesopores in the hierarchical pore structure produced by etching SiCN ceramics, it was explicated that the mesopores (with mean pore size, 3-11 nm) proceeded from etching silicon nitride (Si_3N_4) nano-sized crystals or amorphous Si-N domains, while the micropores came from SiC domains/crystals. It was found that the end-product, highly mesoporous carbon with very high SSA, have potential in practice and can highly be used for applications as sorbents for proteins or large drug molecules, and supports for metal catalyst nanoparticles. It appears that high temperature chlorine etching of PDCs was not a method only enabling the synthesis of porous carbon materials having a very high specific surface area and a large mesoporous volume with well controlled size, but also it can be used to understand the nanostructural phase evolution of PDC materials.

CURRICULUM VITAE

Education:

Ph.D.- Dipartimento di Ingegneria Meccanica-Settore Materiali, 2009.

Università degli Studi di Padova (UNIPD), Padova, Italy.

M.Sc.- Metallurgical & Materials Engineering, 2005.

Middle East Technical University (METU), Ankara, Turkey.

B.S.- Metallurgical & Materials Engineering, 2002.

Middle East Technical University (METU), Ankara, Turkey.

Work Experience:

- Early Stage Researcher (EU Marie Curie Fellowship holder) – University of Padova (ITALY) (November 2006 – 2009).
- Research assistant, (December 2002 to November 2006) – Institute of Applied Mathematics, Middle East Technical University, Ankara, Turkey.

Publications in Journals:

1) P. Colombo, C. Vakifahmetoglu, and S. Costacurta, "Ceramic Components with Hierarchical Porosity – A review," (Manuscript is in preparation, Journal of Material Science, 2010).

2) C. Vakifahmetoglu, S. Carturan, E. Pippel, J. Woltersdorf, and P. Colombo, "Growth of 1D-Nanostructures in Porous Polymer Derived Ceramics by Catalyst-Assisted-Pyrolysis. Part II: Cobalt Catalyst," (Submitted to Journal of the American Ceramic Society (2010)).

3) K. Terauds, P. E. Jimenez–Sanchez, R. Raj, C. Vakifahmetoglu and P. Colombo "Giant Piezoresistivity of Polymer-Derived Ceramics at High Temperatures", (submitted to Journal of the European Ceramic Society (2009).

4) C. Vakifahmetoglu, E. Pippel, J. Woltersdorf, and P. Colombo, "Growth of 1D-Nanostructures in Porous Polymer Derived Ceramics by Catalyst-Assisted-Pyrolysis. Part I: Iron Catalyst", Journal of the American Ceramic Society (in press, 2009).

5) S-H. Yeon, P. Reddington, Y. Gogotsi, J. E. Fischer, C. Vakifahmetoglu, and P. Colombo "Carbide-Derived-Carbons with Hierarchical Porosity from a Preceramic Polymer", Carbon (in press, 2009).

6) C. Vakifahmetoglu, I. Menapace, A. Hirsch, L. Biasetto, R. Hauser, R. Riedel and P. Colombo, "Highly porous macro- and micro-cellular ceramics from a polysilazane precursor", Ceramics International, 35 (2009) 3281–3290.

7) C. Vakifahmetoglu, A. Pauletti, C. Fernandez Martin, F. Babonneau, and P. Colombo, "SiOC ceramic monoliths with hierarchical porosity," *International Journal of Applied Ceramic Technology*, (in press, 2009).

8) C. Vakifahmetoglu, J. Park, F. Korkusuz, A. Ozturk, and M. Timucin, "Production and properties of Apatite-Wollastonite ceramics for biomedical applications," Interceram: International Ceramic Review, 2-3 (2009) 86-90.

9) C. Vakifahmetoglu and P. Colombo, "A Direct Method for the Fabrication of Macro-Porous SiOC Ceramics from Preceramic Polymers," *Advanced Engineering Materials*, 10[3] (2008) 256-259.

Proceedings:

10) C. Vakifahmetoglu and P. Colombo, "Porous Polymer Derived Ceramics Decorated with In-situ Grown Nano-structures," Proceeding of Pac-Rim8, (In press, 2009).

11) C. Vakifahmetoglu, J. Park, F. Korkusuz, A. Ozturk, and M. Timucin, "Production and properties of Apatite-Wollastonite ceramics for biomedical applications," pp.

242-251 in Ceramics, Cells and Tissues topic: Nanotechnology for Functional Repair and Regenerative Medicine the Role of Ceramics as In Bulk and as Coating. Edited by A. Ravaglioli and A. Krajewski, Faenza, Italy, 2008.

12) P. Colombo, L. Biasetto, E. Bernardo, S. Costacurta, C. Vakifahmetoglu, R. Peña-Alonso, G. D. Soraru, E. Pippel, J. Woltersdorf, "Hierarchical porosity ceramic components from preceramic polymers," pp. 3-11 in Ceramic Engineering and Science Proceedings, Vol. 28 (9), Porous, Biological and Geopolymer Ceramics. Edited by M. Brito, E. Darrel., and W.M. Kriven, Wiley, 2007.

13) C. Vakifahmetoglu and M. Timucin, "Production and Characterization of Siliconized Hydroxyapatite Ceramics," 13th International Metallurgy and Materials Congress. Edited, Istanbul, Turkey, Proceedings (CD), 2006.

14) C. Vakifahmetoglu, D. Gungor, E. Arikan, S. Bor, "The Effect of Two Phase Annealing Treatments on Cu-Zn-Al Shape Memory Alloys", 11th International Metallurgy and Materials Congress, Istanbul, Turkey, Proceedings, pp.205, 2002.

Conference talks and posters:

- C. Vakifahmetoglu, J. Woltersdorf, E. Pippel, And P.Colombo "Porous Polymer Derived Ceramic Composites Decorated With In-Situ Grown Nano-Structures" (Oral) and C. Vakifahmetoglu And P.Colombo" Novel Strategies To Produce High Specific Surface Area Ceramic Foams From Preceramic Polymers." (poster), Shaping-4, Madrid, Spain, 15-18 November 2009.
- C. Vakifahmetoglu and P. Colombo "Polymer derived ceramic foams with high specific surface area", EUROMAT 2009, 7-10 September, 2009, Glasgow, UK
- C.Vakifahmetoglu, J. Woltersdorf, E. Pippel and P.Colombo "Polymer derived ceramic composites with special designed nano-structures of different functionalities", 11st International Conference and Exhibition of the European Ceramic Society, XI ECerS Conference, 21-25 June, 2009, Krakow, Poland.

- C. Vakifahmetoglu and P. Colombo "Polymer derived ceramic foams with hierarchical porosity", 8th Pacific Rim Conference on Ceramic and Glass Technology, PacRim8, May 31 - June 5, 2009, Vancouver, British Columbia, Canada.
- C. Vakifahmetoglu and P. Colombo "Ceramic foams with hierarchical porosity from preceramic polymers", 33rd International Conference and Exposition on Advanced Ceramics and Composites, January 18-23, 2009-Daytona Beach, Florida-USA.
- C. Vakifahmetoglu, E. Pippel, J. Woltersdorf, P. Colombo, "A Direct method for the fabrication of porous ceramics with hierarchical porosity from preceramic polymers" 8th Conference on Solid State Chemistry, July 6-11, 2008, Bratislava, Slovakia.
- C. Vakifahmetoglu, J. Park, F. Korkusuz, A. Ozturk, M. Timucin `Production and properties of apatite-wollastonite ceramics for biomedical applications' Ceramics, Cells and Tissues, 11th Annual Seminar & Meeting, Nanotechnology for Functional Repair and Regenerative Medicine, The Role of Ceramics as in Bulk and as Coating, Faenza - Italy, October, 2007, Invited Paper [Awarded in 11th CCT prize as `*Honorable Mention*`].
- C. Vakifahmetoglu and M. Timucin, "Production and Characterization of Siliconized Hydroxyapatite Ceramics", 13th International Metallurgy and Materials Congress, Istanbul, Turkey, 2006.
- C. Vakifahmetoglu and P. Colombo, "Porous ceramics fabricated from a mixture of preceramic polymers", (Poster) 2nd International Conference on Ceramics, June 29-July 4, 2008,Verona, Italy.
- C. Vakifahmetoglu, D. Gungor, E. Arikan, S. Bor, "The Effect of Two Phase Annealing Treatments on Cu-Zn-Al Shape Memory Alloys", (Poster) 11th International Metallurgy and Materials Congress, Istanbul, Turkey, 2002.

Awards:

- 11th CCT (Ceramics, Cells and Tissues) congress prize `Honorable Mention` (2007).
- Thesis of the year award, 2005, M.Sc., Middle East Technical University (METU) given by Prof. Dr. Mustafa N. Parlar Education & Research Foundation.